frontiers | Research Topics

Transmission and infection of arboviruses

Edited by
Ke Liu, Zhiyong Ma and James Weger-Lucarelli

Coordinated by
Muddassar Hameed

Published in
Frontiers in Microbiology

ISSN 1664-8714
ISBN 978-2-8325-4800-4
DOI 10.3389/978-2-8325-4800-4

About Frontiers

Frontiers is more than just an open access publisher of scholarly articles: it is a pioneering approach to the world of academia, radically improving the way scholarly research is managed. The grand vision of Frontiers is a world where all people have an equal opportunity to seek, share and generate knowledge. Frontiers provides immediate and permanent online open access to all its publications, but this alone is not enough to realize our grand goals.

Frontiers journal series

The Frontiers journal series is a multi-tier and interdisciplinary set of open-access, online journals, promising a paradigm shift from the current review, selection and dissemination processes in academic publishing. All Frontiers journals are driven by researchers for researchers; therefore, they constitute a service to the scholarly community. At the same time, the *Frontiers journal series* operates on a revolutionary invention, the tiered publishing system, initially addressing specific communities of scholars, and gradually climbing up to broader public understanding, thus serving the interests of the lay society, too.

Dedication to quality

Each Frontiers article is a landmark of the highest quality, thanks to genuinely collaborative interactions between authors and review editors, who include some of the world's best academicians. Research must be certified by peers before entering a stream of knowledge that may eventually reach the public - and shape society; therefore, Frontiers only applies the most rigorous and unbiased reviews. Frontiers revolutionizes research publishing by freely delivering the most outstanding research, evaluated with no bias from both the academic and social point of view. By applying the most advanced information technologies, Frontiers is catapulting scholarly publishing into a new generation.

What are Frontiers Research Topics?

Frontiers Research Topics are very popular trademarks of the *Frontiers journals series*: they are collections of at least ten articles, all centered on a particular subject. With their unique mix of varied contributions from Original Research to Review Articles, Frontiers Research Topics unify the most influential researchers, the latest key findings and historical advances in a hot research area.

Find out more on how to host your own Frontiers Research Topic or contribute to one as an author by contacting the Frontiers editorial office: frontiersin.org/about/contact

Transmission and infection of arboviruses

Topic editors

Ke Liu — Shanghai Veterinary Research Institute, Chinese Academy of Agricultural Sciences, China

Zhiyong Ma — Shanghai Veterinary Research Institute, Chinese Academy of Agricultural Sciences, China

James Weger-Lucarelli — Virginia Tech, United States

Topic coordinator

Muddassar Hameed — Fralin Life Science Institute, Virginia Tech, United States

Citation

Liu, K., Ma, Z., Weger-Lucarelli, J., Hameed, M., eds. (2024). *Transmission and infection of arboviruses*. Lausanne: Frontiers Media SA.

doi: 10.3389/978-2-8325-4800-4

Table of contents

frontiers | Frontiers in Microbiology

TYPE Original Research
PUBLISHED 12 June 2023
DOI 10.3389/fmicb.2023.1189176

OPEN ACCESS

EDITED BY
Ya-Fang Mei,
Umeå University, Sweden

REVIEWED BY
Luke Alphey,
The Pirbright Institute, United Kingdom
Olivia Wesula Lwande,
Umeå University, Sweden

*CORRESPONDENCE
James Weger-Lucarelli
✉ weger@vt.edu

RECEIVED 18 March 2023
ACCEPTED 16 May 2023
PUBLISHED 12 June 2023

CITATION
Webb EM, Compton A, Rai P, Chuong C, Paulson SL, Tu Z and Weger-Lucarelli J (2023) Expression of anti-chikungunya single-domain antibodies in transgenic *Aedes aegypti* reduces vector competence for chikungunya virus and Mayaro virus.
Front. Microbiol. 14:1189176.
doi: 10.3389/fmicb.2023.1189176

Expression of anti-chikungunya single-domain antibodies in transgenic *Aedes aegypti* reduces vector competence for chikungunya virus and Mayaro virus

Emily M. Webb[1], Austin Compton[2], Pallavi Rai[3], Christina Chuong[3], Sally L. Paulson[1], Zhijian Tu[2,4] and James Weger-Lucarelli[1,3,4]*

[1]Department of Entomology, Fralin Life Sciences Institute, Virginia Polytechnic Institute and State University, Blacksburg, VA, United States, [2]Department of Biochemistry, Fralin Life Sciences Institute, Virginia Polytechnic Institute and State University, Blacksburg, VA, United States, [3]Department of Biomedical Sciences and Pathobiology, VA-MD Regional College of Veterinary Medicine, Virginia Polytechnic Institute and State University, Blacksburg, VA, United States, [4]Center for Emerging, Zoonotic and Arthropod-Borne Pathogens, Fralin Life Sciences Institute, Virginia Polytechnic Institute and State University, Blacksburg, VA, United States

Chikungunya virus (CHIKV) and Mayaro virus (MAYV) are closely related alphaviruses that cause acute febrile illness accompanied by an incapacitating polyarthralgia that can persist for years following initial infection. In conjunction with sporadic outbreaks throughout the sub-tropical regions of the Americas, increased global travel to CHIKV- and MAYV-endemic areas has resulted in imported cases of MAYV, as well as imported cases and autochthonous transmission of CHIKV, within the United States and Europe. With increasing prevalence of CHIKV worldwide and MAYV throughout the Americas within the last decade, a heavy focus has been placed on control and prevention programs. To date, the most effective means of controlling the spread of these viruses is through mosquito control programs. However, current programs have limitations in their effectiveness; therefore, novel approaches are necessary to control the spread of these crippling pathogens and lessen their disease burden. We have previously identified and characterized an anti-CHIKV single-domain antibody (sdAb) that potently neutralizes several alphaviruses including Ross River virus and Mayaro virus. Given the close antigenic relationship between MAYV and CHIKV, we formulated a single defense strategy to combat both emerging arboviruses: we generated transgenic *Aedes aegypti* mosquitoes that express two camelid-derived anti-CHIKV sdAbs. Following an infectious bloodmeal, we observed significant reduction in CHIKV and MAYV replication and transmission potential in sdAb-expressing transgenic compared to wild-type mosquitoes; thus, this strategy provides a novel approach to controlling and preventing outbreaks of these pathogens that reduce quality of life throughout the tropical regions of the world.

KEYWORDS

alphavirus, chikungunya virus (CHIKV), Mayaro virus (MAYV), single-domain antibodies (sdAb), *Aedes* (*Ae.*) *aegypti*, transgenic mosquitoes

Introduction

The widely distributed *Aedes* spp. mosquitoes, notably *Ae. aegypti* and *Ae. albopictus*, are vectors for various debilitating pathogens such as yellow fever virus (YFV), dengue virus (DENV), Zika virus (ZIKV), Rift Valley fever virus (RVFV), and chikungunya virus (CHIKV) (Powell, 2018). The primary method of reducing the spread of most arboviral diseases is limiting the interaction between mosquitoes and their human hosts. This is mainly achieved by educating the public on the use of personal protective equipment (e.g., long-sleeved clothing, screens and/or netting, etc.), the use of insect repellents, and ridding properties of standing water (e.g., tires, buckets, pools, etc.). While these tools have proven to be beneficial, some mosquito species, particularly *Ae. aegypti*, have evolved to live in close proximity to humans and are extremely anthropophilic rendering these methods inadequately effective. Therefore, insecticides are used to reduce populations of mosquitoes in more urban settings; however, the environmental impacts of these potentially toxic chemicals have led to great concern. Due to this concern, modern development is focused on the production of insecticides that require fewer applications, have increased specificity, and do not bioaccumulate (Reeves et al., 2019). However, the limited number of approved insecticides, the potency of available insecticides, and, most importantly, the development of insecticide resistance has all played a major role in the emergence and/or re-emergence of many arthropod-borne (arboviral) diseases (Corbel et al., 2017).

In order to control mosquito populations and/or impede disease transmission, novel strategies including genetic manipulations of mosquitoes have been explored over the last few decades. Recent advances have resulted in the release of genetically modified mosquitoes that carry lethal genes in an attempt to suppress natural mosquito populations and, thus, minimize their interaction with human hosts (i.e., population suppression) (Harris et al., 2012; Carvalho et al., 2015; Waltz, 2021; Wang et al., 2021). Alternatively, scientists have developed control programs that focus on replacing natural disease-carrying mosquito populations with pathogen-refractory mosquito populations (i.e., population modification) (Walker et al., 2011; Aliota et al., 2016; Yakob et al., 2017). While both population suppression and population modification strategies are promising, there are several concerns regarding what the impact of reducing mosquito populations may have on the environment (Fang, 2010) as well as concerns regarding the stability of transinfected organisms, such as *Wolbachia*, within certain environmental conditions (e.g., climate and mosquito diet) (Ross et al., 2019). With this being said, there is still a crucial need for the continued exploration of novel mosquito control strategies in order to combat arboviruses.

CHIKV and Mayaro virus (MAYV) are medically-relevant arboviruses belonging to the *Togaviridae* virus family and *Alphavirus* genus that infect millions of people annually, with CHIKV being responsible for the vast majority of these cases. Infections with these viruses typically result in a febrile illness that is accompanied by incapacitating joint pain that can last for years following infection (Partidos et al., 2011; Elsinga et al., 2017). Both CHIKV and MAYV have become increasingly prevalent throughout the Americas within the past several years. Thus, there is an expanding need for novel approaches to control these viruses. Several studies have been conducted to understand cross-protective immunity among alphaviruses (Hearn, 1961; Latif et al., 1979; Peck et al., 1979; Wust et al., 1987; Partidos et al., 2012; Fox et al., 2015; Webb et al., 2019). In particular, antibodies developed against CHIKV can neutralize and cross-protect against infection with MAYV (Fox et al., 2015; Webb et al., 2019). Our previous studies have characterized a camelid-derived anti-CHIKV single-domain antibody (sdAb) that has potent cross-protective activity against other medically-relevant alphaviruses, including MAYV (Liu et al., 2021). Camelid sdAbs have many advantages when compared to conventional mammalian antibodies, including: increased thermostability, ease of production, and small size (~15 kDa) when compared to conventional mammalian antibodies (Figure 1).

Ultimately, these advantages and the cross-protective capabilities of the aforementioned CHIKV sdAbs provide a unique antiviral strategy. First, we demonstrated potent neutralization of CHIKV and MAYV in the presence of these two anti-CHIKV sdAbs *in vitro*. With these data in mind, we then designed and developed transgenic *Ae. aegypti* mosquitoes that express two different anti-CHIKV sdAbs targeting both CHIKV and MAYV. We then observed a statistically significant reduction of CHIKV and MAYV dissemination and transmission rates in the sdAb-expressing transgenic mosquitoes and reduced viral titers throughout the transgenic mosquitoes, thus limiting the overall transmission potential of both viruses. This transgenic strategy provides a proof of concept for the use of camelid- derived sdAbs in modified mosquito populations and has the potential to be used in future population modification strategies to co-target CHIKV, MAYV, and possibly other closely-related alphaviruses.

Methods and materials

Virus propagation and cell culture

The CHIKV and MAYV strains used in this study were obtained from the World Reference Center for Emerging Viruses and Arboviruses (WRCEVA) at the University of Texas Medical Branch (Galveston, TX), with the exception CHIKV SL-15649 (ECSA lineage), a kind gift from Dr. Mark Heise (Morrison et al., 2011). The viruses obtained from WRCEVA include MAYV 12A (genotype L), MAYV TRVL-4675 (genotype D), and CHIKV H-20235 (Asian lineage). African green monkey kidney (Vero) cells were used to propagate viruses. Vero cells were purchased from American Type Culture Collection (Manassas, VA; CCL-81) and maintained with Dulbecco's Modified Eagle Medium (DMEM; Sigma Aldrich; St. Louis, MO) supplemented with L-glutamine, 5% fetal bovine serum (FBS), and 1% gentamycin (herein referred to as Vero cells maintenance media) and kept at 37°C with 5% CO_2. Vero cells were grown to ~85% confluency before being infected with the respective viruses at an MOI of 0.01 in viral diluent (RPMI-1640 media with 25 mM HEPES, 1% BSA, 50 µg/mL Gentamicin, 2.5 µg/mL Amphotericin B). The cells were infected for 1 h at 37°C, with rocking every 10–15 min. After 1 h of incubation, Vero cell maintenance media was added to the flask. Once 50–75% of cells demonstrated cytopathic effects (CPE), the cellular supernatant was collected and clarified by centrifugation at 4°C before storage at −80°C.

Plaque assays

Virus stocks were titrated by plaque assay before use in subsequent experiments. Serial 10-fold dilutions of each sample were made in

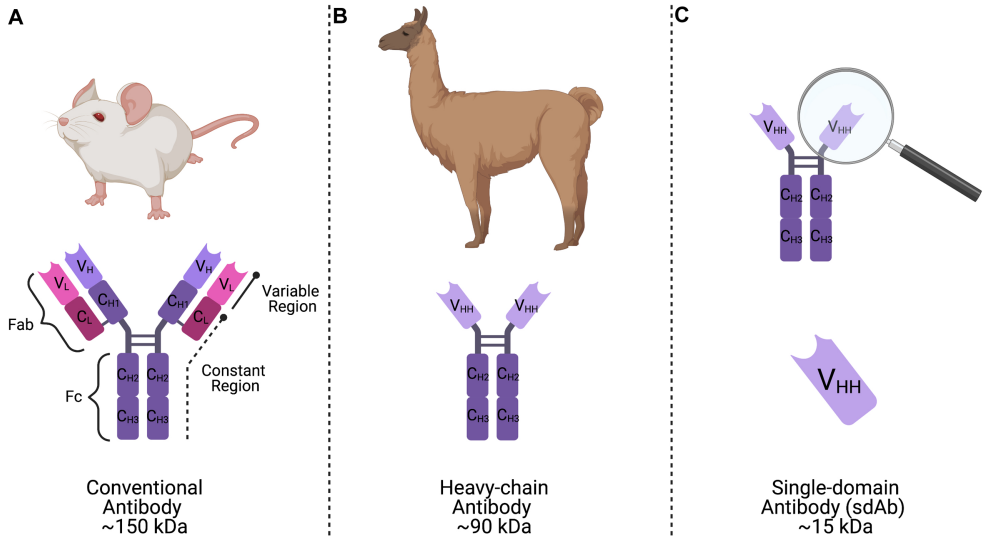

FIGURE 1
Representation of conventional, heavy-chain, and single-domain antibodies. **(A)** Conventional mammalian antibodies are comprised of a basic structure consisting of two variable and constant heavy chains and two variable and constant light chains forming the antigen binding fragment (Fab) region, as well as two constant heavy chains forming the crystallizable fragment (Fc) region. **(B)** Camelid heavy-chain antibodies are composed of two identical constant heavy chains and a variable region (VHH) linked by a curved hinge that is responsible for antigen-binding activity. **(C)** A single-domain antibody (sdAb) is the single antigen binding domain of camelid heavy-chain antibodies, or the VHH region, that has been synthetically produced and retains full functionality.

viral diluent and then added to confluent monolayers of Vero cells. After a 1 h incubation period, an overlay containing 1.5% methylcellulose was added. Plaques were visualized following formalin fixation and staining with crystal violet 3 days post-infection.

Plaque reduction neutralization tests

Purified sdAb samples were serially diluted in viral diluent to the appropriate concentration (10 μg/mL-0.01 μg/mL). Diluted sdAbs, as well as viral diluent (no sdAb) controls, were then mixed with an equal volume of the respective virus at 1,000 PFU/ml. Following a 1.5 h incubation at 37°C, sdAb/virus mixtures were then added to confluent monolayers of Vero cells. After a 1 h incubation period, an overlay containing 1.5% methylcellulose was added. Plaques were visualized following formalin fixation and staining with crystal violet 3 days post-infection. The number of plaques in the wells without sdAbs were counted and taken as control. The average number of plaques from replicates were then expressed as a percentage of that in the control wells.

Cloning the donor construct: AE_CA6CC3

To generate the piggyBac transposon-based plasmid that co-expresses both sdAbs (CA6 and CC3), herein referred to as "AE_CA6CC3," a single coding sequence was designed *in silico* that contained the *Dfurin1* gene of *Drosophila melanogaster* Meigen (Diptera: Drosophilidae) cleavage site (R-Q-K-R) (Cano-Monreal et al., 2010) and *Porcine teschovirus*-1 2A (P2A) self-cleaving peptide (Liu et al., 2017) inserted between the CA6 and CC3 sequences (Figure 2). Sequences for these sdAb can be found in reference [26] (Liu et al., 2019). The entire transcript was codon-optimized for *Drosophila* and commercially synthesized by GENEWIZ, Inc. (South Plainfield, NJ). We then cloned the gene synthesis product containing the *Ae. aegypti* carboxypeptidase A (CpA) promoter, Dfurin 1, P2A, and the sdAb sequences into piggyBac [polyUb GFP] via GeneArt Gibson Assembly cloning (ThermoFisher Scientific, Waltham, MA) per manufacturer's protocol. We sequence-validated the final AE_CA6CC3 construct using Sanger sequencing. All primers for cloning, and subsequent Sanger sequencing, were designed using SnapGene (San Diego, CA) software and obtained from Integrated DNA Technologies. Inc. (IDT; Coralville, IA). AE_CA6CC3 sequence is available through GenBank (accession: OQ921683).

Mosquito rearing

Ae. aegypti Liverpool (LVP) eggs were obtained from BEI resources (Manassas, VA). Mosquitoes were reared and housed at 26°C, relative humidity 60–80%, and 12/12 h light/dark photoperiod. Larvae were fed Nishikoi fish food (Essex, England) and adult mosquitoes were provided with a 10% sucrose solution administered through cotton balls. Mosquitoes were provided defibrinated sheep's blood (Colorado Serum Company; Denver, CO) using artificial membrane feeders for all bloodmeals.

Mosquito transformations

Authors acquired necessary permissions prior to the start of the mosquito experiments. All studies were approved under IBC protocol (18–084) and conducted within an Arthropod Containment Level-3 (ACL-3) facility.

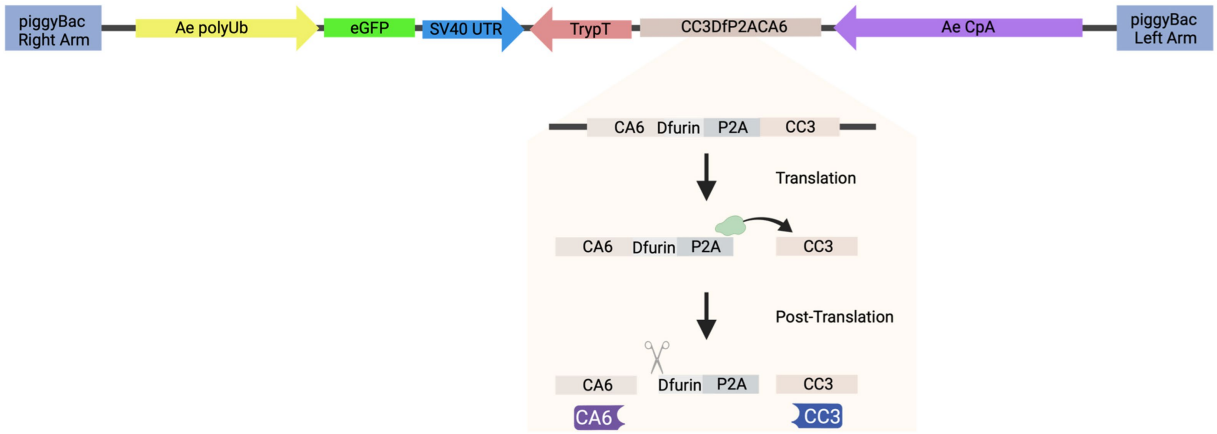

FIGURE 2
Schematic of construct design. AE_CA6CC3 construct design indicating each component of the transformation construct. AE_CA6CC3 was designed to express an eGFP transformation marker (green), constitutively expressed via the *Ae. aegypti* polyubiquitin promoter (Ae polyUb; yellow) to aid in screening and selection of transgenic mosquitoes. Additionally, a fusion peptide consisting of CA6 (i.e., sdAb or VHH), Dfurin 1, P2A, and CC3 (i.e., sdAb or VHH) (beige) was designed under the control of the *Ae. aegypti* carboxypeptidase A promoter (AeCpA; purple) to provide bloodmeal-upregulated, gut-specific gene expression. The P2A linker and Dfurin1 sequences were inserted between the sdAbs so that during translation, ribosomal skipping/translocation is induced (indicated by green ribosome and horizontal arrow) resulting in co-translational cleavage of the polyprotein. Post-translational processing by Dfurin 1 then removes the residual P2A sequence from the upstream gene (CA6; indicated by scissor icon) thus resulting in the production of individual CA6 (purple) and CC3 (blue) sdAbs. AE_CA6CC3 sequence is available through GenBank (accession: OQ921683).

All transformations were carried out by adapting protocols previously described (Chen et al., 2021). PiggyBac donor plasmid (300 ng/μl; piggyBac [AE_CA6CC3]) that contains an enhanced green fluorescent protein (eGFP) transformation marker driven by the *Ae. aegypti* polyubiquitin promoter was co-injected with an *in vitro* transcribed piggyBac mRNA (300 ng/μl) into less than 1 h old embryos of *Ae. aegypti* LVP. The piggyBac-hsp70-transposase plasmid (Handler et al., 1998) was used as a template for *in vitro* transcription using the mMessage mMachine T7 Ultra kit (Thermofisher), followed by MEGAclear (Thermofisher) column purification. Surviving G_0 females were mated to LVP males in pools of 20–25 mosquitoes. Each G_0 male was mated individually with five LVP females in individual cages to isolate each independent line. G_1 larvae were screened for green fluorescence using a Leica M165 FC fluorescence microscope. Positive G_1 individuals were out-crossed to Liverpool mosquitoes to ensure that all transgene cassettes were stably inherited to the G_2 generation.

Western blots

Midguts from WT, AE1, and AE5 mosquitoes ($n = 30$/group; $>G_3$ generation) were dissected 16 h after a bloodmeal and protein was extracted with ice-cold radioimmunoprecipitation assay buffer (RIPA buffer; 50 mM Tris-HCl pH 7.4, 150 mM NaCl, 0.25% Na-deoxy- cholate, 1% NP-40, 1 mM EDTA) containing one cOmplete™, Mini, EDTA-free Protease Inhibitor Cocktail tablet (MilliporeSigma, Burlington, MA). The entire sample was then homogenized and centrifuged at 4°C. Clarified supernatants were transferred to a fresh microcentrifuge tube, pulse-sonicated twice for 10 s each, and mixed with SDS loading buffer. All samples were then placed in a heating block at ~90–95°C for 10 min. Samples were run on a 4–20% SDS-PAGE and transferred to a nitrocellulose membrane. The membranes were then stained with Ponceau S stain to visualize protein transfer. Following destaining, membranes were probed with AffiniPure Goat Anti-Alpaca IgG, VHH domain primary antibody (128–005-232; Jackson ImmunoResearch, West Grove, PA) at a concentration of 15 μg/mL overnight at 4°C. The secondary antibody used was rabbit anti-goat HRP (HAF017; R&D Systems, Minneapolis, MN) at a dilution of 1:1000 per the manufacturer's recommendation. Images were generated by applying Prometheus™ ProSignal™ Pico chemiluminescent ECL reagents (20-300B, Genesee Scientific, San Diego, CA) to the blots and visualized using an Azure c400 gel imaging system (Azure Biosystems, Inc., Dublin, CA).

Vector competence experiments and virus titrations

Vector competence experiments were carried out by adapting protocols previously described (Bates et al., 2021). Female mosquitoes 5–7 days old ($n = 50$) were separated into cartons and sucrose starved for 16 h and H_2O starved for 12 h prior to infection to promote blood-feeding. Mosquitoes were fed virus-spiked bloodmeals containing defibrinated sheep's blood (Colorado Serum Company; Denver, CO) using artificial membrane feeders, and only fully engorged mosquitoes were separated into new containers. Pre- and post-infection blood samples were collected for use as back-titer calculations. Seven days post-infection, mosquitoes were cold-anesthetized and midguts and legs/wings were collected in viral diluent. Saliva was collected through forced salivation for 30 min in immersion oil and then mixed with viral diluent. Samples were stored at −80°C until analyzed by plaque assay. For virus titrations,

all virus-negative mosquito samples were given a value of half the limit of detection (LOD/2) for statistical analyses.

Statistics

For vector competence experiments, data were analyzed via a two-tailed Fisher's exact test. For virus titration experiments, data were analyzed by Kruskal Wallis test with multiple comparisons with undetectable mosquito samples given a value of half the limit of detection (LOD/2) for statistical analyses.

Results

CA6 and CC3 display potent virus neutralization *in vitro*

We previously showed that two anti-CHIKV sdAbs, clones CC3 and CA6, were potent at neutralizing CHIKV (Liu et al., 2019), and that CC3 also has strong neutralizing capacity against MAYV and other related alphaviruses (Liu et al., 2021). We then performed individual sdAb plaque reduction neutralization tests (Figure 3A; PRNTs) and combination PRNTs (Figure 3B). The individual PRNTs were performed to further validate CC3's neutralization activity against MAYV and to demonstrate that CA6 has anti-MAYV activity (Figure 3C). We hypothesized that using both neutralizing sdAbs simultaneously would not interfere with neutralization capacity, thus we performed a series of combination PRNTs to evaluate the level of CHIKV and MAYV neutralization in the presence of both CC3 and CA6 (Figure 3D). These data demonstrate that the use of both CC3 and CA6 at concentrations greater than 0.16 μg/mL, maintain potent neutralization of both CHIKV and MAYV.

Generation of transgenic *Ae. aegypti* colonies expressing sdAbs

We next constructed a piggyBac transposon-based plasmid, herein referred to as "AE_CA6CC3," to co-express both sdAbs in *Ae. aegypti* mosquitoes. AE_CA6CC3 was designed to express both CC3 and CA6 under the control of the *Ae. aegypti* carboxypeptidase A promoter (AeCpA) (Moreira et al., 2000) to provide bloodmeal-upregulated, gut-specific gene expression (Figure 2). The eGFP transformation marker, constitutively expressed via the *Ae. aegypti* polyubiquitin promoter (Ae polyUb) (Anderson et al., 2010), was also included in the design to aid in screening and selection of construct-positive mosquitoes (Figure 4). To generate transgenic mosquitoes, the AE_CA6CC3 donor vector and *piggyBac* mRNA were co-injected into *Ae. aegypti* embryos and the resulting G_0 individuals were outcrossed to wild-type (WT) mosquitoes. In the G_1, GFP-positive individuals identified from each cross in were crossed with WT mosquitoes of the opposite sex to establish multiple independent lines ($n = 5$). Upon further observation, one of the transgenic lines was removed from experimentation due to an apparent male-linked insertion of our construct. The resulting four transgenic lines (AE1, AE2, AE4, and AE5) were reared for multiple generations to expand the colonies for preliminary vector competence studies.

Preliminary analyses allow for selection of optimal transgene phenotype in two transgenic lines

We first performed preliminary vector competence experiments to determine which virus strains should be used to evaluate the transgenic lines. We compared two strains of CHIKV (CHIKV H-20235 and CHIKV SL-15649) and two strains of MAYV (MAYV 12A and MAYV TRVL-4675) in WT *Ae. aegypti* LVP mosquitoes. We spiked bloodmeals with each virus and evaluated virus infection, dissemination, and transmission 7 days post-infection (dpi). Our results indicated the use of CHIKV H-20235 and MAYV 12A for subsequent studies due to the high transmission rates (83 and 75%, respectively; Table 1) in WT mosquitoes. Additionally, both CHIKV H-20235 (Accession: KX262991) and MAYV 12A (Accession: KP842796) were isolated within the last 15 years.

Following the selection of virus strains, the transgenic lines ($n = 4$) were subjected to a preliminary vector competence analysis to assess susceptibility to CHIKV and MAYV. Multiple lines were generated and analyzed because transgene integration is unpredictable when using transposon-based delivery systems and testing of multiple lines facilitates identification of lines with the optimal transgene expression phenotype(s) (Reid et al., 2021). Female mosquitoes from the WT colony and each transgenic line were exposed to either CHIKV or MAYV viremic bloodmeals and infection, dissemination, and transmission rates were calculated 7 days later. AE1 and AE5 were selected for further experimentation since transmission rates were the lowest for each virus (Table 2). Specifically, compared to WT mosquitoes, AE1 transmission was reduced for CHIKV and MAYV ($p = 0.002$ and $p = 0.004$, respectively) and AE5 had a significant reduction ($p = 0.008$) in transmission for CHIKV and a near significant reduction ($p = 0.056$) for MAYV. Interestingly, we observed no differences in dissemination of CHIKV in our transgenic lines, which could be to lower overall systemic titers or due to leaky expression outside of the gut. Further studies can be conducted to assess expression in different compartments.

Transgenic *Ae. aegypti* express CA6 and CC3

To evaluate CA6 and CC3 transgene expression *in vivo*, transgenic *Ae. aegypti* mosquito lines AE1 and AE5 were subjected to Western blot analyses. Midguts from each transgenic line (G_3 and greater) and WT mosquitoes were dissected 16 h post-bloodmeal. Purified CC3 and CA6 sdAbs (a kind gift from Dr. Ellen Goldman) were used as a positive control (Figure 5). As expected, sdAbs were expressed in the midgut tissues of mosquitoes from AE1 and AE5 but not WT mosquitoes. Notably, banding patterns which may suggest unsuccessful ribosomal-skipping of the P2A linker sequence (Liu et al., 2017) thus resulting in a fusion protein of the CA6 and CC3 sdAbs (Figure 5).

AE1 and AE5 reduce overall transmission potential of both CHIKV and MAYV

With selection of the AE1 and AE5 transgenic lines, and evidence of successful sdAb expression in these lines, we performed a larger vector competence experiment to compare infection (virus present in midgut tissues), dissemination (virus present in legs/wings tissues), and transmission (virus present in saliva samples) rates to those of

10.3389/fmicb.2023.1189176

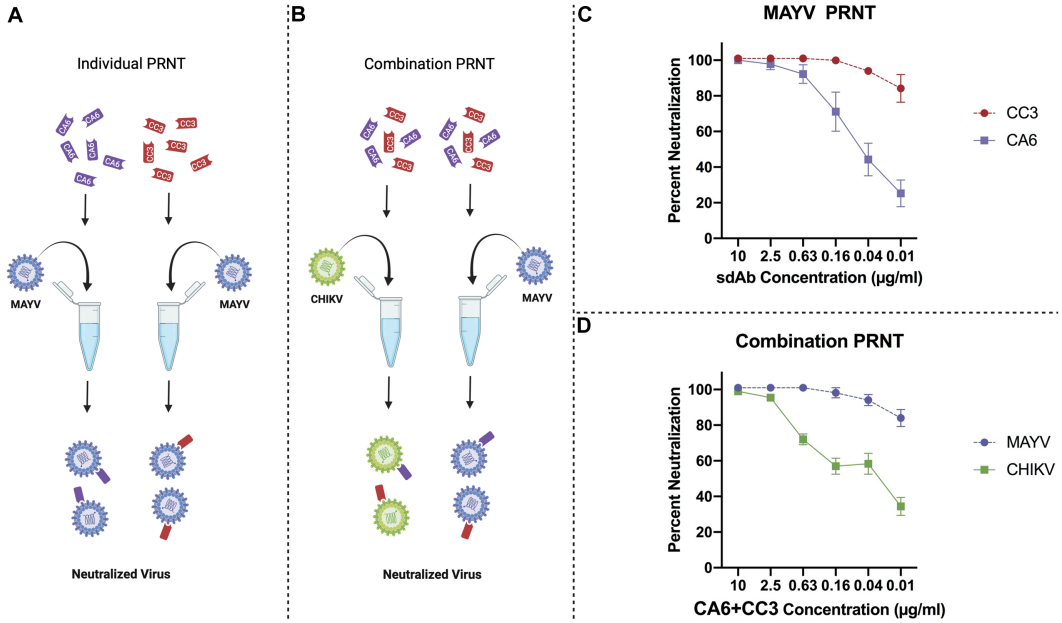

FIGURE 3
General schematic of PRNT methods and virus neutralization data. **(A)** Schematic representing PRNT method of MAYV neutralization using CA6 (dark purple) and CC3 (red). **(B)** Schematic representing combination PRNT method of CHIKV (green) and MAYV (light purple) neutralization via samples mixed with both CA6 (dark purple) and CC3 (red). **(C)** PRNT data provides percent neutralization of MAYV by CC3 (red, circles, dashed line) and CA6 (dark purple, squares, solid line). **(D)** Combination PRNT data provides percent neutralization of MAYV (purple, circles, dashed line) and CHIKV (green, squares, solid line) by mixed samples of both CA6 and CC3. Purified sdAb samples were serially diluted in viral diluent to the appropriate concentration (10 µg/mL–0.01 µg/mL) and then mixed with an equal volume of the respective virus at 1,000 PFU/ml. Data points are representative of six replicates obtained in two independent experiments. Error bars represent SD.

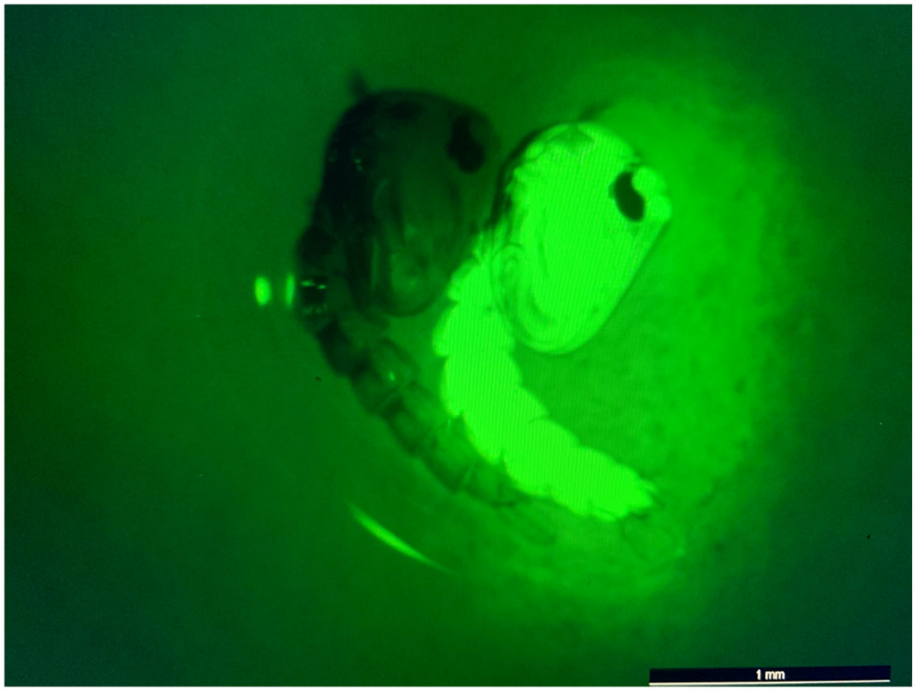

FIGURE 4
eGFP screening process of transgenic pupae. Image of non-transgenic (*left*) and transgenic/eGFP-expressing (*right*) pupae. eGFP screening was performed using a Leica M165 FC fluorescence microscope. All non-transgenic siblings were discarded of and not included in subsequent experiments.

TABLE 1 Preliminary screening of vector competence of WT *Ae. aegypti* LVP mosquitoes for CHIKV and MAYV strains.

Virus	IBM titer	Infection (midgut)	Dissemination (legs/wings)	Transmission (saliva)
CHIKV H-20235 (Asian)	8.53E+07	12/12 (100%)	12/12 (100%)	10/12 (83%)
CHIKV SL-15649 (ECSA)	4.00E+07	11/12 (92%)	9/12 (75%)	3/12 (25%)
MAYV 12A (L)	9.67E+07	12/12 (100%)	12/12 (100%)	9/12 (75%)
MAYV TRVL-4675 (D)	1.40E+08	11/12 (92%)	11/12 (92%)	5/12 (42%)

CHIKV H-20235 (representing the Asian lineage), CHIKV SL-15649 (representing the ECSA lineage), MAYV 12A (representing the L genotype), and MAYV TRVL-4675 (representing the D genotype) were used in these studies. Data are presented as the number of virus positive/number tested with rates of infection (virus present in midgut tissues), dissemination (virus present in legs/wings tissues), and transmission (virus present in saliva samples) indicated by percentages in parentheses. IBM, infectious blood meal.

TABLE 2 Preliminary vector competence of transgenic and WT *Ae. aegypti* mosquitoes for CHIKV H-20235 and MAYV 12A.

Virus	Transgenic line	Infection (midgut)	Dissemination (legs/wings)	Transmission (saliva)
CHIKV H-20235 IBM titer: 6.23E+07	**AE1**	20/20 (100%) *1.000*	17/20 (85%) *0.231*	**2/20 (10%)** ***0.002***
	AE2	20/20 (100%) *1.000*	20/20 (100%) *1.000*	8/20 (40%) *0.343*
	AE4	20/20 (100%) *1.000*	19/20 (95%) *1.000*	9/20 (45%) *0.527*
	AE5	20/20 (100%) *1.000*	18/20 (90%) *0.487*	**3/20 (15%)** ***0.008***
	WT	20/20 (100%) *N/A*	20/20 (100%) *N/A*	12/20 (60%) *N/A*
MAYV 12A IBM titer: 9.87E+06	**AE1**	16/20 (80%) *0.106*	9/20 (45%) ***0.019***	**4/20 (20%)** ***0.004***
	AE2	20/20 (100%) *1.000*	20/20 (100%) *0.231*	14/20 (70%) *1.000*
	AE4	18/20 (90%) *0.487*	12/20 (60%) *0.155*	10/20 (50%) *0.333*
	AE5	18/20 (90%) *0.487*	**10/20 (50%)** ***0.041***	**7/20 (35%)** ***0.056***
	WT	20/20 (100%) *N/A*	17/20 (85%) *N/A*	14/20 (70%) *N/A*

Bold formatting indicates statistical significance. Data are presented as the number of virus-positive/number tested with rates of infection (virus present in midgut tissues), dissemination (virus present in legs/wings tissues), and transmission (virus present in saliva samples) indicated by percentages in parentheses. Two-tailed *p* values of infection, dissemination, and transmission (compared to WT) indicated in italics. Statistical analyses were performed using Fisher's exact test in comparison to WT mosquitoes.
IBM = infectious blood meal.

WT mosquitoes (Table 3). We observed a near-significant reduction in dissemination rate ($p = 0.0547$) and a significant reduction in transmission rate ($p < 0.0001$) for line AE1 with CHIKV. We also observed significant reductions in the dissemination and transmission rates for line AE5 ($p = 0.0053$ and $p < 0.0001$, respectively) with CHIKV. Interestingly, significant reductions in all rates were found with both AE1 and AE5 lines for the MAYV vector competence experiments (Table 3).

As mentioned, we did not see as strong of a reduction in dissemination of CHIKV in our transgenic lines and believed this could be due to lower overall systemic titers within the transgenic mosquitoes. Because of this, we sought to assess the replication of CHIKV and MAYV in these transgene-positive lines by measuring the viral titers present in each of the mosquito groups. We found significant reductions of CHIKV titers in AE1 and AE5 in infection (AE1 $p < 0.0001$; AE5 $p < 0.0001$), dissemination (AE1 $p = 0.016$; AE5 $p = 0.008$), and transmission (AE1 $p < 0.0001$; AE5 $p < 0.0001$) titers when compared to WT (Figure 6). Similarly, we observed significant reductions in MAYV replication in infection (AE1 $p < 0.0001$; AE5 $p = 0.0008$), dissemination (AE1 $p = 0.0008$; AE5 $p = 0.0025$), and transmission (AE1 $p = 0.0003$; AE5 $p = 0.0024$) (Figure 6). Alongside these data, we observed significant reductions in dissemination and transmission rates of infected transgenic mosquitoes when compared to WT mosquitoes (Supplementary Table S1). Altogether, these data demonstrate that both lines expressing sdAbs are more refractory to CHIKV and MAYV than WT mosquitoes.

Discussion

CHIKV and MAYV have become increasingly prevalent in tropical regions of the world within the last few decades, highlighting

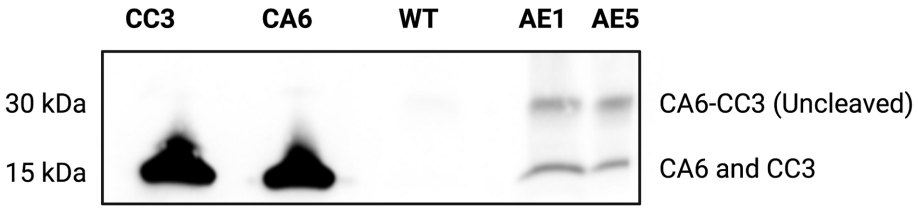

FIGURE 5
Western blot analysis to probe for the expression of sdAbs in AE1 and AE5. Western blots were carried out using homogenized midgut tissues from 16 h post-bloodmeal WT, AE1, and AE5 mosquitoes (n=30/group). Purified CC3 and CA6 sdAbs (Liu et al., 2019) were used as controls and all samples were probed with AffiniPure Goat Anti-Alpaca IgG, VHH domain primary antibody. The presence of a 15 kDa band confirms the expression of the individual, cleaved sdAb proteins (CA6 and CC3) in transgenic, but not in WT, mosquito midgut samples. The presence of a 30kDa band in the transgenic samples may indicate unsuccessful ribosomal skipping of the P2A linker sequence located between the CA6 and CC3 sdAbs, resulting in a (uncleaved) CA6-CC3 fusion protein.

TABLE 3 Vector competence of transgenic and WT *Ae. aegypti* mosquitoes for CHIKV H-20235 and MAYV 12A.

Virus	Transgenic line	Infection (midgut)	Dissemination (legs/wings)	Transmission (saliva)
CHIKV H-20235 IBM titer: 5.63E+07	AE1	39/40 (97.5%) *1.0000*	35/40 (87.5%) *0.0547*	7/40 (17.5%) ***<0.0001***
	AE5	38/40 (95.0%) *0.4937*	32/40 (80.0%) ***0.0053***	10/40 (25.0%) ***<0.0001***
	WT	40/40 (100%) *N/A*	40/40 (100%) *N/A*	33/40 (82.5%) *N/A*
MAYV 12A IBM titer: 3.63E+07	AE1	29/40 (72.5%) ***0.0004***	23/40 (57.5%) ***0.0005***	16/40 (40.0%) ***0.0243***
	AE5	28/40 (70.0%) ***0.0002***	28/40 (70.0%) ***0.0198***	12/40 (30%) ***0.0016***
	WT	40/40 (100%) *N/A*	37/40 (92.5%) *N/A*	27/40 (67.5%) *N/A*

Bold formatting indicates statistical significance. Data are presented as the number of virus-positive/number tested with rates of infection (virus present in midgut tissues), dissemination (virus present in legs/wings tissues), and transmission (virus present in saliva samples) indicated by percentages in parentheses. Two-tailed p values of infection, dissemination, and transmission (compared to WT) indicated in italics. Statistical analyses were performed using Fisher's exact test in comparison to WT mosquitoes. IBM, infectious blood meal.

a crucial need for novel approaches to control the spread of these crippling pathogens. Since 2004, CHIKV has been reported in over 100 countries (Silva et al., 2018; Vairo et al., 2019) and MAYV has the potential to spread similarly. In conjunction with sporadic outbreaks throughout the sub-tropical regions of the Americas, increased global travel to these endemic areas has resulted in imported cases of MAYV, as well as imported cases and autochthonous transmission of CHIKV, within the United States and Europe (Fischer and Staples, 2014; Bocanegra et al., 2016; Gossner et al., 2020). The overall goal of this study was to conceptualize a single control strategy that co-targets these emerging alphaviruses.

Our results demonstrate that the sdAbs, CC3 and CA6, have high neutralizing activity against both CHIKV and MAYV *in vitro* as demonstrated in our initial PRNT experiments (Figure 3). Furthermore, we successfully constructed and cloned a transformation construct (Figure 2) that was used to create several transgenic lines expressing eGFP (Figure 4). Of these transgenic lines, mosquito midgut samples from the AE1 and AE5 transgenic lines were subjected to Western blotting to verify expression of both CA6 and CC3 sdAbs (Figure 5). Interestingly, Western blot analyses revealed a dual banding pattern at ~30 kDa and ~15 kDa which may suggest unsuccessful ribosomal-skipping of the P2A linker sequence thus resulting in a fusion protein of the CA6 and CC3 sdAbs (Liu et al., 2017). Additionally, preliminary vector competence experiments using WT *Ae. aegypti* LVP revealed suitable virus strains of CHIKV and MAYV to be used in the transgenic vector competence experiments (Table 1). Each of the generated transgenic lines were then subjected to another preliminary vector competence experiment to determine which lines had the most refraction to CHIKV and MAYV and these results indicated the AE1 and AE5 transgenic lines were the most refractory to both viruses (Table 2). Thus, we performed a final, larger-scale, vector competence experiment to measure the changes in infection, dissemination, and transmission rates within the AE1 and AE5 lines when compared to WT mosquitoes. This vector competence experiment resulted in statistically significant reductions in dissemination and transmission rates for both lines with MAYV and for the AE5 line with CHIKV (Table 3). The AE1 line resulted in a statistically significant reduction of transmission for CHIKV and a near-significant ($p = 0.0547$) reduction in dissemination. Finally, we compared the overall group viral titers for each line and virus

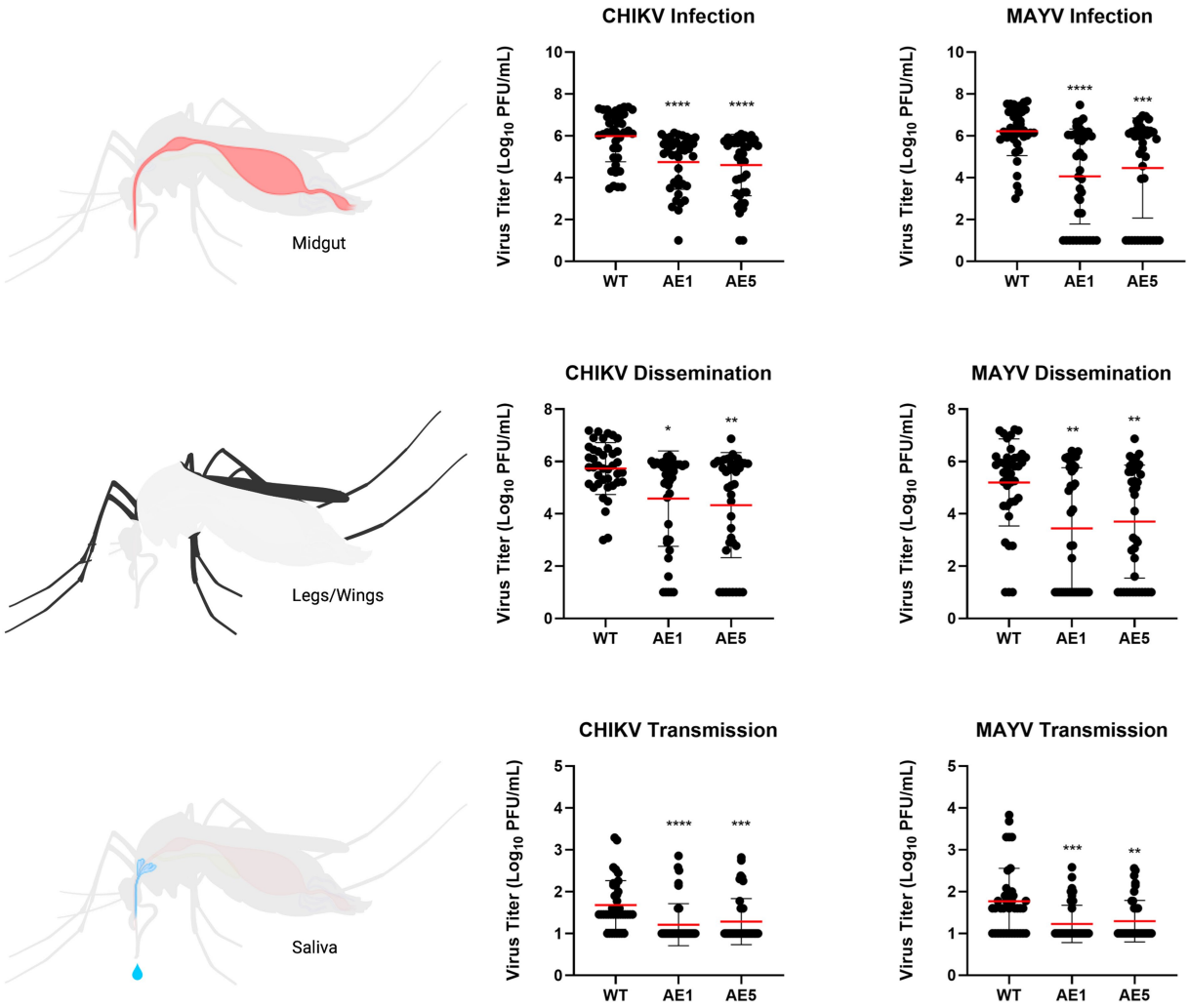

FIGURE 6
Plots of viral titers for CHIKV and MAYV in WT and transgenic mosquitoes. To evaluate the replication of CHIKV and MAYV, we measured viral titers infection (virus present in midgut tissues), dissemination (virus present in legs/wings tissues), and transmission (virus present in saliva samples). Female mosquitoes 5–7 days old were fed virus-spiked bloodmeals using artificial membrane feeders, and only fully engorged mosquitoes were separated into new containers. Seven days post-infection, mosquitoes were cold-anesthetized and individual samples were collected. Viral titers were measured via plaque assay on Vero cells 7 dpi. Data points of the 40 replicates obtained in two independent experiments are depicted on the plot. All undetected mosquito samples were given a value of half the limit of detection (LOD/2) for statistical analyses. Red horizontal bars represent the mean with SD. *p<0.05, **p<0.01, ***p<0.001, ****p<0.0001, Kruskal-Wallis test with Dunn's correction for multiple comparisons. Infectious blood meal (IBM) titers: CHIKV=5.63E+07, MAYV=3.63E+07.

to that of WT titers and found statistically significant reductions of viral titers in each of the lines for both CHIKV and MAYV at the infection, dissemination, and transmission stages (Figure 6). To this end, we have generated transgenic mosquitoes that have refractory activity to both viruses and have therefore likely reduced transmission potential for CHIKV and MAYV in our transgenic mosquitoes.

Researchers have recently exploited genetic manipulation in problematic mosquito species as promising control strategies. Specifically, groups have generated mosquitoes expressing small RNAs or antibody fragments (e.g., scFv) to provide resistance to ZIKV and DENV (Yen et al., 2018; Buchman et al., 2019, 2020); however, our approach is unique based on the use of two camelid-derived sdAbs within a single vector to target two distinct alphaviruses. Importantly, our transgenic lines significantly reduced both CHIKV and MAYV replication and infection, dissemination, and transmission levels. This is particularly noteworthy because these viruses co-circulate throughout South America (Nunes et al., 2015; Vieira et al., 2015; Silva et al., 2018; Lorenz et al., 2019; Ganjian and Riviere-Cinnamond, 2020); thus, this strategy could limit the spread of both pathogens simultaneously.

While these data are promising, future studies are needed to determine the potential for these viruses to escape from sdAb-mediated neutralization within the transgenic mosquitoes. We hypothesized that expressing two individual sdAbs would reduce the probability for these viruses to generate antibody escape variants; however, this hypothesis needs to be tested in future studies. It should be noted that research from previous scFv studies have not indicated the development and/or selection for viral escape mutants (Reid et al., 2021). In addition, the stability of sdAb expression by these transgenic

mosquitoes should also be assessed. As environmental factors such as temperature and mosquito diets affect *Wolbachia* density in transinfected mosquitoes (Ross et al., 2019), there could be similar effects on sdAb expression in our transgenic mosquitoes. Alongside the issues of transgene stability, fitness costs to the transgenic mosquitoes need to be evaluated. However, the stability of our transgene and any potential fitness costs could be circumvented by using this concept in combination with a gene-drive system. Gene-drive systems result in super-Mendelian inheritance and thereby greatly increase the stability of the transgene and can lead to overcoming any fitness costs resulting from the transgene (Macias et al., 2017). Future studies should also consider whether these mosquitoes are refractory to more distantly related alphaviruses, since our previous data has shown substantial cross-neutralization by the CC3 sdAb to a range of alphaviruses (Liu et al., 2021). In addition to these studies, determining the effect this reduction in vector competence has on the vectorial capacity of these transgenic mosquitoes would be crucial in support for this strategy. Vectorial capacity is defined quantitatively and is influenced by variables such as vector density, longevity, vector competence, and extrinsic incubation period. Further studies focusing on the significance of this change in vector competence as well as time-course studies evaluating any shifts in extrinsic incubation period are needed to evaluate the true potential of this concept to reduce transmission in a real-life setting. It should also be noted that the viral titers used in this study may be less than those found in nature as CHIKV viremia can reach high levels (~10^9 copies/ml) during the actue phase of infection (Schwartz and Albert, 2010); however, studies have shown titers as low as ~10^{4-5} PFU/ml is adequate for mosquitoes to become infected on monkeys (Turell et al., 1992). Future studies determining the effect a range of viral titers has on the refractory activity shown here should be performed.

Altogether, our data provide strong support for the effectiveness of using transgenic mosquitoes expressing virus-specific sdAbs to control alphavirus transmission. This study further highlights the ability to target multiple arboviruses simultaneously, and thus has the potential to significantly reduce disease burden of multiple pathogens using a single defense strategy.

Data availability statement

The raw data supporting the conclusions of this article will be made available by the authors, without undue reservation.

Author contributions

EMW, AC, ZT, SLP, and JW-L designed the experiments. EMW, AC, PR, and CC performed all experiments. EMW and JW-L analyzed all data. EMW and JW-L wrote the manuscript and all authors edited the manuscript.

Funding

EMW is supported by a doctoral fellowship from the Institute for Critical Technology and Applied Science (ICTAS) at Virginia Tech.

Acknowledgments

The authors would like to thank Ellen Goldman and George Anderson from the Naval Research Laboratory for sharing the purified sdAbs, Azadeh Aryan for guidance and troubleshooting with mosquito embryonic microinjections, and Omar Akbari's lab for sharing Western blot and midgut dissection protocols.

Conflict of interest

The authors declare that the research was conducted in the absence of any commercial or financial relationships that could be construed as a potential conflict of interest.

Publisher's note

Supplementary material

The Supplementary material for this article can be found online at: https://www.frontiersin.org/articles/10.3389/fmicb.2023.1189176/full#supplementary-material

References

Aliota, M. T., Peinado, S. A., Velez, I. D., and Osorio, J. E. (2016). The wMel strain of Wolbachia reduces transmission of Zika virus by *Aedes aegypti*. *Sci. Rep.* 6:28792. doi: 10.1038/srep28792

Anderson, M. A., Gross, T. L., Myles, K. M., and Adelman, Z. N. (2010). Validation of novel promoter sequences derived from two endogenous ubiquitin genes in transgenic *Aedes aegypti*. *Insect Mol. Biol.* 19, 441–449. doi: 10.1111/j.1365-2583.2010.01005.x

Bates, T. A., Chuong, C., Rai, P., Marano, J., Waldman, A., Klinger, A., et al. (2021). American Aedes japonicus japonicus, *Culex pipiens* pipiens, and *Culex restuans* mosquitoes have limited transmission capacity for a recent isolate of Usutu virus. *Virology* 555, 64–70. doi: 10.1016/j.virol.2020.12.023

Bocanegra, C., Antón, A., Sulleiro, E., Pou, D., Salvador, F., Roure, S., et al. (2016). Imported cases of Chikungunya in Barcelona in relation to the current American outbreak. *J. Travel Med.* 23:tav033. doi: 10.1093/jtm/tav033

Buchman, A., Gamez, S., Li, M., Antoshechkin, I., Li, H.-H., Wang, H.-W., et al. (2020). Broad dengue neutralization in mosquitoes expressing an engineered antibody. *PLoS Pathog.* 16:e1008103. doi: 10.1371/journal.ppat.1008103

Buchman, A., Gamez, S., Li, M., Antoshechkin, I., Li, H.-H., Wang, H.-W., et al. (2019). Engineered resistance to Zika virus in transgenic *Aedes aegypti* expressing a polycistronic cluster of synthetic small RNAs. *Proc. Natl. Acad. Sci.* 116, 3656–3661. doi: 10.1073/pnas.1810771116

Cano-Monreal, G. L., Williams, J. C., and Heidner, H. W. (2010). An arthropod enzyme, Dfurin1, and a vertebrate furin homolog display distinct cleavage site sequence preferences for a shared viral proprotein substrate. *J. Insect Sci.* 10, 1–16. doi: 10.1673/031.010.2901

Carvalho, D. O., McKemey, A. R., Garziera, L., Lacroix, R., Donnelly, C. A., Alphey, L., et al. (2015). Suppression of a field population of *Aedes aegypti* in Brazil by sustained release of transgenic male mosquitoes. *PLoS Negl. Trop. Dis.* 9:e0003864. doi: 10.1371/journal.pntd.0003864

Chen, C., Compton, A., Nikolouli, K., Wang, A., Aryan, A., Sharma, A., et al. (2021). Marker-assisted mapping enables effective forward genetic analysis in the arboviral vector *Aedes aegypti*, a species with vast recombination deserts. *bioRxiv 2021.04.29.442065*

Corbel, V., Fonseca, D. M., Weetman, D., Pinto, J., Achee, N. L., Chandre, F., et al. (2017). International workshop on insecticide resistance in vectors of arboviruses, December 2016, Rio de Janeiro, Brazil. *Parasit. Vectors* 10:278. doi: 10.1186/s13071-017-2224-3

Elsinga, J., Gerstenbluth, I., van der Ploeg, S., Halabi, Y., Lourents, N. T., Burgerhof, J. G., et al. (2017). Long-term Chikungunya Sequelae in Curaçao: burden, determinants, and a novel classification tool. *J. Infect. Dis.* 216, 573–581. doi: 10.1093/infdis/jix312

Fang, J. (2010). Ecology: a world without mosquitoes. *Nature* 466, 432–434. doi: 10.1038/466432a

Fischer, M., and Staples, J. E. (2014). Notes from the field: chikungunya virus spreads in the Americas - Caribbean and South America, 2013-2014. *MMWR Morb. Mortal. Wkly Rep.* 63, 500–501.

Fox, J. M., Long, F., Edeling, M. A., Lin, H., van Duijl-Richter, M. K. S., Fong, R. H., et al. (2015). Broadly neutralizing Alphavirus antibodies bind an epitope on E2 and inhibit entry and egress. *Cells* 163, 1095–1107. doi: 10.1016/j.cell.2015.10.050

Ganjian, N., and Riviere-Cinnamond, A. (2020). Mayaro virus in Latin America and the Caribbean. *Rev. Panam. Salud Publica* 44, e14–e, 1. doi: 10.26633/RPSP.2020.14

Gossner, C. M., Fournet, N., Dias, J. G., Martínez, B. F., Del Manso, M., Young, J. J., et al. (2020). Risks related to Chikungunya infections among European Union travelers, 2012-2018. *Emerg. Infect. Dis.* 26, 1067–1076. doi: 10.3201/eid2606.190490

Handler, A. M., McCombs, S. D., Fraser, M. J., and Saul, S. H. (1998). The lepidopteran transposon vector, piggyBac, mediates germ-line transformation in the Mediterranean fruit fly. *Proc. Natl. Acad. Sci. USA* 95, 7520–7525. doi: 10.1073/pnas.95.13.7520

Harris, A. F., McKemey, A. R., Nimmo, D., Curtis, Z., Black, I., Morgan, S. A., et al. (2012). Successful suppression of a field mosquito population by sustained release of engineered male mosquitoes. *Nat. Biotechnol.* 30, 828–830. doi: 10.1038/nbt.2350

Hearn, H. J. Jr. (1961). Cross-protection between Venezuelan equine encephalomyelitis and eastern equine encephalomyelitis virus. *Proc. Soc. Exp. Biol. Med.* 107, 607–610. doi: 10.3181/00379727-107-26702

Latif, Z., Gates, D., Wust, C. J., and Brown, A. (1979). Cross protection among togaviruses in nude mice and littermates. *J. Gen. Virol.* 45, 89–98. doi: 10.1099/0022-1317-45-1-89

Liu, Z., Chen, O., Wall, J. B. J., Zheng, M., Zhou, Y., Wang, L., et al. (2017). Systematic comparison of 2A peptides for cloning multi-genes in a polycistronic vector. *Sci. Rep.* 7:2193. doi: 10.1038/s41598-017-02460-2

Liu, J. L., Shriver-Lake, L. C., Zabetakis, D., Anderson, G. P., and Goldman, E. R. (2019). Selection and characterization of protective anti-chikungunya virus single domain antibodies. *Mol. Immunol.* 105, 190–197. doi: 10.1016/j.molimm.2018.11.016

Liu, J. L., Webb, E. M., Zabetakis, D., Burke, C. W., Gardner, C. L., Glass, P. J., et al. (2021). Stabilization of a broadly neutralizing anti-Chikungunya virus single domain antibody. *Front. Med.* 8:8. doi: 10.3389/fmed.2021.626028

Lorenz, C., Freitas Ribeiro, A., and Chiaravalloti-Neto, F. (2019). Mayaro virus distribution in South America. *Acta Trop.* 198:105093. doi: 10.1016/j.actatropica.2019.105093

Macias, V. M., Ohm, J. R., and Rasgon, J. L. (2017). Gene drive for mosquito control: where did it come from and where are we headed? *Int. J. Environ. Res. Public Health* 14:1006. doi: 10.3390/ijerph14091006

Moreira, L. A., Edwards, M. J., Adhami, F., Jasinskiene, N., James, A. A., and Jacobs-Lorena, M. (2000). Robust gut-specific gene expression in transgenic *Aedes aegypti* mosquitoes. *Proc. Natl. Acad. Sci. USA* 97, 10895–10898. doi: 10.1073/pnas.97.20.10895

Morrison, T. E., Oko, L., Montgomery, S. A., Whitmore, A. C., Lotstein, A. R., Gunn, B. M., et al. (2011). A mouse model of chikungunya virus-induced musculoskeletal inflammatory disease: evidence of arthritis, tenosynovitis, myositis, and persistence. *Am. J. Pathol.* 178, 32–40. doi: 10.1016/j.ajpath.2010.11.018

Nunes, M. R., Faria, N. R., de Vasconcelos, J. M., Golding, N., Kraemer, M. U., de Oliveira, L. F., et al. (2015). Emergence and potential for spread of Chikungunya virus in Brazil. *BMC Med.* 13:102. doi: 10.1186/s12916-015-0348-x

Partidos, C. D., Paykel, J., Weger, J., Borland, E. M., Powers, A. M., Seymour, R., et al. (2012). Cross-protective immunity against o'nyong-nyong virus afforded by a novel recombinant chikungunya vaccine. *Vaccine* 30, 4638–4643. doi: 10.1016/j.vaccine.2012.04.099

Partidos, C. D., Weger, J., Brewoo, J., Seymour, R., Borland, E. M., Ledermann, J. P., et al. (2011). Probing the attenuation and protective efficacy of a candidate chikungunya virus vaccine in mice with compromised interferon (IFN) signaling. *Vaccine* 29, 3067–3073. doi: 10.1016/j.vaccine.2011.01.076

Peck, R., Wust, C. J., and Brown, A. (1979). Adoptive transfer of cross-protection among alphaviruses in mice requires allogeneic stimulation. *Infect. Immun.* 25, 320–327. doi: 10.1128/iai.25.1.320-327.1979

Powell, J. R. (2018). Mosquito-borne human viral diseases: why *Aedes aegypti*? *Am J Trop Med Hyg.* 98, 1563–1565. doi: 10.4269/ajtmh.17-0866

Reeves, W. R., McGuire, M. K., Stokes, M., and Vicini, J. L. (2019). Assessing the safety of pesticides in food: how current regulations protect human health. *Adv. Nutr.* 10, 80–88. doi: 10.1093/advances/nmy061

Reid, W. R., Olson, K. E., and Franz, A. W. E. (2021). Current effector and gene-drive developments to engineer Arbovirus-resistant *Aedes aegypti* (Diptera: Culicidae) for a sustainable population replacement strategy in the field. *J. Med. Entomol.* 58, 1987–1996. doi: 10.1093/jme/tjab030

Ross, P. A., Turelli, M., and Hoffmann, A. A. (2019). Evolutionary ecology of Wolbachia releases for disease control. *Annu. Rev. Genet.* 53, 93–116. doi: 10.1146/annurev-genet-112618-043609

Schwartz, O., and Albert, M. L. (2010). Biology and pathogenesis of chikungunya virus. *Nat. Rev. Microbiol.* 8, 491–500. doi: 10.1038/nrmicro2368

Silva, J. V. J. Jr., Ludwig-Begall, L. F., Oliveira-Filho, E. F., Oliveira, R. A. S., Durães-Carvalho, R., Lopes, T. R. R., et al. (2018). A scoping review of Chikungunya virus infection: epidemiology, clinical characteristics, viral co-circulation complications, and control. *Acta Trop.* 188, 213–224. doi: 10.1016/j.actatropica.2018.09.003

Turell, M. J., Beaman, J. R., and Tammariello, R. F. (1992). Susceptibility of selected strains of Aedes aegypti and *Aedes albopictus* (Diptera: Culicidae) to chikungunya virus. *J. Med. Entomol.* 29, 49–53. doi: 10.1093/jmedent/29.1.49

Vairo, F., Haider, N., Kock, R., Ntoumi, F., Ippolito, G., and Zumla, A. (2019). Chikungunya: epidemiology, pathogenesis, clinical features, management, and prevention. *Infect. Dis. Clin. N. Am.* 33, 1003–1025. doi: 10.1016/j.idc.2019.08.006

Vieira, C. J., Silva, D. J., Barreto, E. S., Siqueira, C. E., Colombo, T. E., Ozanic, K., et al. (2015). Detection of Mayaro virus infections during a dengue outbreak in Mato Grosso. *Brazil. Acta Trop.* 147, 12–16. doi: 10.1016/j.actatropica.2015.03.020

Walker, T., Johnson, P. H., Moreira, L. A., Iturbe-Ormaetxe, I., Frentiu, F. D., McMeniman, C. J., et al. (2011). The wMel Wolbachia strain blocks dengue and invades caged *Aedes aegypti* populations. *Nature* 476, 450–453. doi: 10.1038/nature10355

Waltz, E. (2021). First genetically modified mosquitoes released in the United States. *Nature* 593, 175–176. doi: 10.1038/d41586-021-01186-6

Wang, G.-H., Gamez, S., Raban, R. R., Marshall, J. M., Alphey, L., Li, M., et al. (2021). Combating mosquito-borne diseases using genetic control technologies. *Nat. Commun.* 12:4388. doi: 10.1038/s41467-021-24654-z

Webb, E. M., Azar, S. R., Haller, S. L., Langsjoen, R. M., Cuthbert, C. E., Ramjag, A. T., et al. (2019). Effects of Chikungunya virus immunity on Mayaro virus disease and epidemic potential. *Sci. Rep.* 9:20399. doi: 10.1038/s41598-019-56551-3

Wust, C. J., Crombie, R., and Brown, A. (1987). Passive protection across subgroups of alphaviruses by hyperimmune non-cross-neutralizing anti-Sindbis serum. *Proc. Soc. Exp. Biol. Med.* 184, 56–63. doi: 10.3181/00379727-184-42446

Yakob, L., Funk, S., Camacho, A., Brady, O., and Edmunds, W. J. (2017). *Aedes aegypti* control through modernized, integrated vector management. *PLoS Curr.*:9. doi: 10.1371/currents.outbreaks.45deb8e03a438c4d088afb4fafae8747

Yen, P. S., James, A., Li, J. C., Chen, C. H., and Failloux, A. B. (2018). Synthetic miRNAs induce dual arboviral-resistance phenotypes in the vector mosquito *Aedes aegypti*. *Commun Biol.* 1:11. doi: 10.1038/s42003-017-0011-5

frontiers | Frontiers in Microbiology

TYPE Original Research
PUBLISHED 12 June 2023
DOI 10.3389/fmicb.2023.1182798

OPEN ACCESS

EDITED BY
James Weger-Lucarelli,
Virginia Tech, United States

REVIEWED BY
David Jesse Sanchez,
Western University of Health Sciences, United States
Masatoshi Kakizaki,
National Institute of Infectious Diseases (NIID), Japan

*CORRESPONDENCE
Ping Zhao
✉ pnzhao@163.com
Lan-Juan Zhao
✉ ljzhao13@163.com

RECEIVED 09 March 2023
ACCEPTED 24 May 2023
PUBLISHED 12 June 2023

CITATION
Tang W-D, Tang H-L, Peng H-R, Ren R-W, Zhao P and Zhao L-J (2023) Inhibition of tick-borne encephalitis virus in cell cultures by ribavirin.
Front. Microbiol. 14:1182798.
doi: 10.3389/fmicb.2023.1182798

Inhibition of tick-borne encephalitis virus in cell cultures by ribavirin

Wan-Da Tang[1], Hai-Lin Tang[1], Hao-Ran Peng[1], Rui-Wen Ren[2], Ping Zhao[1]* and Lan-Juan Zhao[1]*

[1]Department of Microbiology, Faculty of Naval Medicine, Naval Medical University, Shanghai, China, [2]Center for Disease Control and Prevention of Southern Theater Command, Guangzhou, China

Tick-borne encephalitis virus (TBEV) belonging to arboviruses is a major member of zoonotic pathogens. TBEV infection causes severe human encephalitis without specific antiviral drugs. Due to its use of antiviral drug against a wide range of viruses, we investigated antiviral effect of ribavirin against TBEV in susceptible human cell lines A549 and SH-SY5Y. Ribavirin displayed minor cytotoxicity on multiple cell lines. Ribavirin obviously impaired TBEV replication and protected the infected cells from cytopathic effect. Importantly, ribavirin markedly inhibited TBEV propagation, as evidenced by impairment of TBEV production and viral RNA replication. Treatment with ribavirin (co-treatment and post-treatment) led to a dose-dependent reduction in TBEV titers as well as the viral RNA levels. Antiviral protein myxovirus resistance A mRNA expression was significantly up-regulated and signal transducer and activator of transcription 3 was activated in TBEV-infected A549 cells upon the ribavirin treatment. Induction of inflammatory cytokine tumor necrosis factor alpha by TBEV was decreased in A549 cells with the treatment of ribavirin, whereas interleukin 1 beta release appeared to be unaffected. These results suggest that ribavirin might represent a promising safe and effective antiviral drug against TBEV.

KEYWORDS

tick-borne encephalitis virus, ribavirin, myxovirus resistance A, signal transducer and activator of transcription 3, tumor necrosis factor alpha

Introduction

Arboviruses comprise several significant human pathogens such as dengue virus, Zika virus, Japanese encephalitis virus, Crimean-Congo hemorrhagic fever virus, tick-borne encephalitis virus (TBEV), yellow fever virus, West Nile virus and Chikungunya virus. Arboviruses are responsible for considerable morbidity and mortality in vertebrates and humans. TBEV, a major member of arboviruses, is a positive-stranded RNA virus belonging to the *Flavivirus* genus in the Flaviviridae family. TBEV genome encodes a polyprotein that is processed into three structural proteins including capsid, precursor membrane and envelope glycoproteins and seven non-structural (NS) proteins including NS1, NS2A, NS2B, NS3, NS4A, NS4B and NS5 (Blom et al., 2018). In nature, TBEV is maintained in transmission cycles between Ixodes ticks and wild mammalian hosts. Although transmission of unpasteurized milk as well as milk products from infected stock was reported, TBEV, a zoonotic pathogen, is transmitted to humans primarily *via* bites of infected Ixodes ticks (Yoshii, 2019). As a tick-borne viral pathogen of humans, TBEV is becoming an international public health concern.

Infection with TBEV causes severe neurological manifestations including meningitis, encephalitis and meningoencephalitis with and without permanent sequelae and even results in death (Pulkkinen et al., 2018). The geographic distribution of TBEV is considered mainly in large areas of Europe and Asia (Im et al., 2020). In mainland China, TBEV is an endemic pathogen in the Northeast and the Xinjiang and the distribution is closely related to the distribution of tick vectors (Gao et al., 2010). There are five licensed vaccines to TBEV infection on the basis of formalin-inactivated and purified whole virus of TBEV strains. However, some reports have shown the vaccine failures in the particular individuals (Blom et al., 2018). There are no specific antiviral drugs available for TBEV infection (Yoshii, 2019). In recent years, the incidence of diseases caused by TBEV has increased.

Since discovery in 1972 as a synthetic nucleoside analog, ribavirin has been focused due to anticancer and antiviral biological properties. Ribavirin exerted clinical benefit in patients with acute myeloid leukemia and was shown as an anticancer therapy (Borden and Culjkovic-Kraljacic, 2010). The anticancer efficacy of ribavirin has been explored on preclinical models and clinical trials in acute myeloid leukemia, oropharyngeal squamous cell carcinoma, metastatic breast cancer and glioblastoma (Volpin et al., 2017; Casaos et al., 2019). The use of ribavirin as an anticancer agent is apparently instructive. Moreover, ribavirin is well known as a chemotherapeutic agent with activities against a wide range of RNA and DNA viruses. For instance, ribavirin in combination with pegylated interferon alpha (IFN-α) was established as the therapy for chronic hepatitis C (Reddy et al., 2009). Ribavirin therapy was also efficient for hepatitis E (De Winter et al., 2018). Ribavirin was clinically used to treat infection with respiratory syncytial virus as well as other noninfluenza respiratory viruses (Gross and Bryson, 2015; Tejada et al., 2022). Ribavirin has also been used to treat patients infected with Lassa fever virus or Crimean-Congo hemorrhagic fever virus (Ascioglu et al., 2011; Johnson et al., 2018; Cheng et al., 2022). In particular, ribavirin had antiviral efficacy in children with tick-borne encephalitis (Skripchenko et al., 2019). Although ribavirin is regarded as a safe antiviral drug, the effectiveness of ribavirin for the viruses remains to be validated and the precise mechanisms of ribavirin action are still not completely understood.

As no effective anti-TBEV treatments are available, it is necessary to develop antiviral drugs against TBEV for its expanding worldwide. Based on its antiviral activities and the antiviral efficacy in children with tick-borne encephalitis, we wondered whether ribavirin might play active roles in inhibiting TBEV propagation and eliciting antiviral response. In the present study, influence of ribavirin on TBEV propagation was evaluated in susceptible human cell lines by detecting viral protein, viral RNA, virus titer, antiviral protein and inflammatory cytokines. The underlying mechanisms by which ribavirin mediates antiviral and immunomodulatory effects were also discussed.

Materials and methods

Cell culture

Human lung adenocarcinoma A549 cells, human neuroblastoma SH-SY5Y cells, African green monkey kidney Vero cells and porcine kidney PK-15 cells were used in the study. All cell lines were grown in Dulbecco's modified Eagle's medium (DMEM) supplemented with 10% fetal bovine serum (FBS), 1% L-glutamine, 1% non-essential amino acids and 1% penicillin–streptomycin at 37°C under 5% CO_2. These products for cell culture were from Invitrogen (United States). Vero cells were used to propagate TBEV. PK-15 cells were applied to determine virus titer. A549 and SH-SY5Y cells were chosen to evaluate anti-TBEV effects of ribavirin.

Virus propagation

TBEV was stocked in the laboratory as described previously (Ding et al., 2022; Tang et al., 2022). TBEV was propagated in Vero cells, and cell culture supernatants collected at 72 h post-inoculation were centrifuged at 2,500 rpm for 10 min to remove cell debris. Aliquots of supernatant fraction were stored at −80°C until use. Virus titer was titrated on PK-15 cells by plaque assay. The experiments concerning TBEV infection were performed in Biological Safety Level 3 Laboratory in accordance with the guidelines by Committee on Safety of Biomedicine at Naval Medical University.

Cell viability assay

Cells seeded in 96-well plates were cultured overnight to form a confluent monolayer. For 10 mg/mL stock, ribavirin (Millipore, United States) was dissolved in phosphate-buffered saline (PBS). The culture medium was removed and the cells were subsequently incubated with ribavirin at concentrations range of 0 to 300 μg/mL in fresh culture medium. After 48 h of incubation, cell viability was evaluated using One Solution Cell Proliferation Assay kit containing MTS according to the manufacture's instructions (Promega, United States). The absorbance at 490 nm was read on a Synergy 2 Multi-Mode Microplate Reader (BioTek, United States).

Immunofluorescence staining

A549 cells grown in 96-well plates overnight were inoculated with TBEV at a multiplicity of infection (MOI) of 0.1 and different concentrations of ribavirin in fresh culture medium. After 48 h, the medium was removed and the cells were fixed with 4% paraformaldehyde in PBS for 15 min at room temperature, washed twice with PBS, and permeabilized with methanol for 20 min at −20°C. After two washes with PBS and blocking with 3% bovine serum albumin (BSA) in PBS for 2 h, the cells were incubated with formaldehyde-inactivated TBEV immunized mouse ascites recognizing the viral surface antigen (1:500 dilution in 1% BSA) overnight at 4°C. The cells were washed three times with PBS and subsequently labeled with an anti-mouse goat secondary antibody conjugated with Alexa Fluor 488 (1:1,000 dilution in 1% BSA; Abcam, UK) in the dark for 1 h. Finally, the cells were treated with mounting medium with 4′,6′-diamidino-2-phenylindole (DAPI) (Abcam, UK) for 5 min to visualize the cell nuclei. The numbers of infected cells and total cells were counted by using Cytation 5 imaging reader (BioTek, United States), and the infection rate was calculated with Gen5 3.10 software. Images were acquired under a fluorescence inverted microscope (Olympus IX81, Japan).

Ribavirin treatment

A549 or SH-SY5Y cells were seeded into 12-well plates and cultured overnight to form a confluent monolayer. To evaluate which stage of TBEV life cycle was affected by ribavirin, three schemes of ribavirin treatment were applied. For co-treatment, culture medium was removed and the cells were cultured for 48 h in fresh culture medium containing TBEV at an MOI of 0.1 and ribavirin at concentrations ranging from 0 to 50 μg/mL. For post-treatment, the cells were inoculated for 2 h with 0.1 MOI TBEV at 37°C. After removal of the viral inoculum, the cells were washed once with PBS, and grown in fresh culture medium containing ribavirin at the indicated concentrations for 48 h. For pre-treatment, the cells were incubated with ribavirin at the indicated concentrations in fresh culture medium for 12 h. After removal of the medium, the cells were washed once with PBS and inoculated for 2 h with 0.1 MOI TBEV at 37°C. Following the incubation, the viral inoculum was aspirated and replaced with fresh culture medium, and the cells were then cultured for 48 h. The time point was calculated from the end of the 2 h adsorption. As a solvent control, PBS was added to TBEV-infected cells at a final concentration of 0.1% (v/v). Culture supernatants, cellular RNA and cell lysates were collected for the following assays.

Plaque assay

Confluent monolayer of PK-15 cells grown in 12-well plates was inoculated with 10-fold dilutions of the culture supernatants from TBEV-infected cells with and without the ribavirin treatment. After an incubation period of 3 h at 37°C, the viral inoculum was removed, and the cells were washed once with PBS. 2% carboxymethylcellulose (Sigma-Aldrich, United States) overlay medium was added to the cells. After 6 days, the overlay medium was removed, the cells were fixed with 4% paraformaldehyde for 15 min and stained with 1% crystal violet to visualize plaques. After 15 min of staining, the crystal violet was decanted and the plaques were counted. The virus titer was expressed as plaque-forming units (PFU)/mL.

Enzyme-linked immunosorbent assay

The culture supernatants from A549 cells with and without the ribavirin treatment were collected for cytokine measurement. ELISA kits (R&D Systems, United States) were used to determine concentrations of human tumor necrosis factor alpha (TNF-α) and interleukin 1 beta (IL-1β) according to the manufacturer's protocols. The data were acquired on the Synergy 2 Multi-Mode Microplate Reader (BioTek) and analyzed using SigmaPlot 10.0 software (Systat Software Inc.).

Real-time reverse transcription PCR

Total cellular RNA was extracted with Trizol reagent (Invitrogen, United States). cDNA was generated from total RNA by using random hexamer primers and moloney murine leukemia virus reverse transcriptase kit (Promega). Quantitative real-time PCR was performed on cDNA templates using SYBR Green PCR kit (Promega). The signals were acquired on a Rotor-Gene 3,000 Thermal Cycler (Corbett, Australia), and ΔΔCt was calculated with Rotor-Gene 6.1.81 software. Glyceraldehyde-3-phosphate dehydrogenase (GAPDH) RNA levels were quantified as an endogenous reference for normalization of target genes. The primer sequences of target genes were used as follows: TBEV, 5′-TGGAYTTYAGACAGGAAYCAACACA-3′(forward) and 5′-TCCAGAGACTYTGRTCDGTGTGGA-3′(reverse); myxovirus resistance A (MxA), 5′-ACAGGACCATCGGAATCTTG-3′ (forward) and 5′- CCCTTCTTCAGGTGGAACAC-3′ (reverse); GAPDH, 5′-TGGGCTACACTGAGCACCAG-3′ (forward) and 5′-AAGTGGTCGTTGAGGGCAAT-3′ (reverse).

Western blotting

Proteins in A549 cell lysates were electrophoretically separated on sodium dodecyl sulfate polyacrylamide gels and transferred onto polyvinylidene difluoride membranes. After being blocked with 5% nonfat dry milk in 0.1% Tween 20 in tris-buffered saline, the membranes were incubated with rabbit antibodies (1:1,000 dilution; Cell Signaling Technology, United States) for phospho-signal transducer and activator of transcription 3 (P-STAT3) (Tyr705) or GAPDH at 4°C overnight. The membranes were washed three times with 0.1% Tween 20 in tris-buffered saline and subsequently incubated with horseradish peroxidase conjugated goat anti-rabbit IgG (1:2,000 dilution) for 2 h at room temperature. The membranes were washed three times, and target proteins were visualized with enhanced chemiluminescent solution detection reagents (Bio-Rad, United States) on a GeneGnome HR image capture (Cambridge, UK).

Statistical analysis

Data are shown as mean and standard deviation (SD). The statistical analysis was performed with two-tailed unpaired or paired Student's *t*-test (GraphPad Prism 8.0) as indicated. Differences with *p* value <0.05 were considered statistically significant: $^{*}p < 0.05$, $^{**}p < 0.005$, $^{***}p < 0.002$, $^{****}p < 0.001$.

Results

Ribavirin has minor cytotoxicity on multiple cell lines

Some compounds were evaluated for their antiviral efficacy against TBEV on human lung adenocarcinoma A549 cells (Yu et al., 2013; Krol et al., 2019). Human neuroblastoma cell line SH-SY5Y was a valuable cell model for elucidating neuropathogenesis of neurotropic viruses (Yang et al., 2008; Laassri et al., 2011). As TBEV is a neurotropic virus, cell lines of extraneural as well as neuronal origin were chosen to be cell model for evaluating antiviral efficacy of ribavirin. In the present study, antiviral efficacy of ribavirin against TBEV was examined on A549 and SH-SY5Y cell lines.

We previously showed that 100 μg/mL of ribavirin displayed no observable toxicity on human hepatoma Huh7.5.1 cells (Zhao et al., 2012). To initially determine whether ribavirin had any effects on

proliferation of the multiple cell lines used, A549, SH-SY5Y and Vero cells were treated for 48 h with ribavirin at the increasing doses (0–300 μg/mL). The cytotoxicity was determined in terms of cell viability by the MTS assay. As shown in Figure 1, ribavirin was differentially cytotoxic among cell lines and only high doses of ribavirin gave rise to cytotoxicity. In A549 cells, ribavirin did not exert significant cytotoxic effects at doses up to 200 μg/mL. Treatment with 300 μg/mL of ribavirin reduced A549 cell proliferation by 24% and exerted significant inhibitory effects compared with the untreated control (0 μg/mL, $p < 0.05$; Figure 1A). Instead, ribavirin at doses up to 50 μg/mL had little inhibitory effects on SH-SY5Y cell proliferation. The significant inhibitory effects on SH-SY5Y cell proliferation were detectable following the ribavirin treatment at doses of 80 and 100 μg/mL ($p < 0.002$, $p < 0.001$; Figure 1B). Ribavirin treatment was nontoxic to Vero cells even at a high dose of 300 μg/mL (Figure 1C). These results showed that cytotoxicity of ribavirin was associated with cell types and the minor cytotoxic effects may be favorable for its antiviral activity and clinical usage, suggesting a great safety profile of ribavirin. For evaluation of antiviral efficacy, the tested doses of ribavirin did not exceed 60 μg/mL with no cytotoxic effects on the cell lines tested.

Ribavirin obviously impairs TBEV replication in A549 cells

TBEV envelope protein expression was inhibited in the infected cells by some compounds (Eyer et al., 2016, 2017). We analyzed the influence of ribavirin on TBEV protein expression over the course of infection in A549 cells by immunofluorescence. A549 cells were incubated with TBEV and varying doses of ribavirin and the viral protein expression was measured at 48 h post-inocubation. As shown in Figure 2 (left panel), TBEV protein could be clearly detected in the infected cells without the ribavirin treatment (untreated control) and a high percentage of TBEV-positive cells was detectable (right panel), indicating that A549 cells are susceptible to TBEV. Treatment with PBS was used as a solvent control. As expected, PBS showed very minor influence on the viral protein expression. TBEV protein was undetectable in mock-infected A549 cells (data not shown). TBEV protein expression was persistently decreased in the infected cells with the ribavirin treatment compared to the untreated control. Ribavirin at the dose of 40 or 60 μg/mL showed a significant inhibition of the viral protein expression in TBEV-infected cells ($p < 0.05$; Figure 2, right panel). Treatment with 60 μg/mL of ribavirin led to nearly a complete inhibition of TBEV infection. Here immunofluorescence staining showed the dose-dependent inhibition of TBEV protein expression in the ribavirin-treated A549 cells. Moreover, morphological changes of TBEV-infected A549 cells upon ribavirin treatment were observed. In comparison with mock control, cytopathic effect was obviously detectable in the infected A549 cells, and such cytopathic effect was almost abolished due to the 50 μg/mL ribavirin treatment (data not shown). Ribavirin may protect the infected cells from the cytopathic effect by impairing TBEV replication.

Ribavirin markedly inhibits TBEV propagation in A549 and SH-SY5Y cells

Antiviral activity of polyphenol complex from seagrass of the Zosteraceae family against TBEV was analyzed based on several schemes of application of the compound (Krylova et al., 2018). To study the mechanisms of anti-TBEV activity of ribavirin, three schemes of ribavirin treatment were applied to A549 and SH-SY5Y cells. Both TBEV production and the viral RNA replication were examined in the infected cells with and without the ribavirin treatment. At 48 h post-inocubation, the culture supernatants and the cellular RNA were collected from the A549 and SH-SY5Y cells for plaque assay and real-time PCR analysis, respectively. Indeed, TBEV effectively propagated in the cell-based assay systems as evidenced that the peak levels of virus titer were 1.07×10^8 PFU/mL in the culture supernatants from infected A549 cells and 6.67×10^7 PFU/mL from the infected SH-SY5Y cells (Figure 3). For co-treatment, dose-dependent inhibition of TBEV production by ribavirin was observed in A549 and SH-SY5Y cells. TBEV titers from the ribavirin-treated cells were significantly reduced at doses of 10, 20 and 50 μg/mL compared with the untreated cells (0 μg/mL, $p < 0.002$, $p < 0.001$; Figures 3A,B, left panel). Similarly, dose-dependent inhibition of TBEV production by ribavirin post-treatment was also observable in A549 and SH-SY5Y cells. The post-treatment of ribavirin at doses of

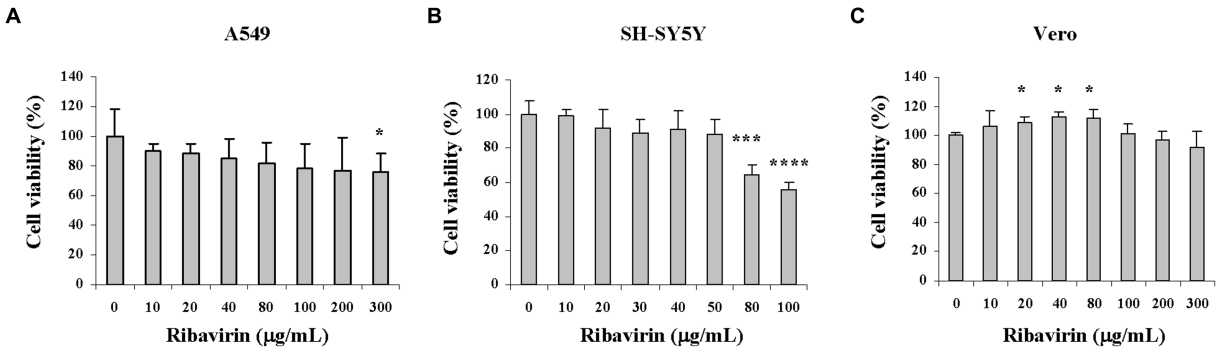

FIGURE 1
Cytotoxicity profile of ribavirin on multiple cell lines. Cells were cultured for 48h in the presence of ribavirin at the indicated concentrations. Cell viability was determined by MTS assay. **(A)** A549 cell viability upon ribavirin treatment. **(B)** SH-SY5Y cell viability upon ribavirin treatment. **(C)** Vero cell viability upon ribavirin treatment. The results are representative of two independent experiments. Data are shown as mean±SD (n=3); *p<0.05, ***p<0.002, ****p<0.001 compared with the untreated control (0μg/mL).

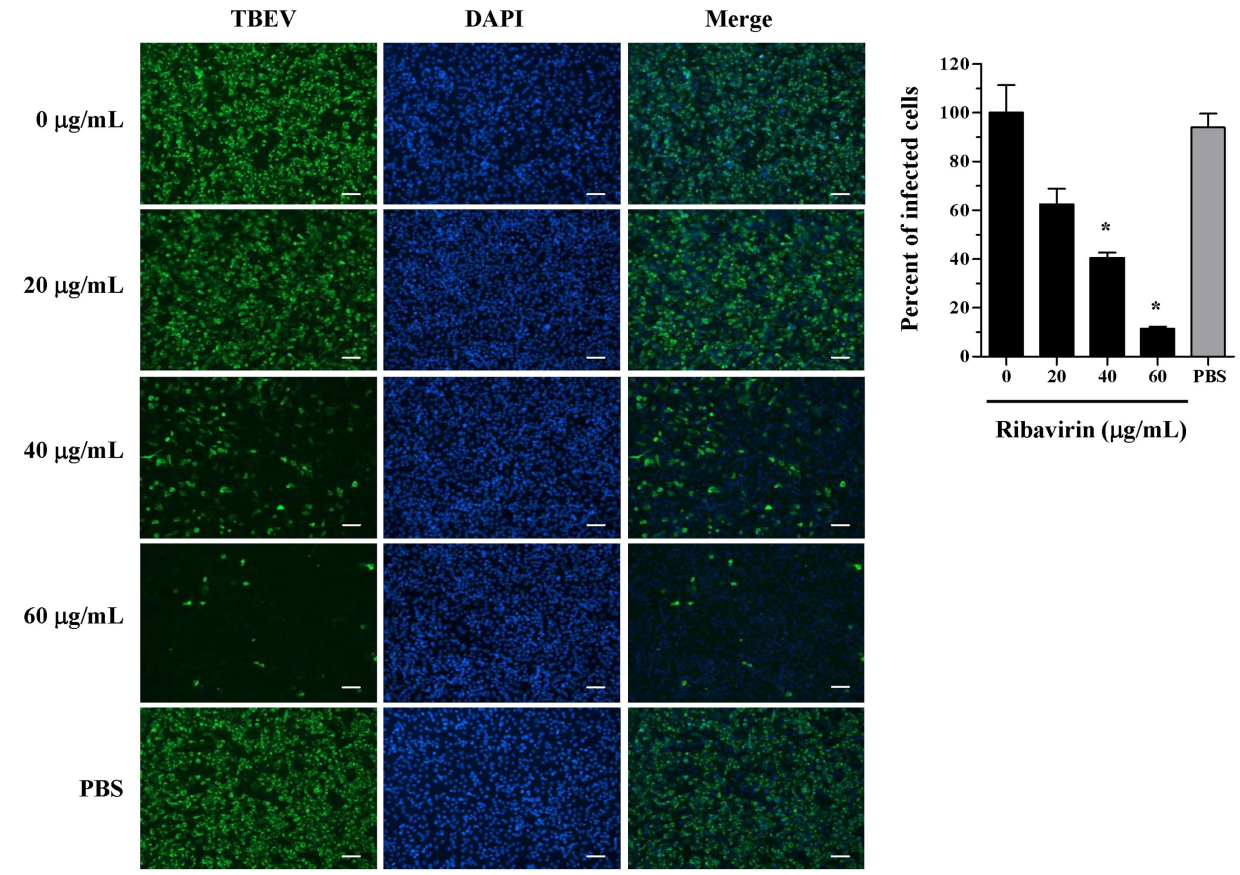

FIGURE 2
Inhibition of TBEV protein expression by ribavirin in A549 cells. A549 cells were incubated with TBEV and ribavirin at the concentrations ranging from 0 to 60μg/mL or 0.1% PBS (solvent control). The cells were fixed at 48h post-inocubation and stained with TBEV immunized mouse ascites and goat anti-mouse secondary antibody conjugated with Alexa Fluor 488 (green) and counterstained with DAPI (blue) by immunofluorescence staining. The representative images of three experiments are shown. Scale bar, 100μm. The percentages of TBEV-infected A549 cells are shown as mean±SD of three experiments (right panel). *p<0.05 compared with the untreated control (0μg/mL).

10, 20 and 50 μg/mL significantly decreased the viral titers ($p < 0.05$; Figures 3A,B, middle panel). In comparison with the untreated cells, the highest tested dose of 50 μg/mL ribavirin led to a reduction in TBEV titer of about 100-fold in A549 cells and 1,000-fold in SH-SY5Y cells. By contrast, there were no antiviral effects of ribavirin pre-treatment observed in A549 and SH-SY5Y cells (Figures 3A,B, right panel). TBEV titers from the ribavirin pre-treated cells were almost the same as those from the untreated cells. As a solvent control, PBS treatment showed little or no effects on the viral titers. By using co-treatment as well as post-treatment scheme of application, the antiviral effects of ribavirin against TBEV were evident in A549 and SH-SY5Y cells. The two schemes of ribavirin treatment were thereby focused in the following assays.

Next, the antiviral effects were further confirmed by measuring TBEV RNA levels in the cells with the co-treatment or post-treatment of ribavirin. In A549 cells, TBEV RNA levels were dose-dependently reduced by ribavirin at the co-treatment as well as the post-treatment scheme and significant differences ($p < 0.05$, $p < 0.005$, $p < 0.001$) were observed at all tested doses as compared with the untreated control (0 μg/mL; Figure 4A). In SH-SY5Y cells, the co-treatment or post-treatment of ribavirin also resulted in a dose-dependent reduction of TBEV RNA levels and such inhibitory effects were significant as compared with the untreated control ($p < 0.05$, $p < 0.001$; Figure 4B). Particularly, a complete inhibition of viral replication was observed at a dose of 50 μg/mL for ribavirin with the two treatment schemes in SH-SY5Y cells, which corresponded to the TBEV titer reduction of about 1,000-fold (Figure 3B, left and middle panel). Whereas there were no inhibitory effects observed on TBEV replication in the infected A549 and SH-SY5Y cells with PBS treatment (solvent control). Furthermore, the inhibition of TBEV replication by ribavirin was comparable with its reduction in the virus production based on the co-treatment as well as the post-treatment scheme. Together, ribavirin markedly inhibited TBEV propagation and exerted potent antiviral effects against TBEV in A549 and SH-SY5Y cells.

Ribavirin up-regulates MxA gene expression and STAT3 phosphorylation in TBEV-infected A549 cells

The following experiments focused on antiviral and anti-inflammatory responses induced by ribavirin, which were investigated in TBEV-infected A549 cells. Since ribavirin exerted the inhibitory effects on TBEV propagation, which downstream elements mediated

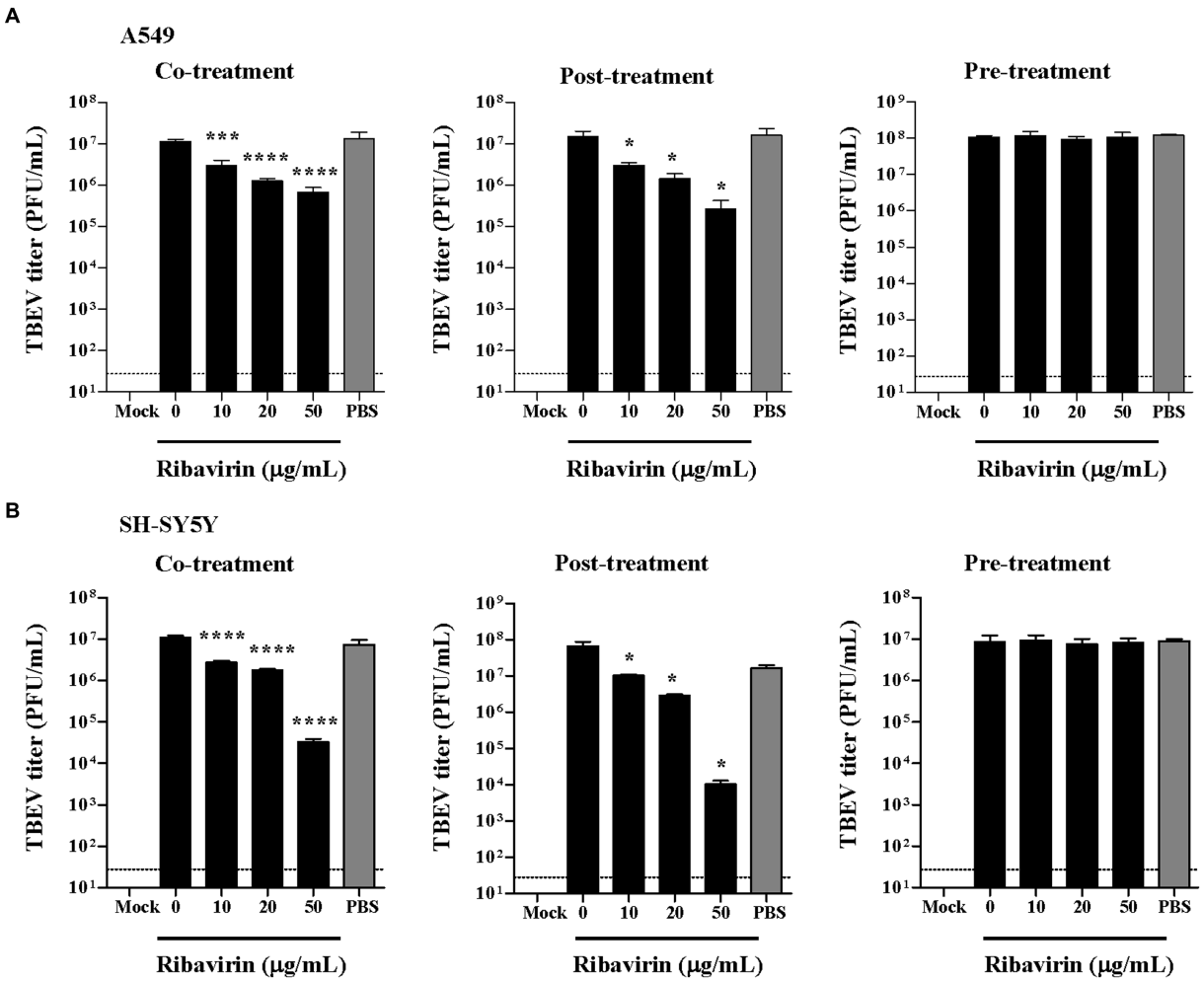

FIGURE 3
Effects of ribavirin on TBEV production in different cell lines. Cells were infected with TBEV and treated with the increasing concentrations of ribavirin at three schemes (co-treatment, post-treatment and pre-treatment). At 48h post-inocubation, culture supernatants were collected and virus titers were monitored by plaque assay. **(A)** TBEV titers in A549 cells. **(B)** TBEV titers in SH-SY5Y cells. Data represent the mean±SD of three experiments (n=3); *p<0.05, ***p<0.002, ****p<0.001 compared with the untreated control (0μg/mL). Uninfected cells were used as a mock control (Mock). PBS was used as a solvent control. The horizontal dashed line indicates the minimum detectable threshold of 1.44 $\log_{10}$ PFU/mL.

the antiviral response were then examined. As a member of IFN-stimulated genes whose protein products mediate a variety of specific antiviral response, MxA gene expression was analyzed in the TBEV-infected A549 cells with and without the ribavirin treatment. At 48 h post-inocubation, the RNA obtained from the cells upon the co-treatment or the post-treatment of ribavirin was also measured for MxA mRNA levels. Real-time PCR analysis showed that the MxA mRNA levels were significantly up-regulated in TBEV-infected A549 cells compared with the mock infected cells (Mock, $p < 0.05$ for the co-treatment, $p < 0.001$ for the post-treatment; Figure 5A), implying TBEV triggered antiviral response at the early stage of infection. The treatment of ribavirin at the co-treatment as well as the post-treatment scheme resulted in a dose-dependent increase in MxA mRNA levels and significant differences ($p < 0.05$, $p < 0.002$, $p < 0.001$) were detectable in the infected A549 cells treated with the ribavirin versus the untreated cells (0 μg/mL). The highest levels of MxA mRNA were detectable in the cells treated with 50 μg/mL of ribavirin. There were no significant differences in MxA mRNA levels in the infected A549 cells alone or along with PBS treatment (solvent control).

STAT3, a member of transcription factor family, is a key regulator of numerous physiological functions, including inflammation, cell proliferation, cell survival and cellular differentiation (Roca Suarez et al., 2018). STAT3 has been documented to play important roles in viral infection and pathogenesis (Chang et al., 2018). STAT3 is activated by tyrosine phosphorylation on Tyr705. At 48 h post-inocubation, the cell lysates obtained from A549 upon the co-treatment or the post-treatment of ribavirin was analyzed for STAT3 phosphorylation by Western blotting. As shown in Figure 5B, levels of phosphorylated STAT3 (P-STAT3) were noticeably impaired in the TBEV-infected cells (0 μg/mL) compared with those in the uninfected cells (Mock). Treatment with the ribavirin at the co-treatment as well as the post-treatment scheme led to a dose-dependent enhancement of STAT3 phosphorylation. PBS treatment had no enhanced effects on the STAT3 phosphorylation. Therefore,

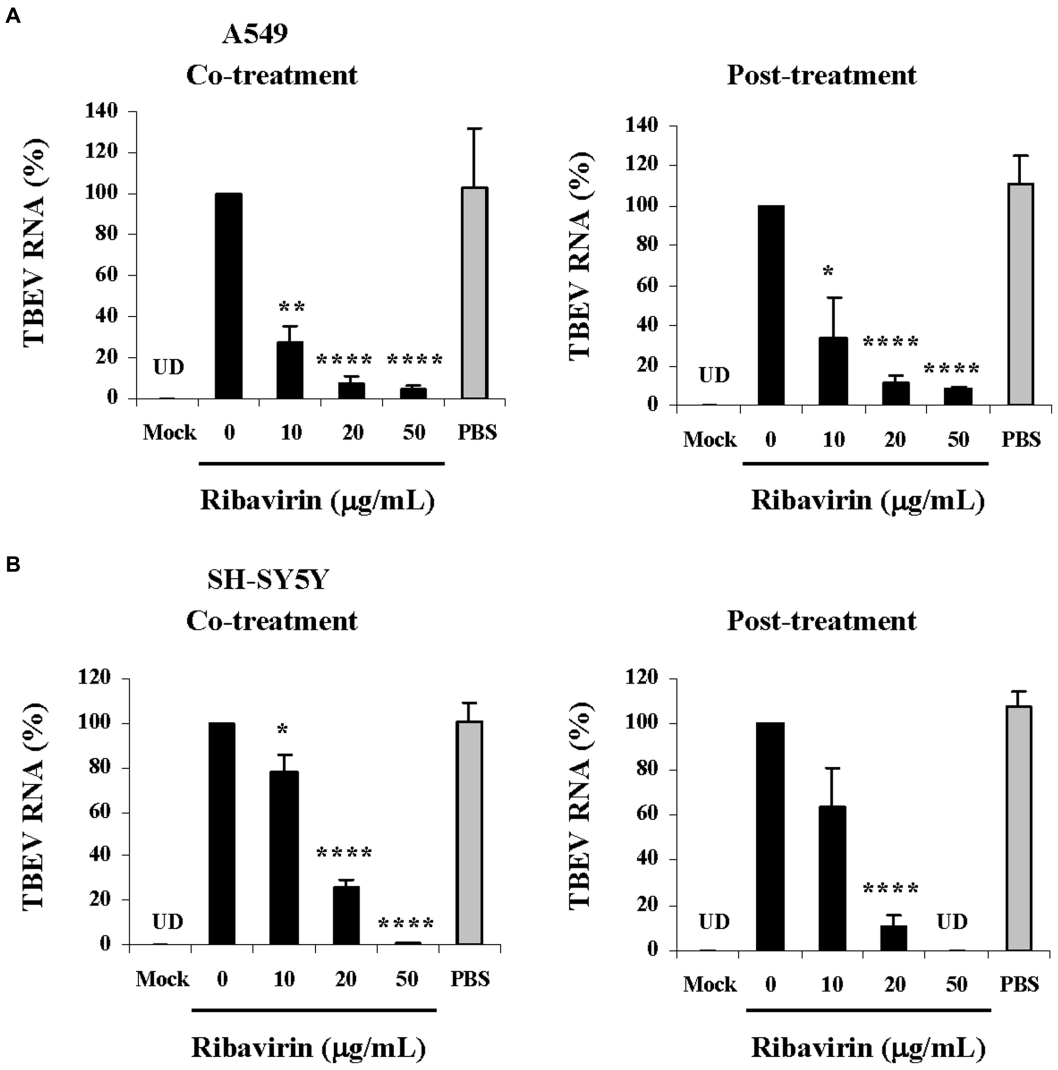

FIGURE 4
Effects of ribavirin on TBEV RNA replication in different cell lines. Cells were infected with TBEV and treated with the increasing concentrations of ribavirin at two schemes (co-treatment and post-treatment). At 48h post-inocubation, total RNA extracts were prepared and levels of TBEV RNA were quantified by real-time reverse transcription PCR. **(A)** TBEV RNA levels in A549 cells. **(B)** TBEV RNA levels in SH-SY5Y cells. TBEV RNA levels are shown as relative percentages of the untreated control (0μg/mL). For each sample, real-time PCR analysis was performed in triplicate. Data are from three experiments and represent the mean±SD (n=3); *p<0.05, **p<0.005, ****p<0.001 compared with the untreated control (0μg/mL). Uninfected cells were used as a mock control (Mock). PBS was used as a solvent control. UD, undetectable.

ribavirin induced activation of STAT3 during TBEV infection. These observations indicate that ribavirin may exert antiviral effects by up-regulating antiviral protein MxA gene expression and STAT3 phosphorylation in A549 cells infected with TBEV.

Ribavirin differentially regulates inflammation cytokine production in TBEV-infected A549 cells

The influence of ribavirin on inflammation response was further evaluated in TBEV-infected A549 cells. At 48 h post-inocubation, the culture supernatants from the cells were collected for measurement of TNF-α and IL-1β release by ELISA. Figure 6A showed that TBEV infection led to strong induction of TNF-α. The peak levels of TNF-α were 108.52pg/mL (the co-treatment) and 68.81pg/mL (the post-treatment) in the culture supernatants from A549 cells infected with TBEV, respectively. Such TNF-α levels were significantly higher as compared with the uninfected cells (Mock; $p < 0.001$ for the co-treatment, $p < 0.002$ for the post-treatment). However, the influence of ribavirin on TBEV-mediated TNF-α release varied among the different treatment schemes. In response to the co-treatment of ribavirin, there was little or no reduction in TNF-α amounts. Whereas the post-treatment of ribavirin resulted in a substantial decrease in TNF-α amounts. Treatment with ribavirin at the dose of 20 or 50 μg/mL significantly reduced TNF-α amounts as compared with the untreated cells (0 μg/mL; $p < 0.05$). Conversely, there were no obvious inhibitory effects of ribavirin on IL-1β amounts in the culture supernatants from the infected A549 cells with the co-treatment as well as post-treatment of ribavirin (Figure 6B). PBS treatment showed

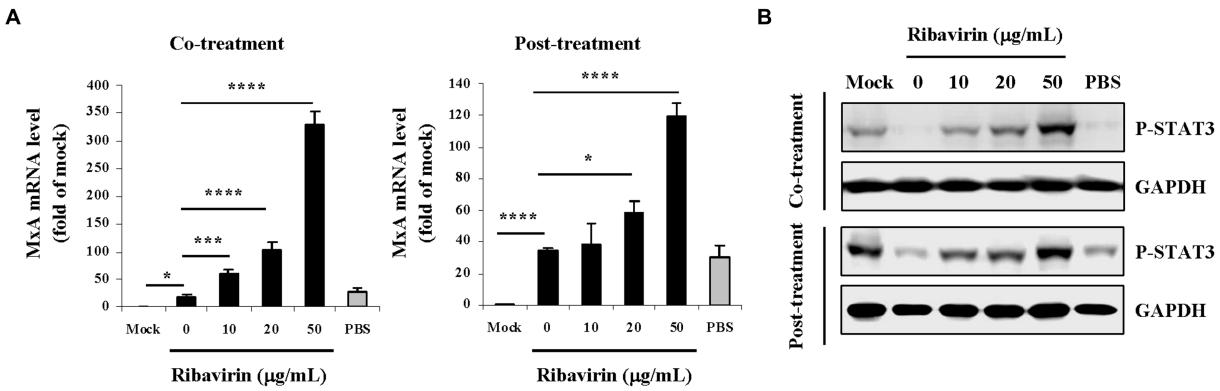

FIGURE 5
Effects of ribavirin on expression of MxA gene and phosphorylation of STAT3 in TBEV-infected A549 cells. Cells were infected with TBEV and treated with the increasing concentrations of ribavirin at two schemes (co-treatment and post-treatment). At 48h post-inocubation, total RNA extracts and cell lysates were prepared. **(A)** MxA mRNA levels were quantified by real-time reverse transcription PCR. MxA mRNA levels are shown as fold of mock control. For each sample, real-time PCR analysis was performed in triplicate. Data are from three experiments and represent the mean±SD (n=3); *p<0.05, ***p<0.002, ****p<0.001. **(B)** P-STAT3 was detected in the cell lysates by Western blotting. GAPDH is shown as a loading control. The results shown are representative of at least three independent experiments. Uninfected cells were used as a mock control (Mock). PBS was used as a solvent control.

no inhibitory effects on the TNF-α and IL-1β amounts in the culture supernatants from the infected cells. Ribavirin exerted differential inhibitory effects on the inflammatory cytokines and the post-treatment of ribavirin reduced TBEV-mediated TNF-α induction in A549 cells.

Discussion

TBEV infection has raised public health concern due to the absence of effective antiviral treatments. With respect to its wide use as a therapeutic antiviral drug, whether ribavirin has anti-TBEV efficiency is taken into consideration. The current study demonstrated that ribavirin exhibited a potent antiviral action during TBEV infection *in vitro*, as evidenced by the inhibition of TBEV propagation as well as the initiation of antiviral and anti-inflammatory responses. Moreover, which stages of TBEV life cycle targeted by ribavirin as well as the molecular elements involved in the antiviral processes were analyzed and discussed.

The development of broad-spectrum antiviral compounds is in progress to improve treatment protocols against highly pathogenic arboviruses. Ribavirin is effective against the several viruses in the clinical management and a number of viruses *in vitro* with multiple effects on virus replication and propagation (Beaucourt and Vignuzzi, 2014). Previous studies showed that ribavirin was inhibitory to yellow fever virus, dengue virus, West Nile virus, Japanese encephalitis virus and TBEV in some cell cultures (Canonico et al., 1984; Huggins et al., 1984; Huggins, 1989; Neyts et al., 1996; Jordan et al., 2000; Crance et al., 2003). Here, we performed systematic experiments to investigate the safety and antiviral efficacy of ribavirin in the A549 and SH-SY5Y cells with TBEV infection. First, ribavirin displayed minor cytotoxicity on the cell lines and such characteristic enabled its clinical usage as an antiviral drug, which was beneficial for the evaluation of anti-TBEV action at a wide range of ribavirin doses in the different types of cells. Next, the dose-dependent inhibition of TBEV protein expression was observed in the infected A549 cells upon ribavirin treatment. In consistent with such inhibition, ribavirin indeed protected the infected cells by reducing the cytopathic effect. Then, the treatment of ribavirin significantly decreased TBEV titers in a dose-dependent manner in both A549 cells and SH-SY5Y cells. At the same time, the ribavirin treatment also exhibited the dose-dependent reduction of TBEV RNA levels. The markedly inhibitory effects of ribavirin on the viral RNA replication were observable in A549 and SH-SY5Y cells. These results demonstrated that ribavirin could strongly inhibit TBEV propagation in the susceptible cells at a non-cytotoxic dose range. In agreement with our results, on the basis of protein-drug interactions, ribavirin potently inhibited TBEV by targeting TBEV NS3 helicase (Singh and Somvanshi, 2009). Ribavirin significantly inhibited the proliferation of the highly virulent strain of the TBEV in the PK cell cultures (Krylova and Leonova, 2016). A recent study also reported that ribavirin exhibited inhibition toward highly and low-virulent strains of TBEV on SPEV cells (Leonova et al., 2020). However, 50 μM of ribavirin displayed no noticeable inhibitory effects on reducing TBEV titers in rat organotypic cerebellum slices (Lenz et al., 2018). We propose that culture models, virulent strains of TBEV and doses of ribavirin may be involved in the differences in anti-TBEV action of ribavirin.

The antiviral action of ribavirin on TBEV was further explored based on its influence in the viral life cycle. The time-of-addition assay was employed to determine which step(s) in the viral life cycle is blocked by an antiviral agent(s) (Chen et al., 2017; Aoki-Utsubo et al., 2018; Krylova et al., 2018). A549 and SH-SY5Y cells infected with TBEV were treated with ribavirin at the three schemes including co-treatment, post-treatment and pre-treatment. The TBEV titers, viral RNA levels and MxA mRNA levels were analyzed and compared. The TBEV titers were significantly reduced in the cells treated with ribavirin at the scheme of co-treatment as well as post-treatment. Conversely, no inhibitory effects on TBEV titers were found in the cells with ribavirin pre-treatment. In parallel with the reduction in TBEV titers, the viral RNA levels were markedly decreased in the cells treated with ribavirin at the scheme of co-treatment as well as post-treatment. These results suggest that ribavirin exhibits antiviral action

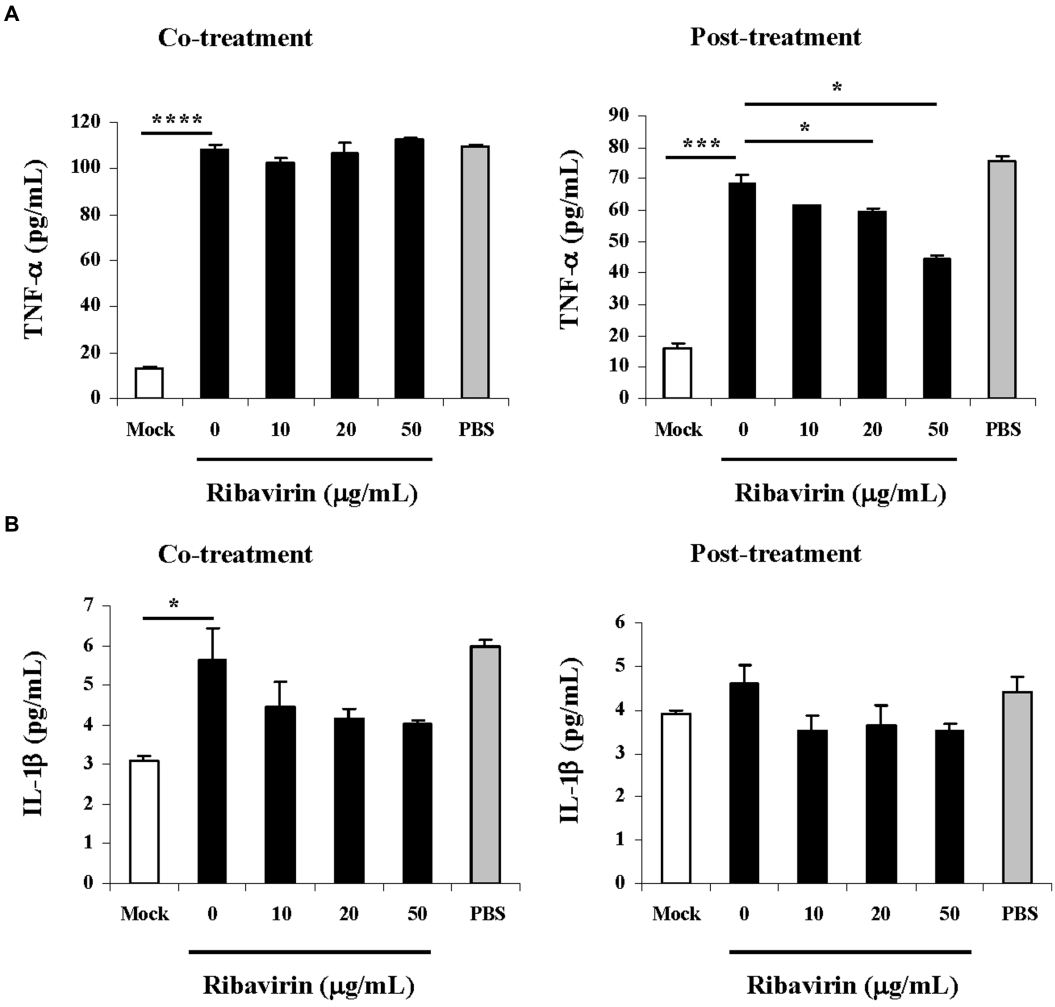

FIGURE 6
Cytokine response in TBEV-infected A549 cells upon ribavirin treatment. A549 cells were infected with TBEV and treated with the increasing concentrations of ribavirin at two schemes (co-treatment and post-treatment). Culture supernatants were harvested at 48h post-inocubation and concentrations of cytokines were measured by ELISA. **(A)** Changes in TNF-α concentration. **(B)** Changes in IL-1β concentration. Data represent the mean±SD of three experiments (n =3); *p <0.05, ***p <0.002, ****p <0.001. Uninfected cells were used as a mock control (Mock). PBS was used as a solvent control.

by targeting TBEV replication stage (co-treatment and post-treatment) rather than early stage of virus penetration into cells (pre-treatment), implying that ribavirin may be used as a promising antiviral drug for the treatment of TBEV infection but not a preventive therapy.

The molecule events underlying the anti-TBEV action of ribavirin were preliminarily investigated in this study. Human MxA is an IFN-induced dynamin-like GTPase with broad antiviral activity through engagement of a diversity of viral proteins (Haller and Kochs, 2011; Mitchell et al., 2013). The expression of MxA in chronic hepatitis C played a role among the mechanisms underlying responsiveness to therapy of pegylated IFN in combination with ribavirin (Giannelli et al., 2004). Ribavirin was also reported to enhance IFN-α-induced mRNA and protein expression of MxA, which was a novel immune modulation mechanism during treatment of hepatitis C virus (Stevenson et al., 2011). It is thus interesting to investigate whether the antiviral action of ribavirin correlates with MxA. In consistent with the inhibitory effects of ribavirin on TBEV propagation, our results demonstrated that MxA mRNA levels were dose-dependently increased in TBEV-infected A549 cells with the co-treatment as well as the post-treatment of ribavirin, indicating that ribavirin may exhibit anti-TBEV action through induction of cellular antiviral response, in particular by up-regulating MxA expression. At the same time, STAT3 was also focused due to its distinct roles in regulating host immune responses and several viral diseases. It is known that STAT3 exhibits a proviral function in several viral infections, whereas STAT3 has an antiviral function in other viral infections (Chang et al., 2018). Moreover, STAT3 is proposed to be a potential target for antiviral therapy (Roca Suarez et al., 2018; Pandey et al., 2022). Inhibition of STAT3 signaling has been implicated in some cell lines during infection with several viruses including Marburg virus, human metapneumovirus, Ebola virus and Kaposi's sarcoma-associated herpesvirus (Valmas et al., 2010; Mitzel et al., 2014; Harrison et al., 2021; Lee et al., 2023). These studies provide fundamental insights into the mechanisms of pathogenesis of viruses. Our results showed that TBEV potently inhibited the STAT3 phosphorylation in A549 cells, which may account for the viral survival and propagation and thereby

establish infection. Recent studies have reported that STAT3 activation is responsible for the antiviral activities, such as STAT3 activation exerted an anti-enterovirus 71 activity; IL-22 suppressed infection of porcine enteric coronaviruses and rotavirus by activating STAT3 pathway; activation of STAT3 signaling was involved in inducing Sindbis virus E2 glycoprotein antibody-mediated viral suppression and viral clearance from neurons; antimicrobial peptide REG3G inhibited replication of Swine coronavirus-porcine epidemic diarrhea virus by up-regulating STAT3 pathway (Chang et al., 2017; Xue et al., 2017; Yeh et al., 2020; Fan et al., 2023). In accordance with the inhibition of TBEV production and the viral RNA replication by ribavirin, we observed that the ribavirin treatment distinctly enhanced the STAT3 phosphorylation in TBEV-infected A549 cells, implying that STAT3 activation might be a key event involved in the antiviral effect of ribavirin.

TBEV infection causes severe central nervous system diseases such as meningitis or encephalitis that is characterized by inflammation. Elucidation of cellular immune response to TBEV infection is important for understanding the viral pathogenesis and developing effective treatment of the diseases. The increased serum levels of TNF-α were found in patients of tick-borne encephalitis (Atrasheuskaya et al., 2003). Indeed, we found that TBEV infection led to strong induction of TNF-α in A549 cells. Ribavirin is known to possess immunomodulatory action. The roles of ribavirin in the induction of cytokines by some viruses were reported. For example, ribavirin suppressed activation of select inflammatory mediators triggered by Andes-virus (Khaiboullina et al., 2013). Treatment with ribavirin decreased the concentrations of TNF-α and IL-1β during murine hepatitis virus strain 3 infection *in vitro* and *in vivo* (Ning et al., 1998; Levy et al., 2006). Treatment of dengue virus-infected cells with ribavirin reduced TNF-α transcription (Rattanaburee et al., 2015). Ribavirin decreased the level of TNF-α and IL-1β in lung of mice infected with influenza virus (Liao et al., 2017). The influence of ribavirin in induction of pro-inflammatory cytokines TNF-α and IL-1β was thereby assessed in the TBEV-infected A549 cells. Our results showed that ribavirin significantly inhibited the production of TNF-α at the scheme of post-treatment, whereas it did not obviously diminish the production of IL-1β. Upon the post-treatment of ribavirin, the suppression of TNF-α release by TBEV-infected A549 cells was in parallel with the inhibition of TBEV propagation and viral RNA replication as well as the up-regulation of MxA mRNA expression and STAT3 phosphorylation, supporting that ribavirin may exhibit antiviral action by targeting TBEV replication stage. Our findings suggest that the suppression of TBEV-induced TNF-α release by ribavirin may attenuate inflammation *via* controlling pro-inflammatory cytokine-mediated immunoinflammatory events. Whether such suppression is associated with the inhibition of TBEV propagation by ribavirin deserves further study.

In conclusion, ribavirin may represent an effective drug toward TBEV infection for its potent inhibition of the virus propagation and limiting immune response in susceptible cell lines. Molecular bases of antiviral effect of ribavirin for TBEV need to be further investigated based on different virulent strains of TBEV and suitable animal models. Ribavirin's precise antiviral mechanisms against TBEV remain to be elucidated and are implicated in the development of specific anti-TBEV treatments.

Data availability statement

The original contributions presented in the study are included in the article/supplementary material, further inquiries can be directed to the corresponding authors.

Author contributions

W-DT and H-LT conducted the study. H-RP analyzed the data. R-WR revised the manuscript. PZ supervised the study. L-JZ designed the study, wrote and revised the manuscript. All authors contributed to the article and approved the submitted version.

Funding

This work was funded by the National Key Research and Development Program of China (2016YFC1202903) to L-JZ.

Acknowledgments

We thank Rong Ye from the School of Basic Medical Sciences Fudan University for kindly providing cell lines including SH-SY5Y, A549 and PK-15, excellent technical assistance and critical reading of the manuscript.

Conflict of interest

The authors declare that the research was conducted in the absence of any commercial or financial relationships that could be construed as a potential conflict of interest.

Publisher's note

All claims expressed in this article are solely those of the authors and do not necessarily represent those of their affiliated organizations, or those of the publisher, the editors and the reviewers. Any product that may be evaluated in this article, or claim that may be made by its manufacturer, is not guaranteed or endorsed by the publisher.

References

Aoki-Utsubo, C., Chen, M., and Hotta, H. (2018). Time-of-addition and temperature-shift assays to determine particular step(s) in the viral life cycle that is blocked by antiviral substance(s). *Bio. Protoc.* 8:e2830. doi: 10.21769/BioProtoc.2830

Ascioglu, S., Leblebicioglu, H., Vahaboglu, H., and Chan, K. A. (2011). Ribavirin for patients with Crimean-Congo haemorrhagic fever: a systematic review and meta-analysis. *J. Antimicrob. Chemother.* 66, 1215–1222. doi: 10.1093/jac/dkr136

Atrasheuskaya, A. V., Fredeking, T. M., and Ignatyev, G. M. (2003). Changes in immune parameters and their correction in human cases of tick-borne encephalitis. *Clin. Exp. Immunol.* 131, 148–154. doi: 10.1046/j.1365-2249.2003.02050.x

Beaucourt, S., and Vignuzzi, M. (2014). Ribavirin: a drug active against many viruses with multiple effects on virus replication and propagation. Molecular basis of ribavirin resistance. *Curr. Opin. Virol.* 8, 10–15. doi: 10.1016/j.coviro.2014.04.011

Blom, K., Cuapio, A., Sandberg, J. T., Varnaite, R., Michaëlsson, J., Björkström, N. K., et al. (2018). Cell-mediated immune responses and immunopathogenesis of human tick-borne encephalitis virus-infection. *Front. Immunol.* 9:2174. doi: 10.3389/fimmu.2018.02174

Borden, K. L., and Culjkovic-Kraljacic, B. (2010). Ribavirin as an anti-cancer therapy: acute myeloid leukemia and beyond? *Leuk. Lymphoma* 51, 1805–1815. doi: 10.3109/10428194.2010.496506

Canonico, P. G., Kende, M., Luscri, B. J., and Huggins, J. W. (1984). In-vivo activity of antivirals against exotic RNA viral infections. *J. Antimicrob. Chemother.* 14, 27–41. doi: 10.1093/jac/14.suppl_a.27

Casaos, J., Gorelick, N. L., Huq, S., Choi, J., Xia, Y., Serra, R., et al. (2019). The use of ribavirin as an anticancer therapeutic: will it go viral? *Mol. Cancer Ther.* 18, 1185–1194. doi: 10.1158/1535-7163

Chang, Z., Wang, Y., Bian, L., Liu, Q., and Long, J. E. (2017). Enterovirus 71 antagonizes the antiviral activity of host STAT3 and IL-6R with partial dependence on virus-induced miR-124. *J. Gen. Virol.* 98, 3008–3025. doi: 10.1099/jgv.0.000967

Chang, Z., Wang, Y., Zhou, X., and Long, J. E. (2018). STAT3 roles in viral infection: antiviral or proviral? *Future Virol.* 13, 557–574. doi: 10.2217/fvl-2018-0033

Chen, M., Aoki-Utsubo, C., Kameoka, M., Deng, L., Terada, Y., Kamitani, W., et al. (2017). Broad-spectrum antiviral agents: secreted phospholipase A_2 targets viral envelope lipid bilayers derived from the endoplasmic reticulum membrane. *Sci. Rep.* 7:15931. doi: 10.1038/s41598-017-16130-w

Cheng, H. Y., French, C. E., Salam, A. P., Dawson, S., McAleenan, A., McGuinness, L. A., et al. (2022). Lack of evidence for ribavirin treatment of Lassa fever in systematic review of published and unpublished studies. *Emerg. Infect. Dis.* 28, 1559–1568. doi: 10.3201/eid2808.211787

Crance, J. M., Scaramozzino, N., Jouan, A., and Garin, D. (2003). Interferon, ribavirin, 6-azauridine and glycyrrhizin: antiviral compounds active against pathogenic flaviviruses. *Antivir. Res.* 58, 73–79. doi: 10.1016/s0166-3542(02)00185-7

De Winter, B. C. M., Hesselink, D. A., and Kamar, N. (2018). Dosing ribavirin in hepatitis E-infected solid organ transplant recipients. *Pharmacol. Res.* 130, 308–315. doi: 10.1016/j.phrs.2018.02.030

Ding, C., Tang, W., Xia, B., Peng, H., Liu, Y., Wang, J., et al. (2022). High-throughput screening of FDA-approved drug library reveals ixazomib is a broad-spectrum antiviral agent against arboviruses. *Viruses* 14:1381. doi: 10.3390/v14071381

Eyer, L., Šmídková, M., Nencka, R., Neča, J., Kastl, T., Palus, M., et al. (2016). Structure-activity relationships of nucleoside analogues for inhibition of tick-borne encephalitis virus. *Antivir. Res.* 133, 119–129. doi: 10.1016/j.antiviral.2016.07.018

Eyer, L., Zouharová, D., Širmarová, J., Fojtíková, M., Štefánik, M., Haviernik, J., et al. (2017). Antiviral activity of the adenosine analogue BCX4430 against West Nile virus and tick-borne flaviviruses. *Antivir. Res.* 142, 63–67. doi: 10.1016/j.antiviral.2017.03.012

Fan, B., Zhou, J., Zhao, Y., Zhu, X., Zhu, M., Peng, Q., et al. (2023). Identification of cell types and transcriptome landscapes of porcine epidemic diarrhea virus-infected porcine small intestine using single-cell RNA sequencing. *J. Immunol.* 210, 271–282. doi: 10.4049/jimmunol.2101216

Gao, X., Nasci, R., and Liang, G. (2010). The neglected arboviral infections in mainland China. *PLoS Negl. Trop. Dis.* 4:e624. doi: 10.1371/journal.pntd.0000624

Giannelli, G., Guadagnino, G., Dentico, P., Antonelli, G., and Antonaci, S. (2004). MxA and PKR expression in chronic hepatitis C. *J. Interf. Cytokine Res.* 24, 659–663. doi: 10.1089/jir.2004.24.659

Gross, A. E., and Bryson, M. L. (2015). Oral ribavirin for the treatment of noninfluenza respiratory viral infections: a systematic review. *Ann. Pharmacother.* 49, 1125–1135. doi: 10.1177/1060028015597449

Haller, O., and Kochs, G. (2011). Human MxA protein: an interferon-induced dynamin-like GTPase with broad antiviral activity. *J. Interf. Cytokine Res.* 31, 79–87. doi: 10.1089/jir.2010.0076

Harrison, A. R., Todd, S., Dearnley, M., David, C. T., Green, D., Rawlinson, S. M., et al. (2021). Antagonism of STAT3 signalling by Ebola virus. *PLoS Pathog.* 17:e1009636. doi: 10.1371/journal.ppat.1009636

Huggins, J. W. (1989). Prospects for treatment of viral hemorrhagic fevers with ribavirin, a broad-spectrum antiviral drug. *Rev. Infect. Dis.* 11, S750–S761. doi: 10.1093/clinids/11.Supplement_4.S750

Huggins, J. W., Robins, R. K., and Canonico, P. G. (1984). Synergistic antiviral effects of ribavirin and the C-nucleoside analogs tiazofurin and selenazofurin against togaviruses, bunyaviruses, and arenaviruses. *Antimicrob. Agents Chemother.* 26, 476–480. doi: 10.1128/AAC.26.4.476

Im, J. H., Baek, J. H., Durey, A., Kwon, H. Y., Chung, M. H., and Lee, J. S. (2020). Geographic distribution of tick-borne encephalitis virus complex. *J. Vector Borne Dis.* 57, 14–22. doi: 10.4103/0972-9062.308794

Johnson, S., Henschke, N., Maayan, N., Mills, I., Buckley, B. S., Kakourou, A., et al. (2018). Ribavirin for treating Crimean Congo haemorrhagic fever. *Cochrane Database Syst. Rev.* 6:CD012713. doi: 10.1002/14651858.CD012713.pub2

Jordan, J., Briese, T., Fischer, N., Lau, J. Y., and Lipkin, W. I. (2000). Ribavirin inhibits West Nile virus replication and cytopathic effect in neural cells. *J. Infect. Dis.* 182, 1214–1217. doi: 10.1086/315847

Khaiboullina, S. F., Rizvanov, A. A., Lombardi, V. C., Morzunov, S. P., Reis, H. J., Palotás, A., et al. (2013). Andes-virus-induced cytokine storm is partially suppressed by ribavirin. *Antivir. Ther.* 18, 575–584. doi: 10.3851/IMP2524

Krol, E., Wandzik, I., Brzuska, G., Eyer, L., Růžek, D., and Szewczyk, B. (2019). Antiviral activity of uridine derivatives of 2-deoxy sugars against tick-borne encephalitis virus. *Molecules* 24:1129. doi: 10.3390/molecules24061129

Krylova, N. V., and Leonova, G. N. (2016). Antiviral activity of various drugs with different mechanisms of action in patients with experimental tick-borne encephalitis. *Vopr. Virusol.* 61, 139–144. doi: 10.18821/0507-4088-2016-61-3

Krylova, N. V., Leonova, G. N., Maystrovskaya, O. S., Popov, A. M., and Artyukov, A. A. (2018). Mechanisms of antiviral activity of the polyphenol complex from seagrass of the Zosteraceae family against tick-borne encephalitis virus. *Bull. Exp. Biol. Med.* 165, 61–63. doi: 10.1007/s10517-018-4099-5

Laassri, M., Bidzhieva, B., Speicher, J., Pletnev, A. G., and Chumakov, K. (2011). Microarray hybridization for assessment of the genetic stability of chimeric West Nile/dengue 4 virus. *J. Med. Virol.* 83, 910–920. doi: 10.1002/jmv.22033

Lee, M. J., Lee, J., Kang, S. K., Wirth, D., Yoo, S. M., Park, C., et al. (2023). CXCL1 confers a survival advantage in Kaposi's sarcoma-associated herpesvirus-infected human endothelial cells through STAT3 phosphorylation. *J. Med. Virol.* 95:28020. doi: 10.1002/jmv.28020

Lenz, N., Engler, O., Grandgirard, D., Leib, S. L., and Ackermann-Gäumann, R. (2018). Evaluation of antivirals against tick-borne encephalitis virus in organotypic brain slices of rat cerebellum. *PLoS One* 13:e0205294. doi: 10.1371/journal.pone.0205294

Leonova, G. N., Maistrovskaya, O. S., and Lubova, V. A. (2020). Molecular and genetic bases of inhibition of tick-borne encephalitis virus replication by eprosartan and ribavirin. *Bull. Exp. Biol. Med.* 170, 53–57. doi: 10.1007/s10517-020-05003-4

Levy, G. A., Adamson, G., Phillips, M. J., Scrocchi, L. A., Fung, L., Biessels, P., et al. (2006). Targeted delivery of ribavirin improves outcome of murine viral fulminant hepatitis via enhanced anti-viral activity. *Hepatology* 43, 581–591. doi: 10.1002/hep.21072

Liao, S. H., Li, Y., Lai, Y. N., Liu, N., Zhang, F. X., and Xu, P. P. (2017). Ribavirin attenuates the respiratory immune responses to influenza viral infection in mice. *Arch. Virol.* 162, 1661–1669. doi: 10.1007/s00705-017-3291-7

Mitchell, P. S., Emerman, M., and Malik, H. S. (2013). An evolutionary perspective on the broad antiviral specificity of MxA. *Curr. Opin. Microbiol.* 16, 493–499. doi: 10.1016/j.mib.2013.04.005

Mitzel, D. N., Jaramillo, R. J., Stout-Delgado, H., Senft, A. P., and Harrod, K. S. (2014). Human metapneumovirus inhibits the IL-6-induced JAK/STAT3 signalling cascade in airway epithelium. *J. Gen. Virol.* 95, 26–37. doi: 10.1099/vir.0.055632-0

Neyts, J., Meerbach, A., McKenna, P., and De Clercq, E. (1996). Use of the yellow fever virus vaccine strain 17D for the study of strategies for the treatment of yellow fever virus infections. *Antivir. Res.* 30, 125–132. doi: 10.1016/0166-3542(96)89697-5

Ning, Q., Brown, D., Parodo, J., Cattral, M., Gorczynski, R., Cole, E., et al. (1998). Ribavirin inhibits viral-induced macrophage production of TNF, IL-1, the procoagulant fgl2 prothrombinase and preserves Th1 cytokine production but inhibits Th2 cytokine response. *J. Immunol.* 160, 3487–3493. doi: 10.4049/jimmunol.160.7.3487

Pandey, P., Al Rumaih, Z., Kels, M. J. T., Ng, E., Kc, R., Chaudhri, G., et al. (2022). Targeting ectromelia virus and TNF/NF-κB or STAT3 signaling for effective treatment of viral pneumonia. *Proc. Natl. Acad. Sci. U. S. A.* 119:e2112725119. doi: 10.1073/pnas.2112725119

Pulkkinen, L. I. A., Butcher, S. J., and Anastasina, M. (2018). Tick-borne encephalitis virus: a structural view. *Viruses* 10:350. doi: 10.3390/v10070350

Rattanaburee, T., Junking, M., Panya, A., Sawasdee, N., Songprakhon, P., Suttitheptumrong, A., et al. (2015). Inhibition of dengue virus production and cytokine/chemokine expression by ribavirin and compound a. *Antivir. Res.* 124, 83–92. doi: 10.1016/j.antiviral.2015.10.005

Reddy, K. R., Nelson, D. R., and Zeuzem, S. (2009). Ribavirin: current role in the optimal clinical management of chronic hepatitis C. *J. Hepatol.* 50, 402–411. doi: 10.1016/j.jhep.2008.11.006

Roca Suarez, A. A., Van Renne, N., Baumert, T. F., and Lupberger, J. (2018). Viral manipulation of STAT3: evade, exploit, and injure. *PLoS Pathog.* 14:e1006839. doi: 10.1371/journal.ppat.1006839

Singh, V., and Somvanshi, P. (2009). Structural modeling of the NS3 helicase of tick-borne encephalitis virus and their virtual screening of potent drugs using molecular docking. *Interdiscip. Sci.* 1, 168–172. doi: 10.1007/s12539-009-0039-4

Skripchenko, N. V., Ivanova, G. P., Skripchenko, E. Y., Pulman, N. F., and Murina, E. A. (2019). The efficacy of anti-viral therapy and serotherapy of tick-borne encephalitis in children. *Zh. Nevrol. Psikhiatr. Im. S S Korsakova* 119, 40–51. doi: 10.17116/hirurgia20190715

Stevenson, N. J., Murphy, A. G., Bourke, N. M., Keogh, C. A., Hegarty, J. E., and O'Farrelly, C. (2011). Ribavirin enhances IFN-α signalling and MxA expression: a novel immune modulation mechanism during treatment of HCV. *PLoS One* 6:e27866. doi: 10.1371/journal.pone.0027866

Tang, H., Liu, Y., Ren, R., Liu, Y., He, Y., Qi, Z., et al. (2022). Identification of clinical candidates against West Nile virus by activity screening in vitro and effect evaluation in vivo. *J. Med. Virol.* 94, 4918–4925. doi: 10.1002/jmv.27891

Tejada, S., Martinez-Reviejo, R., Karakoc, H. N., Peña-López, Y., Manuel, O., and Rello, J. (2022). Ribavirin for treatment of subjects with respiratory syncytial virus-related infection: a systematic review and meta-analysis. *Adv. Ther.* 39, 4037–4051. doi: 10.1007/s12325-022-02256-5

Valmas, C., Grosch, M. N., Schümann, M., Olejnik, J., Martinez, O., Best, S. M., et al. (2010). Marburg virus evades interferon responses by a mechanism distinct from ebola virus. *PLoS Pathog.* 6:e1000721. doi: 10.1371/journal.ppat.1000721

Volpin, F., Casaos, J., Sesen, J., Mangraviti, A., Choi, J., Gorelick, N., et al. (2017). Use of an anti-viral drug, ribavirin, as an anti-glioblastoma therapeutic. *Oncogene* 36, 3037–3047. doi: 10.1038/onc.2016.457

Xue, M., Zhao, J., Ying, L., Fu, F., Li, L., Ma, Y., et al. (2017). IL-22 suppresses the infection of porcine enteric coronaviruses and rotavirus by activating STAT3 signal pathway. *Antivir. Res.* 142, 68–75. doi: 10.1016/j.antiviral.2017.03.006

Yang, M. R., Lee, S. R., Oh, W., Lee, E. W., Yeh, J. Y., Nah, J. J., et al. (2008). West Nile virus capsid protein induces p53-mediated apoptosis via the sequestration of HDM2 to the nucleolus. *Cell. Microbiol.* 10, 165–176. doi: 10.1111/j.1462-5822.2007.01027.x

Yeh, J. X., Schultz, K. L. W., Calvert, V., Petricoin, E. F., and Griffin, D. E. (2020). The NF-κB/leukemia inhibitory factor/STAT3 signaling pathway in antibody-mediated suppression of Sindbis virus replication in neurons. *Proc. Natl. Acad. Sci. U. S. A.* 117, 29035–29045. doi: 10.1073/pnas.2016691117

Yoshii, K. (2019). Epidemiology and pathological mechanisms of tick-borne encephalitis. *J. Vet. Med. Sci.* 81, 343–347. doi: 10.1292/jvms.18-0373

Yu, C., Achazi, K., and Niedrig, M. (2013). Tick-borne encephalitis virus triggers inositol-requiring enzyme 1 (IRE1) and transcription factor 6 (ATF6) pathways of unfolded protein response. *Virus Res.* 178, 471–477. doi: 10.1016/j.virusres.2013.10.012

Zhao, L. J., Wang, W., Liu, Y., Ren, H., and Qi, Z. T. (2012). Interference with ERK and STAT signaling pathways and inhibition of hepatitis C virus replication by ribavirin. *Antivir. Res.* 96, 260–268. doi: 10.1016/j.antiviral.2012.09.002

frontiers | Frontiers in Microbiology

TYPE Original Research
PUBLISHED 14 September 2023
DOI 10.3389/fmicb.2023.1260812

OPEN ACCESS

EDITED BY
James Weger-Lucarelli,
Virginia Tech, United States

REVIEWED BY
Ambuj Shrivastava,
Defence Research and Development Establishment (DRDE), India
Wenn-Chyau Lee,
University of Malaya, Malaysia

*CORRESPONDENCE
Devojit Kumar Sarma
✉ dkbiotek@gmail.com

†These authors have contributed equally to this work

RECEIVED 18 July 2023
ACCEPTED 31 August 2023
PUBLISHED 14 September 2023

CITATION
Sarma DK, Rathod L, Mishra S, Das D, Agarwal A, Sharma G, Singh TA, Kumawat M, Singh S, Verma V, Kumar M, Shubham S, Tiwari RR and Prakash A (2023) Molecular surveillance of dengue virus in field-collected *Aedes* mosquitoes from Bhopal, central India: evidence of circulation of a new lineage of serotype 2.
Front. Microbiol. 14:1260812.
doi: 10.3389/fmicb.2023.1260812

Molecular surveillance of dengue virus in field-collected *Aedes* mosquitoes from Bhopal, central India: evidence of circulation of a new lineage of serotype 2

Devojit Kumar Sarma[1*†], Lokendra Rathod[1†], Sweta Mishra[1†], Deepanker Das[1], Ankita Agarwal[2], Gaurav Sharma[1], Tanim Arpit Singh[3], Manoj Kumawat[1], Samradhi Singh[1], Vinod Verma[4], Manoj Kumar[1], Swasti Shubham[1], Rajnarayan R. Tiwari[1] and Anil Prakash[1]

[1]ICMR-National Institute for Research in Environmental Health, Bhopal, India, [2]State Virology Laboratory, Department of Microbiology, Gandhi Medical College, Bhopal, India, [3]Maharaja Ranjit Singh College of Professional Sciences, Indore, India, [4]Sanjay Gandhi Postgraduate Institute of Medical Sciences, Lucknow, India

Introduction: Dengue fever is hyperendemic in several Southeast and South Asian countries, including India, with all four serotypes (DENV 1–4) circulating at different periods and in different locations. Sustainable and improved virological and entomological surveillance is the only tool to prevent dengue and other vector-borne diseases.

Objectives: The present study has been carried out to detect and characterize the circulating dengue virus (DENV) in field-collected *Aedes* mosquitoes in Bhopal, Central India.

Methods: *Aedes* mosquitoes were collected from 29 localities within Bhopal city during October 2020 to September 2022. DENV infection was assessed in the individual head and thorax regions of *Aedes* mosquitoes using reverse transcriptase PCR. Positive samples were sequenced, and the circulating serotypes and genotypes were determined using phylogenetic analysis.

Results: DENV RNA was detected in 7 *Aedes aegypti* and 1 *Aedes albopictus*, with infection rates of 0.59 and 0.14%, respectively. Phylogenetic analysis revealed all the isolates belonged to DENV serotype 2 and distinctly clustered with the non-Indian lineage (cosmopolitan genotype 4a), which was not recorded from the study area earlier. The time to most common recent ancestor (TMRCA) of these sequences was 7.4 years old, with the highest posterior density (HPD) of 3.5–12.2 years, indicating that this new lineage emerged during the year 2014. This is the first report on the DENV incrimination in both *Ae. aegypti* and *Ae. albopictus* mosquitoes collected from Bhopal, Central India.

Conclusion: The observed emergence of the non-Indian lineage of DENV-2 in Bhopal, which again is a first report from the area, coincides with the gradual increase in DENV cases in Bhopal since 2014. This study emphasizes the importance of DENV surveillance and risk assessment in this strategically important part of the country to decipher its outbreak and severe disease-causing potential.

KEYWORDS

dengue virus, *Aedes* mosquito, surveillance, epidemiology, India font: Italic, complex script font: Italic considering the growing threat

1. Introduction

Dengue fever is caused by the dengue virus (DENV), a single-stranded positive-sense RNA virus of the *Flaviviridae* family. It is the most recognized arbovirus in the world, transmitted by infected female mosquitoes, especially *Aedes aegypti* and *Ae. albopictus* (Hayes and Gubler, 1992). Dengue infections have increased exponentially in the majority of the tropics and subtropics over the past three decades. Currently, one third of the world's population is susceptible to DENV infection. The WHO estimates that the global burden of dengue infection has increased about 10.3-fold in the last two decades (World Health Organization, 2023). This condition is primarily linked to uncontrolled urbanization, climate change, poor water supply and sewage management, rapid movement of people, animals, and trade via air and sea routes, and unsustainable vector control programmes (Wilder-Smith and Gubler, 2008; Gubler, 2011; Bhatia et al., 2022; Romanello et al., 2022).

Dengue infection is caused by four antigenically different serotypes: DENV-1, DENV-2, DENV-3, and DENV-4 (Gubler, 2002) and the disease manifests itself in a range of ways, from asymptomatic infection and mild febrile illness (dengue fever) to more severe forms including dengue hemorrhagic fever (DHF) and dengue shock syndrome (DSS). The most severe clinical manifestation, dengue shock syndrome (DSS), is characterized by coagulation abnormalities, hemorrhage, plasma leakage, and organ failure (Bhatt et al., 2021). The present dengue case classification, according to World Health Organization, comprises symptomatic patients with and without warning signals, as well as severe dengue (World Health Organization, 2009). Based on the genetic make-up of DENV each serotype has been subdivided into 4–5 genotypes (Weaver and Vasilakis, 2009). Furthermore, depending on their phylogenetic classification, each genotype has a range of lineages (Shrivastava et al., 2015). Infection with one serotype results in lifetime immunity against homologous serotypes, while there is no or limited immunity against infection to heterologous dengue serotypes. This secondary infection, which leads to enhanced dengue severity, is primarily caused by antibody-dependent enhancement (ADE), a mechanism mediated mostly by immunoglobulin G (IgG) (Teo et al., 2023). Additionally, certain lineages and genotypes have been associated with severe forms of dengue fever. These genetic variants with modest variations are also responsible for major outbreaks due to rapid transmission in both humans and mosquitoes (Messer et al., 2003). Hence, regular surveillance is necessary for the control and management of dengue.

Recent anthropogenic and climate-related changes have resulted in accelerated transmission of DENV, causing frequent dengue epidemics (Sarma et al., 2022). Previous studies suggested that several Southeast Asian countries demonstrated dengue hyperendemicity that was 18-fold higher than the Americas (Murray et al., 2013). Currently, almost all Indian states are under constant threat of dengue transmission. A nationwide dengue sero-survey during 2017–2018 showed that nearly half of the Indian population (48.7; 95% CI 43.5–54.0) was sero-positive for DENV (Murhekar et al., 2019). Since 2000, the north Indian states, including New Delhi, Rajasthan, Uttar Pradesh, Madhya Pradesh, Haryana, and Punjab, have reported dengue outbreaks at regular intervals (Mishra et al., 2015). Similarly, the western (Maharashtra), eastern (Odisha), and southern states (Kerala, Andhra Pradesh, and Telangana) also reported massive dengue outbreaks along with chikungunya (Anoop et al., 2010; Cecilia et al., 2011; Shrivastava et al., 2015). In view of this, there is an increasing demand for a safe and effective DENV vaccine that elicits immunity against all the four serotypes. At the moment, at least seven DENV vaccines are at various stages of clinical trials or pre-clinical investigations. Three of these, Dengvaxia® (CYT-TDV), Qdenga® (TAK-003) and TV003 (NIAD/Butantan/Merck) have shown promising results in clinical trials (Torres-Flores et al., 2022; Angelin et al., 2023). Dengvaxia®, manufactured by Sanofi Pasteur, has been licensed in 20 countries and approved for use in individuals aged 6–45 years with laboratory confirmed previous dengue infection and living in endemic countries (Thomas and Yoon, 2019; Torres-Flores et al., 2022). However, shortcomings such as vaccine administration limited to dengue immune individuals only, non-availability in non-endemic countries and safety concerns in vaccine recipients who were dengue non-immune at the time of vaccine administration (Hadinegoro et al., 2015) in the case of Dengvaxia® and less protection against DENV-3 (Rivera et al., 2022), as well as a lack of data for elderly individuals (Angelin et al., 2023) in the case of Qdenga®, have posed significant challenges to the widespread and effective control of dengue fever through vaccination efforts. Until an effective vaccine becomes available, vector control will continue to be the primary approach for managing dengue transmission. Furthermore, systematic molecular monitoring of

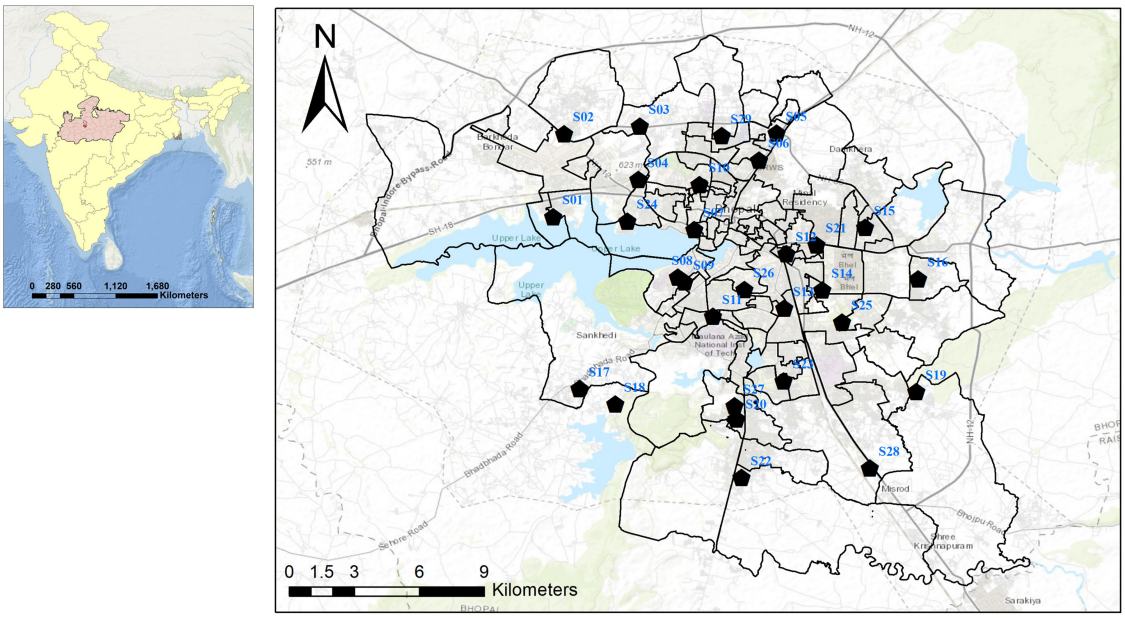

FIGURE 1
Map of Bhopal city showing *Aedes* spp. mosquito collection points.

circulating DENV serotypes in mosquitoes and humans, as well as early detection of any serotype or genotype shift in a geographic area, would aid in the prediction of imminent DENV epidemics and devise targeted public health strategies for dengue control.

This study investigated the phylogenetic relationship of DENV-2 serotypes prevalent in central India (Bhopal, Madhya Pradesh) and reported the emergence of a new lineage (Genotype 4a, cosmopolitan non-Indian lineage) in naturally infected, wild-caught *Ae. aegypti* and *Ae. albopictus* mosquitoes. This study highlights the urgent need of DENV surveillance and clinical characterization of dengue fever in this strategically located part of the country.

2. Materials and methods

2.1. Collection, identification, and pooling of *Aedes* mosquito larvae

The study was conducted in Bhopal, the capital city of Madhya Pradesh in central India. House-frequenting adult *Aedes* mosquitoes were collected from October 2020 to September 2022 during morning and evening hours from 29 different locations in Bhopal (**Figure 1**). Mosquitoes were collected using mechanical aspirators and transported to the laboratory, and then identified to species level using standard taxonomic keys (Tyagi et al., 2015). Each female individual of *Ae. aegypti* and *Ae. albopictus* was bisected into the head, thorax, and abdomen and stored separately in 1.5 mL micro-centrifuge tubes filled with 50 µl of RNAlater^{TM} stabilization solution (Sigma-Aldrich, Cat. # R0901-100ML) at −20°C till further processing. As some of the adult mosquitoes were damaged during transportation, their head and thorax could not be bisected and hence were not processed further. *Aedes* immatures were also collected from the 29 localities in different larval habitats. The collected larvae were transferred to the lab and reared up to the 4th instar. A total of 10 larvae were kept separately in 1.5-ml micro-centrifuge tubes filled with 100 µl of RNAlater^{TM} stabilization solution and stored at −20°C till further processing. The remaining larvae were reared up to adult stage, identified, and stored at 4°C.

2.2. RNA extraction, DENV diagnosis, and sequencing

RNA was extracted from individual mosquito's head-thorax region and from larvae pool (10 larvae/pool) using the Qiagen Viral RNA Mini Kit (Qiagen, cat. # 52906), according to the manufacturer's instructions. DENV infection in the extracted RNA of individual mosquitoes, as well as larval pool was assessed by one-step reverse transcription-PCR (Thermo Fisher Scientific, Cat. # 12594025) targeting the capsid-pre-membrane (*C-prM*) gene region with primers and methods as described (Lanciotti et al., 1992). The 511-bp PCR product of the DENV-positive individuals was gel purified, sequenced in both directions, and used to identify and characterize circulating serotypes and genotypes.

2.3. Phylogenetic analysis

The DENV sequences generated in this study were aligned with representative DENV *C-prM* sequences from India and other countries (**Supplementary Table 1**) using the MUSCLE programme, and a maximum likelihood phylogenetic tree with 1000 bootstrap replicates was reconstructed using the MEGA10 software (Kumar et al., 2018) to identify the serotypes and

TABLE 1 *Aedes* mosquitoes collected, processed and tested positive for DENV in Bhopal city.

Site no.	Site name	*Aedes aegypti*				*Aedes albopictus*			
		Number collected	Number tested for DENV infection	Number found positive for DENV infection	Infection rate (%)	Number collected	Number tested for DENV infection	Number. found positive for DENV infection	Infection rate (%)
S_01	Bairagarh	54	46	0	0.0	2	0	0	0
S_02	Gandhi Nagar	93	87	0	0.0	11	4	0	0
S_03	Sanjiv Nagar	40	19	0	0.0	82	75	0	0
S_04	Lalghati	88	70	1	1.42	13	0	0	0
S_05	Bhanpur	26	14	0	0.0	3	0	0	0
S_06	Gupta Nagar	30	13	0	0.0	15	9	0	0
S_07	Shaid Nagar	43	30	0	0.0	2	0	0	0
S_08	NITTR	28	21	0	0.0	99	88	0	0
S_09	Banganga	38	20	0	0.0	25	24	0	0
S_10	Jamalpura	66	55	1	1.81	4	0	0	0
S_11	Kotra Sultanabad	86	80	1	1.25	157	141	0	0
S_12	Subhash Nagar	81	67	0	0.0	1	0	0	0
S_13	Shankar Nagar	192	181	0	0.0	14	10	0	0
S_14	Anna Nagar	50	38	0	0.0	7	4	0	0
S_15	Nizamuddin Colony	45	38	2	5.26	6	0	0	0
S_16	Awadhpuri	49	41	0	0.0	7	4	0	0
S_17	Neelbad	3	0	0	0.0	31	29	0	0
S_18	NLU	19	12	0	0.0	30	19	0	0
S_19	Katara Hills	18	5	0	0.0	86	76	0	0
S_20	Mahabali Nagar	48	38	0	0.0	7	5	0	0
S_21	BHEL Area	19	15	0	0.0	35	25	0	0
S_22	Priyanka Nagar	33	31	0	0.0	1	0	0	0
S_23	Gulmohar	34	22	0	0.0	11	6	0	0

(Continued)

10.3389/fmicb.2023.1260812

10.3389/fmicb.2023.1260812

TABLE 1 (Continued)

Site no.	Site name	*Aedes aegypti*				*Aedes albopictus*			
		Number collected	Number tested for DENV infection	Number found positive for DENV infection	Infection rate (%)	Number collected	Number tested for DENV infection	Number. found positive for DENV infection	Infection rate (%)
S_24	Khanugaon	26	16	0	0.0	19	13	0	0
S_25	Shakti Nagar	28	16	0	0.0	139	124	1	0.8
S_26	Bheem Nagar	36	25	0	0.0	12	7	0	0
S_27	Kolar Road	97	86	2	2.32	2	0	0	0
S_28	Misroad	27	14	0	0.0	44	36	0	0
S_29	Karond	101	86	0	0.0	8	5	0	0
Total		1498	1186	7	0.59	873	704	1	0.14

genotypes of the DENV isolates. These sequences have been submitted to GenBank with the accession numbers OQ842497-OQ842504. The genetic distance within and between the genotypes was calculated using MEGA10 software. A maximum clade credibility (MCC) tree was used to determine the time to the most recent common ancestor (TMRCA) using DENV-2 genotype 4a and 4b sequences, with sylvatic sequences as the outgroup, using the BEAST 2.5 package (Bouckaert et al., 2019). Based on the lowest BIC (Bayesian Information Criterion) scores, Kimura 2 parameter with discrete gamma distribution (K2 + G) model, assessed through MEGA10 software, was used as the best fit model for Bayesian Markov Chain Monte Carlo (MCMC) analysis. Relaxed uncorrelated lognormal molecular clock model was used and an effective population size of >200 was ensured by running MCMC chains for 4E08 generations with a sampling frequency of 10000 and burn-in of 1000. Tracer v1.7.2, TreeAnnotator v1.10.4 and FigTree v1.4.4 was used to analyze the output and view and annotate the MCC tree.

2.4. Ethical approval

The present study was approved by the Institutional Ethics Committee of the ICMR-National Institute for Research in Environmental Health, Bhopal (NIREH/BPL/IEC/2018-19/3130, dated March 18, 2019).

3. Results

A total of 2,371 adult female *Aedes* mosquitoes (1,498 *Ae. aegypti* and 873 *Ae. albopictus*) were collected. Of these, 1,890 mosquitoes (1,186 *Ae. aegypti* and 704 *Ae. albopictus*) were tested for DENV infection. Similarly, 370 *Aedes* larvae were tested for DENV infection in 37 pools (32 pools for *Ae. aegypti* and 5 pools for *Ae. albopictus*). Based on the RT-PCR amplification of *C-PrM* gene region (**Supplementary Figure 1**), DENV RNA was detected in seven *Ae. aegypti* and one *Ae. albopictus* individuals. Overall DENV infection rates were 0.59 and 0.14% in *Ae. aegypti* and *Ae. albopictus*, respectively. Area wise S_15 (Nizamuddin colony area) recorded the highest DENV infection rate (5.26%), while S_11 (Kotra Sultanabad area) recorded the lowest DENV infection rate (1.25%) for *Ae. aegypti* mosquitoes. *Ae. albopictus* was incriminated only in S_25 (Shakti Nagar) with an infection rate of 0.8% (**Table 1**). No DENV infection was detected in larval pools.

Phylogenetic analysis revealed that all eight DENV *C-prM* sequences were belonged to serotype 2 (**Figure 2**). Analysis of the representative serotype 2 *C-prM* sequences from India and other countries unambiguously clustered these 8 sequences with the non-Indian lineage of DENV-2 (Cosmopolitan genotype 4a) (**Figures 3A, B**). These sequences are substantially divergent from the other genotypes, with nucleotide divergence ranging from 7.4 to 22.2% (**Supplementary Figure 2**). The maximum clade credibility tree indicated a mean TMRCA of 7.4 years (95% HPD: 3.5–12.2) for the sequences in the present study, suggesting that this lineage was introduced in 2014 (95% HPD: 2009.8–2018.5) (**Figure 4**). Other isolates collected in Bhopal in 2016 (GenBank accession nos. MH051272-MH051275) grouped into two distinct clades

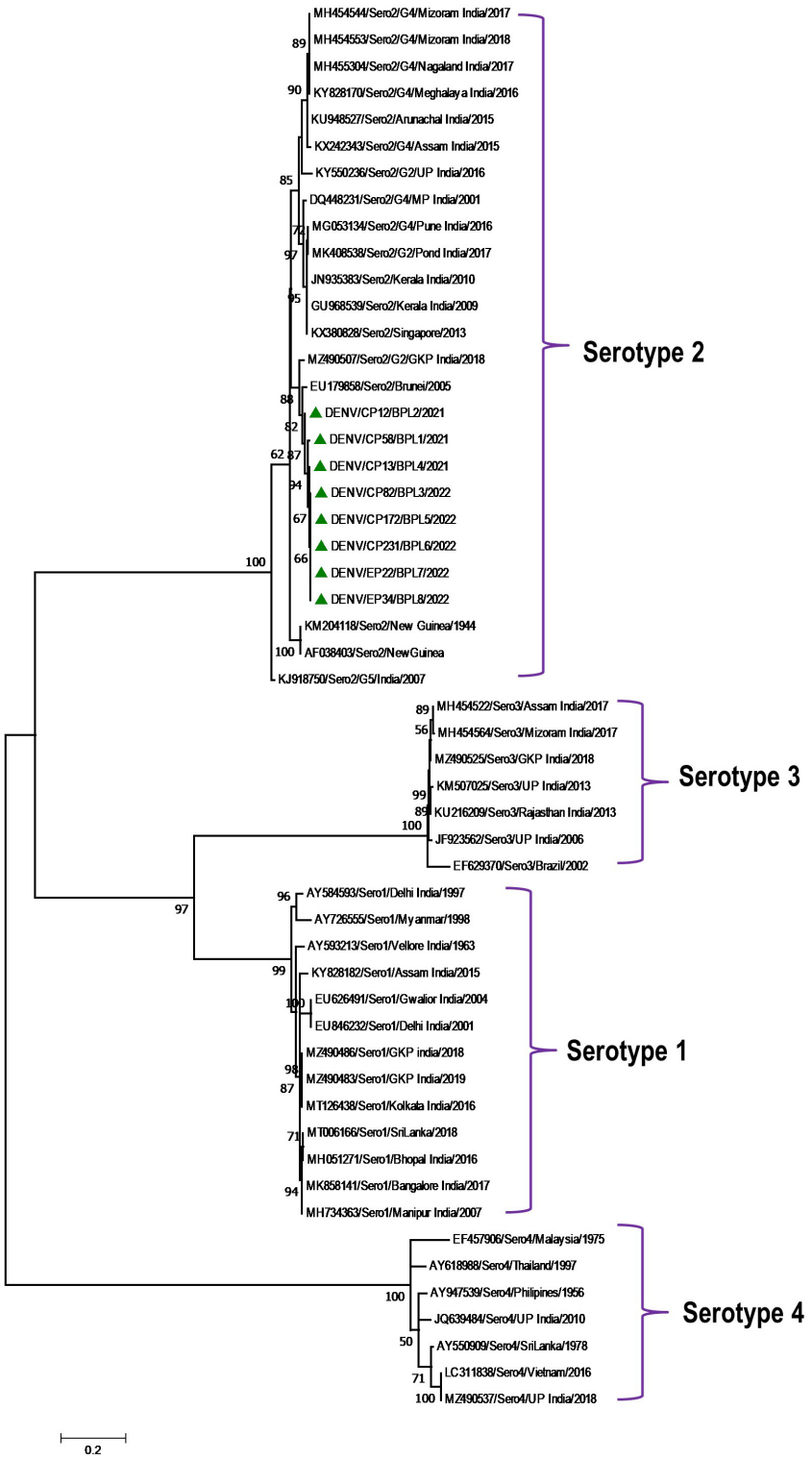

FIGURE 2
Serotype placement and phylogenetic relationship of DENV isolates using C-prM sequences from the present study and other sequences from India and other countries. The sequences with green colored triangle shape indicates sequence generated in this study. Scale bar indicates number of nucleotide substitutions per site.

within the most prevalent cosmopolitan 4b genotype, with identical TMRCA (2014, 95% HPD: 2011–2016), implying that both lineages of the DENV-2 cosmopolitan genotype circulated in Bhopal at the same time. When compared to DENV-2 reference strain KM204118 and other DENV-2 sequences, this lineage showed four significant amino acid alterations, namely E19A, M104I, L108M, and D143N (**Supplementary Table 2**). A statistically significant positive selection was observed in the DENV capsid protein at

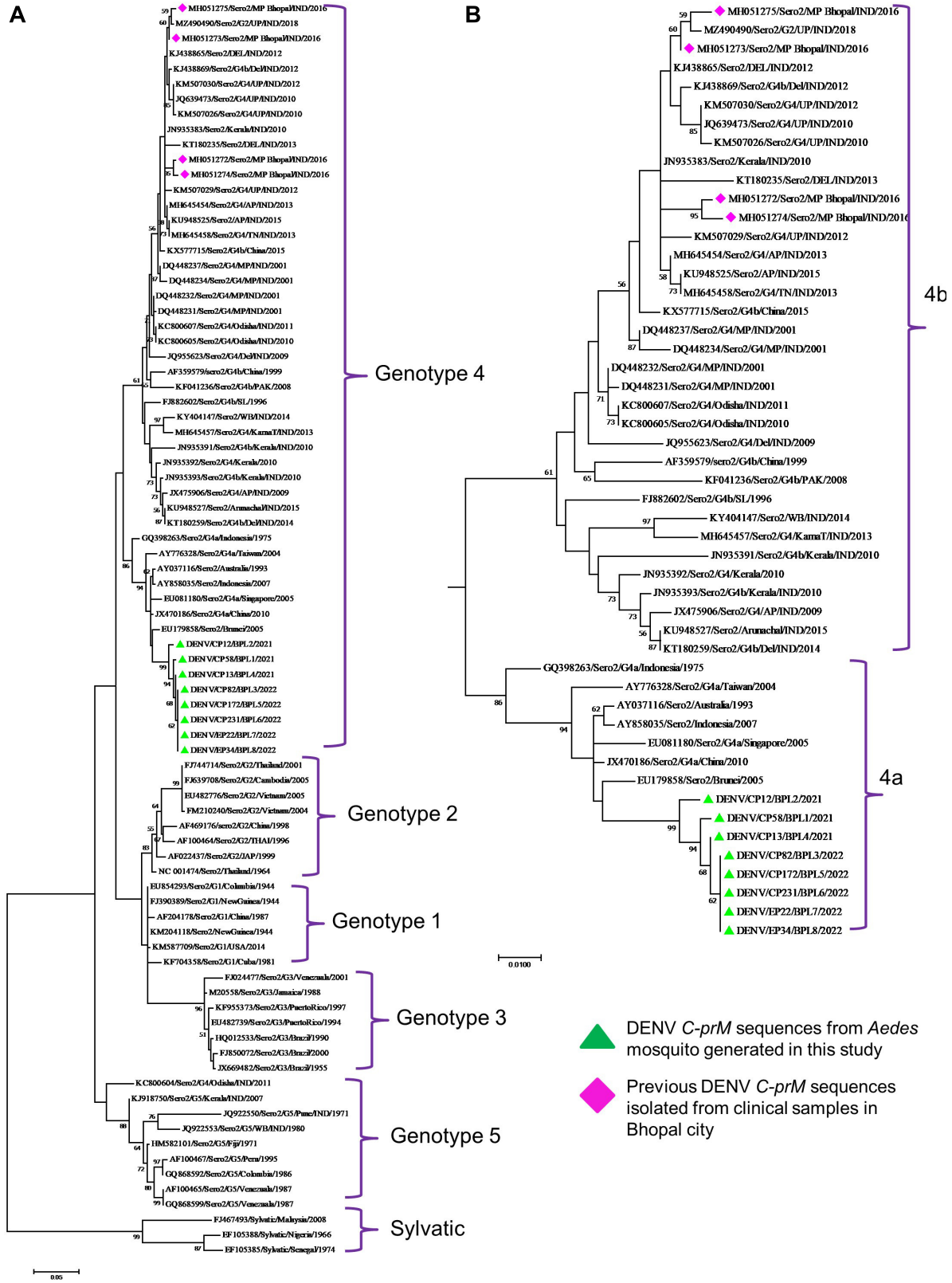

FIGURE 3
(A) Genotypic placement and phylogenetic relationship of DENV-2 isolates using *C-prM* sequences from the present study and from other sequences form India and other countries, **(B)** Phylogenetic tree of DENV-2 corresponding to cosmopolitan genotype (4ab) Sequences. The sequences with green colored triangle shape indicates sequence generated in this study, the sequences with red colored diamond shape indicates previous DENV-2 sequences isolated from clinical samples in Bhopal city. Scale bar indicates number of nucleotide substitutions per site.

TABLE 2 Summary of prevalent DENV serotypes and genotypes detected in *Aedes* mosquitoes across the India.

Location	Vector species	DENV serotype and genotype	Minimum infection rate	Period	References
Malkangiri and Angul (Orissa)	*Aedes aegypti* *Aedes albopictus* *Aedes vittatus*	*Aedes aegypti* DENV–2–Genotype IV *Aedes albopictus* DENV–2–Genotype IV DENV–3–Genotype III	NA	2010–2011	Das et al., 2013
Surat (Gujrat)	*Aedes aegypti*	DENV–3–Genotype III DENV–4–Genotype I	NA	2008–2013	Paingankar et al., 2014
Guwahati (Assam)	*Aedes aegypti* *Aedes albopictus*	*Aedes aegypti* DENV–1–Genotype III	*Aedes aegypti*–1.4	2015–2017	Dutta et al., 2018
Guwahati (Assam) Pasighat (Arunachal Pradesh) Tura (Meghalaya) Dimapur (Nagaland)	*Aedes aegypti* *Aedes albopictus*	*Aedes aegypti* DENV–1 DENV–2 DENV–3 *Aedes albopictus* DENV–1 DENV–2	*Aedes aegypti*–11.95 *Aedes albopictus*–35	2018–2019	Chetry et al., 2020
Lucknow (Uttar Pradesh)	*Aedes aegypti* *Aedes albopictus*	*Aedes aegypti* DENV–1–Genotype III and V DENV–2–Genotype IV DENV–3–Genotype III *Aedes albopictus* DENV–1–Genotype III and V DENV–2–Genotype IV DENV–3–Genotype III	*Aedes aegypti*–5.45 *Aedes albopictus*–5.71	2010–2013	Srivastava et al., 2023
Hyderabad (Telangana)	*Aedes aegypti* *Aedes albopictus*	DENV–1–Genotype III DENV–2–Genotype IV DENV–3–Genotype III DENV–4–Genotype I (Species wise is not available)	DENV–1–16 DENV–2–5.33 DENV–3–8 DENV–4–2.66	2017–2018	Sankoju et al., 2023

amino acid position 19 by different methods (MEME: *p*-value 0.05; FEL: *p*-value 0.09; and FUBER: probability 0.962).

4. Discussion

Dengue is continuing to be the most serious arboviral infection in various Southeast and South Asian nations, including India. This is due to severe environmental changes, rapid urbanization, and increased human long-distance travel, which have resulted in the spread of *Aedes* species in previously unexplored regions (Hussain and Dhiman, 2022). The first virological dengue outbreak in India was reported in 1963 from Kolkata (East India) (Chatterjee et al., 1965). Both *Ae. aegypti* and *Ae. albopictus* have been identified as potential dengue vectors in different parts of the country, with varied incidences of all four known serotypes (**Table 2**). Central India, on the other hand, recorded its first dengue outbreak in 1966 in the Jabalpur district of Madhya Pradesh, with DENV-3 as the causative agent. Subsequently, other districts of Madhya Pradesh, such as Sagar (1966), Sarguja (1997), Gwalior (2002), and Bhopal and Indore (2009), also observed dengue outbreaks with DENV 1, 2, and 3 as causative agents (Sehgal et al., 1967; Mahadev et al., 1997; Parida et al., 2002; Kalpana et al., 2010). According to Mahadev et al. (1997), *Ae. aegypti* was the primary cause of the outbreaks in Madhya Pradesh.

All four serotypes of DENV have been linked to several outbreaks in India in the past (Guo et al., 2017), however, the majority of these outbreaks were associated with DENV-2 (Singh et al., 1999; Dash et al., 2006; Agarwal et al., 2023). The first DHF outbreak caused by DENV-2 occurred in New Delhi in 1996 (Dar et al., 1999). Since 2012, DENV infections in India have steadily increased, with active circulation of the DENV-2 serotype in different regions with varying prevalence (Sankari et al., 2012; Afreen et al., 2016; Murhekar et al., 2019; Alagarasu et al., 2021). However, the prevalence and distribution of DENV-2 in *Aedes* mosquitoes from Bhopal (Central India) remain unknown. The present study reports for the first time the circulation of DENV-2 serotype and its prevalence in both *Ae. aegypti* and *Ae. albopictus* collected from 29 different localities of Bhopal city. It has been observed that most of the DENV incriminated sites were in the South and South-western part of the city (**Figure 1**), which were also known to be the hot-spot area of dengue transmission in Bhopal city (Sarma et al., 2022). This finding further confirms the entomological risk for dengue transmission in these areas.

Dengue virus infection in wild-caught *Aedes* mosquitoes was assessed, and circulating DENV serotypes were characterized by sequence comparison and phylogenetic analysis in Bhopal city during the study. This is crucial because molecular characterization of these viruses aids in the identification of molecular subtypes or genotypes and the introduction of any new lineages. Previously,

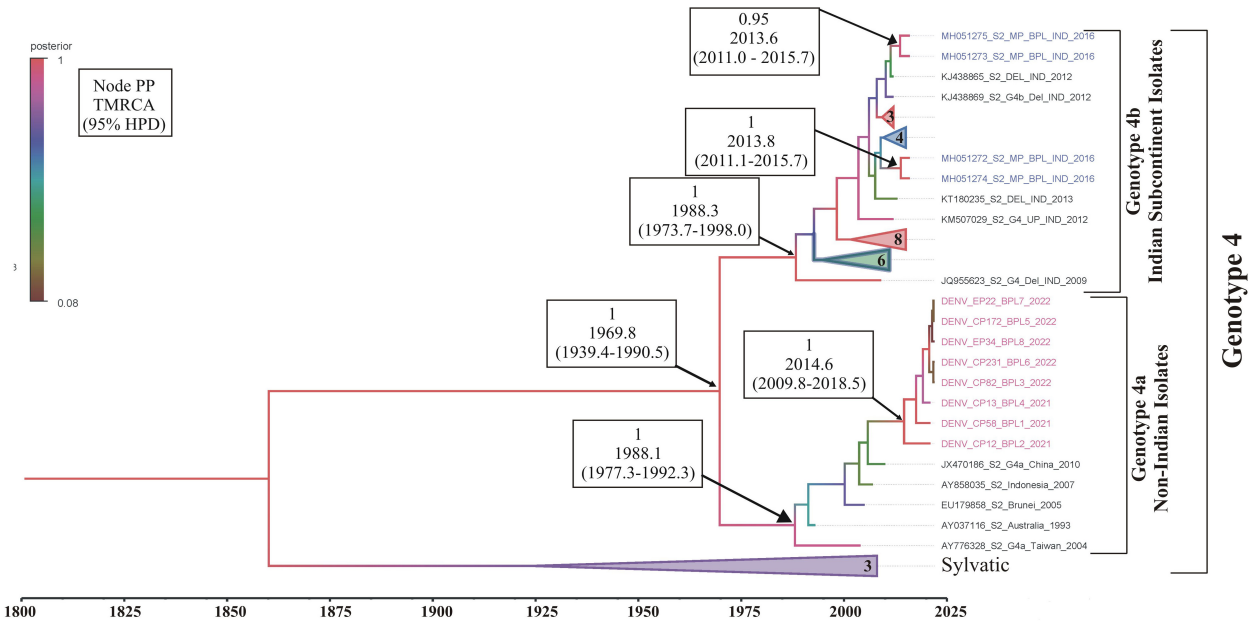

FIGURE 4
Maximum clade credibility (MCC) phylogenetic tree of DENV-2 corresponding to cosmopolitan genotype (4a,b) generated by Bayesian inference method in BEAST calculated using *C-prM* gene sequences. Sequences in pink represents DENV-2 sequences generated in this study, while sequences in blue are the previous sequences generated from the same study area (Bhopal). All horizontal branch lengths are drawn to a scale of years. PP, posterior probability; TMRCA, the mean estimated time to the most recent common ancestor; 95% HPD, 95% highest posterior density interval.

various regions of the dengue genome have been used for molecular phylogenetic analysis, but many studies have reported the *C-prM* gene as a tool in dengue virus genotyping (Murugesan et al., 2020; Titir et al., 2021). We retrieved previously reported *C-prM* gene sequences from the NCBI GenBank database for phylogenetic analysis.

It is evident that cosmopolitan genotypes of the DENV-2 virus are circulating across India (**Table 1**). However, when analyzing the phylogenetic relationship of DENV sequences generated in this study alongside other global sequences, it became evident that they clustered with non-Indian isolates, indicating the establishment of a novel lineage, lineage 4a, of DENV serotype 2 (**Figure 3**) in *Aedes* mosquitoes collected from Central India (Bhopal, Madhya Pradesh). Additionally, the MCC tree indicated that this lineage (4a) was introduced in Bhopal around 2013–2014. Previously, the introduction of a new genotype or lineage was proposed as the root cause of the transmission of a severe strain of dengue sickness in other parts of the world, such as the Americas (Rico-Hesse et al., 1997; Messer et al., 2003). It is pertinent to note that Bhopal experienced severe outbreaks of DENV in 2014 and 2016 (Agarwal et al., 2019), and since then the number of dengue cases has been increasing steadily in Bhopal (Sarma et al., 2022). This might be possible because lineages' extinction and inevitable incursion were connected to a virus's transmission bottleneck. For example, in Thailand, increased viral transmission by a mosquito vector was also recently connected to lineage replacement (Lambrechts et al., 2012). Similarly, Shrivastava et al. (2015) also reported the new lineage of DENV-3 (genotype 4) in eastern India, which was implicated in the dengue outbreak during the year 2011. However, in view of the scarcity of molecular data on the circulating serotypes/genotypes during that time, pinpointing the lineage that possibly triggered those outbreaks is difficult. The MCC tree shows both the lineages (4a and 4b of the cosmopolitan genotype) were circulating in Bhopal, perhaps with different degrees of dominance. The same has been evidenced by a recent hospital based study in the same area, where out of total 154 RT-PCR positive dengue cases, majority (66 nos.) of them belonged to DENV-2 serotype and of these 66 DENV isolates, 13 were sequenced of which 12 were found to belonged to genotype 4a during 2019 and 2021. It was also observed that the new lineage of DENV-2 was also associated with a longer duration of hospitalization ($>10 \pm 3$ days) and hemorrhagic manifestations indicating its role in severity if disease in the studied area (Agarwal et al., 2023). Higher evolutionary and increased transmission rates of one DENV genotype may outnumber the others in the community, resulting in a lineage shift. This shift may be due to several factors, including changes in the mosquito vector population, host immunity, environmental conditions, and international travel (Shrivastava et al., 2015). Bhopal, a central Indian city, is a favorite destination for international tourists and received 316,195 international travelers during 2014 (India Tourism Statistics, 2014). Although most of the incident dengue cases are of local origin, there are some immigrated cases also, which, along with the international travelers, might facilitates the introduction of this new lineage to the study area.

Aedes mosquitoes have the ability to transmit the virus to their offspring, which is identified as vertical transmission. This phenomenon is important to understand as it may contribute to the existence of viruses in the environment in the absence of susceptible hosts. This phenomenon may also be linked to disease endemism, implying that vertical transmission plays an important role in the

establishment of endemicity (Hull et al., 1984). The presence and significance of this transmission in *Aedes* have been reported in previous studies from different regions of the world (Martins et al., 2012; Buckner et al., 2013; Wijesinghe et al., 2021). Within India, natural vertical transmission of DENV was observed in dengue hyper-endemic areas such as Rajasthan (Angel and Joshi, 2008; Bina et al., 2008), Tamil Nadu (Arunachalam et al., 2008), New Delhi (Bina et al., 2008), and Kerala (Thenmozhi et al., 2007). Although no DENV infection was observed in the larvae of *Ae. aegypti* and *Ae. albopictus* in the present study, which may be due to low to mid endemicity of the disease in the studied area and low number of larvae processed, the presence of natural vertical transmission of DENV in the studied area couldn't be ruled out. More molecular surveillance with large numbers larvae is required to confirm the natural vertical transmission of DENV in field collected *Aedes* mosquitoes in this part of India.

5. Conclusion

The present study, for the first time, confirms the prevalence of DENV serotype 2 (genotype 4) in field collected *Aedes* mosquitoes from Bhopal city, Central India. The phylogenetic placement of the DENV sequences with non-Indian lineages indicates the circulation of a new lineage (4a) of cosmopolitan genotype. This lineage transition of DENV-2 is a major cause of concern and requires routine surveillance of viral circulation throughout endemic and non-endemic areas for a better understanding of transmission dynamics and effective control and management of the dengue burden in this central part of India.

Data availability statement

The datasets presented in this study can be found in online repositories. The names of the repository/repositories and accession number(s) can be found in the article/**Supplementary material**.

Author contributions

DS: Conceptualization, Formal Analysis, Funding acquisition, Investigation, Methodology, Project administration, Supervision, Writing—original draft. LR: Data curation, Formal Analysis, Investigation, Methodology, Writing—review and editing. SM: Data curation, Formal Analysis, Investigation, Methodology, Writing—review and editing. DD: Investigation, Methodology, Visualization, Writing—review and editing. AA: Formal Analysis, Investigation, Methodology, Visualization, Writing—review and editing. GS: Formal Analysis, Methodology, Writing—original draft. TS: Formal Analysis, Methodology, Writing—review and editing. MKw: Visualization, Writing—review and editing. SaS: Investigation, Writing—review and editing. VV: Visualization, Writing—review and editing. MK: Investigation, Methodology, Writing—review and editing. SwS: Visualization, Writing—review and editing. RT: Supervision, Writing—review and editing. AP: Conceptualization, Methodology, Supervision, Writing—review and editing.

Funding

The authors declare financial support was received for the research, authorship, and/or publication of this article. This study was funded by Indian Council of Medical Council, New Delhi (https://main.icmr.nic.in/) to DS [award number 6/9-7 (208)/2019-ECD-II].

Acknowledgments

We sincerely thank the District Malaria Officer, Bhopal district and Dr. N. Banerjee for their encouragement to carry out this study. We are grateful to Mr. Kamlesh Mewada and Mr. Mahendra Damle for their assistance in mosquito collection. We also thank Dr. P. K. Mishra, Scientist-F and Head, Molecular Biology Division, ICMR-National Institute for Research in Environmental Health, Bhopal for his critical reviews and suggestion which helped to improve the manuscript substantially.

Conflict of interest

The authors declare that the research was conducted in the absence of any commercial or financial relationships that could be construed as a potential conflict of interest.

The authors declared that they were an editorial board member of Frontiers, at the time of submission. This had no impact on the peer review process and the final decision.

Publisher's note

Supplementary material

The Supplementary Material for this article can be found online at: https://www.frontiersin.org/articles/10.3389/fmicb.2023.1260812/full#supplementary-material

References

Afreen, N., Naqvi, I. H., Broor, S., Ahmed, A., Kazim, S. N., Dohare, R., et al. (2016). Evolutionary analysis of dengue serotype 2 viruses using phylogenetic and Bayesian methods from New Delhi, India. *PLoS Negl. Trop. Dis.* 10:e0004511. doi: 10.1371/journal.pntd.0004511

Agarwal, A., Ganvir, R., Kale, D., Chaurasia, D., and Kapoor, G. (2023). Continued dominance of dengue virus serotype 2 during the recent Central India outbreaks (2019-2021) with evidence of genetic divergence. *Pathog. Glob. Health* doi: 10.1080/20477724.2023.2246712 [Epub ahead of print].

Agarwal, A., Gupta, S., Chincholkar, T., Singh, V., Umare, I. K., Ansari, K., et al. (2019). Co-circulation of dengue virus serotypes in Central India: Evidence of prolonged viremia in DENV-2. *Infect. Genet. Evol.* 70, 72–79. doi: 10.1016/j.meegid.2019.02.024

Alagarasu, K., Patil, J. A., Kakade, M. B., More, A. M., Yogesh, B., Newase, P., et al. (2021). Serotype and genotype diversity of dengue viruses circulating in India: a multi-centre retrospective study involving the Virus Research Diagnostic Laboratory Network in 2018. *Int. J. Infect. Dis.* 111, 242–252. doi: 10.1016/j.ijid.2021.08.045

Angel, B., and Joshi, V. (2008). Distribution and seasonality of vertically transmitted dengue viruses in Aedes mosquitoes in arid and semi-arid areas of Rajasthan, India. *J. Vector Borne Dis.* 45:56.

Angelin, M., Sjölin, J., Kahn, F., Hedberg, A. L., Rosdahl, A., Skorup, P., et al. (2023). Qdenga® -A promising dengue fever vaccine; can it be recommended to non-immune travelers? *Travel Med. Infect. Dis.* 2023:102598. doi: 10.1016/j.tmaid.2023.102598

Anoop, M., Issac, A., Mathew, T., Philip, S., Kareem, N. A., Unnikrishnan, R., et al. (2010). Genetic characterization of dengue virus serotypes causing concurrent infection in an outbreak in Ernakulam, Kerala, South India. *Indian J. Exp. Biol.* 48, 849–857.

Arunachalam, N., Tewari, S. C., Thenmozhi, V., Rajendran, R., Paramasivan, R., Manavalan, R., et al. (2008). Natural vertical transmission of dengue viruses by Aedes aegypti in Chennai, Tamil Nadu, India. *Indian J. Med. Res.* 127, 395–407.

Bhatia, S., Bansal, D., Patil, S., Pandya, S., Ilyas, Q. M., and Imran, S. (2022). A Retrospective Study of Climate Change Affecting Dengue: Evidences, Challenges and Future Directions. *Front. Public Health* 10:884645. doi: 10.3389/fpubh.2022.884645

Bhatt, P., Sabeena, S. P., Varma, M., and Arunkumar, G. (2021). Current understanding of the pathogenesis of dengue virus infection. *Curr. Microbiol* 78, 17–32. doi: 10.1007/s00284-020-02284-w

Bina, P. D., Katyal, R., Abhay, S., Raina, V. K., Saxena, V. K., and Lal, S. (2008). Natural vertical transmission of dengue virus in peak summer collections of Aedes aegypti (Diptera: Culicidae) from urban areas of Jaipur (Rajasthan) and Delhi. *J. Commun. Dis.* 40, 155–157.

Bouckaert, R., Vaughan, T. G., Barido-Sottani, J., Duchêne, S., Fourment, M., Gavryushkina, A., et al. (2019). BEAST 2.5: An advanced software platform for Bayesian evolutionary analysis. *PLoS Comput. Biol.* 15:e1006650. doi: 10.1371/journal.pcbi.1006650

Buckner, E. A., Alto, B. W., and Lounibos, L. P. (2013). Vertical transmission of Key West dengue-1 virus by *Aedes aegypti* and *Aedes albopictus* (Diptera: Culicidae) mosquitoes from Florida. *J. Med. Entomol.* 50, 1291–1297. doi: 10.1603/me13047

Cecilia, D., Kakade, M. B., Bhagat, A. B., Vallentyne, J., Singh, A., Patil, J. A., et al. (2011). Detection of dengue-4 virus in Pune, Western India after an absence of 30 years-its association with two severe cases. *Virol. J.* 8, 1–4. doi: 10.1186/1743-422X-8-46

Chatterjee, S. N., Chakravarti, S. K., Mitra, A. C., and Sarkar, J. K. (1965). Virological investigation of cases with neurological complications during the outbreak of haemorrhagic fever in Calcutta. *J. Indian Med. Assoc.* 45, 314–316.

Chetry, S., Patgiri, S. J., Bhattacharyya, D. R., Dutta, P., and Kumar, N. P. (2020). Incrimination of *Aedes aegypti* and *Aedes albopictus* as vectors of dengue virus serotypes 1, 2 and 3 from four states of Northeast India. *Access Microbiol.* 2:101.

Dar, L., Broor, S., Sengupta, S., Xess, I., and Seth, P. (1999). The first major outbreak of dengue hemorrhagic fever in Delhi, India. *Emerg. Infect. Dis.* 5:589. doi: 10.3201/eid0504.990427

Das, B., Das, M., Dwibedi, B., Kar, S. K., and Hazra, R. K. (2013). Molecular investigations of dengue virus during outbreaks in Orissa state, Eastern India from 2010 to 2011. *Infect. Genet. Evol.* 16, 401–410. doi: 10.1016/j.meegid.2013.03.016

Dash, P. K., Parida, M. M., Saxena, P., Abhyankar, A., Singh, C. P., Tewari, K. N., et al. (2006). Reemergence of dengue virus type-3 (subtype-III) in India: implications for increased incidence of DHF & DSS. *Virol. J.* 3, 1–10. doi: 10.1186/1743-422X-3-55

Dutta, P., Khan, S. A., Chetry, S., and Abdul, M. (2018). Incrimination of *Aedes aegypti* for dengue virus serotype-1 in Assam, Northeast India. *J. Vector Borne Dis.* 55, 330–333. doi: 10.4103/0972-9062.256572

Gubler, D. J. (2002). The global emergence/resurgence of arboviral diseases as public health problems. *Arch. Med. Res.* 33, 330–342. doi: 10.1016/s0188-4409(02)00378-8

Gubler, D. J. (2011). Dengue, urbanization and globalization: the unholy trinity of the 21st century. *Trop. Med. Health* 39, S3–S11. doi: 10.2149/tmh.2011-S05

Guo, C., Zhou, Z., Wen, Z., Liu, Y., Zeng, C., Xiao, D., et al. (2017). Global epidemiology of dengue outbreaks in 1990–2015: a systematic review and meta-analysis. *Front. Cell. Infect.* 7:317. doi: 10.3389/fcimb.2017.00317

Hadinegoro, S. R., Arredondo-García, J. L., Capeding, M. R., Deseda, C., Chotpitayasunondh, T., Dietze, R., et al. (2015). Efficacy and long-term safety of a dengue vaccine in regions of endemic disease. *N. Eng. J. Med.* 373, 1195–1206. doi: 10.1056/NEJMoa1506223

Hayes, E. B., and Gubler, D. J. (1992). Dengue and dengue hemorrhagic fever. *Pediatr. Infect Dis. J.* 11, 311–317. doi: 10.1097/00006454-199204000-00010

Hull, B., Tikasingh, E., de Souza, M., and Martinez, R. (1984). Natural transovarial transmission of dengue 4 virus in Aedes aegypti in Trinidad. *Am. J. Trop. Med. Hyg.* 33, 1248–1250. doi: 10.4269/ajtmh.1984.33.1248

Hussain, S. S. A., and Dhiman, R. C. (2022). Distribution expansion of dengue vectors and climate change in India. *Geohealth* 6:e2021GH000477. doi: 10.1029/2021GH000477

India Tourism Statistics (2014). *Ministry of Tourism, Government of India*. Lucknow: India Tourism Statistics.

Kalpana, B., Kumar, S. P., Mohalia, M. M., and Dhariwal, A. C. (2010). A study on dengue outbreak during 2009 in Bhopal and Indore districts of Madhya Pradesh, India. *J. Commun. Dis.* 42, 273–279.

Kumar, S., Stecher, G., Li, M., Knyaz, C., and Tamura, K. (2018). MEGA X: molecular evolutionary genetics analysis across computing platforms. *Mol. Biol. Evol.* 35:1547. doi: 10.1093/molbev/msy096

Lambrechts, L., Fansiri, T., Pongsiri, A., Thaisomboonsuk, B., Klungthong, C., Richardson, J. H., et al. (2012). Dengue-1 virus clade replacement in Thailand associated with enhanced mosquito transmission. *Virol. J.* 86, 1853–1861. doi: 10.1128/jvi.06458-11

Lanciotti, R. S., Calisher, C. H., Gubler, D. J., Chang, G. J., and Vorndam, A. V. (1992). Rapid detection and typing of dengue viruses from clinical samples by using reverse transcriptase-polymerase chain reaction. *J. Clin. Microbiol.* 30, 545–551. doi: 10.1128/jcm.30.3.545-551.1992

Mahadev, P. V., Prasad, S. R., Ilkal, M. A., Mavale, M. S., Bedekar, S. S., and Banerjee, K. (1997). Activity of dengue-2 virus and prevalence of *Aedes aegypti* in the Chirimiri colliery area, Madhya Pradesh, India. *Southeast Asian J. Trop. Med. Public Health* 28, 126–137.

Martins, V. E. P., Alencar, C. H., Kamimura, M. T., de Carvalho Araujo, F. M., De Simone, S. G., Dutra, R. F., et al. (2012). Occurrence of natural vertical transmission of dengue-2 and dengue-3 viruses in *Aedes aegypti* and *Aedes albopictus* in Fortaleza. Ceará, Brazil. *PLoS One* 7:e41386. doi: 10.1371/journal.pone.0041386

Messer, W. B., Gubler, D. J., Harris, E., Sivananthan, K., and De Silva, A. M. (2003). Emergence and global spread of a dengue serotype 3, subtype III virus. *Emerg. Infect. Dis.* 9:800. doi: 10.3201/eid0907.030038

Mishra, G., Jain, A., Prakash, O., Prakash, S., Kumar, R., Garg, R. K., et al. (2015). Molecular characterization of dengue viruses circulating during 2009–2012 in Uttar Pradesh, India. *J. Med. Virol.* 87, 68–75. doi: 10.1002/jmv.23981

Murhekar, M. V., Kamaraj, P., Kumar, M. S., Khan, S. A., Allam, R. R., Barde, P., et al. (2019). Burden of dengue infection in India, 2017: a cross-sectional population based serosurvey. *Lancet Glob. Health.* 7, 1065–1073. doi: 10.1016/S2214-109X(19)30250-5

Murray, N. E. A., Quam, M. B., and Wilder-Smith, A. (2013). Epidemiology of dengue: past, present and future prospects. *Clin. Epidemiol.* 5, 299–309. doi: 10.2147/CLEP.S34440

Murugesan, A., Aridoss, D., Senthilkumar, S., Sivathanu, L., Sekar, R., Shankar, E. M., et al. (2020). Molecular Diversity of Dengue Virus Serotypes 1–4 during an Outbreak of Acute Dengue Virus Infection in Theni, India. *Indian J. Med. Microbiol.* 38, 401–408. doi: 10.4103/ijmm.IJMM_20_89

Paingankar, M. S., Gokhale, M. D., Vaishnav, K. G., and Shah, P. S. (2014). Monitoring of dengue and chikungunya viruses in field-caught *Aedes aegypti* (Diptera: Culicidae) in Surat city, India. *Curr. Sci.* 106, 1559–1567.

Parida, M. M., Dash, P. K., Upadhyay, C., Saxena, P. J. A., and Jana, A. M. (2002). Serological & virological investigation of an outbreak of. *Indian J. Med. Res.* 116, 248–254.

Rico-Hesse, R., Harrison, L. M., Salas, R. A., Tovar, D., Nisalak, A., and Ramos, C. (1997). Origins of dengue type 2 viruses associated with increased pathogenicity in the Americas. *Virology* 230, 244–251. doi: 10.1006/viro.1997.8504

Rivera, L., Biswal, S., Sáez-Llorens, X., Reynales, H., López-Medina, E., Borja-Tabora, C., et al. (2022). Three-year efficacy and safety of Takeda's dengue vaccine candidate (TAK-003). *Clin. Infect. Dis.* 75, 107–117. doi: 10.1093/cid/ciab864

Romanello, M., Di Napoli, C., Drummond, P., Green, C., Kennard, H., Lampard, P., et al. (2022). The 2022 report of the Lancet Countdown on health and climate change: health at the mercy of fossil fuels. *Lancet* 400, 1619–1654. doi: 10.1016/S0140-6736(22)01540-9

Sankari, T., Hoti, S. L., Singh, T. B., and Shanmugavel, J. (2012). Outbreak of dengue virus serotype-2 (DENV-2) of Cambodian origin in Manipur. India-Association with meteorological factors. *Indian J. Med. Res.* 136:649.

Sankoju, P., Ravinuthala, V. S. U., Mopuri, R., Mutheneni, S. R., and Addlagatta, A. (2023). Genomic characterization and evolutionary analysis of dengue virus from *Aedes* mosquitoes in Telangana, India. *J. Vector Borne Dis.* 60, 179–186. doi: 10.4103/0972-9062.364766

Sarma, D. K., Kumar, M., Balabaskaran Nina, P., Balasubramani, K., Pramanik, M., Kutum, R., et al. (2022). An assessment of remotely sensed environmental variables on Dengue epidemiology in Central India. *PLoS Negl. Trop. Dis.* 16:e0010859. doi: 10.1371/journal.pntd.0010859

Sehgal, P. N., Kalra, N. L., Pattanayak, S., Wattal, B. L., and Shrivastav, J. B. (1967). A study of an outbreak of dengue epidemic in Jabalpur, Madhya Pradesh. *Bull. Indian Soc. Malaria Other Commun. Dis.* 4, 91–108.

Shrivastava, A., Soni, M., Shrivastava, S., Sharma, S., Dash, P. K., Gopalan, N., et al. (2015). Lineage shift of dengue virus in Eastern India: an increased implication for DHF/DSS. *Epidemiol. Infect.* 143, 599–1605.

Singh, U. B., Maitra, A., Broor, S., Rai, A., Pasha, S. T., and Seth, P. (1999). Partial nucleotide sequencing and molecular evolution of epidemic causing dengue 2 strains. *J. Infect. Dis.* 180, 959–965. doi: 10.1086/315043

Srivastava, N. N., Maan, H. S., Dhole, T. N., Singh, J., Sharma, S., Pandey, S. N., et al. (2023). Dengue Virus Serotypes Circulating among *Aedes* Mosquitoes in the Lucknow District of North India: Molecular Identification and Characterization. *J. Pure Appl. Microbiol.* 17, 1141–1153.

Teo, A., Tan, H. D., Loy, T., Chia, P. Y., and Chua, C. L. L. (2023). Understanding antibody-dependent enhancement in dengue: Are afucosylated IgG1s a concern? *PLoS Pathog.* 19:e1011223. doi: 10.1371/journal.ppat.1011223

Thenmozhi, V., Hiriyan, J. G., Tewari, S. C., Samuel, P. P., Paramasivan, R., Rajendran, R., et al. (2007). Natural vertical transmission of dengue virus in Aedes albopictus (Diptera: Culicidae) in Kerala, a southern Indian state. *Jpn. J. Infect. Dis.* 60:245.

Thomas, S. J., and Yoon, I. K. (2019). A review of Dengvaxia®: development to deployment. *Hum. Vaccines Immunother.* 15, 2295–2314. doi: 10.1080/21645515.2019.1658503

Titir, S. R., Paul, S. K., Ahmed, S., Haque, N., Nasreen, S. A., Hossain, K. S., et al. (2021). Nationwide distribution of dengue virus type 3 (Denv-3) genotype I and emergence of denv-3 genotype III during the 2019 outbreak in Bangladesh. *Trop. Med. Infect. Dis.* 6:58. doi: 10.3390/tropicalmed6020058

Torres-Flores, J. M., Reyes-Sandoval, A., and Salazar, M. I. (2022). Dengue vaccines: An update. *BioDrugs* 36, 325–336. doi: 10.1007/s40259-022-00531-z

Tyagi, B. K., Munirathinam, A., and Venkatesh, A. (2015). A catalogue of Indian mosquitoes. *Int. J. Mosq. Res.* 2, 50–97.

Weaver, S. C., and Vasilakis, N. (2009). Molecular evolution of dengue viruses: contributions of phylogenetics to understanding the history and epidemiology of the preeminent arboviral disease. *Infect. Genet. Evol.* 9, 523–540.

Wijesinghe, C., Gunatilake, J., Kusumawathie, P. H. D., Sirisena, P. D. N. N., Daulagala, S. W. P. L., and Iqbal, B. N. (2021). Circulating dengue virus serotypes and vertical transmission in *Aedes* larvae during outbreak and inter-outbreak seasons in a high dengue risk area of Sri Lanka. *Parasit. Vectors.* 14, 1–11. doi: 10.1186/s13071-021-05114-5

Wilder-Smith, A., and Gubler, D. J. (2008). Geographic expansion of dengue: the impact of international travel. *Med. Clin. North Am.* 92, 1377–1390. doi: 10.1016/j.mcna.2008.07.002

World Health Organization (2009). *Special Programme for Research, Training in Tropical Diseases, World Health Organization. Dengue: guidelines for diagnosis, treatment, prevention and control*. Geneva: World Health Organization.

World Health Organization (2023). *Dengue and severe dengue*. Geneva: World Health Organization.

frontiers | Frontiers in Microbiology

TYPE Original Research
PUBLISHED 15 September 2023
DOI 10.3389/fmicb.2023.1201640

OPEN ACCESS

EDITED BY
James Weger-Lucarelli,
Virginia Tech, United States

REVIEWED BY
Ping Zhao,
Second Military Medical University, China
Alberto Anastacio Amarilla Ortiz,
The University of Queensland, Australia

*CORRESPONDENCE
Andres Merits
✉ andres.merits@ut.ee
Delphine Muriaux
✉ delphine.muriaux@irim.cnrs.fr

†These authors have contributed equally to this work and share first authorship

‡These authors share senior authorship

RECEIVED 06 April 2023
ACCEPTED 17 August 2023
PUBLISHED 15 September 2023

CITATION
Cherkashchenko L, Gros N, Trausch A, Neyret A, Hénaut M, Dubois G, Villeneuve M, Chable-Bessia C, Lyonnais S, Merits A and Muriaux D (2023) Validation of flavivirus infectious clones carrying fluorescent markers for antiviral drug screening and replication studies.
Front. Microbiol. 14:1201640.
doi: 10.3389/fmicb.2023.1201640

Validation of flavivirus infectious clones carrying fluorescent markers for antiviral drug screening and replication studies

Liubov Cherkashchenko[1,2†], Nathalie Gros[1†], Alice Trausch[1†], Aymeric Neyret[1], Mathilde Hénaut[1], Gregor Dubois[1], Matthieu Villeneuve[1], Christine Chable-Bessia[1], Sébastien Lyonnais[1], Andres Merits[2*‡] and Delphine Muriaux[1,3*‡]

[1]CEMIPAI UAR3725 CNRS, University of Montpellier, Montpellier, France, [2]Institute of Technology, University of Tartu, Tartu, Estonia, [3]IRIM UMR9004 CNRS, University of Montpellier, Montpellier, France

Flaviviruses have emerged as major arthropod-transmitted pathogens and represent an increasing public health problem worldwide. High-throughput screening can be facilitated using viruses that easily express detectable marker proteins. Therefore, developing molecular tools, such as reporter-carrying versions of flaviviruses, for studying viral replication and screening antiviral compounds represents a top priority. However, the engineering of flaviviruses carrying either fluorescent or luminescent reporters remains challenging due to the genetic instability caused by marker insertion; therefore, new approaches to overcome these limitations are needed. Here, we describe reverse genetic methods that include the design and validation of infectious clones of Zika, Kunjin, and Dengue viruses harboring different reporter genes for infection, rescue, imaging, and morphology using super-resolution microscopy. It was observed that different flavivirus constructs with identical designs displayed strikingly different genetic stabilities, and corresponding virions resembled wild-type virus particles in shape and size. A successful strategy was assessed to increase the stability of rescued reporter virus and permit antiviral drug screening based on quantitative automated fluorescence microscopy and replication studies.

KEYWORDS

flaviviruses, infectious clone, Zika virus, dengue virus, Kunjin virus, fluorescent marker and reporter genes, reverse genetics

Introduction

The Flaviviridae family includes four genera: *Flavivirus*, *Pestivirus*, *Pegivirus*, and *Hepacivirus*.[1] The genus *Flavivirus* includes several arthropod-borne viruses that usually infect insects but some can be responsible for a significant number of human diseases primarily caused by dengue virus (DENV), Zika virus (ZIKV), West Nile virus (WNV), yellow fever virus (YFV), Japanese encephalitis virus (JEV), and tick-borne encephalitis virus (TBEV). In the majority of

1 https://ictv.global/taxonomy

the cases, transmission occurs horizontally between mosquitoes (often *Aedes* or *Culex*) or ticks and vertebrate hosts, whereas mammalians often serve as reservoirs and thus contribute to the adaptation of viruses (Weaver and Barrett, 2004; Pierson and Diamond, 2020). In this study, we focused on investigating three members of the genus *Flavivirus*: DENV (serotypes 2 and 4); ZIKV; and Kunjin virus (KUNV), an Australian subtype of WNV.

The flavivirus genome is a positive-strand RNA of approximately 11,000 bases containing a single open reading frame (ORF) that is flanked by two untranslated regions (UTRs) located at the 5′ and 3′ ends of the virus genome. The genome has a cap structure located at the 5′ end but lacks the 3′ poly(A) tail. The absence of poly(A) is compensated for by the interaction of the 3'UTR with poly(A)-binding protein (PABP). The *Flavivirus* ORF encodes for a polyprotein precursor of viral proteins that is cleaved by viral and host proteases into three structural proteins [C (capsid), prM(M) (membrane), and E (envelope)] and seven non-structural (NS) proteins (NS1, NS2A, NS2B, NS3, NS4A, NS4B, and NS5). The NS proteins play multiple roles in the infection cycle, including in viral RNA replication, the assembly of viral particles, and the evasion of the host immune response. The structural proteins are involved in the formation and release of viral particles (Mazeaud et al., 2018; Choi, 2021).

The spectrum of clinical manifestations of flavivirus infection ranges from mild (asymptomatic) illness to severe disease (Pan et al., 2022). Such a divergence is mostly caused by the different tropisms of viruses or/and their ability to counteract the host immune response. There are approximately 400 million flavivirus infections every year, a large majority of which are caused by four genotypes of DENV (DENV1-4), making it one of the most medically important causative agents of human diseases (Guabiraba and Ryffel, 2014). The clinical presentation of DENV infection includes the development of dengue fever and other more severe diseases—dengue hemorrhagic fever and dengue shock syndrome (Gould and Solomon, 2008; Khanam et al., 2022). By contrast to DENV, symptomatic infection by ZIKV is mostly associated with mild symptoms, such as headache, joint pain, or cutaneous rash. In some cases, ZIKV infection in women during pregnancy can be considered as one of the causative agents of microcephaly in newborns and has been associated with progression into Guillain–Barré syndrome (Wen et al., 2017; Barbi et al., 2018; Lima et al., 2019). Interestingly, WNV has a wider range of vertebrate hosts, and horses and humans represent dead-end hosts. WNV comprises at least seven genetic lineages. KUNV belongs to lineage 1b of WNV and is endemic to Australia. Infection with KUNV mostly leads to the development of mild symptoms in humans but the infection is lethal for horses (Colpitts et al., 2012). Currently, there are no specific treatments for flavivirus infections or efficient methods for controlling the spread of their arthropod vectors. Vaccines capable of preventing infection are available for YFV, JEV, and TBEV. The development of a vaccine for DENV is hampered due to the immunological cross-reaction between different serotypes; in such cases, virus may escape neutralization, which leads to an antibody-dependent enhancement (ADE) believed to be responsible for the establishment of severe forms of DENV disease (van Leur et al., 2021).

Antiviral drug discovery for flaviviruses requires the development of robust screening and antiviral activity assays, which have been the focus of numerous studies. To date, diverse methods have been successfully applied to quantify the effect of antivirals on flavivirus infection; however, they remain time-consuming and expensive (Che et al., 2009; Gurukumar et al., 2009; Shum et al., 2010; McCormick et al., 2012; Cruz et al., 2013; Faye et al., 2013; Wilson et al., 2017; Xu et al., 2017). Therefore, the development of new approaches using reverse genetics of flaviviruses, such as the generation of infectious clones and recombinant flaviviruses harboring marker genes (encoding for fluorescent or luminescent reporters), is necessary. As a part of the study, analysis of the properties of DENV, ZIKV, and KUNV reporter viruses allowed the development of efficient bioluminescence or image-based high-throughput assays applicable to drug discovery (Zou et al., 2011; Schoggins et al., 2012; Fischl and Bartenschlager, 2013; Koishi et al., 2018; Li et al., 2020; Zhang et al., 2021). Nevertheless, genetic stability and durable reporter expression during long-term passage in tissue culture remained a key issue (Aubry et al., 2015).

In the current study, we present the data related to the approaches used for the construction of wt infectious clones of KUNV, DENV2, and DENV4 as well as versions harboring fluorescent and luminescent reporters based on a strategy previously applied to ZIKV (Mutso et al., 2017). Following an assessment of the growth kinetics of viruses rescued from these clones, the genetic stability of the marker-coding viruses was analyzed by monitoring the fluorescence or luminescence signals from the cells infected with the corresponding viruses. Herein, we characterized the structures of the virions and the variations in their sizes and shapes, as well as their distribution in cellular compartments, using transmission electron microscopy (TEM) on fixed infected cells and atomic force microscopy (AFM) on live viruses (Lyonnais et al., 2021). Finally, we validated the use of the obtained recombinant viruses in fluorescent or luminescent-based drug screening assays by testing NITD008 as a reference molecule harboring pan-flavivirus activity.

Results

Design and construction of icDNA clones of DENV2, DENV4, and KUNV

Rescue of the virus from the infectious cDNA (icDNA) clone of an RNA virus enables various modifications and/or manipulations of the RNA genome. The development of reverse genetic systems for different RNA viruses has advanced over the last decades. The RNA transcripts derived from cDNAs of positive-strand RNA viruses are considered to be infectious, i.e., their transfection into susceptible cells results in the replication and successful recovery of the infectious viruses (Ruggli and Rice, 1999). For most positive-strand RNA virus families this approach is relatively straightforward; however, for some viruses, the development and use of reverse genetics is more challenging. Flaviviruses represent an example of the latter. It has been shown that some sequences from flavivirus genome encode proteins with a high level of cytotoxicity for *Escherichia coli*, the bacteria most commonly used to propagate plasmids containing viral icDNAs (Zheng et al., 2016). The expression of such proteins via the activity of cryptic bacterial promoters found in the cDNAs of flaviviruses is therefore harmful to the bacteria harboring the corresponding plasmids, leading to counterselection resulting in the instability of icDNA plasmids.

Here, we aimed to construct icDNAs based on the NCBI sequences for DENV2 (GenBank: U87411.1), DENV4 (GenBank:

AF326573.1), and KUNV (GenBank: AY274504) using a strategy described previously for ZIKV (GenBank database: KJ776791) (Aubry et al., 2015). Briefly, the SP6 promoter was placed upstream of the sequence corresponding to the 5′ end of the virus genome while a cleavage site of restriction endonuclease was placed immediately downstream of the sequence corresponding to the 3′ end of the genome. This allowed run-off *in vitro* transcription to be conducted to obtain transcripts corresponding to the viral genome RNA that could be used for the efficient rescue of infectious viruses. The sequences corresponding to virus genomes were assembled from synthetic DNA fragments; assembly was performed in a single-copy plasmid to ensure the efficient propagation of cloned cDNAs in bacterial cultures and to prevent possible re-arrangements in the cDNAs of flaviviruses (Pu et al., 2011). No instability issues were observed during plasmid construction and the propagation of plasmids containing cDNAs of KUNV, DENV2, and DENV4. Of note, this approach failed with the icDNA of DENV3, probably indicating extreme toxicity of the latter plasmid for *E. coli*.

To extend the study, along with the preparation of the icDNA clones containing the wt sequence of DENV2, DENV4, and KUNV, icDNAs corresponding to recombinant viruses with inserted reporter-encoding genes were also constructed. The reporters allowing the detection of the infection by either quantification of the marker expression/activity (nanoluciferase, NLuc) or visually through the fluorescence of the marker (oxGFP and mCherry) were used. It has been established that the position and insertion strategy of sequence encoding for markers in flavivirus genome play a crucial role in the genetic stability of recombinant virus and affects the speed of loss of marker over passages (Baker et al., 2020). In our study, the design previously used for the construction of stable reporter viruses of ZIKV was applied for DENV2, DENV4, and KUNV. In this design, the sequence encoding marker protein is placed between the native sequence encoding for flavivirus capsid protein and that of the foot-and-mouth disease virus (FMDV) 2A autoprotease followed by a codon-altered copy of sequence encoding for the capsid protein (Figure 1A). Thus, upon translation of the recombinant genome, the marker is released from the first copy of the capsid protein by mechanisms naturally used for the release of flavivirus capsid from the polyprotein, while FMDV 2A cleaves itself from the following copy of the capsid protein, allowing the efficient release of the reporter with no or minimal disturbance of the maturation of flavivirus structural proteins, as was confirmed by immunoblots (Supplementary Figure S1A).

Rescue and properties of wt and reporter-expressing variants of DENV2, DENV4, ZIKV, and KUNV

The rescue of DENV2-wt, DENV4-wt, ZIKV-wt, and KUNV-wt as well as their variants encoding mCherry, oxGFP, or NLuc reporters was performed in Vero cells (Figure 1). A focus forming assay (FFA) using pan-flavivirus E protein-specific mouse MAb (4G2) was used to determine the titers of each of the rescued viruses at different days post-transfection (dpt). Supernatants designated as P_0 stocks were collected at the peak of virus release and used to infect new cells for imaging and further analysis.

It was observed that ZIKV-wt, ZIKV-mCherry, and ZIKV-NLuc were cytopathic and showed similar exponential growth. ZIKV-wt became detectable at 2 dpt and a maximum titer of 6.5×10^7 FFU/mL was reached at 7 dpt (Figure 1B). Curiously, but for unknown reasons, at early time points, ZIKV-oxGFP had titers that were approximately 20× higher than other clone-derived variants of ZIKV, reaching 5.5×10^9 FFU/mL at 5 dpt; however, after that, the titer decreased, and by 8 dpt, had become comparable with the other ZIKV constructs used in the study (Figure 1B). After transfection with transcripts of ZIKV-mCherry, the first mCherry-expressing cells were observed at 4 dpt, and their number increased in the following days (Supplementary Figure S2). Interestingly, despite a high viral titer, ZIKV-oxGFP-infected cells showed a low fluorescent signal-to-noise ratio (SNR ~10), which reduced the interest in ZIKV-oxGFP as a reporter virus. By contrast, ZIKV-mCherry-infected cells showed a robust fluorescent SNR of ~40, thus increasing the value of the use of this virus as a reporter in fluorescence-based experiments, e.g., drug screening.

Cells transfected with transcripts of the icDNAs of KUNV displayed stronger cytopathic effects (CPE) than those observed for ZIKV: a complete CPE was observed already by 7 dpt. Coherently, the rescue of KUNV was also more rapid: at 2 dpt the titer of KUNV-wt was already 2.8×10^5 FFU/mL and reached maximum values of 3.4×10^7 FFU/mL at 4 dpt (Figure 1B). A slight delay in the development of CPE was observed for KUNV-oxGFP and KUNV-NLuc, which was reflected in reduced titers at 2 dpt. Up to 5 dpt, the titers of KUNV-mCherry were the lowest; however, at 6 dpt, they reached a level similar to those of KUNV-wt, KUNV-oxGFP, and KUNV-NLuc (Figure 1B). As an example, mCherry-reporter fluorescence was detected in viral clone-transfected cells at 4, 5, and 7 dpt up to 12 dpt depending on the virus (Supplementary Figure S2). Additionally, the replication of reporter viruses was confirmed by staining with viral envelope (E) antibodies (Figure 1C). Interestingly, fluorescent microscopy showed a distinguishable feature of recombinant KUNV replication: both mCherry and oxGFP signals were mostly detected in large intracytoplasmic structures in infected cells, reflecting the colocalization of capsids, whereas the localization of oxGFP signal in the nucleoli was observed in only a limited number of cells. Viral E proteins were associated with the plasma membrane in both cases (KUNV mCherry and oxGFP) (Figure 1C). The rescue of DENV2 and DENV4 was considerably slower than that of KUNV. Interestingly, in contrast to ZIKV and KUNV, no decrease of viral titers was observed at late time points (up to 12 dpt); instead, virus titers either reached a plateau level (as observed for DENV2-wt) or continued to increase slowly (Figure 1B). Although DENV2-wt rapidly reached high titers (approximately 1.5×10^7 FFU/mL), lower titers were observed for all the reporter-harboring variants of this virus. For DENV2-oxGFP, this was observed for earlier time points and ultimately the virus reached titers similar to those of DENV2-wt. By contrast, for DENV2mCherry and DENV2-NLuc, lower titers were observed at all time points during the experiment and the maximal titer remained as low as 5×10^5 FFU/mL (Figure 1B). Similar "behavior" was observed for reporter variants of DENV4; for all of these (including DENV4-oxGFP), titers remained lower than that of DENV4-wt over the entirety the experiment (Figure 1B). Similar to ZIKV-oxGFP, the fluorescent signal in DENV2-oxGFP and DENV4-oxGFP positive cells remained dim and was detected as foci (DENV2) or was diffusely distributed in the cell cytoplasm and nucleus (DENV4). For all recombinant viruses harboring mCherry or oxGFP markers, viral E protein predominantly accumulated in the cell cytoplasm (Figure 1C), where it colocalized

10.3389/fmicb.2023.1201640

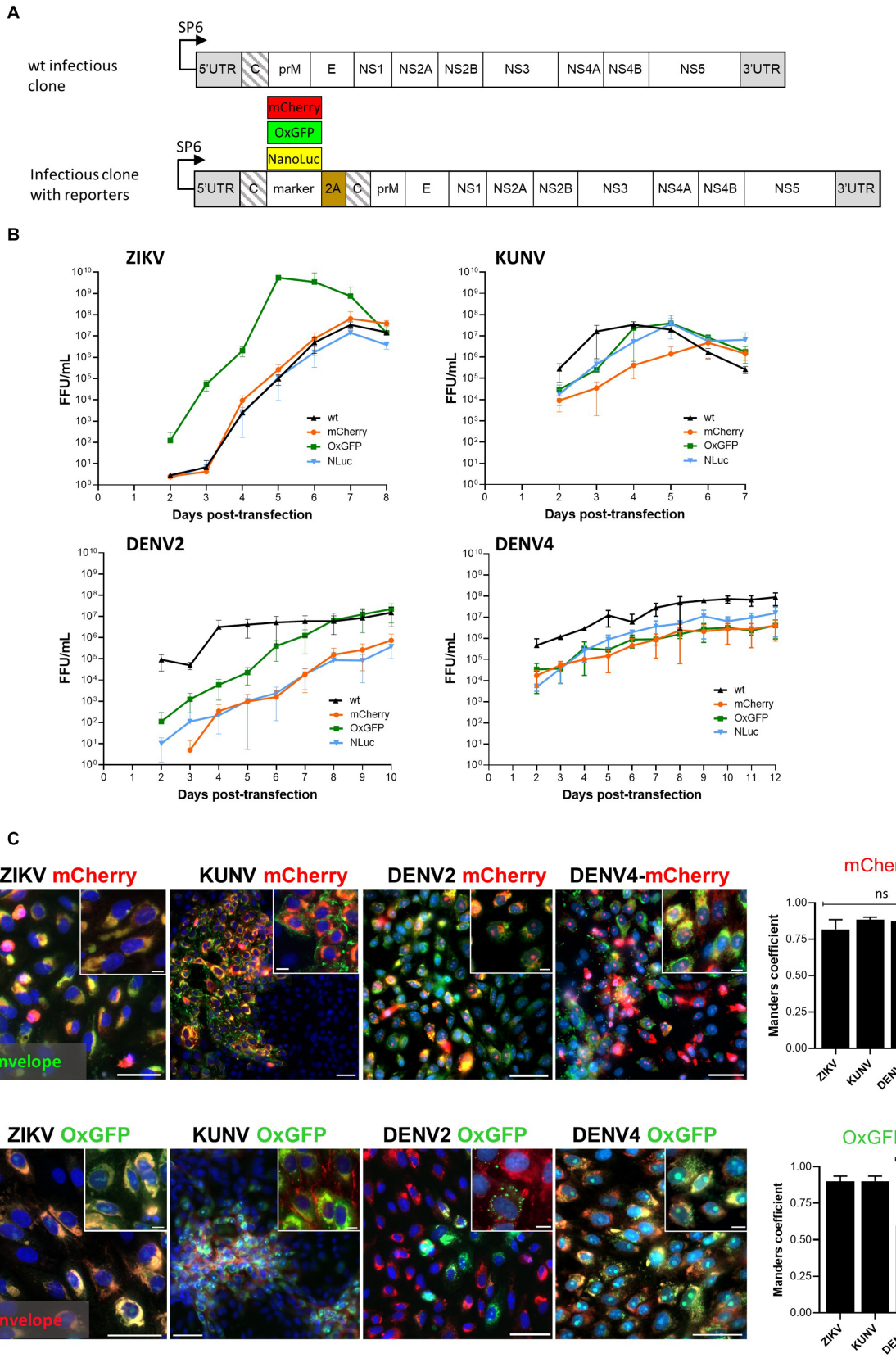

FIGURE 1
Design of the wt and reporter containing the icDNA of flaviviruses. **(A)** Schematic of the viral constructs used in the study. The reporter (mCherry, oxGFP, or NLuc) and foot-and-mouth-disease virus 2A sequence (2A) were placed at the junction of two full-length capsid sequences (shown with slanted lines). The second sequence was codon-altered using synonymous substitutions to avoid homologous recombination. **(B)** Rescue and growth

(Continued)

FIGURE 1 (Continued)
kinetics of recombinant ZIKV, KUNV, DENV2, and DENV4 variants. After transfection of the *in vitro* transcribed RNA, the supernatant was collected at the indicated time points, and the viral titer was quantified using an FFA. Each time point represents the average titer obtained from three independent experiments (N = 3, n = 3 replicates per experiment) with the respective standard deviations. **(C)** Left panels: localization of fluorescent reporter markers and envelope proteins. Vero cells were infected with P_0 stocks of ZIKVmCherry and ZIKV-oxGFP at an MOI of 0.1 and with P_0 stocks of DENV2-oxGFP, DENV2-mCherry, DENV4-mCherry, DENV4-oxGFP, KUNV-oxGFP, and KUNV-mCherry at an MOI of 0.05. At 72 h post-infection, cells were fixed and stained against viral envelope protein (green for cells infected with viruses expressing mCherry, and red for cells infected with viruses expressing oxGFP). mCherry and oxGFP signals were detected using confocal microscopy; nuclei were counterstained with Hoechst (blue). Scale bars: 10 µm. Right panels: colocalization of red and green fluorescence (Manders' coefficient) for ZIKV-mCherry (1,082 cells), KUNV-mCherry (680 cells), DENV2-mCherry (642 cells), DENV4-mCherry (600 cells), ZIKV-oxGFP (716 cells), KUNV-oxGFP (622 cells), DENV2-oxGFP (706 cells), and DENV4-oxGFP (645 cells). One-way ANOVA followed by Tukey's multiple comparisons test was used for statistical analysis; $*p < 0.05$; ns, not significant. Data are mean ± SD from three independent experiments.

with fluorescent marker protein. For DENV4-mCherry and DENV4-oxGFP, colocalization was at 87 and 88% (Manders' coefficient value), respectively; similar colocalization was also observed for ZIKV and KUNV recombinants (Figure 1C). For DENV2-mCherry- and DENV4-mCherry-infected cells, the fluorescent mCherry signal was distributed within the cell cytoplasm and in the nucleus (Figure 1C). The lowest colocalization for viral E protein and the fluorescent marker was observed for DENV2-oxGFP. Most likely, this is not caused by specific properties of the virus/marker combination as estimation of the percentage of the cells positive only for oxGFP in the total population of infected cells revealed a rapid loss or inactivation of oxGFP marker (Figure 1C).

After RT-PCR amplification (Supplementary Figure S3), we also checked by virus sequencing that no mutations were observed in the structural genes of the viruses, 7 days post-transfection of the viral stock P_0, as compared with the WT, and in the markers of the ZIKV, DENV4, DENV2, NanoLuc, mCherry, and Ct-mCherry viruses (Supplementary Figure S4). In some instances, the markers contained a few minor silent mutations. Only, DENV2-oxGFP and KUNV-mCherry-OxGFP presented some deletions of the duplicated capsid associated with the marker or of the marker itself (see Supplementary Figures S4, S5), coherent with what was observed with the genetic stability assay (Figure 2).

Overall, the results of these experiments demonstrated the efficient rescue of recombinant flaviviruses from the RNA transcripts and revealed the dynamics of their replication, allowing us to distinguish specific phenotypic features of infection. In addition, all oxGFP- and mCherry-expressing constructs, with the exception of DENV2-oxGFP, showed a high level (Mander's coefficient value of >80%) of colocalization coefficients between the viral E proteins and their respective markers (Figure 1C). As expected, the replication of ZIKV-wt, KUNV-wt, DENV2-wt, and DENV4-wt was (with the notable exception of ZIKV-oxGFP, which we could not explain reasonably) more robust than that of viruses containing genes encoding for fluorescent or NLuc markers. These data indicate that the insertion of the marker sequences had an impact on the level of RNA replication and/or virion formation and release.

Assessment of the genetic stability of recombinant virus genomes in cell culture

Flaviviruses carrying reporters are known to face instability problems. Owing to mutations and recombination events, the reporter genes are often lost during the serial passaging of these viruses. The stability of recombinant flavivirus genome depends on multiple factors, including virus species, the marker insertion strategy, and the marker gene used (Baker and Shi, 2020). Once the marker is lost, the resulting virus will eventually overgrow the parental recombinant; the speed by which the virus outcompetes the parental recombinant depends on the conditions of infection (MOI) and differences in the growth kinetics of the competing viruses. All marker-containing viruses analyzed in previous experiments, except for ZIKV, replicated slower than their wt counterparts (Figure 1B), demonstrating a growth advantage of the wt virus and indicating that viruses that have lost a sequence encoding for a marker very likely also have a growth advantage. Therefore, we analyzed the marker stability of all the aforementioned viruses with reporters by performing four passages in Vero cells and subsequently quantifying the infectious titer using FFA (immunostaining against E) and analyzing marker expression by fluorescence microscopy (mCherry), fluorescence microscopy with immunostaining (anti-GFP), or measuring luminescence (NLuc) (Figure 2A).

Coherent with a previous study (Mutso et al., 2017), all recombinant variants of ZIKV displayed relatively stable marker expression over four passages, with ≥80% cells infected with P_4 stock of ZIKV-mCherry- or ZIKV-oxGFP (Figure 2B). Results obtained for ZIKV-NLuc showed a larger variation, indicating a partial loss of the inserted sequence during late passages; however, approximately 50% of cells infected with P_3 or P_4 stocks did express NLuc (Figure 2B), as measured by TCID50 using both FFA and direct NLuc measurement. By sharp contrast, a loss of marker expression was already detected for P_1 of KUNV-mCherry and KUNV-oxGFP; cells infected with P_2 of these viruses revealed almost complete (mCherry) or > 50% (oxGFP) loss of marker expression (monitored by FFA with 4G2 antibody labeling). Marker expression was detected in all cells infected by P_1 of KUNV-NLuc; however, in subsequent passages, the percentage of cells infected with the viruses expressing the marker diminished, and by passage 4, marker expression was completely lost (Figure 2B). The effect was similar, albeit even more pronounced, for all recombinant DENV2 variants. Approximately 90% of the loss of marker expression occurred during the first passage, and marker expression was not observed during subsequent passaging (Figure 2B). Somewhat surprisingly, DENV4 reporter-harboring variants were clearly more stable. mCherry expression was almost uniformly detected in cells infected with P_1 of DENV4mCherry followed by a gradual decrease of marker-positive-infected cells over the next three passages. Both DENV4-oxGFP and-NLuc viruses were stable for two passages; however, a rapid loss of

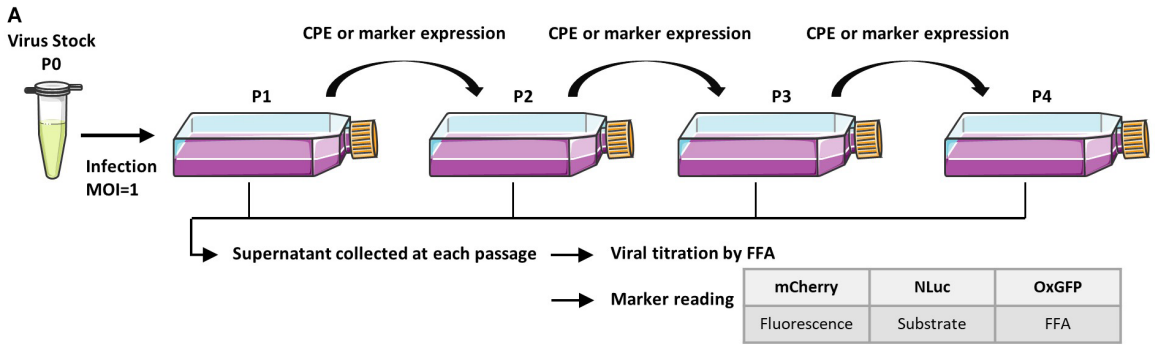

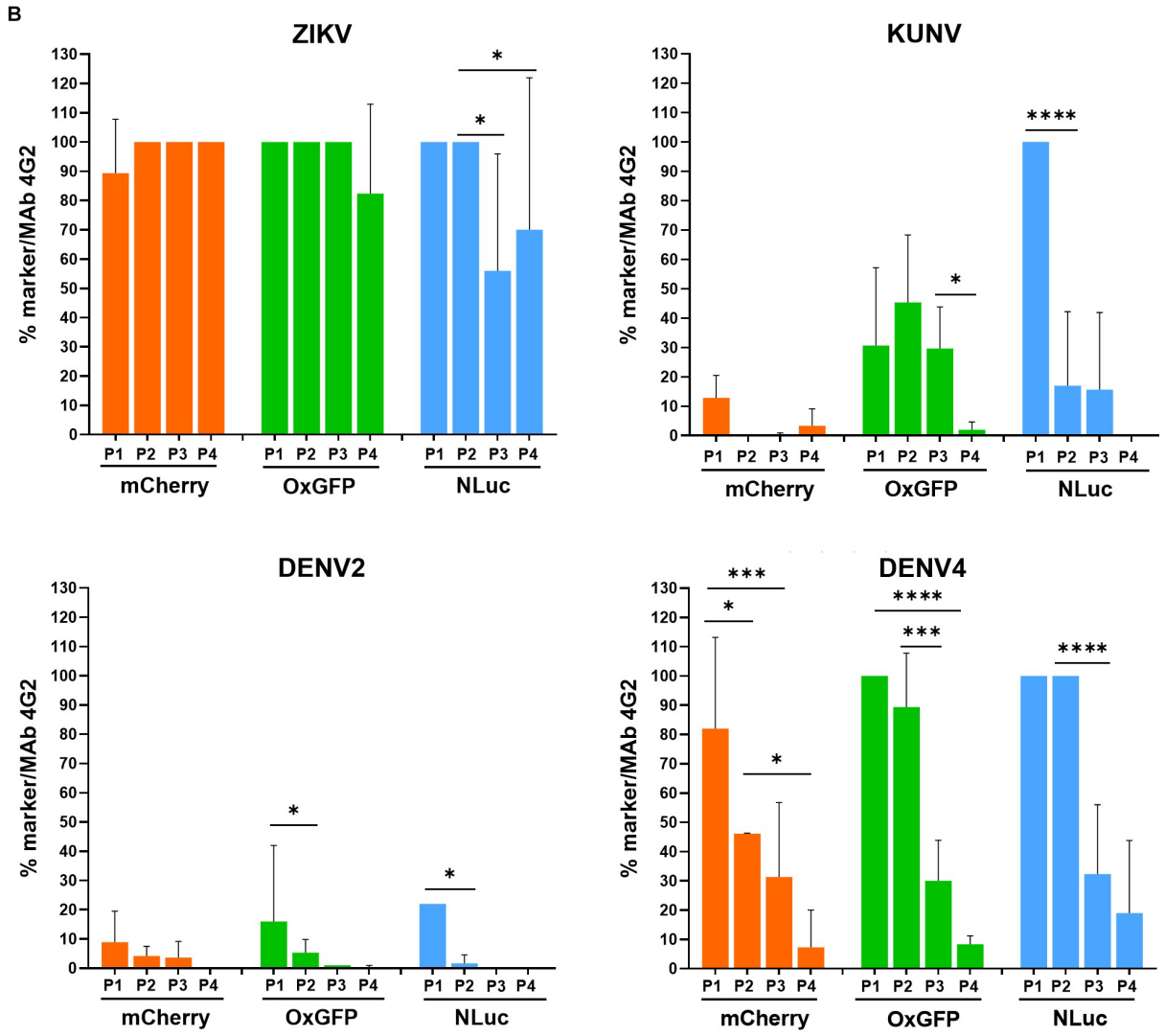

FIGURE 2
Evaluation of the genetic stability of -mCherry, -oxGFP-, and -NLuc reporter-carrying flaviviruses. **(A)** Schematic of the experimental protocol used to perform the marker stability assay. Vero cells were infected at an MOI 1 with P_0 stocks of recombinant ZIKV, KUNV, DENV2, or DENV4 with mCherry, oxGFP, or NLuc markers and incubated until the development of CPE or visible marker expression. P_1 stocks were collected and used to infect Vero cells for the next passage until passage 4 (P_1 to P_4 stocks). Viral stocks were titrated using an FFA with a mouse pan-flavivirus anti-Env antibody (Mab 4G2). mCherry signal was measured by quantifying fluorescence using a Cellomics ArrayScan VTI microscope. oxGFP expression was detected by an immunofluorescence assay using an anti-GFP antibody. For the measurement of NanoLuciferase activity, 96-well plate was infected with P_1 to P_4 stocks according to the end-point titration method, and NLuc was measured using the Nano-Glo Luciferase Assay System after cell lysis, on a microplate reader. **(B)** Evolution of transgene expression through serial passages for each virus. The data represent the expression of the marker reported to the infectious titer. One-way ANOVA followed by the LSD post-hoc test was used to evaluate the significance of the relationship. Each bar represents the mean ± SD ($n = 3$). *$p < 0.05$, ***$p < 0.001$, ****$p < 0.0001$. LSD, least significant difference.

markers was observed for P_3 and P_4 stocks of these viruses (Figure 2B).

DENV2-mCherry can be stabilized by truncating the sequence encoding for the first copy of capsid protein

The instability of reporter-expressing recombinant flaviviruses has led to the development of various approaches aimed to overcome the problem. For viruses harboring markers between two copies of sequences encoding for capsid protein (Figure 1A), shortening of the first (native) copy of the capsid protein gene to a length sufficient for preserving *cis*-active RNA elements located in this region has been successfully used; sometimes, such truncation is combined with additional modifications of the insertion region (Baker et al., 2020; Volkova et al., 2020). For some flaviviruses, the optimal length of the 5′ copy of the capsid encoding sequence has been determined to be 35 or 38 codons; more extensive truncations have been shown to cause unpredictable recombinations of the genome or the loss of the marker (Samsa et al., 2012; Baker et al., 2020). To determine whether this approach can be used to stabilize highly unstable DENV2-mCherry, residues 39–114 in the first copy of capsid were deleted (Figure 3A). The rescue and properties of the corresponding virus (designated as DENV2-Ct-mCherry) were compared with those of DENV2-mCherry (Figures 3B,C).

Higher titers were obtained for DENV2-Ct-mCherry over the time course of the virus rescue experiment than for DENV2-mCherry. By 6 dpt, the titers of DENV2-Ct-mCherry reached a plateau level (around 5×10^6 FFU/mL) that was close to that of DENV2-wt (Figure 3B). Remarkably, improved genetic stability was also observed: all or nearly all cells infected with P_1 or P_2 stocks of DENV2-Ct-mCherry were positive for mCherry expression; in cultures infected with P_3 or P_4 stocks, the loss of the marker became more evident yet 30 to 40% of infected cells were still positive for mCherry (Figure 3C). No clear difference in the time scale of detection of mCherry fluorescence in reporter-positive cells was observed between DENV2mCherry and DENV2-Ct-mCherry (Figure 3D). In both cases, fluorescent signals were detected in the nucleus and cell cytoplasm, with Manders' coefficients of 0.87 and 0.82 for DENV2-mCherry and DENV2-Ct-mCherry, respectively (Figure 3E). The nuclear accumulation of mCherry has also been reported for other DENV2 constructs of a similar design and was most likely caused by the fusion of mCherry with capsid protein or its fragment (Bulich and Aaskov, 1992; Sangiambut et al., 2008; Netsawang et al., 2010). Previously published data indicate that the appearance of the capsid protein in the nucleus of DENV2-infected cells occurs due to the presence of a nuclear localization signal that facilitates interaction with cellular proteins responsible for nuclear transport in its sequence (Sangiambut et al., 2008; Zhang et al., 2021). Taken together, truncation of the first copy of the capsid protein gene had a positive impact on the replication and genetic stability of DENV2 harboring the mCherry marker without any apparent changes in the subcellular distribution of the reporter. Overall, the same approach, i.e., a truncated capsid, can be used to develop flavivirus infectious clones harboring reporters to overcome issues related to the genetic instability of the corresponding recombinant viruses.

Imaging of recombinant virus-infected cells by TEM and purified viruses by Bio-AFM

To image the morphogenesis of virions of clone-derived mCherry-expressing viruses, we performed a cross-analysis of resin-embedded Vero cells infected at an MOI of 1 by P_0 stocks at 3 days post-infection by transmission electron microscopy (TEM). The replication of flaviviruses typically causes dramatic remodeling of the endoplasmic reticulum (ER) membranes, which wrap around the viral replication factories to form viral replication organelles (VRO) (Mackenzie et al., 1996), convoluted membranes/paracrystalline arrays (CMs/PC) (Caldas et al., 2020), and vesicle packets (VP) used as loci for viral genome amplification, RNA translation, and polyprotein processing (Stollar et al., 1967; Westaway et al., 1997; Mackenzie et al., 2001; Welsch et al., 2009; Hamel et al., 2015; Barreto-Vieira et al., 2017; Aktepe and Mackenzie, 2018). Coherently, the infection of Vero cells with ZIKV-mCherry, DENV2-mCherry, DENV4-mCherry, or KUNV-mCherry induced massive ultrastructural ER expansions and reconfigurations, cytoplasm vacuolization, the formation of ER sheets and ER-derived vesicles containing electron-dense viroplasm-like structures, and newly formed virions (Figure 4A, left panels). CMs were usually found in the center of large structures (Figure 4A), as has been previously observed in cells infected with DENV or ZIKV (Welsch et al., 2009; Caldas et al., 2020). VRO and VP were unambiguously observed within subcompartments, including the lumen of large cytoplasmic vacuoles, with a dramatic accumulation of PC and membrane-associated virus particles, often arranged in regular arrays for DENV2- and KUNV-infected cells (Westaway et al., 1997; Mackenzie et al., 2001; Aktepe and Mackenzie, 2018). Tubular-altered ER containing immature viral particles were also observed in close proximity to the VP (Figure 4). All these features have been commonly observed in mammalian cells producing flaviviruses (Mackenzie et al. 1996; Caldas et al., 2020).

Next, Bio-AFM was used to analyze the morphology and integrity of virions released from cells infected with ZIKV-mCherry, DENV2-mCherry, DENV4-mCherry, or KUNV-mCherry. Viral particles were purified from cell supernatants, resuspended/diluted in a buffer solution, and smoothly adsorbed on a poly-L-lysine-coated mica surface. To preserve the structural integrity of the Bio-AFM imaging was performed in a buffer, using a Bio-AFM operating in a BSL3 environment. Figure 4 (right panels) shows topographic AFM images of purified viruses with different magnifications. Interestingly, in all cases, fractions of the viral particles appeared to be clustered, reminiscent of the viral clusters observed in the ER lumen by TEM, which suggests that the virions can be released from the infected culture cells as viral "packages" or, for KUNV-mCherry, can be clustered during ultracentrifugation. Individual virions of ZIKV-mCherry, KUNV-mCherry, DENV2-mCherry, and DENV4-mCherry appeared as roughly spherical particles with some angles suggesting an icosahedral arrangement, as expected from their reported cryoEM structures (Ferreira et al., 2008; Kostyuchenko et al., 2014;Sirohi et al., 2016; Sevvana et al., 2018). Viral particle height measurements obtained from cross-section analysis (Figure 4B) were also consistent with the virion sizes measured by cryoEM or previous AFM studies: 52 ± 8 nm for DENV2-mCherry (Ferreira et al., 2008), 44 ± 7 nm for DENV4-mCherry (Kostyuchenko et al., 2014),

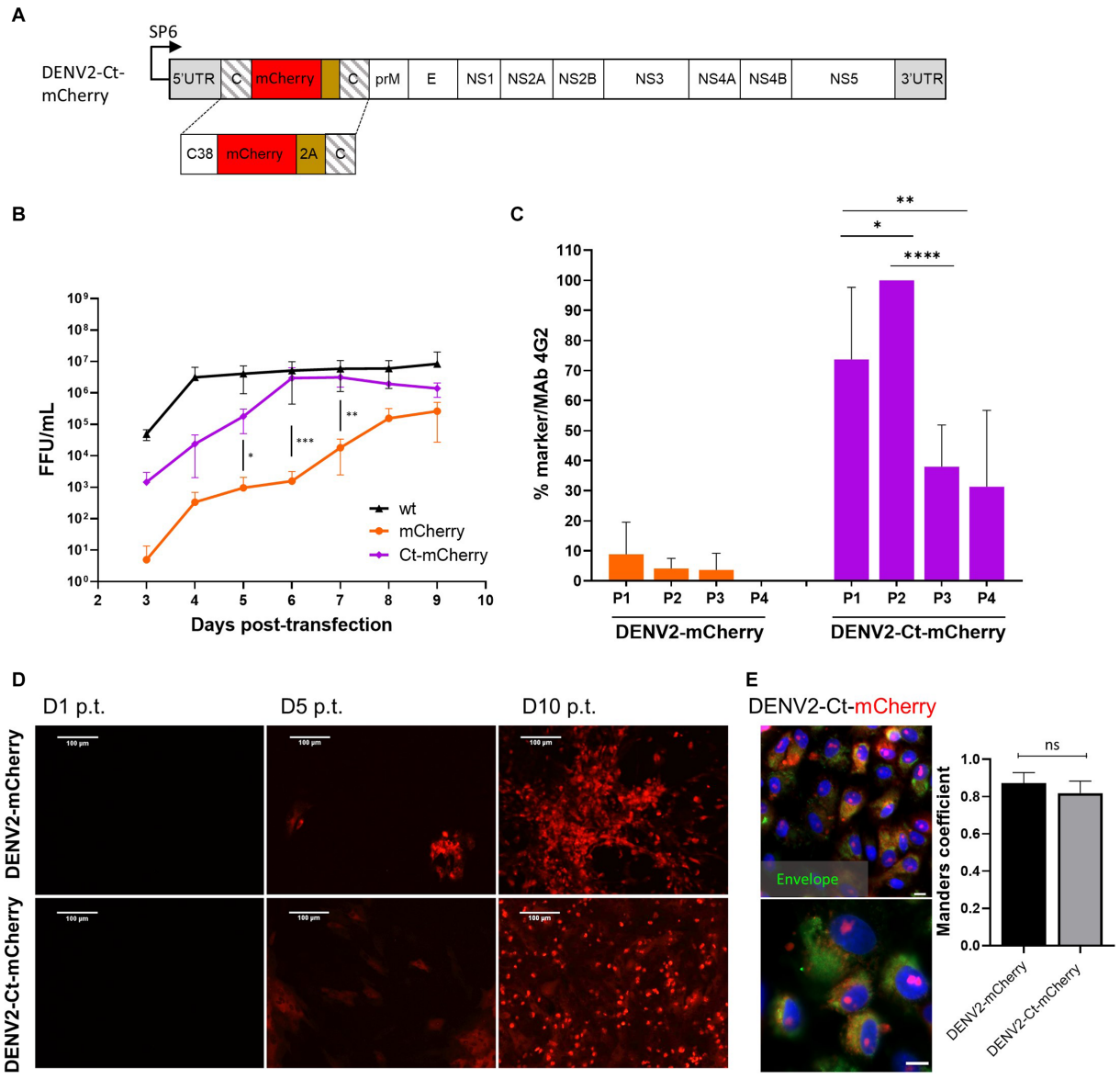

FIGURE 3
Comparison of the growth kinetics and genetic stability of DENV2-mCherry and DENV-Ct-mCherry. **(A)** Schematic representation of the DENV2-Ct-mCherry icDNA clone. The first copy of the capsid protein was truncated by removing residues 39–114. The rest of the design corresponds to the icDNA clones of viruses with full-length capsid duplication. **(B)** Growth kinetics of recombinant DENV2-wt, DENV2-mCherry, and DENV2-Ct-mCherry. Standard deviation is calculated from replicate ($N = 3$; $n = 3$ replicates per experiment) samples tested at each time point. One-way ANOVA was used to evaluate the significance between mCherry and Ct-mCherry clones. Each bar represents the mean ± SD ($n = 3$). **(C)** Comparison of the marker stability of recombinant DENV2-mCherry and DENV2-Ct-mCherry over four passages. One-way ANOVA followed by a least significant difference post-hoc test was used to evaluate the significance of the relationship. Each bar represents the mean ± SD ($n = 3$). **(D)** Evaluation of replication dynamic DENV2-mCherry or DENV2-Ct-mCherry based on the increasing intensity of mCherry signal in the virus-infected cells over the indicated time points. **(E)** Left panels: confocal images of mCherry fluorescence (red) and DENV2 envelope protein (green) at 72 h p.i. at an MOI of 0.05 (scale bars: 50 μm and 10 μm, respectively). Right panel: colocalization of red and green fluorescent signals (Manders' coefficient) for DENV2-mCherry (642 cells) and DENV2-Ct-mCherry (616 cells). Data represent mean ± standard error of mean ($n = 3$). ANOVA was performed followed by Tukey's multiple comparisons test. *$p < 0.05$; **$p < 0.01$; ***$p < 0.001$; ****$p < 0.0001$; ns, not significant.

39 ± 9 nm for ZIKV-mCherry (Sirohi et al., 2016; Sevvana et al., 2018), and 37 ± 8 nm for KUNV-mCherry (Therkelsen et al., 2018). DENV4-mCherry shows morphology similar to DENV2-mCherry, with a slightly smaller mean diameter. These results suggest that modification of the viral genome (adding an extra copy of sequence encoding for capsid protein and a sequence encoding mCherry, i.e., making the genome 10% larger) had no detectable impact on virion size or morphology.

Validation of fluorescent-reporter flaviviruses for antiviral screening

To assess whether the fluorescent (or luminescent) reporter-expressing recombinant flaviviruses could be applied to high-throughput screening for antivirals in a two-dimensional cell culture system, we chose to test the adenosine nucleoside analog NITD008, previously shown to inhibit the replication of mosquito- and

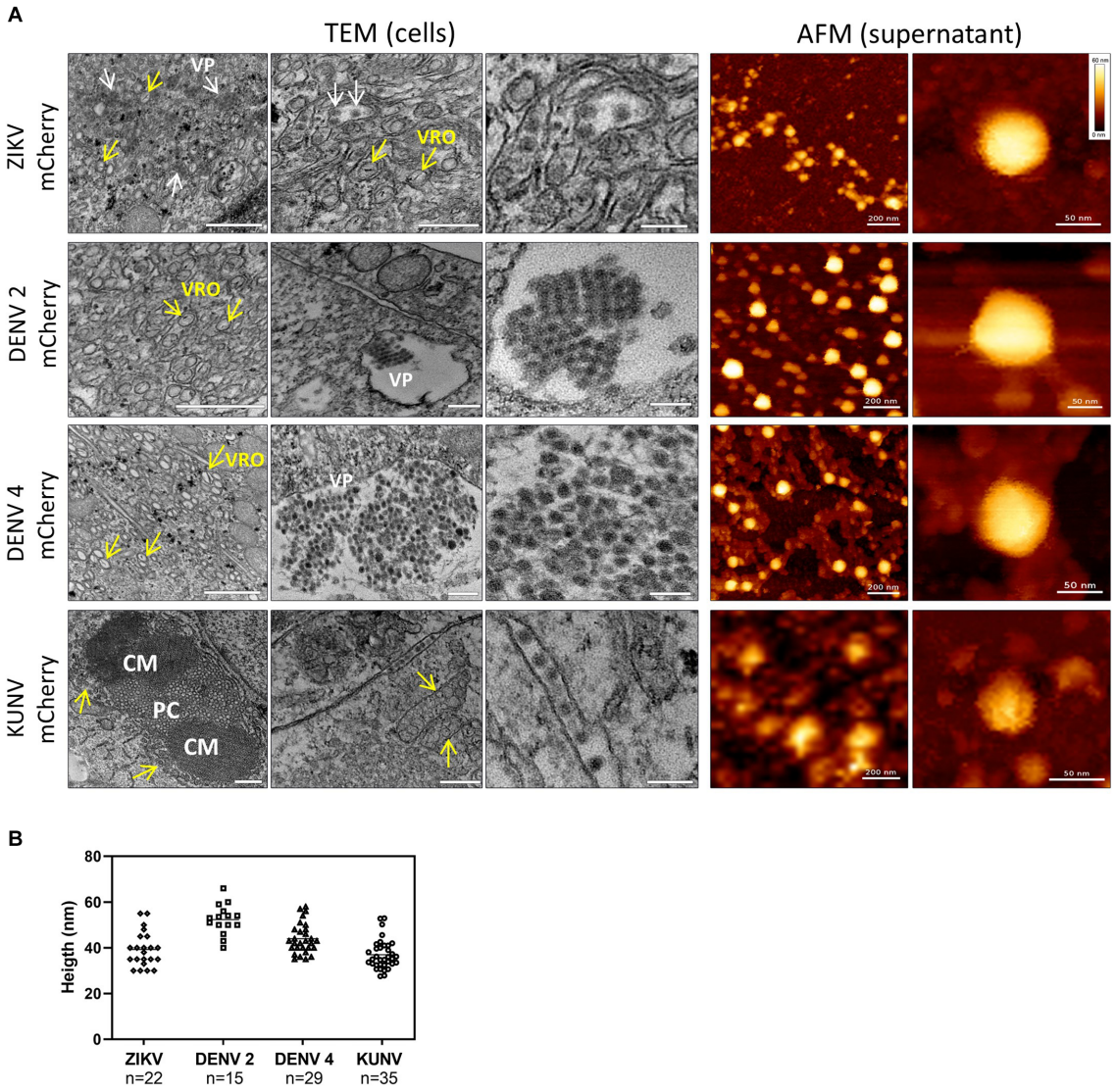

FIGURE 4
TEM and AFM images of mCherry-reporter virions. (**A**, left panel) Transmission electron microscopy of cells infected with DENV2-mCherry, DENV4-mCherry, ZIKV-mCherry, and KUNV-mCherry. Replication organelles derived from the ER were visualized. CM, convoluted membranes; PC, paracrystalline arrays; VP, vesicle packets (white arrows). The localization of viral replication organelles (VRO) are shown with yellow arrows. Scale bars = 200 nm (left and central panels) and 100 nm (right panels). (**A**, right panel) AFM images of mCherry-expressing ZIKV, DENV2, DENV4, and KUNV virions purified from cell supernatants. Virions of ZIKV-mCherry were purified by dialysis in PBS, virions of DENV2mCherry and DENV4-mCherry were purified by Microsep advanced column from the Pall Corporation in Tris-NaCl buffer, and virions of KUNV-mCherry were purified by ultracentrifugation on a sucrose cushion. Scale bars = 200 nm (left panels) and 50 nm (right panels). **(B)** Distribution of the topographical maximal height of viral particles (ZIKV, *n* = 22; DENV2, *n* = 15; DENV4, *n* = 29; and KUNV, *n* = 35) measured from cross-sections of AFM images.

tick-borne flaviviruses, including WNV, DENV, YFV, ZIKV, and TBEV (Yin et al., 2009; Deng et al., 2016). Cells were incubated for 2 h with increasing concentrations of NITD008 and then infected with the corresponding P_0 stocks of the reporter viruses stably expressing inserted marker protein: ZIKV-mCherry, ZIKV-NLuc, or DENV2-Ct-mCherry; ZIKV-wt- or DENV2-wt-infected cells were used for comparison (Figure 5). For ZIKV-mCherry and DENV2-Ct-mCherry, mCherry fluorescence intensity in infected cells was quantified directly on fixed cells by fluorescence microscopy, using nuclei counting for data normalization (Figures 5A,E). For a sake of comparison, cells infected with wt viruses were lysed and total viral RNA was extracted and quantified by RT-qPCR (Figures 5B,D). For ZIKV-NLuc, bioluminescence in lysates of infected cells was quantified by conducting a corresponding enzymatic assay (Figure 5C). The dose–response curves obtained allowed the extraction of the concentrations of NITD008 that inhibited 50% of viral infection (EC_{50}). In accordance with previously reported data (Yin et al., 2009; Deng et al., 2016), NITD008 showed, in all cases, a similar dose-dependent inhibition of virus replication, with EC_{50} values ranging from 0.75 to 1 μM for ZIKV-mCherry and ZIKV-NLuc (Figures 5B,C) and an EC_{50} value of 0.84 μM for DENV2-Ct-mCherry (Figure 5F). Importantly, similar EC_{50} values were obtained for wt viruses with the use of RT-qPCR quantification (Figures 5D,G). These results indicate that ZIKV-mCherry, as well as ZIKV-NLuc and DENV2-Ct-mCherry, can serve as reliable tools for rapid and more direct high-throughput antiviral screening.

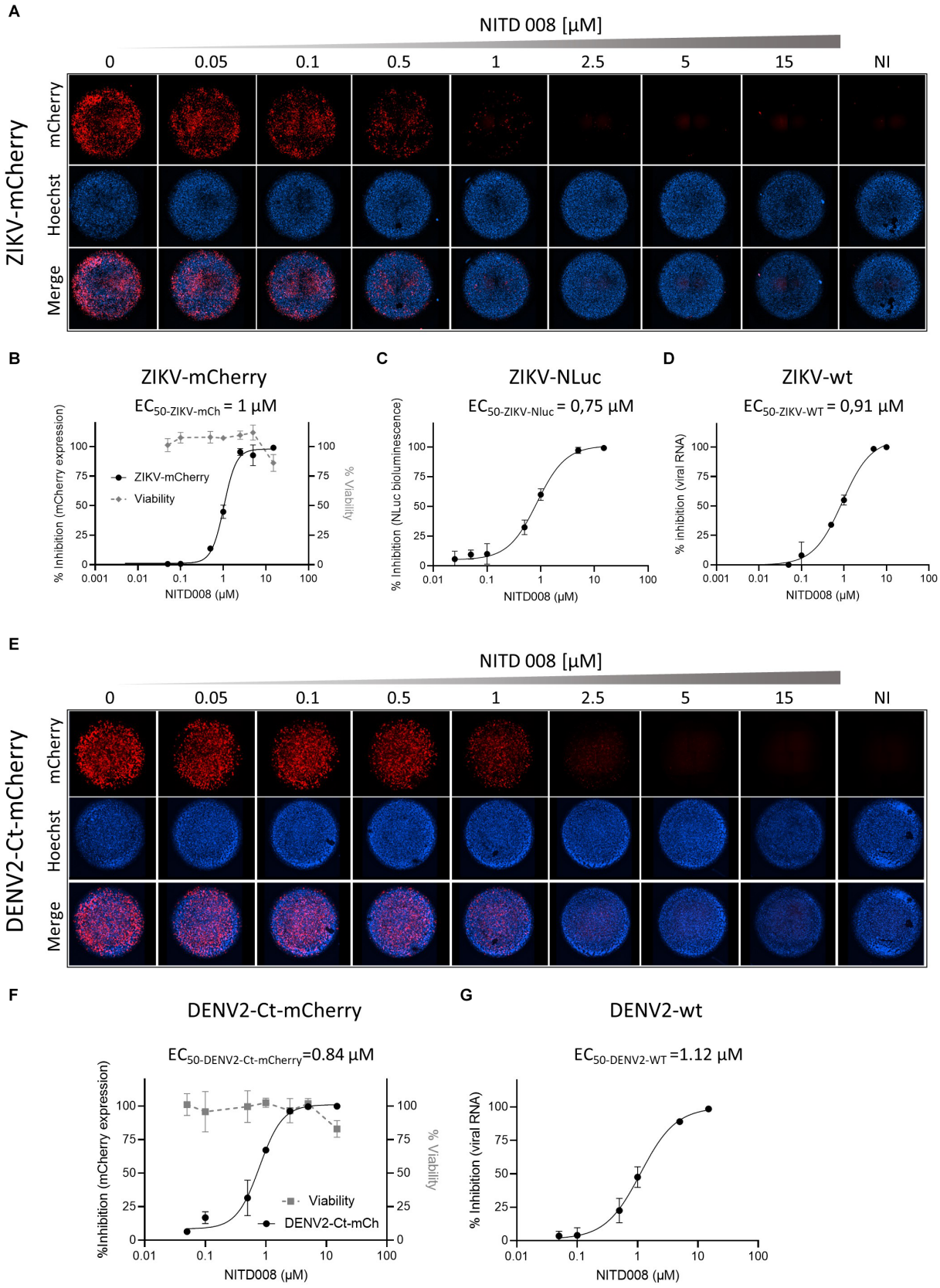

FIGURE 5
Antiviral activity of NITD008 on the reporter-expressing flaviviruses. **(A)** The dose response of NITD008 against ZIKV-mCherry was monitored by fluorescence microscopy. Each panel corresponds to a mosaic image (six tiles) of a single well within a 96-well plate with Vero cells incubated with the indicated increasing concentrations (0.05, 0.1, 0.5, 1, 2.5, 5, and 15 µM) of NITD008 and infected with ZIKV-mCherry at an MOI of 0.05. Upper line,

(Continued)

FIGURE 5 (Continued)
mCherry fluorescence; middle line, cell nuclei stained with Hoechst; bottom line, merged channels. Cell viability at 3 d.p.i. against NITD008 is shown in **(B)**. Dose–response curves for ZIKV-mCherry **(B)**, ZIKV-NLuc **(C)**, and ZIKV-wt **(D)**. **(E)** Dose–response of NIT008 against DENV2-Ct-mCherry monitored by quantitative fluorescence microscopy. Vero cells were treated with increasing concentrations of NITD008 (0.05, 0.1, 0.5, 1, 2.5, 5, and 15 μM) and infected at an MOI of 0.1. Cell viability at 3 d.p.i. against NITD008 is shown in **(F)**. Dose–response curves of NITD008 are shown for DENV2-Ct-mCherry **(F)** and DENV2-wt **(G)**. The corresponding EC_{50} values are indicated in each panel.

Discussion

Over the last decades, reverse genetic approaches have allowed advances in the study of different aspects of flavivirus replication. With these approaches, the construction and manipulation of icDNA clones is essential; however, in contrast to many viruses, the construction and use of these tools for flavivirus studies remain a difficult task due to the instability of the plasmids containing flavivirus cDNAs (Mishin et al., 2001; Aubry et al., 2015). Despite the numerous advantages of high copy number plasmids, they were generally found to be unsuitable for the cloning of flavivirus icDNA as the presence of cryptic prokaryotic promoters in viral sequences leads to the synthesis of mRNAs encoding viral proteins that are toxic to bacteria (Pu et al., 2011). An alternative approach, the use of a low copy number plasmids, can often overcome the instability problem of the virus cDNA by lowering the level of cryptic protein expression and consequently decreasing their cytotoxicity to *E. coli* (Aubry et al., 2015). This strategy was successfully applied to obtain icDNAs for numerous flaviviruses, including YFV, KUNV, ZIKV, and DENV1, 2, and 4 (Santos et al., 2015; Shan et al., 2016; Hu et al., 2022), with DENV3 excluded because the full-length cDNA of this virus appeared to be too toxic to maintain in *E. coli* as a single unit (Santos et al., 2014). Our data reported above are in line with these studies as we could obtain single plasmid icDNA clones for ZIKV, KUNV, DENV2, and DENV4 but not for DENV3. In light of this, additional approaches to resolve the stability problem have been developed. For instance, bacterium-free methods, in particular CPER, have been successfully applied for the development of KUNV icDNA; alternatively, plasmids containing flavivirus icDNAs have been stabilized by the insertion of the intron into virus-derived sequences (Pu et al., 2011; Edmonds et al., 2013; Ávila-Pérez et al., 2018).

The use of icDNAs allows the easy modification of flavivirus genomes; however, on their own, they do not permit the visualization of the course and/or dynamic of the virus infection. A simple concept based on the insertion of the reporter gene(s) into the viral genome allowed us to overcome such a limitation. If successfully applied, recombinant viruses represent a valuable system for tracking and quantifying flavivirus replication *in vitro* and, potentially, *in vivo*. The findings obtained in the current study confirmed that such viral constructs can be used for high-content antiviral screening as well as for the acceleration discovery of antiviral molecules. However, the generation of the reporter viruses containing oxGFP, mCherry, or NLuc markers does encounter another problem—the genetic instability of rescued recombinant viruses observed as a loss of the reporters due to the recombination events during virus replication and the selection for faster-replicating recombinants (lacking a reporter gene) during virus propagation and passaging.

With regard to ZIKV-oxGFP rapid replication growth (Figure 1), viral sequencing of the regions from the beginning of the capsid protein to the end of NS1, including inserted marker sequences, did not reveal any mutations in the viral or inserted sequences. Of note, sequencing of the same region for other variants of ZIKV, as well as those of other variants of ZIKV, DENV2, DENV4, and KUNV, did not detect any mutations in the viral structural proteins of the NS1 region, indicating that such changes are either rare or/and unfavorable for recombinant viruses (see Supplementary Figures S3–S5). Consequently, the accelerated growth of ZIKV-oxGFP was not due to mutations in viral structural proteins or re-arrangements in the inserted marker region. The exact reason(s) for this phenomenon remain unknown and their analysis was beyond the scope of the current study. It can be speculated that accelerated growth may originate from some properties of oxGFP and/or is specific to the experimental conditions (cell line, growth media, etc.) used in this study, as a similar effect has not been observed previously for ZIKV harboring an eGFP insertion (Mutso et al., 2017).

Regarding the loss of the inserted sequences for some of the viruses, the sequencing of regions from the start of the coding region to the end of the NS1 gene revealed truncations, including the deletion of the inserted marker for Denv2-oxGFP, KUNV-mCherry, and -oxGFP, and in some cases, point mutations in the inserted marker gene were detected (see Supplementary Figures S4, S5). These changes are likely responsible for the loss of marker activity (as shown in Figure 2). Interestingly, in several cases, no mutations that can be attributed to the loss of the marker expression was detected. Most likely, this indicates that a large proportion of viral progeny maintained the marker but the corresponding viruses had reduced infectivity and/or fitness and were rapidly outcompeted in subsequent passages. Additionally, our data suggest that monitoring of the expression of the inserted marker is a relevant and effective method for analyzing the stability/infectivity/fitness of flaviviruses harboring recombinant genomes.

Here, we observed that recombinant flaviviruses harboring an NLuc marker were somewhat typically more stable than the ones carrying mCherry or oxGFP markers (Figure 2). Presumably, this was caused by the smaller size of the NLuc insertion (the sequence encoding NLuc is 513 bp long, whereas that for mCherry is 708 bp long). This is consistent with our previous studies with ZIKV, in which the presence of an additional 228 bp insertion encoding ubiquitin resulted in the marked destabilization of viruses encoding for mCherry or GFP reporters (Mutso et al., 2017). Such an effect was not observed for ZIKV encoding NLuc, suggesting the existence of a rather well-defined upper limit for the size of the insert that is tolerated by ZIKV. The data presented in this study suggest that this limit is different for each flavivirus and likely even for sub-types of virus, as observed with DENV2 and DENV4. Interestingly, the stability assay revealed that fluorescent markers were better tolerated by ZIKV than other tested flaviviruses (Figure 2). We observed that previously reported data about the stability of markers in ZIKV-RLuc (Shan et al., 2016), DENV2-mCherry (Li et al., 2020), and DENV2-GFP (Suphatrakul et al., 2018) is consistent with our data. Thus, the findings obtained in the current study clearly underline the high level of instability of all DENV2 and KUNV variants harboring reporters (Figure 2).

It can be speculated that depending on the viral species, genome lengthening by insertions may have a different negative impact on the cyclization of the genome and/or packaging of the viral RNA into the capsid without having a detrimental effect on the virulence of the virus. Of note, one recent discovery demonstrated that JEV had the ability to pack genomic RNA that was much larger in length (up to 15 kb) but the increased genome length was accompanied by a decreased RNA replication efficiency (Yun et al., 2007). Our data indicate that the absolute speed of the replication is not likely the cause, as KUNV variants replicate faster than those of ZIKV or DENV4 (Figure 1). In a recent study, a comparison of the stability of an NLuc insertion for 10 passages was performed for DENV1-4, ZIKV, YFV, and JEV. This study revealed a clear correlation between marker stability and the length of the 5′ copy of the capsid-encoding sequence (Baker and Shi, 2020). Our observation that a reduction in the length of the 5′ copy of the capsid-encoding sequence in DENV2-mCherry has a clear positive impact on the stability of marker expression over passages (Figure 3) is coherent with this data.

Earlier reports also confirmed that some viruses may tolerate less than 10% of an increase in their genome size during packaging into viral capsids, highlighting the importance of the relationship between the size of the viral genome and capsid formation. In this regard, it should be mentioned that we could not find any correlation between the size of the RNA genome and recombinant reporter virus stability, as the sizes of the ZIKV (10,807 nt), KUNV (11,022 nt), DENV2 (10,723 nt), and DENV4 (10,649 nt) genomes are similar. It may be the ratio of the size of the genome to the size of the capsid or the virion that is important—not all viruses may have the same capsid size and the compaction of the viral genome would be higher in a smaller capsid. Clearly, more detailed studies are needed to precisely discover the mechanism(s) responsible for the disadvantage (and therefore counterselection) of flaviviruses with increased genomic RNA lengths.

Capsid protein is known to be a central element in the flavivirus assembly process, which due to the precise physical interactions with the viral genome stabilize the capsid (Tan et al., 2020). The anchor domain (α5 helix) of the capsid possesses a key function in the virion assembly, and in case of its absence, the capsid dimers may remain "locked" within the RNA core, impeding the correct formation of the virions. What is more interesting, the controlled and timely manner of the capsid α5 helix processing was shown as one of the crucial factors necessary for incorporating the nucleocapsid into the virions. Subsequently, α5 helix is removed from the capsid protein but recent investigations demonstrated the opposite for ZIKV: α5 helix is retained for some of the capsid subunits present in virions, indicating other possible (additional) functions in the assembly process (Tan et al., 2020; Barnard et al., 2021). Additionally, the threshold of the positive charges localized in the N-terminal part of the capsid protein, which are necessary for the correct formation of the virions, may be different and thus may affect the stability of flaviviruses to a different extent. Taken together, requirements for the involvement of the capsid protein in the coordination of virion formation are different, which in turn may influence the overall stability of the increased length of the genome or its packaging. Moreover, the functional properties of the RNA elements present within the first 38 codons in the 5′ copy of the capsid gene were different among flaviviruses (Volkova et al., 2020). This indicates that the shortening of this sequence may not affect viral fitness to the same extent for all flaviviruses.

To date, *Flavivirus* particles sizes for ZIKV (49 nm) (Sirohi et al., 2016), DENV2 (50 nm) (Kuhn et al., 2002; Zhang et al., 2003), DENV4 (48 nm) (Kostyuchenko et al., 2014), and KUNV (50 nm) (Therkelsen et al., 2018) have been determined by cryoEM. The AFM measurements performed during this study (Figure 4) with reporter viruses containing an mCherry insertion in their genomes are consistent for DENV2 (52 nm) and DENV4 (44 nm) particle sizes; interestingly, somewhat smaller particle sizes were obtained for ZIKV (40 nm) and KUNV (37 nm). This suggests a slight deformation of ZIKV and KUNV particles during the AFM experiment that could be due either to their adsorption on the surface or the force applied by the AFM tip (or both). On the other hand, DENV2 and DENV4 are maybe more structurally stable in these conditions, showing comparable particle sizes between cryoEM and AFM imaging. However, our results suggest an absence of correlation between particle size and marker stability, as exemplified by ZIKV. Therefore, the size of the virion may be affected—to some extent—by the envelope organization rather than the capsid/genomic RNA size. This leaves the question open. In addition, packages of secreted virions (Figure 4) have not been described so far, to our knowledge, and further exploration is required to attribute this phenomenon to particle preparation for imaging or to a biological behavior.

How does the loss of marker occur? Here, we did not analyze the mechanism directly but some conclusions can be based on the observed speed of the marker loss. Previous studies indicate that the initial loss of the marker occurs through in-frame deletions in the reporter encoding sequence. In most cases, the loss of reporter did not occur (or, at least did not become detectable) during the rescue; instead, it occurred, often very rapidly, during passaging of the rescued virus. It is thus very likely that the main mechanism of how markerless viruses become dominant is not the loss of the marker itself (the timing or frequency of such an event) during viral rescue and replication. Instead, our data is more coherent with the hypothesis that the difference between the growth kinetics of wt virus and virus with a reporter may be the key: the smaller the growth advantage of the wt virus the more stable its variants are with a reporter. The significant growth advantage of wt viruses most likely extends to viruses harboring a deletion in the marker region and allows them to rapidly outcompete the ones that have maintained a marker.

Given these considerations, new approaches directed at increasing the stability of recombinant flavivirus genomes that preserve the properties and virulence similar to the wild-type virus are needed. To date, several strategies have been developed and tested. One of them is the utilization of recombination-dependent lethal mutations. The introduction of such a change into the capsid region of ZIKV and YFV is capable of increasing stability and preventing the formation of defective flavivirus virion in case of recombination events. At the same time, the use of split reporter proteins can also be considered to be one of the most promising approaches due to their already proven robustness and effectiveness. Finally, a recent study has shown that a point nucleotide mutation (T142C) in the 5' CS of JEV, WNV, and DENV leads to the mutation of the capsid protein at position 16 (M16T), which in turn assists genome cyclization with the following stabilization of the reporter-harboring viruses (Li et al., 2017). The question that remains open is whether the combination of several previously mentioned approaches can increase the stabilizing effect.

Materials and methods

Cell culture

Vero cells (African green monkey kidney cells, ATCC CCL-81) were grown in Dulbecco's modified Eagle's medium (DMEM, Lonza) supplemented with 10% fetal bovine serum (FBS, Gibco), 100 U/mL of penicillin, and 100 µg/mL of streptomycin at 37°C with 5% CO_2.

Design and assembly of wt and reporter harboring icDNA clones of flaviviruses

The construction of an icDNA clone of ZIKV (Brazilian isolate), designated as ZIKV-wt, and its variants harboring mCherry and NLuc reporters (ZIKV-mCherry and ZIKV-NLuc), has been described previously (Zheng et al., 2016). To obtain ZIKV expressing green fluorescent marker, NLuc was replaced with an oxidation-resistant GFP marker (McGee et al., 2010); the obtained clone was designated ZIKV-oxGFP. The same cloning strategy was applied for the construction of icDNA clones of DENV2, DENV4, and KUNV. Briefly, synthetic DNA fragments were obtained from Twist Bioscience (San Francisco, CA, USA) and Genscript (New Jersey, USA). The assembly strategy included five steps in which the synthetic fragments were consequentially cloned into the single copy pCCI-Bac plasmid with the SP6 promoter placed upstream of the region corresponding to the 5′ end of the virus genome. The oxGFP, mCherry, and NLuc marker genes were cloned between two copies of capsid sequences in the structural region of the modified genome, as described previously (Zheng et al., 2016). The obtained clones were designated as DENV2-wt (-oxGFP, -mCherry, and -NLuc), DENV4-wt (-oxGFP, -mCherry, and -NLuc), and KUNV-wt (-oxGFP, -mCherry, and -NLuc) (see Supplementary Table S1 for the genomic sequences). To reduce the loss of the mCherry marker, a 228 bp deletion, removing codons 39–114 of the first (native) copy of the region encoding for the capsid protein of DENV2, was introduced into DENV2-mCherry using PCR-based mutagenesis and subcloning procedures; the resulting clone was designated as DENV2-Ct-mCherry. Cloning procedures and amplification of the obtained plasmids containing the icDNAs of the viruses were carried out in *E. coli* EPI300 cells (LGC Biosearch Technologies, United Kingdom). Sequences of all the obtained plasmids were confirmed using Sanger sequencing and are available from the authors upon request.

In vitro transcription and virus rescue

icDNA plasmids (10 µg) of DENV2-wt, DENV4-wt, ZIKV-wt, KUNV-wt, and their reporter-containing variants were linearized using AgeI-HF enzyme (NEB, United States) prior to *in vitro* transcription. The linearized DNAs were purified using a Monarch DNA cleanup kit (NEB, United States) and the capped RNA transcripts were synthesized using an SP6 mMessage mMachine kit (Invitrogen, United States) following the manufacturer's instructions. All virus studies were conducted in a biosafety level 3 facility in CNRS CEMIPAI Montpellier. Vero cells were transfected with the obtained RNA transcripts using Lipofectamine 2000 (Invitrogen) reagent. Briefly, transfection mixtures were incubated at room temperature for 5 min and added to Vero cell monolayers and then incubated for 5–6 h at 37°C. The cells were then washed in 1 × PBS (Eurobio, France) and incubated in growth medium at 37°C. Supernatants (P_0 stocks) were collected at 7 to 15 days post-transfection, clarified by centrifugation at 1,000 × g for 10 min, aliquoted, and stored at −80°C.

Focus forming assay

Viral supernatants were titrated using the end-point titration method. Vero cells were seeded on 96-well plates at 10,000 cells per well and incubated for 4 h at 37°C. Cells were infected with virus dilutions (from 10^{-1} to 10^{-9}) prepared in DMEM supplemented with 2% FBS and a 1% penicillin/streptomycin mixture (Lonza Biosciences). Infected cells were incubated at 37°C for 7–15 days. The medium was then removed, cells were washed once with PBS, and fixed with 4% paraformaldehyde (PFA, Fisher) for 30 min at room temperature. After the removal of PFA, cells were washed with PBS and kept at 4°C until staining. For the staining, cells were permeabilized with PBS containing 0.1% Triton X-100 (Sigma-Aldrich, France) for 5 min and blocked with PBS containing 2% FBS and 0.05% Tween 20 (Sigma-Aldrich, France) for 1 h. Cells were washed once with PBS and incubated with a mouse pan-flavivirus anti-Env antibody (Mab 4G2, Novus Biologicals NBP2) for 1–2 h at room temperature (1:1,000) for viral titration or an anti-GFP antibody (A11122, Invitrogen) for the measurement of oxGFP-positive cells. Following this, cells were washed 3 times for 10 min each time with PBS containing 0.1% Tween 20 and then incubated in the dark with a fluorescent goat anti-mouse IgG secondary antibody conjugated with DyLight 800 (Invitrogen, SA5-35521) for 1–2 h at room temperature. Finally, cells were washed 3 times for 10 min each time with PBS containing 0.1% Tween 20 and the fluorescence was recorded using a microplate reader (Odyssey, Li-Cor Biosciences, United States). Viral titers were calculated using the Spearman–Kärber algorithm.

Genetic stability assay

Vero cells were seeded on 6-well plate at 300,000 cells per well. Cells were infected at an MOI of 1 with P_0 supernatants corresponding to each of the rescued marker expressing viruses. After incubation for 2 h, the viral supernatants were removed, cells were washed once with PBS, and 2 mL of fresh growth medium was added. Cells were incubated for 5–15 days at 37°C. Viral supernatants (P_1 stocks) were collected and used for following passages performed as described above; supernatants from each passage (P_2, P_3, and P_4) were collected. FFA was used to quantify the titers of the rescued viruses in the collected virus stocks. mCherry expression was determined based on the signal intensity measurement using a Cellomics ArrayScan VTI microscope. oxGFP expression was detected using an immunofluorescence assay with an anti-GFP antibody (A11122, Invitrogen). For the measurement of NLuc activity, 96-well plate was infected with P_1 to P_4 stocks, according to the end-point titration method, and NLuc was measured using the Nano-Glo Luciferase Assay System (Promega) after cell lysis with 1X passive lysis buffer (E1941, Promega), using an EnVision plate reader (Plmer). The percentage of the virus-infected cells expressing reporters was calculated based on the ratio of the number of wells positive for the

TABLE 1 Primers used for RT-qPCR for viral RNA quantification.

Gene name	Primer sequences	Product size, bp
ZIKV	F: 5'CCGCTGCCCAACACAAG3'	53
	R: 5'CCACTAACGTTCTTTTGCAGACAT3'	
DENV-2	F: 5'CAGATCTCTGATGAATAACCAACG3'	95
	R: 5'CATTCCAAGTGAGAATCTCTTTGTCA3'	
GAPDH	F: 5'GCTCACTGGCATGGCCTTCCGTG3'	177
	R: 5'TGGAGGAGTGGGTGTCGCTGTTG3'	

marker (mCherry, NLuc, or oxGFP) and the number of wells positive for the virus (detected by staining with 4G2 antibody).

Western blot

Viral supernatant (8 mL) on a 3 mL 20% sucrose cushion was ultracentrifugated for 3 h at 100,000 × g at 4°C using an Optima L80-XP instrument (Beckman Coulter). After ultracentrifugation, the liquid was discarded, the tube was dried with Kimtech paper, and the pellet was resuspended in 80 µL of TNE buffer (10 mM TrisHCl (pH 7.0), 100 mM NaCl, and 1 mM EDTA). The obtained samples were denatured in 1× Laemmli buffer at 95°C for 10 min, and proteins were separated using electrophoresis on a 4–15% mini-protean-TGX-precastgel (Bio-Rad). Proteins were then transferred on nitrocellulose membranes using a semi-dry method using a transblot turbo transfer system (Bio-Rad). The membranes were blocked with 5% skimmed milk powder in Percentage of Tween20 for 30 min and incubated overnight at 4°C with either virus-specific primary capsid antibody (rabbit anti-capsid ZIKV GTX134186 in a 1:10,000 dilution; mouse anti-capsid DENV GTX633632 in a 1:3,000 dilution; and rabbit anti-capsid WNV GTX131947-S in a 1:100 dilution; all antibodies were obtained from GeneTex) or primary anti-pan flavivirus envelope antibody (mouse anti D1-4G2-4-15 [4G2] by NovusBio NBP2-52666 in a 1:1,000 dilution). Membranes were rinsed 3 times for 10 min each time in Percentage of Tween20 prior to incubation with an appropriate secondary antibody (anti-mouse IgG DyLight 800- and anti-rabbit IgG DyLight 800-conjugated antibodies SA5-35521 or SA5-35571 from Invitrogen) for 2 h at room temperature. Membranes were rinsed 3 times for 10 min each time in Percentage of Tween20 before being read on a Li-Cor Odyssey scanner 9120.

Immunofluorescence analysis

A total of 200,000 Vero cells were grown on 35 mm dishes (Fluorodish, Fisher) and infected at a multiplicity of infection (MOI) of 0.05 with P_0 (collected at day 5 post-transfection) stocks of all analyzed viruses. Infected cells were incubated for 3 (ZIKV, DENV2, and KUNV) or 4 (DENV4) days, after which they were fixed with 4% PFA (Fisher) for 30 min at 20°C. Fixed cells were rinsed with PBS, permeabilized with 0.1% Triton X-100, diluted in PBS for 5 min, and blocked with 2% BSA. Then, the cells were incubated in PBS supplemented with the pan-flavivirus anti-Env monoclonal antibody 4G2 (NovusBio, dilution 1:1,000) in the presence of 0.05% Saponin (Sigma-Aldrich, France) for 1 h, washed three times with PBS, and incubated with anti-mouse IgG secondary antibodies conjugated with Alexa647 (ab150107, Abcam, 1:1,000 dilution) or Alexa488 (A21202, Invitrogen, 1:10,000 dilution) for 2 h at 4°C in the dark. Nuclei were stained with 10 µg/mL Hoechst 33342 (Invitrogen) for 15 min. The stained cells were washed with PBS and epifluorescence and confocal images were acquired using a Cell-Discoverer 7 microscope (Carl Zeiss SAS, France) at 10× and 25× magnification. Mander's coefficients were calculated based on the images obtained using Zen Blue software (Zeiss).

RT-qPCR

The cells were infected with ZIKV and DENV2 and lysed using Luna Cell Ready Lysis reagent (New England Biolabs, United Kingdom). Quantification of viral RNA was performed with cell lysates using virus-specific primers, and their levels were normalized to GAPDH mRNA (Table 1). For these analyses, a Luna Universal One-Step RT-qPCR Kit (New England Biolabs) and a CFX opus real-time 384 system (Bio-Rad) were used. Cycling conditions were as follows: reverse transcription at 55°C for 15 min, followed by an initial polymerase activation at 95°C for 1 min, and then 45 cycles of denaturation at 95°C for 10 s and an annealing/extension at 60°C for 45 s. The calibration of the assay was performed with control plasmids containing sequences encoding ZIKV NS1 and DENV2 capsid proteins (Eurofins Genomics, Germany; GenBank accession numbers KU365778.1 and U87411.1, respectively). Primers were obtained from Eurofins Genomics (Germany).

Virus sequencing

Viral RNA (140 µL) from P_0 stocks collected at 7 days post-transfection were extracted using a QIAamp Viral RNA Extraction Kit (Qiagen). RT-PCRs were performed for each virus using TranscriptII One-Step RT-PCR SuperMix (Transgenbiotech, France) and the primers listed in Supplementary Table S1. Cycling conditions were as follows: reverse transcription at 50°C for 30 min, followed by an initial polymerase activation at 95°C for 5 min, and then 35 cycles of denaturation at 94°C for 30 s, annealing at 60°C for 30 s and an extension at 72°C for 4.5 min. Amplified cDNA fragments were separated by agarose gel electrophoresis and extracted from the gel using a Nucleospin Gel Clean-Up Kit (Macherey-Nagel). DNA sequencing was performed by Plasmidsaurus (Eugene, United States).

Antiviral assay

NITD008 (Bio-Techne 6045/1) was initially dissolved in 100% dimethyl sulfoxide (DMSO D8418, Sigma) at 10 mM and subsequently diluted in DMEM to the desired concentrations (0.05–15 µM). DMSO (0.5%) was set as the vehicle control. Cells were incubated with increasing concentrations of NITD008 for 2 h prior to infection. For cell fluorescence counting, 9,000 cells per well were cultured in a black opaque 96-well Microplate (PerkinElmer), infected with virus stock at an MOI of 0.01 (ZIKV-mCherry) or MOI 0.05 (DENV2-Ct-mCherry), and prepared for imaging at 72 h post-infection. Briefly, cells were fixed with 4% PFA and stained with 10 µg/mL Hoechst 33342 for 15 min and

washed with PBS. Image tiles acquisitions (3 × 2 per well) were performed at a magnification of 2.5 in wide-field on a Cell-Discoverer 7 microscope (Carl Zeiss SAS, France). Image analysis was performed using ZEN Blue software for segmenting of the stained nuclei and mCherry positive cells. The number of nuclei were sorted per well. The sum of fluorescence intensity was weighted against the normalized number of nuclei. For the measurement of NLuc activity, 20,000 cells were plated on a transparent 96-well plate and infected with ZIKV-NLuc at an MOI of 0.05. Luminescence was measured at 1 day post-infection using the Nano-Glo Luciferase Assay System (Promega) on the EnVision plate reader after cell lysis with 1X passive lysis buffer (E1941, Promega). Results were normalized to the total protein amount per well, which was determined using a BCA protein assay kit (Pierce). For wt viruses, 20,000 cells were cultured in a transparent 96-well plate and infected with DENV2-wt or ZIKV-wt at an MOI of 0.01 and 0.05, respectively. Seventy-two hours post-infection, cells were lysed and total viral RNA was extracted and quantified by RT-qPCR, as described above. In all cases, the 50% effective concentration (EC_{50}) was calculated by fitting the dose–response curves traced from 4parameter non-linear regression with GraphPad Prism v9.0, based on the following calculations: % Inhibition $=100-\left(drug-cell\ DMSO / infected\ cells-cell\ DMSO\right)\times 100$.

Transmission electron microscopy

Vero cells were infected at an MOI of 1, incubated for 3 days, fixed with 2.5% glutaraldehyde in PHEM buffer (PIPES 60 mM, HEPES 25 mM, EGTA 10 mM, and MgCl2 2 mM, all provided by Merck-Sigma, Germany), post-fixed in 1% OsO_4/0.8% $K_4Fe(CN)_6$, and then dehydrated in successive ethanol baths (50/70/90/100%).

Samples were then infiltrated in propylene oxide (MERCK-SIGMA, Germany)/EMbed812 (EMS, USA) mixes, embedded in EMbed812, and polymerized at 60°C. Ultrathin sections (70 nm) were cut using a PowerTome XL ultramicrotome (RMC, Tucson, AZ, United States), stained in 0.2% OTE/lead citrate, and observed on a Tecnai G2 F20 (200 kV FEG) TEM at the platform Plateau de Microscopie Electronique COMET, INM.

Atomic force microscopy

AFM imaging was performed on a JPK-Bruker Nanowizard IV XP atomic force microscope (JPK BioAFM, Bruker Nano GmbH, Berlin, Germany) operating in BSL-3 (Lyonnais et al., 2021). *Flavivirus* virions were imaged in imaging buffer (10 mM Tris–HCl [pH 7.5] and 100 mM NaCl) shortly after being adsorbed on a freshly cleaved muscovite surface (mica grade v1, Ted Pella) glued on a glass slide. Before virus adsorption, the mica was functionalized with 100 µL of Poly-L-lysine 0.1% (P8920, Sigma) for 10 min, then washed three times in imaging buffer. A three-dimensional printed plastic O-ring was glued around the mica to form a small liquid cell. Viral samples (20 µL) were deposited on the functionalized mica from 15 min to 1 h, and the volume was completed to 200 µL with the imaging buffer. AFM topographic images were obtained using the quantitative imaging (QI) mode using qp-Bio-AC CB2 (Nanosensors), BL-AC40TS (Olympus), or MLCT-Bio (Bruker) cantilevers. Before each set of acquisitions, the sensitivity and spring constant of the cantilever were calibrated (thermal noise method). The applied force was kept at 150–200 pN, 100 nm Z-length, and 20 msec/pixel speed. Using JPK SPM-data processing software, images were flattened with a polynomial/histogram line fit. Low-pass Gaussian and/or median filtering was applied to remove minor noise from the images. The Z-color scale in all images is given as relative after processing. Particle height analysis, based on the height (measured) channel of the QI mode, was performed using the cross section of the analysis software to calculate the maximal central height on each particle.

Statistical analysis

Statistical analysis was performed using GraphPad Prism 9.3.0 software. The results of marker expression were represented with error bars indicating the standard deviation (SD). One-way ANOVA followed by Tukey's multiple comparisons test was used for statistical analysis, as indicated in the figures.

Data availability statement

The datasets presented in this study can be found in online repositories. The names of the repository/repositories and accession number(s) can be found in the article/Supplementary material.

Ethics statement

Ethical approval was not required for the studies on animals in accordance with the local legislation and institutional requirements because only commercially available established cell lines were used.

Author contributions

LC, AT, NG, MH, MV, AN, GD, CC-B, AM, and SL performed the experiments. LC and AM constructed the icDNA clones. LC, AT, NG, MH, GD, and CC-B performed virus production, purification, viral titers, sequencing, immunoblots, infection kinetics, FFA, and data analysis. AT and SL performed AFM analysis. MV and SL performed fluorescence microscopy imaging and analysis. AN performed TEM imaging. NG, SL, AM, and DM conceived, directed, and supervised the study. SL, LC, NG, AT, AM, and DM wrote and edited the manuscript. AM and DM raised funding. All authors contributed to the article and approved the submitted version.

Funding

The BSL3 Bio-AFM was funded by the REDSAIM program at Montpellier University, the BSL3 Cell-Discoverer 7 microscope was funded by Occitanie FEDER. AM and LC were supported by the Estonian Research Council (PRG1154). DM was supported by CNRS, University of Montpellier, Region Occitanie and FEDER EU programme.

Acknowledgments

We thank Yannick Simonin from the University of Montpellier (France) for helpful discussions, Benoît Bordignon from MRI (CNRS Montpellier, France), and Julien Kissenberger from ZEISS France for help with data acquisition and image analysis. We thank the CNRS and Montpellier University for funding.

Conflict of interest

The authors declare that the research was conducted in the absence of any commercial or financial relationships that could be construed as a potential conflict of interest.

Publisher's note

All claims expressed in this article are solely those of the authors and do not necessarily represent those of their affiliated organizations, or those of the publisher, the editors and the reviewers. Any product that may be evaluated in this article, or claim that may be made by its manufacturer, is not guaranteed or endorsed by the publisher.

Supplementary material

The Supplementary material for this article can be found online at: https://www.frontiersin.org/articles/10.3389/fmicb.2023.1201640/full#supplementary-material

References

Aktepe, T. E., and Mackenzie, J. M. (2018). Shaping the flavivirus replication complex: it is curvaceous! *Cell. Microbiol.* 20:e12884. doi: 10.1111/cmi.12884

Aubry, F., Nougairède, A., Gould, E. A., and de Lamballerie, X. (2015). Flavivirus reverse genetic systems, construction techniques and applications: a historical perspective. *Antivir. Res.* 114, 67–85. doi: 10.1016/j.antiviral.2014.12.007

Ávila-Pérez, G., Nogales, A., Martín, V., Almazán, F., and Martínez-Sobrido, L. (2018). Reverse genetic approaches for the generation of recombinant Zika virus. *Viruses* 10:597. doi: 10.3390/v10110597

Baker, C., Liu, Y., Zou, J., Muruato, A., Xie, X., and Shi, P. Y. (2020). Identifying optimal capsid duplication length for the stability of reporter flaviviruses. *Emerg. Microbes Infect.* 9, 2256–2265. doi: 10.1080/22221751.2020.1829994

Baker, C., and Shi, P. Y. (2020). Construction of stable reporter Flaviviruses and their applications. *Viruses* 12:1082. doi: 10.3390/v12101082

Baker, C., Xie, X., Zou, J., Muruato, A., Fink, K., and Shi, P. Y. (2020). Using recombination-dependent lethal mutations to stabilize reporter flaviviruses for rapid serodiagnosis and drug discovery. *EBioMedicine* 57:102838. doi: 10.1016/j.ebiom.2020.102838

Barbi, L., Coelho, A. V. C., Alencar, L. C. A., and Crovella, S. (2018). Prevalence of Guillain-Barré syndrome among Zika virus infected cases: a systematic review and meta-analysis. *Braz. J. Infect. Dis.* 22, 137–141. doi: 10.1016/j.bjid.2018.02.005

Barnard, T. R., Abram, Q. H., Lin, Q. F., Wang, A. B., and Sagan, S. M. (2021). Molecular determinants of flavivirus virion assembly. *Trends Biochem. Sci.* 46, 378–390. doi: 10.1016/j.tibs.2020.12.007

Barreto-Vieira, D. F., Jácome, F. C., da Silva, M. A. N., Caldas, G. C., de Filippis, A. M. B., de Sequeira, P. C., et al. (2017). Structural investigation of C6/36 and Vero cell cultures infected with a Brazilian Zika virus. *PLoS One* 12:e0184397. doi: 10.1371/journal.pone.0184397

Bulich, R., and Aaskov, J. G. (1992). Nuclear localization of dengue 2 virus core protein detected with monoclonal antibodies. *J. Gen. Virol.* 73, 2999–3003. doi: 10.1099/0022-1317-73-11-2999

Caldas, L. A., Azevedo, R. C., da Silva, J. L., and de Souza, W. (2020). Microscopy analysis of Zika virus morphogenesis in mammalian cells. *Sci. Rep.* 10:8370. doi: 10.1038/s41598-020-65409-y

Che, P., Wang, L., and Li, Q. (2009). The development, optimization and validation of an assay for high throughput antiviral drug screening against dengue virus. *Int. J. Clin. Exp. Med.* 2, 363–373

Choi, K. H. (2021). The role of the stem-loop a RNA promoter in flavivirus replication. *Viruses* 13:1107. doi: 10.3390/v13061107

Colpitts, T. M., Conway, M. J., Montgomery, R. R., and Fikrig, E. (2012). West Nile virus: biology, transmission, and human infection. *Clin. Microbiol. Rev.* 25, 635–648. doi: 10.1128/CMR.00045-12

Cruz, D. J., Koishi, A. C., Taniguchi, J. B., Li, X., Milan, B. R., No, J. H., et al. (2013). High content screening of a kinase-focused library reveals compounds broadly-active against dengue viruses. *PLoS Negl. Trop. Dis.* 7:e2073. doi: 10.1371/journal.pntd.0002073

Deng, Y. Q., Zhang, N. N., Li, C. F., Tian, M., Hao, J. N., Xie, X. P., et al. (2016). Adenosine analog NITD008 is a potent inhibitor of Zika virus. *Open Forum Infect. Dis.* 3:ofw175. doi: 10.1093/ofid/ofw175

Edmonds, J., van Grinsven, E., Prow, N., Bosco-Lauth, A., Brault, A. C., Bowen, R. A., et al. (2013). A novel bacterium-free method for generation of flavivirus infectious DNA by circular polymerase extension reaction allows accurate recapitulation of viral heterogeneity. *J. Virol.* 87, 2367–2372. doi: 10.1128/JVI.03162-12

Faye, O., Faye, O., Diallo, D., Diallo, M., Weidmann, M., and Sall, A. A. (2013). Quantitative real-time PCR detection of Zika virus and evaluation with field-caught mosquitoes. *Virol. J.* 10:311. doi: 10.1186/1743-422X-10-311

Ferreira, G. P., Trindade, G. S., Vilela, J. M., Da Silva, M. I., Andrade, M. S., and Kroon, E. G. (2008). Climbing the steps of viral atomic force microscopy: visualization of dengue virus particles. *J. Microsc.* 231, 180–185. doi: 10.1111/j.1365-2818.2008.02028.x

Fischl, W., and Bartenschlager, R. (2013). High-throughput screening using dengue virus reporter genomes. *Methods Mol. Biol.* 1030, 205–219. doi: 10.1007/978-1-62703-484-5_17

Gould, E. A., and Solomon, T. (2008). Pathogenic flaviviruses. *Lancet* 371, 500–509. doi: 10.1016/S0140-6736(08)60238-X

Guabiraba, R., and Ryffel, B. (2014). Dengue virus infection: current concepts in immune mechanisms and lessons from murine models. *Immunology* 141, 143–156. doi: 10.1111/imm.12188

Gurukumar, K. R., Priyadarshini, D., Patil, J. A., Bhagat, A., Singh, A., Shah, P. S., et al. (2009). Development of real time PCR for detection and quantitation of dengue viruses. *Virol. J.* 6:10. doi: 10.1186/1743-422X-6-10

Hamel, R., Dejarnac, O., Wichit, S., Ekchariyawat, P., Neyret, A., Luplertlop, N., et al. (2015). Biology of Zika virus infection in human skin cells. *J. Virol.* 89, 8880–8896. doi: 10.1128/JVI.00354-15

Hu, M., Wu, T., Yang, Y., Chen, T., Hao, J., Wei, Y., et al. (2022). Development and characterization of a genetically stable infectious clone for a genotype I isolate of dengue virus serotype 1. *Viruses* 14:2073. doi: 10.3390/v14092073

Khanam, A., Gutiérrez-Barbosa, H., Lyke, K. E., and Chua, J. V. (2022). Immune-mediated pathogenesis in dengue virus infection. *Viruses* 14:2575. doi: 10.3390/v14112575

Koishi, A. C., Suzukawa, A. A., Zanluca, C., Camacho, D. E., Comach, G., and Duarte Dos Santos, C. N. (2018). Development and evaluation of a novel high-throughput image-based fluorescent neutralization test for detection of Zika virus infection. *PLoS Negl. Trop. Dis.* 12:e0006342. doi: 10.1371/journal.pntd.0006342

Kostyuchenko, V. A., Chew, P. L., Ng, T. S., and Lok, S. M. (2014). Near-atomic resolution cryo-electron microscopic structure of dengue serotype 4 virus. *J. Virol.* 88, 477–482. doi: 10.1128/JVI.02641-13

Kuhn, R. J., Zhang, W., Rossmann, M. G., Pletnev, S. V., Corver, J., Lenches, E., et al. (2002). Structure of dengue virus: implications for flavivirus organization, maturation, and fusion. *Cells* 108, 717–725. doi: 10.1016/s0092-8674(02)00660-8

Li, L. H., Kaptein, S. J. F., Schmid, M. A., Zmurko, J., Leyssen, P., Neyts, J., et al. (2020). A dengue type 2 reporter virus assay amenable to high-throughput screening. *Antivir. Res.* 183:104929. doi: 10.1016/j.antiviral.2020.104929

Li, X. F., Li, X. D., Deng, C. L., Dong, H. L., Zhang, Q. Y., Ye, Q., et al. (2017). Visualization of a neurotropic flavivirus infection in mouse reveals unique viscerotropism controlled by host type I interferon signaling. *Theranostics* 7, 912–925. doi: 10.7150/thno.16615

Lima, M. E. S., Bachur, T. P. R., and Aragão, G. F. (2019). Guillain-Barre syndrome and its correlation with dengue, Zika and chikungunya viruses infection based on a literature review of reported cases in Brazil. *Acta Trop.* 197:105064. doi: 10.1016/j.actatropica.2019.105064

Lyonnais, S., Hénaut, M., Neyret, A., Merida, P., Cazevieille, C., Gros, N., et al. (2021). Atomic force microscopy analysis of native infectious and inactivated SARS-CoV-2 virions. *Sci. Rep.* 11:11885. doi: 10.1038/s41598-021-91371-4

Mackenzie, J. M., Jones, M. K., and Young, P. R. (1996). Improved membrane preservation of flavivirus-infected cells with cryosectioning. *J. Virol. Methods* 56, 67–75. doi: 10.1016/0166-0934(95)01916-2

Mackenzie, J. M., Khromykh, A. A., and Westaway, E. G. (2001). Stable expression of noncytopathic Kunjin replicons simulates both ultrastructural and biochemical characteristics observed during replication of Kunjin virus. *Virology* 279, 161–172. doi: 10.1006/viro.2000.0691

Mazeaud, C., Freppel, W., and Chatel-Chaix, L. (2018). The multiples fates of the Flavivirus RNA genome during pathogenesis. *Front. Genet.* 9:595. doi: 10.3389/fgene.2018.00595

McCormick, K. D., Liu, S., Jacobs, J. L., Marques, E. T. Jr., Sluis-Cremer, N., and Wang, T. (2012). Development of a robust cytopathic effect-based high-throughput screening assay to identify novel inhibitors of dengue virus. *Antimicrob. Agents Chemother.* 56, 3399–3401. doi: 10.1128/AAC.06425-11

McGee, C. E., Shustov, A. V., Tsetsarkin, K., Frolov, I. V., Mason, P. W., Vanlandingham, D. L., et al. (2010). Infection, dissemination, and transmission of a West Nile virus green fluorescent protein infectious clone by *Culex pipiens* quinquefasciatus mosquitoes. *Vector Borne Zoonotic Dis.* 10, 267–274. doi: 10.1089/vbz.2009.0067

Mishin, V. P., Cominelli, F., and Yamshchikov, V. F. (2001). A 'minimal' approach in design of flavivirus infectious DNA. *Virus Res.* 81, 113–123. doi: 10.1016/s01681702(01)00371-9

Mutso, M., Saul, S., Rausalu, K., Susova, O., Žusinaite, E., Mahalingam, S., et al. (2017). Reverse genetic system, genetically stable reporter viruses and packaged subgenomic replicon based on a Brazilian Zika virus isolate. *J. Gen. Virol.* 98, 2712–2724. doi: 10.1099/jgv.0.000938

Netsawang, J., Noisakran, S., Puttikhunt, C., Kasinrerk, W., Wongwiwat, W., Malasit, P., et al. (2010). Nuclear localization of dengue virus capsid protein is required for DAXX interaction and apoptosis. *Virus Res.* 147, 275–283. doi: 10.1016/j.virusres.2009.11.012

Pan, Y., Cai, W., Cheng, A., Wang, M., Yin, Z., and Jia, R. (2022). Flaviviruses: innate immunity, Inflammasome activation, inflammatory cell death, and cytokines. *Front. Immunol.* 13:829433. doi: 10.3389/fimmu.2022.829433

Pierson, T. C., and Diamond, M. S. (2020). The continued threat of emerging flaviviruses. *Nat. Microbiol.* 5, 796–812. doi: 10.1038/s41564-020-0714-0

Pu, S. Y., Wu, R. H., Yang, C. C., Jao, T. M., Tsai, M. H., Wang, J. C., et al. (2011). Successful propagation of flavivirus infectious cDNAs by a novel method to reduce the cryptic bacterial promoter activity of virus genomes. *J. Virol.* 85, 2927–2941. doi: 10.1128/JVI.01986-10

Ruggli, N., and Rice, C. M. (1999). Functional cDNA clones of the Flaviviridae: strategies and applications. *Adv. Virus Res.* 53, 183–207. doi: 10.1016/s0065-3527(08)60348-6

Samsa, M. M., Mondotte, J. A., Caramelo, J. J., and Gamarnik, A. V. (2012). Uncoupling cis-acting RNA elements from coding sequences revealed a requirement of the N-terminal region of dengue virus capsid protein in virus particle formation. *J. Virol.* 86, 1046–1058. doi: 10.1128/JVI.05431-11

Sangiambut, S., Keelapang, P., Aaskov, J., Puttikhunt, C., Kasinrerk, W., Malasit, P., et al. (2008). Multiple regions in dengue virus capsid protein contribute to nuclear localization during virus infection. *J. Gen. Virol.* 89, 1254–1264. doi: 10.1099/vir.0.83264-0

Santos, J. J., Cordeiro, M. T., Bertani, G. R., Marques, E. T., and Gil, L. H. (2014). A two-plasmid strategy for engineering a dengue virus type 3 infectious clone from primary Brazilian isolate. *An. Acad. Bras. Cienc.* 86, 1749–1759. doi: 10.1590/0001-3765201420130332

Santos, J. J., Magalhães, T., Silva Junior, J. V., Silva, A. N., Cordeiro, M. T., and Gil, L. H. (2015). Full-length infectious clone of a low passage dengue virus serotype 2 from Brazil. *Mem. Inst. Oswaldo Cruz* 110, 677–683. doi: 10.1590/0074-02760150053

Schoggins, J. W., Dorner, M., Feulner, M., Imanaka, N., Murphy, M. Y., Ploss, A., et al. (2012). Dengue reporter viruses reveal viral dynamics in interferon receptor-deficient mice and sensitivity to interferon effectors in vitro. *Proc. Natl. Acad. Sci. U. S. A.* 109, 14610–14615. doi: 10.1073/pnas.1212379109

Sevvana, M., Long, F., Miller, A. S., Klose, T., Buda, G., Sun, L., et al. (2018). Refinement and analysis of the mature Zika virus Cryo-EM structure at 3.1 Å resolution. *Structure* 26, 1169–1177.e3. doi: 10.1016/j.str.2018.05.006

Shan, C., Xie, X., Muruato, A. E., Rossi, S. L., Roundy, C. M., Azar, S. R., et al. (2016). An infectious cDNA clone of Zika virus to study viral virulence, mosquito transmission, and antiviral inhibitors. *Cell Host Microbe* 19, 891–900. doi: 10.1016/j.chom.2016.05.004

Shum, D., Smith, J. L., Hirsch, A. J., Bhinder, B., Radu, C., Stein, D. A., et al. (2010). High-content assay to identify inhibitors of dengue virus infection. *Assay Drug Dev. Technol.* 8, 553–570. doi: 10.1089/adt.2010.0321

Sirohi, D., Chen, Z., Sun, L., Klose, T., Pierson, T. C., Rossmann, M. G., et al. (2016). The 3.8 Å resolution cryo-EM structure of Zika virus. *Science* 352, 467–470. doi: 10.1126/science.aaf5316

Stollar, V., Schlesinger, R. W., and Stevens, T. M. (1967). Studies on the nature of dengue viruses. III. RNA synthesis in cells infected with type 2 dengue virus. *Virology* 33, 650–658. doi: 10.1016/0042-6822(67)90065-7

Suphatrakul, A., Duangchinda, T., Jupatanakul, N., Prasittisa, K., Onnome, S., Pengon, J., et al. (2018). Multi-color fluorescent reporter dengue viruses with improved stability for analysis of a multi-virus infection. *PLoS One* 13:e0194399. doi: 10.1371/journal.pone.0194399

Tan, T. Y., Fibriansah, G., Kostyuchenko, V. A., Ng, T. S., Lim, X. X., Zhang, S., et al. (2020). Capsid protein structure in Zika virus reveals the flavivirus assembly process. *Nat. Commun.* 11:895. doi: 10.1038/s41467-020-14647-9

Therkelsen, M. D., Klose, T., Vago, F., Jiang, W., Rossmann, M. G., and Kuhn, R. J. (2018). Flaviviruses have imperfect icosahedral symmetry. *Proc. Natl. Acad. Sci. U. S. A.* 115, 11608–11612. doi: 10.1073/pnas.1809304115

van Leur, S. W., Heunis, T., Munnur, D., and Sanyal, S. (2021). Pathogenesis and virulence of flavivirus infections. *Virulence* 12, 2814–2838. doi: 10.1080/21505594.2021.1996059

Volkova, E., Tsetsarkin, K. A., Sippert, E., Assis, F., Liu, G., Rios, M., et al. (2020). Novel approach for insertion of heterologous sequences into full-length ZIKV genome results in superior level of gene expression and insert stability. *Viruses* 12:61. doi: 10.3390/v12010061

Weaver, S. C., and Barrett, A. D. (2004). Transmission cycles, host range, evolution and emergence of arboviral disease. *Nat. Rev. Microbiol.* 2, 789–801. doi: 10.1038/nrmicro1006

Welsch, S., Miller, S., Romero-Brey, I., Merz, A., Bleck, C. K., Walther, P., et al. (2009). Composition and three-dimensional architecture of the dengue virus replication and assembly sites. *Cell Host Microbe* 5, 365–375. doi: 10.1016/j.chom.2009.03.007

Wen, Z., Song, H., and Ming, G. L. (2017). How does Zika virus cause microcephaly? *Genes Dev.* 31, 849–861. doi: 10.1101/gad.298216.117

Westaway, E. G., Mackenzie, J. M., Kenney, M. T., Jones, M. K., and Khromykh, A. A. (1997). Ultrastructure of Kunjin virus-infected cells: colocalization of NS1 and NS3 with double-stranded RNA, and of NS2B with NS3, in virus-induced membrane structures. *J. Virol.* 71, 6650–6661. doi: 10.1128/JVI.71.9.6650-6661.1997

Wilson, H. L., Tran, T., Druce, J., Dupont-Rouzeyrol, M., and Catton, M. (2017). Neutralization assay for Zika and dengue viruses by use of real-time-PCR-based endpoint assessment. *J. Clin. Microbiol.* 55, 3104–3112. doi: 10.1128/JCM.00673-17

Xu, H. T., Colby-Germinario, S. P., Hassounah, S. A., Fogarty, C., Osman, N., Palanisamy, N., et al. (2017). Evaluation of Sofosbuvir (β-D-2′-deoxy2′-α-fluoro-2'-β-C-methyluridine) as an inhibitor of dengue virus replication. *Sci. Rep.* 7:6345. doi: 10.1038/s41598-017-06612-2

Yin, Z., Chen, Y. L., Schul, W., Wang, Q. Y., Gu, F., Duraiswamy, J., et al. (2009). An adenosine nucleoside inhibitor of dengue virus. *Proc. Natl. Acad. Sci. U. S. A.* 106, 20435–20439. doi: 10.1073/pnas.0907010106

Yun, S. I., Choi, Y. J., Yu, X. F., Song, J. Y., Shin, Y. H., Ju, Y. R., et al. (2007). Engineering the Japanese encephalitis virus RNA genome for the expression of foreign genes of various sizes: implications for packaging capacity and RNA replication efficiency. *J. Neurovirol.* 13, 522–535. doi: 10.1080/13550280701684651

Zhang, W., Chipman, P., Corver, J., Johnson, P. R., Zhang, Y., Mukhopadhyay, S., et al. (2003). Visualization of membrane protein domains by cryo-electron microscopy of dengue virus. *Nat. Struct. Mol. Biol.* 10, 907–912. doi: 10.1038/nsb990

Zhang, J. W., Wang, H., Liu, J., Ma, L., Hua, R. H., and Bu, Z. G. (2021). Generation of a stable GFP-reporter Zika virus system for high-throughput screening of Zika virus inhibitors. *Virol. Sin.* 36, 476–489. doi: 10.1007/s12250-020-00316-0

Zhang, X., Zhang, Y., Jia, R., Wang, M., Yin, Z., and Cheng, A. (2021). Structure and function of capsid protein in flavivirus infection and its applications in the development of vaccines and therapeutics. *Vet. Res.* 52:98. doi: 10.1186/s13567-021-00966-2

Zheng, X., Tong, W., Liu, F., Liang, C., Gao, F., Li, G., et al. (2016). Genetic instability of Japanese encephalitis virus cDNA clones propagated in *Escherichia coli*. *Virus Genes* 52, 195–203. doi: 10.1007/s11262-016-1289-y

Zou, G., Xu, H. Y., Qing, M., Wang, Q. Y., and Shi, P. Y. (2011). Development and characterization of a stable luciferase dengue virus for high-throughput screening. *Antivir. Res.* 91, 11–19. doi: 10.1016/j.antiviral.2011.05.001

frontiers | Frontiers in Microbiology

TYPE Original Research
PUBLISHED 12 October 2023
DOI 10.3389/fmicb.2023.1258810

OPEN ACCESS

EDITED BY
Ke Liu,
Chinese Academy of Agricultural Sciences, China

REVIEWED BY
Mel C. Melendrez,
Anoka-Ramsey Community College, United States
Devojit Kumar Sarma,
ICMR-National Institute for Research in Environmental Health, India

*CORRESPONDENCE
Jun Hang
jun.hang.civ@health.mil

†These authors have contributed equally to this work

RECEIVED 04 August 2023
ACCEPTED 27 September 2023
PUBLISHED 12 October 2023

CITATION
Potter-Birriel JM, Pollio AR, Knott BD, Chunashvili T, Fung CK, Conte MA, Reinbold-Wasson DD and Hang J (2023) Metagenomics analysis reveals presence of the Merida-like virus in Georgia.
Front. Microbiol. 14:1258810.
doi: 10.3389/fmicb.2023.1258810

Metagenomics analysis reveals presence of the Merida-like virus in Georgia

Jennifer M. Potter-Birriel[1†], Adam R. Pollio[1†], Brian D. Knott[2], Tamar Chunashvili[2], Christian K. Fung[1], Matthew A. Conte[1], Drew D. Reinbold-Wasson[2] and Jun Hang[1*]

[1]Walter Reed Army Institute of Research, Silver Spring, MD, United States, [2]U.S. Army Medical Research Directorate – Georgia (USAMRD-G), Walter Reed Army Institute of Research, Tbilisi, Georgia

Arbovirus surveillance is fundamental for the discovery of novel viruses and prevention of febrile vector-borne illnesses. Vector-borne pathogens can rapidly expand and adapt in new geographic and environmental conditions. In this study, metagenomic surveillance was conducted to identify novel viruses in the Country of Georgia. A total of 521 mosquitoes were captured near a military training facility and pooled from species *Culex pipiens* (Linnaeus) (87%) and *Aedes albopictus* (Skuse) (13%). We decided to further analyze the *Culex pipiens* mosquitoes, due to the more extensive number of samples collected. Our approach was to utilize an unbiased total RNA-seq for pathogen discovery in order to explore the mosquito virome. The viral reads from this analysis were mostly aligned to Insect-specific viruses from two main families, the *Iflaviridae*; a positive-stranded RNA virus and the *Rhabdoviridae*; a negative- and single-stranded RNA virus. Our pathogen discovery analysis revealed viral reads aligning to the Merida-like virus Turkey (MERDLVT) strain among the *Rhabdoviridae*. To further validate this result, we conducted a BLAST sequence comparison analysis of our samples with the MERDLVT strain. Our positive samples aligned to the MERDLVT strain with 96–100% sequence identity and 99.7–100% sequence coverage. A bootstrapped maximum-likelihood phylogenetic tree was used to evaluate the evolutionary relationships among these positive pooled specimens with the (MERDLVT) strain. The Georgia samples clustered most closely with two strains from Turkey, the Merida-like virus KE-2017a isolate 139-1-21 and the Merida-like virus Turkey isolate P431. Collectively, these results show the presence of the MERDLVT strain in Georgia.

KEYWORDS

mosquito, *Culex pipiens*, pathogen discovery, vector control, Merida like-virus, NGS

Introduction

Vector-borne pathogens (VBPs) are one of the main causes of human infections worldwide (Kilpatrick and Randolph, 2012; de Almeida et al., 2021). The geographic boundaries of these vectors continue to expand and adapt around the world's changing climate (Kilpatrick and Randolph, 2012). For this reason, pathogen discovery becomes increasingly important for arbovirus surveillance and the prevention of VBPs. The most prominent and emerging viruses belong to the *Flaviviridae* family. Flaviviruses are positive-stranded RNA viruses, that are recognized to have the capacity to globally infect and cause a spectrum of several diseases (Pierson and Diamond, 2020; Cuevas-Juarez et al., 2021). This family include several significant human pathogens including Yellow Fever virus (YFV), Zika virus (ZIKV), and Dengue virus

(DENV) (Pierson and Diamond, 2020; Cuevas-Juarez et al., 2021). Another major vector-borne virus family, *Rhabdoviridae*, are single-stranded negative RNA viruses, characterized for being ubiquitous, with the ability to infect a wide range of species including plants, vertebrates, and invertebrates (Dietzgen et al., 2017). Two well-known rhabdoviruses include the rabies virus which causes disease in various animals and the infectious hematopoietic necrosis virus which causes disease in salmonid fish. Rhabdoviruses have been shown to exhibit rapid mutation rates and complex genome evolution including gains and losses of genes (Walker et al., 2015). This constant evolution of new variants has made it difficult to the scientific community to develop new vaccines. For this reason, efforts to expand mosquito-borne surveillance in developing countries must continue to be a main priority to keep up with the evolution of emerging viral diseases.

The advances of sequencing metagenomic analysis has led to the discovery of new viruses worldwide, leading to the detection and prevention of emerging viruses. A group of viruses that continues to be detected in mosquitoes are the Insect-specific viruses (ISVs). ISVs can naturally infect and replicate in arthropod hosts. An example of ISVs is the Culex Iflavi-like virus 4 which belongs to the *Iflaviridae* family; a positive-stranded RNA virus (Valles et al., 2017). In recent studies, researchers conducted studies to understand how these ISVs interact with pathogenic arboviruses and how it can be of benefit for vector borne disease control. Continued research will help to develop biotechnology tools that can serve as vector controls to reduce or restrict arboviral diseases (Liu et al., 2011; Bolling et al., 2012; Agboli et al., 2019). In addition, other groups are using ISVs as expression tools against arboviruses for the development of new vaccines (Erasmus et al., 2018). ISVs is gaining interest as potential vectors to restrict pathogenic hosts due to its inability to infect vertebrates (Agboli et al., 2019).

Here, we report the presence of the Merida virus in Senaki, a town within the country of Georgia. The Merida virus was discovered in *Culex pipiens* mosquitoes collected in various sites of a Georgia military facility. Metagenomic analysis was executed using the Chan Zuckerberg ID (CZ ID) cloud-based pipeline; results were further evaluated using phlyogenetics to determine the likely evolutionary origin of our samples. The Merida virus is classified as a rhabdovirus, a single-stranded, negative RNA virus that was originally discovered in the Yucatan Peninsula of Mexico (Charles et al., 2016).

Materials and methods

Mosquito collection

Adult host seeking mosquitoes were collected using multiple traps: BG Sentinel 2 (Biogents AG, Regensburg, Germany), CDC light trap (Model 1,012 and 1,212, John W. Hock Company, Gainesville, FL), Stealth Trap (Model 214, John W. Hock Company, Gainesville, FL), and Fay-Prince Trap (Model 812, John W. Company, Gainesville, FL). Collection traps were placed on a tree that was either next to a pond or a pile of tires. Larval dipping collection focused on small water filled containers and larger water pools in order to collect immature mosquitoes. The larval mosquitoes were then allowed to mature in sealed containers then collected as adults. Mosquito collections were conducted between August 2018 and June 2019, in the town of Senaki, located in the Samegrelo-Zemo Svaneti region of Georgia. Mosquitoes were morphologically identified using a stereomicroscope (Leica S4E, Leica microsystems, Germany) and the ECDC MosKey Tool.[1] Female mosquitoes were sorted into pools of no more than 20 individuals and stored at −80°C. Specimens were shipped frozen from Tbilisi, Georgia to Silver Spring, Maryland, United States. Where they were processed for advanced molecular characterization at the Walter Reed Army Institute of Research, Viral Detection Branch (WRAIR VDB).

RNA extraction of mosquito pools

Mosquitos were homogenized by bead-beating with the Bio Spec Mini-Bead Beater 16 (Bio Spec Products Inc., Bartlesville, OK, United States). The mosquitos' homogenates were centrifuged, and the supernatant was treated with DNase I, Benzonase nuclease and RNase A as described in Sanborn et al. (2019). Lysis and RNA extraction was performed using the 5XMag MAX Pathogen RNA/DNA kit (Cat# 4462359) with the Thermo Scientific Kingfisher Flex by following the manufacturer's user guides.

RNA amplification, library preparation, and sequencing

Random reverse transcription and PCR amplification (RT-PCR) was conducted on the purified nucleic acid as described by Sanborn et al. (2019). The RT-PCR amplicons were purified and quantified using the Quant-iT™ Pico Green™ dsDNA Assay (Thermo Fisher Scientific). Library prep was made using the DNA Prep library prep kit (Illumina, San Diego, CA, United States) (Product # 20060059). Libraries were quantitated using Tape Station, D5000 Screen Tape (Agilent Technologies, Inc., Santa Clara, CA, United States), pooled at equal molar concentrations, and sequenced using Illumina MiSeq system and Sequencing Reagent Kit v3 (600-cycle) (Product # MS-102-3003).

Metagenomics data analyses

Data analysis was performed by uploading MiSeq raw sequence read data to CZID.org (Ramesh et al., 2019; Saha et al., 2019; Kalantar et al., 2020) followed by the metagenomic analysis function within the site. The data was then sorted by reference from the NCBI database. Heat maps were also generated by CZID.org.

We further verified our results by using our in-house *de novo* pipeline previously described (Kilianski et al., 2015).This is a preprocessing step using Cutadapt (Martin, 2011) and Prinseq (Schmieder and Edwards, 2011), followed by a de-novo assembly using RAY Meta (Boisvert et al., 2012). The resulting contigs are then further combined using Cap3 (Huang and Madan, 1999). The final scaffold is then categorized with iterative BLAST against the NCBI nucleotide database (nr/nt).

The Merida-like virus KE-2017a (accession number NC_040532.1) was used as a reference to map sequence reads on Geneious prime. The resulting sequences were then aligned to remove sequencing artifacts followed by a BLAST to show sequence similarity and identity. We then identified the individual ORFs using BLASTp for our annotation.

RASTtk (Brettin et al., 2015) with the "correct frame shift" option was used to annotate the assembled genome sequence. We referenced Merida virus (Taxon ID: 1803034) to build and identify ORFs.

1 https://www.medilabsecure.com/moskeytool.html

We then compared those results using the protein search tool BLASTp (Altschul et al., 1990). Proteins with low similarity were not reported.

Phylogenetic analyses

We compared 10 whole genome Merida-like virus (Georgia) sequences with 30 publicly available Merida-like viruses sequences, including Hirame rhabdovirus, Infectious hematopoietic necrosis virus, Zahedan rhabdovirus, Long Island tick rhabdovirus, Moussa virus, Arborteum virus, Puerto Almendras virus, Bovine ephemeral fever virus, Kimberley virus, Coastal Plain virus, Tibrogargan virus, Shayang Fly Virus 2 strain, *Drosophila melanogaster* sigmavirus AP30, Wuhan Louse Fly Virus 9 strain, Iriri virus nucleoprotein, European bat 1 lyssavirus, Australian bat lyssavirus, Rabies virus, Bole Tick Virus 2 strain, Culex tritaeniorhynchus rhabdovirus, Culex rhabdovirus strain CRV (Ticino, Switzerland), Merida virus isolate XY14959 nucleoprotein, Merida virus isolate CC_H, Culex rhabdovirus strain CRV (Kern, California), Merida virus isolate MERDV-2020, Merida virus isolate CMS002, Merida virus isolate MERD-Mex07, Merida virus OTU4, Merida-like virus KE-2017a isolate, and Merida-like virus isolate P431. The sequences were aligned using MAFFT version v7.475 using the high-speed setting (Katoh and Standley, 2013). This alignment quality was inspected and confirmed in Geneious, and a phylogenetic tree was constructed using IQ-TREE version 2.0.3 with Model Finder to determine the most appropriate model and the following specific settings: "-ninit 2 -bb 1,000 -nt 4" (Kalyaanamoorthy et al., 2017; Hoang et al., 2018). The resulting tree was edited using FigTree version 1.4.4.

Results and discussion

Mosquito collections in the country of Georgia

Mosquito sampling was conducted at 10 sites in Senaki, a town in Samegrelo-Zemo Svaneti region located in western Georgia. These collections were made in 2018 and 2019 on a Georgia military training base, the coordinates of each site were recorded using the Global Positioning System (GPS) (Figure 1A; Supplementary Table S1). A total of 521 mosquitoes were captured and distributed into 45 pools from species *Culex pipiens* (87%) and *Aedes albopictus* (13%) (Figure 1B). Due to the more extensive number of samples collected, we decided to further analyze *Culex pipiens* mosquitoes. Figure 1C illustrates the number of *Culex pipiens* mosquitoes collected each year.

Detection of the Merida-like virus KE-2017a in pooled specimens collected in Senaki

To explore the viral diversity of the town of Senaki, we conducted an unbiased total RNA-seq approach to identify viruses in this specific

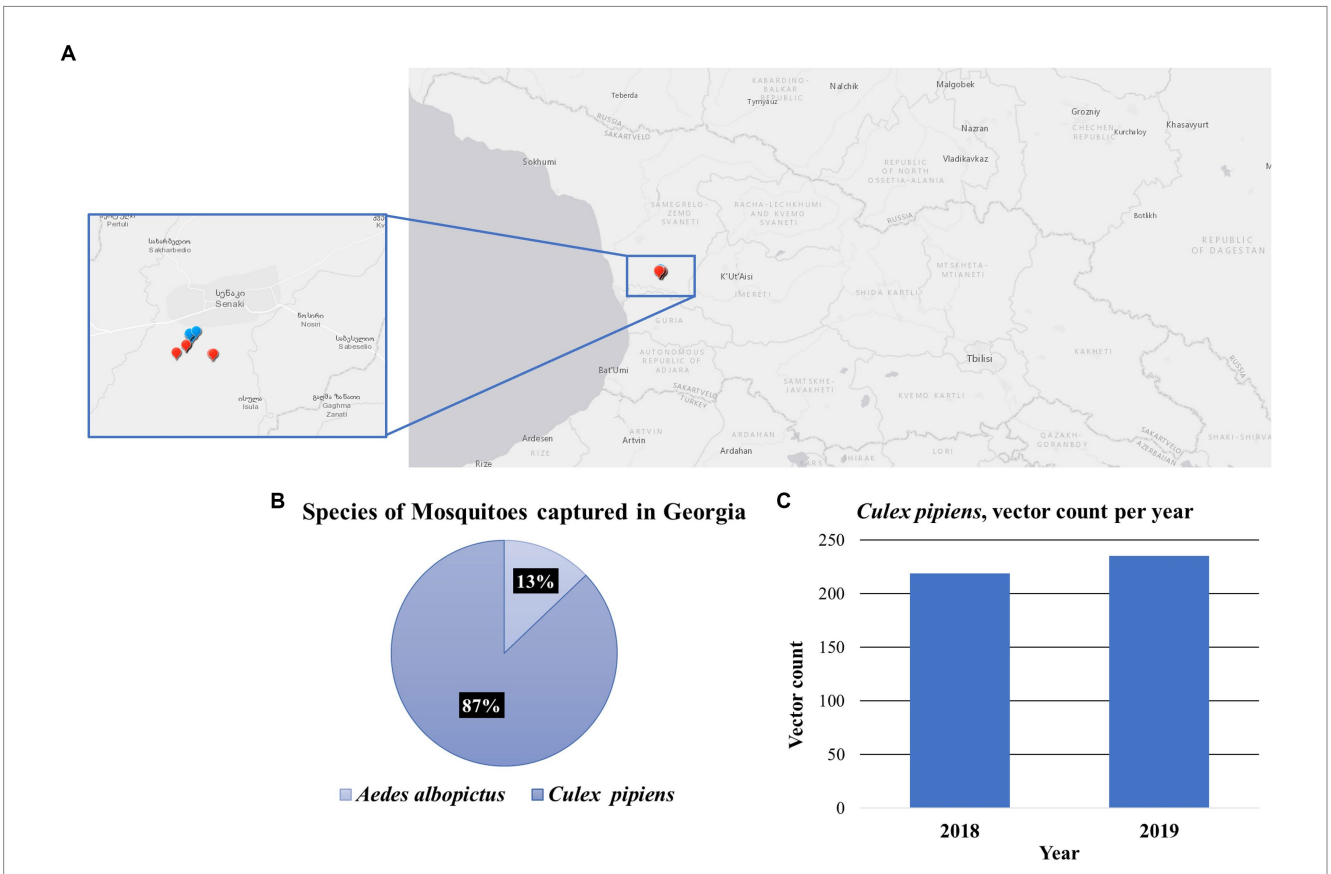

FIGURE 1
Mosquito collections in the Country of Georgia. **(A)** A map containing the location for each collection site, in the Senaki area. Each dot represents the collection site, 2018 (blue) and 2019 (red). **(B)** Species of mosquitoes captured in Georgia. Chart illustrates the percentage of the two species of mosquitoes captured, the *Culex pipiens* 87% and the *Aedes albopictus* 13%. **(C)** The vector count of *Culex pipiens* mosquitoes captured per year, 2018 (*N*=219) and 2019 (*N*=235).

area. This methodology was previously described and published by us (Hang et al., 2012; Sanborn et al., 2019; Pollio et al., 2022). A total of 37 pooled samples were prepared using the Illumina sequencing system. To analyze our Next-generation sequencing (NGS) raw data, we utilized the CZ ID cloud-based pipeline, a computational tool to detect microbial pathogens (Kalantar et al., 2020). With this computational tool, we obtained an average read passing filter per sample of 203,822. Sequences were aligned to the NCBI's database of nucleotide sequences to calculate rPM (reads per million) and classified into three kingdoms. The total reads per kingdom are the following: Bacteria (1,430,993,14%), Eukaryote (445,670, 4%) and Virus (8,775,711, 82%) (Figure 2A). Most of our sequencing reads were aligned to viruses (82%); thus, we decided to further explore and compare the viral diversity between the years 2018 and 2019 (Figure 2B).

A heat map was built, to analyze the presence and abundance of viral reads in our samples. The heat map was set to NT rPM > =10 which shows viruses with at least 10 reads per million aligned reads to simplify our overall analysis (Figure 3). The most abundant viruses aligned to ISVs including: the Culex Iflavi-like virus 4 (2,167,511.86), and the Merida-like virus KE-2017a (1,304,966.73) (Supplementary Figure S1). These results indicate the abundance of two main families in our pooled samples: the *Iflaviridae*; a positive-stranded RNA virus and the

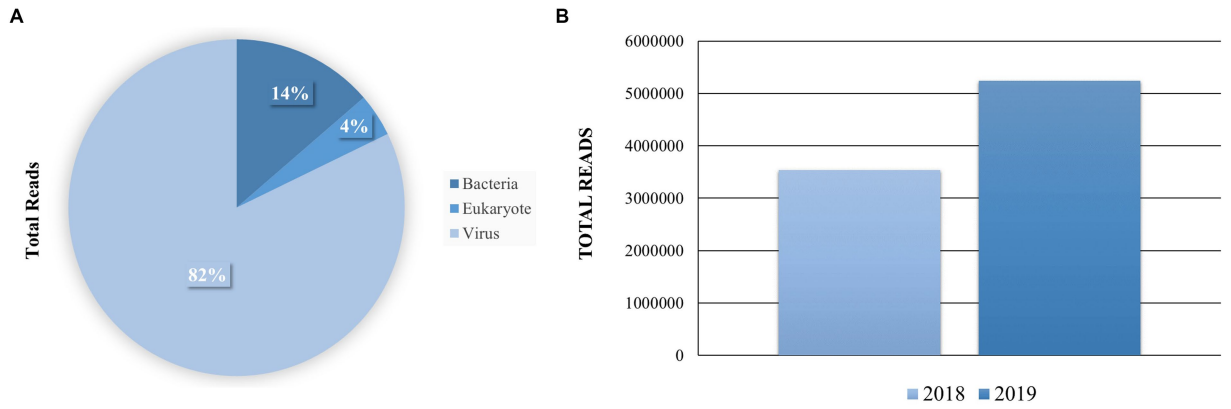

FIGURE 2
Distribution of the total reads per sample and taxonomy kingdom. **(A)** The total reads per sample were queried to the NCBI database using CZ ID and STAR. The mapped Super kingdom data is shown Bacteria 1,430,993 (14%), Eukaryote 445,670 (4%) and Virus 8,775,711 (82%). **(B)** Comparison of sequencing reads that were aligned to viruses per sample.

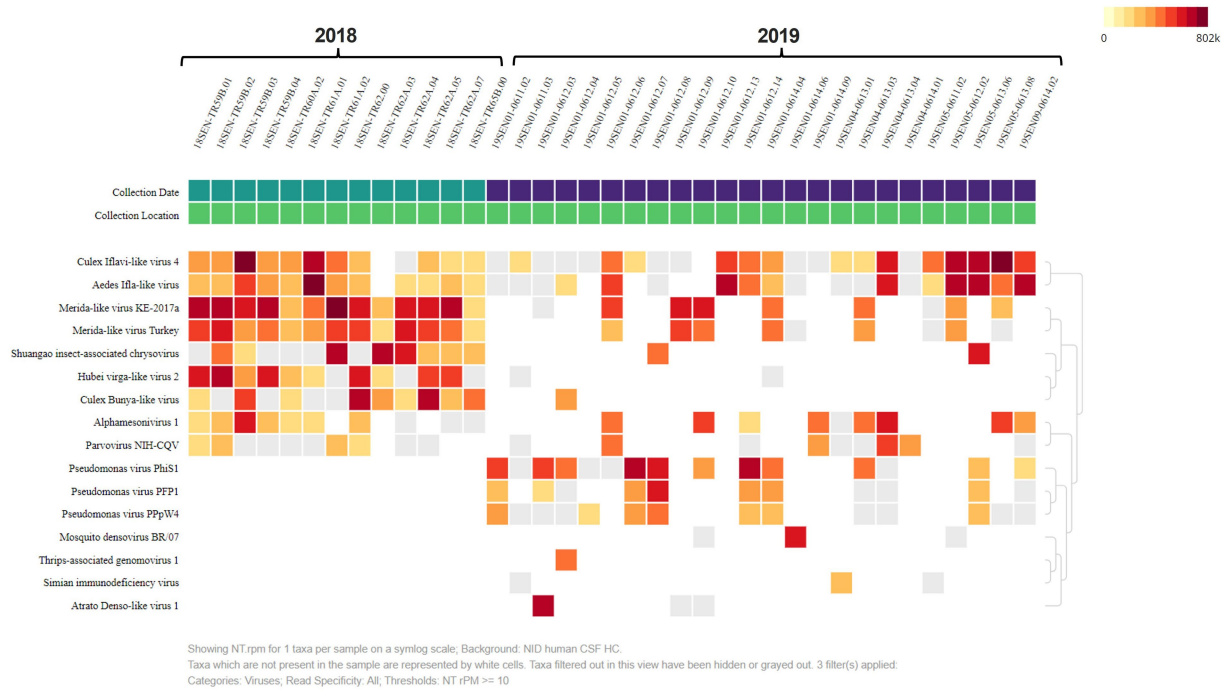

FIGURE 3
Heat Map analysis shows virus diversity in collected samples. The heat map was set to NT rPM > =10 which only shows viruses with at least 10 reads per million. Samples are divided by collection date. The most abundant viruses aligned to insect-specific viruses including: the Culex Iflavi-like virus 4, Merida-like virus KE-2017a and the Merida-like virus Turkey.

Rhabdoviridae; a single-stranded, negative RNA virus. We found the Merida-like virus KE-2017a in most of the collected pooled samples from 2018 (Figure 3). The Merida virus was first detected in the *Culex quinquefasciatus* species in the Yucatan Peninsula of Mexico and classified as a Rhabdovirus (Charles et al., 2016). This virus has been detected in other places around the world (Charles et al., 2016; Ergunay et al., 2017; Sadeghi et al., 2018; da Silva Neves et al., 2021). Airborne surveillance conducted in Thrace and Anatolia, two regions from Turkey recently identified the Merida-like virus Turkey (MERDLVT) (Ergunay et al., 2017). This virus is closely related to the Merida virus detected in Mexico. Due to the proximity of Georgia to Turkey, these results could imply a migration of the Merida virus.

Evolutionary analysis confirms the presence of the Merida-like virus

We used phylogenetic tools to further evaluate the relationship of these positive pooled specimens with the Merida virus. The phylogenetic analysis indicates that our positive samples are closely related to two viruses from mosquitoes collected in Turkey, the Merida-like virus KE-2017a and the MERDLVT (Figure 4). 81% of ultrafast bootstrap replicates supported the common ancestor node that places the two samples from Turkey with two samples from Georgia (Merida_virus_Georgia_OQ725976 and Merida_virus_Georgia_OQ725975). To further confirm the previous analysis, we used the BLAST

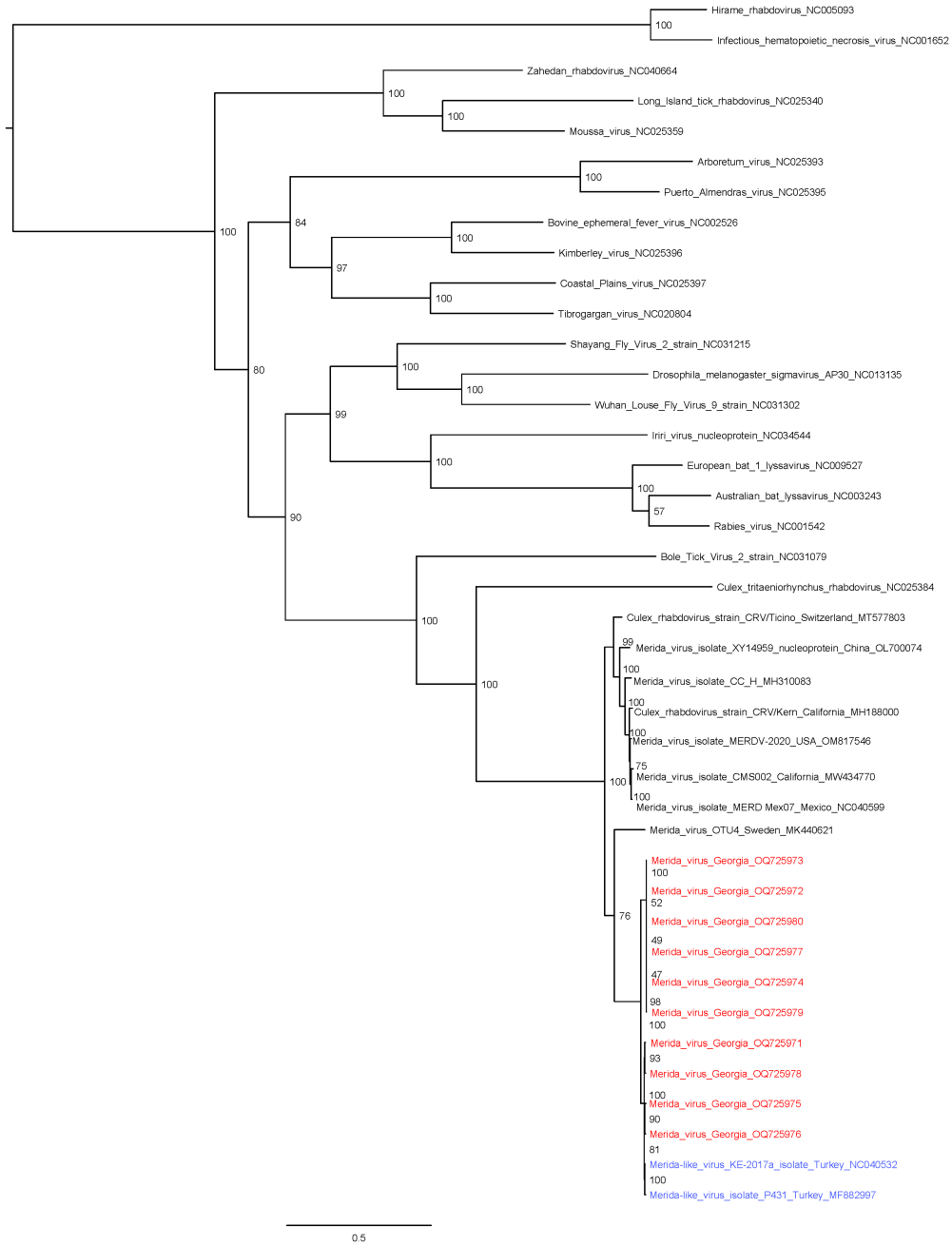

FIGURE 4
Maximum likelihood tree of rhabdovirus family including Merida virus and Merida-like virus samples. Merida virus genomes from Georgia samples are highlighted in red and closely related MERDLVT samples are highlighted in blue. Node confidence values represent ultrafast bootstrap replicate support.

sequencing alignment tool to evaluate and compare the sequence identity between the Georgia samples and the MERLDVT strain. Our positive samples aligned to the MERDLVT strain with 96%–100% sequence identity with 99.7%–100% aligned genome sequence coverage.

Our aim was to explore unique viral communities to expand our knowledge in mosquito virome populations. To explore the viral component of the town of Senaki we used an unbiased metagenomic approach. Pooled specimens of *Culex pipiens* mosquitoes were studied to reveal mosquito virome. In both years, most viral reads belonged to the Culex Iflavi-like virus 4. In addition, we found most samples containing the Merida-like virus KE-2017a in pooled specimens from 2018. A phylogenetic analysis revealed that these positive pooled samples shared a common ancestor with the Merida-like virus KE-2017a isolate 139-1-21 and the Merida-like virus Turkey isolate P431. The known Merida viruses shown in this phylogenetic analysis cluster geographically.

The Merida virus was initially detected in *Culex quinquefasciatus* mosquitoes and assigned to the genus Merhavirus within the *Rhabdoviridae* family (Charles et al., 2016). Since then, the virus has been detected in metagenomic analyses conducted in other mosquito species and around the world (Charles et al., 2016; Ergunay et al., 2017). However, the pathology of the Merida virus has not been further explored.

Controlling vector populations has become widely implemented approach to prevent the endemic spread of VBPs. With the continuous expansion of vector habitats, it is critical to monitor vector populations for potential emerging viral diseases to better prepare for new threats. Our work has added contributed NGS data and curated genome assemblies of novel Merida-like viruses that can be further used to better understand viral communities within the mosquito population. These data have the potential in combination with additional surveys to identify new and emerging diseases.

Data availability statement

The datasets presented in this study can be found in online repositories. The names of the repository/repositories and accession number(s) can be found at: https://www.ncbi.nlm.nih.gov/genbank/, OQ725971; https://www.ncbi.nlm.nih.gov/genbank/, OQ725972; https://www.ncbi.nlm.nih.gov/genbank/, OQ725973; https://www.ncbi.nlm.nih.gov/genbank/, OQ725974; https://www.ncbi.nlm.nih.gov/genbank/, OQ725975; https://www.ncbi.nlm.nih.gov/genbank/, OQ725976; https://www.ncbi.nlm.nih.gov/genbank/, OQ725977; https://www.ncbi.nlm.nih.gov/genbank/, OQ725978; https://www.ncbi.nlm.nih.gov/genbank/, OQ725979; https://www.ncbi.nlm.nih.gov/genbank/, OQ725980.

Author contributions

JP-B: Formal analysis, Methodology, Writing – original draft, Writing – review & editing, Conceptualization, Investigation, Visualization. AP: Formal analysis, Methodology, Writing – original draft, Writing – review & editing, Conceptualization, Investigation. BK: Methodology, Project administration, Writing – review & editing, Investigation, Formal analysis. TC: Methodology, Writing – review & editing, Investigation. CF: Formal analysis, Methodology, Software, Visualization, Writing – review & editing, Validation. MC: Formal analysis, Methodology, Writing – review & editing, Software, Visualization, Validation. DR-W: Formal analysis, Funding acquisition, Methodology, Project administration, Supervision, Writing – review & editing, Investigation, Resources. JH: Formal analysis, Funding acquisition, Methodology, Project administration, Supervision, Writing – review & editing, Investigation, Resources, Validation, Visualization.

Funding

The author(s) declare financial support was received for the research, authorship, and/or publication of this article. Funding was provided by the Global Emerging Infections Surveillance and Response System (GEIS), Division by the Armed Forces Health Surveillance Branch, projects P0092_18_GA, P0031_19_GA, P0171_21_WR, P0175_22_WR.

Acknowledgments

We thank James S. Hilaire, Nicole R. Nicholas, Tuan K. Nguyen, and April N. Griggs for their assistance in project management and sample tracking, storage, and retrieval.

Conflict of interest

The authors declare that the research was conducted in the absence of any commercial or financial relationships that could be construed as a potential conflict of interest.

The author(s) declared that they were an editorial board member of Frontiers, at the time of submission. This had no impact on the peer review process and the final decision.

Publisher's note

Author disclaimer

Material has been reviewed by the authors' respective institutions. There is no objection to its presentation and/or publication. The views expressed here are those of the authors and do not reflect the official policy of the Department of the Army, Department of Defense or US Government. This is the work of US government employees and may not be copyrighted (17 USC 105).

Supplementary material

The Supplementary material for this article can be found online at: https://www.frontiersin.org/articles/10.3389/fmicb.2023.1258810/full#supplementary-material

References

Agboli, E., Leggewie, M., Altinli, M., and Schnettler, E. (2019). Mosquito-specific viruses-transmission and interaction. *Viruses* 11:873. doi: 10.3390/v11090873

Altschul, S. F., Gish, W., Miller, W., Myers, E. W., and Lipman, D. J. (1990). Basic local alignment search tool. *J. Mol. Biol.* 215, 403–410. doi: 10.1016/S0022-2836(05)80360-2

Boisvert, S., Raymond, F., Godzaridis, E., Laviolette, F., and Corbeil, J. (2012). Ray Meta: scalable de novo metagenome assembly and profiling. *Genome Biol.* 13:R122. doi: 10.1186/gb-2012-13-12-r122

Bolling, B. G., Olea-Popelka, F. J., Eisen, L., Moore, C. G., and Blair, C. D. (2012). Transmission dynamics of an insect-specific flavivirus in a naturally infected *Culex pipiens* laboratory colony and effects of co-infection on vector competence for West Nile virus. *Virology* 427, 90–97. doi: 10.1016/j.virol.2012.02.016

Brettin, T., Davis, J. J., Disz, T., Edwards, R. A., Gerdes, S., Olsen, G. J., et al. (2015). RASTtk: a modular and extensible implementation of the RAST algorithm for building custom annotation pipelines and annotating batches of genomes. *Sci. Rep.* 5:8365. doi: 10.1038/srep08365

Charles, J., Firth, A. E., Lorono-Pino, M. A., Garcia-Rejon, J. E., Farfan-Ale, J. A., Lipkin, W. I., et al. (2016). Merida virus, a putative novel rhabdovirus discovered in Culex and Ochlerotatus spp. mosquitoes in the Yucatan peninsula of Mexico. *J. Gen. Virol.* 97, 977–987. doi: 10.1099/jgv.0.000424

Cuevas-Juarez, E., Pando-Robles, V., and Palomares, L. A. (2021). Flavivirus vaccines: virus-like particles and single-round infectious particles as promising alternatives. *Vaccine* 39, 6990–7000. doi: 10.1016/j.vaccine.2021.10.049

da Silva Neves, N. A., Pinto, A. Z. L., Melo, F. L., Maia, L. M. S., da Silva Ferreira, R., de Carvalho, M. S., et al. (2021). Sialovirome of Brazilian tropical anophelines. *Virus Res.* 302:198494. doi: 10.1016/j.virusres.2021.198494

de Almeida, J. P., Aguiar, E. R., Armache, J. N., Olmo, R. P., and Marques, J. T. (2021). The virome of vector mosquitoes. *Curr. Opin. Virol.* 49, 7–12. doi: 10.1016/j.coviro.2021.04.002

Dietzgen, R. G., Kondo, H., Goodin, M. M., Kurath, G., and Vasilakis, N. (2017). The family Rhabdoviridae: mono- and bipartite negative-sense RNA viruses with diverse genome organization and common evolutionary origins. *Virus Res.* 227, 158–170. doi: 10.1016/j.virusres.2016.10.010

Erasmus, J. H., Seymour, R. L., Kaelber, J. T., Kim, D. Y., Leal, G., Sherman, M. B., et al. (2018). Novel insect-specific Eilat virus-based chimeric vaccine candidates provide durable, mono- and multivalent, single-dose protection against lethal alphavirus challenge. *J. Virol.* 92, e01274–e01217. doi: 10.1128/JVI.01274-17

Ergunay, K., Brinkmann, A., Litzba, N., Gunay, F., Kar, S., Oter, K., et al. (2017). A novel rhabdovirus, related to Merida virus, in field-collected mosquitoes from Anatolia and Thrace. *Arch. Virol.* 162, 1903–1911. doi: 10.1007/s00705-017-3314-4

Hang, J., Forshey, B. M., Kochel, T. J., Li, T., Solorzano, V. F., Halsey, E. S., et al. (2012). Random amplification and pyrosequencing for identification of novel viral genome sequences [research support, U.S. Gov't, non-P.H.S.]. *J. Biomol. Tech.* 23, 4–10. doi: 10.7171/jbt.12-2301-001

Hoang, D. T., Chernomor, O., von Haeseler, A., Minh, B. Q., and Vinh, L. S. (2018). UFBoot2: improving the ultrafast bootstrap approximation. *Mol. Biol. Evol.* 35, 518–522. doi: 10.1093/molbev/msx281

Huang, X., and Madan, A. (1999). CAP3: a DNA sequence assembly program. *Genome Res.* 9, 868–877. doi: 10.1101/gr.9.9.868

Kalantar, K. L., Carvalho, T., de Bourcy, C. F. A., Dimitrov, B., Dingle, G., Egger, R., et al. (2020). IDseq-an open source cloud-based pipeline and analysis service for metagenomic pathogen detection and monitoring. *Gigascience* 9:giaa111. doi: 10.1093/gigascience/giaa111

Kalyaanamoorthy, S., Minh, B. Q., Wong, T. K. F., von Haeseler, A., and Jermiin, L. S. (2017). ModelFinder: fast model selection for accurate phylogenetic estimates. *Nat. Methods* 14, 587–589. doi: 10.1038/nmeth.4285

Katoh, K., and Standley, D. M. (2013). MAFFT multiple sequence alignment software version 7: improvements in performance and usability. *Mol. Biol. Evol.* 30, 772–780. doi: 10.1093/molbev/mst010

Kilianski, A., Carcel, P., Yao, S., Roth, P., Schulte, J., Donarum, G. B., et al. (2015). Pathosphere.org: pathogen detection and characterization through a web-based, open source informatics platform. *BMC Bioinformatics* 16:416. doi: 10.1186/s12859-015-0840-5

Kilpatrick, A. M., and Randolph, S. E. (2012). Drivers, dynamics, and control of emerging vector-borne zoonotic diseases. *Lancet* 380, 1946–1955. doi: 10.1016/S0140-6736(12)61151-9

Liu, S., Vijayendran, D., and Bonning, B. C. (2011). Next generation sequencing technologies for insect virus discovery. *Viruses* 3, 1849–1869. doi: 10.3390/v3101849

Martin, M. (2011). Cutadapt removes adapter sequences from high-throughput sequencing reads. *EMBnet Journal* 17, 10–12. doi: 10.14806/ej.17.1.200

Pierson, T. C., and Diamond, M. S. (2020). The continued threat of emerging flaviviruses. *Nat. Microbiol.* 5, 796–812. doi: 10.1038/s41564-020-0714-0

Pollio, A. R., Jiang, J., Lee, S. S., Gandhi, J. S., Knott, B. D., Chunashvili, T., et al. (2022). Discovery of Rickettsia spp. in mosquitoes collected in Georgia by metagenomics analysis and molecular characterization. *Front. Microbiol.* 13:961090. doi: 10.3389/fmicb.2022.961090

Ramesh, A., Nakielny, S., Hsu, J., Kyohere, M., Byaruhanga, O., de Bourcy, C., et al. (2019). Metagenomic next-generation sequencing of samples from pediatric febrile illness in Tororo. *Uganda. PLoS One* 14:e0218318. doi: 10.1371/journal.pone.0218318

Sadeghi, M., Altan, E., Deng, X., Barker, C. M., Fang, Y., Coffey, L. L., et al. (2018). Virome of > 12 thousand Culex mosquitoes from throughout California. *Virology* 523, 74–88. doi: 10.1016/j.virol.2018.07.029

Saha, S., Ramesh, A., Kalantar, K., Malaker, R., Hasanuzzaman, M., Khan, L. M., et al. (2019). Unbiased metagenomic sequencing for pediatric meningitis in Bangladesh reveals Neuroinvasive chikungunya virus outbreak and other unrealized pathogens. *MBio* 10, e02877–e02819. doi: 10.1128/mBio.02877-19

Sanborn, M. A., Klein, T. A., Kim, H. C., Fung, C. K., Figueroa, K. L., Yang, Y., et al. (2019). Metagenomic analysis reveals three novel and prevalent mosquito viruses from a single Pool of *Aedes vexans* nipponii collected in the Republic of Korea. *Viruses* 11:222. doi: 10.3390/v11030222

Schmieder, R., and Edwards, R. (2011). Quality control and preprocessing of metagenomic datasets. *Bioinformatics* 27, 863–864. doi: 10.1093/bioinformatics/btr026

Valles, S. M., Chen, Y., Firth, A. E., Guerin, D. M. A., Hashimoto, Y., Herrero, S., et al. (2017). ICTV virus taxonomy profile: Iflaviridae. *J. Gen. Virol.* 98, 527–528. doi: 10.1099/jgv.0.000757

Walker, P. J., Firth, C., Widen, S. G., Blasdell, K. R., Guzman, H., Wood, T. G., et al. (2015). Evolution of genome size and complexity in the rhabdoviridae. *PLoS Pathog.* 11:e1004664. doi: 10.1371/journal.ppat.1004664

frontiers | Frontiers in Microbiology

TYPE Opinion
PUBLISHED 25 October 2023
DOI 10.3389/fmicb.2023.1284838

OPEN ACCESS

EDITED BY
Ke Liu,
Chinese Academy of Agricultural Sciences (CAAS), China

REVIEWED BY
Rui-De Xue,
University of the Sciences, Philadelphia, United States

*CORRESPONDENCE
Andrew W. Taylor-Robinson
andrew.tr@vinuni.edu.vn

RECEIVED 29 August 2023
ACCEPTED 10 October 2023
PUBLISHED 25 October 2023

CITATION
Taylor-Robinson AW (2023) Harnessing artificial intelligence to enhance key surveillance and response measures for arbovirus disease outbreaks: the exemplar of Australia. *Front. Microbiol.* 14:1284838. doi: 10.3389/fmicb.2023.1284838

Harnessing artificial intelligence to enhance key surveillance and response measures for arbovirus disease outbreaks: the exemplar of Australia

Andrew W. Taylor-Robinson [1,2,3,4]*

[1]College of Health Sciences, VinUniversity, Hanoi, Vietnam, [2]VinUniversity-University of Illinois Smart Health Center, VinUniversity, Hanoi, Vietnam, [3]Center for Global Health, Perelman School of Medicine, University of Pennsylvania, Philadelphia, PA, United States, [4]College of Health and Human Sciences, Charles Darwin University, Casuarina, NT, Australia

KEYWORDS

Research topic: Transmission and infection of arboviruses, surveillance, response, outbreak, public health, artificial intelligence, Australia

1. Contributions to the field statement

Arboviruses present a significant public health risk to the Australian population. Both the many indigenous arboviruses and imported cases of major global pathogens contribute to this burden. Effective surveillance measures, which involve monitoring for mosquitoes responsible for transmission, the signs and symptoms of disease in humans, and a range of environmental and climactic factors, are essential to detect and respond early to local outbreaks. This is particularly crucial in regional Australia, a vast area that is underserved but is now becoming a focal point for economic and social development. As this transformation progresses, there will be increased human interaction with native reservoir animal hosts and vector mosquitoes, creating a potential scenario for a higher prevalence of neglected indigenous arbovirus infections. Additionally, the impact of climate change in the tropical north of the country is predicted to lead to a population boom of arbovirus-transmitting mosquitoes, further exacerbating the situation. Hence, it is imperative to maintain diligent attention to vector monitoring and control efforts. Integrating artificial intelligence to rapidly process large volumes of data should enhance surveillance by improving data analysis, prediction, and decision-making. More accurate and quicker detection of arboviral disease outbreaks will enable proactive and effective public health responses.

2. Introduction: the public health problem

Viruses that are transmitted between vertebrate hosts by biting, blood-feeding arthropods (primarily mosquitoes and ticks) are called *ar*thropod-*bo*rne viruses or, for short, arboviruses. The transmission of arboviruses to humans poses a significant and accelerating global public health risk (Madewell, 2020). It is estimated that 3.9 billion people, approaching half of the world's population is at risk (World Health Organization, 2022), leading to hundreds of millions of symptomatic infections, a disease burden of tens of thousands of deaths and up to 5 million disability-adjusted life years lost annually (Labeaud et al., 2011). Notable examples of pathogens include dengue (DENV), chikungunya, yellow fever, Japanese encephalitis (JEV), West Nile, Zika and Mayaro viruses. For several of these,

humans serve as the primary reservoir host, with many causing pandemics over the last few decades (Mayer et al., 2017). Mild infection is typically associated with influenza-like symptoms such as fever, headache, muscle or joint pain, and/or a skin rash. Less commonly, severe infection is characterised by rapid onset of haemorrhagic fever (with internal bleeding) or life-threatening shock syndrome (with circulatory collapse). Signs and symptoms of encephalitis include confusion, tremors, seizures, paralysis, and loss of consciousness (Labeaud et al., 2011; Mayer et al., 2017).

The distribution of an arbovirus is restricted by the territory of its mosquito vector(s) of transmission, which tends to be limited to tropical and subtropical zones. Yet, due to the effects of climate change (involving rainfall patterns) the geographical range of common vectors may be predicted to expand in future (Madewell, 2020). Thus, locations that at present are currently not affected should not be complacent that they will always remain free of arboviruses. The dramatic emergence and re-emergence of arboviral diseases has been greatly exacerbated by a combination of global meteorological, demographic, and societal changes, principally increasing rates and levels of climate change, urbanisation, globalisation, and international mobility (Bellone et al., 2023). These environmental and anthropogenic factors have facilitated viral etiological agents to break out of their natural ecological zones to become established in novel geographical sites where susceptible arthropod vectors and human hosts provide conditions supportive to their causing epidemics (Madewell, 2020).

3. The usual suspects

DENV is an arbovirus of global concern but for which local outbreaks in Australia are restricted to Queensland, where the vector mosquito *Aedes aegypti* is established (Beebe et al., 2009). Community acquired infections have been reported only from urban areas in the northeast of the state, where the vector is most abundant. However, historical data show that much of Australia has previously sustained both the virus and the vector mosquito (Russell et al., 2009). Factors such as increased DENV activity in neighbouring countries like Indonesia and Papua New Guinea, plus the growing human population of northern Australia contribute to the risk of DENV transmission (Gyawali et al., 2016a). Climate change projections also suggest potential rises in dengue incidence and distribution associated with increasing temperatures (Williams et al., 2014). This also applies to JEV, the recent and rapid emergence of which in several states is a cause for concern (Williams et al., 2022).

Imported cases of DENV and other arboviruses, including JEV, also pose a risk to public health in Australia. With increased global travel and trade, there is a potential for the introduction of arboviruses through infected travellers or imported vectors (Mackenzie and Williams, 2009). The spread of arboviruses to regions without established vectors, such as *Ae. aegypti* and *Ae. albopictus*, can occur through international air and sea ports (Gyawali et al., 2016a). Therefore, surveillance and control measures at ports of entry are crucial to prevent the importation and establishment of arboviruses in Australia. The most recent national report, for 2016, shows 2,227 notifications of DENV, of which 31 were locally acquired and the remainder travel-related, mostly tourists visiting Bali (Australian Government Department of Health, 2021).

4. The less usual suspects

The threat presented by emerging indigenous arboviruses in Australia is arguably undervalued (Gyawali et al., 2016b). More than 75 arboviruses have been identified that are unique to the continent. While several are recognised to cause disease in humans, information on the potential human pathogenicity of most of these indigenous viruses is negligible (Gyawali et al., 2017a). Ross River (RRV) and Barmah Forest (BFV) viruses trigger an often debilitating and sometimes chronic type of arthritis that affects several joints at once. Murray Valley encephalitis (MVEV) and West Nile Kunjin strain (KUNV) viruses cause inflammation of the brain.

One of the key arboviruses of concern is RRV, which is endemic and enzootic in the country and Papua New Guinea (Kuleshov et al., 2022). The major vector in inland areas is the freshwater-breeding *Culex annulirostris*, whereas *Ochlerotatus vigilax* and *O. camptorhynchus* transmit in brackish coastal waters. RRV infection in humans can cause peripheral polyarthralgia or arthritis, with disease notifications averaging 5,000 per year in Australia since the start of this century. Yet, there is considerable annual fluctuation of confirmed case reports; for instance, 9,555 notifications in 2015 but 3,677 in the following year (Australian Government Department of Health, 2021).

As with RRV, human infections with BFV have been reported from all states and territories in Australia. Moreover, serological surveys indicate that this is a widespread phenomenon. Clinical manifestations often include fever, rash, chronic fatigue and polyarthritis. BFV is transmitted primarily by *Cx. annulirostris* and *Aedes funereus* in inland and in coastal regions, respectively. The reported incidence is usually close to 1,000 cases per annum since routine testing by immunoassay antibody detection became widely available (Gyawali and Taylor-Robinson, 2017).

MVEV is endemic in northern Australia, with sporadic outbreaks occurring (Broom et al., 2003). The virus is transmitted primarily by *Cx. annulirostris* mosquitoes, and its activity is influenced by rainfall and flooding. Other emerging arboviruses, such as KUNV, have been detected in this and other ornithophilic mosquitoes and pose a potential public health threat (Broom et al., 2003). The presence of competent vectors and the potential for virus introduction through travel and trade increase the risk of emerging indigenous arboviruses in Australia (Mackenzie and Williams, 2009).

Other Australian arboviruses, such as Alfuy, Edge Hill, Gan Gan, Kokobera, Sindbis and Stratford, are also associated with human disease (Gyawali et al., 2019). However, they appear to cause predominantly mild symptoms and a major outbreak has not yet been reported. While the epidemiology of these neglected viruses is poorly understood, they are likely maintained in zoonotic cycles rather than by human-to-human transmission. Hence, they are harboured by apathogenic, persistent infections in native Australian reservoir mammals (such as kangaroos and wallabies) and birds (including herons and

egrets) (e.g., Gyawali et al., 2020), with occasional spillover into humans.

5. Need for improved early detection

For many years it was speculated that infection with arboviruses may be a cause of febrile illness in Australia, as elsewhere in the world. This was confirmed with the discovery of the now frequently diagnosed RRV in 1959 and BFV in 1974. Yet, even after identification of these viruses it took almost 15 years for routine laboratory tests (involving detection of virus-specific immunoglobulin (Ig) M and IgG) to diagnose infection to become available (Gyawali et al., 2017a). While paired serology of RRV and BBV is considered clinical best practise, it requires careful interpretation considering the high rates of false positive and negative results, plus the long-term persistence of IgM in some individuals. Incorrect interpretation risks misdiagnosis and therefore inappropriate patient treatment (Gyawali et al., 2017b).

Compounding this problem of inaccurate viral infection case reporting is the fact that more than half of so-called undifferentiated fevers (those with non-specific symptoms) in Australia still go undiagnosed (Gyawali et al., 2017a). In many instances this is because the treating physician may consider the cost of testing is not justified or the causative agent is novel, not known to cause human disease or no routine diagnostic test is available. In such cases, an association could be assumed but not proved between arboviruses and feverish illness. Hence, establishing a robust surveillance system would enable the early warning of an infection outbreak. Developing accurate diagnostic tools would aid early diagnosis and correct treatment of febrile primary care patients.

Unforeseen climatic and environmental variations, such as the increased incidence of cyclones, heavy rainfall, and resultant intensified flooding associated with outbreaks of RRV (Tall et al., 2014) and MVEV (Selvey et al., 2014), have been occurring of late with disconcerting regularity, potentially effectuating an ecological change for Australian arboviruses (Young, 2018). The projected future climatic suitability of Northern Australia for competent vector mosquito species needs to be evaluated. In this context, improved epidemiological surveillance of prevailing environmental conditions, mosquito vector species and reservoir host animals, should be considered a public health priority.

6. A proposed solution

In order to prepare effectively for the emergence of an arbovirus outbreak of public health concern, both globally (Weaver and Reisen, 2010), and in particular in regional Australia (Gyawali and Taylor-Robinson, 2017), key surveillance measures are essential. These include the following five actions:

1. *Vector surveillance*: monitoring and mapping the distribution and abundance of mosquito vectors is crucial. This involves regular trapping and identification of vector species, as well as testing them for the presence of arboviruses. Vector surveillance helps identify areas at risk and informs targeted control measures.
2. *Environmental surveillance*: monitoring environmental factors, such as temperature, rainfall, and humidity, can provide insights into vector breeding and arbovirus transmission dynamics. This information helps predict and anticipate outbreaks, enabling timely interventions.
3. *Animal surveillance*: monitoring arboviral infections in animal populations, particularly in sentinel species, can serve as an early warning system for human outbreaks. Animals, such as marsupials and water birds, can act as reservoir hosts or environmental indicators of arbovirus activity.
4. *Disease surveillance*: active surveillance for human cases of arboviral infections is vital. This involves monitoring and reporting suspected cases, conducting microbiology laboratory testing for confirmation, and analysing epidemiological data to identify trends and patterns. Early detection and reporting of cases allow for prompt public health responses.
5. *Syndromic surveillance*: implementing surveillance systems that monitor specific clinical symptoms or syndromes associated with arboviral infections can provide early indications of outbreaks. Health indicators that are discernible before confirmed diagnosis include monitoring febrile illnesses, neurological symptoms, and other relevant clinical presentations.

7. A novel approach

Artificial intelligence (AI) can play a prominent role in enhancing arbovirus surveillance at scales ranging from local to global. AI algorithms can analyze large volumes of data, including environmental, epidemiological, and entomological data. Integrating human, pathogen, vector, and climatic variables from various existing surveillance sources into a unified system can enhance pattern recognition and generate probabilistic risk models for outbreak spread and severity (Pley et al., 2021). This allows epidemiologists to detect patterns, predict outbreaks, and inform targeted interventions more accurately using such high-throughput techniques as metatranscriptomic sequencing (Batovska et al., 2022). Moreover, AI can automate data processing, improve data integration, assist in modelling, and provide real-time monitoring and analysis of multiple variables. This enables public health authorities to identify areas at high risk, to allocate resources more efficiently and thereby to make more proactive and effective responses (Batovska et al., 2019; Pley et al., 2021).

In the context of arbovirus surveillance, AI can assist in the identification and tracking of mosquito vectors, processes that are crucial for understanding the transmission dynamics of arboviruses. By analysing data on mosquito populations, AI algorithms can identify trends and patterns that may indicate increased virus activity or the novel emergence of a virus in a location (Ramírez et al., 2018). This information can then be used to guide control and preventive measures. For example, AI can analyze satellite imagery and climate data, mosquito surveillance data, and human case data to reveal vector habitats,

identify high-risk areas for disease outbreaks, and predict disease transmission dynamics (Kurucz et al., 2022). AI algorithms can also analyze social media and internet search data for disease outbreaks and public concerns to help to develop early warning systems and decision support tools (Batovska et al., 2022). Additionally, AI can assist in data integration and modelling to improve disease forecasting and inform targeted interventions by public health authorities.

Research conducted in Kenya has demonstrated the effectiveness of mosquito-based arbovirus surveillance in diverse ecological zones (Ochieng et al., 2013). Similarly, in Burkina Faso, AI has been employed to enhance surveillance during dengue outbreaks, leading to improved understanding of the burden of arboviral diseases (Sanou et al., 2018). These experiences highlight the potential of AI in strengthening surveillance and response measures for arbovirus disease outbreaks globally. Therefore, the use of AI in arbovirus surveillance is not limited to Australia. Yet, this affluent developed nation is particularly suited to integrating AI into outbreak preparedness procedures (van den Hurk et al., 2012). It has the infrastructure and resources to leverage AI better than most countries, while also having plenty to gain by mitigating a neglected public health threat, especially in rural and regional locations that are relatively underserved.

8. Conclusion

Arboviruses pose a significant public health threat to the population of Australia. There is a risk of emerging indigenous arboviruses, while imported cases also contribute to the burden. Surveillance measures, including monitoring vectors, diseases, and environmental factors, are crucial for early detection and response to outbreaks. This is particularly impactful in regional Australia, a historically underinvested region that is set to become a focus of economic and social development. This will increasingly bring humans into close contact with native reservoir hosts and vector mosquitoes. Such a convergence of factors could trigger an increased prevalence of infection with neglected indigenous arboviruses. Moreover, the escalating rate and effects of climate change that are observed in the tropical north of the country will likely drive a population boom of arbovirus-transmitting mosquitoes. As a commensurate response, continuing assiduous attention to vector monitoring and control is required. It is anticipated that the integration of artificial intelligence to process large volumes of data rapidly will enhance surveillance efforts by improving data analysis, prediction, and decision-making, ultimately leading to improved accuracy in detecting arboviral disease outbreaks and enabling more proactive and effective public health responses. The lessons learned from this Australian experience can help to better prepare government agencies in other nations to adopt AI technology in their enhanced surveillance efforts. In particular, this applies to low- and lower-middle income countries in tropical and subtropical zones where the rising incidence of arboviral diseases is a major public health concern.

Author contributions

AWT-R: Conceptualisation, Formal analysis, Investigation, Writing—original draft, Writing—review and editing.

Funding

The author(s) declare that no financial support was received for the research, authorship, and/or publication of this article.

Acknowledgments

Past and present arboviral research colleagues are thanked warmly for expert advice and insightful discussions over several years that informed the views expressed in this article. These include John Aaskov (Queensland University of Technology), Narayan Gyawali and Gregor Devine (QIMR Berghofer Medical Research Institute), and Richard Bradbury (Federation University Australia).

Conflict of interest

The author declares that the research was conducted in the absence of any commercial or financial relationships that could be construed as a potential conflict of interest.

Publisher's note

References

Australian Government Department of Health (2021). Australia's notifiable disease status, 2016: Annual report of the National Notifiable Diseases Surveillance System. *Commun. Dis. Intell.* 45, 1–196. doi: 10.33321/cdi.2021.45.28

Batovska, J., Mee, P. T., Lynch, S. E., Sawbridge, T. I., and Rodoni, B. C. (2019). Sensitivity and specificity of metatranscriptomics as an arbovirus surveillance tool. *Sci. Rep.* 9, 19398. doi: 10.1038/s41598-019-55741-3

Batovska, J., Mee, P. T., Sawbridge, T. I., Rodoni, B. C., and Lynch, S. E. (2022). Enhanced arbovirus surveillance with high-throughput metatranscriptomic processing of field-collected mosquitoes. *Viruses* 14, 2759. doi: 10.3390/v1412 2759

Beebe, N. W., Cooper, R. D., Mottram, P., and Sweeney, A. W. (2009). Australia's dengue risk driven by human adaptation to climate change. *PLoS Negl. Trop. Dis.* 3, e429. doi: 10.1371/journal.pntd.0000429

Bellone, R., Lechat, P., Mousson, L., Gilbart, V., Piorkowski, G., Bohers, C., et al. (2023). Climate change and vector-borne diseases: a multi-omics approach of temperature-induced changes in the mosquito. *J. Travel. Med.* 30, taad062. doi: 10.1093/jtm/taad062

Broom, A. K., Lindsay, M. D., Wright, A. E., Smith, D. W., and Mackenzie, J. S. (2003). Epizootic activity of Murray Valley encephalitis and Kunjin viruses in an aboriginal community in the southeast Kimberley region of Western Australia: results of mosquito fauna and virus isolation studies. *Am. J. Trop. Med. Hyg.* 69, 277–283. doi: 10.4269/ajtmh.2003.69.277

Gyawali, N., Bradbury, R. S., Aaskov, J. G., and Taylor-Robinson, A. W. (2017a). Neglected Australian arboviruses: quam gravis? *Microbes Infect.* 19, 388–401. doi: 10.1016/j.micinf.2017.05.002

Gyawali, N., Bradbury, R. S., Aaskov, J. G., and Taylor-Robinson, A. W. (2017b). Neglected Australian arboviruses and undifferentiated febrile illness: addressing public health challenges arising from the 'Developing Northern Australia' government policy. *Front. Microbiol.* 8, 2150. doi: 10.3389/fmicb.2017.02150

Gyawali, N., Bradbury, R. S., and Taylor-Robinson, A. W. (2016a). The epidemiology of dengue infection: Harnessing past experience and current knowledge to support implementation of future control strategies. *J. Vector Borne. Dis.* 53, 293–304.

Gyawali, N., Bradbury, R. S., and Taylor-Robinson, A. W. (2016b). Do neglected Australian arboviruses pose a global epidemic threat? *Aust. N. Z. J. Public Health.* 40, 596. doi: 10.1111/1753-6405.12582

Gyawali, N., and Taylor-Robinson, A. W. (2017). Confronting the emerging threat to public health in northern Australia of neglected indigenous arboviruses. *Trop. Med. Infect. Dis.* 2, 55. doi: 10.3390/tropicalmed2040055

Gyawali, N., Taylor-Robinson, A. W., Bradbury, R. S., Pederick, W., Faddy, H. M., and Aaskov, J. G. (2019). Neglected Australian arboviruses associated with undifferentiated febrile illnesses. *Front. Microbiol.* 10, 2818. doi: 10.3389/fmicb.2019.02818

Gyawali, N., Taylor-Robinson, A. W., Bradbury, R. S., Potter, A., and Aaskov, J. G. (2020). Infection of Western Gray Kangaroos (*Macropus fuliginosus*) with Australian arboviruses associated with human infection. *Vector Borne Zoonotic Dis.* 20, 33–39. doi: 10.1089/vbz.2019.2467

Kuleshov, Y., Wei, Y., Inape, K., and Liu, G. J. (2022). Spatio-temporal distribution of vector borne diseases in Australia and Papua New Guinea vis-à-vis climatic factors. *J. Vector Borne Dis.* 59, 115–126. doi: 10.4103/0972-9062.337510

Kurucz, N., McMahon, J. L., Warchot, A., Hewitson, G., Barcelon, J., Moore, F., et al. (2022). Nucleic acid preservation card surveillance is effective for monitoring arbovirus transmission on crocodile farms and provides a One Health benefit to northern Australia. *Viruses* 14, 1342. doi: 10.3390/v14061342

Labeaud, A. D., Bashir, F., and King, C. H. (2011). Measuring the burden of arboviral diseases: the spectrum of morbidity and mortality from four prevalent infections. *Popul. Health Metr.* 9, 1. doi: 10.1186/1478-7954-9-1

Mackenzie, J. S., and Williams, D. T. (2009). The zoonotic flaviviruses of southern, south-eastern and eastern Asia, and Australasia: the potential for emergent viruses. *Zoonoses Public Health* 56, 338–356. doi: 10.1111/j.1863-2378.2008.01208.x

Madewell, Z. J. (2020). Arboviruses and their vectors. *South. Med. J.* 113, 520–523. doi: 10.14423/SMJ.0000000000001152

Mayer, S. V., Tesh, R. B., and Vasilakis, N. (2017). The emergence of arthropod-borne viral diseases: a global prospective on dengue, chikungunya and zika fevers. *Acta Trop.* 166, 155–163. doi: 10.1016/j.actatropica.2016.11.020

Ochieng, C., Lutomiah, J., Makio, A., Koka, H., Chepkorir, E., Yalwala, S., et al. (2013). Mosquito-borne arbovirus surveillance at selected sites in diverse ecological zones of Kenya; 2007–2012. *Virol. J.* 10, 140. doi: 10.1186/1743-422X-10-140

Pley, C., Evans, M., Lowe, R., Montgomery, H., and Yacoub, S. (2021). Digital and technological innovation in vector-borne disease surveillance to predict, detect, and control climate-driven outbreaks. *Lancet Planet. Health* 5, e739–e745. doi: 10.1016/S2542-5196(21)00141-8

Ramírez, A. L., van den Hurk, A. F., Meyer, D. B., and Ritchie, S. A. (2018). Searching for the proverbial needle in a haystack: advances in mosquito-borne arbovirus surveillance. *Parasit. Vectors* 11, 320. doi: 10.1186/s13071-018-2901-x

Russell, R. C., Currie, B. J., Lindsay, M. D., Mackenzie, J. S., Ritchie, S. A., and Whelan, P. I. (2009). Dengue and climate change in Australia: predictions for the future should incorporate knowledge from the past. *Med. J. Aust.* 190, 265–268. doi: 10.5694/j.1326-5377.2009.tb02393.x

Sanou, A. S., Dirlikov, E., Sondo, K. A., Kagoné, T. S., Yameogo, I., Sow, H. E., et al. (2018). Building laboratory-based arbovirus sentinel surveillance capacity during an ongoing dengue outbreak, Burkina Faso, 2017. *Health Secur.* 16, S103–S110. doi: 10.1089/hs.2018.0048

Selvey, L. A., Johansen, C. A., Broom, A. K., Antão, C., Lindsay, M. D., Mackenzie, J. S., et al. (2014). Rainfall and sentinel chicken seroconversions predict human cases of Murray Valley encephalitis in the north of Western Australia. *BMC Infect. Dis.* 14, 672. doi: 10.1186/s12879-014-0672-3

Tall, J. A., Gatton, M. L., and Tong, S. (2014). Ross River virus disease activity associated with naturally occurring nontidal flood events in Australia: a systematic review. *J. Med. Entomol.* 51, 1097–1108. doi: 10.1603/ME14007

van den Hurk, A. F., Hall-Mendelin, S., Johansen, C. A., Warrilow, D., and Ritchie, S. A. (2012). Evolution of mosquito-based arbovirus surveillance systems in Australia. *J. Biomed. Biotechnol.* 2012, 325659. doi: 10.1155/2012/325659

Weaver, S. C., and Reisen, W. K. (2010). Present and future arboviral threats. *Antiviral Res.* 85, 328–345. doi: 10.1016/j.antiviral.2009.10.008

Williams, C. R., Mincham, G., Ritchie, S. A., Viennet, E., and Harley, D. (2014). Bionomic response of *Aedes aegypti* to two future climate change scenarios in far north Queensland, Australia: implications for dengue outbreaks. *Parasit. Vectors* 7, 447. doi: 10.1186/1756-3305-7-447

Williams, C. R., Webb, C. E., Higgs, S., and van den Hurk, A. F. (2022). Japanese encephalitis virus emergence in Australia: public health importance and implications for future surveillance. *Vector Borne Zoonotic Dis.* 22, 529–534. doi: 10.1089/vbz.2022.0037

World Health Organization (2022). *Launch of the Global Arbovirus Initiative.* Available online at: https://www.who.int/news-room/events/detail/2022/03/31/default-calendar/global-arbovirus-initiative (accessed August 28, 2023).

Young, P. R. (2018). Arboviruses: a family on the move. *Adv. Exp. Med. Biol.* 1062, 1–10. doi: 10.1007/978-981-10-8727-1_1

frontiers | Frontiers in Microbiology

TYPE Review
PUBLISHED 30 October 2023
DOI 10.3389/fmicb.2023.1257024

OPEN ACCESS

EDITED BY
Ke Liu,
Chinese Academy of Agricultural Sciences, China

REVIEWED BY
Luciana Barros Arruda,
Federal University of Rio de Janeiro, Brazil
Lauro Velazquez-Salinas,
Agricultural Research Service (USDA), United States

*CORRESPONDENCE
Sébastien Nisole
✉ sebastien.nisole@inserm.fr

RECEIVED 11 July 2023
ACCEPTED 11 October 2023
PUBLISHED 30 October 2023

CITATION
Zoladek J and Nisole S (2023) Mosquito-borne flaviviruses and type I interferon: catch me if you can!
Front. Microbiol. 14:1257024.
doi: 10.3389/fmicb.2023.1257024

Mosquito-borne flaviviruses and type I interferon: catch me if you can!

Jim Zoladek and Sébastien Nisole*

Viral Trafficking, Restriction and Innate Signaling, CNRS, Institut de Recherche en Infectiologie de Montpellier (IRIM), Université de Montpellier, Montpellier, France

Mosquito-borne flaviviruses include many viruses that are important human pathogens, including Yellow fever virus, Dengue virus, Zika virus and West Nile virus. While these viruses have long been confined to tropical regions, they now pose a global public health concern, as the geographical distribution of their mosquito vectors has dramatically expanded. The constant threat of flavivirus emergence and re-emergence underlines the need for a better understanding of the relationships between these viruses and their hosts. In particular, unraveling how these viruses manage to bypass antiviral immune mechanisms could enable the design of countermeasures to limit their impact on human health. The body's first line of defense against viral infections is provided by the interferon (IFN) response. This antiviral defense mechanism takes place in two waves, namely the induction of type I IFNs triggered by viral infection, followed by the IFN signaling pathway, which leads to the synthesis of interferon-stimulated genes (ISGs), whose products inhibit viral replication. In order to spread throughout the body, viruses must race against time to replicate before this IFN-induced antiviral state hinders their dissemination. In this review, we summarize our current knowledge on the multiple strategies developed by mosquito-borne flaviviruses to interfere with innate immune detection and signaling pathways, in order to delay, if not prevent, the establishment of an antiviral response.

KEYWORDS

flavivirus, type I interferon, viral antagonists, innate signaling, antiviral immunity

1. Introduction

Flaviviridae is a family of enveloped, positive-strand RNA viruses, many of which are spread by arthropod vectors (mainly ticks and mosquitoes). Within this viral family, the orthoflavivirus genus (hereafter referred to as flavivirus for simplicity) comprises arboviruses with a significant impact on public health (Smith, 2017; Pierson and Diamond, 2020), including Yellow fever virus (YFV), Dengue virus (DENV), Zika virus (ZIKV), Japanese encephalitis virus (JEV), and West Nile virus (WNV). These viruses are transmitted by the bite of mosquitoes, mainly of the genera *Aedes* and *Culex* (Figure 1). Once introduced in the skin, flaviviruses are capable of disseminating throughout the body and replicating in numerous organs. Flaviviruses can be classified according to the type of infection they cause in humans, which can be visceral (such as YFV, DENV, or ZIKV) and/or neurotropic (such as WNV, JEV, and ZIKV). In both cases, infections are often asymptomatic, but can cause severe and sometimes fatal symptoms, including hemorrhages, encephalitis, myelitis, paralysis or congenital malformations.

Given the recent and spectacular geographical expansion of these mosquitoes, in particular *Aedes albopictus* and *Aedes aegypti*, arboviruses have become a global health problem. Indeed,

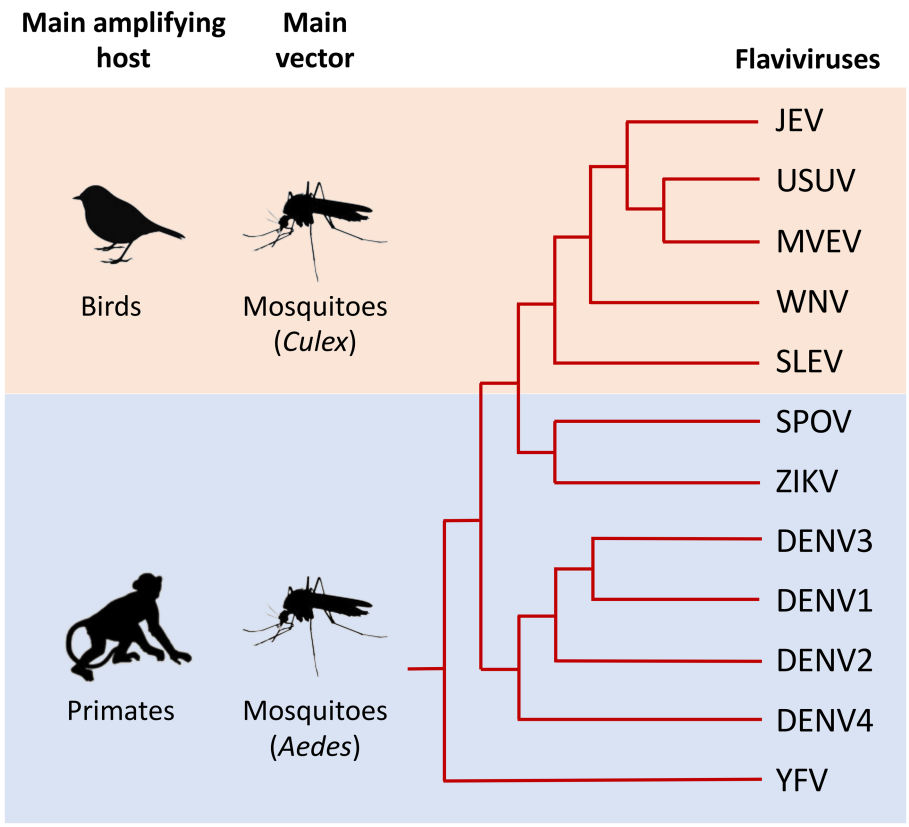

FIGURE 1
Schematic phylogeny illustrating the genetic relationships between the main flaviviruses transmitted by mosquitoes that are pathogenic to humans. Main amplifying hosts and vectors of the selected viruses are indicated on the left. The relationships between selected flaviviruses are shown in the dendrogram on the right. Evolutionary distance is not represented in this figure. Japanese encephalitis virus (JEV), Usutu virus (USUV), Murray Valley encephalitis virus (MVEV), West Nile virus (WNV), St. Louis encephalitis virus (SLEV), Spondweni virus (SPOV), Zika virus (ZIKV), Dengue virus 1, 2, 3, and 4 (DENV1, 2, 3, and 4), Yellow fever virus (YFV). Adapted from Mukhopadhyay et al. (2005), Lazear and Diamond (2016), and Foulongne et al. (2018).

whereas they were restricted to tropical and sub-tropical regions until recently, flaviviruses now represent a threat also in temperate regions (Smith, 2017; Pierson and Diamond, 2020). Among them, Dengue is the most common and important arthropod-borne viral disease in humans. Its global incidence has grown dramatically in recent decades and all four dengue virus serotypes (DENV1-4) now threaten about half of the world population (Bhatt et al., 2013; Messina et al., 2019). Although DENV infection is often asymptomatic, it can cause a spectrum of illnesses, ranging from flu-like symptoms (Dengue fever) to the more severe and sometimes fatal Dengue hemorrhagic fever, which can progress to Dengue shock syndrome (Rigau-Pérez et al., 1998). According to the World Health Organization (WHO), the number of reported Dengue fever cases has increased from 500,000 cases in 2000 to more than 5 million in 2019 (source WHO, Dengue and severe dengue. Available at: https://www.who.int/news-room/fact-sheets/detail/dengue-and-severe-dengue. Accessed August, 2023).

ZIKV has also emerged as a major threat to human health. Indeed, while only sporadic infections were described in Africa and Asia from the 1960s until the 2000s, no major epidemics occurred until 2007, the year of the first outbreak of ZIKV-related disease on the Yap Island in Micronesia (Duffy et al., 2009). In the following years, two far greater epidemics occurred, the first in French Polynesia in 2013–2014 and the second which started in Brazil in 2015 and then spread to the rest of South America as well as in Central America in 2015–2016 (Zanluca et al., 2015; Faria et al., 2016). The epidemic had important impacts on the health of populations, coinciding with cases of Guillain-Barré syndrome in some adults and an unexpected epidemic of newborns with microcephaly and other neurological deficiencies, following *in utero* exposure to the virus (Mlakar et al., 2016). In February 2016, the WHO declared Zika-related microcephaly a Public Health Emergency of International Concern. This alert has now been lifted, but the virus remains under close surveillance by health authorities (Musso et al., 2019).

Unlike DENV and ZIKV, whose amplifying hosts are primates (including humans), WNV mainly infects birds, and humans are only incidental hosts (Campbell et al., 2002; McVey et al., 2015). Nevertheless, this emerging virus has caused major human epidemics over the last 20 years, including in New York in 1999, in Israel in 2000 and in Greece in 2010 (Jia et al., 1999; Bin et al., 2001; Hayes, 2001; Danis et al., 2011). The global emergence of WNV is perfectly illustrated by its recent rapid expansion in the United States. Indeed, since its sudden emergence in New York in 1999, the virus has quickly spread across the United States, resulting in over 56,000 reported cases and more than 2,700 deaths [source CDC, Historic Data (1999–2022). Available at: https://www.cdc.gov/westnile/statsmaps/historic-data.html. Accessed August, 2023]. It is currently considered one of the zoonotic diseases of greatest concern for the US population (Ronca et al., 2021). WNV belongs to the Japanese encephalitis virus (JEV)

serocomplex (Chan et al., 2022). Both WNV and JEV are neurotropic viruses that can cause severe neurological symptoms, including encephalitis, meningitis or acute flaccid paralysis. However, while WNV circulates throughout most of the world, JEV is predominantly found in Asia, where it represents the leading cause of viral encephalitis (Le Flohic et al., 2013; Caldwell et al., 2022).

YFV is found in tropical and subtropical areas of Africa and South America (Chen and Wilson, 2020; Tuells et al., 2022). In these regions, yellow fever (YF) remains a widespread threat despite a very efficient, safe and affordable live-attenuated vaccine (Chen and Wilson, 2020; Tuells et al., 2022). The clinical spectrum of YF ranges from mild non-specific viral symptoms to a severe clinical course culminating in liver failure, renal failure, cardiovascular instability, which can be fatal. Most cases of YF are reported in Africa, and a modeling study based on African data sources estimated that in 2013, yellow fever caused 84,000–170,000 severe cases and 29,000–60,000 deaths (Garske et al., 2014).

In addition to these main human pathogens, many other flaviviruses transmitted by mosquitoes are responsible for sporadic cases or local epidemics, including the Usutu virus (USUV), Murray Valley encephalitis virus (MVEV), St. Louis encephalitis virus (SLEV) or Spondweni virus (SPOV) (Figure 1).

The factors that govern the severity of infections are still not completely understood, but both viral and host factors exist (Fernandez-Garcia et al., 2009; Pierson and Diamond, 2020; van Leur et al., 2021). Among host factors, antiviral innate immunity is likely to play a central role, since it is the first line of defense against viral infections and, depending on its capacity to control viral replication in the early stages of infection, it allows or not viruses to disseminate within the whole body (Fernandez-Garcia et al., 2009; van Leur et al., 2021). As a result, flaviviruses have developed multiple strategies to interfere with innate immunity, and in particular with the interferon (IFN) response, the armed wing of antiviral defenses.

The first descriptions of flavivirus-encoded proteins that inhibit the IFN response date from the early 2000s (Muñoz-Jordán et al., 2003, 2005; Lin et al., 2004; Guo et al., 2005; Jones et al., 2005; Liu et al., 2005), and subsequent research aimed at elucidating the multiple mechanisms involved has been intense. This topic has already been the subject of excellent reviews, including (Gack and Diamond, 2016; Cumberworth et al., 2017; Miorin et al., 2017). In this review, we aim to provide an update on the state of the art, given the constant progression of this field. Specifically, we summarize the state of knowledge on how infected cells trigger the IFN response following flavivirus infection and how these viruses manage to inhibit every single step of this response, focusing on mosquito-borne pathogenic viruses. We detail common and virus-specific strategies that allow flaviviruses to escape detection, block signaling pathways leading to IFN synthesis, and also prevent IFN signaling, in order to escape its powerful antiviral activity and thus be able to propagate.

2. Structure and replication cycle of flaviviruses

Flaviviruses are small enveloped viruses, whose genome consists of a 10 to 11 kb positive-sense single-stranded RNA, which contains a single open reading frame (ORF), flanked by 5′ and 3′ non-coding regions. This ORF encodes a single polyprotein which is co- and post-translationally processed by host and viral proteases into 10 proteins: 3 structural proteins, the capsid (Cap), a precursor of the membrane protein (prM) and the envelope glycoprotein (Env), as well as 7 non-structural proteins (NS1, NS2A, NS2B, NS3, NS4A, NS4B, and NS5). The Cap proteins constitute the icosahedral capsid which contains the viral genome, while the prM and Env proteins are incorporated into the membrane of the virions. The NS1 protein is a non-structural glycoprotein, important for the replication of flaviviruses. It exists as dimers, which are associated to membranes and as hexamers, which are secreted by the infected cells (Rastogi et al., 2016). NS2B is a transmembrane protein and serves as a cofactor of the NS3 protein, the viral protease, which is involved in the proteolytic cleavage of the polyprotein. While NS3 carries a serine protease activity in its N-terminal domain, its C-terminal domain possesses 5′-RNA triphosphatase (RTPase), nucleoside triphosphatase (NTPase), and helicase activities. NS5 is the viral RNA-dependent RNA polymerase. It also contains a methyltransferase activity in its N-terminal part, necessary for the methylation of the 5′ cap of the viral RNA (Ray et al., 2006). NS2A, NS4A, and NS4B are transmembrane proteins anchored to the endoplasmic reticulum (ER). Together with the other NS proteins, they participate in viral RNA replication and also in the evasion of host immune response.

Following the bite of an infected female mosquito, the skin is the first organ to be infected. Flaviviruses can replicate in fibroblasts, keratinocytes, and also in resident immune cells of the skin (Garcia et al., 2017). If flaviviruses can infect so many different cell types, it is because they are able to use many receptors to enter cells, including phosphatidylserine receptors and C-type lectins (Laureti et al., 2018). Following the interaction of envelope glycoproteins with their receptors, most flaviviruses penetrate their target cells by clathrin-dependent endocytosis (Figure 2). Once in late endosomes, the drop in pH induces a change in the conformation of the Env proteins, allowing the fusion of the viral and endosomal membranes (Mukhopadhyay et al., 2005) (Figure 2). Following its uncoating in the cytoplasm, the viral RNA is translated by ribosomes into polyproteins, which will then be cleaved by cellular and viral proteases (Rice et al., 1985) (NS2B/3).

Viruses replicate in invaginations of the ER membrane (Welsch et al., 2009; Den Boon and Ahlquist, 2010; Gillespie et al., 2010) (Figure 2). Within these virus-induced compartments, non-structural proteins form replication complexes, in which viral RNA is replicated. Viral assembly takes place at the ER membrane, close to sites of viral RNA replication (Welsch et al., 2009; Gillespie et al., 2010). These new immature virions will bud in the lumen of the endoplasmic reticulum then transit to the Golgi complex. It is in this compartment that furin cleaves the pr domain of the prM protein, allowing the release of mature infectious virions from the cell (Mukhopadhyay et al., 2005) (Figure 2).

3. The interferon response

The body's first line of defense against viral infections is provided by the IFN response. IFNs are a family of antiviral cytokines that have been discovered more than 60 years ago (Isaacs and Lindenmann, 1957). They have no intrinsic antiviral properties, but act through the induction of hundreds of interferon-stimulated genes (ISGs), whose products confer the cells a so-called antiviral

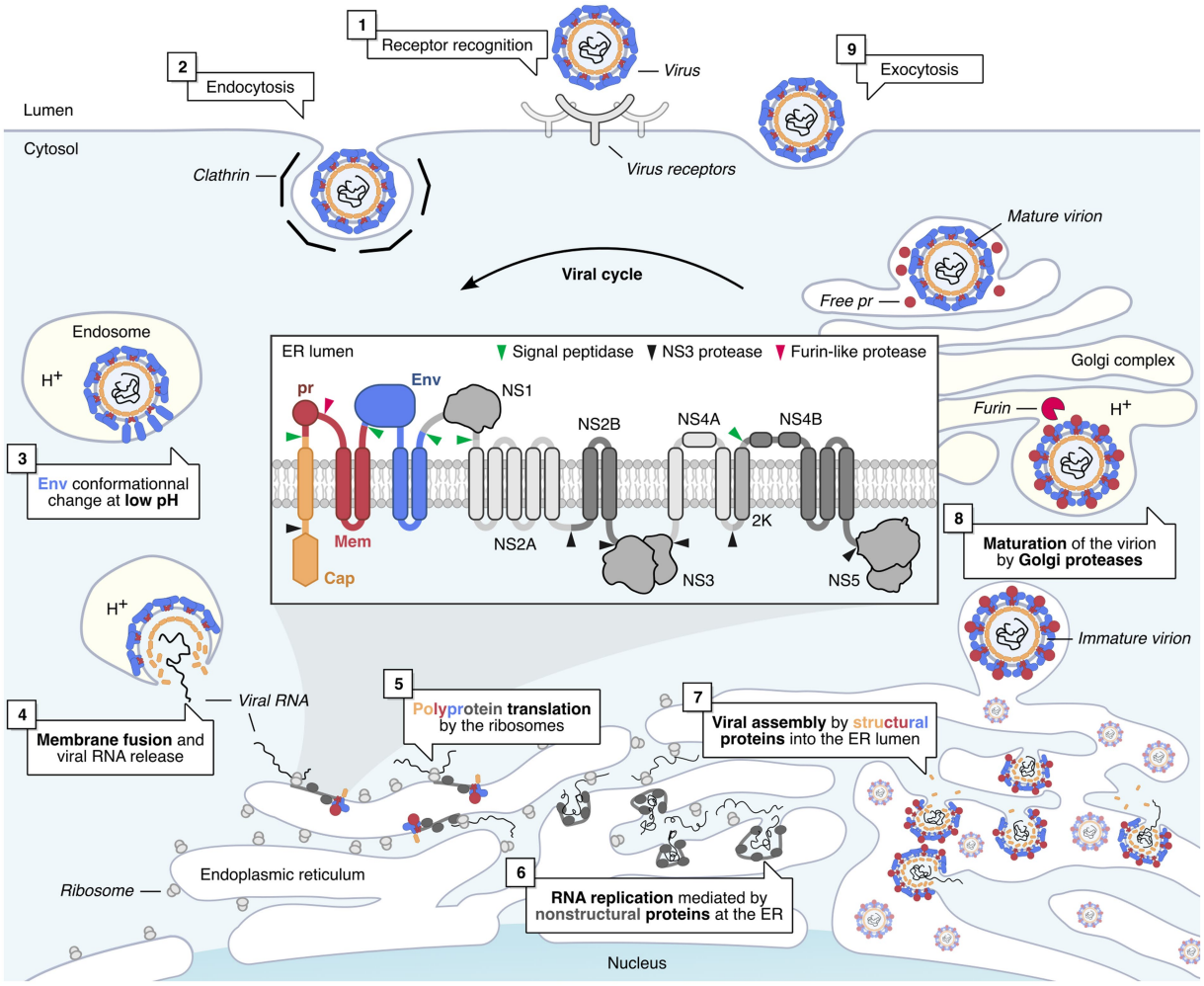

FIGURE 2
Flavivirus life cycle in mammalian cells. Flavivirus infection is initiated by the recognition of the virus by cell receptors (1) (Laureti et al., 2018). This triggers the clathrin-mediated endocytosis of the virus (2). The virus is then transported to the late endosomes (3), where the pH drops, triggering the Envelope-mediated fusion with the endosome membrane (4) (Mukhopadhyay et al., 2005). Once released in the cytoplasm, the viral genome is translated by host ribosomes into the viral polyprotein, which is co-translationally processed and cleaved by viral and cellular proteases into individual proteins (5) (Rice et al., 1985). Non-structural (NS) viral proteins form replication factories, which replicate viral RNA genomes within invaginated endoplasmic reticulum (ER) compartments (6) (Welsch et al., 2009; Gillespie et al., 2010). Structural proteins are assembled around newly replicated viral RNA, and the newly formed virions bud into the lumen of the ER and are then transported to the Golgi complex (7) (Mukhopadhyay et al., 2005). In the Golgi, immature virions are matured by a furin-like protease, which cleaves the pr peptide from prM, resulting in infectious virions (8) (Mukhopadhyay et al., 2005). The viral progeny is then released by exocytosis (9).

state. IFNs are typically divided into three classes: Type I (mainly IFN-α and -β), type II (IFN-γ), and type III (IFN-λs) (Schneider et al., 2014). While the direct antiviral effects of type II IFN are limited, type I and III IFNs induce a potent antiviral state within target cells, but with a different spectrum of action (Schneider et al., 2014). Indeed, while almost all nucleated cells are able to respond to IFN type I, the response to IFN type III is limited to epithelial cells and certain immune cells (Sommereyns et al., 2008). For this reason, we will only discuss the relationship between flaviviruses and IFN type I in this review.

This antiviral defense mechanism proceeds in two waves, namely the induction of type I IFN, triggered by viral infection, and the type I IFN signaling pathway, which leads to the synthesis of ISGs. These two steps of the IFN response are detailed below.

3.1. Innate immune sensing

Cellular sensors called pattern-recognition receptors (PRRs) are able to detect pathogens through the recognition of specific pathogen-associated molecular patterns, or PAMPs (Kumar et al., 2011; Dolasia et al., 2018; Zhu and Fernandez-Sesma, 2020). In the case of viruses, it is essentially the viral genetic material that is detected by these PRRs. Once activated, these receptors trigger two main signaling pathways: the NF-κB pathway, which leads to the production of inflammatory cytokines, and the IRF3/IRF7 pathway, which results in the expression of IFNs. To induce the expression of type I IFNs, each PRR engages its own signaling pathway, but they all converge to a common event, namely the activation of the TBK1 and IKKε kinases, which phosphorylate the transcription factors

IRF3 and IRF7, inducing their translocation into the nucleus where they induce the transcription of type I IFNs (mainly IFN-α and -β) (Figure 3).

PRRs can be classified into different categories, depending on their subcellular localization and on the type of PAMPs that they can sense. The first category consists of TLRs (for "Toll-like receptors"), which are located at the cell surface or within the endosomes, and which are mainly expressed by immune cells (Kawai and Akira, 2010; Fitzgerald and Kagan, 2020). There are 10 TLRs in humans, which differ in their subcellular location, but also in the molecules they detect. Among the TLRs that can detect viral RNAs, TLR3 and TLR7/8 recognize dsRNA and ssRNA within endosomes, respectively. In order to trigger activation pathways, TLRs require TIR-domain-containing adaptors (O'Neill and Bowie, 2007). There are 5 of these adaptors, including Myd88, necessary for the signaling downstream of many TLRs and TRIF, which is specific for TLR3. It is the recruitment of this adaptor at the level of the TLR which induces the activation of TBK1 and IKKε, ultimately leading to the induction of type I IFN.

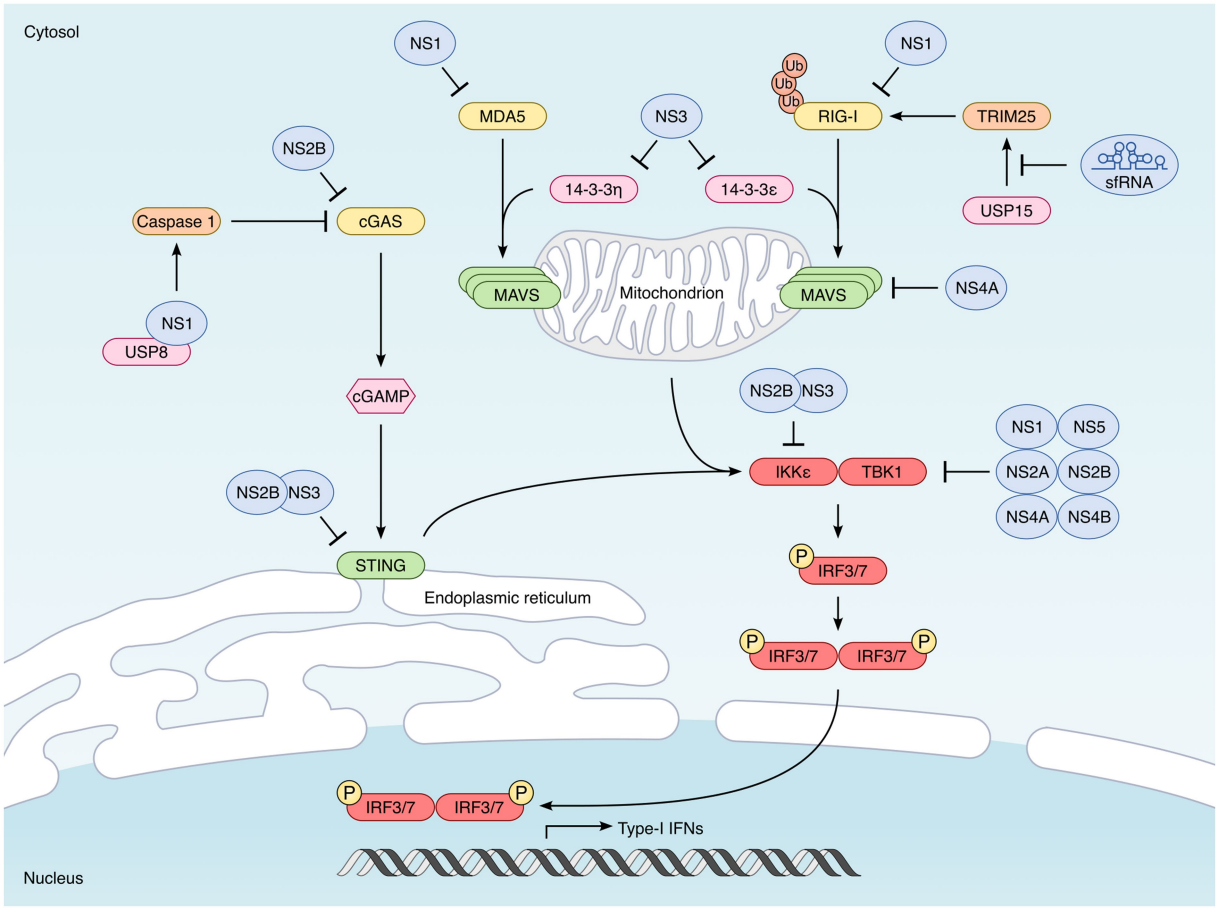

FIGURE 3
Strategies developed by mosquito-borne flaviviruses to interfere with type I IFN synthesis. Induction of type I IFN is triggered by the recognition of specific pathogen-associated molecular patterns (PAMPs) by cellular sensors known as pattern-recognition receptors (PRRs). In the case of viruses, it is essentially their genomes that are detected. The main PRRs triggered by flavivirus infection are the cytoplasmic RIG-I-like receptors (RLRs), RIG-I and MDA5. Once activated, RIG-I and MDA5 interact with the downstream signaling MAVS, located in the outer membrane of the mitochondria. This interaction leads to the activation of TBK1 and IKKε kinases which phosphorylate the transcription factors IRF3 and IRF7, inducing their translocation into the nucleus where they induce the transcription of type I IFNs. Flaviviruses also activate the cytoplasmic DNA sensor cGAS, not directly, but through the cytoplasmic leakage of mitochondrial DNA they induce (Kato et al., 2011; Goubau et al., 2013). Upon activation, cGAS dimerizes and catalyzes the synthesis of 2′,3′-cyclic GMP–AMP (cGAMP). This second messenger is recognized by STING, localized at the endoplasmic reticulum, which leads to the activation TBK1 and IKKε. Flaviviruses have developed multiple strategies to counteract each step of these signaling pathways leading to type I IFN synthesis. The main antagonists are indicated in the picture. One of them is not a viral protein but highly structured non-coding RNAs called sfRNA (for "subgenomic flavivirus RNA"), derived from the 3′ non-coding region of viral genomes (Pijlman et al., 2008; Chapman et al., 2014). sfRNA inhibit RIG-I by preventing its polyubiquitination by TRIM25 (Manokaran et al., 2015). The NS1 protein encoded by WNV acts directly on PRRs, and promotes the degradation of RIG-I, MDA5 (Zhang et al., 2017) and also cGAS (Zheng et al., 2018). DENV NS2B also binds to and induces cGAS degradation (Aguirre et al., 2017). Downstream of PRRs, the NS3 proteins encoded by DENV, WNV and ZIKV inhibit the cytosolic-to mitochondrial translocation of RIG-I, by preventing its interaction with the chaperone protein 14-3-3ε (Chan and Gack, 2016; Riedl et al., 2019). ZIKV NS3 can bind additionally to 14-3-3η, thus preventing the translocation of MDA5 (Lin J. P. et al., 2019; Riedl et al., 2019). MAVS is also targeted by viral antagonists, such as the NS4A protein encoded by DENV and ZIKV, which prevents the interaction between RIG-I and MAVS (He et al., 2016; Ma et al., 2018; Hu et al., 2019). STING has been shown to be degraded by the NS2B/3 protease complex of many mosquito-borne flaviviruses, including DENV, ZIKV, WNV, and JEV (Rodriguez-Madoz et al., 2010; Aguirre et al., 2012; Yu et al., 2012; Ding et al., 2018). IKKε is also targeted by the DENV NS2B/3 protease complex (Angleró-Rodríguez et al., 2014), while TBK1 can be targeted by multiple flavivirus non-structural proteins, including NS1 (ZIKV) NS2A (DENV and ZIKV), NS2B (ZIKV), NS4A (DENV), NS4B (DENV, ZIKV, and WNV) and NS5 (ZIKV) (Dalrymple et al., 2015; Lubick et al., 2015; Wu et al., 2017; Xia et al., 2018; Lin S. et al., 2019).

The other category of PRR are RIG-I-like receptors (RLRs), including RIG-I and MDA5, which detect viral RNA in the cytoplasm of most cells. Once activated, RIG-I and MDA5 interact with the downstream signaling adaptor called Mitochondrial antiviral-signaling protein (MAVS, also designated IPS-1, VISA, or Cardif), via their CARD domain. This interaction leads to the recruitment of TRAF3 and the subsequent activation of TBK1 and IKKε kinases (Takeuchi and Akira, 2010; Loo and Gale, 2011) (Figure 3).

Finally, there are also some cytoplasmic DNA sensors, such as cGAS (Kato et al., 2011; Goubau et al., 2013). Upon detection of DNA in the cytoplasm, cGAS dimerizes and catalyzes the synthesis of 2′,3′-cyclic GMP–AMP (cGAMP). This second messenger is then recognized by STING (for "stimulator of interferon genes"), localized at the endoplasmic reticulum, which leads to the activation TBK1 and IKKε (Ishikawa and Barber, 2008; Gao et al., 2013; Sun et al., 2013) (Figure 3).

3.2. Type I IFN signaling

Once their transcription is induced by IRF3/7, type I IFNs get translated and secreted. They act in an autocrine and paracrine manner, by binding to the heterodimeric IFNAR receptor, consisting of the IFNAR1 and IFNAR2 subunits (Takaoka and Yanai, 2006; Ivashkiv and Donlin, 2014) (Figure 4). This binding leads to the activation of the kinases TYK2 and JAK1, which then phosphorylate the transcription factors STAT1 and STAT2. Activated STAT1 and STAT2 heterodimerize and associate with IRF9 to form the ISGF3 complex, which translocates in the nucleus and binds to the Interferon-Stimulated Response Elements (ISRE) present in the promoter of ISGs (Figure 4) (Fu et al., 1990; Schindler et al., 1992). It is the expression of these ISGs that will protect the cells from infections (Schoggins et al., 2011; Schneider et al., 2014; Berthoux, 2020; Martin and Nisole, 2020).

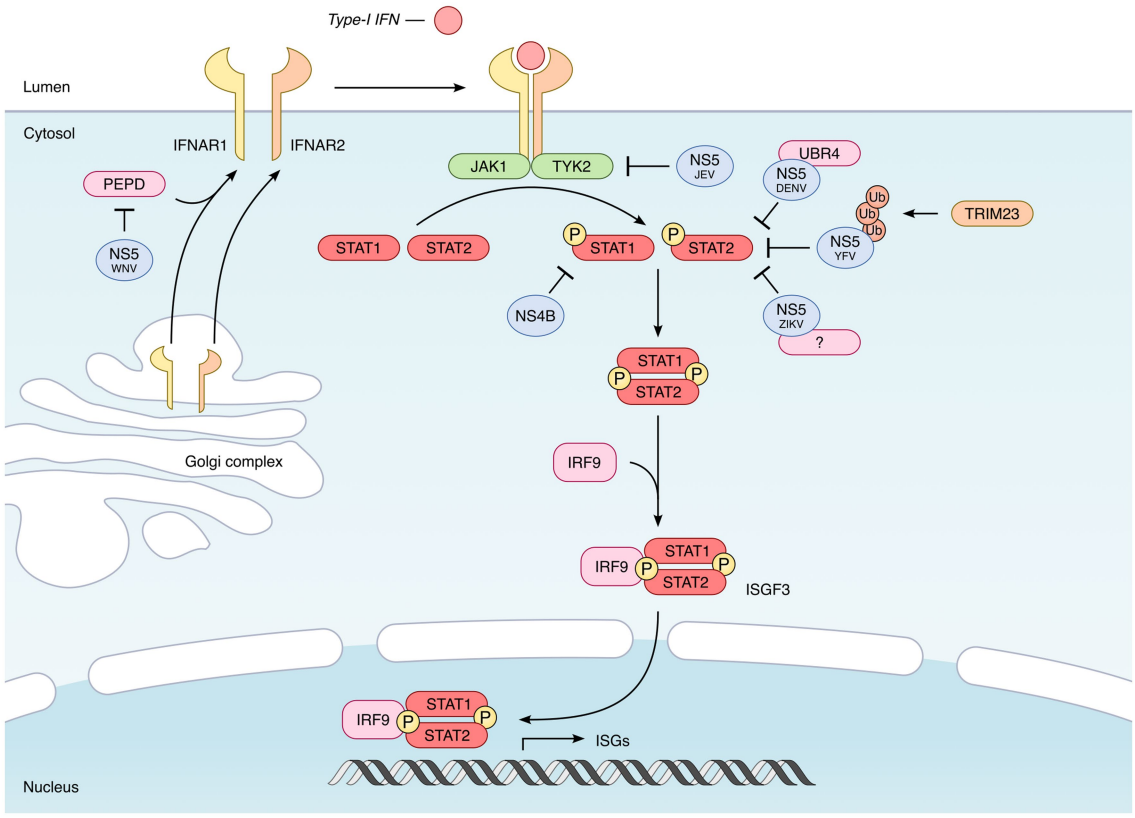

FIGURE 4
Inhibition of the IFN signaling by mosquito-borne flaviviruses. Once secreted by infected cells, type I IFNs bind to their receptor, which consists of the IFNAR1 and IFNAR2 subunits. This binding leads to the activation of the TYK2 and JAK1 kinases, which phosphorylate the transcription factors STAT1 and STAT2. Phosphorylated STAT1–STAT2 heterodimers then recruit IRF9 to form the ISGF3 complex, which translocates in the nucleus and activates the expression of hundreds of IFN-induced genes (ISGs). In the case of all mosquito-borne flaviviruses tested, the NS5 protein proved to be the main viral agonist of the JAK–STAT pathway, but through different mechanisms. The NS5 protein encoded by DENV, ZIKV, and YFV targets STAT2 and induces its proteasomal degradation (Jones et al., 2005; Ashour et al., 2009; Mazzon et al., 2009; Laurent-Rolle et al., 2014; Grant et al., 2016; Kumar et al., 2016). However, while DENV NS5 was found to recruit the E3 ubiquitin ligase UBR4 (Morrison et al., 2013) in order to induce STAT2 degradation, ZIKV and YFV-encoded NS5 do not require UBR4 (Laurent-Rolle et al., 2014; Grant et al., 2016; Kumar et al., 2016). In the case of YFV, NS5-STAT2 interaction requires the IFN-induced phosphorylation of STAT1 and the TRIM23-induced K63-linked polyubiquitination of NS5 (Laurent-Rolle et al., 2014). The NS5 protein encoded by JEV also inhibits the JAK/STAT pathway, but presumably by preventing Tyk2 phosphorylation (Lin et al., 2004, 2006; Yang et al., 2013). Finally, WNV NS5 inhibits the expression of IFNAR1 by recruiting prolidase (PEPD), a cellular peptidase (Laurent-Rolle et al., 2010; Lubick et al., 2015). Besides NS5, other flavivirus-encoded proteins could also participate in the inhibition of type I IFN signaling. This is the case of NS4B, which interferes with the phosphorylation of STAT1 and its nuclear translocation, as shown for several flaviviruses, including DENV, YFV, ZIKV, and WNV (Liu et al., 2005; Muñoz-Jordán et al., 2005; Fanunza et al., 2021b).

4. Sensing of flaviviruses

Endosomal TLRs, and in particular TLR3, participate in the detection of flaviviruses in certain cell types, as well as in the physiopathology of infection, but their involvement in the induction of the IFN response is relatively modest. Indeed, while the ability of TLR3 to trigger type I IFN synthesis has been demonstrated in certain cell models following infection by DENV (Tsai et al., 2009; Nasirudeen et al., 2011), the results obtained with other flaviviruses, in particular ZIKV or WNV, are less clear (Fredericksen and Gale, 2006; Hamel et al., 2015). It has been shown in a mouse model that the absence of TLR3 does not influence the replication of WNV in peripheral tissues, nor the IFN-α/β response, but leads to a higher mortality of mice, probably because of a protective role of TLR3 in the central nervous system (Daffis et al., 2008). A study has recently shown that, in human neural progenitor cells, TLR3 is involved in the synthesis of pro-inflammatory cytokines following ZIKV infection, but not in the synthesis of type I IFN (Plociennikowska et al., 2021). Furthermore, the authors showed that TLR3 activation inhibits RIG-I-induced type I IFN production (Plociennikowska et al., 2021). TLR3 therefore seems to be involved in the proinflammatory response and the physiopathology of flavivirus infections, but not or only modestly in the IFN response. Flaviviruses can also be sensed by TLR7 within endosomes, but this only occurs in plasmacytoid dendritic cells (pDCs) (Wang et al., 2006; Sun et al., 2009; Assil et al., 2019).

Unlike TLRs, numerous studies have demonstrated the predominant role of RIG-I and MDA-5 in the recognition of flavivirus RNAs and IFN response upon infection in most cells (Kato et al., 2006; Fredericksen et al., 2008; Loo et al., 2008). These two PRRs recognize double-stranded viral RNA in the cytoplasm and are partially redundant. In the case of flavivirus infections, they act in a coordinated manner, with an IFN response in two stages, first involving RIG-I, then MDA5 (Fredericksen and Gale, 2006; Fredericksen et al., 2008; Loo et al., 2008).

Besides the RNA sensors TLR3, RIG-I, and MDA5, the cGAS-STING axis, triggered by the presence of DNA in the cytoplasm, has also been shown to be involved in flavivirus infections (Schoggins et al., 2014). For instance, DENV infection causes mitochondrial membrane disruptions, leading to the leakage of mitochondrial DNA into the cytoplasm, thereby triggering the cGAS-STING pathway (Aguirre et al., 2017; Sun B. et al., 2017). As a consequence, cGAS$^{-/-}$ mice are more susceptible to flavivirus infection (Schoggins et al., 2014; Zheng et al., 2018).

5. How flaviviruses avoid or counteract innate sensing and signaling

Once the synthesis of IFN-induced expression of ISGs is engaged, cells become virtually uninfectable. This is the reason why viruses engage in a race against time to replicate before this IFN-induced antiviral state hinders their dissemination (Katze et al., 2002). To ensure victory, viruses have developed various strategies to prevent the synthesis of IFN, to limit the induction of ISGs or to inhibit the activities of antiviral mediators. In this context, flaviviruses master the art and manner of inhibiting every single step of the innate immune response, in order to delay, if not prevent, the establishment of an antiviral response (Katze et al., 2002).

5.1. Cloaking strategies

The surest way to evade the IFN response is to go unnoticed. In higher eukaryotic organisms, the cap of cellular mRNAs is 2′O-methylated by a methyltransferase in order to avoid their detection by MDA5 as non-self (Züst et al., 2011). While viruses whose replication takes place in the nucleus can take advantage of the cellular machinery to cap their RNAs and make them invisible to the vigilance of PRRs, viruses replicating in the cytoplasm must either steal the cap from cellular mRNAs, or possess their own enzymatic machinery (Decroly et al., 2012). It is this last strategy that flaviviruses use so that their genomic RNA is perceived as self. It is the NS5 protein that is responsible for the methylation of the cap, via its methyltransferase activity at its N-terminal domain (Ray et al., 2006).

In addition to evading detection by MDA5, the 2′O-methylation of the cap of flaviviruses also allows them to escape the antiviral activity of IFIT proteins (IFN-induced proteins with tetratricopeptide repeats), ISGs that inhibit the translation of unmethylated RNAs (Daffis et al., 2010).

The other strategy employed by flaviviruses to evade the detection by PRRs is to sequester their replication within endoplasmic reticulum invaginations where viral factories assemble (Welsch et al., 2009; Den Boon and Ahlquist, 2010; Gillespie et al., 2010), and which shields dsRNA replication intermediates from detection (Uchida et al., 2014).

5.2. Counteracting RLR functions

In addition to cloaking strategies, flaviviruses have also developed more aggressive mechanisms to block the activation of PRRs as well as downstream signaling pathways. First of all, it is the activation of RIG-I which is targeted. Following viral RNA recognition, RIG-I must undergo K63 polyubiquitination by the E3 ubiquitin ligase TRIM25, which allows its oligomerization and subsequent interaction with MAVS, in order to trigger the IFN response (Gack et al., 2007). To induce this ubiquitination, TRIM25 must itself be deubiquitinated beforehand by the ubiquitin-specific protease, USP15 (Pauli et al., 2014).

To interfere with the IFN response, flaviviruses use an original strategy, which involves subgenomic RNAs, designated sfRNA (for "subgenomic flavivirus RNA"). sfRNAs are highly structured non-coding RNAs measuring 0.3–0.5 kb in length, originating from the 3′ non-coding region, and generated by the partial degradation of viral RNAs by the exonuclease Xrn1 (Pijlman et al., 2008; Chapman et al., 2014). A WNV unable to generate sfRNAs was first shown to have attenuated replication in wild-type mice, but not in IRF3/7 KO or IFNAR KO mice (Schuessler et al., 2012). Later, Manokaran et al. demonstrated that the sfRNAs produced by DENV were able to interact directly with TRIM25 and inhibit its deubiquitination by USP15, thus preventing the activation of RIG-I (Manokaran et al., 2015) (Figure 3).

In addition to sfRNAs, a recent study showed that flavivirus capsid proteins could interact with TRIM25 and prevent it from

ubiquitinating RIG-I, thus inhibiting IFN synthesis (Airo et al., 2022) (Figure 3). This observation, made with the capsids of several flaviviruses, including ZIKV, DENV, YFV, JEV, MVEV, and SLEV, suggests that structural proteins may also be involved in the inhibition of the IFN response.

Besides TRIM25, the chaperone protein 14-3-3ε has also been described as an important cofactor of RIG-I, to which it binds in order to facilitate its translocation to mitochondria and interaction with MAVS (Liu et al., 2012) (Figure 3). Recent studies have shown that this chaperone protein can be targeted by flaviviruses in order to interfere with downstream RIG-I signaling, through their NS3 proteins. Indeed, a phosphomimetic motif within the NS3 proteins of DENV, WNV, and ZIKV has been shown to interact with 14-3-3ε, thus preventing its interaction with RIG-I and subsequent mitochondrial translocation (Chan and Gack, 2016; Riedl et al., 2019). In contrast, the NS3 protein of YFV is unable to interact with 14-3-3ε (Chan and Gack, 2016), while ZIKV NS3 can bind additionally to 14-3-3η, thus preventing the cytosolic-to mitochondrial translocation of MDA5 (Lin J. P. et al., 2019; Riedl et al., 2019) (Figure 3).

Downstream of RIG-I and MDA5, MAVS is also targeted by flavivirus-encoded antagonists. This is the case of the NS4A protein of DENV, which can interfere with the interaction between RIG-I and MAVS, by binding directly to MAVS (He et al., 2016) (Figure 3). This NS4A activity was also observed in the case of ZIKV (Ma et al., 2018; Hu et al., 2019). However, these two studies were carried out only under conditions of overexpression of the viral protein in cell lines, and these results must therefore be confirmed under infection conditions.

In addition, some studies have described the capacity of certain flavivirus proteins to directly inhibit RLRs. The NS1 encoded by WNV, in particular, can bind directly to RIG-I and MDA5 and cause their degradation by the proteasome (Zhang et al., 2017) (Figure 3). Recently, it is the prM protein of certain flaviviruses, including ZIKV, which has been proposed to interact with MDA5 and MAVS, thus preventing the interaction between these two proteins (Sui et al., 2023). However, these observations need to be confirmed by further studies.

5.3. Interfering with cytoplasmic DNA sensing

In addition to RLRs, flaviviruses have also evolved different strategies to inhibit the STING pathway, illustrating the importance of the DNA sensing axis (Schoggins et al., 2014). Here, it is the NS2B/3 protease complex that plays a decisive role, since it is able to recognize STING and to cleave it (Aguirre et al., 2012; Yu et al., 2012; Zhu et al., 2022) (Figure 3). This activity of the DENV NS2B/3 protease complex was previously shown to be important for the inhibition of IFN production in monocyte-derived dendritic cells (MDDCs), infected with DENV (Rodriguez-Madoz et al., 2010). It was subsequently shown that the anti-STING NS2B/3 activity described for DENV was also conserved in other flaviviruses, including ZIKV, WNV, and JEV, but not YFV (Ding et al., 2018).

In addition to its involvement in the NS2B/3 complex, the DENV NS2B protein alone was shown to interact with cGAS and to induce its degradation in an autophagy-lysosome-dependent mechanism (Aguirre et al., 2017) (Figure 3). Thus, during DENV infection, the protease NS3 and its cofactor NS2B can, on their own, inhibit the entire cGAS-STING pathway and prevent the mitochondrial DNA released into the cytoplasm from triggering the IFN response.

In the case of ZIKV, it is the NS1 protein that has been proposed to antagonize cGAS functions (Zheng et al., 2018). Mechanistically, ZIKV NS1 appears to promote the degradation of cGAS by caspase-1, by stabilizing the expression of the latter. The recruitment of the deubiquitinase USP8 by NS1 was shown to allow the cleavage of the poly-ubiquitin chains of caspase-1, thus preventing its proteosomal degradation (Zheng et al., 2018) (Figure 3).

5.4. Inhibiting downstream signaling pathways

Whether the trigger is viral RNA or mitochondrial DNA, all signaling pathways converge to TBK1 and IKKε, the two kinases that are responsible for IRF3 phosphorylation (Fitzgerald et al., 2003). It is therefore hardly surprising that flaviviruses prey on these two kinases in order to prevent the synthesis of IFN. First, it was proposed that the NS2B/3 protease complex of DENV binds directly to IKKε and prevents it from phosphorylating IRF3 (Angleró-Rodríguez et al., 2014) (Figure 3). Surprisingly, a catalytically inactive mutant of the viral protease is endowed with the same activity, suggesting that this catalysis-independent inhibition is probably due to steric hindrance (Angleró-Rodríguez et al., 2014).

TBK1 is also targeted by flavivirus non-structural proteins. In particular, the ectopic expression of the NS2A and NS4B proteins of DENV serotypes 1, 2, and 4 inhibits the autophosphorylation of TBK1 and therefore the phosphorylation of IRF3 (Dalrymple et al., 2015) (Figure 3). The NS4B protein of WNV also has this ability. Moreover, in the case of DENV1, NS4A was also shown to inhibit TBK1 (Dalrymple et al., 2015) (Figure 3). However, the authors did not evaluate whether the viral proteins could interact directly or not with TBK1, so the effect observed may be indirect (Dalrymple et al., 2015).

For ZIKV, it is NS1 and NS4B whose ectopic expression reduces TBK1 phosphorylation and IFN expression (Wu et al., 2017) (Figure 3). In this case, however, the co-immunoprecipitation of ZIKV NS1 and NS4B with exogenous TBK1 suggests that the effect could be direct (Wu et al., 2017). Additionally, a specific residue within ZIKV NS1 was found to be important for TBK1 inhibition (Xia et al., 2018). Indeed, the NS1 protein of an epidemic ZIKV mutant carries an A188V substitution, which allows it to interact with TBK1 and to inhibit its phosphorylation (Xia et al., 2018). Particularly convincingly, the introduction of this mutation in a non-epidemic strain decreases its ability to trigger IFN synthesis, while the reversion of this same mutation in the epidemic strain restores its ability to induce IFN- β (Xia et al., 2018).

In addition to NS1 and NS4B, the overexpression of ZIKV NS2A, or NS2B in HEK293T was also found to inhibit TBK1 phosphorylation (Xia et al., 2018), while ZIKV NS5 has been proposed to inhibit TBK1 by binding to its ubiquitin-like domain, thus preventing its interaction with TRAF6 (Lin S. et al., 2019) (Figure 3). Another study found ZIKV NS5 to rather act at a step downstream of IRF3 phosphorylation, through a direct interaction with IRF3 (Xia et al., 2018).

While TBK1 is obviously an interesting target for viruses, given its central role in the signaling pathways leading to type I IFN synthesis, it is nonetheless surprising that so many viral proteins could target a single cellular protein. It is therefore important that all studies carried out under overexpression conditions be confirmed in the context of infection.

6. How flaviviruses counteract IFN signaling

All tested flaviviruses proved capable of blocking the JAK/STAT signaling pathway, in order to prevent the synthesis of ISGs, in particular DENV (Muñoz-Jordán et al., 2003), ZIKV (Kumar et al., 2016), WNV (Guo et al., 2005), JEV (Lin et al., 2004), and YFV (Laurent-Rolle et al., 2014). Again, many non-structural proteins have been implicated in this inhibition, but NS5 appears to be the most effective viral antagonist. However, while all flaviviruses seem to inhibit type I IFN signaling through NS5, the mechanisms involved are virus-specific (Best, 2017).

The NS5 protein of DENV was shown to target STAT2 and to induce its degradation by the proteasome (Jones et al., 2005; Ashour et al., 2009; Mazzon et al., 2009), by recruiting the E3 ubiquitin ligase UBR4 (Morrison et al., 2013) (Figure 4).

ZIKV NS5 also binds to STAT2 and induces its proteosomal degradation, but, unlike DENV, it does not require UBR4, suggesting that another cellular protein may be involved (Grant et al., 2016; Kumar et al., 2016) (Figure 4). Whether it depends on other cellular proteins or not remains to be addressed. However and interestingly, it was recently reported that ZIKV sfRNAs potentiated the inhibitory effect of NS5, by binding to the viral protein and stabilizing it (Slonchak et al., 2022).

Surprisingly, the NS5 protein encoded by SPOV, a virus that is phylogenetically close to ZIKV, does not interact with STAT2 nor interfere with its phosphorylation (Grant et al., 2016). Given that SPOV NS5 is nonetheless capable of inhibiting type I IFN signaling, these observations suggest that it may act downstream of the pathway (Grant et al., 2016).

In the case of YFV again, NS5 was found to interact with STAT2, but only when cells have been previously stimulated with type I IFN (Laurent-Rolle et al., 2014). Indeed, this interaction was found to require the IFN-induced phosphorylation of STAT1 and the TRIM23-induced K63-linked polyubiquitination of NS5 (Laurent-Rolle et al., 2014) (Figure 4). As for ZIKV, this interaction is UBR4-independent.

JEV NS5 has also been shown to inhibit the JAK/STAT pathway, presumably by preventing Tyk2 tyrosine phosphorylation (Lin et al., 2004, 2006; Yang et al., 2013) (Figure 4).

Finally, WNV NS5 does not target STAT2 nor Tyk2, but the type I IFN receptor subunit IFNAR1 (Laurent-Rolle et al., 2010; Lubick et al., 2015), thus explaining why IFNAR1 is depleted in WNV-infected cells (Evans et al., 2011). Specifically, NS5 inhibits the expression of IFNAR1 by recruiting prolidase (PEPD), a cellular peptidase (Lubick et al., 2015). According to this study, PEPD would be involved in IFNAR1 biosynthesis, by facilitating its trafficking through the ER-to-golgi network (Lubick et al., 2015) (Figure 4).

NS5 seems therefore to play a predominant role for flaviviruses in order to counteract the antiviral effect of type I IFN. However, it is striking to note such a convergence of NS5 function in several flaviviruses, but with such a heterogeneity of mechanisms. Besides NS5, other flavivirus-encoded proteins could also participate in the inhibition of type I IFN signaling.

This is the case of NS4B which, in several flaviviruses, including DENV, YFV, ZIKV, and WNV, interferes with the phosphorylation of STAT1 and its nuclear translocation (Liu et al., 2005; Muñoz-Jordán et al., 2005; Fanunza et al., 2021b) (Figure 4). The involvement of the NS2B/3 protease complex of ZIKV has also been proposed, since its ectopic expression leads to the degradation of JAK1 (Wu et al., 2017). Finally, when overexpressed in HEK293T cells, ZIKV NS2A induces the degradation of STAT1 and STAT2 in a proteasome-dependent manner, suggesting an anti-IFN activity of this protein (Fanunza et al., 2021a). However, once again, these observations will have to be confirmed, particularly in the context of infection.

7. IFN and flaviviruses: from *in vitro* data to *in vivo* outcomes

As discussed above, many studies demonstrate that flaviviruses possess an important arsenal, consisting of sfRNAs, non-structural and possibly even structural proteins to prevent type I IFN synthesis and signaling. Importantly, the ability of flaviviruses to interfere with the IFN response has not only been observed *in vitro*, but also in infected patients. For example, RNA sequencing-based transcriptional profiling studies performed on cells isolated from ZIKV-infected patients revealed that the transcription of type I IFNs and ISGs was unaffected in infected patients, thus demonstrating the capacity of ZIKV to inhibit type I IFN production and type I IFN signaling *in vivo* (Sun X. et al., 2017; Carlin et al., 2018; Hu et al., 2019).

A large number of studies have also shown that the ability to efficiently antagonize the IFN response confers an important selective advantage to flaviviruses. There is therefore a correlation between the IFN resistance of a given virus and its replication efficiency, pathogenicity and/or epidemiological fitness (Keller et al., 2006; Manokaran et al., 2015; Xia et al., 2018; Castro-Jiménez et al., 2022).

However, although flaviviruses can inhibit IFN-induced responses, type I IFN still restricts viral replication *in vitro*, but only when added prior to infection, since it is much less effective once the infection is established (Diamond et al., 2000; Anderson and Rahal, 2002; Crance et al., 2003; Lin et al., 2004; Ho et al., 2005; Samuel and Diamond, 2005). Type I IFN is also able to effectively inhibit flavivirus replication and spread *in vivo*. In this respect, mice lacking the type I IFN receptor ($IFNAR^{-/-}$) or key components of the IFN signaling pathway such as STAT1 and STAT2, show markedly enhanced lethality and viral replication when infected with DENV (Shresta et al., 2004; Ashour et al., 2010), ZIKV (Lazear et al., 2016; Tripathi et al., 2017), YFV (Meier et al., 2009; Erickson and Pfeiffer, 2013), WNV (Samuel and Diamond, 2005; Keller et al., 2006), USUV (Martín-Acebes et al., 2016) or MVEV (Lobigs et al., 2003). Interestingly, in these IFN response-deficient mice, increased infection is observed in normally resistant cell populations and tissues, suggesting that type I IFN acts in part to restrict viral tropism.

The capacity of type I IFN to restrict flavivirus infection has also been confirmed in therapeutic disease models, since pretreatment with IFN-α or inducers of IFN-α has been shown to attenuate viral dissemination and to improve clinical outcome in mice or hamsters

infected by several viruses (Brooks and Phillpotts, 1999; Leyssen et al., 2003; Morrey et al., 2004; Julander et al., 2007; Chan et al., 2016).

However, despite these promising results in preclinical models, the therapeutic efficacy of type I IFN in patients has been disappointing. During a severe DENV epidemic in Cuba in 1981, IFN-α was administered to patients (Limonta Vidal et al., 1984). Although some clinical improvement was noted, no other trials have been reported and it is therefore difficult to draw conclusions from this single study. Another study reported the case of two patients with severe Japanese encephalitis, out of a group of four, who showed improvement in clinical signs and recovered from the infection after treatment with IFN-α, whereas the two patients who did not receive IFN died (Harinasuta et al., 1985). However, a randomized double-blind placebo-controlled trial performed on 112 Vietnamese children with suspected Japanese encephalitis concluded that IFN-α did not improve the outcome of patients (Solomon et al., 2003).

While the use of type I IFN in the treatment of flavivirus infections is therefore an unlikely prospect, other therapeutic strategies could exploit its antiviral potency. For example, an inhibitor of YFV NS4B was recently described as able to suppress viral replication as well as enhance IFN-β expression in infected cells (Gao et al., 2022). Therefore, compounds that counteract flavivirus-induced inhibition of the IFN response might be an interesting perspective.

8. Concluding remarks

Higher eukaryotes have developed sophisticated mechanisms to prevent the spread of viruses in the body. Type I IFN is the armed wing of these defenses. Extremely fast and efficient, the IFN response can abolish the replication of any virus, at least in theory. Indeed, most viruses have developed strategies to avoid detection, to inhibit IFN synthesis by infected cells or to prevent the establishment of an IFN-induced antiviral state in neighboring cells. As detailed in this review, flaviviruses are experts in terms of countermeasures, as they are able to interfere with every single step of the IFN response. The fact that all the proteins encoded by these viruses are involved in hijacking cellular defenses perfectly illustrates the incredible selection pressure that these defenses exert on viruses in general, and flaviviruses in particular. Strikingly, even the viral RNA is implicated, since flaviviruses have developed a particularly original mechanism involving non-coding subgenomic RNAs to prevent their detection. Our understanding of all these strategies has considerably progressed over the past decade, even if many gray areas remain. For instance, some degree of uncertainty remains for the many observations that were made by overexpressing individual flavivirus proteins, and which need to be confirmed under conditions of infection. Furthermore, while the involvement of non-structural viral proteins in the inhibition of the IFN response is very well documented, recent descriptions of a potential role for structural proteins will need to be confirmed by further studies (Airo et al., 2022; Sui et al., 2023). Finally, it is still not fully understood how the balance between the IFN response and viral antagonists influences the dissemination of flaviviruses in the body, and in particular how IFN manages to control viral replication in certain organs but not in others.

Elucidating the molecular mechanisms that allow flaviviruses to bypass cellular defenses in order to spread is an important issue, especially for the development of future vaccines and antivirals.

Author contributions

JZ: Writing – original draft, Writing – review & editing, Visualization. SN: Writing – original draft, Writing – review & editing, Conceptualization, Funding acquisition.

Funding

The author(s) declare financial support was received for the research, authorship, and/or publication of this article. This work was financially supported by the Agence Nationale de la Recherche (ANR-21-CE15-0041).

Acknowledgments

We thank Nathalie J. Arhel (CNRS, IRIM, Montpellier) for the critical reading of our manuscript.

Conflict of interest

The authors declare that the research was conducted in the absence of any commercial or financial relationships that could be construed as a potential conflict of interest.

The author(s) declared that they were an editorial board member of Frontiers, at the time of submission. This had no impact on the peer review process and the final decision.

Publisher's note

References

Aguirre, S., Luthra, P., Sanchez-Aparicio, M. T., Maestre, A. M., Patel, J., Lamothe, F., et al. (2017). Dengue virus NS2B protein targets cGAS for degradation and prevents mitochondrial DNA sensing during infection. *Nat. Microbiol.* 2:17037. doi: 10.1038/nmicrobiol.2017.37

Aguirre, S., Maestre, A. M., Pagni, S., Patel, J. R., Savage, T., Gutman, D., et al. (2012). DENV inhibits type I IFN production in infected cells by cleaving human STING. *PLoS Pathog.* 8:e1002934. doi: 10.1371/journal.ppat.1002934

Airo, A. M., Felix-Lopez, A., Mancinelli, V., Evseev, D., Lopez-Orozco, J., Shire, K., et al. (2022). Flavivirus capsid proteins inhibit the interferon response. *Viruses* 14:968. doi: 10.3390/v14050968

Anderson, J. F., and Rahal, J. J. (2002). Efficacy of interferon alpha-2b and ribavirin against West Nile virus *in vitro*. *Emerg. Infect. Dis.* 8, 107–108. doi: 10.3201/eid0801.010252

Angleró-Rodríguez, Y. I., Pantoja, P., and Sariol, C. A. (2014). Dengue virus subverts the interferon induction pathway via NS2B/3 protease-IκB kinase epsilon interaction. *Clin. Vaccine Immunol.* 21, 29–38. doi: 10.1128/CVI.00500-13

Ashour, J., Laurent-Rolle, M., Shi, P.-Y., and García-Sastre, A. (2009). NS5 of dengue virus mediates STAT2 binding and degradation. *J. Virol.* 83, 5408–5418. doi: 10.1128/JVI.02188-08

Ashour, J., Morrison, J., Laurent-Rolle, M., Belicha-Villanueva, A., Plumlee, C. R., Bernal-Rubio, D., et al. (2010). Mouse STAT2 restricts early dengue virus replication. *Cell Host Microbe* 8, 410–421. doi: 10.1016/j.chom.2010.10.007

Assil, S., Coléon, S., Dong, C., Décembre, E., Sherry, L., Allatif, O., et al. (2019). Plasmacytoid dendritic cells and infected cells form an Interferogenic synapse required for antiviral responses. *Cell Host Microbe* 25, 730–745.e6. doi: 10.1016/j.chom.2019.03.005

Berthoux, L. (2020). The Restrictome of Flaviviruses. *Virol. Sin.* 35, 363–377. doi: 10.1007/s12250-020-00208-3

Best, S. M. (2017). The many faces of the Flavivirus NS5 protein in antagonism of type I interferon signaling. *J. Virol.* 91, e01970–e01916. doi: 10.1128/JVI.01970-16

Bhatt, S., Gething, P. W., Brady, O. J., Messina, J. P., Farlow, A. W., Moyes, C. L., et al. (2013). The global distribution and burden of dengue. *Nature* 496, 504–507. doi: 10.1038/nature12060

Bin, H., Grossman, Z., Pokamunski, S., Malkinson, M., Weiss, L., Duvdevani, P., et al. (2001). West Nile fever in Israel 1999-2000: from geese to humans. *Ann. N. Y. Acad. Sci.* 951, 127–142. doi: 10.1111/j.1749-6632.2001.tb02691.x

Brooks, T. J., and Phillpotts, R. J. (1999). Interferon-alpha protects mice against lethal infection with St Louis encephalitis virus delivered by the aerosol and subcutaneous routes. *Antivir. Res.* 41, 57–64. doi: 10.1016/s0166-3542(98)00063-1

Caldwell, M., Boruah, A. P., and Thakur, K. T. (2022). Acute neurologic emerging flaviviruses. *Ther. Adv. Infect. Dis.* 9:204993612211026. doi: 10.1177/20493612211026664

Campbell, G. L., Marfin, A. A., Lanciotti, R. S., and Gubler, D. J. (2002). West Nile virus. *Lancet Infect. Dis.* 2, 519–529. doi: 10.1016/S1473-3099(02)00368-7

Carlin, A. F., Vizcarra, E. A., Branche, E., Viramontes, K. M., Suarez-Amaran, L., Ley, K., et al. (2018). Deconvolution of pro- and antiviral genomic responses in Zika virus-infected and bystander macrophages. *Proc. Natl. Acad. Sci. U. S. A.* 115, E9172–E9181. doi: 10.1073/pnas.1807690115

Castro-Jiménez, T. K., Gómez-Legorreta, L. C., López-Campa, L. A., Martínez-Torres, V., Alvarado-Silva, M., Posadas-Mondragón, A., et al. (2022). Variability in susceptibility to type I interferon response and subgenomic RNA accumulation between clinical isolates of dengue and Zika virus from Oaxaca Mexico correlate with replication efficiency in human cells and disease severity. *Front. Cell. Infect. Microbiol.* 12:890750. doi: 10.3389/fcimb.2022.890750

Chan, Y. K., and Gack, M. U. (2016). A phosphomimetic-based mechanism of dengue virus to antagonize innate immunity. *Nat. Immunol.* 17, 523–530. doi: 10.1038/ni.3393

Chan, K. R., Ismail, A. A., Thergarajan, G., Raju, C. S., Yam, H. C., Rishya, M., et al. (2022). Serological cross-reactivity among common flaviviruses. *Front. Cell. Infect. Microbiol.* 12:975398. doi: 10.3389/fcimb.2022.975398

Chan, J. F.-W., Zhang, A. J., Chan, C. C.-S., Yip, C. C.-Y., Mak, W. W.-N., Zhu, H., et al. (2016). Zika virus infection in dexamethasone-immunosuppressed mice demonstrating disseminated infection with multi-organ involvement including Orchitis effectively treated by recombinant type I interferons. *EBioMedicine* 14, 112–122. doi: 10.1016/j.ebiom.2016.11.017

Chapman, E. G., Costantino, D. A., Rabe, J. L., Moon, S. L., Wilusz, J., Nix, J. C., et al. (2014). The structural basis of pathogenic subgenomic flavivirus RNA (sfRNA) production. *Science* 344, 307–310. doi: 10.1126/science.1250897

Chen, L. H., and Wilson, M. E. (2020). Yellow fever control: current epidemiology and vaccination strategies. *Trop. Dis. Travel Med. Vaccines* 6:1. doi: 10.1186/s40794-020-0101-0

Crance, J. M., Scaramozzino, N., Jouan, A., and Garin, D. (2003). Interferon, ribavirin, 6-azauridine and glycyrrhizin: antiviral compounds active against pathogenic flaviviruses. *Antivir. Res.* 58, 73–79. doi: 10.1016/s0166-3542(02)00185-7

Cumberworth, S. L., Clark, J. J., Kohl, A., and Donald, C. L. (2017). Inhibition of type I interferon induction and signalling by mosquito-borne flaviviruses. *Cell. Microbiol.* 19:e12737. doi: 10.1111/cmi.12737

Daffis, S., Samuel, M. A., Suthar, M. S., Gale, M., and Diamond, M. S. (2008). Toll-like receptor 3 has a protective role against West Nile virus infection. *J. Virol.* 82, 10349–10358. doi: 10.1128/JVI.00935-08

Daffis, S., Szretter, K. J., Schriewer, J., Li, J., Youn, S., Errett, J., et al. (2010). 2′-O methylation of the viral mRNA cap evades host restriction by IFIT family members. *Nature* 468, 452–456. doi: 10.1038/nature09489

Dalrymple, N. A., Cimica, V., and Mackow, E. R. (2015). Dengue virus NS proteins inhibit RIG-I/MAVS signaling by blocking TBK1/IRF3 phosphorylation: dengue virus serotype 1 NS4A is a unique interferon-regulating virulence determinant. *mBio* 6, e00553–e00515. doi: 10.1128/mBio.00553-15

Danis, K., Papa, A., Theocharopoulos, G., Dougas, G., Athanasiou, M., Detsis, M., et al. (2011). Outbreak of West Nile virus infection in Greece, 2010. *Emerg. Infect. Dis.* 17, 1868–1872. doi: 10.3201/eid1710.110525

Decroly, E., Ferron, F., Lescar, J., and Canard, B. (2012). Conventional and unconventional mechanisms for capping viral mRNA. *Nat. Rev. Microbiol.* 10, 51–65. doi: 10.1038/nrmicro2675

Den Boon, J. A., and Ahlquist, P. (2010). Organelle-like membrane compartmentalization of positive-strand RNA virus replication factories. *Annu. Rev. Microbiol.* 64, 241–256. doi: 10.1146/annurev.micro.112408.134012

Diamond, M. S., Roberts, T. G., Edgil, D., Lu, B., Ernst, J., and Harris, E. (2000). Modulation of dengue virus infection in human cells by alpha, beta, and gamma interferons. *J. Virol.* 74, 4957–4966. doi: 10.1128/jvi.74.11.4957-4966.2000

Ding, Q., Gaska, J. M., Douam, F., Wei, L., Kim, D., Balev, M., et al. (2018). Species-specific disruption of STING-dependent antiviral cellular defenses by the Zika virus NS2B3 protease. *Proc. Natl. Acad. Sci. U. S. A.* 115, E6310–E6318. doi: 10.1073/pnas.1803406115

Dolasia, K., Bisht, M. K., Pradhan, G., Udgata, A., and Mukhopadhyay, S. (2018). TLRs/NLRs: shaping the landscape of host immunity. *Int. Rev. Immunol.* 37, 3–19. doi: 10.1080/08830185.2017.1397656

Duffy, M. R., Chen, T.-H., Hancock, W. T., Powers, A. M., Kool, J. L., Lanciotti, R. S., et al. (2009). Zika virus outbreak on Yap Island, Federated States of Micronesia. *N. Engl. J. Med.* 360, 2536–2543. doi: 10.1056/NEJMoa0805715

Erickson, A. K., and Pfeiffer, J. K. (2013). Dynamic viral dissemination in mice infected with yellow fever virus strain 17D. *J. Virol.* 87, 12392–12397. doi: 10.1128/JVI.02149-13

Evans, J. D., Crown, R. A., Sohn, J. A., and Seeger, C. (2011). West Nile virus infection induces depletion of IFNAR1 protein levels. *Viral Immunol.* 24, 253–263. doi: 10.1089/vim.2010.0126

Fanunza, E., Carletti, F., Quartu, M., Grandi, N., Ermellino, L., Milia, J., et al. (2021a). Zika virus NS2A inhibits interferon signaling by degradation of STAT1 and STAT2. *Virulence* 12, 1580–1596. doi: 10.1080/21505594.2021.1935613

Fanunza, E., Grandi, N., Quartu, M., Carletti, F., Ermellino, L., Milia, J., et al. (2021b). INMI1 Zika virus NS4B antagonizes the interferon signaling by suppressing STAT1 phosphorylation. *Viruses* 13:2448. doi: 10.3390/v13122448

Faria, N. R., Azevedo, R., Kraemer, M. U. G., Souza, R., Cunha, M. S., Hill, S. C., et al. (2016). Zika virus in the Americas: early epidemiological and genetic findings. *Science* 352, 345–349. doi: 10.1126/science.aaf5036

Fernandez-Garcia, M.-D., Mazzon, M., Jacobs, M., and Amara, A. (2009). Pathogenesis of Flavivirus infections: using and abusing the host cell. *Cell Host Microbe* 5, 318–328. doi: 10.1016/j.chom.2009.04.001

Fitzgerald, K. A., and Kagan, J. C. (2020). Toll-like receptors and the control of immunity. *Cells* 180, 1044–1066. doi: 10.1016/j.cell.2020.02.041

Fitzgerald, K. A., McWhirter, S. M., Faia, K. L., Rowe, D. C., Latz, E., Golenbock, D. T., et al. (2003). IKKepsilon and TBK1 are essential components of the IRF3 signaling pathway. *Nat. Immunol.* 4, 491–496. doi: 10.1038/ni921

Foulongne, V., Clé, M., Gutierrez, S., Perre, P. V., Salinas, S., and Simonin, Y. (2018). Usutu virus: let's be vigilant. *Virologie (Montrouge)* 22, 233–236. doi: 10.1684/vir.2018.0749

Fredericksen, B. L., and Gale, M. (2006). West Nile virus evades activation of interferon regulatory factor 3 through RIG-I-dependent and -independent pathways without antagonizing host defense signaling. *J. Virol.* 80, 2913–2923. doi: 10.1128/JVI.80.6.2913-2923.2006

Fredericksen, B. L., Keller, B. C., Fornek, J., Katze, M. G., and Gale, M. (2008). Establishment and maintenance of the innate antiviral response to West Nile virus involves both RIG-I and MDA5 signaling through IPS-1. *J. Virol.* 82, 609–616. doi: 10.1128/JVI.01305-07

Fu, X. Y., Kessler, D. S., Veals, S. A., Levy, D. E., and Darnell, J. E. (1990). ISGF3, the transcriptional activator induced by interferon alpha, consists of multiple interacting polypeptide chains. *Proc. Natl. Acad. Sci. U. S. A.* 87, 8555–8559. doi: 10.1073/pnas.87.21.8555

Gack, M. U., and Diamond, M. S. (2016). Innate immune escape by dengue and West Nile viruses. *Curr. Opin. Virol.* 20, 119–128. doi: 10.1016/j.coviro.2016.09.013

Gack, M. U., Shin, Y. C., Joo, C.-H., Urano, T., Liang, C., Sun, L., et al. (2007). TRIM25 RING-finger E3 ubiquitin ligase is essential for RIG-I-mediated antiviral activity. *Nature* 446, 916–920. doi: 10.1038/nature05732

Gao, D., Wu, J., Wu, Y.-T., Du, F., Aroh, C., Yan, N., et al. (2013). Cyclic GMP-AMP synthase is an innate immune sensor of HIV and other retroviruses. *Science* 341, 903–906. doi: 10.1126/science.1240933

Gao, Z., Zhang, X., Zhang, L., Wu, S., Ma, J., Wang, F., et al. (2022). A yellow fever virus NS4B inhibitor not only suppresses viral replication, but also enhances the virus activation of RIG-I-like receptor-mediated innate immune response. *PLoS Pathog.* 18:e1010271. doi: 10.1371/journal.ppat.1010271

Garcia, M., Wehbe, M., Lévêque, N., and Bodet, C. (2017). Skin innate immune response to flaviviral infection. *Eur. Cytokine Netw.* 28, 41–51. doi: 10.1684/ecn.2017.0394

Garske, T., Van Kerkhove, M. D., Yactayo, S., Ronveaux, O., Lewis, R. F., Staples, J. E., et al. (2014). Yellow fever in Africa: estimating the burden of disease and impact of mass

vaccination from outbreak and serological data. *PLoS Med.* 11:e1001638. doi: 10.1371/journal.pmed.1001638

Gillespie, L. K., Hoenen, A., Morgan, G., and Mackenzie, J. M. (2010). The endoplasmic reticulum provides the membrane platform for biogenesis of the flavivirus replication complex. *J. Virol.* 84, 10438–10447. doi: 10.1128/JVI.00986-10

Goubau, D., Deddouche, S., and Reis e Sousa, C. (2013). Cytosolic sensing of viruses. *Immunity* 38, 855–869. doi: 10.1016/j.immuni.2013.05.007

Grant, A., Ponia, S. S., Tripathi, S., Balasubramaniam, V., Miorin, L., Sourisseau, M., et al. (2016). Zika virus targets human STAT2 to inhibit type I interferon signaling. *Cell Host Microbe* 19, 882–890. doi: 10.1016/j.chom.2016.05.009

Guo, J.-T., Hayashi, J., and Seeger, C. (2005). West Nile virus inhibits the signal transduction pathway of alpha interferon. *J. Virol.* 79, 1343–1350. doi: 10.1128/JVI.79.3.1343-1350.2005

Hamel, R., Dejarnac, O., Wichit, S., Ekchariyawat, P., Neyret, A., Luplertlop, N., et al. (2015). Biology of Zika virus infection in human skin cells. *J. Virol.* 89, 8880–8896. doi: 10.1128/JVI.00354-15

Harinasuta, C., Nimmanitya, S., and Titsyakorn, U. (1985). The effect of interferon-alpha a on two cases of Japanese encephalitis in Thailand. *Southeast Asian J. Trop. Med. Public Health* 16, 332–336.

Hayes, C. G. (2001). West Nile virus: Uganda, 1937, to new York City, 1999. *Ann. N. Y. Acad. Sci.* 951, 25–37. doi: 10.1111/j.1749-6632.2001.tb02682.x

He, Z., Zhu, X., Wen, W., Yuan, J., Hu, Y., Chen, J., et al. (2016). Dengue virus subverts host innate immunity by targeting adaptor protein MAVS. *J. Virol.* 90, 7219–7230. doi: 10.1128/JVI.00221-16

Ho, L.-J., Hung, L.-F., Weng, C.-Y., Wu, W.-L., Chou, P., Lin, Y.-L., et al. (2005). Dengue virus type 2 antagonizes IFN-alpha but not IFN-gamma antiviral effect via down-regulating Tyk2-STAT signaling in the human dendritic cell. *J. Immunol. Baltim. Md* 174, 8163–8172. doi: 10.4049/jimmunol.174.12.8163

Hu, Y., Dong, X., He, Z., Wu, Y., Zhang, S., Lin, J., et al. (2019). Zika virus antagonizes interferon response in patients and disrupts RIG-I-MAVS interaction through its CARD-TM domains. *Cell Biosci.* 9:46. doi: 10.1186/s13578-019-0308-9

Isaacs, A., and Lindenmann, J. (1957). Virus interference. I. The interferon. *Proc. R. Soc. Lond. B Biol. Sci.* 147, 258–267. doi: 10.1098/rspb.1957.0048

Ishikawa, H., and Barber, G. N. (2008). STING is an endoplasmic reticulum adaptor that facilitates innate immune signalling. *Nature* 455, 674–678. doi: 10.1038/nature07317

Ivashkiv, L. B., and Donlin, L. T. (2014). Regulation of type I interferon responses. *Nat. Rev. Immunol.* 14, 36–49. doi: 10.1038/nri3581

Jia, X. Y., Briese, T., Jordan, I., Rambaut, A., Chi, H. C., Mackenzie, J. S., et al. (1999). Genetic analysis of West Nile New York 1999 encephalitis virus. *Lancet (North American ed)* 354, 1971–1972. doi: 10.1016/s0140-6736(99)05384-2

Jones, M., Davidson, A., Hibbert, L., Gruenwald, P., Schlaak, J., Ball, S., et al. (2005). Dengue virus inhibits alpha interferon signaling by reducing STAT2 expression. *J. Virol.* 79, 5414–5420. doi: 10.1128/JVI.79.9.5414-5420.2005

Julander, J. G., Morrey, J. D., Blatt, L. M., Shafer, K., and Sidwell, R. W. (2007). Comparison of the inhibitory effects of interferon alfacon-1 and ribavirin on yellow fever virus infection in a hamster model. *Antivir. Res.* 73, 140–146. doi: 10.1016/j.antiviral.2006.08.008

Kato, H., Takahasi, K., and Fujita, T. (2011). RIG-I-like receptors: cytoplasmic sensors for non-self RNA. *Immunol. Rev.* 243, 91–98. doi: 10.1111/j.1600-065X.2011.01052.x

Kato, H., Takeuchi, O., Sato, S., Yoneyama, M., Yamamoto, M., Matsui, K., et al. (2006). Differential roles of MDA5 and RIG-I helicases in the recognition of RNA viruses. *Nature* 441, 101–105. doi: 10.1038/nature04734

Katze, M. G., He, Y., and Gale, M. (2002). Viruses and interferon: a fight for supremacy. *Nat. Rev. Immunol.* 2, 675–687. doi: 10.1038/nri888

Kawai, T., and Akira, S. (2010). The role of pattern-recognition receptors in innate immunity: update on toll-like receptors. *Nat. Immunol.* 11, 373–384. doi: 10.1038/ni.1863

Keller, B. C., Fredericksen, B. L., Samuel, M. A., Mock, R. E., Mason, P. W., Diamond, M. S., et al. (2006). Resistance to alpha/beta interferon is a determinant of West Nile virus replication fitness and virulence. *J. Virol.* 80, 9424–9434. doi: 10.1128/JVI.00768-06

Kumar, A., Hou, S., Airo, A. M., Limonta, D., Mancinelli, V., Branton, W., et al. (2016). Zika virus inhibits type-I interferon production and downstream signaling. *EMBO Rep.* 17, 1766–1775. doi: 10.15252/embr.201642627

Kumar, H., Kawai, T., and Akira, S. (2011). Pathogen recognition by the innate immune system. *Int. Rev. Immunol.* 30, 16–34. doi: 10.3109/08830185.2010.529976

Laurent-Rolle, M., Boer, E. F., Lubick, K. J., Wolfinbarger, J. B., Carmody, A. B., Rockx, B., et al. (2010). The NS5 protein of the virulent West Nile virus NY99 strain is a potent antagonist of type I interferon-mediated JAK-STAT signaling. *J. Virol.* 84, 3503–3515. doi: 10.1128/JVI.01161-09

Laurent-Rolle, M., Morrison, J., Rajsbaum, R., Macleod, J. M. L., Pisanelli, G., Pham, A., et al. (2014). The interferon signaling antagonist function of yellow fever virus NS5 protein is activated by type I interferon. *Cell Host Microbe* 16, 314–327. doi: 10.1016/j.chom.2014.07.015

Laureti, M., Narayanan, D., Rodriguez-Andres, J., Fazakerley, J. K., and Kedzierski, L. (2018). Flavivirus receptors: diversity, identity, and cell entry. *Front. Immunol.* 9:2180. doi: 10.3389/fimmu.2018.02180

Lazear, H. M., and Diamond, M. S. (2016). Zika virus: new clinical syndromes and its emergence in the Western hemisphere. *J. Virol.* 90, 4864–4875. doi: 10.1128/JVI.00252-16

Lazear, H. M., Govero, J., Smith, A. M., Platt, D. J., Fernandez, E., Miner, J. J., et al. (2016). A mouse model of Zika virus pathogenesis. *Cell Host Microbe* 19, 720–730. doi: 10.1016/j.chom.2016.03.010

Le Flohic, G., Porphyre, V., Barbazan, P., and Gonzalez, J.-P. (2013). Review of climate, landscape, and viral genetics as drivers of the Japanese encephalitis virus ecology. *PLoS Negl. Trop. Dis.* 7:e2208. doi: 10.1371/journal.pntd.0002208

Leyssen, P., Drosten, C., Paning, M., Charlier, N., Paeshuyse, J., De Clercq, E., et al. (2003). Interferons, interferon inducers, and interferon-ribavirin in treatment of flavivirus-induced encephalitis in mice. *Antimicrob. Agents Chemother.* 47, 777–782. doi: 10.1128/AAC.47.2.777-782.2003

Limonta Vidal, M., Ramírez Albajes, V., López Saura, P., Aguilera, A., Pentón, E., Barcelona, S., et al. (1984). Use of leukocyte interferon during an epidemic outbreak of haemorragic dengue (type II) in Cuba. *Interf. Biotecnol.* 1, 15–22.

Lin, R.-J., Chang, B.-L., Yu, H.-P., Liao, C.-L., and Lin, Y.-L. (2006). Blocking of interferon-induced Jak-Stat signaling by Japanese encephalitis virus NS5 through a protein tyrosine phosphatase-mediated mechanism. *J. Virol.* 80, 5908–5918. doi: 10.1128/JVI.02714-05

Lin, J. P., Fan, Y.-K., and Liu, H. M. (2019). The 14-3-3η chaperone protein promotes antiviral innate immunity via facilitating MDA5 oligomerization and intracellular redistribution. *PLoS Pathog.* 15:e1007582. doi: 10.1371/journal.ppat.1007582

Lin, R.-J., Liao, C.-L., Lin, E., and Lin, Y.-L. (2004). Blocking of the alpha interferon-induced Jak-Stat signaling pathway by Japanese encephalitis virus infection. *J. Virol.* 78, 9285–9294. doi: 10.1128/JVI.78.17.9285-9294.2004

Lin, S., Yang, S., He, J., Guest, J. D., Ma, Z., Yang, L., et al. (2019). Zika virus NS5 protein antagonizes type I interferon production via blocking TBK1 activation. *Virology* 527, 180–187. doi: 10.1016/j.virol.2018.11.009

Liu, H. M., Loo, Y.-M., Horner, S. M., Zornetzer, G. A., Katze, M. G., and Gale, M. (2012). The mitochondrial targeting chaperone 14-3-3ε regulates a RIG-I translocon that mediates membrane association and innate antiviral immunity. *Cell Host Microbe* 11, 528–537. doi: 10.1016/j.chom.2012.04.006

Liu, W. J., Wang, X. J., Mokhonov, V. V., Shi, P.-Y., Randall, R., and Khromykh, A. A. (2005). Inhibition of interferon signaling by the New York 99 strain and Kunjin subtype of West Nile virus involves blockage of STAT1 and STAT2 activation by nonstructural proteins. *J. Virol.* 79, 1934–1942. doi: 10.1128/JVI.79.3.1934-1942.2005

Lobigs, M., Müllbacher, A., Wang, Y., Pavy, M., and Lee, E. (2003). Role of type I and type II interferon responses in recovery from infection with an encephalitic flavivirus. *J. Gen. Virol.* 84, 567–572. doi: 10.1099/vir.0.18654-0

Loo, Y.-M., Fornek, J., Crochet, N., Bajwa, G., Perwitasari, O., Martinez-Sobrido, L., et al. (2008). Distinct RIG-I and MDA5 signaling by RNA viruses in innate immunity. *J. Virol.* 82, 335–345. doi: 10.1128/JVI.01080-07

Loo, Y.-M., and Gale, M. (2011). Immune signaling by RIG-I-like receptors. *Immunity* 34, 680–692. doi: 10.1016/j.immuni.2011.05.003

Lubick, K. J., Robertson, S. J., McNally, K. L., Freedman, B. A., Rasmussen, A. L., Taylor, R. T., et al. (2015). Flavivirus antagonism of type I interferon signaling reveals Prolidase as a regulator of IFNAR1 surface expression. *Cell Host Microbe* 18, 61–74. doi: 10.1016/j.chom.2015.06.007

Ma, J., Ketkar, H., Geng, T., Lo, E., Wang, L., Xi, J., et al. (2018). Zika virus non-structural protein 4A blocks the RLR-MAVS signaling. *Front. Microbiol.* 9:1350. doi: 10.3389/fmicb.2018.01350

Manokaran, G., Finol, E., Wang, C., Gunaratne, J., Bahl, J., Ong, E. Z., et al. (2015). Dengue subgenomic RNA binds TRIM25 to inhibit interferon expression for epidemiological fitness. *Science* 350, 217–221. doi: 10.1126/science.aab3369

Martin, M.-F., and Nisole, S. (2020). West Nile virus restriction in mosquito and human cells: a virus under confinement. *Vaccine* 8:256. doi: 10.3390/vaccines8020256

Martín-Acebes, M. A., Blázquez, A.-B., Cañas-Arranz, R., Vázquez-Calvo, Á., Merino-Ramos, T., Escribano-Romero, E., et al. (2016). A recombinant DNA vaccine protects mice deficient in the alpha/beta interferon receptor against lethal challenge with Usutu virus. *Vaccine* 34, 2066–2073. doi: 10.1016/j.vaccine.2016.03.015

Mazzon, M., Jones, M., Davidson, A., Chain, B., and Jacobs, M. (2009). Dengue virus NS5 inhibits interferon-alpha signaling by blocking signal transducer and activator of transcription 2 phosphorylation. *J. Infect. Dis.* 200, 1261–1270. doi: 10.1086/605847

McVey, D. S., Wilson, W. C., and Gay, C. G. (2015). West Nile virus. *Rev. Sci. Tech. Int. Off. Epizoot.* 34, 431–439. doi: 10.20506/rst.34.2.2369

Meier, K. C., Gardner, C. L., Khoretonenko, M. V., Klimstra, W. B., and Ryman, K. D. (2009). A mouse model for studying viscerotropic disease caused by yellow fever virus infection. *PLoS Pathog.* 5:e1000614. doi: 10.1371/journal.ppat.1000614

Messina, J. P., Brady, O. J., Golding, N., Kraemer, M. U. G., Wint, G. R. W., Ray, S. E., et al. (2019). The current and future global distribution and population at risk of dengue. *Nat. Microbiol.* 4, 1508–1515. doi: 10.1038/s41564-019-0476-8

Miorin, L., Maestre, A. M., Fernandez-Sesma, A., and García-Sastre, A. (2017). Antagonism of type I interferon by flaviviruses. *Biochem. Biophys. Res. Commun.* 492, 587–596. doi: 10.1016/j.bbrc.2017.05.146

Mlakar, J., Korva, M., Tul, N., Popović, M., Poljšak-Prijatelj, M., Mraz, J., et al. (2016). Zika virus associated with microcephaly. *N. Engl. J. Med.* 374, 951–958. doi: 10.1056/NEJMoa1600651

Morrey, J. D., Day, C. W., Julander, J. G., Blatt, L. M., Smee, D. F., and Sidwell, R. W. (2004). Effect of interferon-alpha and interferon-inducers on West Nile virus in mouse and hamster animal models. *Antivir. Chem. Chemother.* 15, 101–109. doi: 10.1177/095632020401500202

Morrison, J., Laurent-Rolle, M., Maestre, A. M., Rajsbaum, R., Pisanelli, G., Simon, V., et al. (2013). Dengue virus co-opts UBR4 to degrade STAT2 and antagonize type I interferon signaling. *PLoS Pathog.* 9:e1003265. doi: 10.1371/journal.ppat.1003265

Mukhopadhyay, S., Kuhn, R. J., and Rossmann, M. G. (2005). A structural perspective of the flavivirus life cycle. *Nat. Rev. Microbiol.* 3, 13–22. doi: 10.1038/nrmicro1067

Muñoz-Jordán, J. L., Laurent-Rolle, M., Ashour, J., Martínez-Sobrido, L., Ashok, M., Lipkin, W. I., et al. (2005). Inhibition of alpha/beta interferon signaling by the NS4B protein of flaviviruses. *J. Virol.* 79, 8004–8013. doi: 10.1128/JVI.79.13.8004-8013.2005

Muñoz-Jordán, J. L., Sánchez-Burgos, G. G., Laurent-Rolle, M., and García-Sastre, A. (2003). Inhibition of interferon signaling by dengue virus. *Proc. Natl. Acad. Sci.* 100, 14333–14338. doi: 10.1073/pnas.2335168100

Musso, D., Ko, A. I., and Baud, D. (2019). Zika virus infection — after the pandemic. *N. Engl. J. Med.* 381, 1444–1457. doi: 10.1056/NEJMra1808246

Nasirudeen, A. M. A., Wong, H. H., Thien, P., Xu, S., Lam, K.-P., and Liu, D. X. (2011). RIG-I, MDA5 and TLR3 synergistically play an important role in restriction of dengue virus infection. *PLoS Negl. Trop. Dis.* 5:e926. doi: 10.1371/journal.pntd.0000926

O'Neill, L. A. J., and Bowie, A. G. (2007). The family of five: TIR-domain-containing adaptors in toll-like receptor signalling. *Nat. Rev. Immunol.* 7, 353–364. doi: 10.1038/nri2079

Pauli, E.-K., Chan, Y. K., Davis, M. E., Gableske, S., Wang, M. K., Feister, K. F., et al. (2014). The ubiquitin-specific protease USP15 promotes RIG-I-mediated antiviral signaling by deubiquitylating TRIM25. *Sci. Signal.* 7:ra3. doi: 10.1126/scisignal.2004577

Pierson, T. C., and Diamond, M. S. (2020). The continued threat of emerging flaviviruses. *Nat. Microbiol.* 5, 796–812. doi: 10.1038/s41564-020-0714-0

Pijlman, G. P., Funk, A., Kondratieva, N., Leung, J., Torres, S., van der Aa, L., et al. (2008). A highly structured, nuclease-resistant, noncoding RNA produced by flaviviruses is required for pathogenicity. *Cell Host Microbe* 4, 579–591. doi: 10.1016/j.chom.2008.10.007

Plociennikowska, A., Frankish, J., Moraes, T., Del Prete, D., Kahnt, F., Acuna, C., et al. (2021). TLR3 activation by Zika virus stimulates inflammatory cytokine production which dampens the antiviral response induced by RIG-I-like receptors. *J. Virol.* 95, e01050–e01020. doi: 10.1128/JVI.01050-20

Rastogi, M., Sharma, N., and Singh, S. K. (2016). Flavivirus NS1: a multifaceted enigmatic viral protein. *Virol. J.* 13:131. doi: 10.1186/s12985-016-0590-7

Ray, D., Shah, A., Tilgner, M., Guo, Y., Zhao, Y., Dong, H., et al. (2006). West Nile virus 5′-cap structure is formed by sequential guanine N-7 and ribose 2'-O methylations by nonstructural protein 5. *J. Virol.* 80, 8362–8370. doi: 10.1128/JVI.00814-06

Rice, C. M., Lenches, E. M., Eddy, S. R., Shin, S. J., Sheets, R. L., and Strauss, J. H. (1985). Nucleotide sequence of yellow fever virus: implications for flavivirus gene expression and evolution. *Science* 229, 726–733. doi: 10.1126/science.4023707

Riedl, W., Acharya, D., Lee, J.-H., Liu, G., Serman, T., Chiang, C., et al. (2019). Zika virus NS3 mimics a cellular 14-3-3-binding motif to antagonize RIG-I- and MDA5-mediated innate immunity. *Cell Host Microbe* 26, 493–503.e6. doi: 10.1016/j.chom.2019.09.012

Rigau-Pérez, J. G., Clark, G. G., Gubler, D. J., Reiter, P., Sanders, E. J., and Vorndam, A. V. (1998). Dengue and dengue haemorrhagic fever. *Lancet Lond. Engl.* 352, 971–977. doi: 10.1016/s0140-6736(97)12483-7

Rodriguez-Madoz, J. R., Belicha-Villanueva, A., Bernal-Rubio, D., Ashour, J., Ayllon, J., and Fernandez-Sesma, A. (2010). Inhibition of the type I interferon response in human dendritic cells by dengue virus infection requires a catalytically active NS2B3 complex. *J. Virol.* 84, 9760–9774. doi: 10.1128/JVI.01051-10

Ronca, S. E., Ruff, J. C., and Murray, K. O. (2021). A 20-year historical review of West Nile virus since its initial emergence in North America: has West Nile virus become a neglected tropical disease? *PLoS Negl. Trop. Dis.* 15:e0009190. doi: 10.1371/journal.pntd.0009190

Samuel, M. A., and Diamond, M. S. (2005). Alpha/beta interferon protects against lethal West Nile virus infection by restricting cellular tropism and enhancing neuronal survival. *J. Virol.* 79, 13350–13361. doi: 10.1128/JVI.79.21.13350-13361.2005

Schindler, C., Shuai, K., Prezioso, V. R., and Darnell, J. E. (1992). Interferon-dependent tyrosine phosphorylation of a latent cytoplasmic transcription factor. *Science* 257, 809–813. doi: 10.1126/science.1496401

Schneider, W. M., Chevillotte, M. D., and Rice, C. M. (2014). Interferon-stimulated genes: a complex web of host defenses. *Annu. Rev. Immunol.* 32, 513–545. doi: 10.1146/annurev-immunol-032713-120231

Schoggins, J. W., Mac Duff, D. A., Imanaka, N., Gainey, M. D., Shrestha, B., Eitson, J. L., et al. (2014). Pan-viral specificity of IFN-induced genes reveals new roles for cGAS in innate immunity. *Nature* 505, 691–695. doi: 10.1038/nature12862

Schoggins, J. W., Wilson, S. J., Panis, M., Murphy, M. Y., Jones, C. T., Bieniasz, P., et al. (2011). A diverse range of gene products are effectors of the type I interferon antiviral response. *Nature* 472, 481–485. doi: 10.1038/nature09907

Schuessler, A., Funk, A., Lazear, H. M., Cooper, D. A., Torres, S., Daffis, S., et al. (2012). West Nile virus noncoding subgenomic RNA contributes to viral evasion of the type I interferon-mediated antiviral response. *J. Virol.* 86, 5708–5718. doi: 10.1128/JVI.00207-12

Shresta, S., Kyle, J. L., Snider, H. M., Basavapatna, M., Beatty, P. R., and Harris, E. (2004). Interferon-dependent immunity is essential for resistance to primary dengue virus infection in mice, whereas T- and B-cell-dependent immunity are less critical. *J. Virol.* 78, 2701–2710. doi: 10.1128/jvi.78.6.2701-2710.2004

Slonchak, A., Wang, X., Aguado, J., Sng, J. D. J., Chaggar, H., Freney, M. E., et al. (2022). Zika virus noncoding RNA cooperates with the viral protein NS5 to inhibit STAT1 phosphorylation and facilitate viral pathogenesis. *Sci. Adv.* 8:eadd8095. doi: 10.1126/sciadv.add8095

Smith, D. R. (2017). Waiting in the wings: the potential of mosquito transmitted flaviviruses to emerge. *Crit. Rev. Microbiol.* 43, 405–422. doi: 10.1080/1040841X.2016.1230974

Solomon, T., Dung, N. M., Wills, B., Kneen, R., Gainsborough, M., Diet, T. V., et al. (2003). Interferon alfa-2a in Japanese encephalitis: a randomised double-blind placebo-controlled trial. *Lancet* 361, 821–826. doi: 10.1016/s0140-6736(03)12709-2

Sommereyns, C., Paul, S., Staeheli, P., and Michiels, T. (2008). IFN-lambda (IFN-lambda) is expressed in a tissue-dependent fashion and primarily acts on epithelial cells *in vivo*. *PLoS Pathog.* 4:e1000017. doi: 10.1371/journal.ppat.1000017

Sui, L., Zhao, Y., Wang, W., Chi, H., Tian, T., Wu, P., et al. (2023). Flavivirus pr M interacts with MDA5 and MAVS to inhibit RLR antiviral signaling. *Cell Biosci.* 13:9. doi: 10.1186/s13578-023-00957-0

Sun, P., Fernandez, S., Marovich, M. A., Palmer, D. R., Celluzzi, C. M., Boonnak, K., et al. (2009). Functional characterization of *ex vivo* blood myeloid and plasmacytoid dendritic cells after infection with dengue virus. *Virology* 383, 207–215. doi: 10.1016/j.virol.2008.10.022

Sun, X., Hua, S., Chen, H.-R., Ouyang, Z., Einkauf, K., Tse, S., et al. (2017). Transcriptional changes during naturally-acquired Zika virus infection render dendritic cells highly conducive to viral replication. *Cell Rep.* 21, 3471–3482. doi: 10.1016/j.celrep.2017.11.087

Sun, B., Sundström, K. B., Chew, J. J., Bist, P., Gan, E. S., Tan, H. C., et al. (2017). Dengue virus activates cGAS through the release of mitochondrial DNA. *Sci. Rep.* 7:3594. doi: 10.1038/s41598-017-03932-1

Sun, L., Wu, J., Du, F., Chen, X., and Chen, Z. J. (2013). Cyclic GMP-AMP synthase is a cytosolic DNA sensor that activates the type I interferon pathway. *Science* 339, 786–791. doi: 10.1126/science.1232458

Takaoka, A., and Yanai, H. (2006). Interferon signalling network in innate defence. *Cell. Microbiol.* 8, 907–922. doi: 10.1111/j.1462-5822.2006.00716.x

Takeuchi, O., and Akira, S. (2010). Pattern recognition receptors and inflammation. *Cells* 140, 805–820. doi: 10.1016/j.cell.2010.01.022

Tripathi, S., Balasubramaniam, V. R. M. T., Brown, J. A., Mena, I., Grant, A., Bardina, S. V., et al. (2017). A novel Zika virus mouse model reveals strain specific differences in virus pathogenesis and host inflammatory immune responses. *PLoS Pathog.* 13:e1006258. doi: 10.1371/journal.ppat.1006258

Tsai, Y.-T., Chang, S.-Y., Lee, C.-N., and Kao, C.-L. (2009). Human TLR3 recognizes dengue virus and modulates viral replication *in vitro*. *Cell. Microbiol.* 11, 604–615. doi: 10.1111/j.1462-5822.2008.01277.x

Tuells, J., Henao-Martínez, A. F., and Franco-Paredes, C. (2022). Yellow fever: a perennial threat. *Arch. Med. Res.* 53, 649–657. doi: 10.1016/j.arcmed.2022.10.005

Uchida, L., Espada-Murao, L. A., Takamatsu, Y., Okamoto, K., Hayasaka, D., Yu, F., et al. (2014). The dengue virus conceals double-stranded RNA in the intracellular membrane to escape from an interferon response. *Sci. Rep.* 4:7395. doi: 10.1038/srep07395

van Leur, S. W., Heunis, T., Munnur, D., and Sanyal, S. (2021). Pathogenesis and virulence of flavivirus infections. *Virulence* 12, 2814–2838. doi: 10.1080/21505594.2021.1996059

Wang, J. P., Liu, P., Latz, E., Golenbock, D. T., Finberg, R. W., and Libraty, D. H. (2006). Flavivirus activation of Plasmacytoid dendritic cells delineates key elements of TLR7 signaling beyond endosomal recognition 1. *J. Immunol.* 177, 7114–7121. doi: 10.4049/jimmunol.177.10.7114

Welsch, S., Miller, S., Romero-Brey, I., Merz, A., Bleck, C. K. E., Walther, P., et al. (2009). Composition and three-dimensional architecture of the dengue virus replication and assembly sites. *Cell Host Microbe* 5, 365–375. doi: 10.1016/j.chom.2009.03.007

Wu, Y., Liu, Q., Zhou, J., Xie, W., Chen, C., Wang, Z., et al. (2017). Zika virus evades interferon-mediated antiviral response through the co-operation of multiple nonstructural proteins *in vitro*. *Cell Discov.* 3:17006. doi: 10.1038/celldisc.2017.6

Xia, H., Luo, H., Shan, C., Muruato, A. E., Nunes, B. T. D., Medeiros, D. B. A., et al. (2018). An evolutionary NS1 mutation enhances Zika virus evasion of host interferon induction. *Nat. Commun.* 9:414. doi: 10.1038/s41467-017-02816-2

Yang, T.-C., Li, S.-W., Lai, C.-C., Lu, K.-Z., Chiu, M.-T., Hsieh, T.-H., et al. (2013). Proteomic analysis for type I interferon antagonism of Japanese encephalitis virus NS5 protein. *Proteomics* 13, 3442–3456. doi: 10.1002/pmic.201300001

Yu, C.-Y., Chang, T.-H., Liang, J.-J., Chiang, R.-L., Lee, Y.-L., Liao, C.-L., et al. (2012). Dengue virus targets the adaptor protein MITA to subvert host innate immunity. *PLoS Pathog.* 8:e1002780. doi: 10.1371/journal.ppat.1002780

Zanluca, C., De Melo, V. C. A., Mosimann, A. L. P., Santos, G. I. V. D., Santos, C. N. D. D., and Luz, K. (2015). First report of autochthonous transmission of Zika virus in Brazil. *Mem. Inst. Oswaldo Cruz* 110, 569–572. doi: 10.1590/0074-02760150192

Zhang, H.-L., Ye, H.-Q., Liu, S.-Q., Deng, C.-L., Li, X.-D., Shi, P.-Y., et al. (2017). West Nile virus NS1 antagonizes interferon Beta production by targeting RIG-I and MDA5. *J. Virol.* 91, e02396–e02316. doi: 10.1128/JVI.02396-16

Zheng, Y., Liu, Q., Wu, Y., Ma, L., Zhang, Z., Liu, T., et al. (2018). Zika virus elicits inflammation to evade antiviral response by cleaving cGAS via NS1-caspase-1 axis. *EMBO J.* 37:e99347. doi: 10.15252/embj.201899347

Zhu, T., and Fernandez-Sesma, A. (2020). Innate immune DNA sensing of Flaviviruses. *Viruses* 12:979. doi: 10.3390/v12090979

Zhu, T., Webb, L. G., Veloz, J., Wilkins, M., Aguirre, S., and Fernandez-Sesma, A. (2022). Generation and characterization of human-mouse STING chimeras that allow DENV replication in mouse cells. *mSphere* 7:e0091421. doi: 10.1128/msphere.00914-21

Züst, R., Cervantes-Barragan, L., Habjan, M., Maier, R., Neuman, B. W., Ziebuhr, J., et al. (2011). Ribose 2'-O-methylation provides a molecular signature for the distinction of self and non-self mRNA dependent on the RNA sensor Mda5. *Nat. Immunol.* 12, 137–143. doi: 10.1038/ni.1979

frontiers | Frontiers in Microbiology

TYPE Original Research
PUBLISHED 20 November 2023
DOI 10.3389/fmicb.2023.1214148

OPEN ACCESS

EDITED BY
Ke Liu,
Chinese Academy of Agricultural Sciences, China

REVIEWED BY
Diogo Antonio Tschoeke,
Federal University of Rio de Janeiro, Brazil
Kim-Kee Tan,
University of Malaya, Malaysia
Fabiana Feitosa-Suntheimer,
Boston University, United States

*CORRESPONDENCE
Joanne Macdonald
jmacdon1@usc.edu.au
Nina M. Pollak
npollak@usc.edu.au
David J. McMillan
dmcmill1@usc.edu.au

RECEIVED 29 April 2023
ACCEPTED 06 November 2023
PUBLISHED 20 November 2023

CITATION
Balea R, Pollak NM, Hobson-Peters J, Macdonald J and McMillan DJ (2023) Development and pre-clinical evaluation of a Zika virus diagnostic for low resource settings. *Front. Microbiol.* 14:1214148. doi: 10.3389/fmicb.2023.1214148

Development and pre-clinical evaluation of a Zika virus diagnostic for low resource settings

Rickyle Balea[1,2], Nina M. Pollak[1,2]*, Jody Hobson-Peters[3,4], Joanne Macdonald[2,5]* and David J. McMillan[1,2]*

[1]Centre for Bioinnovation, University of the Sunshine Coast, Sippy Downs, QLD, Australia, [2]School of Science, Technology and Engineering, University of the Sunshine Coast, Sippy Downs, QLD, Australia, [3]School of Chemistry and Molecular Biosciences, The University of Queensland, St Lucia, QLD, Australia, [4]Australian Infectious Diseases Research Centre, The University of Queensland, St Lucia, QLD, Australia, [5]BioCifer Pty Ltd., Auchenflower, QLD, Australia

Introduction: Zika virus (ZIKV) is a re-emerging flavivirus that poses a significant public health threat. ZIKV exhibits a wide array of non-vector borne human transmission routes, such as sexual transmission, transplacental transmission and blood transfusion. Detection and surveillance of ZIKV is considered paramount in prevention of major outbreaks. With the majority of cases reported in low-resource locations, simple, low-cost detection methods are considered highly desirable.

Materials and Methods: Here we have developed a sensitive and specific ZIKV diagnostic using reverse transcription recombinase-aided amplification (RT-RAA) coupled with lateral flow detection (LFD) targeting a highly conserved region of the ZIKV NS1 gene.

Results: We show our rapid, isothermal-ZIKV-diagnostic (Iso-ZIKV-Dx) can detect 500 copies of synthetic ZIKV RNA/μL in under 30min at a constant 39°C. Using simulated urine samples, we observed that Iso-ZIKV-Dx also detects as low as 34.28 RNA copies/reaction of ZIKV (MR766 strain). Specificity testing confirmed that our test does not detect any co-circulating flaviviruses (dengue, West Nile, Japanese encephalitis, Murray Valley encephalitis and yellow fever viruses) or chikungunya virus. Sample processing results show complete inactivation of ZIKV (MR766 strain) in 5min at room temperature using our novel viral RNA sample preparation reagent. Furthermore, lateral flow strips testing demonstrates positive diagnoses in as little as 5min in running buffer.

Discussion: Contrary to conventional RT-qPCR, our Iso-ZIKV-Dx does not require expensive machinery, specialised laboratory settings or extensively trained personnel. Pre-clinical evaluation demonstrates that our test exhibits robust, in-field capabilities without compromising sensitivity or specificity. When compared to the gold-standard RT-qPCR, our Iso-ZIKV-Dx test offers an array of applications that extend beyond diagnostics alone, including potential for surveillance and monitoring of ZIKV vector competency.

KEYWORDS

Zika virus, NS1 gene, recombinase aided amplification, lateral flow detection, point-of-care, rapid test

Highlights

- Development of a low-resource rapid Zika virus diagnostic test.
- Rapid one-step sample processing protocol inactivating Zika virus in 5 min.
- Test format utilising isothermal amplification coupled with lateral flow detection.
- Achieved detection of highly virulent ZIKV MR766 in under 30 min.
- Rapid Zika virus test 4 times faster than RT-qPCR.

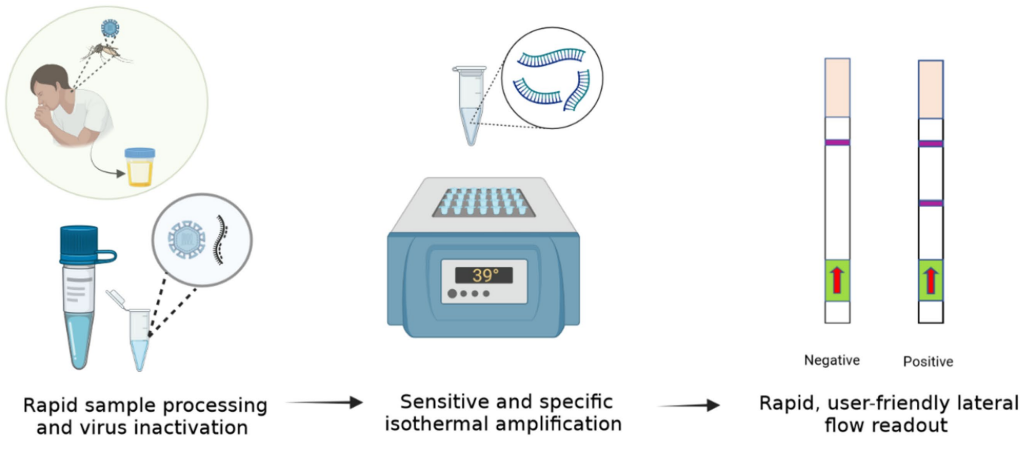

GRAPHICAL ABSTRACT

Introduction

Zika virus (ZIKV), a member of the *Flaviviridae* family, was first isolated in 1947 from the serum of a rhesus monkey in Uganda (Dick et al., 1952). In 2007, an outbreak on Yap Island (Hayes, 2009) resulting in the first instance of ZIKV transmission outside of Africa and Asia was reported. ZIKV outbreaks have subsequently been reported in multiple locations including French Polynesia (Roth et al., 2014), Papua New Guinea (Chang et al., 2016), New Caledonia (Dupont-Rouzeyrol et al., 2015), and Brazil (Wen et al., 2017). Spanning throughout nearly all seven continents, ZIKV remains a priority disease by World Health Organisation (WHO) (TwistDx™, 2023b). Although predominantly transmitted via mosquitos (*Aedes albopictus* and *aegypti*) (Azar and Weaver, 2019), blood transfusion and sexual transmission have also been reported (Gregory et al., 2017). Historically ZIKV transmission was primarily observed in remote, developing countries (Paixão et al., 2016). However, in 2019, the first locally acquired cases of ZIKV transmission were reported in southern Europe (Brady and Hay, 2019), initiating the prevalence and spread of ZIKV in developed nations. Most ZIKV infections manifest in mild, flu like symptoms (Mumtaz et al., 2016). In severe cases, medical complications such as Guillain Barre (Hendel-Paterson et al., 2016) and severe thrombocytopenia (Sharp et al., 2016) have been reported. ZIKV infection mechanisms also allow for cross placental infections, resulting in microcephaly in developmental infants (Wen et al., 2017).

With no approved vaccine or therapeutics (Da Silva et al., 2018), rapid and accurate detection of ZIKV is a crucial component in predicting and monitoring potential outbreaks (Heukelbach et al., 2016). The majority of ZIKV-positive individuals, including pregnant women are also asymptomatic (Paixao et al., 2018). Crucially delayed diagnosis among pregnant women is particularly concerning due to the inherent risk of congenital abnormalities. Current ZIKV detection and diagnostic strategies utilise both nucleic acid amplification tests (NAATs) (Gourinat et al., 2015) or antibody-based detection-based techniques (Kadkhoda et al., 2017). Due to antigenic cross-reactivity between Zika antigens and other flaviviruses (Stettler et al., 2016), serology based testing such as Enzyme Linked Immunosorbent Assay (ELISA) are less favoured. Reverse Transcription-Quantitative Polymerase Chain Reaction (RT-qPCR) therefore, still remains the 'gold standard' for detection and diagnostics among arboviruses (Dong et al., 2012). While accurate and sensitive, a draw-back for RT-qPCR is the need for specialised equipment and trained personnel that restricts these tests to centralised laboratories.

A diagnostic platform that enables in-field or point-of-care (POC) detection without the need for highly trained personnel or specialised equipment offers beneficial attributes to both clinical diagnostics and surveillance of not just ZIKV, but arboviruses alike (Ahmed et al., 2022). Isothermal NAAT's address all these issues and have been described as potential alternatives to RT-qPCR for viruses such as Zika (Cheikh Tidiane Diagne et al., 2020). As of recent years, innovation and proliferation of various isothermal amplification tests have taken significant strides within the field of rapid diagnostics (Xue et al., 2020). Recombinase aided amplification (RAA) (Jiangsu Qitian Gene Biotechnology Co., Ltd, 2023) is a promising isothermal technique that utilises similar molecular mechanisms as Recombinase Polymerase Amplification (RPA) (TwistDx™, 2023a). For RNA viruses such as ZIKV, a reverse transcriptase enzyme is added to the RAA reaction. Comparable to RT-qPCR, reverse transcriptase-recombinase aided amplification (RT-RAA) has been shown to be both rapid (Xue et al., 2020) and clinically sensitive (Wang et al., 2020). However, NAAT test uptake for low-resource detection of disease is hampered by the lack of field-friendly sample preparation techniques, instead requiring purification of RNA using magnetic beads or column-based laboratory technologies (Pollak et al., 2022).

Here we describe a rapid, isothermal ZIKV diagnostic (Iso-ZIKV-Dx). Our test format combines a unique low-resource sample preparation reagent with RT-RAA amplification, and lateral flow detection (LFD) to enable ZIKV detection in urine in under 30 min without the need for expensive nor advanced instrumentation. As such, our Iso-ZIKV-Dx exhibits promising diagnostic capabilities suitable for low-resource settings.

Materials and methods

Plasmids and RNA template preparation

Plasmids (pBIC-A) containing regions of the ZIKV Envelope (E) gene fragment (OM964568.1, 901–2,412 nt) and non-structural 1

(NS1) gene fragment (MW015936, 249–3,545 nt) of ZIKV were obtained from Bioneer Pacific Pty Ltd., Victoria, AUS. The pBIC-A-NS1 and E gene vector was transformed into *E. coli*. A single colony of *E. coli* containing the pBIC-A- NS1 plasmid was streaked onto LB broth agar supplemented with 100 µg/mL of ampicillin and incubated at 37°C. The selected colony was grown in liquid LB broth supplemented with 100 µg/mL of ampicillin for plasmid isolation using the 'NucleoBond Xtra Midi' kit (Machery-Nagel, GER). MEGAscript (Ambion, Austin USA) *in vitro* transcription kit was used to yield RNA transcript from pBIC-A- NS1 plasmids. XhoI was the chosen restriction enzyme to digest the linearize plasmid in preparation for *in vitro* transcription. Transcribed RNA from pBIC-A-NS1 plasmid was quantified using Quibit RNA Hs Kit. Using software, a calculation of an approximate numerical quantity of RNA copies/µL from extracted RNA was established (Pollak et al., 2023c). RNA transcripts were then stored at −80°C as working stocks and used as reference RNA standards for qRT-PCR.

RAA primer and probe design

A total of 967 ZIKV NS1 genes obtained from NCBI's databank representing both the African and Asian were aligned using Geneious Prime (version 2023.0.4) (Kearse et al., 2012). The first phylogenetic tree was created to isolate only unique ZIKV NS1 sequences. A total of 105 unique sequences were isolated and then imported to Geneious Prime for re-alignment using MAFFT (Nakamura et al., 2018). To assess the range of ZIKV sequences targeted by the primers and probes, a maximum likelihood (ML) phylogenetic tree (Figure 1) was constructed using IQTREE2 (Minh et al., 2020), utilising 10,000 bootstrap replicates and the TEST function. A consensus sequence of all unique ZIKV NS1 gene sequences was created using BioEdit 7.2 (Informer Technologies, INC, GER). Primers and probes were then designed using the most conserved region of the NS1 gene within the consensus sequence. Primer and probe design were further evaluated (primer dimers, secondary structures and GC content) using an oligoevaluator (Sigma-Aldrich Co. LLC, 2014). ALL primers and probes were bioinformatically evaluated to ensure no non-specific annealing to other flavivirus NS1 sequences occurred. Probes and primers (Table 1) were synthesised by (Bioneer Pacific Pty Ltd., Victoria, AUS) and purified via PAGE and HPLC, respectively.

Iso-ZIKV-Dx test

Rapid sample processing

ZIKV MR766 culture was mixed into urine and RPMI media samples at a ratio of 1:1 with TNA-Cifer Reagent E (BioCifer, Auchenflower, AUS) at room temperature for 5 min. Urine and RPMI media samples were diluted 1:5 in nuclease free H_20.

RT-RAA amplification

Each RT-RAA test was performed using the RAA kit (Jiangsu Qitian Gene Biotechnology Co. Ltd., Wuxi City China) with final reaction conditions of 0.83x RAA rehydration buffer, 1/5 RAA pellet, forward primer (350 nM), reverse primer (350 nM), probe (200 nM), Endonuclease IV (2U; New England Biolabs, Victoria, AUS), Moloney Murine Leukemia virus reverse transcriptase enzyme (M-MLV, 60U; Biocifer Pty Ltd., Auchenflower, AUS), magnesium acetate (MgOAc, 23.33 mM) and 2 µL template in a final reaction volume of 12 µL. MgOAc was added to the cap of each 0.2 mL PCR tube. Once template had been added, tubes were centrifuged and incubated at 39°C for 20 min using a heating block.

Lateral flow strip detection

HybriDetect lateral flow strips (LFS) (Milenia Biotec, Giessen, GER) were treated with 8 µL of 0.4% casein blocking buffer for pre-activation (Rames and Macdonald, 2019). To each strip, 2 µL of amplicon was pipetted on to the sample pad. The LFS strips were placed into 2 mL Eppendorf tubes containing 100 µL of LFS Running Buffer (Li et al., 2019) for 5 min. LFS were scanned using an Epson Perfection V39 Flatbed Scanner (Epson, New South Wales, AUS). The scanned images were converted to greyscale using Irfan View 64 and then imported to ImageJ for analysis. Band intensity analysis and statistical quantification were conducted as previously described (Pollak et al., 2023b).

Sensitivity and specificity testing

Analytical sensitivity testing for Iso-ZIKV-Dx tests were performed using a 10-fold serial dilution of purified, synthetic RNA transcripts coding for ZIKV E and NS1 gene fragments. Analytical specificity testing utilised purified RNA of various virus strains (Table 2). Synthetic ZIKV RNA transcript (1×10^6 copies/µL) was used as a positive control for validation of specificity.

Simulated-infected urine

ZIKV culture 3.56×10^8 $TCID_{50}$/ml was spiked into Pickering Laboratories #1700–0018 Artificial urine medium for growing urological pathogens (Walker Scientific Pty Ltd., Joondalup DC, AUS).

Viruses and cell culture

All viral strains used in this study are listed in Table 2. Excluding ZIKV, all viruses were obtained from Hobson-Peters lab (University of Queensland, St Lucia, QLD) and were cultured at high titres as previously described (Hobson-Peters et al., 2013).

Cell culture

Aedes albopictus larvae cells C6/36 (ATCC-CRL-1660™) were obtained from the ATCC. Cell lines were cultured in Gibco (USA) 1640 RPMI supplemented with 5% Foetal Bovine Serum (FBS), 2 mM L-glutamine, Gibco (USA) 1x Antibiotic/Antimycotic at 28°C in a 5% $C0_2$ incubator until approximately 80% confluent (Pollak et al., 2023b).

ZIKV infection and titre determination

Virus culture

ZIKV MR766 culture (accession MK105975) was used to infect C6/36 cells at a multiplicity of Infection (MOI) of 0.01 for 5 and 7 days, respectively (Pollak et al., 2023a). Virus culture media was harvested after centrifugation at 4°C for 10 min at 130× *g* and then stored at −80°C.

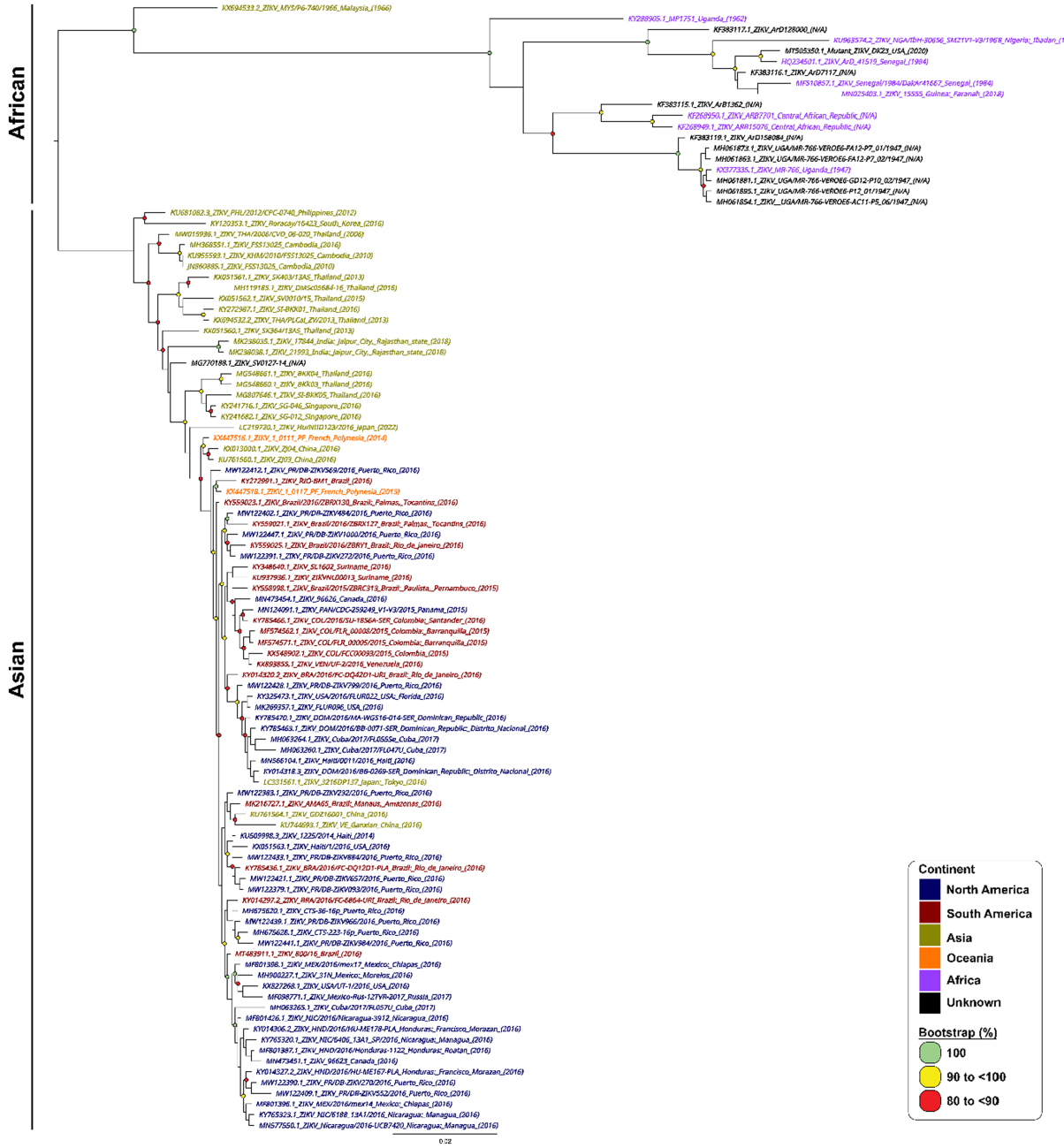

FIGURE 1
Phylogenetic tree of 105 unique ZIKV NS1 gene sequences. Phylogenetic relationships among 105 ZIKV NS1 sequences. ZIKV NS1 sequences are named by their corresponding GenBank accession number/strain/country of origin, with text being coloured according to their continent of isolation. The midpoint-rooted maximum likelihood phylogenetic trees were constructed using IQTREE2, which automatically incorporates the most appropriate nucleotide substitution model (TN + F + G4). The scale bar indicates the number of nucleotide substitutions per site. Bootstrap values above 80% are displayed next to the node of each clade and are coloured according to the figure legend.

TABLE 1 Primer and probe sequences for rapid Iso-ZIKV-Dx test.

Oligonucleotide	Sequence
Forward primer	GAAATYCGGTTTGAGGAATGYCCAGGHACYAAGG
Reverse primer	[5' Biotin]GGTTCYTTYCTGGGCCTTATCTCCATTCCATACC
Probe	[5'FAM]GAGGACCATCTCTGAGATCAACYACTGCAAG[Internal dS Spacer] GGAAGGGTSATHGAG [3' C3 spacer]

TABLE 2 Virus strains used in this study.

Virus	Abbreviation	Strain	GenBank accession number
Zika virus	ZIKV	MR766	KX830960
Chikungunya virus	CHIKV	Mauritius 2006	MH229986
Dengue virus serotype 1	DENV-1	ET00.243	JN415499
Dengue virus serotype 2	DENV-2	ET00.300	JN568254
Dengue virus serotype 3	DENV-3	East Timor 2000	JN575585
Dengue virus serotype 4	DENV-4	ET00.288	JN571853
Japanese encephalitis virus	JEV	Nakayama	EF571853
Murray Valley encephalitis virus	MVEV	1–51	AF161266
West Nile virus	WNV_{KUNV}	Kunjin strain NSW 2011	JN887352
Yellow fever virus	YFV	17D	MT505351

Titre determination

ZIKV titre determination was evaluated by standard $TCID_{50}$ assays and fixed-cell ELISAs using C6/36 cells in a 96 well plate as previously described (Pollak et al., 2023b). Titres were calculated using the Reed and Muench method (Reed and Muench, 1938).

ZIKV inactivation testing

ZIKV inactivation testing was performed using ZIKV culture (3.56×10^8 $TCID_{50}$/ml) mixed with TNA-Cifer Reagent E (TCE; BioCifer, Auchenflower, AUS) at different ratios (1:1 and 2:1, ZIKV culture to TCE) and incubated from 0 min up to 10 min. Titre was determined as previously described (Pollak et al., 2023b).

RNA purification

RNA from viral stocks were purified using TRIzol™ (Invitrogen by Thermo Fisher Scientific Pty Ltd., Victoria, AUS) or column-based kit (NucleoSpin RNA Virus Isolation Mini kit, Machery-Nagel, Duren, GER) following protocols outlined by the manufacturer. Viral RNA was eluted into 150 µL of nuclease free H_2O and stored at −80°C.

ZIKV RT-qPCR

For a ZIKV RT-qPCR comparative, TaqMan™ Fast Virus 1-Step Master Mix (Thermo Fisher Pty Ltd., Victoria, AUS) was used in conjunction with primers and probes previously described (de Moraes et al., 2018). Parameters for RT-qPCR were implemented as per manufacturer's instructions.

Results

In designing our primers and probes, we performed stringent bioinformatic analysis to ensure our primers and probes target as many strains and isolates of ZIKV from all existing lineages as possible. We mapped out all known ZIKV sequences from NCBI covering both Asian and African lineages of ZIKV and constructed a phylogenetic tree using the most unique 105 sequences (Figure 1).

Analytical sensitivity

In developing a rapid, low-resource reliant diagnostic for ZIKV, we strategically designed RT-RAA primers and probes to target a highly conserved region of the NS1 gene. To test analytical sensitivity, serial dilutions of RNA transcripts were assessed. Our RT-RAA tests exhibited a limit of detection (LOD) of 500 RNA copies/µL (Figure 2).

Analytical specificity

The analytical specificity of Iso-ZIKV-Dx was assessed against RNA from eight common flaviviruses that co-circulate with ZIKV (Table 2). Alphavirus chikungunya virus (CHIKV) (Table 2) was also included due to its common co-circulation with ZIKV. Our results showed that none of the common co-circulating viruses were detected using Iso-ZIKV-Dx (Figure 3). In addition, bioinformatic analysis of different ZIKA isolates indicated that the designed primers and probes are homologous to all ZIKV strains (African and Asian lineages) (Supplementary Figure 1).

Sample preparation inactivates ZIKV

A rapid diagnostic suitable for low-resource implementation requires a simple sample preparation procedure. Here we assessed the capacity of TNA-Cifer Reagent E (TCE) (BioCifer, Auchenflower, QLD, AUS) as a sample preparation reagent for rapid inactivation and sample preparation of ZIKV. Our results showed that ZIKV MR766 (3.56×10^8 $TCID_{50}$/mL) was completely inactivated after 5 min when using a 1:1 ratio of sample to TCE, and 10 min when using a 2:1 ratio (Figure 4).

Detection of ZIKV in synthetic urine and RPMI medium

A key principle of our rapid Iso-ZIKV-Dx is operation in a manner that is not dependant on intricate resources or involve complex methodology. As such, the use of urine as a clinical matrix (Gourinat et al., 2015; Bonaldo et al., 2016; Lamb et al., 2016) eliminates the requirement for excessive sample collection procedures such as phlebotomy and/or serum and plasma extraction. Here

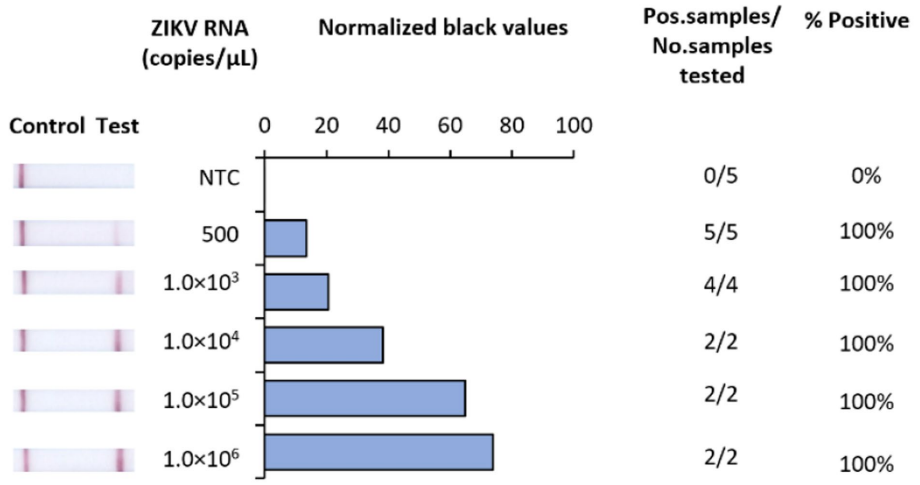

FIGURE 2
Analytical sensitivity of Iso-ZIKV-Dx using synthetic RNA transcripts. Sensitivity tests used 10-fold serially diluted synthetic ZIKV RNA. Scanned images of lateral flow strips with two lines (control and test) indicating positive detection of ZIKV and one being negative; no template control (NTC) consisted of nuclease free H_2O in place of RNA (left). Normalised pixel density (black shifted) contrasted with the white space on lateral flow strips (middle). Number of positive samples detected over number of samples tested along with calculated percentage accuracy of positive results for each dilution series (right).

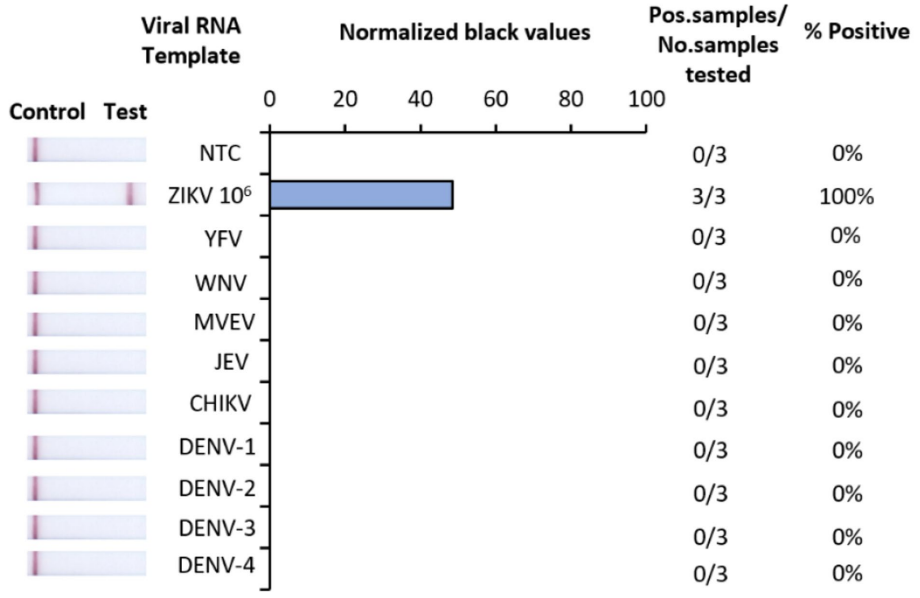

FIGURE 3
Analytical specificity of Iso-ZIKV-Dx using co-circulating flaviviruses and chikungunya virus. Specificity tests used synthetic RNA from ZIKV (PTC) and TRIzol extracted RNA from yellow fever virus (YFV), West $Nile_{Kunjin}$ virus (WNV_{KUN}), Murray Valley Encephalitis virus (MVEV), Japanese Encephalitis virus (JEV), chikungunya virus (CHIKV), dengue 1, 2, 3 and 4 virus (DENV-1, 2, 3, and 4). Scanned images of lateral flow strips with two lines (control and test) indicating positive detection of ZIKV and one being negative; no template control (NTC) consisted of nuclease free H_2O in place of RNA (left). Normalised pixel density (black shifted) contrasted with the white space on lateral flow strips (middle). Number of positive samples detected over number of samples tested along with calculated percentage accuracy of positive results (right).

we trialled synthetic urine and RPMI media spiked with MR766 ZIKV culture as the simulated clinical matrix for our rapid Iso-ZIKV-Dx. Using the same spiked samples, we performed our Iso-ZIKV-Dx test concurrently with virus isolation and TaqMan RT-qPCR for a comprehensive comparison. The rapid Iso-ZIKV-Dx test exhibited a LOD of 3.56×10^7 $TCID_{50}$/mL of ZIKV in both synthetic urine (Figure 5) and RPMI media (Supplementary Figure 2). In RPMI culture media, this was quantified by TaqMan RT-qPCR to be equivalent to a Ct value of 35.91 and 449 copies/reaction. In urine, our LOD was quantified by TaqMan RT-qPCR to be equivalent to a Ct value of 37.71 and 34.28 copies/reaction.

Discussion

Due to the lack of approved vaccines or specific therapeutics for ZIKV, rapid detection remains crucial in predicting and controlling potential outbreaks. ZIKV outbreaks often occur in rural and remote

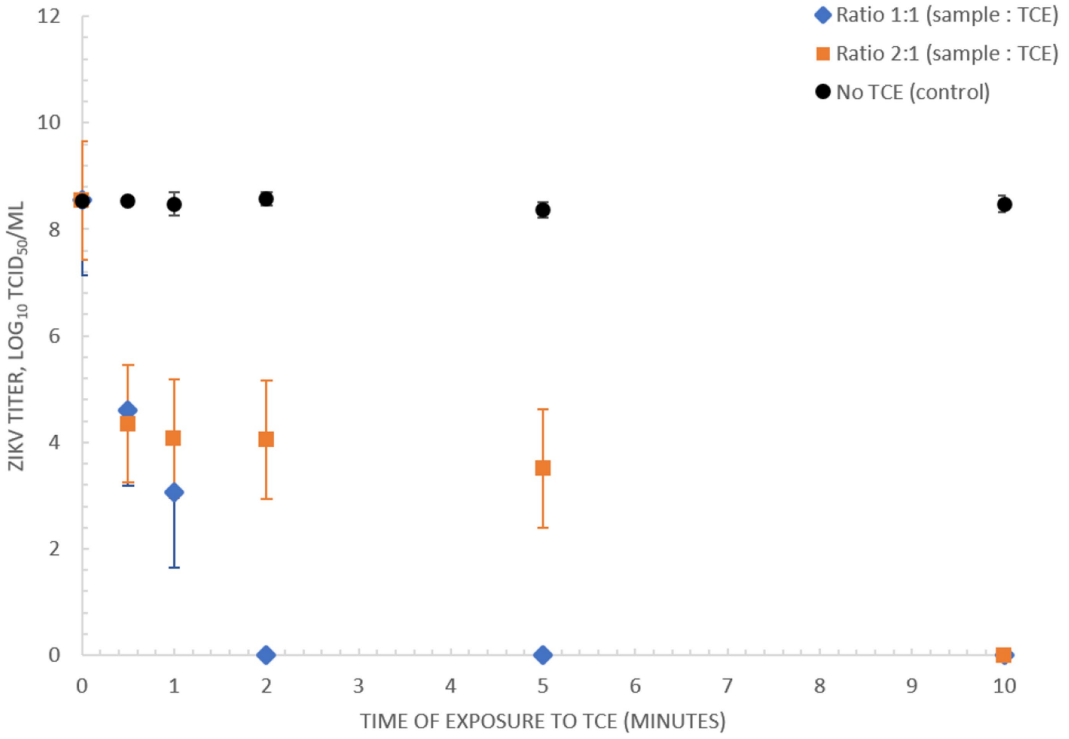

FIGURE 4
Inactivation of ZIKV (MR766) culture using TNA-Cifer Reagent E. Inactivation of 3.56×10^8 $TCID_{50}$/mL ZIKV (MR766) culture using TNA-Cifer Reagent E (TCE) at 1:1 and 2:1 ratio (sample to TCE) incubated for 0, 0.5, 1, 2, 5, and 10 min at room temperature.

areas, making it necessary for ZIKV diagnostics to be suitable for use in resource-limited settings, whilst still meeting the requirement for sensitive and accurate detection of ZIKV infection. Isothermal NAAT techniques are a potential solution, especially when combined with safe and simple sample preparation methods, as they could be easily deployed in low-resource settings with minimal training requirements for healthcare workers. In this study, we evaluated a novel rapid ZIKV diagnostic (Iso-ZIKV-Dx) which combines a low-resource sample preparation, RT-RAA test, and LFD. We used a phylogenetically divergent and highly virulent strain (MR766) of ZIKV (Shao et al., 2017). In this study we demonstrated the analytical sensitivity of our RT-RAA test to be 500 copies/μL when using synthetic ZIKV RNA, and confirmed the test did not detect other co-circulating viruses. It should be noted that our synthetic ZIKV RNA generated from RNA transcripts of the NS1 gene whilst the co-circulating viruses consisted of total viral RNA. The rapid Iso-ZIKV-Dx detected 3.56×10^7 $TCID_{50}$/mL, equivalent to 34.28 copies/reaction RT-qPCR in synthetic urine spiked with ZIKV MR766 and offers improved safety for low-resource testing as the virus is inactivated in the very first step of the procedure. The novel sample preparation reagent, TNA-Cifer Reagent E, has previously been shown to inactivate other pathogens, such as DENV (Calvert et al., 2017), Nipah virus (Rossini et al., 2017) and Hendra virus (Jiangsu Qitian Gene Biotechnology Co., Ltd, 2023), ensuring operator safety in the event of other potential pathogens within the clinical sample. Our data emphasises the benefits of our uncomplicated sample preparation protocol, which proved effective in detecting ZIKV in urine samples. It is noteworthy that ZIKV RNA is known to have limited stability at room temperature, making it challenging to detect within a specific time frame (Tan et al., 2017). Of note, a comparative analysis on current RT-qPCR tests for ZIKV reported discrepancies in detection sensitivity and specificity amongst Asian versus African lineages (de Moraes et al., 2018) with particular emphasis on the difficulty observed among African lineages specifically. Therefore, the primers and probes used in this study were strategically designed to target highly conserved regions of the NS1 gene among both ZIKV lineages as illustrated via our bioinformatic alignment analysis of the most unique NS1 gene sequences.

RT-qPCR is still considered the most reliable technique for diagnosing ZIKV in clinical pathology, and is widely recognised as the gold standard method for detection. However, due to the RNA stability issues at room temperature reported in urine (Tan et al., 2017), methods such as RT-qPCR that require sample storage favour clinical matrices such as plasma, serum or whole blood. For comparison, in serum and plasma, ZIKV RT-qPCRs typically demonstrate detection limits between 1 and 64 copies/reaction ($n = 31$) (Pessôa et al., 2016). A comparative study of RT-qPCR versus RT-LAMP using urine to detect ZIKV, however, demonstrated a detection limit of 6 copies/reaction ($n = 8$) for RT-qPCR (Calvert et al., 2017). Our rapid Iso-ZIKV-Dx test showed similar levels of sensitivity, detecting as low as 34 copies/reaction in ZIKV-spiked synthetic urine. The Range of reported ZIKV concentration in urine was observed to be between 0.7 and 220^6 copies/mL (Gourinat et al., 2015). The vastness of this range is thought to be due to the variability in ZIKV RNA stability, further supporting the need for a rapid sample processing method. Non-invasive clinical sample collections such as urine (Lamb et al., 2016) offer significant advantages for isothermal, POC compatible methods such as RT-RAA, RT-RPA, and RT-LAMP, due to the prolonged period of ZIKV RNA detectable throughout the infection period (Rossini et al., 2017). As such, our rapid Iso-ZIKV-Dx

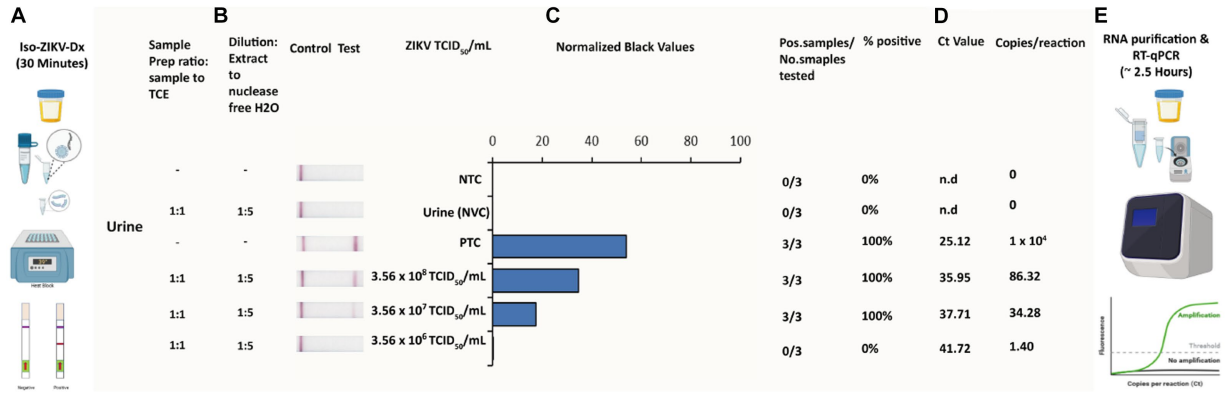

FIGURE 5
Rapid Iso-ZIKV-Dx of simulatedurine samples spiked with ZIKV (MR766). **(A)** Workflow, equipment needed and time frame of Iso-ZIKV-Dx. **(B)** Sample processing conditions including sample to reagent ratio and processed sample dilution ratio. **(C)** Sample description and quantities (NTC, non-template control; PTC, positive template control, synthetic ZIKV RNA transcripts 10^6 copies/µl); NVC, no virus control, urine. Scanned lateral flow strips showing test and control bands observable by naked eye. Normalised pixel densities (black values) from the displayed lateral flow strips. **(D)** Comparative Ct values and copies/reaction quantified via TaqMan RT-qPCR. **(E)** Workflow, equipment and time frame involved in conventional ZIKV RT-qPCR diagnostic.

test could be valuable in overcoming the obstacle of testing urine samples by potentially detecting ZIKV directly at the point of sample collection. One study using RT-LAMP reported a LOD of 6.6 copies/reaction in urine ($n = 63$) (Castro et al., 2018), whilst another study achieved 6 copies/reaction in urine ($n = 178$) (Calvert et al., 2017). Although both RT-qPCR and RT-LAMP offer slightly improved sensitivity compared to the Iso-ZIKV-Dx test, their application as POC diagnostics in low-resource settings is limited. RT-qPCR requires highly skilled personnel, expensive machinery and laboratory-based sample preparation. While RT-LAMP is known for its simplicity, sensitivity and speed which resulted in wide scale application in low resource settings, it still needs heating machines capable of attaining temperatures of 55–65°C. In contrast, RT-RAA, similarly to RT-RPA can be performed at near-ambient temperature (37–40°C) and moreover has a higher tolerance to PCR inhibitors (Li et al., 2020). Both have previously required laboratory-based purification of RNA, whereas our Iso-ZIKV-Dx test does not require any sophisticated laboratory equipment, providing potential the entire procedure, from sample to result, be performed in low-resource near-patient settings. The ideal rapid POC test should provide a range of detection and diagnostic capabilities, as defined by the REASSURED criteria – Real-time connectivity, Ease of specimen collection, Affordable, Sensitive, Specific, User-friendly, Rapid, Equipment-free, and Deliverable to end-users (Land et al., 2019). Our data suggests that the Iso-ZIKV-Dx (sample preparation, RT-RAA, LFD) has potential to meet the REASSURED criteria, providing real-time connectivity through direct analogue reading of the result which could be performed at or near the patient in a low-resource clinic. Insofar as our assay has met pre-clinical and REASSURED criteria, our next phase of evaluation will involve clinical and in-field evaluation of the assay to evaluate clinical efficacy and performance among pathology of ZIKV infections. As our study only involved live MR766 strain of ZIKV, our hope would be to evaluate our ZIKV test with multiple strains within these clinical trials.

Due to manual steps in our assay, it should be acknowledged that screening of large-scale clinical samples would not occur as rapidly as standard RT-PCR assays. However, unlike RT-PCR, our rapid ZIKV test has been designed to be field deployable, requiring minimal resources and minimally trained staff. As a result, the time from sample preparation to diagnostic result is considerably faster than when compared to transportation and processing within central laboratory. Moreover, this particular attribute of our ZIKV test renders it a potential early warning screening tool in the face of a sudden outbreaks. A second potential challenge for our ZIKV test, and indeed many in-field nucleic acid amplification assays (Tang et al., 2016), is the risk of post amplification cross-contamination. A potential solution to this issue is the substitution of dTTP with dUTP in the amplification reactions. This approach has been shown to reduce cross-contamination in LAMP assays (Kil et al., 2015). However, to the authors knowledge, the feasibility of implementing such measure in recombinase-aided amplification assays has yet to be assessed. Therefore, a more feasible alternative is to utilise 'U-Star' disposable cartridges (TwistDx™, 2023b), which would reduce cross contamination occurrences by limiting external exposure of lateral flow strips to the environment.

Rapid detection of arboviruses such as ZIKV play a crucial role in limiting outbreaks that have already emerged or are currently on going. Additionally, surveillance and monitoring can serve to identify early signs of the pathogen and thereby prevent outbreaks through vector control. The study of vector competency and transovarial transmission of arboviruses such as ZIKV thus remain a particular area of focus. Due to factors such as climate change and increased urbanisation (Li et al., 2017) vector competency continues to broaden, further implicating the emergence of novel and existing viruses. A tool with in-field capabilities that provides robust and rapid results could be highly beneficial in epidemiology for monitoring ZIKV. To that end, further studies are warranted to determine if our Iso-ZIKV-Dx is compatible for detection of virus in mosquitoes, as was similarly performed for the TNA-Cifer Reagent E combined with RPA-LFD for detection of dengue virus in *Aedes aegpytii* mosquitoes. This would allow our Iso-ZIKV-Dx test to be extended beyond diagnostics alone, in potentially offering strategies toward aiding in surveillance and

monitoring of viral vectors (Pollak et al., 2023b) and possibly reservoir hosts for arboviruses such as ZIKV.

Conclusion

In conclusion, we developed a rapid, isothermal test for ZIKV that only requires incubation at 39°C and produces a real-time result in 30 min. Pre-clinical evaluation suggests that our Iso-ZIKV-Dx could offer promising innovations for diagnostics in ZIKV endemic areas. We demonstrate that our ZIKV test was able to detect as low as 500 copies/μL of synthetic ZIKV RNA and also, does not detect any other co-circulating arbovirus. We successfully established a simple sample preparation procedure which demonstrated that we were able to completely inactivate one of the highest virulent strains of ZIKV (MR766, African lineage) in 5 min at room temperature, whilst at the same time, extracting sufficient quantities of viral RNA for detection. By combining our simple sample preparation procedure with RT-RAA and Lateral Flow Strip detection, we successfully developed a robust rapid isothermal ZIKV diagnostic. Our data illustrated that our ZIKV test operates five times faster than 'gold standard' RT-qPCR and exhibited a detection limit of 34 RNA copies/reaction in spiked synthetic urine. Furthermore, due to the simplistic nature of our ZIKV test, we surmise that the applications of our Iso-ZIKV-Dx extend beyond detection alone, and could potentially provide innovations toward surveillance and monitoring for ZIKV and arboviruses alike.

Data availability statement

The original contributions presented in the study are included in the article/Supplementary material, further inquiries can be directed to the corresponding authors.

Author contributions

RB: conceptualization, data curation, formal analysis, investigation, methodology, resources, supervision, validation, visualization, writing – original draft, and writing – review and editing. NP, JM, and DM: conceptualization, formal analysis, funding acquisition, methodology, project administration, resources, supervision, and writing – review and editing. JH-P: resources and writing – review and editing. All authors contributed to the article and approved the submitted version.

Funding

This study was supported by the Research Training Program (RTP) Commonwealth Research Scholarship (https://www.education.gov.au/research-block-grants/research-training-program), in accordance with the Higher Education Support act 2003 with the University of the Sunshine Coast (QLD, Australia). This work was also supported, in part by the Bill & Melinda Gates foundation (OPP1140133).

Acknowledgments

We wish to thank BioCifer Pty Ltd. for generously providing TNA-Cifer Reagent E and Reverse Transcriptase used to develop the ZIKV diagnostic test. We also wish to thank Vasilli Kasimov (Centre for Bioinnovation, University of the Sunshine Coast) for assisting in the bioinformatic analysis and formulation of the phylogenetic tree for our primer and probe design.

Conflict of interest

RB reports supplies were provided by BioCifer Pty Ltd. JM reports financial support was provided by Bill and Melinda Gates Foundation. JM reports a relationship with BioCifer Pty Ltd. that includes: board membership and equity or stocks.

The remaining authors declare that the research was conducted in the absence of any commercial or financial relationships that could be construed as a potential conflict of interest.

Publisher's note

All claims expressed in this article are solely those of the authors and do not necessarily represent those of their affiliated organizations, or those of the publisher, the editors and the reviewers. Any product that may be evaluated in this article, or claim that may be made by its manufacturer, is not guaranteed or endorsed by the publisher.

Supplementary material

The Supplementary material for this article can be found online at: https://www.frontiersin.org/articles/10.3389/fmicb.2023.1214148/full#supplementary-material

References

Ahmed, M., Nath, N. S., Hugo, L. E., Devine, G. J., Macdonald, J., and Pollak, N. M. (2022). Rapid detection of kdr mutation F1534C in *Aedes aegypti* using recombinase polymerase amplification and lateral flow dipsticks. *Pestic. Biochem. Physiol.* 187:105209. doi: 10.1016/j.pestbp.2022.105209

Azar, S. R., and Weaver, S. C. (2019). Vector competence: what has Zika virus taught us? *Viruses* 11:867. doi: 10.3390/v11090867

Bonaldo, M. C., Ribeiro, I. P., Lima, N. S., dos Santos, A. A. C., Menezes, L. S. R., da Cruz, S. O. D., et al. (2016). Isolation of infective Zika virus from urine and saliva of patients in Brazil. *PLoS Negl. Trop. Dis.* 10:e0004816. doi: 10.1371/journal.pntd.0004816

Brady, O. J., and Hay, S. I. (2019). The first local cases of Zika virus in Europe. *Lancet* 394, 1991–1992. doi: 10.1016/S0140-6736(19)32790-4

Calvert, A. E., Biggerstaff, B. J., Tanner, N. A., Lauterbach, M., and Lanciotti, R. S. (2017). Rapid colorimetric detection of Zika virus from serum and urine specimens by reverse transcription loop-mediated isothermal amplification (RT-LAMP). *PLoS One* 12:e0185340. doi: 10.1371/journal.pone.0185340

Castro, T., Sabalza, M., Barber, C., Abrams, W., da Costa, A. C., de Pádua Milagres, F. A., et al. (2018). Rapid diagnosis of Zika virus through saliva and urine by loop-mediated isothermal amplification (LAMP). *J. Oral Microbiol.* 10:1510712. doi: 10.1080/20002297.2018.1510712

Chang, C., Ortiz, K., Ansari, A., and Gershwin, M. E. (2016). The Zika outbreak of the 21st century. *J. Autoimmun.* 68, 1–13. doi: 10.1016/j.jaut.2016.02.006

Cheikh Tidiane Diagne, M. F., Lopez-Jimena, B., El Wahed, A. A., Loucoubar, C., Fall, C., Mencatelli, G., et al. (2020). Comparative analysis of Zika virus detection by

RT-qPCR, RT-LAMP, and RT-RPA, in methods in molecular biology. *Methods Mol. Biol.* 2142, 165–179. doi: 10.1007/978-1-0716-0581-3_14

Da Silva, S., Martins, D. O. S., and Jardim, A. C. G. (2018). A review of the ongoing research on Zika virus treatment. *Viruses* 10:255. doi: 10.3390/v10050255

de Moraes, F. M., Espósito, D. L. A., Klein, T. M., and da Fonseca, B. A. L. (2018). Searching for the best real-time RT-PCRs to detect Zika virus infections: the importance of comparing several protocols. *Braz. J. Med. Biol. Res.* 51:e7221. doi: 10.1590/1414-431x20187221

Dick, G. W. A., Kitchen, S. F., and Haddow, A. J. (1952). Zika virus (I). Isolations and serological specificity. *Trans. R. Soc. Trop. Med. Hyg.* 46, 509–520. doi: 10.1016/0035-9203(52)90042-4

Dong, D., Fu, S. H., Wang, L. H., Lv, Z., Li, T. Y., and Liang, G. D. (2012). Simultaneous detection of three arboviruses using a triplex RT-PCR enzyme hybridization assay. *Virol. Sin.* 27, 179–186. doi: 10.1007/s12250-012-3246-9

Dupont-Rouzeyrol, M., O'Connor, O., Calvez, E., Daurès, M., John, M., Grangeon, J. P., et al. (2015). Co-infection with Zika and dengue viruses in 2 patients, New Caledonia, 2014. *Emerg. Infect. Dis.* 21, 381–382. doi: 10.3201/eid2102.141553

Gourinat, A. C., O'Connor, O., Calvez, E., Goarant, C., and Dupont-Rouzeyrol, M. (2015). Detection of Zika virus in urine. *Emerg. Infect. Dis.* 21, 84–86. doi: 10.3201/eid2101.140894

Gregory, C. J., Oduyebo, T., Brault, A. C., Brooks, J. T., Chung, K. W., Hills, S., et al. (2017). Modes of transmission of Zika virus. *J. Infect. Dis.* 216, S875–S883. doi: 10.1093/infdis/jix396

Hayes, E. B. J. E. I. D. (2009). Zika virus outside. *Africa* 15, 1347–1350. doi: 10.3201/eid1509.090442

Hendel-Paterson, B., Anderson, K., Fabrizius, R. G., Walker, P. F., Maalim, S., and Kaiser, R. M. (2016). Guillain-Barré syndrome associated with Zika virus infection in a traveler returning from Guyana. *Am J Trop Med Hyg* 95, 1161–1165. doi: 10.4269/ajtmh.16-0397

Heukelbach, J., Alencar, C. H., Kelvin, A. A., de Oliveira, W. K., and Pamplona de Góes Cavalcanti, L. (2016). Zika virus outbreak in Brazil. *J. Infect. Dev. Ctries.* 10, 116–120. doi: 10.3855/jidc.8217

Hobson-Peters, J., Yam, A. W. Y., Lu, J. W. F., Setoh, Y. X., May, F. J., Kurucz, N., et al. (2013). A new insect-specific flavivirus from northern Australia suppresses replication of West Nile virus and Murray Valley encephalitis virus in co-infected mosquito cells. *PLoS One* 8:e56534. doi: 10.1371/journal.pone.0056534

Jiangsu Qitian Gene Biotechnology Co., Ltd. (2023). Recombinase aided amplification. 2012–2023. Available at: http://en.qt-bio.com/.

Kadkhoda, K., Gretchen, A., and Racano, A. (2017). Evaluation of a commercially available Zika virus IgM ELISA: specificity in focus. *Diagn. Microbiol. Infect. Dis.* 88, 233–235. doi: 10.1016/j.diagmicrobio.2017.04.002

Kearse, M., Moir, R., Wilson, A., Stones-Havas, S., Cheung, M., Sturrock, S., et al. (2012). Geneious basic: an integrated and extendable desktop software platform for the organization and analysis of sequence data. *Bioinformatics* 28, 1647–1649. doi: 10.1093/bioinformatics/bts199

Kil, E. J., Kim, S., Lee, Y. J., Kang, E. H., Lee, M., Cho, S. H., et al. (2015). Advanced loop-mediated isothermal amplification method for sensitive and specific detection of tomato chlorosis virus using a uracil DNA glycosylase to control carry-over contamination. *J. Virol. Methods* 213, 68–74. doi: 10.1016/j.jviromet.2014.10.020

Lamb, L. E., Bartolone, S. N., Kutluay, S. B., Robledo, D., Porras, A., Plata, M., et al. (2016). Advantage of urine based molecular diagnosis of Zika virus. *Int. Urol. Nephrol.* 48, 1961–1966. doi: 10.1007/s11255-016-1406-9

Land, K. J., Boeras, D. I., Chen, X. S., Ramsay, A. R., and Peeling, R. W. (2019). REASSURED diagnostics to inform disease control strategies, strengthen health systems and improve patient outcomes. *Nat. Microbiol.* 4, 46–54. doi: 10.1038/s41564-018-0295-3

Li, C.-X., Guo, X. X., Deng, Y. Q., Xing, D., Sun, A. J., Liu, Q. M., et al. (2017). Vector competence and transovarial transmission of two *Aedes aegypti* strains to Zika virus. *Emerg. Microbes Infect.* 6, 1–7. doi: 10.1038/emi.2017.8

Li, J., Macdonald, J., and von Stetten, F. (2020). Correction: review: a comprehensive summary of a decade development of the recombinase polymerase amplification. *Analyst* 145, 1950–1960. doi: 10.1039/C9AN90127B

Li, J., Pollak, N. M., and Macdonald, J. J. A. O. (2019). Multiplex detection of nucleic acids using recombinase polymerase amplification and a molecular colorimetric 7-segment display 4, 11388–11396. doi: 10.1021/acsomega.9b01097,

Minh, B. Q., Schmidt, H. A., Chernomor, O., Schrempf, D., Woodhams, M. D., von Haeseler, A., et al. (2020). IQ-TREE 2: new models and efficient methods for phylogenetic inference in the genomic era. *Mol. Biol. Evol.* 37, 1530–1534. doi: 10.1093/molbev/msaa015

Mumtaz, N., van Kampen, J. J. A., Reusken, C. B. E. M., Boucher, C. A. B., and Koopmans, M. P. G. (2016). Zika virus: where is the treatment? *Curr. Treat. Options Infect. Dis.* 8, 208–211. doi: 10.1007/s40506-016-0083-7

Nakamura, T., Yamada, K. D., Tomii, K., and Katoh, K. (2018). Parallelization of MAFFT for large-scale multiple sequence alignments. *Bioinformatics* 34, 2490–2492. doi: 10.1093/bioinformatics/bty121

Paixão, E. S., Barreto, F., da Glória Teixeira, M., da Conceição N. Costa, M., and Rodrigues, L. C. (2016). History, epidemiology, and clinical manifestations of Zika: a systematic review. *Am. J. Public Health* 106, 606–612. doi: 10.2105/AJPH.2016.303112

Paixao, E. S., Leong, W. Y., Rodrigues, L. C., and Wilder-Smith, A. (2018). Asymptomatic prenatal Zika virus infection and congenital Zika syndrome. *Open Forum Infect. Dis.* 5:ofy073. doi: 10.1093/ofid/ofy073

Pessôa, R., Patriota, J. V., Lourdes de Souza, M., Felix, A. C., Mamede, N., and Sanabani, S. S. (2016). Investigation into an outbreak of dengue-like illness in Pernambuco, Brazil, revealed a Cocirculation of Zika, chikungunya, and dengue virus type 1. *Medicine* 95, –e3201. doi: 10.1097/MD.0000000000003201

Pollak, N. M., Fais, O., Kristoffersen, J., Phuthaworn, C., Knibb, W., and Macdonald, J. (2022). Rapid sample preparation and low-resource molecular detection of hepatopancreatic parvoviruses (HPV) by recombinase polymerase amplification lateral flow detection assay in shrimps (*Fenneropenaeus merguiensis*). *PLoS One* 17:e0276164. doi: 10.1371/journal.pone.0276164

Pollak, N. M., Marsh, G. A., Olsson, M., McMillan, D., and Macdonald, J. (2023a). Rapid, sensitive, and specific, low-resource molecular detection of Hendra virus. *One Health* 16:100504. doi: 10.1016/j.onehlt.2023.100504

Pollak, N. M., Olsson, M., Ahmed, M., Tan, J., Lim, G., Setoh, Y. X., et al. (2023b). Rapid diagnostic tests for the detection of the four dengue virus serotypes in clinically relevant matrices. *Microbiol. Spectr.* 11:e0279622. doi: 10.1128/spectrum.02796-22

Pollak, N. M., Olsson, M., Marsh, G. A., Macdonald, J., McMillan, D., et al. (2023c). Evaluation of three rapid low-resource molecular tests for Nipah virus. *Front. Microbiol.* 13:1101914. doi: 10.3389/fmicb.2022.1101914

Rames, E. K., and Macdonald, J. (2019). Rapid assessment of viral water quality using a novel recombinase polymerase amplification test for human adenovirus. *Appl. Microbiol. Biotechnol.* 103, 8115–8125. doi: 10.1007/s00253-019-10077-w

Reed, L. J., and Muench, H. J. A. J. O. E. (1938). A simple method of estimating fifty per cent endpoints 27, 493–497. doi: 10.1093/oxfordjournals.aje.a118408,

Rossini, G., Gaibani, P., Vocale, C., Cagarelli, R., and Landini, M. P. (2017). Comparison of Zika virus (ZIKV) RNA detection in plasma, whole blood and urine – case series of travel-associated ZIKV infection imported to Italy, 2016. *J. Infect.* 75, 242–245. doi: 10.1016/j.jinf.2017.05.021

Roth, A., Mercier, A., Lepers, C., Hoy, D., Duituturaga, S., Benyon, E., et al. (2014). Concurrent outbreaks of dengue, chikungunya and Zika virus infections – an unprecedented epidemic wave of mosquito-borne viruses in the Pacific 2012–2014. *Eur. Secur.* 19:20929. doi: 10.2807/1560-7917.ES2014.19.41.20929

Shao, Q., Herrlinger, S., Zhu, Y. N., Yang, M., Goodfellow, F., Stice, S. L., et al. (2017). The African Zika virus MR-766 is more virulent and causes more severe brain damage than current Asian lineage and dengue virus. *Development* 144, 4114–4124. doi: 10.1242/dev.156752

Sharp, T. M., Muñoz-Jordán, J., Perez-Padilla, J., Bello-Pagán, M. I., Rivera, A., Pastula, D. M., et al. (2016). Zika virus infection associated with severe thrombocytopenia. *Clin. Infect. Dis.* 63, 1198–1201. doi: 10.1093/cid/ciw476

Sigma-Aldrich Co. LLC (2014). OligoEvaluator. Available at: http://www.oligoevaluator.com/LoginServlet

Stettler, K., Beltramello, M., Espinosa, D. A., Graham, V., Cassotta, A., Bianchi, S., et al. (2016). Specificity, cross-reactivity, and function of antibodies elicited by Zika virus infection 353, 823–826. doi: 10.1126/science.aaf8505,

Tan, S. K., Sahoo, M. K., Milligan, S. B., Taylor, N., and Pinsky, B. A. (2017). Stability of Zika virus in urine: specimen processing considerations and implications for the detection of RNA targets in urine. *J. Virol. Methods* 248, 66–70. doi: 10.1016/j.jviromet.2017.04.018

Tang, Y., Chen, H., and Diao, Y. (2016). Advanced uracil DNA glycosylase-supplemented real-time reverse transcription loop-mediated isothermal amplification (UDG-rRT-LAMP) method for universal and specific detection of Tembusu virus. *Sci. Rep.* 6:27605. doi: 10.1038/srep27605

TwistDx™. (2023a). Recombinase polymerase amplification, or RPA, is the breakthrough, isothermal replacement to PCR. Available at: https://www.twistdx.co.uk/rpa/.

TwistDx™. (2023b). U-star disposable nucleic acid lateral flow detection units products. Available at: https://www.twistdx.co.uk/product/u-star-disposable-nucleic-acid-lateral-flow-detection-units-pack-of-20/

Wang, Y., Cui, Y., Yu, Z., Li, Y., Bai, C., Sun, P., et al. (2020). Development of a recombinase-aided amplification assay for detection of orf virus. *J. Virol. Methods* 280:113861. doi: 10.1016/j.jviromet.2020.113861

Wen, Z., Song, H., and Ming, G. L. (2017). How does Zika virus cause microcephaly? *Genes Dev.* 31, 849–861. doi: 10.1101/gad.298216.117

Xue, G., Li, S., Zhang, W., du, B., Cui, J., Yan, C., et al. (2020). Reverse-transcription recombinase-aided amplification assay for rapid detection of the 2019 novel coronavirus (SARS-CoV-2). *Anal. Chem.* 92, 9699–9705. doi: 10.1021/acs.analchem.0c01032

frontiers | Frontiers in Microbiology

TYPE Original Research
PUBLISHED 12 December 2023
DOI 10.3389/fmicb.2023.1314538

OPEN ACCESS

EDITED BY
Ke Liu,
Chinese Academy of Agricultural Sciences, China

REVIEWED BY
Tatjana Vilibic-Cavlek,
Croatian Institute of Public Health, Croatia
Ljubo Barbic,
University of Zagreb, Croatia

*CORRESPONDENCE
Pavle Banović
✉ pavle.banovic@mf.uns.ac.rs

RECEIVED 10 October 2023
ACCEPTED 14 November 2023
PUBLISHED 12 December 2023

CITATION
Banović P, Mijatović D, Bogdan I, Simin V, Meletis E, Kostoulas P, Resman Rus K, Knap N, Korva M, Avšič-Županc T and Cabezas-Cruz A (2023) Evidence of tick-borne encephalitis virus neutralizing antibodies in Serbian individuals exposed to tick bites. *Front. Microbiol.* 14:1314538. doi: 10.3389/fmicb.2023.1314538

Evidence of tick-borne encephalitis virus neutralizing antibodies in Serbian individuals exposed to tick bites

Pavle Banović[1,2]*, Dragana Mijatović[3], Ivana Bogdan[4], Verica Simin[4], Eleftherios Meletis[5], Polychronis Kostoulas[5], Katarina Resman Rus[6], Nataša Knap[6], Miša Korva[6], Tatjana Avšič-Županc[6] and Alejandro Cabezas-Cruz[7]

[1]Clinic for Lyme Borreliosis and Other Tick-Borne Diseases, Pasteur Institute Novi Sad, Novi Sad, Serbia, [2]Department of Microbiology with Parasitology and Immunology, Faculty of Medicine in Novi Sad, University of Novi Sad, Novi Sad, Serbia, [3]Department for Research and Monitoring of Rabies and Other Zoonoses, Pasteur Institute Novi Sad, Novi Sad, Serbia, [4]Department of Microbiology, Pasteur Institute Novi Sad, Novi Sad, Serbia, [5]Faculty of Public and One Health, School of Health Sciences, University of Thessaly, Karditsa, Greece, [6]Institute of Microbiology and Immunology, Faculty of Medicine, University of Ljubljana, Ljubljana, Slovenia, [7]Anses, INRAE, Ecole Nationale Vétérinaire d'Alfort, UMR BIPAR, Laboratoire de Santé Animale, Maisons-Alfort, France

Introduction: Tick-borne encephalitis (TBE) is an emerging vector-borne and food-borne disease caused by the tick-borne encephalitis virus (TBEV; *Orthoflavivirus encephalitidis*), with a distribution spanning the Eurasian continent. Despite its significant public health impact in various European regions, TBE remains largely underdiagnosed in Serbia due to limited awareness and diagnostic challenges. In response to this, our study aimed to comprehensively assess TBEV exposure in individuals infested with ticks and to identify potential TBEV foci within Serbia.

Materials and methods: From 2019 to 2021, we conducted an observational study involving 450 patients who reported tick infestations.

Results: Our demographic analysis revealed a median age of 38 years, with a slight male predominance among the participants. We documented tick infestations in 38 municipalities across 14 districts of Serbia, with a notable concentration in proximity to Fruška Gora Mountain. The ticks most frequently removed were *Ixodes ricinus*, with nymphs and adult females being the predominant stages. On average, nymphs were removed after about 27.1 hours of feeding, while adult females remained attached for approximately 44.4 hours. Notably, we found age as a significant predictor of infestation time for both nymphs and adult females. Furthermore, we detected TBEV-neutralizing antibodies in 0.66% of the serum samples, shedding light on potential TBEV foci, particularly in Fruška Gora Mountain and other regions of Serbia.

Conclusion: Our study emphasizes the urgent need for active TBE surveillance programs, especially in areas suspected of hosting TBEV foci, in order to assess the true TBE burden, identify at-risk populations, and implement effective preventive measures.

KEYWORDS

ticks, TBEV, seroprevalence, TBEV-neutralizing antibodies, Serbia

1 Introduction

Tick-borne encephalitis (TBE) is an emerging vector-borne and food-borne disease caused by the TBE virus, a member of the *Orthoflavivirus* genus, Flaviviridae family (Elbaz et al., 2022; Kunze et al., 2022; Postler et al., 2023). This virus is distributed across the Euroasian continent, forming a "TBE belt" stretching from Western Europe to the easternmost regions of Asia (Kunze et al., 2022). TBEV is classified into five subtypes based on antigenic characteristics, disease severity, and geographic distribution: European (TBEV-Eu), Siberian (TBEV-Sib), Far Eastern (TBEV-Fe), Baikalian (TBEV-Bkl), and Himalayan (TBEV-Him; Dai et al., 2018).

Tick-borne encephalitis-European primarily infects humans through the bites of infected *Ixodes ricinus* tick and occasionally via the consumption of unpasteurized milk products contaminated with TBEV. This European subtype is prevalent in Western, Central, and Southeastern Europe and is generally less virulent compared to TBEV-Sib and TBEV-Fe. Consequently, it is associated with milder forms of central nervous system (CNS) infections, more favorable outcome, and fewer long-term complications in survivors. Nonetheless, TBE remains a significant public health concern, particularly in Central and North-eastern Europe, with the highest number of cases reported in the Baltic countries, Czechia, Switzerland, Slovakia, Slovenia, Austria, and Germany (Steffen, 2016; Kunze et al., 2022).

Following exposure to TBEV, individuals can develop subclinical, abortive, or clinical infections. It is estimated that the majority of TBEV-Eu infections are subclinical, while approximately 30% progress to the febrile stage (Stage I) with concurrent viremia. Among these, 70% will clear the virus and have an abortive infection, while the remaining 30% will experience CNS involvement and develop manifest TBE (Barp et al., 2020; Bogovič et al., 2022a,b).

Due to the short viremia period and non-specific disease signs during Stage I (i.e., most patients seek medical attention when neurological symptoms appear), the definitive diagnosis of TBE relies on indirect methods, and most commonly enzyme-linked immunosorbent assays (ELISAs; Kunze et al., 2022). In regions where both TBEV and West Nile virus (*Orthoflavivirus nilense*; WNV) infections occur, such as Serbia, Hungary, Croatia, and Romania (Popescu et al., 2018; Zana et al., 2020; Petrović et al., 2021), ELISA results may lead to misdiagnosis of TBE as West Nile encephalitis and vice versa due to antibody cross-reactivity. Therefore, neutralization assays are often necessary for accurate differentiation (Potkonjak et al., 2017; Kunze et al., 2022).

Despite TBE being a notifiable disease in Serbia since 2004, there is limited awareness of the disease among medical practitioners (Vasić et al., 2022). The most recent detection of TBEV in ticks in Serbia dates back to 2017 (Potkonjak et al., 2017). Additionally, TBEV-reactive antibodies have been recently detected in individuals recovering from viral meningitis/encephalitis of unknown origin and in tick-infested patients (Banović et al., 2021, 2022a). Until recently, there was no active TBE surveillance program focused on serological or molecular screening of patients with CNS infection symptoms, and the assay for detecting TBEV-neutralizing antibodies (TBEV-NAb) was not available (Popović Dragonjić et al., 2022).

To assess the extent of TBEV exposure in the Serbian population and identify risk groups and high-incidence areas, we conducted a prospective observational study between 2019 and 2021. This study aimed to determine the prevalence of TBEV-NAbs in individuals who had been infested with ticks.

2 Materials and methods

2.1 Study design and participant enrollment

This observational study leveraged medical records obtained during routine operations at the Clinic for Lyme Borreliosis and Other Tick-Borne Diseases, Pasteur Institute Novi Sad (PI Novi Sad) between January 1, 2019 and December 31, 2021. Serum samples were collected from patients with tick infestations. The medical records included basic demographic information (age, gender), tick-borne disease development, and data related to the ticks removed from patients (e.g., species, life stage, and feeding duration). Serum samples were taken at least 4 weeks after tick removal from patients that met the inclusion criteria and provided informed consent, for the detection and quantification of TBEV-neutralizing antibodies. Additionally, samples showing neutralizing effect to TBEV were examined for WNV-neutralizing antibodies to rule out cross-reactivity.

To be eligible for enrollment and serum sampling, patients needed to meet the following criteria: (i) patients who reported to PI Novi Sad with ticks still attached or recently removed and submitted them for entomologic examination; (ii) patients who underwent a total of three medical examinations during a 2-month follow-up period, including a visit for blood sampling at least 4 weeks after tick removal; (iii) patients or their caregivers provided informed consent for study inclusion, medical record analysis, and blood sampling; and (iv) patients had not been immunized against TBE or yellow fever.

2.2 Tick collection and classification

All ticks collected from patients were identified by species, sex, and life stage based on morphological features and standard taxonomic keys as described by Estrada-Peña (2004). Patients also provided information about where they suspected they acquired the ticks. When patients were uncertain about the time between tick bite and detection, attachment time was estimated from approximate feeding time, assessed using the coxal index (for tick attachments lasting <24 h) and the scutal index (for tick attachments lasting 24 h or more; Gray et al., 2005). Since feeding time assessed by measurement of scutal or coxal index is expressed in hours, we divided final values by 24 and expressed infestation time as number of days.

2.3 Blood sample collection and sera extraction

At least 4 weeks after tick removal and with informed consent obtained from each patient or their caregivers (for underage individuals), a 3 mL blood sample was collected using BD Vacutainer® SST™ Tubes (BD, Franklin Lakes, NJ, United States). The blood samples were allowed to clot at room temperature, followed by centrifugation at 2,000 × g for 10 min to extract and store the serum at −80°C until further analysis.

2.4 Detection of TBEV-Nabs

The TBEV strain Neudörfl (National Collection of Pathogenic Viruses, United Kingdom; Cat. No 0201139v) was cultured in a biosafety level 2+ Laboratory for Vector Borne Pathogens at Pasteur Institute Novi Sad using a monolayer of BHK-21/C13 cells (BS CL 8, Istituto Zooprofilattico Sperimentale Brescia, Italy). Virus stocks were prepared at a concentration of 100 Tissue Culture Infectious Dose (TCID)/100 µL and stored at −80°C. The micro-neutralization test (micro-NT) was conducted using a 96-well cell culture plate (Thermo Scientific™, MA, United States, Cat. No 130338). Serum samples were first inactivated at 56°C for 30 min and tested in duplicate with serial dilutions ranging from 1:5 to 1:40 in Glasgow Minimal Essential Medium (Biowest, France; Cat. No P0120). Each test run included positive and negative controls, a cell control, and virus back-titration. A total of 100 TCID of virus stock was added to the respective serum dilutions and incubated for 1 h at 37°C. After incubation, the serum-virus mixture was transferred to wells containing BHK21/C13 cells seeded at a concentration of 2×10^5 cells and incubated for 5 days at 37°C with 5% CO2. The cytopathic effect (CPE) was observed in both wells for each sample. The dilution of the sample resulting in virus neutralization in 50% of the replicates (NT_{50}) was calculated using the Spearman and Karber method (Ramakrishnan, 2016) and represented as the reciprocal value of the same dilution.

2.5 External validation of TBEV neutralization assay

The TBEV neutralization assay was performed in a biosafety level 3 facility. First, Vero E6 cells (ATTC CRL-1586) were seeded at 10^5 cells/well in 96-well plates (TPP, 92196) supplemented with growth medium consisting of DMEM with GlutaMAX supplement (Thermo Fisher Scientific, 61965026) and 10% FBS (Euroclone, ECS0180L) and incubated for 24 h at 37°C in 5% CO2. Two-fold serial dilutions (initial dilution was 1:10) of heat-inactivated sera samples (56°C, 30 min) were incubated with 100 $TCID_{50}$ of TBEV (TBEV strain Ljubljana 1; deposited in the EVA-GLOBAL Virus Archive under reference number Ref-SKU: 007 V-EVA71) for 1 h at 37°C. Then, 50 µL of the serum dilution-virus mixture was inoculated in triplicate into a 96-well plate containing an 80% confluent Vero E6 monolayer. The plates were incubated for 5 days at 37°C before being fixed with 50 µL of 4% formaldehyde. Plates were then examined microscopically for cytopathic effect (CPE) and the cell monolayer was additionally visualized by crystal violet staining. The neutralization endpoint titer was defined as the endpoint plasma dilution that inhibited TBEV-induced cytopathic effect in at least two out of three parallels. Positive and negative control sera were included in each plate.

2.6 Detection of cross-reactivity via West Nile virus neutralization assay

To exclude the possibility of antibody cross-reactivity, we also performed a West Nile virus neutralization assay using 100 $TCID_{50}$ of WNV (strain: Eg101; deposited in the EVA-GLOBAL Virus Archive under reference number Ref-SKU: 007 V-03213) according to the protocol described in Knap et al. (2020).

2.7 Bias identification and management

The most significant bias identified in this clinical observational study is the proximity of our center to patients' homes. Patients residing in urban and suburban areas of Novi Sad are more likely to seek medical attention at PI Novi Sad compared to those who need to travel longer distances for follow-up examinations. To address this bias, general practitioners across the Vojvodina autonomous province (North Serbia) were instructed to encourage patients to visit PI Novi Sad regardless of whether they acquired ticks within or outside their home city. This approach allowed us to analyze ticks from various locations across Serbia, not limited to patients' municipalities of residence.

2.8 Statistical analysis

In this study, we employed the Cox proportional hazards mixed-effects model, referred to as the Cox mixed-effects model, to analyze the time taken until tick removal, which was the event of interest (dependent variable). For all patients, a tick was removed, and thus, the event was coded as 1 for each individual. The primary objective of the analysis was to identify the most influential predictors for the time until tick removal. The independent variables examined were demographic information, including age, gender, and place of residence. We conducted separate analyses for nymphs and adult females. Additionally, to visually depict the time until removal for specific clusters, such as age groups divided into 10-year intervals and gender, Kaplan–Meier survival curves were constructed. The analysis and visualization were performed using the R programming language (R-Project, 2023).

Regarding the number of seroreactive samples, the data analysis was limited to descriptive statistics of laboratory findings. Fisher's exact test was used to assess differences in demographic characteristics within the examined cohort, with statistical significance considered for $p < 0.05$. Statistical analysis and visualization were conducted using GraphPad software v.9 (GraphPad Software Inc., La Jolla, CA, United States).

3 Results

3.1 Ethics statement

This study was approved by the ethical committee of Medical faculty Novi Sad, University of Novi Sad (Ethical approval No. 01-39/261/1 from 17.09.2020) and conducted according to the Declaration of Helsinki and The Patient Rights Law of the Republic of Serbia.

3.2 Participants enrollment

Between January 1, 2019 and December 31, 2021, a total of 1,447 patients sought medical consultation at PI Novi Sad, reporting tick bites and tick-associated infections. To be eligible for study inclusion, patients needed to either bring the tick removed from their skin or present with an attached tick. Out of these patients, 1,225 were

confirmed to have been exposed to tick bites, while 222 individuals reported with various biologic materials of different origins, such as fabric fragments, crusts, small warts, spiders, or coagulated blood. Informed consent for study enrollment was obtained from 545 individuals (44.48%) among those confirmed to be exposed to tick bites. However, during the 4-week follow-up period, 45 participants dropped out due to low compliance, and an additional 50 patients refused to have their blood sampled after the follow-up period. Ultimately, the cohort of tick-exposed patients comprised 450 individuals who completed the observation period and underwent blood sampling (Figure 1).

3.3 Characteristics of enrolled patients and tick exposure locations

Demographic analysis revealed that the median age of tick-infested individuals included in the study was 38 years (interquartile range: 10–58 years). In terms of gender, males constituted a non-significant majority (237/450; 52.66%, Fisher exact test value 0.4632; $p > 0.05$).

An epidemiological survey, supplemented by determination of tick feeding time, indicated that tick infestations occurred in 38 municipalities spanning 14 districts across Serbia (Figure 2). Tick infestations were most frequent in municipalities proximate to Fruška Gora Mountain, particularly within the Srem and South Bačka districts.

3.4 Characteristics of ticks removed from patients, assessment of tick attachment time

Ixodes ricinus accounted for the overwhelming majority of ticks removed from patients (432/450; 96%). Other tick species, such as *Dermacentor reticulatus* (4/450; 0.88%, all adult females), *Dermacentor marginatus* (4/450; 0.88%, all adult females), *Rhipicephalus sanguineus* (6/450; 1.33%, two adult males and four adult females), and *Haemaphysalis punctata* (4/450; 0.88%, all adult females), were observed less frequently.

Among *I. ricinus* ticks, nymphs (235/432; 54.39%) and adult females (184/432; 42.59%) were the most prevalent. Infestations caused by larvae and adult males were rare (11/432; 2.54% and 2/432; 0.46%, respectively). On average, nymphs were removed after approximately 27.1 h of feeding (95% CI 38–49.2), while adult females achieved infestations lasting approximately 44.4 h (95% CI 33.84–54.96).

The Cox proportional hazards mixed model identified age as a parameter associated with the duration of *I. ricinus* nymph feeding. Specifically, the age group of 10–20 years exhibited a statistically significant relationship with the outcome (i.e., infestation period assessed by scutal/coxal indices). The reported odds ratio was 1.54 (95% CI 1.06–2.22), with a value of p of 0.022, suggesting that patients aged 10–20 years may have a distinct relationship with the shorter time required to remove infesting ticks when compared to the reference level or other age groups (Figure 3A).

The Cox proportional hazards mixed model for the infestation time of adult females showed a p value of <0.05, indicating the possibility of one or more age groups differing from the others (Figure 3B). Further investigation through pairwise comparisons of Kaplan-Mayer curves revealed a statistically significant difference between the age group of 10–20 years and the age group of 60–70 years ($p = 0.014$), where the age group of 10–20 years was associated shorter infestation period, despite this not being captured or reported in the model.

3.5 Prevalence of TBEV-neutralizing antibodies

Out of the 450 serum samples examined at PI Novi Sad, TBEV $NT_{50} \geq 10$ was observed in three samples, with one sample recording $NT_{50} = 5$, categorized as borderline. Subsequent analysis conducted at the Institute of Microbiology and Immunology, Faculty of Medicine, in Ljubljana (University of Ljubljana, Slovenia) confirmed the presence of TBEV-neutralizing antibodies in all three samples initially identified as positive in PI Novi Sad, with no neutralization effect against WNV. Additionally, the sample initially categorized as borderline (TBEV $NT_{50} = 5$) exhibited a significant neutralization effect against WNV (WNV $NT_{50} = 80$), with no neutralization effect against TBEV, ultimately being classified as negative for TBEV-neutralizing antibodies. Three samples initially identified as negative in PI Novi Sad were confirmed to be absent of TBEV-neutralizing antibodies as well as WNV-neutralizing antibodies. In summary, the presence of TBEV-neutralizing antibodies was confirmed in three serum samples (3/450; 0.66%), with NT_{50} values of 10, 160, and > 1,280. None of the patients with TBEV-neutralizing antibodies exhibited signs of stage I or II TBEV infection, and denied previous immunization against TBE and yellow fever, as well as medical history of aseptic meningitis and/or encephalitis. All three individuals were infested with *I. ricinus* ticks in 2021 (one larva, one nymph, and one adult female, respectively). The suspected locations of tick infestation for the three seropositive patients were Ledinci village (Fruška Gora Mountain, Municipality of Novi Sad), Divčibare Mountain (Municipality of Valjevo), and Bukulja Mountain (Municipality of Aranđelovac; Figure 2).

4 Discussion

Tick-borne encephalitis virus foci are intricate microecosystems heavily influenced by a multitude of biotic and abiotic factors that can either facilitate or hinder virus transmission and the amplification chain (Cabezas-Cruz and Banović, 2023). The European continent is currently witnessing the expansion of TBEV endemic regions, primarily driven by climate changes, various anthropogenic factors, and the resulting migration of animals that serve as tick hosts (Kunze et al., 2022). Variation in these factors can result in disappearance of existing TBEV foci when the maintenance and transmission of the virus between vectors (i.e., *Ixodidae*) and reservoirs (e.g., small rodents of the genera *Apodemus* and *Myodes*) are disturbed (Knap and Avšič-Županc, 2015; Bournez et al., 2020). As TBEV foci expand, the incidence of TBE is on the rise across Europe, even in higher-altitude regions of Central Europe and previously considered TBEV-free areas such as Scandinavian countries (Kunze et al., 2022).

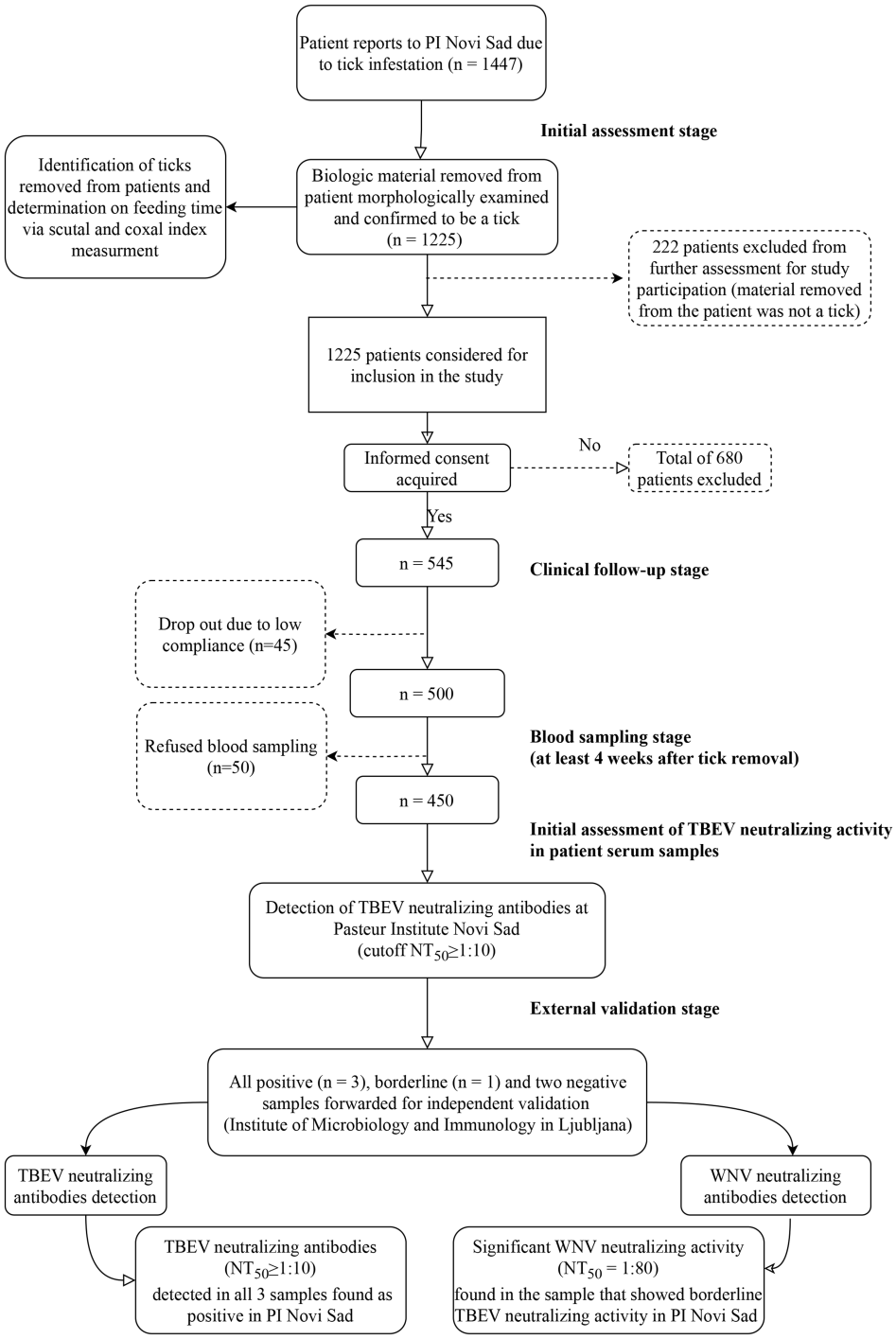

FIGURE 1
Study flowchart. PI Novi Sad, Clinic for Lyme borreliosis and other Tick-Borne Diseases of the Pasteur Institute Novi Sad; TBEV, Tick-borne encephalitis virus; WNV, West Nile virus; NT_{50}, titer that neutralizes 50% of challenge virus. Flowchart generated using open-source software draw.io (https://app.diagrams.net/).

Despite TBE being a notifiable disease in Serbia, reported cases are infrequent due to low awareness among healthcare workers (Vasić et al., 2022). Another challenge in TBE diagnostics has been the absence of a gold standard diagnostic assay, as the detection of TBEV-neutralizing antibodies in Serbia only became possible in 2022 (Popović Dragonjić et al., 2022). Unlike many European countries where concerns over TBEV are growing, Serbia lacks an active surveillance program to assess the prevalence of TBEV infection in ticks and/or rodents. The last detection of TBEV in Serbia occurred in 2017 when infected *I. ricinus* ticks were collected in various locations within the suburbs of Belgrade and Fruška Gora Mountain (Potkonjak et al., 2017).

The existence of TBEV foci in different regions of Serbia was evident when tick-infested patients exhibited a higher likelihood of

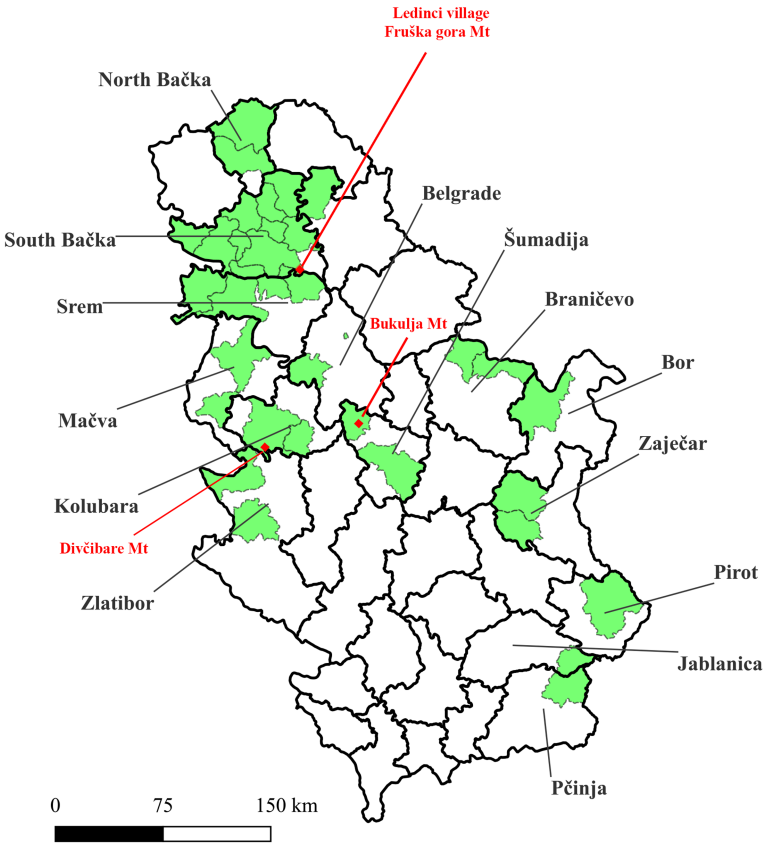

District	Municipality	Sample size (*n*)	%
Belgrade		**4**	**0.89**
	Obrenovac	2	0.44
	Stari Grad	2	0.44
Bor		**5**	**1.11**
	Majdanpek	5	1.11
Braničevo		**8**	**2.00**
	Veliko Gradište	2	0.67
	Golubac	6	1.33
Jablanica		**2**	**0.44**
	Crna Trava	2	0.44
Kolubara		**7**	**1.56**
	Valjevo	4	0.89
	Mionica	3	0.67
Mačva		**6**	**1.33**
	Krupanj	2	0.44
	Šabac	4	0.89
North Bačka		**7**	**1.56**
	Subotica	1	0.22
	Bačka Topola	6	1.33
Pčinja		**1**	**0.44**
	Surdulica	1	0.44
Pirot		**5**	**1.11**
	Pirot	5	1.11
South Bačka		**316**	**70.22**
	Bač	2	0.44
	Bačka Palanka	8	1.78
	Bački Petrovac	2	0.44
	Bečej	8	1.78
	Beočin	49	10.89
	Novi Sad	141	31.33
	Petrovaradin	39	8.67
	Srbobran	2	0.44
	Sremska Kamenica	27	6.00
	Sremski Karlovci	20	4.44
	Temerin	4	0.89
	Vrbas	4	0.89
	Žabalj	10	2.22
Srem		**45**	**10.00**
	Indija	20	4.44
	Irig	11	2.44
	Šid	2	0.44
	Sremska Mitrovica	12	2.67
Šumadija		**5**	**1.11**
	Kragujevac	2	0.44
	Aranđelovac	3	0.67
Zaječar		**3**	**0.67**
	Boljevac	2	0.44
	Sokobanja	1	0.22
Zlatibor		**5**	**1.11**
	Čajetina	1	0.22
	Bajina Bašta	4	0.89
N/A	Fruška gora Mountain	29	6.44

FIGURE 2
Map of Serbia showing Geographical locations where tick infestations occurred in patients reported to Pasteur Institute Novi Sad. The sample distribution is presented by municipalities (green color), across 14 districts of Serbia. Red dots are used to mark locations where tick infestation occurred for three patients whose serum had TBEV-neutralizing capability. Mt., Mountain. The shape file for mapping at district and municipality levels is available at the GADM database of Global Administrative Areas (v4.1, July 2022; https://gadm.org/). The map was generated by using QGIS v3.12 (QGIS Development Team 2020).

seroreactivity to TBEV antigens compared to blood donors from the same region (Banović et al., 2021). Further awareness arose when TBEV-reactive IgG were discovered in 20% of individuals recovering from viral encephalitis of unknown origin (Banović et al., 2022a; Cabezas-Cruz and Banović, 2023). However, a significant limitation of these studies is that TBEV exposure was inferred through assays not designed to differentiate anti-TBEV antibodies from the humoral response generated against other orthoflaviviruses circulating in Serbia (e.g., *Orthoflavivirus usutuense* and WNV). Indeed, when a neutralization assay was applied in a two-center seroprevalence study conducted in Novi Sad (Serbia) and Skopje (North Macedonia), no TBEV-neutralizing antibodies were found in the Serbian cohort exposed to tick bites (Jakimovski et al., 2023). This result may be influenced by the small number of participants included in the Serbian cohort ($n = 51$), compared with the cohort examined in this study ($n = 450$).

Among the 450 individuals exposed to tick bites, TBEV-neutralizing antibodies were found in three patients, representing a seroprevalence of 0.66%. This seroprevalence is considerably lower than the prevalence of IgG reactivity to TBEV in tick-infested individuals from Serbia (13.27%; Banović et al., 2021). This discrepancy is expected, as several members of genus *Orthoflavivirus* are circulating within Serbian population and causing development of specific immunoglobulins (Petrović et al., 2019, 2021) that can cross-react with other members of the *Orthoflavivirus* genus. In addition, TBEV-Nabs are only a subset of total anti-TBEV antibodies generated after exposure to TBEV. Although, TBEV-Nab seroprevalence in our cohort is higher compared to Norwegian, Romanian and Serbian blood donors (0.66 vs. 0.4% and 0.08 and 0%, respectively; Marvik et al., 2021; Coroian et al., 2022; Jakimovski et al., 2023) and much lower compared to residents of Czechia (0.66% vs. 26.3%; Kriz et al., 2015).

To identify potential TBEV foci in Serbia, we integrated anamnestic data and an epidemiological survey with scutal/coxal index values of ticks removed from patients with TBEV-neutralizing antibodies. We identified potential locations within three mountains: Fruška Gora Mountain, Divčibare Mountain, and Bukulja Mountain. Among these, Fruška Gora Mountain is the only locality previously suspected in seroprevalence and field studies to have an environment conducive to the maintenance of TBEV foci (Potkonjak et al., 2017; Banović et al., 2021). Regarding the tick species responsible for human infestations, our finding that *I. ricinus* was the most frequently removed tick aligns with previous studies conducted in Serbia (Banović et al., 2022b, 2023). Although *I. ricinus* ticks were removed

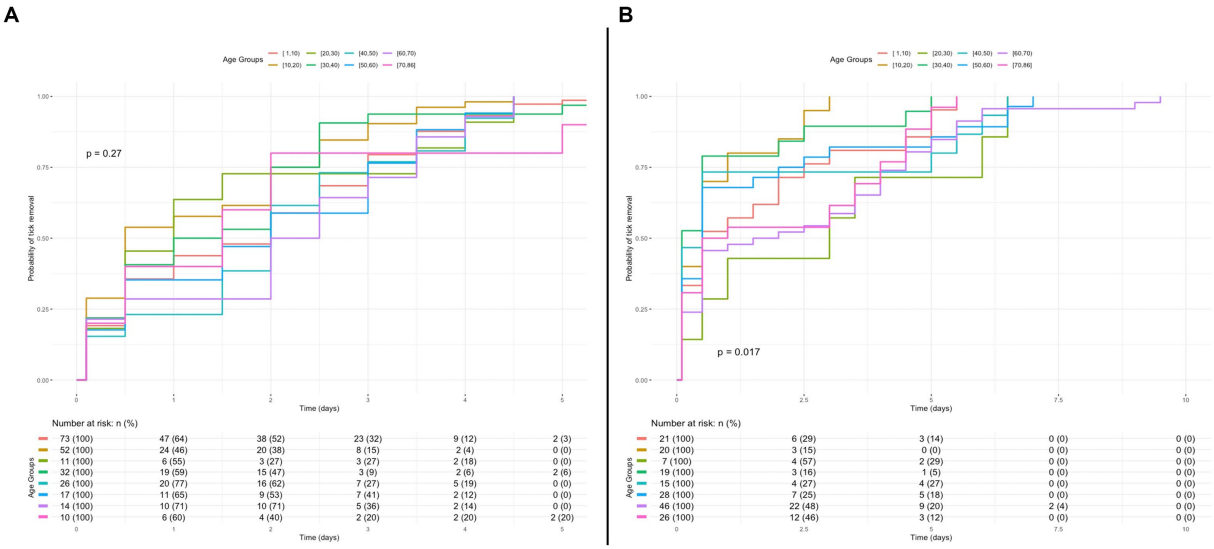

FIGURE 3
Kaplan–Meier curve of probability for removal of *Ixodes ricinus* removal in the course of time for different age groups. **(A)** Kaplan–Meier curve for probability of *I. ricinus* nymph removal in the course of time for the different patient age groups of the study. A *p* value higher than 5% indicates no statistically significant difference between groups. **(B)** Kaplan–Meier curve for probability of *I. ricinus* adult female removal in the course of time for the patient different age groups of the study.

from all three patients in whom TBEV-neutralizing antibodies were detected, we are not able to claim that TBEV exposure occurred during most recent infestation. Concerning the infestation time, the significance of age as a predictor level and the output of the Cox model used here necessitate further investigation. When a level of a predictor variable (age group) in a Cox proportional hazards model has a *p* value greater than 5%, it suggests that overall, that specific age group might not have a statistically significant difference in infestation time compared to other age groups. However, when conducting pairwise comparisons among levels of the predictor (i.e., age groups), it might be found that one particular age group significantly differs from another, even if its overall relationship in the main model was not statistically significant (Hosmer et al., 2011; Agresti, 2012).

A major limitation of this study is the absence of attempts to isolate and/or detect TBEV in ticks removed from humans, which could confirm recent exposure to the virus in patients with TBEV-neutralizing antibodies. Additionally, a 4-week period between tick infestation and serum sampling may not be long enough for all TBEV-exposed persons to develop detectable levels of TBEV-neutralizing antibodies. Uneven distribution of samples across the country limits the representativeness of the results for all districts of Serbia, necessitating further studies where several centers will be engaged in serum collection, where period between tick infestation and serum sampling should be expanded to at least 5 weeks. Nevertheless, this study is the first to provide unequivocal evidence of TBEV exposure in tick-infested individuals from Serbia. Since anti-TBEV IgM reactivity and anti-TBEV IgG avidity were not determined, we are not able to claim that most recent (i.e., observed) tick infestation is linked with virus exposure in patients with TBEV-neutralizing antibodies. Therefore, infestation locations should be considered as potential natural foci, warranting future surveillance campaigns. Healthcare institutions should initiate surveillance programs and test all cases of viral meningitis/encephalitis of unknown origin for the presence of TBEV-neutralizing antibodies, especially those responsible for the residents of Fruška Gora, Divčibare, and Bukulja mountains. This approach will enable the assessment of the TBE burden in the Serbian population, identification of risk groups, field research, and the implementation of prevention measures, including immunization and educational campaigns.

5 Conclusion

In this study, we have unveiled critical insights into the seroprevalence of TBEV-neutralizing antibodies and epidemiological significance of TBEV in Serbia. Although we were not able to provide the evidence of recent infection in tested patients, our findings suggest the existence of potential TBEV foci within Serbia, notably in regions proximal to Fruška Gora Mountain, Divčibare Mountain, and Bukulja Mountain. The detection of TBEV-neutralizing antibodies in tick-infested individuals, albeit at a relatively low prevalence of 0.66%, underscores the need for heightened surveillance efforts. The identification of TBEV exposure in these regions highlights the urgency of implementing active TBE surveillance programs. Furthermore, our study has shed light on the demographics of tick-infested individuals and the characteristics of tick infestations, including attachment times of different tick stages. Age was identified as a significant predictor of infestation time, emphasizing the importance of considering age-related factors in future TBE research and surveillance. Research efforts as presented in this paper are crucial for assessing the true burden of TBE, identifying high-risk groups, conducting further field research, and ultimately implementing effective prevention measures to mitigate the spread of this emerging disease.

Data availability statement

The original contributions presented in the study are included in the article/supplementary material, further inquiries can be directed to the corresponding author.

Ethics statement

This study was approved by the ethical committee of Medical faculty Novi Sad, University of Novi Sad (Ethical approval No. 01-39/261/1 from 17.09.2020.) and conducted according to the Declaration of Helsinki and The Patient Rights Law of the Republic of Serbia. The studies involving humans were approved by Komisija za etičnost kliničkih ispitivanja Medicinskog fakulteta u Novom Sadu. The studies were conducted in accordance with the local legislation and institutional requirements. Written informed consent for participation in this study was provided by the participants' legal guardians/next of kin. The manuscript presents research on animals that do not require ethical approval for their study.

Author contributions

PB: Conceptualization, Formal analysis, Funding acquisition, Investigation, Methodology, Project administration, Validation, Visualization, Writing – original draft, Writing – review & editing. DM: Formal analysis, Investigation, Methodology, Writing – original draft. IB: Conceptualization, Investigation, Methodology, Writing – original draft. VS: Conceptualization, Data curation, Investigation, Methodology, Writing – review & editing. EM: Formal analysis, Investigation, Methodology, Software, Visualization, Writing – review & editing. PK: Investigation, Methodology, Software, Supervision, Visualization, Writing – review & editing. KR: Formal analysis, Investigation, Methodology, Validation, Writing – review & editing. NK: Investigation, Methodology, Validation, Writing – review & editing. MK: Data curation, Investigation, Resources, Validation, Writing – review & editing. TA-Ž: Conceptualization, Methodology, Resources, Supervision, Validation, Writing – review & editing. AC-C: Data curation, Formal analysis, Methodology, Supervision, Writing – review & editing.

Funding

The author(s) declare financial support was received for the research, authorship, and/or publication of this article. The BSL3+ work at Institute of Microbiology and Immunology, Faculty of Medicine, University of Ljubljana was supported by Slovenian Research and Innovation Agency (grant number P3-0083), Network of Infrastructure Centers of the University of Ljubljana (MRIC-UL-IC-BSL3+), and the European Union's Horizon 2020 research and innovation program—EVA GLOBAL project (Grant agreement no. 871029). The BSL2+ work at Pasteur Institute Novi Sad was supported by an independent medical grant from Pfizer. The funders had no role in the design of the study; in the collection, analyses or interpretation of data; in the writing of the manuscript or in the decision to publish the results.

Conflict of interest

The authors declare that the research was conducted in the absence of any commercial or financial relationships that could be construed as a potential conflict of interest.

The author(s) declared that they were an editorial board member of Frontiers, at the time of submission. This had no impact on the peer review process and the final decision.

Publisher's note

References

Agresti, A. (2012). *Categorical Data Analysis*. Hoboken, New Jersey, USA: John Wiley & Sons.

Banović, P., Díaz-Sánchez, A. A., Durić, S., Sević, S., Turkulov, V., Lendak, D., et al. (2022a). Unexpected TBEV Seropositivity in Serbian patients who recovered from viral meningitis and encephalitis. *Pathogens* 11:371. doi: 10.3390/pathogens11030371

Banović, P., Díaz-Sánchez, A. A., Foucault-Simonin, A., Mateos-Hernandez, L., Wu-Chuang, A., Galon, C., et al. (2023). Emerging tick-borne spotted fever group rickettsioses in the Balkans. *Infect. Genet. Evol.* 107:105400. doi: 10.1016/j.meegid.2022.105400

Banović, P., Díaz-Sánchez, A. A., Simin, V., Foucault-Simonin, A., Galon, C., Wu-Chuang, A., et al. (2022b). Clinical aspects and detection of emerging Rickettsial pathogens: a "one health" approach study in Serbia, 2020. *Front. Microbiol.* 12:797399. doi: 10.3389/fmicb.2021.797399

Banović, P., Obregón, D., Mijatović, D., Simin, V., Stankov, S., Budakov-Obradović, Z., et al. (2021). Tick-borne encephalitis virus Seropositivity among tick infested individuals in Serbia. *Pathogens* 10:301. doi: 10.3390/pathogens10030301

Barp, N., Trentini, A., Di Nuzzo, M., Mondardini, V., Francavilla, E., and Contini, C. (2020). Clinical and laboratory findings in tick-borne encephalitis virus infection. *Paras. Epidemiol. Control* 10:e00160. doi: 10.1016/j.parepi.2020.e00160

Bogovič, P., Kastrin, A., Lotrič-Furlan, S., Ogrinc, K., Avšič Županc, T., Korva, M., et al. (2022a). Comparison of laboratory and immune characteristics of the initial and second phase of tick-borne encephalitis. *Emerg. Microbes Infect.* 11, 1647–1656. doi: 10.1080/22221751.2022.2086070

Bogovič, P., Kastrin, A., Lotrič-Furlan, S., Ogrinc, K., Županc, T. A., Korva, M., et al. (2022b). Clinical and laboratory characteristics and outcome of illness caused by tick-borne encephalitis virus without central nervous system involvement. *Emerg. Infect. Dis.* 28, 291–301. doi: 10.3201/eid2802.211661

Bournez, L., Umhang, G., Moinet, M., Boucher, J.-M., Demerson, J.-M., Caillot, C., et al. (2020). Disappearance of TBEV circulation among rodents in a natural focus in Alsace, eastern France. *Pathogens* 9:930. doi: 10.3390/pathogens9110930

Cabezas-Cruz, A., and Banović, P. (2023). Understanding tick-borne encephalitis virus foci, a tale of two mountains. *Pathogens* 12:265. doi: 10.3390/pathogens12020265

Coroian, M., Mihalca, A. D., Dobler, G., Euringer, K., Girl, P., Borşan, S.-D., et al. (2022). Seroprevalence rates against West Nile, Usutu, and tick-borne encephalitis viruses in blood-donors from North-Western Romania. *Int. J. Environ. Res. Public Health* 19:8182. doi: 10.3390/ijerph19138182

Dai, X., Shang, G., Lu, S., Yang, J., and Xu, J. (2018). A new subtype of eastern tick-borne encephalitis virus discovered in Qinghai-Tibet plateau, China. *Emerg. Microbes Infect.* 7:74. doi: 10.1038/s41426-018-0081-6

Elbaz, M., Gadoth, A., Shepshelovich, D., Shasha, D., Rudoler, N., and Paran, Y. (2022). Systematic review and Meta-analysis of foodborne tick-borne encephalitis, Europe, 1980-2021. *Emerg. Infect. Dis.* 28, 1945–1954. doi: 10.3201/eid2810.220498

Estrada-Peña, A. (2004). *Ticks of Domestic Animals in the Mediterranean Region: A Guide to Identification of Species*. Zaragoza, Spain: University of Zaragoza.

Gray, J., Stanek, G., Kundi, M., and Kocianova, E. (2005). Dimensions of engorging *Ixodes ricinus* as a measure of feeding duration. *Int. J. Med. Microbiol.* 295, 567–572. doi: 10.1016/j.ijmm.2005.05.008

Hosmer, D. W., Lemeshow, S., and May, S. (2011). *Applied Survival Analysis: Regression Modeling of Time-to-Event Data*. Hoboken, New Jersey, USA: John Wiley & Sons.

Jakimovski, D., Mateska, S., Dimitrova, E., Bosilkovski, M., Mijatović, D., Simin, V., et al. (2023). Tick-borne encephalitis virus and *Borrelia burgdorferi* Seroprevalence in Balkan tick-infested individuals: a two-Centre study. *Pathogens* 12:922. doi: 10.3390/pathogens12070922

Knap, N., and Avšič-Županc, T. (2015). Factors affecting the ecology of tick-borne encephalitis in Slovenia. *Epidemiol. Infect.* 143, 2059–2067. doi: 10.1017/S0950268815000485

Knap, N., Korva, M., Ivović, V., Kalan, K., Jelovšek, M., Sagadin, M., et al. (2020). West Nile Virus in Slovenia. *Viruses* 12:720. doi: 10.3390/v12070720

Kriz, B., Hubalek, Z., Marek, M., Daniel, M., Strakova, P., and Betasova, L. (2015). Results of the screening of tick-borne encephalitis virus antibodies in human sera from eight districts collected two decades apart. *Vector Borne Zoonotic Dis* 15, 489–493. doi: 10.1089/vbz.2014.1747

Kunze, M., Banović, P., Bogovič, P., Briciu, V., Čivljak, R., Dobler, G., et al. (2022). Recommendations to improve tick-borne encephalitis surveillance and vaccine uptake in Europe. *Microorganisms* 10:1283. doi: 10.3390/microorganisms10071283

Marvik, Å., Tveten, Y., Pedersen, A.-B., Stiasny, K., Andreassen, Å. K., and Grude, N. (2021). Low prevalence of tick-borne encephalitis virus antibodies in Norwegian blood donors. *Infect Dis* 53, 44–51. doi: 10.1080/23744235.2020.1819561

Petrović, T., Šekler, M., Petrić, D., Vidanović, D., Debeljak, Z., Lazić, G., et al. (2021). Intensive West Nile virus circulation in Serbia in 2018—results of integrated surveillance program. *Pathogens* 10:1294. doi: 10.3390/pathogens10101294

Petrović, T., Šekler, M., Petrić, D., Vidanović, D., Potkonjak, A., Hrnjaković Cvjetković, I., et al. (2019). Flaviviruses at the territory of Serbia—present situation and challenges. *AVM* 11, 53–70. doi: 10.46784/e-avm.v11i2.26

Popescu, C. P., Florescu, S. A., Cotar, A. I., Badescu, D., Ceianu, C. S., Zaharia, M., et al. (2018). Re-emergence of severe West Nile virus neuroinvasive disease in humans in Romania, 2012 to 2017-implications for travel medicine. *Travel Med. Infect. Dis.* 22, 30–35. doi: 10.1016/j.tmaid.2018.03.001

Popović Dragonjić, L., Vrbić, M., Tasić, A., Simin, V., Bogdan, I., Mijatović, D., et al. (2022). Fatal case of imported tick-borne encephalitis in South Serbia. *Trop. Med. Infect. Dis.* 7:434. doi: 10.3390/tropicalmed7120434

Postler, T. S., Beer, M., Blitvich, B. J., Bukh, J., de Lamballerie, X., Drexler, J. F., et al. (2023). Renaming of the genus Flavivirus to Orthoflavivirus and extension of binomial species names within the family Flaviviridae. *Arch. Virol.* 168:224. doi: 10.1007/s00705-023-05835-1

Potkonjak, A., Petrović, T., Ristanović, E., Lalić, I., Vračar, V., Savić, S., et al. (2017). Molecular detection and serological evidence of tick-borne encephalitis virus in Serbia. *Vect. Borne Zoonot. Dis.* 17, 813–820. doi: 10.1089/vbz.2017.2167

Ramakrishnan, M. A. (2016). Determination of 50% endpoint titer using a simple formula. *World J. Virol.* 5, 85–86. doi: 10.5501/wjv.v5.i2.85

R-Project (2023). The R Project for Statistical Computing. Available at: https://www.r-project.org/ (Accessed July 19, 2023).

Steffen, R. (2016). Epidemiology of tick-borne encephalitis (TBE) in international travellers to Western/Central Europe and conclusions on vaccination recommendations. *J. Travel Med.* 23:taw018. doi: 10.1093/jtm/taw018

Vasić, A., Bjekić, J., Veinović, G., Mihaljica, D., Sukara, R., Poluga, J., et al. (2022). Knowledge, attitudes, and practices on tick-borne encephalitis virus and tick-borne diseases within professionally tick-exposed persons, health care workers, and general population in Serbia: a questionnaire-based study. *Int. J. Environ. Res. Public Health* 19:867. doi: 10.3390/ijerph19020867

Zana, B., Erdélyi, K., Nagy, A., Mezei, E., Nagy, O., Takács, M., et al. (2020). Multi-approach investigation regarding the West Nile virus situation in Hungary, 2018. *Viruses* 12:123. doi: 10.3390/v12010123

frontiers | Frontiers in Microbiology

TYPE Original Research
PUBLISHED 14 December 2023
DOI 10.3389/fmicb.2023.1309650

OPEN ACCESS

EDITED BY
James Weger-Lucarelli,
Virginia Tech, United States

REVIEWED BY
Shandian Gao,
Lanzhou Veterinary Research Institute, Chinese Academy of Agricultural Sciences, China
Hongzhuan Wu,
Alabama State University, United States

*CORRESPONDENCE
Li-Na Zhang
✉ zln_tiantang@163.com
Lei Zhang
✉ zhanglei_tcs@126.com

†These authors have contributed equally to this work and share first authorship

RECEIVED 08 October 2023
ACCEPTED 20 November 2023
PUBLISHED 14 December 2023

CITATION
Liu H, Hu J, Li L-X, Lu Z-S, Sun X-T, Lu H-J, Jin N-Y, Zhang L and Zhang L-N (2023) Seroepidemiological investigation of Getah virus in the China-Myanmar border area from 2022-2023.
Front. Microbiol. 14:1309650.
doi: 10.3389/fmicb.2023.1309650

Seroepidemiological investigation of Getah virus in the China-Myanmar border area from 2022-2023

Hao Liu[1†], Jin Hu[1†], Li-Xia Li[1], Zi-Shuo Lu[1], Xiu-Tao Sun[2], Hui-Jun Lu[3], Ning-Yi Jin[3], Lei Zhang[4*] and Li-Na Zhang[5*]

[1]School of Life Sciences and Engineering, Foshan University, Foshan, China, [2]Honghe Animal Disease Prevention and Control Center, Mengzi, China, [3]Institute of Military Veterinary Medicine, Academy of Military Medical Sciences, Changchun, China, [4]Institute of Special Economic Animal and Plant Sciences, Chinese Academy of Agricultural Sciences, Changchun, China, [5]Eco-Engineering Department, Guangdong Eco-Engineering Polytechnic, Guangzhou, China

Getah Virus (GETV) is an RNA virus that is transmitted by mosquitoes and can cause disease or death in a variety of vertebrates. Its prevalence is increasingly severe in Asia. This study conducted a GETV epidemiological investigation on 1,300 bovine sera collected in the Honghe Prefecture of Yunnan Province on the China-Myanmar border from 2022 to 2023. The positive rate of GETV antibodies in bovine serum in Honghe Prefecture was determined to be 20.25% through indirect Enzyme-linked immunosorbent test (ELISA) methods. Using Real-time PCR methods to detect GETV RNA in bovine serum, the positive rate was 0.23% (3/1300), and viral nucleic acids were only detected in three bovine sera in Jianshui area in 2022. The YN2305 strain was successfully isolated from mouse neuroblastoma (N2a) cells and the complete gene sequence was obtained. All the above results indicate the existence of GETV infection in cattle in Honghe Prefecture, Yunnan Province. Homology and genetic evolution analysis found that the isolated strain has a high homology with the JL1808 strain isolated from cattle in 2018, with a nucleotide identity of 100%, and a nucleotide identity of 99.8% with the SD17-09 strain isolated from foxes in 2017. Compared with the nucleotides of 44 virus strains published in Genbank, YN2305 has multiple nucleotide site mutations in the structural gene E2 and non-structural gene NS. The nucleotide and amino acid identity of the E2 gene are 94.2–100% and 96.4–100%, respectively. Genetic evolution analysis found that this virus strain is most closely related to the bovine origin JL1808, and it is in gene group III with HuN1, Kochi-01, SD17-09, MI-110-C1, and MI-110-C2 strains that causes significant clinical symptoms in Chinese pig, fox and horse populations, belonging to the same evolutionary branch. This study determined the infection rate, genotype, and main prevalence areas of GETV in bovine sera in the China-Myanmar border area. Therefore, the epidemiological investigation of GETV infection in multiple animal hosts should be further expanded, and research on its pathogenicity and vectors should be carried out.

KEYWORDS

Getah virus, virus Isolation, sequence determination and analysis, phylogenetic analysis, seroepidemiological investigation, cattle

1 Introduction

Getah virus (GETV) is an arbovirus, belonging to the *Alphavirus* genus of the *Togaviridae* family, along with Chikungunya virus (CHIKV) and Venezuelan equine encephalitis virus (VEEV) (Zhai et al., 2008; Shi et al., 2022a). GETV was first isolated from *Culex gelidus* mosquitoes in Malaysia in 1955 (Zhai et al., 2008; Ren et al., 2020; Xing et al., 2020; Shi et al., 2022a; Sun et al., 2022). Since then, GETV has rapidly expanded its host range and geographical distribution (Zhai et al., 2008). Currently, it has appeared and become prevalent in 12 countries including China, Russia, South Korea, Japan, Thailand, and Australia (Zhai et al., 2008; Yang et al., 2018; Rattanatumhi et al., 2022). Since its first isolation from mosquitoes in Hainan Province, China in 1964, it has broken out and become prevalent in 17 provinces and cities (Zhai et al., 2008). So far, the virus RNA or antibodies have been detected in horses, pigs, cattle, sheep, blue foxes, kangaroos, monkeys, red pandas, and some poultry (Nemoto et al., 2015; Li et al., 2017, 2019; Yang et al., 2018; Ren et al., 2020; Xing et al., 2020; Rattanatumhi et al., 2022; Shi et al., 2022a; Zhao et al., 2022). Of particular note is that neutralizing antibodies against GETV have been found in human serum in Malaysia, Australia, and China (Zhai et al., 2008; Shi et al., 2022b), and the specific antibody titers in febrile populations are significantly higher than in healthy populations, indicating that GETV infection is related to human diseases. Yunnan Province, located in southwestern China, borders Myanmar, Laos, and Vietnam. Frequent tourism and animal trade have accelerated the spread of arboviruses locally, which may pose a threat to livestock and human health. In recent years, most GETV strains in China have come from four genera and seven species of mosquito specimens in Yunnan Province (Li et al., 2019). Cattle are the primary reservoir hosts of arboviruses, however, there have been no reports on cattle infection with GETV in the border areas of Yunnan Province. Therefore, this study conducted a GETV epidemiological investigation on bovine serum samples in the China-Myanmar border area from 2022-2023 using indirect ELISA and real-time PCR methods, to provide data support for disease prevention and control.

2 Materials and methods

2.1 Animal serum collection

From 2022 to 2023, a total of 1,300 bovine sera were collected in Honghe Prefecture, Yunnan Province, including Luxi (400), Jianshui (420), and Mile (480). All samples were stored in a −80°C freezer.

2.2 RNA detection

RNA was extracted from the bovine serum samples using the QIAamp Viral RNA Mini Kit (Qiagen). The RNA was then converted to cDNA using the Vazyme HiScript II First Strand cDNA Synthesis Kit (Vazyme Biotech Co., Ltd, China). The detection was carried out using the previously established quantitative reverse transcription PCR (RT-qPCR) detection method for GETV non-structural protein 1 (nsP1) (Shi et al., 2018).

2.3 Enzyme-linked immunosorbent test (ELISA)

The amino acid sequence of the E2 protein of GETV virus strain in Genbank was used, and after codon optimization, the gene was artificially synthesized and directionally cloned into the pGEX-6P-1 vector. After correct identification by enzyme cleavage and sequencing, it was transformed into the host bacterium BL-21 for induced expression. The identification of the recombinant E2 (rE2) protein was achieved by employing Western blot and SDS-PAG techniques subsequent to the completion of GST tag purification. Subsequently, the rE2 protein was employed as a diagnostic antigen in order to establish an indirect ELISA method for the detection of GETV antibodies, in accordance with prior literature (Sun et al., 2022). The cross-reactivity of the rE2-based indirect ELISA was assessed by examining the anti-sera from various common bovine and porcine viruses, such as BVDV, FMDV, PRRSV, BATV, JEV, and PEDV. Additionally, the sensitivity of the Indirect ELISA was analyzed by testing different dilutions of bovine GETV positive serum.

2.4 Virus isolation and amplification of whole gene sequence

The serum with GETV nucleic acid positive was filtered through a 0.22°μm filter (Millipore, Billerica, MA, USA) and inoculated into N2a monolayer cells in a six-well plate. After incubating at 37°C for 1°h, the cells were washed twice with PBS, and preserved in 2% FBS (Gibco) MEM in a 5% CO_2 incubator. The cytopathic effect (CPE) of the cells was observed daily. After five continuous cell passages, the cell suspension was collected and the isolated GETV strain was sequenced for the whole genome (Ren et al., 2020).

2.5 Alignment and phylogenetic analysis of GETV genome sequences

To analyze the homology relationship between GETV YN2305 isolate and other various GETV strains, the MegAlign software was used to perform homology analysis on the full gene and E2 gene sequences of the YN2305 isolate. Other GETV strains are from those registered in Genbank. MEGA 7 software was used to perform phylogenetic analysis on 44 full genes and 58 E2 gene groups of GETV that have been published in Genbank and YN2305. The Tamura-Nei model and the maximum likelihood method of gamma distribution rate heterogeneity were used in MEGA 7.

2.6 Statistical analysis

The binom.confint function in R version 3.5.0 was used to calculate the seroprevalence and 95% confidence interval (95% CI).

3 Results

3.1 Results of the serological tests

From 2022 to 2023, a total of 1,300 bovine sera were collected in Honghe Prefecture, Yunnan Province, with a total positive rate of 20.25% (108/534, 95% CI: 17.04−27.84). Among them, 1,000 bovine serum samples collected in Jianshui, Mile, and Luxi regions of Honghe Prefecture in Yunnan Province in 2022 were tested, with a positive rate of 20.78% (53/255, 95% CI: 16.26−26.18). The positive rates in each region were 24.74% (23/93, 95% CI: 17.08−34.38), 12.17% (9/74, 95% CI: 6.53−21.53), and 23.86% (21/88, 95% CI: 16.17−33.74), respectively. In 2023, the positive rate of GETV antibodies in 300 bovine serum samples collected in Honghe Prefecture was 19.71% (55/279, 95% CI: 15.47−24.78), with Jianshui, Mile, and Luxi counties at 8.6% (8/93, 95% CI: 4.42−16.07), 36.56% (34/93, 95% CI:27.49−46.7), and 13.98% (13/93, 95% CI: 8.35−22.46), respectively, (**Table 1**).

3.2 GETV RNA test results

All bovine serum samples were tested for GETV RNA using RT-qPCR method, with a positive rate of 0.23% (3/1300).

3.3 Enzyme-linked immunosorbent test (ELISA)

Following the process of GST label purification, the E2 protein underwent identification through SDS-PAGE and Western blot techniques, which revealed a protein size of 74.6 kDa, aligning with the anticipated value (Technical Appendix **Supplementary Figure 1**). The average outcomes of the antisera for BVDV, FMDV, PRRSV, BATV, JEV, and PEDV indicated negativity, thereby confirming the absence of cross-reactivity with the established rE2 indirect ELISA. Consequently, the indirect ELISA exhibited a significant of specificity. In addition, the serum from bovines infected with GETV were subjected to testing at various dilutions, ranging from 1:100 to 1:51200. The results indicated that the lowest detectable dilution using this methodology was 1:6400.

3.4 GETV homology and genetic evolution analysis

The full gene sequence of GETV YN2305 strain was obtained by PCR method with a length of 11,689 nt and submitted to Genbank (Genbank number: OR371719). Homology analysis was carried out with 44 GETV strains registered in Genbank, revealing that the YN2305 strain has the highest nucleotide homology with the bovine-derived JL1808 strain, with an identity of 100%. The nucleotide identity with the fox-derived SD17-09 strain and pig-derived Kochi-01 strain were 99.8 and 99.5%, respectively. Similarly, comparison with 58 E2 gene nucleotide sequences revealed that the identity of YN2305 strain with JL1808 was 100%, while the identity with E2 genes of other strains was 94.2−99.8% (**Table 2**). Through the phylogenetic analysis of the full gene and E2, YN2305 belongs to the GETV gene group III, and is most closely related to the bovine-derived JL1808 in genetic evolution, belonging to the same branch (Li et al., 2017; **Figures 1A, B**).

4 Discussion

Getah virus (GETV) was first discovered in Hainan Province, China in 1964 (Li et al., 2019; Lu et al., 2019). In recent years, the widespread distribution of GETV has been found in mosquitoes and animals in 21 provinces and cities including Yunnan, Sichuan, Guizhou, Gansu, Jilin, Hebei, and Shanxi. Prior to 2006, only six provinces in China were known to be affected by GETV (Zhai et al., 2008), but by 2018, the number of provinces affected had dramatically increased to 15 (Lu et al., 2019; Xia et al., 2021). Yunnan Province, bordering Laos, Myanmar, and Vietnam, has frequent trade and a climate conducive to mosquito breeding, facilitating the transmission of GETV. Reports indicate that there are high titers of GETV neutralizing antibodies in many livestock in Yunnan Province, and the positive antibody rate in pigs is high (Li et al., 2019), indicating that cattle, as livestock, face the risk of infection from pig-derived GETV. This study detected the highest positive rate of GETV antibodies in bovine serum in Jianshui County, Honghe Prefecture, Yunnan Province in 2022 at 24.74% using indirect ELISA methods. In 2023, the positive rate in Jianshui decreased by 16.14%, which related to the implementation of local pest and mosquito control measures and the seasonal prevalence of

TABLE 1 The positive rate of GETV in bovine serum in 2022-2023.

Species	Region	Year			
		2022		2023	
		Positive rate	95% CI	Positive rate	95% CI
Cattle	JS	24.74 (23/93)	17.08−34.38	8.6 (8/93)	4.42−16.07
	ML	12.17 (9/74)	6.53−21.53	36.56 (34/93)	27.49−46.7
	LX	23.86 (21/88)	16.17−33.74	13.98 (13/93)	8.35−22.46
	Total	20.78 (53/255)	16.26−26.18	19.71 (55/279)	15.47−24.78

*JS, Jianshui County; ML, Mile City; LX, Luxi County.

TABLE 2 Nucleotide sequences and identity analysis of YN2305 and the other GETV strains.

Virus isolates	YH2305 (%)	
	E2 genome	Complete genome
	nt	nt
AY702913.1	97.6	98.1
GETV-GDFS2	97.4	97.6
GETV-GDFS9	97.4	97.6
GETV-JX-CHN-22	96.9	97.5
GETV-JX-CHN-22-P7	97.2	97.5
GETV-V1	97.3	97.8
GETV-XJ	97.4	97.7
GZ201808	97.2	97.6
HB0234	96.8	97.9
HNJZ-S1	97.2	97.8
HNJZ-S2	97.4	97.8
HNNY-1	97.3	97.8
HNNY-2	97.2	97.8
HNPDS-1	97.3	97.8
HNPDS-2	97.3	97.8
HuN1	99.7	99.5
JL1707	97.2	97.8
JL1708	96.8	97.8
JL1808	100	100
Kochi-01	99.2	99.5
LEIV 16275 Mag	97.2	97.5
LEIV 17741 MPR	98.2	98.6
M1	97.4	98
MI-110-C1	98	98.5
MI-110-C2	98.1	98.5
NC_006558.1	97.6	98.1
NMDK1813-1	97.2	97.6
Sagiyama virus	96.4	97.2
SC266	97.2	97.5
SC1210	97.1	97.8
SC201807	97.5	97.7
SD17-09	99.8	99.8
YN0540	97.3	97.9
YN12031	95.8	96.3
YN12042	97.2	97.8
12IH26	97.4	97.8
14-I-605-C1	97.3	97.7
14-I-605-C2	97.3	97.7
15-I-752	97.3	97.7
15-I-1105	97.3	97.7
16-I-599	97.3	97.7
16-I-674	97.3	97.7
16-I-676	97.3	97.7
AH9192	97.1	97.6
Sagiyama virus original	96.6	—
dog202206	96.5	—
GDJM2022	97.2	—
GDQY2022	97.3	—
GETV-SCrph129	97.3	—
GETV-SW	95.1	—
GETV-YL	97.2	—
GS11-155	97.2	—
GX201808	99	—
HNDZ1712-1	97.2	—
MM 2021	94.2	—
SC202010	96.9	—
SC483	97.3	—
SCZY202010	97.3	—

vector-borne viruses. While the positive rate in Mile County increased by 24.39% compared to the previous year. Based on these serological survey results, we speculate that there is a trend for GETV virus to spread from border areas to inland areas. The YN2305 strain was successfully isolated from cattle in Yunnan Province (Genbank Number: OR371719), and this isolate has the highest nucleotide identity and the closest genetic evolutionary relationship with the previously isolated bovine-derived JL1808 strain in Jilin Province. It also has high identity and close phylogenetic relationships with the fox-derived SD17-09 strain and the pig-derived HuN1 strain, which causes fever, anorexia, and neurological symptoms in host animals, but there are multiple mutations in the E2 gene and NS gene of GETV, which may be related to host differences (Shi et al., 2022b). In addition, phylogenetic analysis shows that YN2305, along with Kochi-01, MI-110-C1, and MI-110-C2 strains that causes significant clinical symptoms in Chinese pig and horse populations, belongs to gene group III and the same evolutionary branch (Nemoto et al., 2015). These results indicate that GETV is widely present in various animal hosts with differences in nucleotide sequences. As cattle are in close contact with humans and other animals, the bovine-derived isolate YN2305 may pose a threat to other livestock, wildlife, and even humans. To reduce the impact of GETV virus on humans and animals, it is necessary to further expand the scope of monitoring and carry out long-term serological surveys.

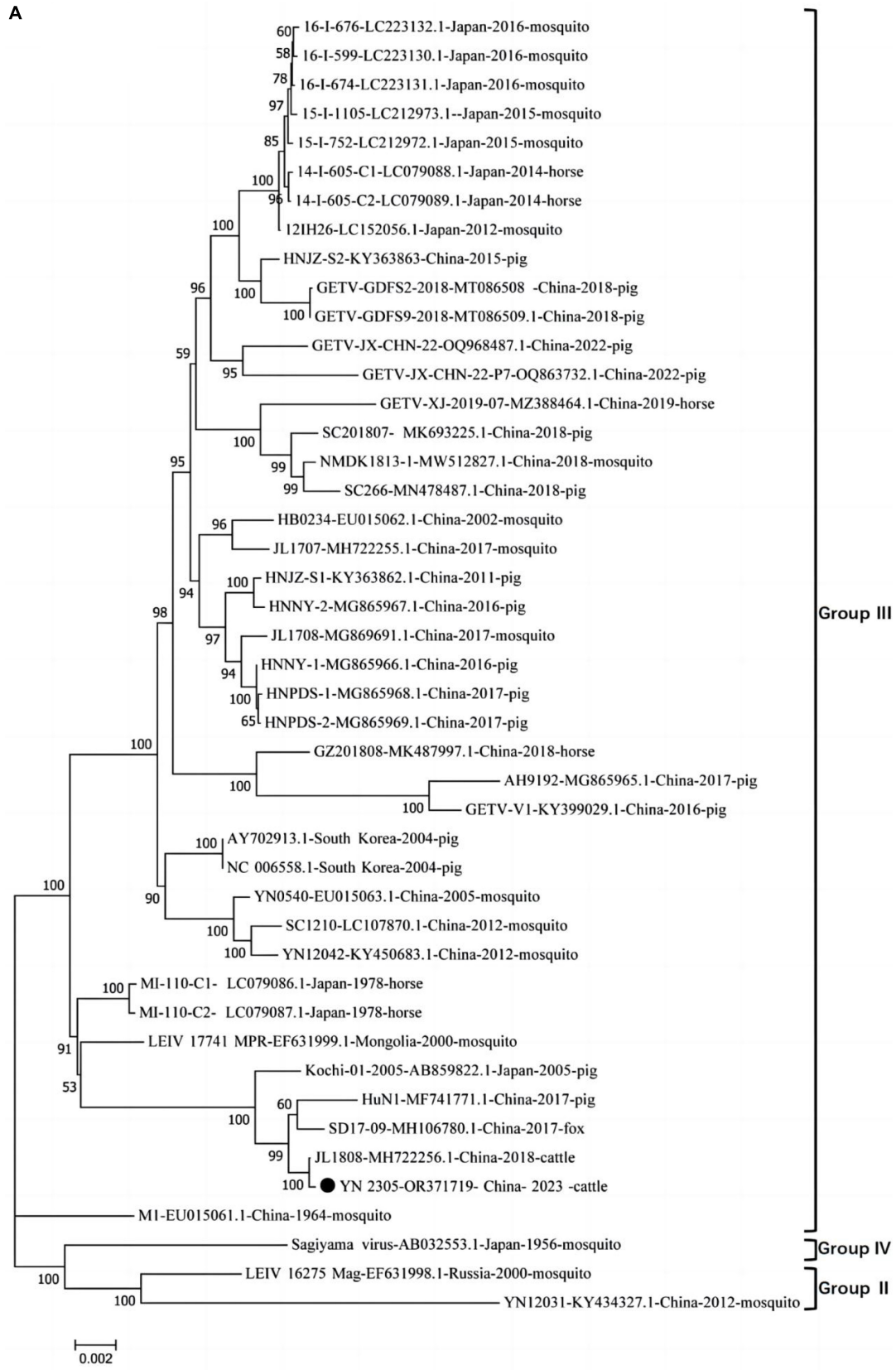

FIGURE 1
(Continued)

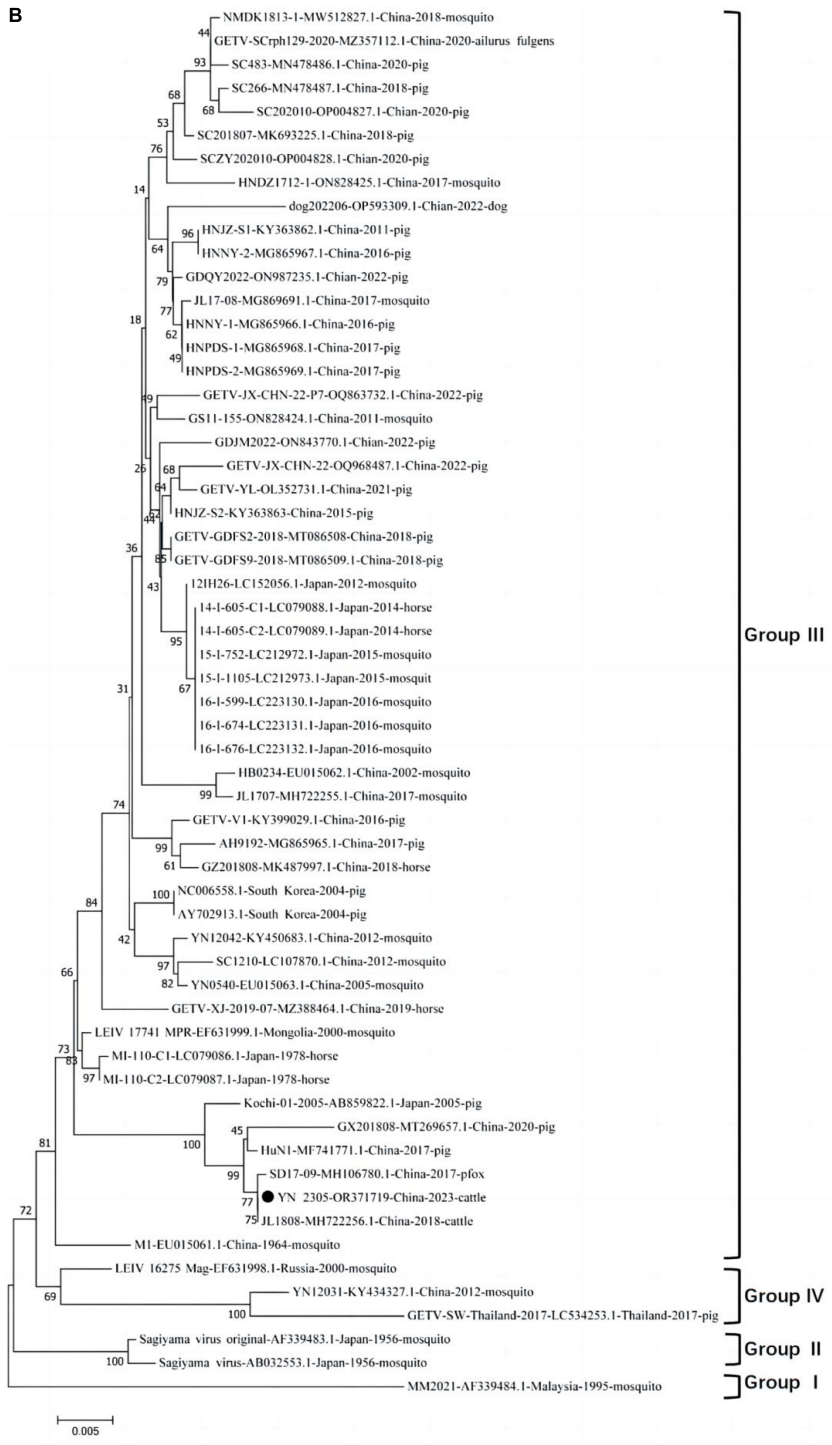

FIGURE 1
(A) Diagrammatic representation of a tree based on the complete genome sequence of GETV YN2305 and the available complete GETV genomes from the GenBank. **(B)** Diagrammatic representation of a tree based on the complete E2 gene nucleotide sequences of GETVs.

5 Conclusion

In conclusion, this study indicates that GETV is present and prevalent in cattle in the China-Vietnam border region, with the highest positive rate of bovine serum antibodies in Jianshui and Mile counties, and a trend to spread inland. In addition, GETV YN2305 strain has the highest homology with bovine isolate JL1808, but there are genetic differences in the E2 and NS genes with closely related fox and pig derived isolates. The isolate may pose a threat to other livestock and humans. This study fills the gap in information on the infection rate and prevalence of GETV in livestock in the Yunnan border region, providing data support for the prevention and control of the epidemic.

Data availability statement

The original contributions presented in the study are publicly available. This data can be found here: https://www.ncbi.nlm.nih.gov/; OR371719.

Ethics statement

The animal studies were approved by the Institutional Animal Care and Use Ethics Committee (IACUC) of the Chinese Academy of Military Medical Science. The studies were conducted in accordance with the local legislation and institutional requirements. Written informed consent was obtained from the owners for the participation of their animals in this study.

Author contributions

HL: Funding acquisition, Investigation, Writing – original draft. JH: Investigation, Writing – original draft, Data curation, Formal Analysis. L-XL: Software, Validation, Writing – review & editing. Z-SL: Software, Validation, Writing – review & editing. X-TS: Resources, Writing – review & editing. H-JL: Resources, Writing – review & editing. N-YJ: Resources, Supervision, Writing – review & editing. LZ: Supervision, Writing – review & editing. L-NZ: Supervision, Writing – review & editing, Funding acquisition.

Funding

The author(s) declare financial support was received for the research, authorship, and/or publication of this article. This work was supported by the National Natural Sciences Foundation of China (32273097), Key Laboratory for prevention and control of Avian Influenza and Other Major Poultry Diseases, Ministry of Agriculture and Rural Affairs, P.R. China; Key Laboratory of Livestock Disease Prevention of Guangdong Province (YDWS202205).

Conflict of interest

The authors declare that the research was conducted in the absence of any commercial or financial relationships that could be construed as a potential conflict of interest.

Publisher's note

All claims expressed in this article are solely those of the authors and do not necessarily represent those of their affiliated organizations, or those of the publisher, the editors and the reviewers. Any product that may be evaluated in this article, or claim that may be made by its manufacturer, is not guaranteed or endorsed by the publisher.

Supplementary material

The Supplementary Material for this article can be found online at: https://www.frontiersin.org/articles/10.3389/fmicb.2023.1309650/full#supplementary-material

References

Li, Y., Fu, S., Guo, X., Li, X., Li, M., Wang, L., et al. (2019). Serological survey of getah virus in domestic animals in Yunnan Province, China. *Vector Borne Zoonot. Dis.* 19, 59–61. doi: 10.1089/vbz.2018.2273

Li, Y.-Y., Liu, H., Fu, S.-H., Li, X.-L., Guo, X.-F., Li, M.-H., et al. (2017). From discovery to spread: The evolution and phylogeny of Getah virus. *Infect. Genet. Evol.* 55, 48–55. doi: 10.1016/j.meegid.2017.08.016

Lu, G., Ou, J., Ji, J., Ren, Z., Hu, X., Wang, C., et al. (2019). Emergence of Getah virus infection in horse with fever in China, 2018. *Front. Microbiol.* 10:1416.

Nemoto, M., Bannai, H., Tsujimura, K., Kobayashi, M., Kikuchi, T., Yamanaka, T., et al. (2015). Getah virus infection among racehorses, Japan, 2014. *Emerg. Infect. Dis.* 21, 883–885. doi: 10.3201/eid2105.141975

Rattanatumhi, K., Prasertsincharoen, N., Naimon, N., Kuwata, R., Shimoda, H., Ishijima, K., et al. (2022). A serological survey and characterization of Getah virus in domestic pigs in Thailand, 2017–2018. *Transbound. Emerg. Dis.* 69, 913–918. doi: 10.1111/tbed.14042

Ren, T., Mo, Q., Wang, Y., Wang, H., Nong, Z., Wang, J., et al. (2020). Emergence and phylogenetic analysis of a Getah virus isolated in Southern China. *Front. Vet. Sci.* 7:552517. doi: 10.3389/fvets.2020.552517

Shi, N., Liu, H., Li, L., Hu, B., Zhang, L., Zhao, C., et al. (2018). Development of a TaqMan probe-based quantitative reverse transcription PCR assay for detection of Getah virus RNA. *Arch. Virol.* 163, 2877–2881. doi: 10.1007/s00705-018-3927-2

Shi, N., Qiu, X., Cao, X., Mai, Z., Zhu, X., Li, N., et al. (2022a). Molecular and serological surveillance of Getah virus in the Xinjiang Uygur Autonomous Region, China, 2017–2020. *Virol. Sin.* 37, 229–237. doi: 10.1016/j.virs.2022.02.004

Shi, N., Zhu, X., Qiu, X., Cao, X., Jiang, Z., Lu, H., et al. (2022b). Origin, genetic diversity, adaptive evolution and transmission dynamics of Getah virus. *Transbound. Emerg. Dis.* 69, e1037–e1050. doi: 10.1111/tbed.14395

Sun, Q., Xie, Y., Guan, Z., Zhang, Y., Li, Y., Yang, Y., et al. (2022). Seroprevalence of Getah virus in pigs in Eastern China determined with a recombinant E2 protein-based indirect ELISA. *Viruses* 14:2173. doi: 10.3390/v14102173

Xia, Y., Shi, Z., Wang, X., Li, Y., Wang, Z., Chang, H., et al. (2021). Development and application of SYBR Green I real-time quantitative reverse transcription PCR assay for detection of swine Getah virus. *Mol. Cell. Probes* 57:101730. doi: 10.1016/j.mcp.2021.101730

Xing, C., Jiang, J., Lu, Z., Mi, S., He, B., Tu, C., et al. (2020). Isolation and characterization of Getah virus from pigs in Guangdong province of China. *Transbound. Emerg. Dis.* doi: 10.1111/tbed.13567 [Epub ahead of print].

Yang, T., Li, R., Hu, Y., Yang, L., Zhao, D., Du, L., et al. (2018). An outbreak of Getah virus infection among pigs in China, 2017. *Transbound. Emerg. Dis.* 65, 632–637. doi: 10.1111/tbed.12867

Zhai, Y., Wang, H.-Y., Sun, X., Fu, S., Wang, H., Attoui, H., et al. (2008). Complete sequence characterization of isolates of Getah virus (genus Alphavirus, family Togaviridae) from China. *J. Gen. Virol.* 89, 1446–1456. doi: 10.1099/vir.0.83607-0

Zhao, M., Yue, C., Yang, Z., Li, Y., Zhang, D., Zhang, J., et al. (2022). Viral metagenomics unveiled extensive communications of viruses within giant pandas and their associated organisms in the same ecosystem. *Sci. Total Environ.* 820:153317. doi: 10.1016/j.scitotenv.2022.153317

frontiers | Frontiers in Microbiology

TYPE Original Research
PUBLISHED 22 December 2023
DOI 10.3389/fmicb.2023.1286519

OPEN ACCESS

EDITED BY
Ke Liu,
Chinese Academy of Agricultural Sciences, China

REVIEWED BY
Pradip Barde,
National Institute for Research in Tribal Health (ICMR), India
Stephen Higgs,
Kansas State University, United States

*CORRESPONDENCE
Malcolm J. Fraser Jr.
✉ fraser.1@nd.edu

†PRESENT ADDRESSES
Priya Mishra,
Office of Research Affairs, Rush University Medical Center, Chicago, IL, United States

Velmurugan Balaraman,
Department of Diagnostic Medicine and Pathobiology, Center of Excellence for Emerging and Zoonotic Animal Diseases, Kansas State University, Manhattan, KS, United States

‡These authors share senior authorship

RECEIVED 31 August 2023
ACCEPTED 14 November 2023
PUBLISHED 22 December 2023

CITATION
Mishra P, Balaraman V and Fraser MJ Jr (2023) Maxizyme-mediated suppression of chikungunya virus replication and transmission in transgenic *Aedes aegypti* mosquitoes. *Front. Microbiol.* 14:1286519. doi: 10.3389/fmicb.2023.1286519

Maxizyme-mediated suppression of chikungunya virus replication and transmission in transgenic *Aedes aegypti* mosquitoes

Priya Mishra†‡, Velmurugan Balaraman†‡ and Malcolm J. Fraser Jr.*

Department of Biological Sciences, Eck Institute for Global Health, University of Notre Dame, Notre Dame, IN, United States

Chikungunya virus (CHIKV) is an emerging mosquito-borne pathogen of significant public health importance. There are currently no prophylactic vaccines or therapeutics available to control CHIKV. One approach to arbovirus control that has been proposed is the replacement of transmission-competent mosquitoes with those that are refractory to virus infection. Several transgene effectors are being examined as potentially useful for this population replacement approach. We previously demonstrated the successful use of hammerhead ribozymes (hRzs) as an antiviral effector transgene to control CHIKV infection of, and transmission by, Aedes mosquitoes. In this report we examine a maxizyme approach to enhance the catalytic activity and prevent virus mutants from escaping these ribozymes. We designed a maxizyme containing minimized (monomer) versions of two hRzs we previously demonstrated to be the most effective in CHIKV suppression. Three versions of CHIKV maxizyme were designed: Active (Mz), inactive (ΔMz), and a connected CHIKV maxizyme (cMz). The maxizymes with their expression units (Ae-tRNA ^{val} promoter and its termination signal) were incorporated into lentivirus vectors with selection and visualization markers. Following transformation, selection, and single-cell sorting of Vero cells, clonal cell populations were infected with CHIKV at 0.05 and 0.5 MOI, and virus suppression was assessed using $TCID_{50}$-IFA, RT-qPCR, and caspase-3 assays. Five transgenic mosquito lines expressing cMz were generated and transgene insertion sites were confirmed by splinkerette PCR. Our results demonstrate that Vero cell clones expressing Mz exhibited complete inhibition of CHIKV replication compared to their respective inactive control version or the two parent hRzs. Upon oral challenge of transgenic mosquitoes with CHIKV, three out of the five lines were completely refractory to CHIKV infection, and all five lines tested negative for salivary transmission. Altogether, this study demonstrates that maxizymes can provide a higher catalytic activity and viral suppression than hRzs.

KEYWORDS

maxizyme (Mz), hammerhead ribozyme (hRz), chikungunya (CHIKV), connected maxizyme (cMz), mosquito transmission

Introduction

Chikungunya virus (CHIKV) is an enveloped, single-stranded, positive-sense RNA virus that belongs to the genus *Alphavirus* and family *Togaviridae*. CHIKV is transmitted to humans by *Aedes aegypti* and *Ae. albopictus* mosquitoes (Weaver and Lecuit, 2015; Higgs and Vanlandingham, 2018), causing chikungunya fever (CF), which is characterized by

symptoms such as fever, myalgia, and debilitating joint pain that may last for months (Pialoux et al., 2007; Weaver and Lecuit, 2015; Halstead, 2018), and in some cases, can result in fatality (Cardona-Ospina et al., 2015). The disease can impact the economy in several spheres, significantly affecting the health system and national economies (Costa et al., 2023). Currently there are no effective prophylactic or therapeutic measures to control CF, although a putative vaccine is making its way through clinical trials (Schmidt and Schnierle, 2022; Schneider et al., 2023).

Since arboviruses such as CHIKV require mosquitoes to complete their transmission cycle (Franz et al., 2006), alternative approaches aimed at reducing or replacing naturally competent mosquitoes with virus refractory mosquitoes expressing various transgene effectors have been pursued to control arboviruses (Gantz et al., 2015; Aliota et al., 2016; Williams et al., 2020; Reid et al., 2021).

In our lab we have been exploring the potential of several types of antiviral ribozymes including hammerhead ribozyme (hRz) and maxizyme (Mz), among others (Nawtaisong et al., 2009; Carter et al., 2015; Mishra et al., 2016). Hammerhead ribozymes are small catalytic RNA molecules that can cleave target RNA in a sequence-specific manner. In contrast, maxizymes (Mz) are dual-catalytic RNA molecules capable of simultaneously cleaving multiple target sequences in an RNA molecule.

We previously identified two hRzs, #9 and #14, targeting the sub-genomic region of CHIKV that were effective at inhibiting CHIKV 181/25 replication both *in vitro* and *in vivo* (Mishra et al., 2016). However, these single hRzs target regions of 19 nt in size, making them potentially susceptible to escape variants.

In this study, we utilized a maxizyme approach to enhance the ribozyme activity and provide broad spectrum activity against escape variants (Haasnoot et al., 2007). Maxizymes (Mz) utilize minimized versions of two hRzs by combining them into a single catalytic unit (Kuwabara et al., 1998). A maxizyme consists of two minizymes (minimized hRz) that lack stem loop II of the hammerhead structure (Figure 1). While minizymes have lower catalytic activity compared to their parental hRzs, some have cleavage activity similar to or better than their parental hRzs when they are configured into a dimeric form such as maxizymes (Iyo et al., 2002, 2004; Kuwabara et al., 2002) (Figure 1).

Previous research has demonstrated that Mzs are catalytically more active compared to hRzs (Kuwabara et al., 1998, 2002; Hamada et al., 1999). The binding of one target site enhances unwinding of RNA secondary structures in the targeted RNA and serves as an alternative approach to the recruitment of RNA helicases, thereby cleaving less accessible sites in the target RNA molecule through binding two arms rather than one (Kuwabara et al., 2002).

Our maxizyme constructs demonstrated greater effectiveness against CHIKV infection than the hRzs they were derived from when expressed in both transformed cell cultures and transgenic mosquitoes. These results suggest that maxizyme can be an effective antiviral for arboviruses like CHIKV, DENV, and Zika as mosquito transgene effectors.

Materials and methods

Cells and viruses

African monkey kidney (Vero) cells (ATCC, USA) were maintained on Dulbecco's modified eagle medium (DMEM; Sigma Aldrich, USA) supplemented with 10% fetal bovine serum (FBS, Atlanta Biological, Flowery Branch, GA, USA) and non-essential amino acids [(1x), Gibco, USA)]. The CHIKV 181/25 strain is an attenuated vaccine strain (a gift from Dr. Scott Weaver, UTMB, Galveston) that was used for testing the effectiveness of our maxizymes *in vitro* and *in vivo*. We chose this strain for safety reasons since we do not have appropriate containment facilities for handling a virulent strain. Additionally, while the 181/25 strain is attenuated for human virulence, it does not exhibit significant reduction in mosquito infection.

Design and cloning strategy for CHIKV maxizyme

We designed two versions of a CHIKV maxizyme, active Mz and inactive ΔMz, by combining the most effective anti-CHIKV hammerhead ribozymes (hRzs) #9 and #14 (Mishra et al., 2016). Each maxizyme version consists of two monomers, I and II, with the following components: $tRNA^{val}$ promoter, partial target binding sites of hRz# 9 and #14, catalytic core (active: CTG, or inactive: CTA), and a termination signal (Figure 1 and Table 1).

The active Mz was cloned into an Aedes expression lentivirus plasmid, pLAeARH (Nawtaisong et al., 2009), in two steps. The first step amplified Mz monomer I from the pLAeRz#9ARH vector along with the promoter and termination signals using PCR primers Mz-I F and Mz-I R (Table 1) and cloned the amplified sequence into *Bam HI* and *Not* I sites of pLAeARH. In the second step, the Mz-II was amplified from the Mz-II template using the primers Mz-II F and Mz-II R (Table 2), and cloned into *Pme* I and *Not* I sites of the lentivirus plasmid pLAeMzIARH downstream of Mz-I to construct pLAeMzIAeMzIIARH.

The inactive ΔMz was made by introduction of a point mutation (CTG-CTA) to disrupt the catalytic activity of the maxizyme. Cloning of this inactive ΔMz involved generation of the ΔMz monomer I from the pLAeMzIARH vector with active monomer I through PCR amplification using Mz-I F and ΔMz R primers (Table 2). The amplified sequence was inserted at the restriction sites *Bam HI* and *Not* I pLAeARH, as described above. The remaining portion of inactive ΔMz was created by amplification from the template ΔMz monomer II using primers Mz-II F and ΔMz II R MI (Table 2) and cloned into *Pme* I and *Not* I sites of the lentivirus plasmid pLAeΔMzIARH. The final vector was pLAeΔMzIAeΔMzIIARH. Finally, a CMV-ds RED fluorescent marker was cloned into both the maxizyme plasmids, as previously described (Mishra et al., 2016).

Generation of clonal cell populations

Vero cells were seeded into 6 well plates and 24 hours (hrs) later the ribozyme expression plasmids were transfected

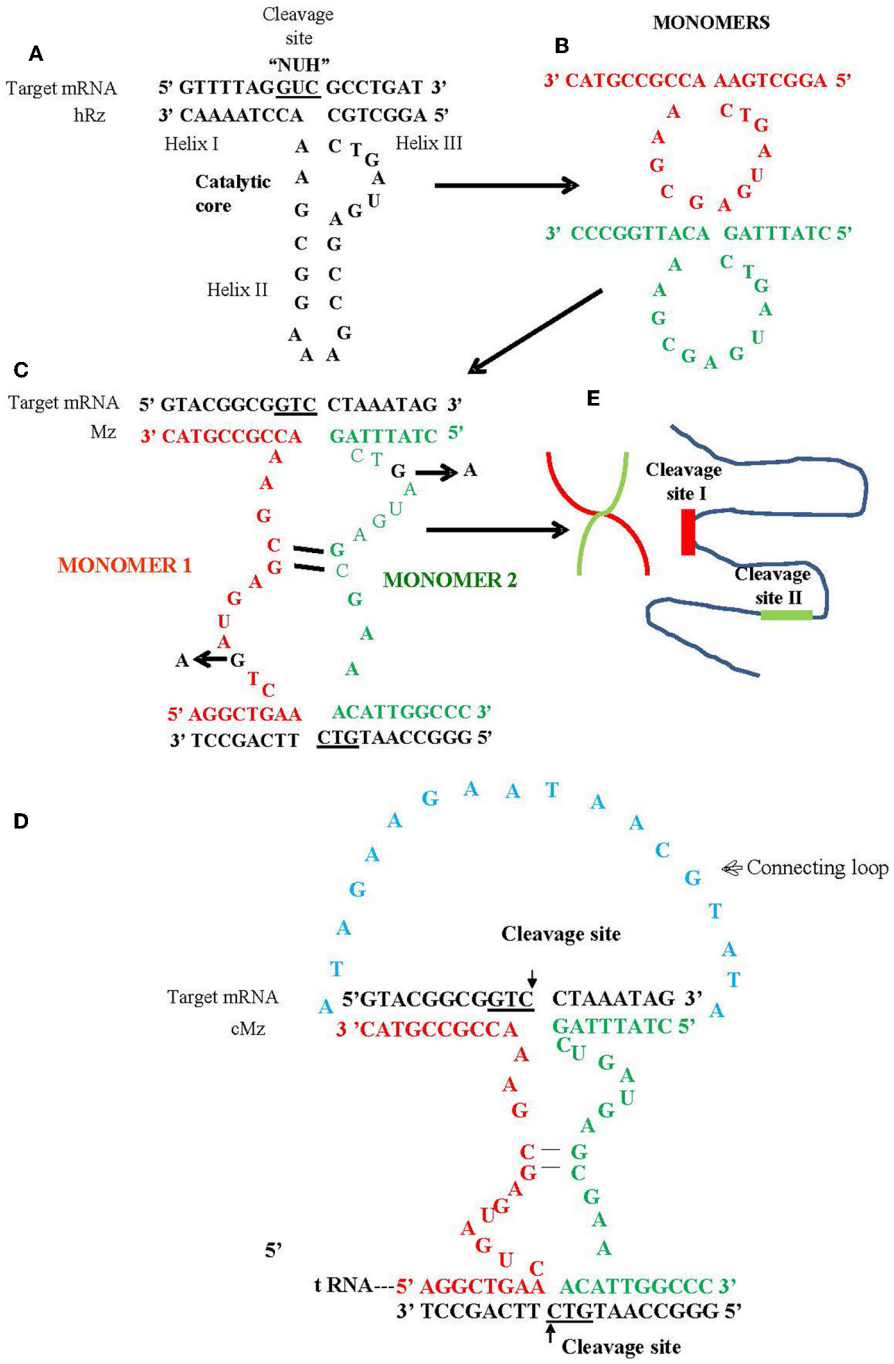

FIGURE 1
Schematic of hammerhead ribozyme (hRz) and maxizymes. **(A)** Structure of hRz. **(B)** Monomers derived from hRzs by deletion of helix II stem loop structure. **(C)** Monomers (Red or Green) undergoing bimolecular interaction leading to the formation of heterodimer/maxizyme, (guanine: G in Black) in the catalytic core for both monomers replaced by adenine (A) to generate inactive version of maxizyme **(D)** connected maxizyme with 13 nucleotide connecting chain (Blue) **(E)** Maxizyme binding to two different target sites on viral RNA.

using lipofectamine LTX and plus reagent (Invitrogen, USA), following the manufacturer's instructions. Forty-eight hrs later, the transfected cells were selected using 200 μg/ml of hygromycin B (Invitrogen, USA) and maintained for two passages before sorting into 96 well plates. Cell sorting and screening was performed as previously described (Mishra et al., 2016).

RT-PCR based detection of ribozyme expression

Total cellular RNA was TRIzol-extracted following the manufacturer's protocol (Invitrogen, USA). The concentration of extracted RNA was determined spectrophotometrically using a NanoDrop ND-1000 UV-Vis Spectrophotometer. A total of

TABLE 1 Sequence of maxizymes: each maxizyme sequence includes the Ae-tRNA ^{val} promoter (Black), monomer I (Red), monomer II (Green) and stop signal sequence (Purple).

Ribozyme	Sequence
Maxizyme (Mz)	ACCGTTGGTTTCCGTAGTGTAGTGGTTATCACGTCTGCTTCACACGCAGAAGGTCCCCGGTTCGAACCCGG GCACTACAAAAACCAACTTT AGGCTGAACTGATGACGCAAACCGCCGTACTTTTTTTACCGTTGGTTTCCG TAGTGTAGTGGTTATCACGTCTGCTTCACACGCAGAAGGTCCCCGGTTCGAACCCGGGCACTACAAAAACC AACTTT CTATTTAGCTGATGACGCAAACATTGGCCCTTTTTTT
Maxizyme (inactive) (ΔMz)	ACCGTTGGTTTCCGTAGTGTAGTGGTTATCACGTCTGCTTCACACGCAGAAGGTCCCCGGTTCGAACCCG GGCACTACAAAAACCAACTTT AGGCTGAACTAATGACGCAAACCGCCGTACTTTTTTTACCGTTGGTT TCCGTAGTGTAGTGGTTATCACGTCTGCTTCACACGCAGAAGGTCCCCGGTTCGAACCCGGGCACTACAA AAACCAACTTT CTATTTAG CTAATGACGCAAACATTGGCCCTTTTTTT
Maxizyme (cMz)	ACCGTTGGTTTCCGTAGTGTAGTGGTTATCACGTCTGCTTCACACGCAGAAGGTCCCCGGTTCGAA CCCGGGCACTACAAAAACCAACTTTAGGCTGAACTGATGACGCAAACCGCCGTACATAGAAGAATAACGT ATACTATTTAGCTGATGACGCAAACATTGGCCCTTTTTTT

For the inactive maxizyme, the guanine in the catalytic core was replaced by adenine (A) nucleotide underlined. For the connected maxizyme both Monomer I and Monomer II are connected via a connecting loop (Blue) expressed under a single Ae-tRNA ^{val} promoter.

TABLE 2 Primers/oligos used for the construction of anti-CHIKV maxizyme and connected maxizyme, and for confirmation of maxizyme expression.

Name	Sequence (5′-3′)
Mz-I F	TTTTTTTTTGGATCCACGGATCCTCTAGACCGTTGGA
Mz-I R	AATGCATGAGCGGCCGCGTTTAAACAAAAAAAGTACGGCGGTTTCGCTCATCAGTTCAGCCTTTGTTGGTTTTTGTAGTGCCCG
Mz-II	CGCTCATCAGCTAAATAGTTGTTGGTTTTTGTAGTGCCCGGGTTCGAACCGGGGACCTTCTGCGTGTGAAGCAGACGTG
Mz-II F	ATATACGTGTTTAAACACCGTTGGTTTCCGTAGTGTAGTGGTTATCACGTCTGCTTCACACGC
Mz-II R	TGATGCTGAGCGGCCGCAAAAAAAGGGGCCAATGTTTCGCTCATCAGCTAAATAGTTG
ΔMz-I R	AATGCATGAGCGGCCGCGTTTAAACAAAAAAAGTACGGCGGTTTCGCTCATTAGTTCAGCCTTTGTTGGTTTTTGTAGTGCCCG
ΔMz-II R	TGATGCTGAGCGGCCGCAAAAAAAGGGGCCAATGTTTCGCTCATAAGCTAAATAGTTG.
ΔMz-II	CGCTCATAAGCTAAATAGTTGTTGGTTTTTGTAGTGCCCGGGTTCGAACCGGGGACCTTCTGCGTGTGAAGCAGACGTG
cMz-sense	AAACAGGCTGAACTGATGACGCAAACCGCCGTAC ATAGAAGAATAACGTATACTATTTAGCTGATGACGCAAACATTGGCC CTTTTTTTGC
cMz-antisense	GGCCGCAAAAAAAGGGCCAATGTTTGCGTCATCAGCTAAATAGTATACGTTATTCT TCTATGTACGGCGGTTTGCGTCATCAGTTCAGCCTGTTT
Common tRNA F	ACCGTTGGTTTCCGTAGTGTAGTG
hRz#9 R	ATAAGAATGCGGCCGCGTTTAACGTACGGCGGTTTCGGCCTTTCG
hRz#14 R	ATAAGAATGCGGCCGCGTTTAACGGGCCAATGTTTCGGCCTTTC
Mz-II R	GCCAATGTTTGCGTCATCAGC
ΔMz-MII (inactive)	TGATGCTGAGCGGCCGCAAAAAAAGGGGCCAATGTTTCGCTCATAAGCTAAATAGTTG
Ae-tRNA ^{val} F	TTTTTTTTTTGTCGACACCGTTGGTTTCCGTAGTGTAG
Ae-tRNA ^{val} R	TTTTTTTTTGCGGCCGCGTTTAAACTCTAGAAAAGTTGGTTTTTGTAGTGCCC
Transgene F	TTTAAATTTCCGCGGACCGTTGGTTTCCGTAGTGTAGTGG
Transgene R	TTTAAATTTAGATCTTGAGGGGATCTGCGGCCG
Poly A R	TATATCCTGAGGGGATCTGCG

5μg of RNA was treated with Turbo DNase I (Ambion, USA) and directly used for reverse transcriptase (RT) positive and negative reactions using the Superscript III one step RT-PCR kit (Invitrogen, USA). For the RT negative reaction, Taq DNA polymerase (Invitrogen) was used. A common Ae-tRNA ^{val} forward primer was used along with ribozyme-specific reverse primers (Table 2). The RT-PCR products were resolved on 2.0% agarose gels (Ethidium bromide concentration 10 mg/ml) at 105 V for 1 h. Similarly, RT-PCR was performed using twenty mosquitoes per reaction to check for the expression of maxizyme in transgenic mosquitoes.

For mosquito analysis, we collected mosquitoes and organized them into groups of 20. We manually homogenized these groups in 500 μL of Trizol (Invitrogen, USA) followed by centrifugation at 12, 000 g for 10 min at 4°C. After centrifugation, we processed the resulting supernatant for RNA extraction, following the manufacturer's instructions (Invitrogen, USA).

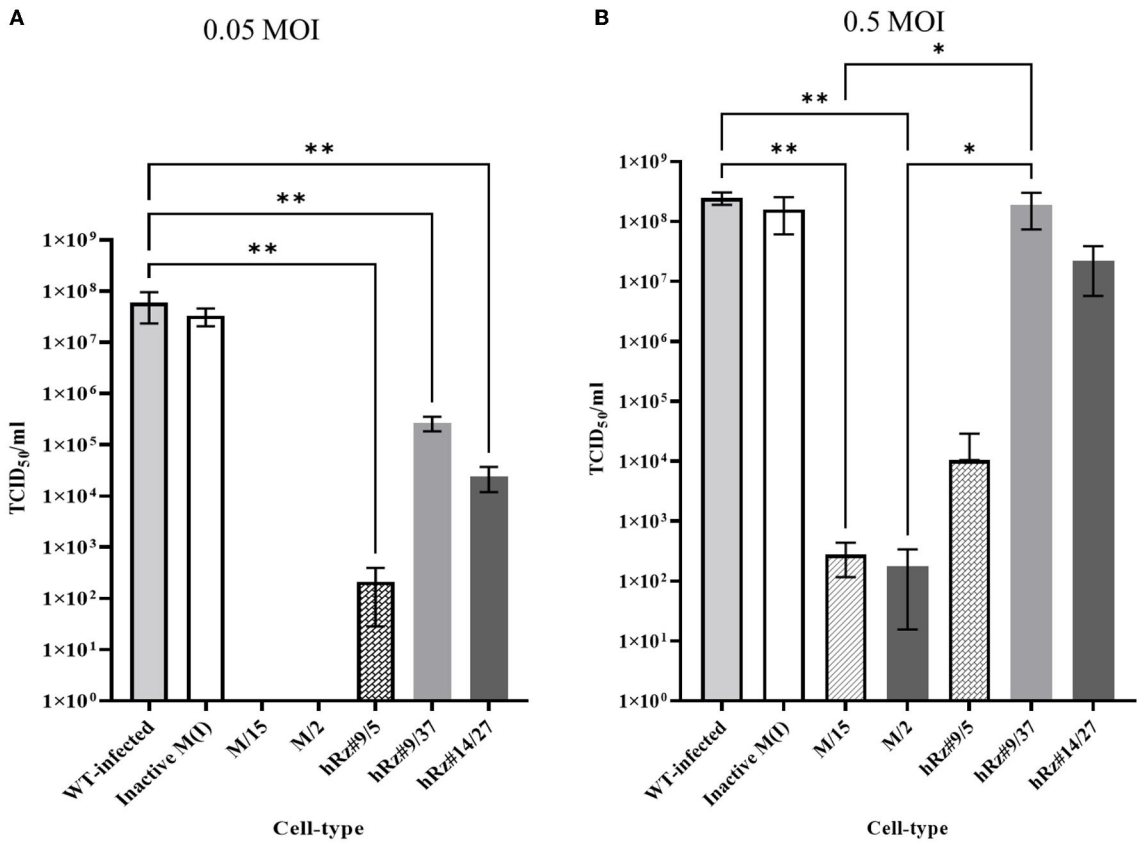

FIGURE 2
$TCID_{50}$-IFA analysis of clonal populations expressing CHIKV specific maxizymes and hammerhead ribozymes with two different MOI. **(A)** Challenge MOI of 0.05 and **(B)** Challenge MOI of 0.5, cells were fixed and stained with anti-CHIKV capsid specific antibody 3 dpi. WT: Untransformed wild type Vero cells and M (I): inactive control for maxizyme. Each clone is represented as maxizyme or hRz number / clone number. Each bar represents an average CHIKV titer from three independent experiments. Error bars represent the standard deviation among the three independent replicates for each clone. Statistical analysis was performed using the Two-way ANOVA test and Tukey's multiple comparisons test (* $p < 0.05$,** $p < 0.005$).

CHIKV infection of vero cells

Wild-type Vero cells and selected clonal Vero cells expressing effector molecules specific to CHIKV were plated at a density of 1 $\times$ 10^5 cells per well. After overnight incubation at 37 °C, the cells were washed once with serum-free DMEM and were challenged with CHIKV 181/25 at an MOI of 0.05 or 0.5 for 2 h. The infected cells were fed with fresh DMEM supplemented with 10% FBS. Two days post infection (dpi) supernatants were collected for $TCID_{50}$, RT-qPCR, and caspase 3 assays.

$TCID_{50}$-IFA analysis

CHIKV cell supernatants were collected at 2 dpi for assay. Briefly, 10-fold serial dilutions of virus supernatant were prepared in DMEM plus 10% FBS, and 100 µl of each dilution was aliquoted into 10 wells of a 96 well plate pre-seeded with 1 $\times$ 10^5 cells per well. After 3 dpi, the plates were fixed and stained with a primary antibody (1:100) specific to CHIKV capsid protein (Virostat, USA). Infected positive cells were recognized using a biotinylated secondary antibody (GE healthcare) and streptavidin detection system (Invitrogen). An inverted fluorescent microscope (Nikon, Japan) was used for observation of cytoplasmic fluorescence. Wells scored positive for the presence of green cytoplasmic fluorescence. The numbers of positive wells were counted and the virus titers calculated according to Karber's method (Kärber, 1931). The titer was expressed as $\log_{10}TCID_{50}$/ml.

Caspase 3 assay

The caspase assay was performed using the Caspase-glo 3/7 kit (Promega, USA) according to the manufacturer protocol. Vero cells were plated in 96 well plates 24 h before infection. The cells were then infected with the clones exhibiting complete suppression at an MOI of 0.05. At 2dpi, the cells were incubated with Caspase-glo reagent for 1 h in the dark at room temperature. The caspase activity was measured by detecting the luminescence using LMAX-2 luminometer (Molecular Devices).

Quantitative real time PCR

Viral RNA was isolated from 2 dpi supernatants collected from clones exhibiting complete suppression at an MOI of 0.05

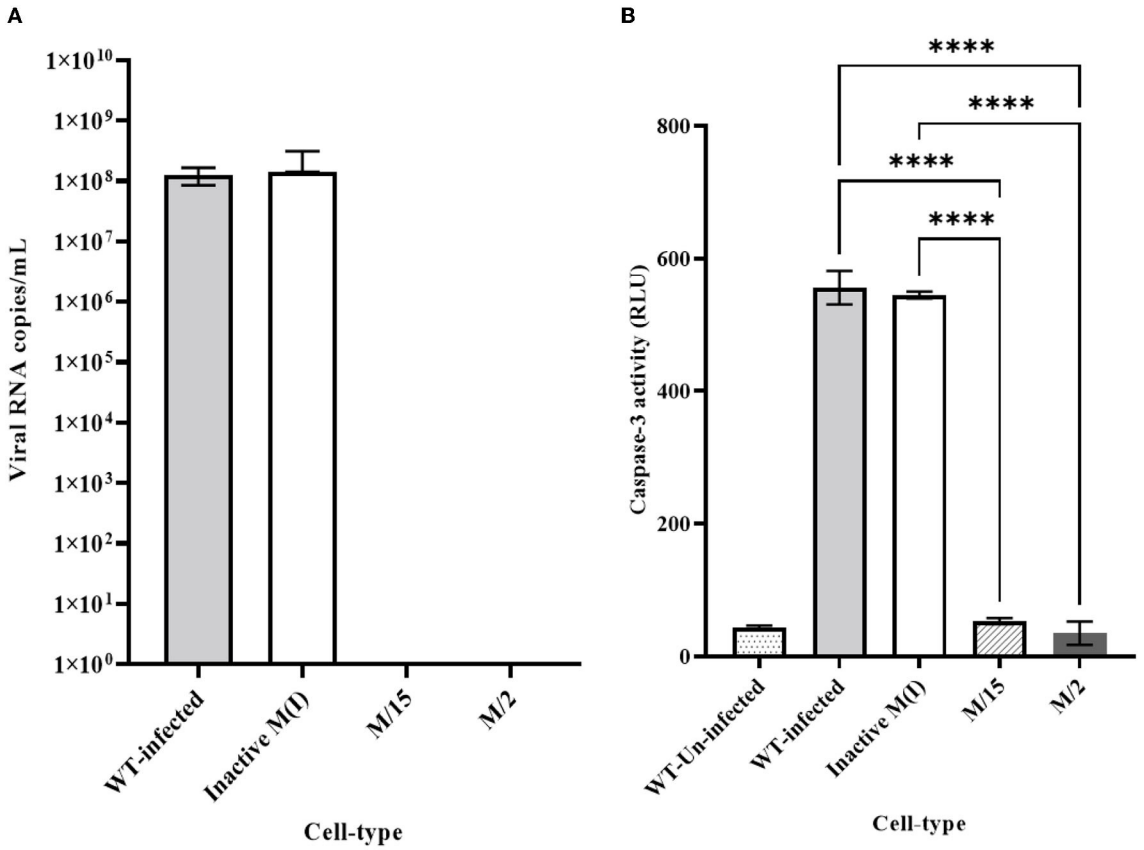

FIGURE 3
Quantitative RT-qPCR and caspase 3 analysis for clonal expressing antiviral ribozymes specific to CHIKV. **(A)** RT-qPCR performed on viral RNA isolated from the infected cell culture supernatants collected 2 dpi challenged at an MOI of 0.05. nsP2 specific primer were employed for quantification. **(B)** Caspase 3 analysis performed by infecting healthy control and transformed clonal cells using supernatant collected from 2dpi challenge experiment at an MOI of 0.05. WT designates untransformed Vero cells, either infected with virus as the infected control, or incubated with media as the Unifected control. M-maxizyme, M(I)- maxizyme Inactive, each clone is represented as maxizyme/clone number. Each bar is an average of three independent infection experiments. Bars denote the standard deviation among the three independent replicates done for each clone. Statistical analysis was performed using the Two-way ANOVA test and Tukey's multiple comparisons test (**** $p < 0.0001$).

for CHIKV, using the viral RNA mini kit (Qiagen, Germany). All isolated nucleic acids were quantitated using a Nanodrop ND-1000 spectrophotometer (Thermofisher). Stock virus with known titer was used as a control to generate the standard curve. Complementary DNA synthesis was carried out using the Gene Amp RNA PCR MULV reverse transcriptase kit (Applied Biosystem) both for samples and standards. For CHIKV, the primer targeting the nsP2 region of the virus, nsP2 reverse: aaattcggcctgaaccttct, was utilized (Ho et al., 2010). One cycle of 30 minutes at 42°C and 5 min at 99°C was performed (Mishra et al., 2016). The absolute quantification was performed on the 7500 fast real-time PCR system (Applied Biosystem) using Power sybr green master mix (Applied Biosystem) at a particular thermocyclic condition of one cycle for 2 min at 50°C, one cycle for 10 min at 95°C, 40 cycles for 15 s at 95°C, and 1 min at 60°C. For quantification of CHIKV, the above mentioned primer nsP2 reverse along with nsP2 forward: ttctgggggtcagagaaaga was used (Ho et al., 2010). Beta-actin was used as an internal control for all RT-qPCR assays. The slope of the standard curve was −2.8 and the R^2 value was 0.97. The absolute quantification of viral RNA copies/ml in the samples was performed by comparing them to the corresponding standards with known viral titer.

Construction of connected maxizyme-expressing transgenes in the *piggyBac* vector and mosquito injections

For the generation of transgenic mosquitoes expressing maxizymes, we adopted the connected maxizyme approach. In this approach, both monomers of the CHIKV-Mz were connected using a 13-nucleotide long linker sequence (atagaagaataacgtata) and expressed using a single Ae-tRNA^{val} promoter (Figure 1). This was done to increase the efficiency of formation of a bi-molecular heterodimeric maxizyme structure (Hamada et al., 1999; Kuwabara et al., 2002) and reduce the chance of inactive homodimer formation. The cloning of the transgene into the *piggyBac* vector, pXL-BacII-3xP3-ECFP, involved PCR amplification of the Ae-tRNA ^{val} pol III promoter from the pLAeARz#9RH vector using the Ae-tRNA ^{val} F and R primers (Table 2) and inserting it into

10.3389/fmicb.2023.1286519

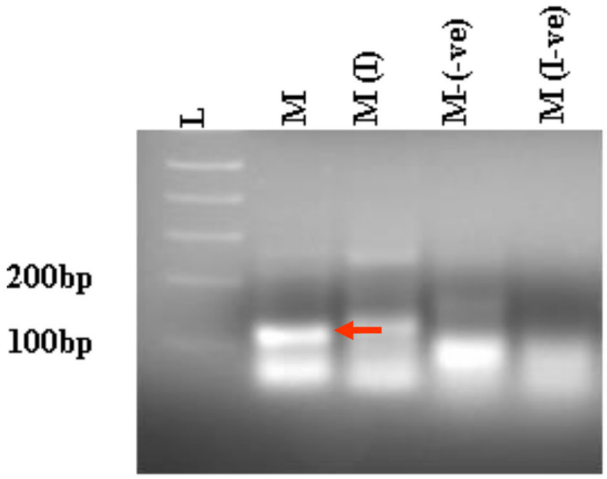

FIGURE 4
RT-PCR analysis of selected clonal cell populations expressing antiviral ribozyme constructs specific to CHIKV. The presence of the desired band specific to each CHIKV maxizyme is evident, where M: active maxizyme, M (I): inactive maxizymes, M(-ve) and M(I-ve) is RT-negative reaction. The presence of the correct band (110 bp size) is indicated by the red arrow. L- 1kb plus DNA ladder.

the pLAeARH plasmid *Sal* I and *Not* I sites. The complementary oligonucleotides of connected maxizyme (cMz-sense and cMz-antisense, Table 2) were annealed together and cloned into the *Bam* HI and *Not* I sites downstream of the promoter in pLAeARH, resulting in the plasmid pLAeAcMzRH. The connected Mz and expression units were PCR amplified from the pLAeAcMzRH vector using transgene F and R (Table 2) primers and subcloned into the *Sac* II and *Bgl* II sites of the *piggyBac* vector.

Generation of transgenic mosquitoes and identification of transgene integration sites using splinkertte PCR

Transgenic mosquitoes were generated by embryo injection of *piggBac* cMz expression vectors into mosquito embryos, essentially as previously described (Mishra et al., 2016). Higgs White Eye (HWE) mosquitoes were used in this study, facilitating detection of the 3×P3-ECFP eye-specific transgene marker gene and allowing transgenic mosquitoes to be detected from UV fluorescence in the eyes. Mosquitoes were reared in an Arthropod containment level-2 (ACL-2) facility at 28°C with 60–80% relative humidity. They were maintained on 10% sucrose solution and water and artificially fed with citrated sheep's blood (Colorado Serum Company, Denver, CO, USA) and 1 mM/10 ml of phagostimulant ATP. During infections, virus-infected cell culture medium was mixed with an equal volume of feeding solution.

A total of five independent transgenic lines were established and a splinkerette protocol was adopted from Potter and Luo (2010) to assess the genomic location of each *piggyBac*-integrated transgene as previously described (Mishra et al., 2016). All five transgenic mosquito lines exhibited unique integration sites in *Ae. aegypti* genome (Table 3).

TABLE 3 Location of transgene in the mosquito genome.

Transgenic line	Chromosome number	Supercontig number
CMCM1	3q	1.13
CMCM46	No	1.648
CMCM75	No	1.891
CMCF4	No	1.187
CMCM80	No	1.1431

The transgene integration sites in chromosomes and supercontigs of Aedes mosquitoes. 3q-chromosome number 3; no-chromosome number not known.

Analysis of CHIKV infection in cMz transgenic mosquitoes

Control and transgenic lines were fed infectious blood meals with a viral titer of 3×10^9 $TCID_{50}$/mL. Both the infected controls and cMz transgenics were maintained for seven days on 10% sucrose solution prior to feeding infected bloodmeals. For each transgenic line, a total of 15 mosquitoes in small containers were allowed to feed for 2 h on 700 µL probing solution (50% FBS (164 mM) + NaCl (100 mM) + $NaHCO_3$ (0.2 mM) + ATP (50 µg) + sucrose, pH 7.0) contained between two parafilm membranes, as described by Franz et al. (2006). Successful feeding was confirmed by observation of fully engorged mosquitoes in all groups. Mosquito homogenates were processed as previously described (Mishra et al., 2016).

Statistical analysis

The statistical analysis performed in this study is described in figure legends. All the statistical tests were carried out using GraphPad Prism version 9.3.0.3.

Results

Effect of maxizyme on CHIKV replication *in vitro*

To compare the effect of our maxizyme on CHIKV replication, we successfully constructed two lentivirus expression constructs with maxizyme: Mz, and ΔMz. Then, we transformed these maxizyme expression plasmids along with plasmids expressing the parental hRz #9 and # 14 and isolated several clonal cell populations for each. All these clonal populations were challenged with CHIKV at two different MOIs, and the effect was evaluated by the presence or absence of CPE. Our screening results revealed clones #2 and #15 of Mz, clones #5 and #27 of hRz#9, and clone #37 of hRz#14 were resistant to CHIKV CPE. However, all the clones from the inactive ΔMz had marked CPE (data not shown).

We employed two different MOIs in our study to more thoroughly assess the effectiveness of maxizyme against CHIKV replication. At a lower MOI (0.05), the Mz clones #M2 and #M15 showed eight logs of CHIKV suppression as compared

10.3389/fmicb.2023.1286519

to the negative controls: i.e., untransformed wild-type and ΔMz transformed Vero cells (Figure 2A). However, the hRzs #9/5, #9/37, and #14/27clones showed six and three logs of suppression relative to the negative controls (Figure 2A). We also determined the CHIKV viral RNA copies by RT-qPCR assay in the supernatant collected of the infected maxizyme clones. The results revealed that Mz clones M/2 and M/15 completely suppressed viral RNA production, unlike the negative controls (Figure 3A). Additionally, we performed a caspase-3 assay to measure the virus-induced apoptosis. The infected virus supernatant collected from the Mz clones was tested for caspase-3 activity and the supernatants of both Mz clones exhibited caspase-3 activity similar to the levels of uninfected Vero cells (Figure 3B). However, the supernatant of the negative control, ΔMz, showed 500 times more activity than uninfected controls and Mz clones (Figure 3B), reflecting no effect on CHIKV replication.

Next, we compared the level of CHIKV suppression for the hRz and Mz clones at a higher MOI of 0.5. Our initial tests at a lower MOI of 0.05 demonstrated that the maxizyme was highly effective in suppressing CHIKV replication. However, it was important for us to understand how this maxizyme performed across a range of virus concentrations, as this reflects the diverse conditions found in the field. The results revealed the Mz clones # M5 and # M2 suppressed CHIKV replication by six logs as compared to the negative controls. However, the suppression level of hRz clones #9/5, #9/37, and #14/27 clones dropped to four, zero and half a log, respectively. The maxizyme expression in the clones was confirmed by RT-PCR (Figure 4). Overall, under *in vitro* conditions, the maxizyme was more effective in suppressing CHIKV replication than the parental hammerhead ribozymes.

Effect of maxizyme on CHIKV replication in transgenic mosquitoes

To test the effectiveness of Mz in controlling CHIKV transmission, we generated five transgenic lines of *Ae. aegypti* mosquitoes. For transgenesis, we used a connected maxizyme (cMz) approach for ease of integration into *piggyBac* vector (pXL-Bac-II-ECFP) and to increase the efficiency of formation of active heterodimeric structures. The pXL-Bac-II-ECFP-cMz expression and transposase helper plasmids were co-injected into *Ae. aegypti* embryos as previously described (Mishra et al., 2016), and the transformation efficiency ranged from 0.5 to 20% (Table 4). A percentage fluorescence of 57–96% was obtained from all the transgenic lines at G5 (data not shown). Generation 5 positive mosquitoes were then backcrossed to wild-type HWE mosquitoes as previously described (Mishra et al., 2016) to generate a heterozygous G6 transgenic mosquito population. cMz expression in these transgenic lines was confirmed by RT-PCR (Figure 5). Each of the integration sites of these five lines were identified in the mosquito genome at different super contigs (Table 3).

Challenge of transgenic mosquitoes with CHIKV

Heterozygous G6 transgenic lines were challenged with CHIKV by oral exposure to infectious CHIKV blood meal, as previously described (Mishra et al., 2016). Mosquitoes were collected at 7

TABLE 4 **Percentage transformation frequency for cMz containing transgenic lines.**

Transgenic lines	Total screened	Positives	% transformation
CMCM1	340	11	3.2
CMCF4	299	4	1.3
CMCM80	252	7	2.7
CMCM46	108	21	20
CMCM75	612	3	0.5

Screening for transgenic mosquitoes was performed based upon eye specific cyan fluorescent protein.

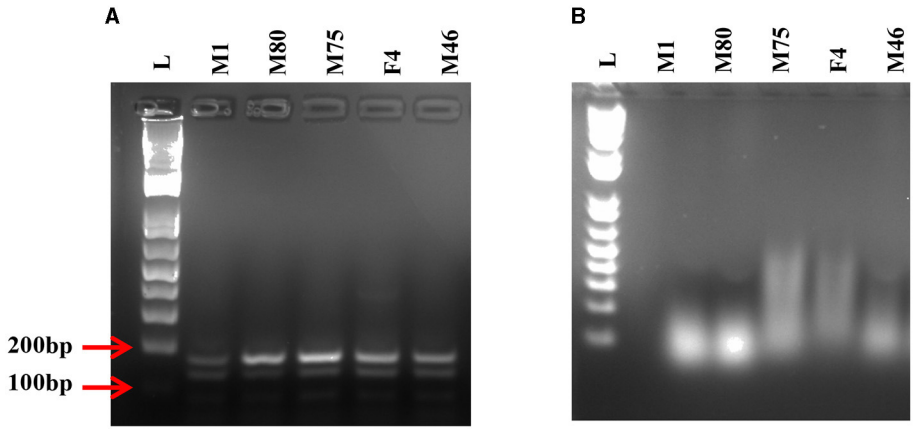

FIGURE 5
RT-PCR on transgenic mosquitoes. **(A)** Agarose gel displays the presence of desired 170 bp band confirming the expression of the connected maxizyme in each transgenic mosquito line. **(B)** RT negative reaction run using Taq polymerase shows the absence of the desired band. L- 1kb plus DNA ladder and M1, M80, M75, F4 and M46 are transgenic lines.

10.3389/fmicb.2023.1286519

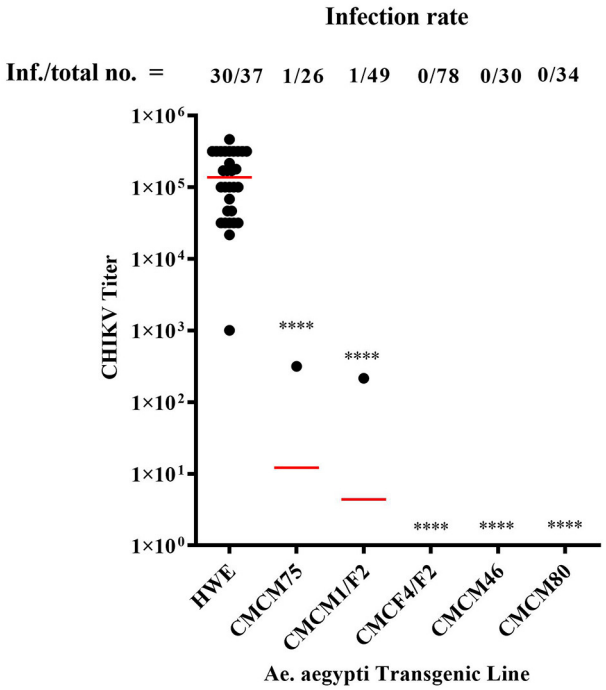

FIGURE 6
$TCID_{50}$- IFA performed on CHIKV challenged transgenic G6 heterozygous mosquito population. $TCID_{50}$-IFA was performed on homogenates of single transgenic mosquito fed an infectious blood meal compared to control HWE mosquitoes. Analysis was performed seven days post infectious blood meal. "Inf." indicates the number of infected mosquitoes analyzed and "total no." indicates the total number of mosquitoes analyzed. HWE-Higgs White Eye mosquitoes, CMCM75, CMCM1/F2, CMCF4/F2, CMCM46 and CMCM80 are connected maxizyme expressing transgenic mosquitoes. Statistical analysis was performed using the Two-way ANOVA test and Tukey's multiple comparisons test. All the transgenic lines had a statistical significance of $^{****}p < 0.0001$ as compared to the HWE line.

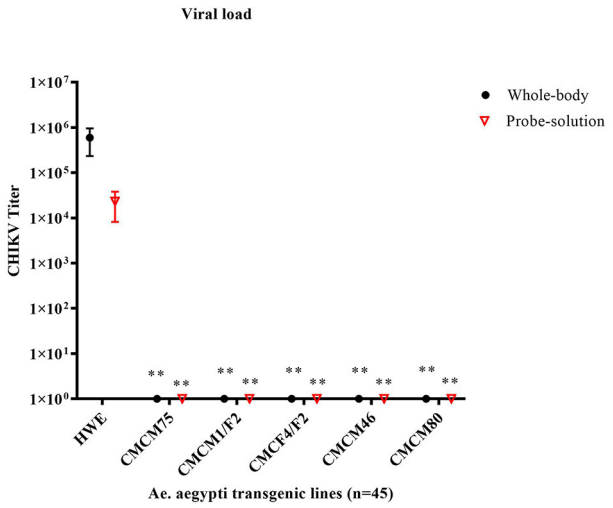

FIGURE 7
$TCID_{50}$- IFA performed on the probe solution (saliva) and whole-body of CHIKV challenged transgenic G6 heterozygous mosquito population. Briefly, pooled probe solutions and whole-body homogenates were collected from the infected transgenic and infected wild-type mosquitoes at 7dpbm. The virus titer of these samples was determined by $TCID_{50}$-IFA. Statistical analysis was performed using the Two-way ANOVA test and Tukey's multiple comparisons test. All the transgenic lines (whole body and probe solution) had a statistical significance of $^{**}p < 0.005$ as compared to the HWE line.

days post-blood meal (7 dpbm) and individual homogenates were made of each mosquito in 200 µl of DMEM. Homogenates were filtered through a 0.2 µM membrane filter for further analysis. Mosquitoes from three of the lines, CMCM80, CMCM46, and CMCF4/F2, exhibited complete suppression and had a 0% infection rate. However, non-transgenic (wild-type) HWE mosquitoes had an infection rate of 81 % with an average infectious virus titre of 2×10^5 $TCID_{50}$/ml (Figure 6). In contrast, the transgenic mosquito lines CMCM75 and CMCM1/F2 had an infection rate of 3.8 and 2 %, and infectious virus titer of 3.2×10^2 and 2.2×10^2 $TCID_{50}$/ml, respectively (Figure 6).

Next, we tested the transmission potential of these transgenic mosquitoes. As expected, the wild-type HWE mosquitoes effectively transmitted CHIKV to probe solution with an average titer of 2.3×10^4 $TCID_{50}$/ml, along with an average whole-body titer of 5.9×10^5 $TCID_{50}$/ml (Figure 7). However, no infectious virus was detected from either the probe solution or the whole-body homogenates of the five transgenic mosquito lines (Figure 7). Overall, these results indicate that the transgenic mosquito line expressing cMz completely inhibited CHIKV infection and transmission and did so from a heterozygous genetic background.

Discussion

Anti-pathogen effectors have been investigated for several arboviruses such as CHIKV (Mishra et al., 2016), DENV-2 (Franz et al., 2006), DENV3 and CHIKV (Yen et al., 2018), and Zika (Buchman et al., 2019). The presumptive outcome of such investigations is the development of transgenic mosquitoes that could eventually be used for replacement of naturally arboviruses competent mosquitoes (Marshall et al., 2019). Thus, far, researchers have come close to releasing some of these transgenic approaches, but the caveat remaining is the difficulty of introgression into wild-type mosquitoes due to possible position effects on efficient expression, the presence of multiple strains of virus circulating in the target areas, and the size of the transgene. *Wolbachia* infection of mosquitoes has been successful at controlling arboviruses in various countries, however the stability and the effect of such use is not yet clear (Yen and Failloux, 2020). To overcome these limitations, we have developed a strategy of using maxizymes, which has the potential advantages of small size transgene, higher potency, effectiveness against escape variants, and possible adaptability to target multiple arboviruses simultaneously.

We first demonstrated the effectiveness of our maxizyme in inhibiting CHIKV replication by measuring virus production, viral RNA, and virus-induced apoptosis in Vero cells. To mimic the variability of virus doses in nature we tested the effectiveness of Mz under lower (0.05 MOI) and higher doses (0.5 MOI). The Mz was effective at inhibiting CHIKV replication at both doses of virus as compared to the parental hRzs. The observation two 2 logs of virus production at higher MOIs in Mz clones could be due to higher

doses of the virus skewing the target-enzyme ratio, or it could be due to weaker expression of both the monomers (Figure 2). Nevertheless, the CHIKV suppression was more significant than the controls and parental hRzs (Mishra et al., 2016). Overall, Mz showed a higher potency and effectiveness in controlling CHIKV replication as compared to the parental counterparts *in vitro*.

We utilized a connected maxizyme in the transgenic mosquitoes owing to the advantages discussed in the results section. All five transgenic lines were highly refractory to CHIKV infection and prevented virus transmission, and this was true in a heterozygous state. This latter observation is important because if we envision release of these transgenes in a population control strategy, heterozygotes will predominate in the first and subsequent generations. Additionally, this approach is not susceptible to gene position effects, as demonstrated by cMz expression and CHIKV inhibition irrespective of the integration loci (Table 4).

Although these results are promising, our study has the following limitations. First, we have not tested the effectiveness of Mz against a virulent strain of CHIKV due to the unavailability of BSL-3 facility. While the 181/25 CHIKV strain is attenuated for human infection, and lacks the A226V mutation attributed to recent epidemic outbreaks of CHIKV, the maxizyme targets we chose are present in both the attenuated and virulent strains. Additionally, based upon our results in this and prior studies, infection of cell cultures and mosquitoes is not appreciably affected by the dual mutations in the E2 protein responsible for the attenuation in humans (Gorchakov et al., 2012). Second, the stability of the transgene and its effectiveness over generations in our transgenic mosquitoes was not addressed. This will take additional time and analyses, and we will pursue this in our future studies.

These results confirm that maxizymes can be potent inhibitors of CHIKV replication in mammalian cells or transmission in transgenic mosquitoes. Additionally, we could use this approach to design Mz against multiple arboviruses and possibly develop a universal transgenic mosquito resistant to several arboviruses (Carter et al., 2015).

Data availability statement

The original contributions presented in the study are included in the article/supplementary material, further inquiries can be directed to the corresponding author.

Ethics statement

Ethical approval was not required for the studies on animals in accordance with the local legislation and institutional requirements because only commercially available established cell lines were used.

Author contributions

PM: Conceptualization, Investigations, Validation, Resources, Data curation, Formal analysis, Methodology, Writing—original draft, Writing—review & editing. VB: Resources, Writing—original draft, Writing—review & editing. MF: Conceptualization, Funding acquisition, Resources, Supervision, Writing—review & editing.

Funding

The author(s) declare financial support was received for the research, authorship, and/or publication of this article. This research was supported by NIH/NIAID grant 1R01AI097554 to Principal Investigator MF.

Acknowledgments

The authors would like to thank Scott Weaver (University of Texas Medical Branch, Galveston, TX, USA), for providing the attenuated strain of CHIKV 181/25. We also acknowledge the invaluable instruction and assistance of Tresa Fraser in maintenance of cell cultures and in mosquito blood feeding and maintenance, Cheryl Kucharski in facilitating cell sorting and Pruksa Nawtaisong for providing the pLAeARH vector.

Conflict of interest

The authors declare that the research was conducted in the absence of any commercial or financial relationships that could be construed as a potential conflict of interest.

Publisher's note

References

Aliota, M. T., Walker, E. C., Uribe Yepes, A., Dario Velez, I., Christensen, B. M., Osorio, J. E., et al. (2016). The wMel strain of Wolbachia reduces transmission of chikungunya virus in *Aedes aegypti*. *PLoS Negl. Trop. Dis.* 10, e0004677. doi: 10.1371/journal.pntd.0004677

Buchman, A., Gamez, S., Li, M., Antoshechkin, I., Li, H-. H., Wang, H-. W., et al. (2019). Engineered resistance to Zika virus in transgenic *Aedes aegypti* expressing a polycistronic cluster of synthetic small RNAs. *Proc. Nat. Acad. Sci.* 116, 3656–61. doi: 10.1073/pnas.1810771116

Cardona-Ospina, J. A., Henao-San Martin, V., Paniz-Mondolfi, A. E., and Rodríguez-Morales, A. J. (2015). Mortality and fatality due to Chikungunya virus infection in Colombia. *J. Clin. Virol.* 70, 14–5. doi: 10.1016/j.jcv.2015.07.001

Carter, J. R., Taylor, S., Fraser, T. S., Kucharski, C. A., Dawson, J. L., Fraser, M. J., et al. (2015). Suppression of the arboviruses dengue and chikungunya using a dual-acting group-i intron coupled with conditional expression of the Bax C-terminal domain. *PLoS ONE* 10, e0139899. doi: 10.1371/journal.pone.0139899

Costa, L. B., Barreto, F. K. A., Barreto, M. C. A., Santos, T. H. P., Andrade, M. M. O., Farias, L. A. B. G., et al. (2023). Epidemiology and economic burden of chikungunya: a systematic literature review. *Trop. Med. Inf. Dis.* 8, 301. doi: 10.3390/tropicalmed8060301

Franz, A. W. E., Sanchez-Vargas, I., Adelman, Z. N., Blair, C. D., Beaty, B. J., James, A. A., et al. (2006). Engineering RNA interference-based resistance to dengue virus type 2 in genetically modified *Aedes aegypti*. *Proc. Nat. Acad. Sci.* 103, 4198–203. doi: 10.1073/pnas.0600479103

Gantz, V. M., Jasinskiene, N., Tatarenkova, O., Fazekas, A., Macias, V. M., Bier, E., et al. (2015). Highly efficient Cas9-mediated gene drive for population modification of the malaria vector mosquito *Anopheles stephensi*. *Proc. Nat. Acad. Sci.* 49, 112. doi: 10.1073/pnas.1521077112

Gorchakov, R., Wang, E., Leal, G., Forrester, N. L., Plante, K., Rossi, S. L., et al. (2012). Attenuation of chikungunya virus vaccine strain 181/clone 25 is determined by two amino acid substitutions in the E2 envelope glycoprotein. *J Virol.* 86, 6084–96. doi: 10.1128/JVI.06449-11

Haasnoot, J., Westerhout, E. M., and Berkhout, B. R. N. A. (2007). interference against viruses: strike and counterstrike. *Nat. Biotechnol.* 25, 1435–43. doi: 10.1038/nbt1369

Halstead, S. B. (2018). *Chikungunya and Zika Disease*. Amsterdam: Elsevier, 69–85.

Hamada, M., Kuwabara, T., Warashina, M., Nakayama, A., and Taira, K. (1999). Specificity of novel allosterically trans - and cis - activated connected maxizymes that are designed to suppress BCR-ABL expression. *FEBS Lett.* 461, 77–85. doi: 10.1016/S0014-5793(99)01367-8

Higgs, S., and Vanlandingham, D. L. (2018). *Chikungunya Virus and Zika Virus Transmission Cycles*. Amsterdam: Elsevier, 15–68.

Ho, P. S., Ng, M. M. L., and Chu, J. J. H. (2010). Establishment of one-step SYBR green-based real time-PCR assay for rapid detection and quantification of chikungunya virus infection. *Virol J.* 7, 13. doi: 10.1186/1743-422X-7-13

Iyo, M., Kawasaki, H., Miyagishi, M., and Taira, K. (2004). Allosterically Controlled Ribozymes as Artificial Ribonucleases. *Artif. Nucl.* 12, 89–109. doi: 10.1007/978-3-642-18510-6_7

Iyo, M., Kawasaki, H., and Taira, K. (2002). Allosterically controllable maxizymes for molecular gene therapy. *Curr. Opin. Mol. Ther.* 4, 154–65. doi: 10.1016/B978-012476249-7/50013-8

Kärber, G. (1931). Beitrag zur kollektiven Behandlung pharmakologischer Reihenversuche. *Naunyn-Schmiedebergs Archiv. Für Exp. Pathol. Und Pharmakol.* 162, 480–3. doi: 10.1007/BF01863914

Kuwabara, T., Warashina, M., Orita, M., Koseki, S., Ohkawa, J., Taira, K., et al. (1998). Formation of a catalytically active dimer by tRNAVal -driven short ribozymes. *Nat. Biotechnol.* 16, 961–5. doi: 10.1038/nbt1098-961

Kuwabara, T., Warashina, M., and Taira, K. (2002). Cleavage of an inaccessible site by the maxizyme with two independent binding arms: an alternative approach to the recruitment of RNA helicases. *J. Biochem.* 132, 149–55. doi: 10.1093/oxfordjournals.jbchem.a003193

Marshall, J. M., Raban, R. R., Kandul, N. P., Edula, J. R., León, T. M., Akbari, O. S., et al. Winning the tug-of-war between effector gene design and pathogen evolution in vector population replacement strategies. *Front. Genet.* (2019) 10:1072. doi: 10.3389/fgene.2019.01072

Mishra, P., Furey, C., Balaraman, V., and Fraser, M. (2016). Antiviral hammerhead ribozymes are effective for developing transgenic suppression of chikungunya virus in *Aedes aegypti* mosquitoes. *Viruses* 8, 163. doi: 10.3390/v8060163

Nawtaisong, P., Keith, J., Fraser, T., Balaraman, V., Kolokoltsov, A., Davey, R. A., et al. (2009). Effective suppression of dengue fever virus in mosquito cell cultures using retroviral transduction of hammerhead ribozymes targeting the viral genome. *Virol J.* 6, 73. doi: 10.1186/1743-422X-6-73

Pialoux, G., Gaüzère, B-. A., Jauréguiberry, S., and Strobel, M. (2007). Chikungunya, an epidemic arbovirosis. *Lancet Infect Dis.* 7, 319–27. doi: 10.1016/S1473-3099(07)70107-X

Potter, C. J., and Luo, L. (2010). Splinkerette PCR for mapping transposable elements in drosophila. *PLoS ONE* 5, e10168. doi: 10.1371/journal.pone.0010168

Reid, W. R., Olson, K. E., and Franz, A. W. E. (2021). Current effector and gene-drive developments to engineer arbovirus-resistant *Aedes aegypti* (Diptera: Culicidae) for a sustainable population replacement strategy in the field. *J. Med. Entomol.* 58, 1987–96. doi: 10.1093/jme/tjab030

Schmidt, C., and Schnierle, B. S. (2022). Chikungunya vaccine candidates: current landscape and future prospects. *Drug Design Dev. Ther.* 16, 3663–73. doi: 10.2147/DDDT.S366112

Schneider, M., Narciso-Abraham, M., Hadl, S., McMahon, R., Toepfer, S., Fuchs, U., et al. (2023). Safety and immunogenicity of a single-shot live-attenuated chikungunya vaccine: a double-blind, multicentre, randomised, placebo-controlled, phase 3 trial. *Lancet* 401, 2138–47. doi: 10.1016/S0140-6736(23)00641-4

Weaver, S. C., and Lecuit, M. (2015). Chikungunya virus and the global spread of a mosquito-borne disease. *New Eng. J. Med.* 372, 1231–9. doi: 10.1056/NEJMra1406035

Williams, A., Franz, A., Reid, W., and Olson, K. (2020). Antiviral effectors and gene drive strategies for mosquito population suppression or replacement to mitigate arbovirus transmission by *Aedes aegypti*. *Insects* 11, 52. doi: 10.3390/insects11010052

Yen, P-. S., and Failloux, A-. B. (2020). A review: Wolbachia-based population replacement for mosquito control shares common points with genetically modified control approaches. *Pathogens* 9, 404. doi: 10.3390/pathogens9050404

Yen, P. S., James, A., Li, J-. C., Chen, C-. H., and Failloux, A-. B. (2018). Synthetic miRNAs induce dual arboviral-resistance phenotypes in the vector mosquito *Aedes aegypti*. *Commun. Biol.* 1, 11. doi: 10.1038/s42003-017-0011-5

frontiers | Frontiers in Microbiology

TYPE Original Research
PUBLISHED 05 January 2024
DOI 10.3389/fmicb.2023.1325473

OPEN ACCESS

EDITED BY
Ke Liu,
Chinese Academy of Agricultural Sciences, China

REVIEWED BY
Devojit Kumar Sarma,
ICMR-National Institute for Research in Environmental Health, India
Gianmarco Ferrara,
University of Naples Federico II, Italy

*CORRESPONDENCE
Sandra Junglen
✉ sandra.junglen@charite.de
David P. Tchouassi
✉ dtchouassi@icipe.org

†These authors have contributed equally to this work

RECEIVED 21 October 2023
ACCEPTED 13 December 2023
PUBLISHED 05 January 2024

CITATION
Ogola EO, Bastos ADS, Slothouwer I, Getugi C, Osalla J, Omoga DCA, Ondifu DO, Sang R, Torto B, Junglen S and Tchouassi DP (2024) Viral diversity and blood-feeding patterns of Afrotropical *Culicoides* biting midges (Diptera: Ceratopogonidae). *Front. Microbiol.* 14:1325473. doi: 10.3389/fmicb.2023.1325473

Viral diversity and blood-feeding patterns of Afrotropical *Culicoides* biting midges (Diptera: Ceratopogonidae)

Edwin O. Ogola[1,2], Armanda D. S. Bastos[2], Inga Slothouwer[3], Caroline Getugi[1], Josephine Osalla[1], Dorcus C. A. Omoga[1], Dickens O. Ondifu[1], Rosemary Sang[1], Baldwyn Torto[1,2], Sandra Junglen[3*†] and David P. Tchouassi[1*†]

[1]International Centre of Insect Physiology and Ecology (icipe), Nairobi, Kenya, [2]Department of Zoology and Entomology, University of Pretoria, Pretoria, South Africa, [3]Institute of Virology, Charité Universitätsmedizin Berlin, Corporate Member of Free University Berlin, Humboldt-University Berlin, and Berlin Institute of Health, Berlin, Germany

Introduction: *Culicoides* biting midges (Diptera: Ceratopogonidae) are vectors of arboviral pathogens that primarily affect livestock represented by Schmallenberg virus (SBV), epizootic hemorrhagic disease virus (EHDV) and bluetongue virus (BTV). In Kenya, studies examining the bionomic features of *Culicoides* including species diversity, blood-feeding habits, and association with viruses are limited.

Methods: Adult *Culicoides* were surveyed using CDC light traps in two semi-arid ecologies, Baringo and Kajiado counties, in Kenya. Blood-fed specimens were analysed through polymerase chain reaction (PCR) and sequencing of cytochrome oxidase subunit 1 (*cox1*) barcoding region. *Culicoides* pools were screened for virus infection by generic RT-PCR and next-generation sequencing (NGS).

Results: Analysis of blood-fed specimens confirmed that midges had fed on cattle, goats, sheep, zebra, and birds. *Cox1* barcoding of the sampled specimens revealed the presence of known vectors of BTV and epizootic hemorrhagic disease virus (EHDV) including species in the Imicola group (*Culicoides imicola*) and Schultzei group (*C. enderleni*, *C. kingi*, and *C. chultzei*). *Culicoides leucostictus* and a cryptic species distantly related to the Imicola group were also identified. Screening of generated pools (11,006 individuals assigned to 333 pools) by generic RT-PCR revealed presence of seven phylogenetically distinct viruses grouping in the genera *Goukovirus*, *Pacuvirus* and *Orthobunyavirus*. The viruses showed an overall minimum infection rate (MIR) of 7.0% (66/333, 95% confidence interval (CI) 5.5-8.9). In addition, full coding sequences of two new iflaviruses, tentatively named Oloisinyai_1 and Oloisinyai_2, were generated by next-generation sequencing (NGS) from individual homogenate of *Culicoides* pool.

Conclusion: The results indicate a high genetic diversity of viruses in Kenyan biting midges. Further insights into host-vector-virus interactions as well as investigations on the potential clinical significance of the detected viruses are warranted.

KEYWORDS

arbovirus surveillance, vertebrate hosts, next generation sequencing, *Culicoides* biting midges, *Goukovirus*, *Pacuvirus*, *Orthobunyavirus*, Iflavirus

Introduction

Culicoides or biting midges (Diptera: Ceratopogonidae) are tiny insects measuring about 1–3 mm in length, commonly identified by unique wing pigmentation and macrotrichia pattern (Mathieu et al., 2012; Kirk-Spriggs and Sinclair, 2017; Borkent and Dominiak, 2020). They have a global distribution with species important for veterinary and public health mainly grouped into the genus *Culicoides* Latreille (Diptera: Ceratopogonidae) comprising about 1,340 species. The Afrotropical region is home to diverse *Culicoides* species, with over 120 species described in southern Africa alone (Garros et al., 2019; Borkent and Dominiak, 2020). Examples of medically important *Culicoides* species include invasive species of the *Culicoides imicola* complex (*C. imicola, C. brevitarsis and C. bolitinos*) and Schultzei group (*C. enderleni, C. kingi*, and *C. schultzei*) (Bakhoum et al., 2013; Leta et al., 2019).

Both sexes of *Culicoides* feed on plants as a primary energy source, but females also blood-feed on vertebrates such as mammals, birds and lizards to acquire additional protein to fertilize their eggs (Martínez-de la Puente et al., 2015; Borkent and Dominiak, 2020). Some *Culicoides* species rely on insect haemolymph as a protein source (Lassen et al., 2012). Further, there is a record of *C. anophelis* and *C. nubeculosus* feeding on engorged mosquitoes (Kremer et al., 1974; Ma et al., 2013). Like other insects, *Culicoides* harbour insect-specific viruses of the genera *Iflavirus* (Langat et al., 2021). Iflaviruses are arthropod-infecting viruses which are not known to be pathogenic to animals and have been largely identified in arthropods of the orders Lepidoptera and Hemiptera (Carrillo-Tripp et al., 2014).

The hematophagous feeding tendency ranks *Culicoides* among arthropods of veterinary and public health importance as they transmit parasites, protozoa and arboviruses that can cause severe disease, such as Schmallenberg virus (SBV) (family *Peribunyaviridae*, genus *orthobunyavirus*) and Bluetongue virus (BTV) (family *Reoviridae,* genus *orbivirus*) (Elbers et al., 2008; Santiago-Alarcon et al., 2012; Elbers et al., 2013; Sick et al., 2019; Žiegytė et al., 2021). Schmallenberg virus is grouped into the simbu serogroup together with Akabane virus (AKV) and Shuni virus (SHUV) and predominantly infects domestic ruminants causing fever, diarrhoea, and serious fetal malformation in gestating cattle and sheep (Saeed et al., 2001). Other viruses in the simbu serogroup include Oropouche virus (OROV) which has been associated with febrile illness in humans and is common in the neotropics (Romero-Alvarez and Escobar, 2018; Gaillet et al., 2021). On the other hand, viruses of the genus *Orbivirus* such as epizootic hemorrhagic disease virus (EHDV) and BTV are known to cause haemorrhagic disease and high morbidity in livestock leading to movement bans and strict trade restrictions which cause huge economic losses (Elbers et al., 2008; Rivera et al., 2021). Outbreaks of *Culicoides*-borne viruses have been common in Europe, for instance SBV in Germany, Italy, Netherlands, UK and Belgium (Hoffmann et al., 2012,; Elbers et al., 2013; Stokes et al., 2018; Ferrara et al., 2023a,b), but there are also reports of EHDV in Canada and North-eastern United States (Stallknecht et al., 2015; Allen et al., 2019). In Africa, BTV is endemic in South Africa, Morocco and Algeria (Youssef et al., 2015; Grewar, 2016; Moustafa et al., 2016; Durr et al., 2017).

The epizootics of *Culicoides*-borne viruses demonstrate the important role of neglected insect groups in veterinary health as outbreaks often mirror distribution of vectors (Purse et al., 2004). While the development and host biting rate of vectors such as *C. enderleni* and *C. imicola* are associated with warm temperatures, colder temperatures distinctly enable sustained EHDV and BTV transmission in an episystem (Grimaud et al., 2019; Mayo et al., 2020; Ferrara et al., 2023a,b). Another factor facilitating sustained virus transmission is the availability of vertebrate hosts that support large insect populations and may also serve as reservoir and maintenance hosts (Kuno et al., 2017). To understand the transmission dynamics of *Culicoides*-borne viruses, it is important to identify blood-meal sources of the vectors and abundant vector species. However, apart from reports highlighting active circulation of BTV serotypes in Kenya, studies on *Culicoides*-borne viruses are generally scarce in Africa (Toye et al., 2013; Onyango et al., 2015; Langat et al., 2021). In this study, we sought to identify *Culicoides*-borne viruses in two arid ecosystems, Baringo and Kajiado counties in Kenya using generic RT-PCR assays and next-generation sequencing (NGS). We further examined the vertebrate blood-meal sources of *Culicoides* in this area and identified abundant species by molecular barcoding.

Methods

Study location

Adult *Culicoides* were collected between August 2019 and July 2020 in Baringo and Kajiado counties at the end of rainy season and coinciding with peak abundance (Diarra et al., 2014). The study spanned 4 sites, Ntepes, Sandai, Logumgum, and Kapkuikui, in Baringo County, and 2 sites in Kajiado county, namely Soweto and Oloisinyai (Figure 1). The 2 study areas have similar semi-arid ecologies. Baringo had mean daily temperatures of 21.4°C, mean daily rainfall of 3.0 mm and a mean relative humidity of 66.8% during the sample collection periods. In Kajiado, the mean daily temperature was 23.7°C, mean daily rainfall was 0.3 mm and mean relative humidity 66.0% during sampling period. Using GIS-coordinates, the weather variable data were retrived from https://power.larc.nasa.gov/, and mean daily temperature and humidity in Kajiado documented using Thermochron iButton (Sunnyvale, CA) attached to each trap. The sparse human population in both areas rely on nomadic pastoralism as the major economic activity. A typical family has large herds of cattle, goat and/or sheep which they move from one place to another in search of water and pasture. The areas also have conservancies haboring wild animals including Kiborgoch community conservancy in Baringo and Olkirimatian conservancy in Kajiado. Some of the common wild animals in the conservancies include zebra, impala antelope and diverse bird species, including ostriches.

Culicoides collection and identification

Centers for Disease Control (CDC) light traps model 512 (John W. Hock Company, Gainesville, United States) were used to catch adult *Culicoides* as part of a larger arbovirus surveillance project. Eight CDC light traps were baited with yeast-produced CO_2 (Laguna-Aguilar et al., 2012), and deployed overnight from 18:00 h to 06:00 h for 3 consecutive nights at each sampling site. The traps were deployed outdoors with an inter-trap distance of about 25 m geo-referenced

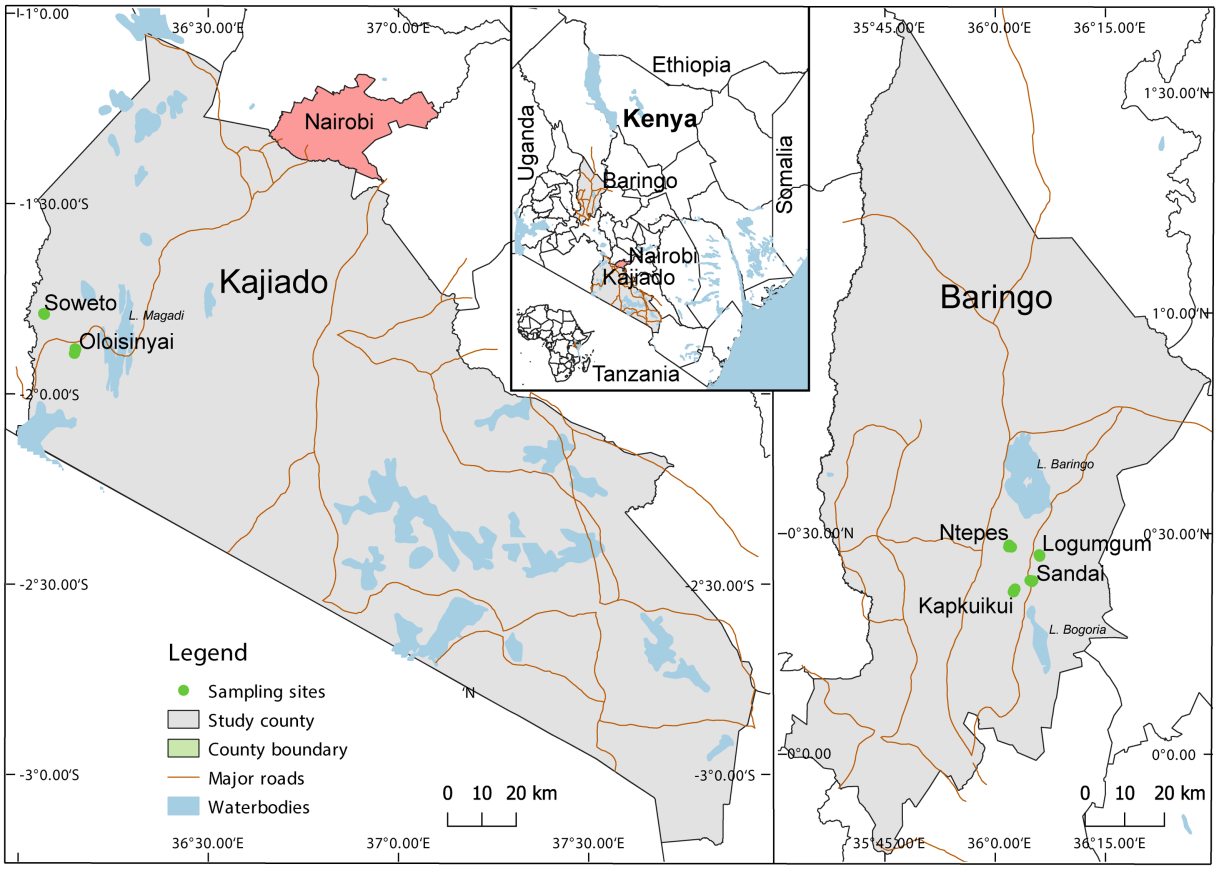

FIGURE 1
Map showing specimen collection sites in two semi-arid counties Kajiado and Baringo, in Kenya during entomological surveillance activities conducted between August 2019 and July 2020. The map was generated in QGIS 2.12 with shape files provided by Natural Earth (http://www.naturalearthdata.com/) and Africa Open data (https://africaopendata.org/dataset/kenya-counties-shapefile) (QGIS Development Team, 2019).

positions near farms/animal shelters (in the vicinity of human-settlement) as well as inside wild animal conservancies. After retrieval, the samples were initially taken to a temporary field laboratory. Biting midges were anesthetized with triethylamine and cryopreserved in liquid nitrogen for transportation to the laboratory at *icipe* in Nairobi and stored at −80°C until further analysis. In the laboratory, the *Culicoides* were sorted from other insects on a pre-chilled ice pack under a dissecting microscope (Stemi 2000-C microscope, Zeiss, Germany) (Glick, 1990; Bakhoum et al., 2018). Unfed *Culicoides* were pooled in groups of 2 to 50 according to collection date and sampling site. Engorged (blood-fed) specimen were analyzed individually.

Homogenization of midge samples

The collected *Culicoides* were homogenized for 30 s in 1.5 mL microcentrifuge tubes containing 2.0 mm zirconia beads and DPBS (Dulbeccos phosphate-buffered saline, pH 7.4) using a Mini-Beadbeater-16 (Biospec, Bartlesville, OK, United States). For each pool, 1 mL of DPBS was used, whereas for individual engorged specimens the volume was reduced to 500 µL. The homogenate was centrifuged for 10 min in a bench top centrifuge (Eppendorf, United States) at 2500 revolutions per minute (rpm) at 4°C. After phase separation, the supernatant was used for virus screening and isolation. The pellet of individual engorged samples were preserved for DNA analyzes inclusive of species identification and blood-meal source determination.

Molecular identification of engorged *Culicoides* species and blood-meal source detection

DNA was extracted from the homogenate pellets of individual engorged *Culicoides* using DNeasy Blood and Tissue Kit (Qiagen, Hilden, Germany) following manufacturer's recommendations and stored at −20°C until further use. *Culicoides* species molecular identification involved polymerase chain reaction (PCR) and Sanger sequencing of a 710 bp region of the cytochrome oxidase subunit 1 (*cox1*) gene as previously described (Folmer et al., 1994). To identify different blood meal host sources a different *cox1* fragment was targeted using vertebrate specific primers (Reeves et al., 2018). ExoSAP-IT (USB Corporation, Cleveland, OH, United States) was used to remove unincorporated dNTPs and PCR primers from the amplicons before submitting purified amplicons for Sanger sequencing (Microsynth Seqlab GmbH, Göttingen, Germany). Sequences were edited in Geneious prime and used to query Barcode of Life (BOLD) and GenBank databases (Altschul et al., 1990; Ratnasingham and Hebert, 2007).

Detection and characterization of viruses

Viral RNA was extracted from 140 µL of the homogenate supernatants using the Viral RNA Mini Kit (Qiagen, Hilden, Germany) as described by the manufacturer. Double-stranded cDNA was synthesized using random hexamer primers (Endoh et al., 2005) and High Capacity cDNA Reverse Transcription (RT) kit (Life Technologies, CA, United States) following the manufacturers' protocol. Pan-PCR assays targeting the RNA-dependent RNA polymerase (RdRp) gene of peribunyaviruses and phenuiviruses were utilized to screen for viral infections as described earlier (Hermanns et al., 2023). The resulting PCR products were examined on 1.5% agarose gels stained with ethidium bromide and amplicons of the correct size were purified for Sanger sequencing (Macrogen, Amsterdam, Netherlands) using ExoSAP-IT (USB Corporation, Cleveland, OH, United States).

Virus isolation

Virus-positive samples were inoculated onto semi-confluent monolayers of mammalian Vero E6 (*Ceropithecus aethiops*) and insect C6/36 (*Aedes albopictus*) and KC (*Drosophila melanogaster*) cell lines, as described previously (Junglen et al., 2009). Briefly, Vero E6 cells were maintained in Dulbecco's modified Eagle's medium (DMEM) supplemented with 5% fetal calf serum (FCS) and 1% l-glutamine. C6/36 and KC cells were maintained in Leibovitz's L-15 medium (L-15) supplemented with 5% FCS. Vero E6 cells were maintained in a 5% CO_2 incubator at 37°C while C6/36 and KC cells were maintained at 28°C incubator without CO_2. The cells were observed regularly for up to 7 days for occurrence of cytopathic effects (CPE). Samples were passaged on fresh cells 8 days after inoculation and a 75 µL aliqout of cell culture supernatant was taken from each sample. The blind passage was repeated 3 times and aliquots from cell culture supernatants from each passage were tested for viral replication.

Library preparation and next-generation sequencing

Sequencing libraries were constructed using the KAPA HyperPlus kit (Roche Diagnostics, Rotkreuz, Switzerland) following the manufacturers' instructions. Sequencing was performed on the Illumina MiSeq platform (Illumina, United States) as described (Marklewitz et al., 2019). Low-quality reads and adaptor sequences were removed from paired-end reads using BBDuk (filterk = 27, trimk = 30; http://jgi.doe.gov/data-and-tools/bb-tools/). After quality control, the cleaned reads were *de novo* assembled using Spades v3.11 implemented in Geneious Prime (Kearse et al., 2012). The resulting contigs were queried against the NCBI reference sequence database using BLASTn search.

Sequence and phylogenetic analyzes

Sequences were analyzed using Geneious prime (Kearse et al., 2012). Obtained sequences were compared to publicly available sequences in BOLD and GenBank (Altschul et al., 1990; Ratnasingham and Hebert, 2007). Sequences were aligned to related sequences using MAFFT as implemented in Geneious prime (Kearse et al., 2012). Maximum likelihood (ML) phylogenetic analyzes were executed using PhyML v. 2.2.4 in Geneious prime with each of the aligned *cox1* nucleotide datasets. Nodal support was assessed by 1,000 bootstrap replicates using standard parameters (Guindon et al., 2010). Flavivirus and iflavirus genome organization were predicted using interProScan executed in Geneious prime (Kearse et al., 2012; Jones et al., 2014).

Statistical analysis

Metadata including *Culicoides* trap catches, sampling area, GPS coordinates, collection date, trapping method and abdominal status were captured in Microsoft Excel (2020) and relative abundance of *Culicoides* in sampling areas analyzed in R version 4.1.2 using funrar package (R Core Team, 2016). Minimum infection rate (MIR) was determined using PooledInfRate (https://github.com/CDCgov/PooledInfRate) under the assumption that there was at least one infected specimen in every positive *Culicoides* pool (Ségard et al., 2018). The relative abundance of *Culicoides* was estimated binomially and evaluated by Chi square tests at 95% confidence intervals in R version 4.1.2 (R Core Team, 2016).

Results

Culicoides abundance in Kenya

A total of 11,006 *Culicoides* were collected from the six sampling sites in the two counties using CDC light traps (Table 1). More *Culicoides* were collected from Baringo County (55.9%, $n = 6,149$) than from Kajiado County (44.1%, $n = 4,857$) (Table 1). Overall, the majority of *Culicoides* specimens were collected in Oloisinyai, Kajiado County (42.0%; $n = 4,622$). In Baringo County, Logumgum (23.8%, $n = 2,620$) and Kaptombes (13.3%, $n = 1,462$) yielded the highest numbers of *Culicoides*. Seventy-four individuals (0.7% of the total collection) were engorged (blood-fed) specimens.

Blood-meal sources of engorged *Culicoides* species

Seventy-four blood-fed specimens mainly originating from Baringo (93.2%, $n = 69$) and only few from Kajiado county (6.8%, $n = 5$) were identified to species by PCR. Most prevalent species were *C. imicola* (45.9%, $n = 34$) followed by *C. enderleni* (37.8%, $n = 28$). Other species identified in the blood-fed cohorts included *C. kingi* (6.8%, n = 5), *C. leucostictus* (1.4%, $n = 1$) and *C. schultzei* (1.4%, $n = 1$). Five samples could not be identified to species level by *cox1* gene analyzes. The sequences of these 5 samples showed maximum nucleotide similarity of 85–86% to *C. brevitarsis* and *C. imicola*, and grouped in a distinct monophyletic clade in distant relationship to the Imicola group (Figure 2A). Among the collected blood-fed specimen, the highest species richness was observed in Kaptombes, Baringo County. Only one species (*C. enderleni*) was found in Sandai and Ntepes in Baringo County. *Culicoides enderleni* was common at all sampling sites, while *C. schultzei* was identified in Oloisinyai, Kajiado County, only.

TABLE 1 Relative abundance of *Culicoides* sampled from Baringo and Kajiado counties, Kenya.

County	Habitat type	Sampling site	*n* (%)	Blood-fed (%)
Baringo (55.9%, *n* = 6,149)	Animal conservancy	Kaptombes	1,462 (13.3)	34 (45.9)
	Farm/animal shelter	Logumgum	2,620 (23.8)	17 (23.0)
		Ntepes	891 (8.1)	1 (1.4)
		Kapkuikui	825 (7.5)	16 (21.6)
		Sandai	351 (3.2)	1 (1.4)
		n (%)	**6,149 (55.9)**	**69 (93.2)**
Kajiado (44.1%, n = 4,857)	Animal conservancy	Oloisinyai	4,622 (42.0)	5 (6.8)
	Farm/ animal shelter	Soweto	235 (2.1)	0 (0.0)
		n (%)	**4,857 (44.1)**	**5 (6.8)**
n (%)			**11,006 (100.0)**	**74 (100.1)**

n, number of specimens. Bold values highlight the total number of specimen in sub-sections.

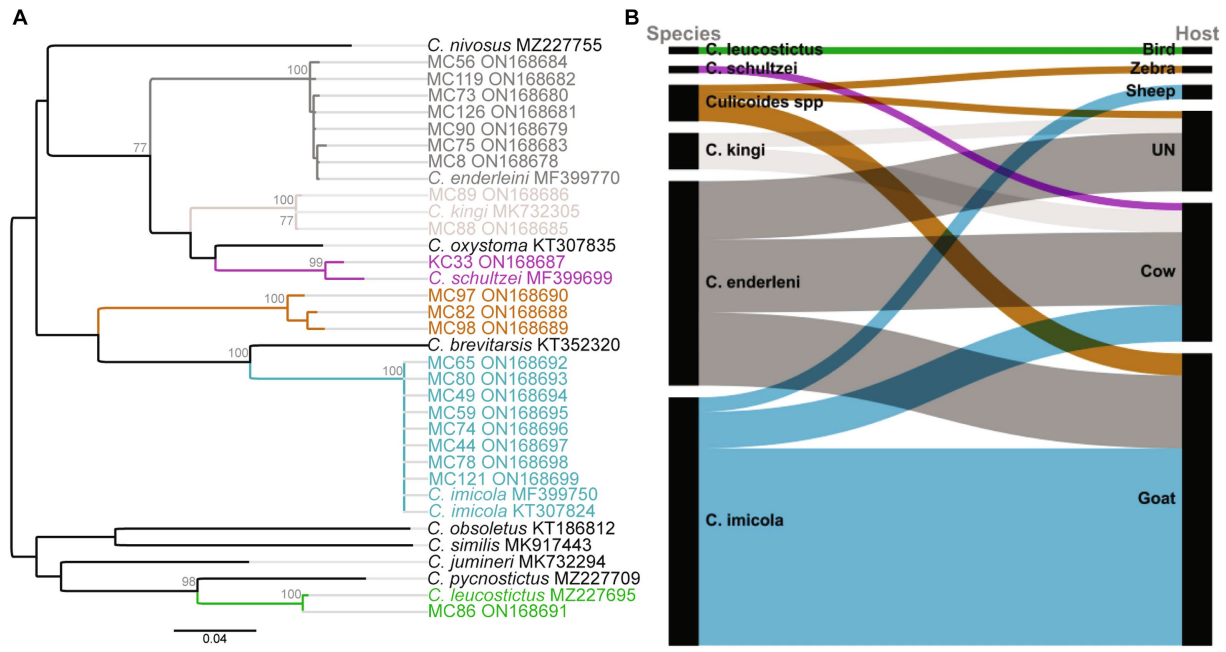

FIGURE 2
Phylogenetic relationship of identified *Culicoides* species and their blood-feeding patterns. **(A)** Maximum likelihood phylogenetic analysis based on the *Cox1* (nt 710 bp) gene inferred with PhyML v. 2.2.4 using the GTR substitution model. Bootstrap values of 70% and above are shown. **(B)** Alluvial diagram showing *Culicoidies* species blood-meal sources. The diagram was visualized in RAWGraphs (Mauri et al., 2017). UN: Unknown blood-meal source (identification was not successful).

In total, blood-meal sources were successfully identified from 63 *Culicoides* specimens (85.1%, 63/74; Table 2). Five different vertebrate blood-meal hosts were identified including livestock such as cattle (*Bos taurus*), goat (*Capra hircus*) and sheep (*Ovis aries*), and wild animals exemplified by zebra (*Equus burchelli boehmi*) and birds (*Crinifer piscator*) (Table 2; Figure 2B). *Culicoides imicola* showed the most diverse blood-meal sources having fed on cattle, goat and sheep followed by *C. enderleni* which had fed on cattle and goat. The other species *C. kingi* and *C. schultzei* were found to have fed on cattle only while *C. leucostictus* blood meals were from birds. Analysis of sequence chromatograms did not show evidence for mixed blood-meal sources. No human blood-meal source was identified, despite the trapping conducted in the vicinity of human-settlements.

Identification of phenuiviruses, peribunyaviruses and iflaviruses

All collected 11,006 *Culicoides* specimens were tested in pools ($n = 333$, ≤50 *Culicoides*/pool) for infections with phenui- and peribunyaviruses. Iflaviruses were detected during analysis of NGS data from *Culicoides* homogenates. An overall minimum infection rate (MIR) of 7.0% (66/333, 95% confidence interval (CI) 5.5–8.9) was found (Table 3). Highest MIR were registered in Sandai (MIR = 47.0, 95% CI 18.3–107.8) and Ntepes (MIR = 11.8, 95% CI 5.4–22.2), both in Baringo County (Table 3).

Two potential *Goukovirus* species were detected in 56 samples (MIR of 5.7, 95% CI 4.3–7.3, 56/333). The viral sequences were

10.3389/fmicb.2023.1325473

TABLE 2 Summary of blood-meal sources identified in blood-fed *Culicoides*.

County	Sampling site	Culicoides species	n (%)	Vertebrate host					
				Goats	Cattle	Sheep	Birds	Zebras	UN
Baringo	Kapkuikui	*C. enderleni*	7	4	0	0	0	0	3
		C. imicola	7	7	0	0	0	0	0
		Culicoides sp.	2	2	0	0	0	0	0
	Kaptombes	*C. enderleni*	6	1	5	0	0	0	0
		C. imicola	22	16	4	2	0	0	0
		C. kingi	2	0	0	0	0	0	2
		C. leucostictus	1	0	0	0	1	0	0
		Culicoides sp.	3	1	0	0	0	1	1
	Logumgum	*C. enderleni*	12	5	3	0	0	0	4
		C. imicola	5	4	1	0	0	0	0
	Ntepes	*C. enderleni*	1	0	1	0	0	0	0
	Sandai	*C. enderleni*	1	0	0	0	0	0	1
Kajiado	Oloisinyai	*C. enderleni*	1	0	1	0	0	0	0
		C. kingi	3	0	3	0	0	0	0
		C. schultzei	1	0	1	0	0	0	0
n (%)			74	40 (54.1)	19 (25.7)	2 (2.7)	1 (1.4)	1 (1.4)	11 (14.9)

n: numbers of blood-fed *Culicoides*; UN: Unknown blood-meal source (identification was not successful).

TABLE 3 Viral detections at the six sampling sites in Baringo and Kajiado counties, Kenya.

County	Sampling	No. of pools	No. of positive	MIR (95% CI)			
	Site	Tested	Pools (%)	All positives	Phenuiviruses	peribunyaviruses	Iflaviruses
Baringo	Kapkuikui	53	4 (1.2)	5.2 (1.6–12.0)	4.0 (1.0–10.3)	0	0
	Kaptombes	75	5 (1.5)	3.6 (1.3–7.8)	2.9 (0.9–6.7)	0	0
	Logumgum	72	7 (2.1)	2.8 (1.2–5.5)	2.8 (1.2–5.5)	0	0
	Ntepes	19	8 (2.4)	11.8 (5.4–22.2)	8.2 (3.2–16.6)	2.4 (0.4–7.3)	0
	Sandai	8	7 (2.1)	47.0 (18.3–107.8)	21.2 (7.5–47.1)	6.7 (1.1–20.7)	0
Kajiado	Oloisinyai	100	34 (10.2)	9.1 (6.4–12.6)	7.5 (5.1–10.6)	0	0.4 (0.1–1.3)
	Soweto	6	1 (0.3)	4.8 (0.3–21.0)	4.8 (0.3–21.0)	0	0
Total		**333**	**66 (19.8)**	**7.0 (5.5–8.9)**	**5.7 (4.3–7.3)**	**0.7 (0.3–1.4)**	**0**

MIR, minimum infection rate; CI, confidence interval.

detected at all sampling sites in Baringo and Kajiado counties. Detections were made in *C. enderleni* that had fed on cattle and in *C. imicola* with a blood-meal from a goat (Figure 3A). The 2 potential *Goukovirus* species showed 98–100% and 89–100% nucleotide identities among each at the RdRp gene of 521–233 nucleotides in length. Maximum pairwise amino acid identities of 57 to 71% were found to *Gouleako* virus described in mosquitoes from Cote d'Ivoire (Supplementary Figure S1) (Marklewitz et al., 2011). The phylogenetic tree revealed that the 56 viruses characterized in this study clustered within a monophyletic clade sister to *Gouleako* goukovirus.

Eight RdRp gene sequences that fell within the family *Peribunyaviridae* were identified (Figure 3B; MIR of 0.7%; 95% CI 0.2–1.4, 8/333). BLAST analysis showed that the sequence of the sample MC1 from Sandai, Baringo county, shared 90% amino acid identity to Bahig virus from the Tete serogroup that was isolated from birds in Egypt (Shchetinin et al., 2015). Sample KC97 from Oloisinyai, Kajiado was distantly related to the clade comprising Akhtuba and Khurdun viruses isolated from birds in Russia (Figure 3B) (Al'kovskhovskiĭ et al., 2013). Another sample MC18 was distantly related to Pacui virus (genus *Pacuvirus*) detected in Brazilian rodents (Rodrigues et al., 2014). The remaining samples from Baringo and Kajiado counties clustered together forming a unique monophyletic clade. A distance matrix of pairwise similarity scores of detected viruses and representative peribunyaviruses is shown in Figure S2. There was no peribunyavirus detection in blood-fed specimens.

Seventeen *Culicoides* homogenate pools positive by Pan-PCR assay were randomly selected and analyzed by NGS. Analysis of NGS data from revealed full coding sequences of two novel iflaviruses (tentatively named Oloisinyai_1 and Oloisinyai_2) in sample KC102 collected from Oloisinyai (Kajiado County) with overall MIR of 0.2%

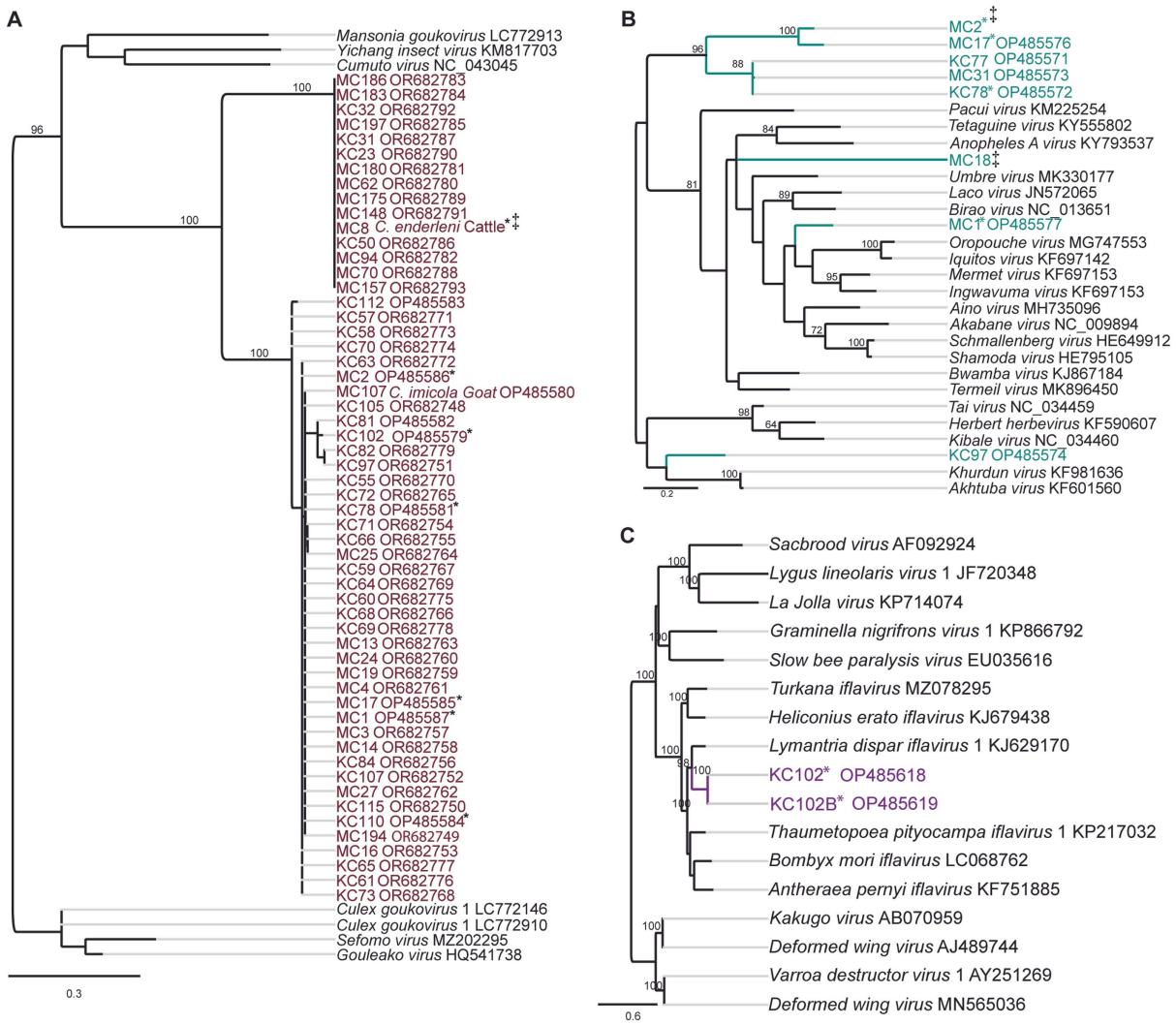

FIGURE 3
Maximum likelihood RNA-dependent RNA polymerase (RdRp) gene phylogenies depicting the genetic relatedness of **(A)** goukoviruses and samples sequenced in the present study; **(B)** peribunyaviruses and members of the *Peribunyaviridae* family; **(C)** iflaviruses and members of the *Iflaviridae* family. The phylogenetic trees were inferred with PhyML v. 2.2.4. *: Samples with mixed infection; ‡: sequence not deposited to GeneBank due to short length.

(95% CI 0.0–0.6, 2/17). Comparison of the two sequences against the GenBank database using BLASTx showed 80–82% amino acid similarity to *Lymantria dispar iflavirus 1* isolated in the US (Carrillo-Tripp et al., 2014) (Figure 3C). The detected viral sequences had 85% nucleotide similarity to each other. Genome annotation of Oloisinyai_1 and Oloisinyai_2 revealed a single-stranded positive sense RNA [ssRNA (+)] genome and a genomic organization that includes a capsid protein at N-terminal end and non-structural proteins (helicase and RNA-dependent RNA polymerase) at the C-terminal end (Figure 4). Attempts to isolate the detected phenuiviruses, peribunyaviruses and iflaviruses in KC, C6/36, and Vero E6 cell lines were not successful.

Discussion

Culicoides are vectors of several arboviral pathogens of veterinary and public health importance (Elbers et al., 2008; Romero-Alvarez and Escobar, 2018; Sick et al., 2019; Gaillet et al., 2021). Similar to earlier association of *Culicoides* abundance with warm temperatures, the high *Culicoides* collection in Baringo and Kajiado counties can be attributed to the favorable weather conditions observed in study sites (Grimaud et al., 2019; Mayo et al., 2020). Although the present study involved barcoding of a limited number of blood-fed *Culicoides* ($n = 74$), it revealed the presence of established/known vectors including members of Imicola group (*C. imicola*) and Schultzei group (*C. enderleni, C. kingi*, and *C. schultzei*) (Bakhoum et al., 2013). The rarely encountered species *C. leucostictus* and a cryptic *Culicoides* sp. distantly related to the Imicola group species (*C. imicola* and *C. brevitarsis*) were also identified (Table 2; Figure 2A). *Culicoides imicola* was the most abundant blood-fed *Culicoides*. This finding is similar to an earlier survey in Senegal showing higher collections of *C. imicola* in traps set near farms/animal shelters suggesting that animal shelters provide dung important for successful breeding of the vector (Acevedo et al., 2010; Diarra et al., 2014, 2015).

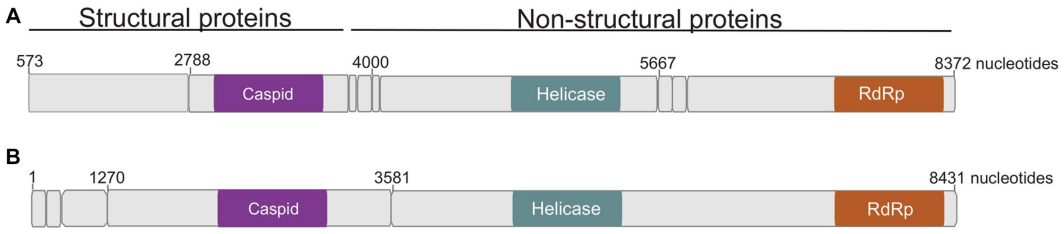

FIGURE 4
Genome organization of detected Oloisinyai_1 and Oloisinyai_2 iflaviruses. Colored sections highlight regions of functional significance. **(A)** Oloisinyai_1 virus; **(B)** Oloisinyai_2 virus.

Culicoides imicola is a known vector of BTV and its presence in Kenya provides an important avenue for the virus transmission (Sick et al., 2019). It is noteworthy that there was no record of blood-fed *C. imicola* in Kajiado County. However, the presence of *C. imicola* in the region cannot be excluded since only blood-fed *Culicoides* species were barcoded. *Culicoides* schultzei group species identified in the present study are known vectors of EHDV and BTV (Mellor et al., 1984; Bakhoum et al., 2016) and have been previously described in Kenya (Walker and Boreham, 1976; Cornet and Brunhes, 1994). Their presence highlight the risk of the virus' transmission and is notable in light of reports of high BTV and EHDV prevalence in western part of the country (Toye et al., 2013). Considering the relatively low numbers of *Culicoides* samples that were barcoded, it is possible that more species and haplotypes could be identified with analysis of larger number of samples. Additional *Culicoides* species characterization would provide valuable information on vector species composition in the region.

Culicoides have diverse blood-meal sources. Therefore, information about their blood-feeding pattern is important in elucidating vector-host interactions and *Culicoides*-borne virus eco-epidemiology. Overall, our data confirmed five blood-meal hosts including cattle, goats, sheep, zebras, and birds in agreement with previous studies which reported diverse hosts for *Culicoides* species sampled in Romania (Tomazatos et al., 2020). All *Culicoides* species demonstrated mammophilic blood-feeding habits except *C. leucostictus* which had fed on birds (Table 2; Figure 2B). While ornithophilic tendencies in *C. leucostictus* has been reported before, there is little information on the role of the species in virus transmission (Scheffer et al., 2012). At each sampling site, there appeared to be a correlation between available vertebrate hosts and the blood-meal source detected. For example, at Kaptombes there is a wildlife conservancy inhabited by zebra explaining their detection in *Culicoides* blood-meals. The finding that *Culicoides* were feeding on livestock hosts such as cattle, goat and sheep confirm opportunistic feeding habits, underscoring the role of large animal herds serving as blood-meal sources for vectors (Table 2; Figure 2B). Although hosts availability seemed to influence the observed blood-feeding pattern, it is interesting that human blood-meals were not detected, an indication of potential impact on veterinary rather than human health by *Culicoides*-associated viruses in these ecological settings. A blood-meal source could not be established for 14.9% ($n = 11$) of the blood-fed *Culicoides* (Table 2). The blood-meal analysis involved nested PCR using 3 primer pair combinations of which one, targeting a shorter *cox1* gene of 244 bp, is ideal for detecting degraded host DNA (Reeves et al., 2018). Therefore, blood-meal source identification failure can be attributed to highly degraded host DNA due to advanced digestion in the insect gut. Nevertheless, the study shows that *Culicoides* species in the two counties take diverse blood-meal sources and that the vertebrate hosts can potentially act as reservoirs of *Culicoides*-borne viruses. However, the observed blood-feeding pattern should be interpreted with caution due to the small sample size. A wider study focused on blood-fed *Culicoides* would provide greater insight into *Culicoides* feeding patterns and vector-host interactions.

Virus screening assays revealed the presence of seven potential virus species belonging to the genera *Goukovirus, Pacuvirus, Orthobunyavirus* and *Iflavirus* (Table 3). The family *Phenuiviridae* represents both medically important viruses such as Rift Valley fever virus and the recently discovered sandfly-borne phleboviruses in Baringo County, as well as insect specific viruses like the *gouleako* virus, prototype of the genus *Goukovirus* (Marklewitz et al., 2011; Tchouassi et al., 2019; Marklewitz et al., 2020). Since the discovery of Gouleako virus, several further mosquito-associated goukoviruses have been described (Lefkowitz et al., 2018). However, information associating *Culicoides* with goukoviruses transmission is scarce. The data presented here expand the list of viruses in the genus, describing detection of uncharacterised goukoviruses identified in *Culicoides*. These viruses had a MIR of 5.7% (95% CI 4.3–7.3, 56/333) and were widely distributed, occurring at all sampling sites (Table 3). Further, the viruses were detected in established vectors of EHDV and BTV (*C. enderleni* and *C. imicola*) that had fed on cattle and goat.

One detected vial sequence (MC1) clustered with the pathogenic Simbu group including SBV, AKV, and OROV (Saeed et al., 2001; Romero-Alvarez and Escobar, 2018; Gaillet et al., 2021). Further, sample KC97 was related to Akhtuba and Khurdun viruses isolated from birds in Russia (Al'kovskhovskiĭ et al., 2013; Rodrigues et al., 2014). These virus detections are not surprising as the genus is probably the most medically relevant one within the family *Peribunyaiviridae* and comprises the majority of *Culicoides*-borne viruses (Lefkowitz et al., 2018). Orthobunyaviruses are known to have a wide vertebrate host range inclusive of humans, livestock and birds. In the present study, there was no detection of orthobunyaviruses in *Culicoides* that had fed on livestock and birds, however, this cannot be ruled out due to the small sample

size. Unfortunately, attempts to generate more sequence information of the detected peribunyaviruses failed, as well as virus isolation attempts were not successful. Hence, further studies including genome sequencing and analyzes as well as phenotypic studies with virus isolates in cell culture are needed for further classification and assessment.

In the present study, seventeen samples were analyzed by NGS revealing two insect-specific viruses of genus *Iflaviruses* were detected. The low diversity of detected viruses in relation to a similar study could be attributed to the few representative samples that were analyzed by NGS (Langat et al., 2021). The identified iflaviruses showed 80–82% amino acid similarity to *Lymantria dispar iflavirus* 1 (LdIV1) isolated in the US (Carrillo-Tripp et al., 2014), suggesting that the identified iflaviruses represent novel species in the genus as stipulated in the Executive Committee (EC) 51, 2019 report (Lefkowitz et al., 2018). Apart from recent report of iflaviruses in *Culicoides* in Kenya, reports of *Culicoides* iflaviruses infection in the country remains scarce (Langat et al., 2021).

Conclusion

This study has provided evidence that established *Culicoides* vectors (*C. imicola, C. enderleni, C. kingi*, and *C. schultzei*) of BTV and EHDV were feeding mainly on livestock host in Kenya. Blood-meal analyzes revealed opportunistic feeding of *Culicoides* species on livestock and wildlife and the potential for spillover of viruses of veterinary importance. Expanded studies on vector-host-virus interactions, inclusive of *Culicoides* blood-meal source determination, virus genome characterization and seroprevalence studies are needed to establish the clinical and modulatory impacts of *Culicoides*-borne viruses.

Data availability statement

The datasets presented in this study can be found in online repositories. The names of the repository/repositories and accession number(s) can be found in the article/supplementary material.

Ethics statement

The animal study was approved by Kenya Medical Research Institute Scientific and Ethics Review Unit (KEMRI-SERU). The study was conducted in accordance with the local legislation and institutional requirements.

Author contributions

EO: Conceptualization, Data curation, Formal analysis, Investigation, Methodology, Software, Validation, Visualization, Writing – original draft, Writing – review & editing. AB: Conceptualization, Resources, Supervision, Writing – review & editing. IS: Writing – review & editing, Formal analysis, Investigation. CG: Formal analysis, Investigation, Writing – review & editing. JO: Writing – review & editing, Formal analysis, Investigation. DOm: Formal analysis, Investigation, Writing – review & editing. DOn: Formal analysis, Investigation, Writing – review & editing. RS: Conceptualization, Funding acquisition, Resources, Supervision, Writing – review & editing. BT: Conceptualization, Funding acquisition, Resources, Supervision, Writing – review & editing. SJ: Conceptualization, Formal analysis, Funding acquisition, Methodology, Resources, Supervision, Validation, Writing – review & editing. DT: Conceptualization, Formal analysis, Funding acquisition, Methodology, Resources, Supervision, Validation, Writing – review & editing.

Funding

The author(s) declare financial support was received for the research, authorship, and/or publication of this article. The work was funded by the Deutsche Forschungsgemeinschaft (JU 2857/9-1 / and -2 to SJ). Edwin Ogola was supported by a German Academic Exchange Service (DAAD) through the *icipe* ARPPIS-DAAD scholarship and a UP postgraduate bursary. DT received support from the Norad-funded project Combatting Arthropod Pests for better Health, Food and Climate Resilience (CAP-Africa; project number RAF-3058 KEN-18/0005). We also gratefully acknowledge the financial support and technical support of ICIPE core donors: Swiss Agency for Development and Cooperation (SDC), Switzerland; Swedish International Development Cooperation Agency (Sida), Sweden; Australian Centre for International Agricultural Research (ACIAR), Federal Democratic Republic of Ethiopia and the Government of the Republic of Kenya. The views expressed herein do not necessarily reflect the official opinion of the donors. The funders had no role in study design, data collection and analysis, decision to publish, or preparation of the manuscript.

Acknowledgments

We are grateful for the technical support of Christian Hieke and Verena Hyde of Institute of Virology, Charité Universitätsmedizin Berlin, and Gibert Rotich of *icipe*'s ML-EID laboratory.

Conflict of interest

The authors declare that the research was conducted in the absence of any commercial or financial relationships that could be construed as a potential conflict of interest.

The author(s) declared that they were an editorial board member of Frontiers, at the time of submission. This had no impact on the peer review process and the final decision.

Publisher's note

All claims expressed in this article are solely those of the authors and do not necessarily represent those of their affiliated organizations, or those of the publisher, the editors and the reviewers. Any product

that may be evaluated in this article, or claim that may be made by its manufacturer, is not guaranteed or endorsed by the publisher.

Supplementary material

The Supplementary material for this article can be found online at: https://www.frontiersin.org/articles/10.3389/fmicb.2023.1325473/full#supplementary-material

SUPPLEMENTARY FIGURE 1
Goukoviruses distance matrix. Distance matrix of the RdRp gene showing representative viruses of genus *Goukovirus* and samples sequenced in the present study. Light grey to dark shades highlights amino acid distances.

SUPPLEMENTARY FIGURE 2
Peribunyaviruses distance matrix. Distance matrix of the RdRp gene showing representative viruses and samples sequenced in the present study (bold). Light grey to dark shades indicates nucleotide distances.

References

Acevedo, P., Ruiz-Fons, F., Estrada, R., Márquez, A. L., Miranda, M. A., Gortázar, C., et al. (2010). A broad assessment of factors determining *Culicoides imicola* abundance: modelling the present and forecasting its future in climate change scenarios. *PLoS One* 5:e14236. doi: 10.1371/JOURNAL.PONE.0014236

Al'kovskhovskiĭ, S. V., Shchetinin, A. M., Lvov, D. K., Shchelkanov, M. I., Deriabin, P. G., L'vov, D. N., et al. (2013). The Khurdun virus (KHURV): a new representative of the orthobunyavirus (Bunyaviridae). *Vopr. Virusol.* 58, 10–13.

Allen, S. E., Rothenburger, J. L., Jardine, C. M., Ambagala, A., Hooper-McGrevy, K., Colucci, N., et al. (2019). Epizootic hemorrhagic disease in white-tailed deer, Canada. *Emerg. Infect. Dis.* 25, 832–834. doi: 10.3201/eid2504.180743

Altschul, S. F., Gish, W., Miller, W., Myers, E. W., and Lipman, D. J. (1990). Basic local alignment search tool. *J. Mol. Biol.* 215, 403–410. doi: 10.1016/S0022-2836(05)80360-2

Bakhoum, M. T., Fall, M., Fall, A. G., Bellis, G. A., Gottlieb, Y., Labuschagne, K., et al. (2013). First record of *Culicoides oxystoma* Kieffer and diversity of species within the Schultzei group of Culicoides Latreille (Diptera: Ceratopogonidae) biting midges in Senegal. *PLoS One* 8:e84316. doi: 10.1371/journal.pone.0084316

Bakhoum, M. T., Fall, M., Seck, M. T., Gardes, L., Fall, A. G., Diop, M., et al. (2016). Foraging range of arthropods with veterinary interest: new insights for Afrotropical *Culicoides* biting midges (Diptera: Ceratopogonidae) using the ring method. *Acta Trop.* 157, 59–67. doi: 10.1016/J.ACTATROPICA.2016.01.023

Bakhoum, M. T., Sarr, M., Fall, A. G., Huber, K., Fall, M., Sembène, M., et al. (2018). DNA barcoding and molecular identification of field-collected *Culicoides* larvae in the Niayes area of Senegal. *Parasit. Vectors* 11:615. doi: 10.1186/s13071-018-3176-y

Borkent, A., and Dominiak, P. (2020). Catalog of the biting midges of the world (Diptera: Ceratopogonidae). *Zootaxa* 4787, 1–377. doi: 10.11646/zootaxa.4787.1.1

Carrillo-Tripp, J., Krueger, E. N., Harrison, R. L., Toth, A. L., Miller, W. A., and Bonning, B. C. (2014). *Lymantria dispar* iflavirus 1 (LdIV1), a new model to study iflaviral persistence in lepidopterans. *J. Gen. Virol.* 95, 2285–2296. doi: 10.1099/vir.0.067710-0

Cornet, M., and Brunhes, J. (1994). Révision des espèces de Culicoides apparentés à *C. schultzei* (Enderlein, 1908) dans la région afrotropicales (Diptera, Ceratopogonidae). *Bull. Soc. entomol. Fr.* 99, 149–164. doi: 10.3406/BSEF.1994.17053

Diarra, M., Fall, M., Fall, A. G., Diop, A., Seck, M. T., Garros, C., et al. (2014). Seasonal dynamics of *Culicoides* (Diptera: Ceratopogonidae) biting midges, potential vectors of African horse sickness and bluetongue viruses in the Niayes area of Senegal. *Parasit. Vectors* 7:147. doi: 10.1186/1756-3305-7-147/FIGURES/4

Diarra, M., Fall, M., Lancelot, R., Diop, A., Fall, A. G., Dicko, A., et al. (2015). Modelling the abundances of two major Culicoides (Diptera: Ceratopogonidae) species in the Niayes area of Senegal. *PLoS One* 10:e0131021. doi: 10.1371/JOURNAL.PONE.0131021

Durr, P. A., Graham, K., and van Klinken, R. D. (2017). Sellers' revisited: a big data reassessment of historical outbreaks of bluetongue and African horse sickness due to the long-distance wind dispersion of Culicoides midges. *Front. Vet. Sci.* 4:98. doi: 10.3389/fvets.2017.00098

Elbers, A. R., Backx, A., Meroc, E., Gerbier, G., Staubach, C., Hendrickx, G., et al. (2008). Field observations during the bluetongue serotype 8 epidemic in 2006. Detection of first outbreaks and clinical signs in sheep and cattle in Belgium, France and the Netherlands. *Prev. Vet. Med.* 87, 21–30. doi: 10.1016/j.prevetmed.2008.06.004

Elbers, A. R., Meiswinkel, R., van Weezep, E., van Oldruitenborgh-Oosterbaan, M. M. S., and Kooi, E. A. (2013). Schmallenberg virus in *Culicoides* spp. biting midges, the Netherlands, 2011. *Emerg. Infect. Dis.* 19, 106–109. doi: 10.3201/eid1901.121054

Endoh, D., Mizutani, T., Kirisawa, R., Maki, Y., Saito, H., Kon, Y., et al. (2005). Species-independent detection of RNA virus by representational difference analysis using non-ribosomal hexanucleotides for reverse transcription. *Nucleic Acids Res.* 33:e65. doi: 10.1093/nar/gni064

Ferrara, G., Improda, E., Piscopo, F., Esposito, R., Iovane, G., Pagnini, U., et al. (2023b). Bluetongue virus seroprevalence and risk factor analysis in cattle and water buffalo in southern Italy (Campania region). *Vet. Res. Commun.* 1–6. doi: 10.1007/s11259-023-10215-w

Ferrara, G., Wernike, K., Iovane, G., Pagnini, U., and Montagnaro, S. (2023a). First evidence of Schmallenberg virus infection in southern Italy. *BMC Vet. Res.* 19:95. doi: 10.1186/s12917-023-03666-5

Folmer, O., Black, M., Hoeh, W., Lutz, R., and Vrijenhoek, R. (1994). DNA primers for amplification of mitochondrial cytochrome C oxidase subunit I from diverse metazoan invertebrates. *Mol. Mar. Biol. Biotechnol.* 5, 294–299. doi: 10.1371/journal.pone.0013102

Gaillet, M., Pichard, C., Restrepo, J., Lavergne, A., Perez, L., Enfissi, A., et al. (2021). Outbreak of Oropouche virus in French Guiana. *Emerg. Infect. Dis.* 27, 2711–2714. doi: 10.3201/eid2710.204760

Garros, C., Labuschagne, K., Dommergues, L., Balenghien, T., Muñoz, F., Bakhoum, M. T., et al. (2019). *Culicoides Latreille* in the sun: faunistic inventory of *Culicoides* species (Diptera: Ceratopogonidae) in Mayotte (Comoros archipelago, Indian Ocean). *Parasit. Vectors* 12:135. doi: 10.1186/s13071-019-3379-x

Glick, J. I. (1990). Culicoides biting midges (Diptera: Ceratopogonidae) of Kenya. *J. Med. Entomol.* 27, 85–195. doi: 10.1093/jmedent/27.2.85

Grewar, J. D. (2016). The economic impact of bluetongue and other orbiviruses in sub-Saharan Africa, with special reference to southern Africa. *Vet. Ital.* 52, 375–381. doi: 10.12834/VetIt.503.2427.3

Grimaud, Y., Guis, H., Chiroleu, F., Boucher, F., Tran, A., Rakotoarivony, I., et al. (2019). Modelling temporal dynamics of Culicoides Latreille (Diptera: Ceratopogonidae) populations on Reunion Island (Indian Ocean), vectors of viruses of veterinary importance. *Parasit. Vectors* 12, 562–517. doi: 10.1186/s13071-019-3812-1

Guindon, S., Dufayard, J. F., Lefort, V., Anisimova, M., Hordijk, W., and Gascuel, O. (2010). New algorithms and methods to estimate maximum-likelihood phylogenies: assessing the performance of PhyML 3.0. *Syst. Biol.* 59, 307–321. doi: 10.1093/sysbio/syq010

Hermanns, K., Marklewitz, M., Zirkel, F., Kopp, A., Kramer-Schadt, S., and Junglen, S. (2023). Mosquito community composition shapes virus prevalence patterns along anthropogenic disturbance gradients. *elife* 12:e66550. doi: 10.7554/eLife.66550

Hoffmann, B., Scheuch, M., Höper, D., Jungblut, R., Holsteg, M., Schirrmeier, H., et al. (2012). Novel orthobunyavirus in cattle, Europe, 2011. *Emerg. Infect. Dis.* 18, 469–472. doi: 10.3201/eid1803.111905

Jones, P., Binns, D., Chang, H. Y., Fraser, M., Li, W., McAnulla, C., et al. (2014). InterProScan 5: genome-scale protein function classification. *Bioinformatics* 30, 1236–1240. doi: 10.1093/BIOINFORMATICS/BTU031

Junglen, S., Kopp, A., Kurth, A., Pauli, G., Ellerbrok, H., and Leendertz, F. H. (2009). A new *flavivirus* and a new vector: characterization of a novel flavivirus isolated from *Uranotaenia* mosquitoes from a tropical rain Forest. *J. Virol.* 83, 4462–4468. doi: 10.1128/JVI.00014-09

Kearse, M., Moir, R., Wilson, A., Stones-Havas, S., Cheung, M., Sturrock, S., et al. (2012). Geneious basic: an integrated and extendable desktop software platform for the organization and analysis of sequence data. *Bioinformatics* 28, 1647–1649. doi: 10.1093/bioinformatics/bts199

Kirk-Spriggs, A. H., and Sinclair, B. J. (2017). *Manual of Afrotropical Diptera, volume 2: Nematocera & Lower Brachycera | NHBS Academic & Professional Books*. SANBI Publishing. Coimbatore

Kremer, M., Molet, B., Rebholtz-hirtzel, C., and Delecolle, J. C. (1974). *Culicoides nubeculosus* (Ceratopogonidae) feeding on engorged *Aedes aegypti* under laboratory conditions. *Mosq. News* 34, 471–472.

Kuno, G., Mackenzie, J. S., Junglen, S., Hubálek, Z., Plyusnin, A., and Gubler, D. J. (2017). Vertebrate reservoirs of arboviruses: myth, synonym of amplifier, or reality? *Viruses* 9, 1–28. doi: 10.3390/v9070185

Laguna-Aguilar, M., Alvarado-Moreno, M. S., Sánchez-Rodríguez, O. S., Ramírez-Jiménez, R., Zárate-Nahón, E. A., Sánchez-Casas, R. M., et al. (2012). Field evaluation of a novel trap baited with carbon dioxide produced by yeast for the collection of female *Aedes aegypti* mosquitoes in Mexico. *Southwest. Entomol.* 37, 495–504. doi: 10.3958/059.037.0407

Langat, K. S., Eyase, F., Bulimo, W., Lutomiah, J., Oyola, S. O., Imbuga, M., et al. (2021). Profiling of RNA viruses in biting midges (Ceratopogonidae) and related Diptera from Kenya using metagenomics and metabarcoding analysis. *mSphere* 6, e00551–e00521. doi: 10.1128/mSphere.00551-21

Lassen, S. B., Nielsen, S. A., and Kristensen, M. (2012). Identity and diversity of blood meal hosts of biting midges in Denmark. *Parasit. Vectors* 5:143. doi: 10.1186/1756-3305-5-143

Lefkowitz, E. J., Dempsey, D. M., Hendrickson, R. C., Orton, R. J., Siddell, S. G., and Smith, D. B. (2018). Virus taxonomy: the database of the international committee on taxonomy of viruses (ICTV). *Nucleic Acids Res.* 46, D708–D717. doi: 10.1093/nar/gkx932

Leta, S., Fetene, E., Mulatu, T., Amenu, K., Jaleta, M. B., Beyene, T. J., et al. (2019). Updating the global occurrence of *Culicoides imicola*, a vector for emerging viral diseases. *Sci. Data* 6, 185–188. doi: 10.1038/s41597-019-0197-0

Ma, Y., Xu, J., Yang, Z., Wang, X., Lin, Z., Zhao, W., et al. (2013). A video clip of the biting midge *Culicoides anophelis* ingesting blood from an engorged Anopheles mosquito in Hainan, China. *Parasit. Vectors* 6:326. doi: 10.1186/1756-3305-6-326/TABLES/1

Marklewitz, M., Dutari, L. C., Paraskevopoulou, S., Page, R. A., Loaiza, J. R., and Junglen, S. (2019). Diverse novel phleboviruses in sandflies from the Panama Canal area, Central Panama. *J. Gen. Virol.* 100, 938–949. doi: 10.1099/jgv.0.001260

Marklewitz, M., Handrick, S., Grasse, W., Kurth, A., Lukashev, A., Drosten, C., et al. (2011). Gouleako virus isolated from west African mosquitoes constitutes a proposed novel genus in the family Bunyaviridae. *J. Virol.* 85, 9227–9234. doi: 10.1128/jvi.00230-11

Marklewitz, M., Tchouassi, D. P., Hieke, C., Heyde, V., Torto, B., Sang, R., et al. (2020). Insights into the evolutionary origin of Mediterranean sandfly fever viruses. *mSphere* 5, e00598–e00520. doi: 10.1128/mSphere.00598-20

Martínez-de la Puente, J., Figuerola, J., and Soriguer, R. (2015). Fur or feather? Feeding preferences of species of Culicoides biting midges in Europe. *Trends Parasitol.* 31, 16–22. doi: 10.1016/j.pt.2014.11.002

Mathieu, B., Cêtre-Sossah, C., Garros, C., Chavernac, D., Balenghien, T., Carpenter, S., et al. (2012). Development and validation of IIKC: an interactive identification key for Culicoides (Diptera: Ceratopogonidae) females from the Western Palaearctic region. *Parasit Vectors* 5, 1–11. doi: 10.1186/1756-3305-5-137

Mauri, M., Elli, T., Caviglia, G., Uboldi, G., and Azzi, M. (2017). RAWGraphs: a visualisation platform to create open outputs. *Proc. ACM Int. Conf. Part F131371* 28, 1–5. doi: 10.1145/3125571.3125585

Mayo, C., McDermott, E., Kopanke, J., Stenglein, M., Lee, J., Mathiason, C., et al. (2020). Ecological dynamics impacting bluetongue virus transmission in North America. *Front. Vet. Sci* 7:186. doi: 10.3389/fvets.2020.00186

Mellor, P. S., Osborne, R., and Jennings, D. M. (1984). Isolation of bluetongue and related viruses from Culicoides spp. in the Sudan. *Epidemiol. Infect.* 93, 621–628. doi: 10.1017/S0022172400065190

Moustafa, K., Pam, D. L., and Meriem, H. B. (2016). Sero-epidemiology of bluetongue in Algerian ruminants. *Afr. J. Biotechnol.* 15, 868–871. doi: 10.5897/ajb2016.15343

Onyango, M. G., Michuki, G. N., Ogugo, M., Venter, G. J., Miranda, M. A., Elissa, N., et al. (2015). Delineation of the population genetic structure of Culicoides imicola in east and South Africa. *Parasit. Vectors* 8:660. doi: 10.1186/s13071-015-1277-4

Purse, B. V., Baylis, M., Tatem, A. J., Rogers, D. J., Mellor, P. S., Van Ham, M., et al. (2004). Predicting the risk of bluetongue through time: climate models of temporal patterns of outbreaks in Israel. *Rev. Sci. Tech.* 23, 761–775. doi: 10.20506/rst.23.3.1515

QGIS Development Team, (2019). Welcome to the QGIS project. Available at: https://qgis.org/en/site/ (accessed June 11, 2019).

R Core Team, (2016). *R: A language and environment for statistical computing*. Vienna, Austria: R Foundation for Statistical Computing.

Ratnasingham, S., and Hebert, P. D. N. (2007). BOLD: the barcode of life data system (http://www.barcodinglife.org). *Mol. Ecol. Notes* 7:355-64. doi: 10.1111/J.1471-8286.2007.01678.X

Reeves, L. E., Gillett-Kaufman, J. L., Kawahara, A. Y., and Kaufman, P. E. (2018). Barcoding blood meals: new vertebrate-specific primer sets for assigning taxonomic identities to host DNA from mosquito blood meals. *PLoS Negl. Trop. Dis.* 12:e0006767. doi: 10.1371/journal.pntd.0006767

Rivera, N. A., Varga, C., Ruder, M. G., Dorak, S. J., Roca, A. L., Novakofski, J. E., et al. (2021). Bluetongue and epizootic Hemorrhagic disease in the United States of America at the wildlife-livestock Interface. *Pathogens* 10:915. doi: 10.3390/pathogens10080915

Rodrigues, D. S. G., Medeiros, D. B. D. A., Rodrigues, S. G., Martins, L. C., de Lima, C. P. S., de Oliveira, L. F., et al. (2014). Pacui virus, Rio Preto da Eva virus, and Tapirape virus, three distinct viruses within the family Bunyaviridae. *Genome Announcents* 2, e00923–e00914. doi: 10.1128/genomeA.00923-14

Romero-Alvarez, D., and Escobar, L. E. (2018). Oropouche fever, an emergent disease from the Americas. *Microbes Infect.* 20, 135–146. doi: 10.1016/j.micinf.2017.11.013

Saeed, M. F., Li, L., Wang, H., Weaver, S. C., and Barrett, A. D. T. (2001). Phylogeny of the Simbu serogroup of the genus bunyavirus. *J. Gen. Virol.* 82, 2173–2181. doi: 10.1099/0022-1317-82-9-2173

Santiago-Alarcon, D., Havelka, P., Schaefer, H. M., and Segelbacher, G. (2012). Bloodmeal analysis reveals avian plasmodium infections and broad host preferences of culicoides (diptera: Ceratopogonidae) vectors. *PLoS One* 7:e31098. doi: 10.1371/journal.pone.0031098

Scheffer, E. G., Venter, G. J., Labuschagne, K., Page, P. C., Mullens, B. A., MacLachlan, N. J., et al. (2012). Comparison of two trapping methods for Culicoides biting midges and determination of African horse sickness virus prevalence in midge populations at Onderstepoort, South Africa. *Vet. Parasitol.* 185, 265–273. doi: 10.1016/J.VETPAR.2011.09.037

Ségard, A., Gardès, L., Jacquier, E., Grillet, C., Mathieu, B., Rakotoarivony, I., et al. (2018). Schmallenberg virus in *Culicoides* Latreille (Diptera: Ceratopogonidae) populations in France during 2011-2012 outbreak. *Transbound Emerg. Dis.* 65, e94–e103. doi: 10.1111/tbed.12686

Shchetinin, A. M., Lvov, D. K., Deriabin, P. G., Botikov, A. G., Gitelman, A. K., Kuhn, J. H., et al. (2015). Genetic and phylogenetic characterization of Tataguine and Witwatersrand viruses and other Orthobunyaviruses of the anopheles a, Capim, Guamá, Koongol, Mapputta, Tete, and Turlock serogroups. *Viruses* 7, 5987–6008. doi: 10.3390/V7112918

Sick, F., Beer, M., Kampen, H., and Wernike, K. (2019). *Culicoides* biting midges-underestimated vectors for arboviruses of public health and veterinary importance. *Viruses* 11:376. doi: 10.3390/v11040376.MDPIAG

Stallknecht, D. E., Allison, A. B., Park, A. W., Phillips, J. E., Goekjian, V. H., Nettles, V. F., et al. (2015). Apparent increase of reported hemorrhagic disease in the midwestern and northeastern USA. *J. Wildl. Dis.* 51, 348–361. doi: 10.7589/2013-12-330

Stokes, J. E., Tarlinton, R. E., Lovatt, F., Baylis, M., Carson, A., and Duncan, J. S. (2018). Survey to determine the farm-level impact of Schmallenberg virus during the 2016-2017 United Kingdom lambing season. *Vet. Rec.* 183:690. doi: 10.1136/vr.104866

Tchouassi, D. P., Marklewitz, M., Chepkorir, E., Zirkel, F., Agha, S. B., Tigoi, C. C., et al. (2019). Sand fly-associated Phlebovirus with evidence of neutralizing antibodies in humans, Kenya. *Emerg. Infect. Dis.* 25, 681–690. doi: 10.3201/eid2504.180750

Tomazatos, A., Jöst, H., Schulze, J., Spînu, M., Schmidt-Chanasit, J., Cadar, D., et al. (2020). Blood-meal analysis of *Culicoides* (Diptera: Ceratopogonidae) reveals a broad host range and new species records for Romania. *Parasit. Vectors* 13:79. doi: 10.1186/s13071-020-3938-1

Toye, P. G., Batten, C. A., Kiara, H., Henstock, M. R., Edwards, L., Thumbi, S., et al. (2013). Bluetongue and epizootic haemorrhagic disease virus in local breeds of cattle in Kenya. *Res. Vet. Sci.* 94, 769–773. doi: 10.1016/j.rvsc.2012.11.001

Walker, A. R., and Boreham, P. F. L. (1976). Blood feeding of *Culicoides* (Diptera, Ceratopogonidae) in Kenya in relation to the epidemiology of bluetongue and ephemeral fever. *Bull. Entomol. Res.* 66, 181–188. doi: 10.1017/S000748530000660X

Youssef, L., Mounir, K., Mohamed, B., El Harrak, M., and Fihri, O. F. (2015). Spatial and seasonal distribution of Culicoides species in Morocco in relation to the transmission of bluetongue viruses. *Br. J. Virol.* 2, 88–95. doi: 10.17582/journal.bjv/2015.2.6.88.95

Žiegytė, R., Platonova, E., Kinderis, E., Mukhin, A., Palinauskas, V., and Bernotienė, R. (2021). Culicoides biting midges involved in transmission of haemoproteids. *Parasit. Vectors* 14:27. doi: 10.1186/S13071-020-04516-1/TABLES/2

frontiers | Frontiers in Microbiology

TYPE Original Research
PUBLISHED 05 January 2024
DOI 10.3389/fmicb.2023.1165378

OPEN ACCESS

EDITED BY
Julianne H. Grose,
Brigham Young University, United States

REVIEWED BY
Zheng Chen,
Jiangxi Agricultural University, China
Arup Banerjee,
Regional Centre for Biotechnology (RCB), India
Dengyuan Zhou,
Huazhong Agricultural University, China

*CORRESPONDENCE
Ke Liu
✉ liuke@shvri.ac.cn
Zhiyong Ma
✉ zhiyongma@shvri.ac.cn
Xiuli Feng
✉ xiulifeng@njau.edu.cn

RECEIVED 14 February 2023
ACCEPTED 11 December 2023
PUBLISHED 05 January 2024

CITATION
Chen M, Kang L, Zhang T, Zheng J, Chen D, Shao D, Li Z, Li B, Wei J, Qiu Y, Feng X, Ma Z and Liu K (2024) Circular RNA network plays a potential antiviral role in the early stage of JEV infection in mouse brain. *Front. Microbiol.* 14:1165378. doi: 10.3389/fmicb.2023.1165378

Circular RNA network plays a potential antiviral role in the early stage of JEV infection in mouse brain

Mengli Chen[1,2], Lei Kang[1,2], Tong Zhang[1], Jiayang Zheng[1], Dishi Chen[3], Donghua Shao[1], Zongjie Li[1], Beibei Li[1], Jianchao Wei[1], Yafeng Qiu[1], Xiuli Feng[2]*, Zhiyong Ma[1]* and Ke Liu[1]*

[1]Shanghai Veterinary Research Institute, Chinese Academy of Agricultural Science, Shanghai, China, [2]Key Laboratory of Animal Disease Diagnostic and Immunology, Department of Veterinary Medicine College, Nanjing Agricultural University, Nanjing, Jiangsu, China, [3]Sichuan Animal Disease Prevention and Control Center, Chengdu, China

Japanese encephalitis is one of the most important insect-borne infectious disease with public health concern. The virus can break the blood–brain barrier and cause death or long-term sequela in infected humans or animals. Viral encephalitis is an important clinical feature of JEV infection. In recent studies, CircRNAs and related ceRNAs data illustrated the regulative role in many aspects of biological process and disease duration. It is believed that CircRNA regulates JEV infection in a ceRNA-dependent mechanism. In this study, brain tissues of experimental mice were sequenced and analysised. 61 differentially expressed circRNAs, 172 differentially expressed miRNAs and 706 differentially expressed mRNAs were identified by RNA-Sequencing and statistical analysis. CX3CR1 was determined as a key host factor impact JEV infection by microRNA interference measurement. CX3CR1 interaction network indicated circStrbp/miR709/CX3CR1 as a functional regulation axis. Further sequencing in BV2 cell shown CX3CR1 is a special target of miR-709 only during JEV infection. In summary, our study presented a new ceRNA pathway that impact JEV infection *in vivo* and *in vitro*, which could be a therapeutic target to fight against JEV.

KEYWORDS

circular RNA, Japanese encephalitis, Japanese encephalitis virus, ceRNA, miR-709

1 Introduction

Japanese encephalitis is a zoonotic infectious disease transmitted by mosquitoes, and the pathogen, Japanese encephalitis virus (JEV), belong to *Flaviviridae* which is an important part of arboviruses (Huang et al., 2014). JEV infection can cause viral encephalitis in humans and nervous system or organ infection in animals (Daep et al., 2014). Related to mosquito-borne vectors, Japanese encephalitis mainly spreads in tropical and subtropical regions. Cases of Japanese encephalitis in China mainly occur in southern regions (Zheng et al., 2012; Le Flohic et al., 2013). JEV infection can cause fatal viral encephalitis or viral encephalitis with sequelae in humans, orchitis in boars and abortion in sows, and different diseases in birds (Di et al., 2020; Hameed et al., 2021; Bharucha et al., 2022; Pichl et al., 2022).

Therefore, Japanese encephalitis is an infectious disease that endangers public health (Daep et al., 2014).

The greatest threat of JEV infection is the destruction of the host's brain tissue. Once the virus invades the brain tissue, it will cause an uncontrollable inflammatory response in a short period of time, leading to host fatality (Yun and Lee, 2014). Even if the host survives, the risk of sequelae is 50%. From the perspective of cytokines, this process mainly involves TNF-α, interleukins, and chemokines (Liu et al., 2018). Among them, inflammatory chemokines and homeostasis-regulating chemokines play important roles. We found in previous studies that CCR5- and CCR2-related chemokines (CCL3, CCL4, and CCL5) play key roles in Japanese encephalitis and that these chemokines are potential targets for the treatment of viral encephalitis (Liu et al., 2018). We also found that the brain- and liver-specific chemokine CX3CL1 was downregulated during JEV infection. CX3CL1 is a bifunctional chemokine that participates in the regulation of inflammation and tissue homeostasis. No study has clarified the relationship between the downregulated expression of CX3CL1-CX3CR1 axis and JEV infection of brain. In this study, we explored this issue from the perspective of circRNA-miRNA-mRNA.

In 2013, a large number of circRNAs were discovered with the help of high-throughput sequencing technology, proving that circRNAs are important RNA components in organisms (Memczak et al., 2013). With advancements in research, circRNAs have been proven to act as miRNA sponges and protein sponges and affecting protein expression (Chen, 2016). circRNAs, which act as miRNA sponges, adsorb miRNAs and further regulate the expression of mRNAs, which is the most studied function of circRNAs (Hansen et al., 2013). circRNA-miRNA-mRNA has been proven to play an important role in chronic diseases such as cancer, brain tissue disease, and vascular disease (Wang et al., 2021; Zhu et al., 2021; Xie et al., 2022). The abnormal expression of circRNA slowly promotes changes in miRNA–mRNA expression and gradually leads to the occurrence of chronic diseases. Among the many studies on circRNA-miRNA-mRNA, only a few have focused on circRNA-miRNA-mRNA related to viral infection (Lu et al., 2020; Hu et al., 2021; Li et al., 2021; Shi et al., 2021; Zhao et al., 2021; Chen et al., 2022), in particular acute viral infection, probably due to the weak regulatory effect of circRNA-miRNA-mRNA on viruses. However, a JEV infection model has been shown to be useful for research on viral circRNA-miRNA-mRNA. JEV infection of mouse brain tissue can cause significant changes in circRNA_0000220 and the downstream targets of circRNA_0000220, i.e., miR-326-3p and BCL3/MK2/TRIM25, ultimately affecting the occurrence of viral encephalitis (Li et al., 2020).

In this study, we focused on the early stages of JEV infection of mouse brain tissue and mouse microglia cell. Through high-throughput sequencing, we discovered the network through which circRNA-miRNA regulates CX3CR1 and demonstrated the inhibitory effect of this regulation on JEV. The findings indicate that the changes in circRNA-miRNA in the early stage of infection can regulate the expression of CX3CR1 and affect the early stage of virus infection.

2 Materials and methods

2.1 Ethics statement

Mouse experiments were performed in compliance with the Guidelines on the Human Treatment of Laboratory Animals (Ministry of Science and Technology of the People's Republic of China, Policy No. 2006 398) and were approved by the Institutional Animal Care and Use Committee at the Shanghai Veterinary Research Institute (IACUC No: Shvri-Pi-0124).

2.2 Cells, viruses and mice

Mouse microglia (BV2) cells, Baby hamster kidney (BHK-21) cells and African green monkey kidney (Vero) cells were purchased from the ATCC (Rockville, Maryland) and maintained in Dulbecco's modified Eagle's medium (DMEM) supplemented with 10% fetal bovine serum (FBS) at 37°C in a 5% CO2 incubator.

JEV NJ2008 strain (Genbank No. GQ918133) was used in study. Virus was propagated in BHK-21 cells and titrated in Vero cells.

8 weeks specific pathogen free (SPF) female C57BL/6 mice were grouped and infected in this study. Mice were purchased from Shanghai SLAC Laboratory Animal Co., Ltd. and maintained under pathogen-free conditions.

2.3 Mouse infection and sampling

Grouped C57BL/6 mice were injected intraperitoneally (i.p.) with 4×10^6 PFU of JEV or phosphate buffered saline (PBS). All infected or mock infected mice were maintained under pathogen-free conditions in animal central of Shanghai Veterinary Research Institute. The mice were sacrificed at 5, 7, 8, 9 and 10 days after injection, then mouse brain, blood, lymph nodes were collected. Brain samples collected at 7 day post injection were send for CircRNA-miRNA-mRNA sequencing. Other samples for qPCR detection were stored at minus 80°C.

2.4 RNA sequencing analysis

Three biological replicates of the infected and mock infected samples at 7 day after injection were used for circRNA, miRNA and mRNA sequencing. For circRNA sequencing, total RNA was extracted and digested with RNase R to degest linear RNA and was further purified by using RNeasy MinElute Cleanup Kit (Qiagen). NEBNext Ultra Directional RNA Library Prep Kit for Illumina was used for constructing the strand-specific library according to the manufacturer's instructions. The miRNA sequencing libraries were generated by using the Small RNA Sample Pre Kit (Illumina) and the mRNA were enriched by using Oligo(dT) magnetic beads. The next step was similar with circRNAs sequencing. To get the clean data (clean reads), reads containing poly-N or adapter sequence and reads of low-quality were removed. Candidate circRNAs were subjected to blast in the circBase database for annotation, and unannotated circRNAs were recognized as novel ones. miRNAs and mRNAs were aligned by using bowtie tools or to the mouse reference genome (GRCm38/mm10), respectively. The DESeq2 package and the edgeR package (http://www.r-project.org/, accessed 21 May 2019) were applied to analyze differentially expressed circRNAs and mRNAs, respectively. Candidates were considered significantly differentially expressed ones if a fold change 2 and a p value <0.05.

In addition to combined sequencing, BV2 cells transfected with siRNA were subjected to RNA-Seq sequencing. Three biological

replicates of the infected and mock infected samples were collected, treated and analysed as above.

2.5 Quantitative PCR

For circRNA, miRNA, and mRNA expression analysis, total RNA was extracted from mice brain using TRIzol Reagent (Life Technologies). cDNA was immediately reverse-transcribed using RT Master Mix (TaKaRa, Tokyo, Japan). JEV or gene mRNA levels were detected by a SYBR quantitative PCR (qPCR). PCR was performed using an ABI Prism 7,900 sequence-detection system (Applied Biosystems, Foster City, CA, United States), using SYBR Green PCR Master Mix. The amount of target gene expression was calculated from the respective standard curves and normalized using glyceraldehyde-3-phosphate dehydrogenase (GAPDH), and displayed as fold change. Briefly, mock infected mice collected at the same time points were measured and set as 1. Then, JEV infected mice were calculated referenced to mock and presented as fold change. Relative gene expression to the control was determined by the standard $2^{-\Delta\Delta Ct}$ method. Mice chemokine primer was a kindly gift from Dr. Clive S. McKimmie and Dr. Gerard J. Graham.

2.6 RNA interference

Small interfering RNAs (siRNAs) targeting the indicated genes were synthesized chemically. A negative siRNA without known target genes was synthesized as control. The siRNA sequences are shown in S1 Table. BV2 cells were plated in DMEM medium containing 10% FBS at 37°C overnight, washed with PBS, and transfected with siRNA at a concentration of 20 nM using Lipofectamine 2000 (Thermo Fisher Scientific), according to the manufacturer's protocol. The transfectants were re-cultured at 37°C for 24 h and subsequently inoculated with JEV at a MOI of 0.1. JEV replication in the transfectants was determined by qPCR at 24 h post-infection (hpi).

2.7 Statistical analysis

All the measurements were conducted in triplicate in at least three independent experiments. Mean values ± standard deviation (SD) was calculated using Microsoft Excel. Statistical analysis was done by Student's t test or log rank test and values were considered significant when $p < 0.05$. Figures were made using the GraphPad™ Prism 5.0 software.

3 Results

3.1 Expression characteristics of circRNAs in JEV-infected mouse brain tissue

To analyze the characteristics of circRNA expression changes in JEV-infected mouse brain tissue in the early stage, JEV was intraperitoneally injected into mice, and brain tissue samples were collected 7 days after infection (Figure 1A). The samples were processed for high-throughput sequencing analysis.

First, the differential expression of circRNAs in JEV-infected mouse brain tissue was analyzed. Through second-generation high-throughput sequencing, a total of 29,129 circRNAs were detected in mouse brain tissue samples (Supplementary Figure S1A). A total of 74.82% of these circRNAs were 100 to 2,500 nt long, and 15.86% of these circRNAs were longer than 10,000 nt (Supplementary Figure S1B). Therefore, most of the identified circRNAs fell within these 2 length ranges. Chromosomes derived from circRNAs were evenly distributed, and the chromosomal origins of circRNAs were not significantly different between the JEV-infected group and the uninfected group (mock group), both with chr2 as the main origin (Supplementary Figure S1C).

The differential expression of total circRNAs between the JEV-infected and mock groups was analyzed (2-fold change in expression, false discovery rate (FDR) < 0.05), and 61 circRNAs were found to be differentially expressed between the 2 groups (Figure 1B). In a comparison with the circRNAs in the mock group, there were 33 downregulated circRNAs and 28 upregulated circRNAs in the JEV-infected group (Figure 1C). A total of 90.16% of the 61 differentially expressed circRNAs were derived from exons (Figure 1D), and 88.52% of the 61 differentially expressed circRNAs were 100 to 2,500 nt long (Figure 1E). The small portion (61/29,129) of differentially expressed circRNAs after JEV infection indicates that the circRNAs were generally little affected by JEV infection. This result is consistent with the results of the previously published article (Li et al., 2020).

3.2 Cerna network in the brain tissue of JEV-infected mice

In addition to circRNAs, high-throughput sequencing of miRNAs and mRNAs in mouse brain tissue was also performed. A total of 172 differentially expressed (fold change>2, $p < 0.05$) miRNAs (Supplementary Figures S2A,B) and 706 differentially expressed mRNAs (Supplementary Figures S2C,D) were obtained from the analysis of total miRNAs and mRNAs. Then, the competing endogenous RNA (ceRNA) network was obtained from a correlation analysis of circRNAs, miRNAs and mRNAs. In the circRNA-miRNA-mRNA interaction network (Figure 2A), circRNAs act as adsorption sponges with mRNAs as the ultimate targets, and miRNAs bridge circRNAs and mRNAs and act as mediators that directly interact with circRNAs and mRNAs (Hansen et al., 2013). Therefore, we organized a structure of the ceRNA interaction network centered on miRNA. There were 136 miRNAs in the ceRNA network, most of which were upregulated, to a maximum fold change of 20. Each miRNA generally adsorbed 1–11 circRNAs, but most miRNAs adsorbed 2–5 circRNAs. Each miRNA generally targeted 1–42 mRNAs, but most miRNAs targeted approximately 10 mRNAs (Supplement files). The number of genes adsorbed and targeted and the binding efficiency of miRNAs are key factors that affect the effectiveness of miRNAs. Using circMir software, the free energy of an miRNA binding with circRNAs and mRNAs was analyzed to estimate the binding efficiency of the miRNA. miRNA background expression level and fold change are other factors that affect the effectiveness of miRNAs. Specifically, the higher the expression of a functional miRNA, the stronger is the potential biological effect of the miRNA. The binding targets of each miRNA were scored based on the

10.3389/fmicb.2023.1165378

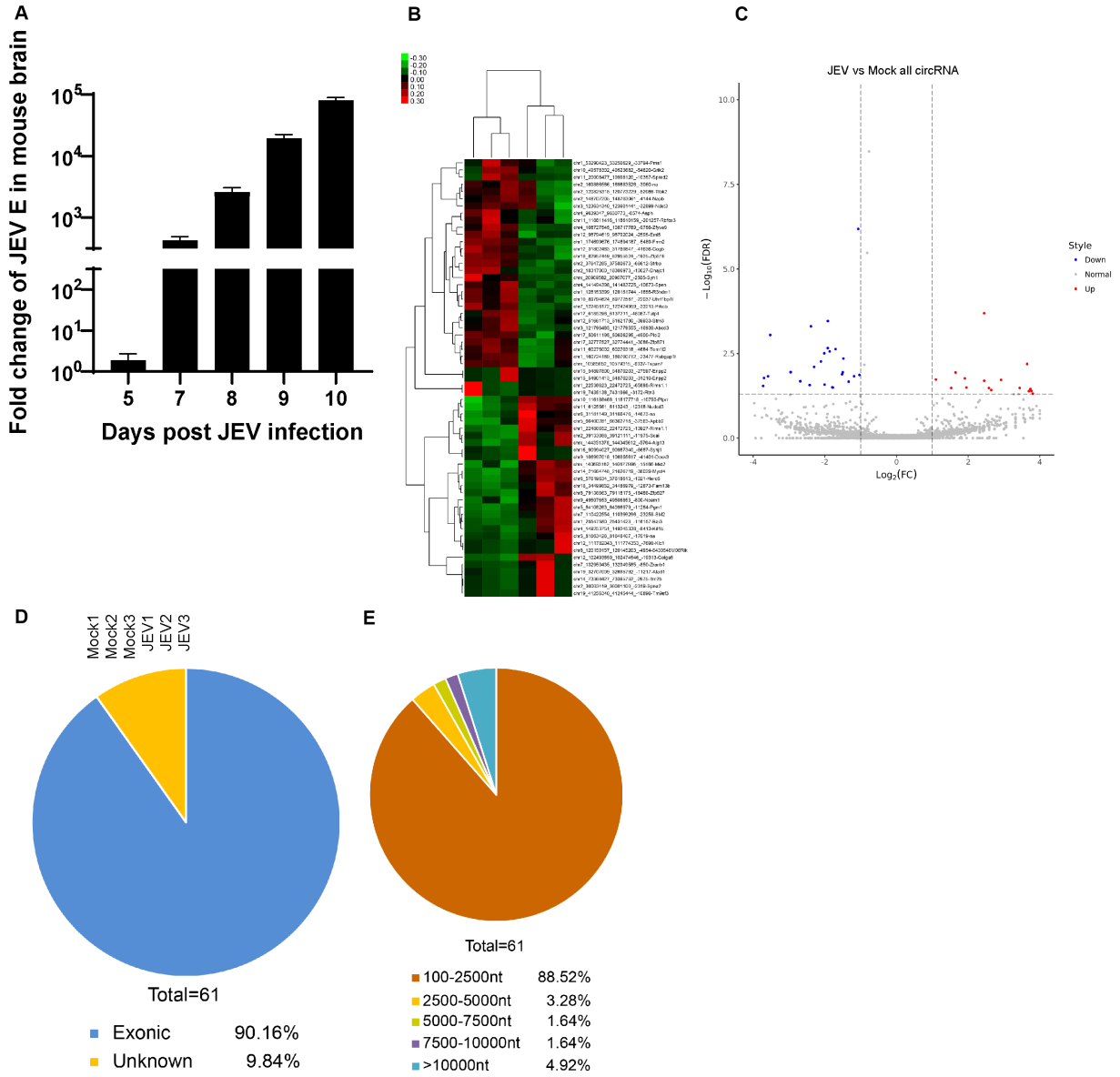

FIGURE 1
The characteristics of circRNA during JEV infection in mouse brain. **(A)** Viral fold change in mouse brain. JEV (4×10^6 PFU) was injected intraperitoneally. The viral load was determined by detecting JEV envelope **(E)** gene and normalized with mouse GAPDH. All fold changes were measured by Real-time PCR. Data are shown as the mean ± standard error (SEM). Six mice for each group were detected, and the experiments were repeated three times. **(B,C)** Heat map **(B)** and Volcanic map **(C)** of differently expressed circRNAs enriched in mouse brain. Red color represents up-regulations and other colors represent down-regulatons. Difference were calculated as significant if a fold change >2 and a *p* value <0.05. **(D)** The genomic distribution of differently expressed circRNAs. Exonic, intron and unknown distribution were measured. **(E)** The length distribution of differently expressed circRNAs. Length range from 100 to more than 10,000 were analysed.

targets, free energy, and expression levels in the ceRNA data. A ceRNA interaction network diagram was obtained using the ceRNA interaction network and these scores (Table 1).

For the ceRNA network, the circRNAs (downregulated) Tulp4 and zfyve9, miRNAs (upregulated) miR-6974-3p and miR-3547-5p, and mRNAs (downregulated) Bmp7, Kcne2, Nrarp, and Mlc1 were randomly selected for qPCR validation analysis. High-throughput sequencing samples indicated differential changes at one time point. To further understand these biological processes, we infected mice with the same titer of JEV for validation and collected tissue samples 5–10 days after infection to detect changes in gene expression in a time-dependent manner. The expression levels of Tulp4 and zfyve9 were significantly lower in the brain tissue of infected mice than in the brain tissue of mice in the mock group, and zfyve9 expression was generally stable in the infected mice, showing a slow downward trend over time after infection (Figure 2B). The expression levels of miR-6974-3p and miR-3547-5p were significantly higher in the brain tissue of infected mice than in the brain tissue of mice in the mock group and increased with over time after infection. The expression levels of Bmp7, Kcne2, Nrarp and Mlc1 were significantly lower in the JEV-infected group than in the mock group. Except for Nrarp, the expression levels of the other mRNAs decreased over time after

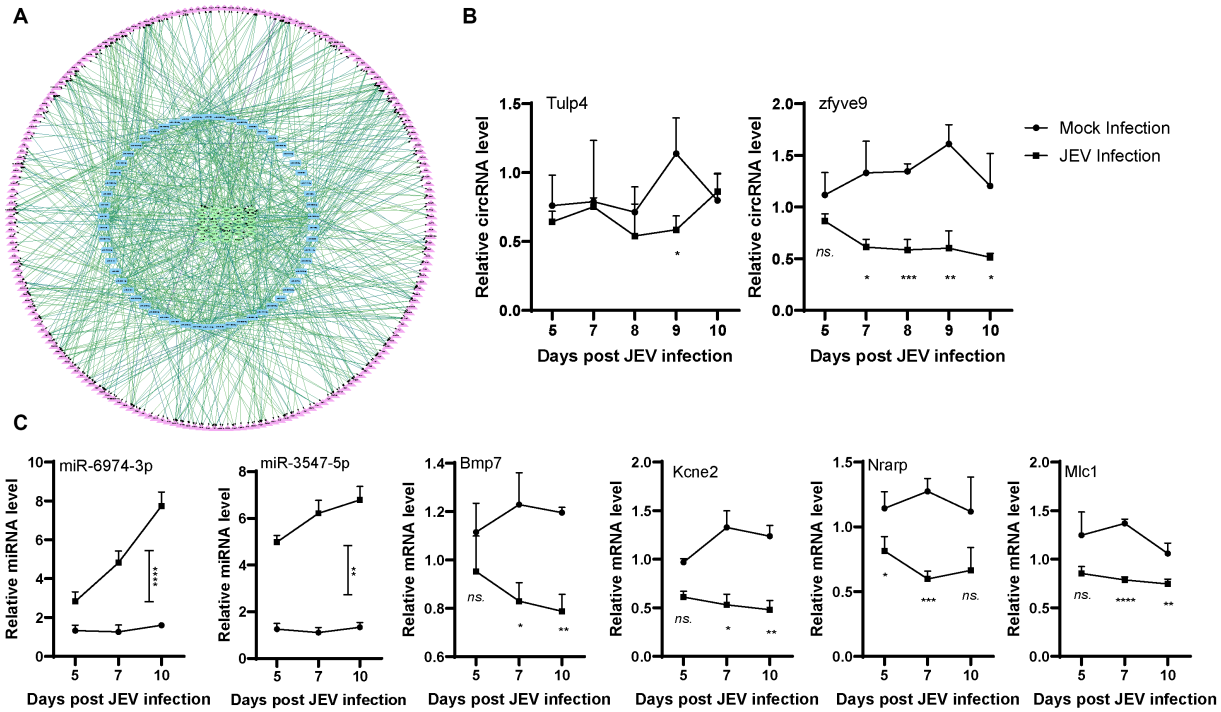

FIGURE 2
Network of differently expressed ceRNA. **(A)**. circRNA (green)-miRNA (blue)-mRNA (purple) interaction network. CircRNA is inside the circle with green frame, miRNA is in the middle of the circle with blue frame, mRNA is outside the circle with purple frame. **(B,C)**. Validation of circRNAs, miRNAs and mRNAs expression in infected mouse. Mice were infected or mock infected with JEV. Mouse brain was sampled in the indicated time points, then representative circRNAs, miRNAs and mRNAs were detected by qPCR.

infection (Figure 2C). These findings are mostly consistent with the ceRNA high-throughput sequencing results, indicating that the ceRNA high-throughput sequencing results were reliable and that the changes in expression for each gene in the ceRNA network after JEV infection are time dependent.

3.3 The chemokine CX3CR1 is regulated by circRNA-miRNA

The ceRNA network regulates many target genes and exerts complex biological functions. We sought to identify a ceRNA network related to viral encephalitis. The sequencing data indicted that CX3CR1 is affected by a series of miRNAs and circRNAs. To better analyze the central role of miRNAs, we scored individual miRNAs according to expression level, binding free energy and number of target genes. High expression levels and low free energy are important factors for adding scores. In addition, we hypothesized that too many target molecules of miRNA would reduce the biological functional strength of miRNAs, so the number of target molecules is negatively correlated with miRNA scoring (Yang et al., 2021). In our ceRNA network, 9 miRNAs targeted CX3CR1, and these 9 miRNAs were scored based on expression, binding free energy and number of targets comprehensively (Table 2). Among the 9 miRNAs, miR-709 had the highest score, implying that miR-709 is an important miRNA that may affect the expression of CX3CR1. These miRNAs are upregulated (4 to 8-fold) after JEV infection, and each miRNA adsorbed 2 to 9 circRNAs, among which Strbp, Tulp4, and Zfyve9 were the most frequently occurring circRNAs, indicating that these 3 circRNAs are likely to bind miRNAs through adsorption and further regulate the expression of CX3CR1.

The ceRNA network is complex, and miRNAs and circRNAs targeting CX3CR1 also regulate other genes (Figure 3A; Table 2). From another perspective, the network serves to selectively regulates the expression of CX3CR1, further reflecting the complexity of biology. To confirm that CX3CR1 is regulated by circRNA-miRNA, we selected the highest scoring miRNA, miR-709, for *in vitro* validation. First, qPCR was used to analyze the expression of miR-709, circStrbp, and CX3CR1 in JEV-infected mouse brain tissue, with miR-3547 used as a control. The results indicated that the expression level of miR-709 increased over time after infection and that the expression levels of circStrbp and CX3CR1 decreased over time after infection (Figure 3B). The trend of circStrbp-miR-709-CX3CR1 expression detected by qPCR was consistent with the ceRNA results obtained by high-throughput sequencing, indicating a potential regulatory relationship among circStrbp-miR-709-CX3CR1.

To further analysis the ceRNA network function in JEV infection, circStrbp RNAi method was employed. The BV2 cells were transfected with circStrbp siRNA or normal control (NC), then inoculated with 0.1 MOI of JEV 24 h after transfection, and collected for detection 24 h after infection. Interference efficiency of circStrbp siRNA was firstly measured by using qPCR. circStrbp was significantly decreased in siRNA transfeced cells (Figure 3C). As expected, circStrbp related miR-709 and CX3CR1 mRNA were significantly changed after

10.3389/fmicb.2023.1165378

TABLE 1 Profile of ceRNA in JEV infected mouse brain based on miRNA.

miRNA	Log2FC	FDR	Style	Number of miRNA-mRNA	Number of miRNA-CircRNA
mmu-miR-1198-3p	4.354	0.000049599122204674	Up	5	1
mmu-miR-1224-3p	6.318	0.0351095494688527	Up	24	3
mmu-miR-136-5p	−1.822	0.0487122507988076	down	1	4
mmu-miR-141-3p	3.212	0.0174460832523778	up	4	4
mmu-miR-142a-3p	2.780	0.0362638626102003	up	2	2
mmu-miR-149-3p	4.232	0.000319079971256809	up	35	2
mmu-miR-155-5p	4.285	0.000634899620817067	up	2	2
mmu-miR-1668	5.258	0.0251796787996459	up	6	3
mmu-miR-1892	7.261	0.0407966651019063	up	24	5
mmu-miR-1893	7.007	0.00899413636337472	up	1	1
mmu-miR-1897-5p	4.832	0.000342747015051776	up	4	3
mmu-miR-1903	4.029	0.00384701087453602	up	11	11
mmu-miR-1904	3.837	0.00331039855704739	up	16	7
mmu-miR-1906	5.117	0.00412344272229418	up	30	5
mmu-miR-191-5p	−1.861	0.04255097434091	down	1	1
mmu-miR-1934-3p	5.337	1.67489304823256E-07	up	4	3
mmu-miR-1934-5p	5.071	0.0000669276227204325	up	11	6
mmu-miR-1943-5p	4.051	0.00234750264197207	up	32	3
mmu-miR-1946a	5.411	8.93702845873959E-06	up	7	3
mmu-miR-1946b	5.228	0.0000193173326343373	up	7	1
mmu-miR-1954	4.545	0.00141347398704677	up	15	3
mmu-miR-1957a	5.641	2.80951635748803E-10	up	4	1
mmu-miR-1957b	4.206	0.000431442637061225	up	5	1
mmu-miR-1967	6.135	0.000997225904950666	up	8	2
mmu-miR-199b-5p	−1.901	0.0340954165590419	down	13	6
mmu-miR-200c-5p	5.198	0.00141347398704677	up	1	2
mmu-miR-219a-1-3p	4.980	0.00625810142621969	up	3	2
mmu-miR-21a-3p	2.172	0.0494699059120279	up	12	4
mmu-miR-2861	7.318	0.00385392970056958	up	13	4
mmu-miR-3061-5p	4.403	0.00163651041239826	up	10	1
mmu-miR-3112-3p	4.299	0.0277535892236198	up	2	3
mmu-miR-320-5p	5.102	0.0259077898099045	up	21	7
mmu-miR-326-3p	−2.988	0.000103988200795178	down	21	9
mmu-miR-329-5p	−1.927	0.0273670106681081	down	7	4
mmu-miR-346-3p	6.484	2.46384407557472E-11	up	34	3
mmu-miR-3470a	5.605	2.35273705619275E-09	up	9	5
mmu-miR-3470b	5.850	2.40270286547131E-11	up	11	2
mmu-miR-3473a	5.422	0.0000400854861074338	up	8	2
mmu-miR-3473b	6.386	2.46384407557472E-11	up	18	4
mmu-miR-3473c	5.956	4.97147489813369E-11	up	19	5
mmu-miR-3473e	6.984	1.06955113712167E-12	up	18	3
mmu-miR-3547-5p	6.587	0.00036619368479388	up	37	9

(Continued)

10.3389/fmicb.2023.1165378

TABLE 1 (Continued)

miRNA	Log2FC	FDR	Style	Number of miRNA-mRNA	Number of miRNA-CircRNA
mmu-miR-3620-5p	5.693	0.00287623388474358	up	18	5
mmu-miR-376a-3p	−1.864	0.0425997704711526	down	1	1
mmu-miR-3960	7.308	0.00141347398704677	up	5	1
mmu-miR-455-3p	−2.341	0.00891332667445275	down	14	6
mmu-miR-466i-5p	4.276	0.0000334778362810868	up	28	1
mmu-miR-466j	3.803	0.0166799939343183	up	20	3
mmu-miR-466 k	4.700	7.96549854883085E-06	up	29	3
mmu-miR-495-3p	−1.910	0.0314062492584068	down	4	2
mmu-miR-5098	4.775	0.000174242767966446	up	1	1
mmu-miR-5106	8.347	1.08005791442604E-12	up	16	4
mmu-miR-5112	4.523	0.0000530957128344883	up	11	3
mmu-miR-5114	4.496	0.0169258868672246	up	15	5
mmu-miR-5121	6.117	0.00141347398704677	up	4	2
mmu-miR-5128	6.121	0.0020577634593746	up	5	1
mmu-miR-5130	6.368	0.0173183661799466	up	9	1
mmu-miR-532-5p	−2.423	0.0088738742848416	down	11	5
mmu-miR-543-3p	−1.859	0.0487122507988076	down	1	3
mmu-miR-615-5p	6.624	0.00141347398704677	up	6	2
mmu-miR-6238	4.213	0.000174548270725916	up	1	1
mmu-miR-6366	5.179	0.0127278535486286	up	12	1
mmu-miR-6368	3.974	0.0234283989841492	up	25	7
mmu-miR-6372	5.018	0.0407966651019063	up	6	6
mmu-miR-6380	4.625	0.0159604685145588	up	4	2
mmu-miR-6393	8.166	0.00385392970056958	up	9	2
mmu-miR-6404	6.210	0.0296114257249124	up	19	7
mmu-miR-652-5p	−2.241	0.0373874212508746	down	8	1
mmu-miR-665-3p	−1.961	0.0325912135152282	down	33	8
mmu-miR-677-3p	5.031	0.0032312965958258	up	22	5
mmu-miR-680	7.085	0.00504177392794773	up	10	5
mmu-miR-683	2.568	0.0456928790631196	up	7	7
mmu-miR-690	6.103	2.29537891480982E-09	up	2	2
mmu-miR-692	6.005	0.00190160169504928	up	4	5
mmu-miR-6921-5p	6.131	0.0407966651019063	up	16	4
mmu-miR-6925-5p	6.151	0.02019673764755	up	26	3
mmu-miR-6931-5p	6.986	0.000297048033031346	up	42	3
mmu-miR-6936-5p	5.273	0.0174460832523778	up	11	3
mmu-miR-6937-5p	4.823	0.0000418802801207815	up	10	3
mmu-miR-6955-3p	5.719	0.00759222820514879	up	8	3
mmu-miR-6957-5p	8.234	7.32101541376813E-10	up	14	4
mmu-miR-696	10.141	2.18807307533137E-10	up	4	1
mmu-miR-6961-5p	20	0.00839672354830158	up	8	4
mmu-miR-6963-3p	4.086	0.0374168535124453	up	11	4

(Continued)

TABLE 1 (Continued)

miRNA	Log2FC	FDR	Style	Number of miRNA-mRNA	Number of miRNA-CircRNA
mmu-miR-6963-5p	5.294	0.0484222299598572	up	18	5
mmu-miR-6971-5p	5.890	0.0251085195447356	up	27	2
mmu-miR-6973a-5p	12.804	4.0347785792735E-07	up	9	1
mmu-miR-6973b-5p	6.025	0.0243289483982281	up	10	1
mmu-miR-6974-3p	6.904	0.0313736349917696	up	19	6
mmu-miR-6978-5p	5.493	0.000742500462525439	up	8	1
mmu-miR-6979-5p	4.473	0.0251085195447356	up	14	1
mmu-miR-6981-3p	20	0.0238138902402119	up	11	2
mmu-miR-6981-5p	5.266	0.000375612841723136	up	34	3
mmu-miR-6989-5p	5.119	0.0494699059120279	up	13	3
mmu-miR-6992-5p	4.582	0.0243289483982281	up	16	9
mmu-miR-6995-3p	4.504	0.000963078614648598	up	10	4
mmu-miR-7007-5p	4.943	0.00442283369163749	up	24	3
mmu-miR-7011-3p	5.346	0.0000814711849479471	up	13	2
mmu-miR-7011-5p	4.755	0.00418383682182131	up	26	1
mmu-miR-7014-5p	4.709	0.0127123630058442	up	15	3
mmu-miR-7017-3p	6.107	0.0251153852432307	up	12	2
mmu-miR-7023-5p	6.398	0.0427202026166347	up	23	2
mmu-miR-7025-5p	4.678	0.014602157096298	up	18	1
mmu-miR-7028-3p	9.172	0.0205384032785827	up	32	7
mmu-miR-7032-5p	5.301	0.00134000605927864	up	21	4
mmu-miR-7033-5p	6.178	4.98773663785387E-06	up	38	10
mmu-miR-7042-3p	20	0.0422811649114925	up	10	3
mmu-miR-7044-5p	4.936	0.0374168535124453	up	14	3
mmu-miR-7045-5p	5.464	0.0242939518092793	up	7	1
mmu-miR-7051-3p	5.078	0.000584840384232765	up	17	6
mmu-miR-7068-5p	4.369	0.0137436651698999	up	13	2
mmu-miR-7070-5p	4.943	0.00571628977371187	up	19	4
mmu-miR-7075-5p	7.202	0.00322989034525318	up	27	3
mmu-miR-7082-5p	5.284	0.00812302360336593	up	8	2
mmu-miR-7084-3p	7.307	0.0000970351783144778	up	10	5
mmu-miR-709	7.799	1.8644972480033E-16	up	28	5
mmu-miR-7118-5p	6.996	0.0316024941145538	up	39	4
mmu-miR-712-3p	7.126	1.13403265924996E-13	up	2	2
mmu-miR-712-5p	7.589	1.06955113712167E-12	up	9	5
mmu-miR-7212-5p	7.727	0.0000772767854116384	up	20	2
mmu-miR-7213-3p	6.582	1.09497097213404E-12	up	3	2
mmu-miR-7216-5p	4.638	0.0315857216967794	up	29	3
mmu-miR-7225-3p	5.331	0.0407966651019063	up	3	2
mmu-miR-761	4.228	0.0211170875064135	up	13	2
mmu-miR-762	7.740	5.35534475331443E-16	up	36	7
mmu-miR-7654-3p	5.229	0.0250692218211853	up	1	2
mmu-miR-7654-5p	7.801	0.000282589868205336	up	1	2

(Continued)

TABLE 1 (Continued)

miRNA	Log2FC	FDR	Style	Number of miRNA-mRNA	Number of miRNA-CircRNA
mmu-miR-7669-3p	3.834	0.0029078687003109	up	24	3
mmu-miR-8097	6.564	0.0127278535486286	up	4	1
mmu-miR-8102	4.973	0.00516535079654147	up	2	1
mmu-miR-8104	6.019	0.020721000301402	up	12	4
mmu-miR-8106	20	0.00565663613096242	up	2	3
mmu-miR-8112	3.216	0.00188488077250827	up	3	1
mmu-miR-8115	4.552	0.00152129494770112	up	2	2
mmu-miR-8119	5.095	0.0000811944763272297	up	20	3
mmu-miR-92b-3p	−2.518	0.0020577634593746	down	1	1

circStrbp RNAi consistent with mouse results (Figures 3D,E). The same results were observed both in the JEV-infected and uninfected groups. Next, JEV mRNA levels were compared in circStrbp RNAi and NC cells. JEV mRNA levels were significantly decreased in circStrbp RNAi cells (Figure 3F). This results implied CX3CR1 enhance JEV infection in BV2 cell which regulated by circStrbp-miR709-CX3CR1 axis.

3.4 Mir-709 is an important regulatory miRNA in JEV infection

miR-709 has been shown to play a role in regulating JEV infection. As a multitarget miRNA, miR-709 has many potential targets. To further clarify the target molecules of miR-709 and the network of miR-709 in JEV infection, BV2 cells were employed to study miR-709. JEV mRNA levels were measured in 0 to 6 h after JEV infection (MOI = 0.5, 1, 5) (Figure 4A). JEV growth curve was observed in different time points. Therefore, we detected early JEV infection in BV2 cells, consistent with the stage of infection in mice brain. The expression of miR-709 was increased within 1 h of JEV infection, then gradually decreased, and remained relatively low after 6 h (Figures 4B–D). This gradually decreasing may be due to the characteristics of BV2 cells. During the entire infection process, the expression of miR-709 in the JEV-infected group was higher than that in the mock group, and the trend of miR-709 expression in BV2 cells was consistent with that in mouse brain tissue, indicating that BV2 cells can be used as a cell model for studying miR-709. Further validation of the targeting effect of miR-709 on CX3CR1 and JEV was performed using BV2 cells. The BV2 cells were transfected with miR-709 or normal control (NC), inoculated with 0.1 MOI of JEV 24 h after transfection, and collected for detection 24 h after inoculation. The results indicated that miR-709 interfered with the expression of CX3CR1 and that the CX3CR1 mRNA expression was significantly decreased in miR-709-transfected cells (Figure 4F). JEV mRNA expression was lower in CX3CR1 knockdown cells. CX3CR1 promoted the JEV infection of microglia (Figure 4E). The above results demonstrate that miR-709 is regulated by circRNAs and changes the expression of CX3CR1 in the ceRNA regulatory network. Changes in CX3CR1 expression can affect the process of JEV infection.

We then performed high-throughput RNA-seq of mRNAs in miR-709 transfected BV2 cells (Supplementary Figure S4). In uninfected BV2 cells, 123 genes were downregulated after miR-709 transfection (Figure 4G). In JEV-infected BV2 cells, 12 genes were downregulated after miR-709 transfection include CX3CR1 (Figure 4H). Hence, JEV infection greatly affects the performance of miR-709 on target genes through complex interactions. The downregulated genes in the mock and JEV-infected groups were not completely consistent. The CX3CR1 gene was significantly downregulated only in the JEV-infected group, a finding that was consistent with the results of the ceRNA sequencing analysis of mouse brain tissue. Interestingly, no significant downregulation of CX3CR1 was observed in the mock group. Hence, the downregulation of CX3CR1 was apparently related to JEV infection. We speculate that circRNA-miRNA-mRNA is a very complex regulatory network but not an evenly distributed network; neither the binding of circRNA to miRNAs nor the downstream regulatory target mRNAs are fixed. The regulatory effect of circRNA-miRNA-mRNA may be selective and can only be activated under certain conditions. The Strbp-miR-709-CX3CR1 regulatory pathway in mouse brain may activate by JEV infection.

Through high-throughput sequencing of miR-709-transfected BV2 cells, we further demonstrated the regulatory effect of miR-709 on CX3CR1, a finding that indicates that miR-709-CX3CR1 plays a role in the process of JEV infection in mouse brain. Additionally, as seen from the interaction network for miR-709, there is more than one circRNA that affects miR-709, and CX3CR1 is not the only mRNA targeted by miR-709. The regulatory pathway of X circRNA-miR-709-X mRNA may play different roles in different stages of JEV infection.

Finally, we demonstrate that the circStrbp-miR709-CX3CR1 axis changes in response to JEV infection and subsequently influence JEV replication (Figure 5) which is a representative ceRNA net in JEV infection.

4 Discussion

Japanese encephalitis is a zoonotic infectious disease that infects humans and animals and is a serious threat in the Asia-Pacific region (Le Flohic et al., 2013). The most important clinical infectious feature

10.3389/fmicb.2023.1165378

TABLE 2 Cx3cr1 related miRNA-circRNA.

miRNA	Log2FC	FDR	Style	miRNA-mRNA	CX3CR1 target score	miRNA-circRNA	CircRNA name
mmu-miR-709	7.799	1.8644972480033E-16	up	28	177	5	na Uhrf1bp1l Strbp Tulp4 Strn3
mmu-miR-3473c	5.956	4.97147489813369E-11	Up	19	171	5	Ttbk2 Rims1.1 Plcl2 Eml5 Strn3
mmu-miR-3547-5p	6.587	0.00036619368479388	up	37	155	9	na Grik2 Zfyve9 Cog5 Zfp516 Rims1.1 Strbp Zfp871 Spen
mmu-miR-6936-5p	5.273	0.0174460832523778	up	11	154	3	Zfyve9 Zfp516 Syn1
mmu-miR-6937-5p	4.823	0.0000418802801207815	up	10	150	3	Uhrf1bp1l Zfp871 Spen
mmu-miR-6963-5p	5.294	0.0484222299598572	up	18	154	5	na Rbfox3 Zfyve9 Strbp Zfp871
mmu-miR-6971-5p	5.890	0.0251085195447356	up	27	152	2	na Zfp516
mmu-miR-6992-5p	4.582	0.0243289483982281	up	16	160	9	na Grik2 Rbfox3 Uhrf1bp1l Zfp516 Strbp Plcl2 Spen Tulp4
mmu-miR-7023-5p	6.398	0.0427202026166347	up	23	166	2	Zfyve9 Zfp516

of Japanese encephalitis is the occurrence of viral encephalitis. The fine and complex structure of brain tissue has been a challenge of Japanese encephalitis research (Chen et al., 2019). At present, the precise pathogenic mechanism of viral encephalitis caused by JEV infection has not been fully elucidated. In this study, high-throughput sequencing analysis was performed to discover the regulatory role of ceRNAs in the process of JEV infection of brain tissue and to demonstrate the regulatory effect of Strbp-miR-709-CX3CR1 on JEV infection.

High-throughput sequencing was performed using JEV-infected mouse brain tissue, and changes in the expression levels of circRNAs, miRNAs and mRNAs were analyzed. The differentially expressed circRNA, miRNA, and mRNA data obtained herein were not identical to the data reported in

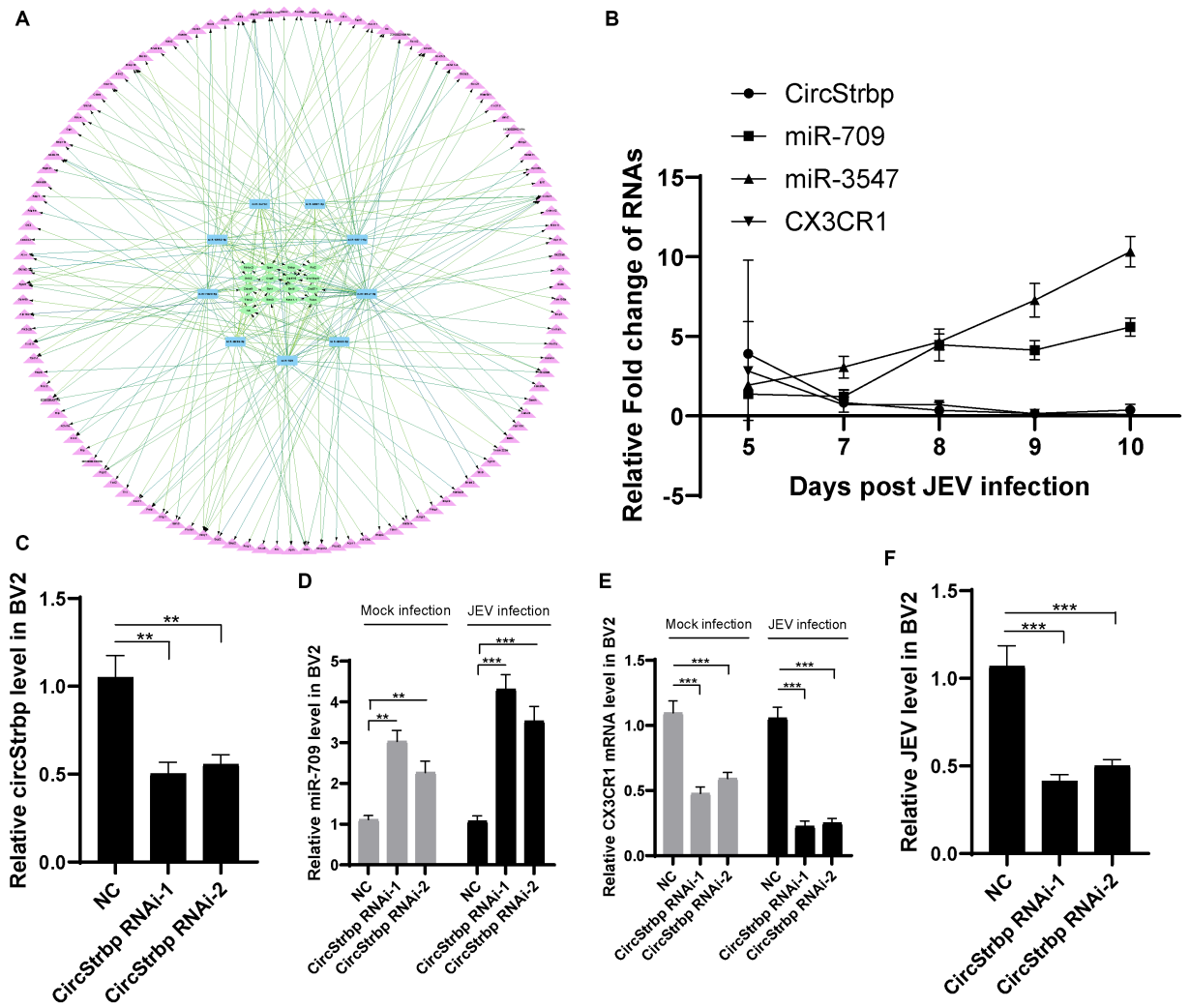

FIGURE 3
Network of CX3CR1 related ceRNA. **(A)** circRNA (green)-miRNA (blue)-mRNA (purple) interaction network. **(B)** Validation of CX3CR1 related circRNAs, miRNAs and mRNAs expression in infected mouse. Each genes were measured by qPCR using $2^{-\Delta\Delta Ct}$ method and then normalized by a mock sample at day 5 to calculate fold change. **(C)** RNA interference efficiency of circStrbp. CircStrbp gene was measured by qPCR with primers target to linkage sequences of circStrbp. **(D)** Detection of miR-709 levels in BV2 cell after circStrbp knock-down. **(E)** Detection of CX3CR1 mRNA levels in BV2 cell after circStrbp knock-down. **(F)** Detection of JEV mRNA levels in BV2 cell after circStrbp knock-down. All experiments were measured by qPCR using $2^{-\Delta\Delta Ct}$ method and then normalized by a mock. All experiments were repeated three times. Data are shown as means ± standard errors of the means.

previously published studies (Li et al., 2020; Lu et al., 2020; Hu et al., 2021). This difference may be caused by the difference in sampling time of infected mice and the presence of different differentially expressed genes at different stages of JEV infection. The ceRNA regulatory network may also change over time after infection. Li found that the ceRNA pathways of circ_0000220, miR-326-3p and BCL3/MK2/TRIM25 played roles in viral encephalitis, demonstrating that viral encephalitis caused by JEV infection is regulated by a complex ceRNA network (Li et al., 2020). Our study revealed that Strbp-miR-709-CX3CR1 had a regulatory effect on JEV infection. These results demonstrate that the ceRNA network plays different roles during JEV infection.

The abundant circRNAs indicate that ceRNAs are abundant in brain tissue. It is speculated that circRNA-miRNA-mRNA regulation plays an important role in brain tissue. From our experimental results, circRNA-miRNA-mRNA was greatly affected by JEV infection. The high-throughput sequencing results from miR-709 transfected BV2 cells showed that the cellular changes caused by JEV infection affect gene expression and ceRNA network. One possibility of this result is that JEV infection directly affects the production of circRNAs and the expression of miRNAs, resulting in the activation of some specific circRNA-miRNA-mRNA pathways. Another possibility is that JEV infection leads to changes in the expression of some terminal target mRNAs, resulting in the failure to detect the targeting effect of ceRNA network on mRNAs. Based on the results reported herein, the overall expression and differences in expression of miR-709 are more obvious in the early stage of infection, and thus, circRNA-miRNA-mRNA is more likely to play a role in the early stage of virus infection. In the late stage of infection, the regulatory effect of various cytokines and proteins seems to be greater (Bian et al., 2020).

10.3389/fmicb.2023.1165378

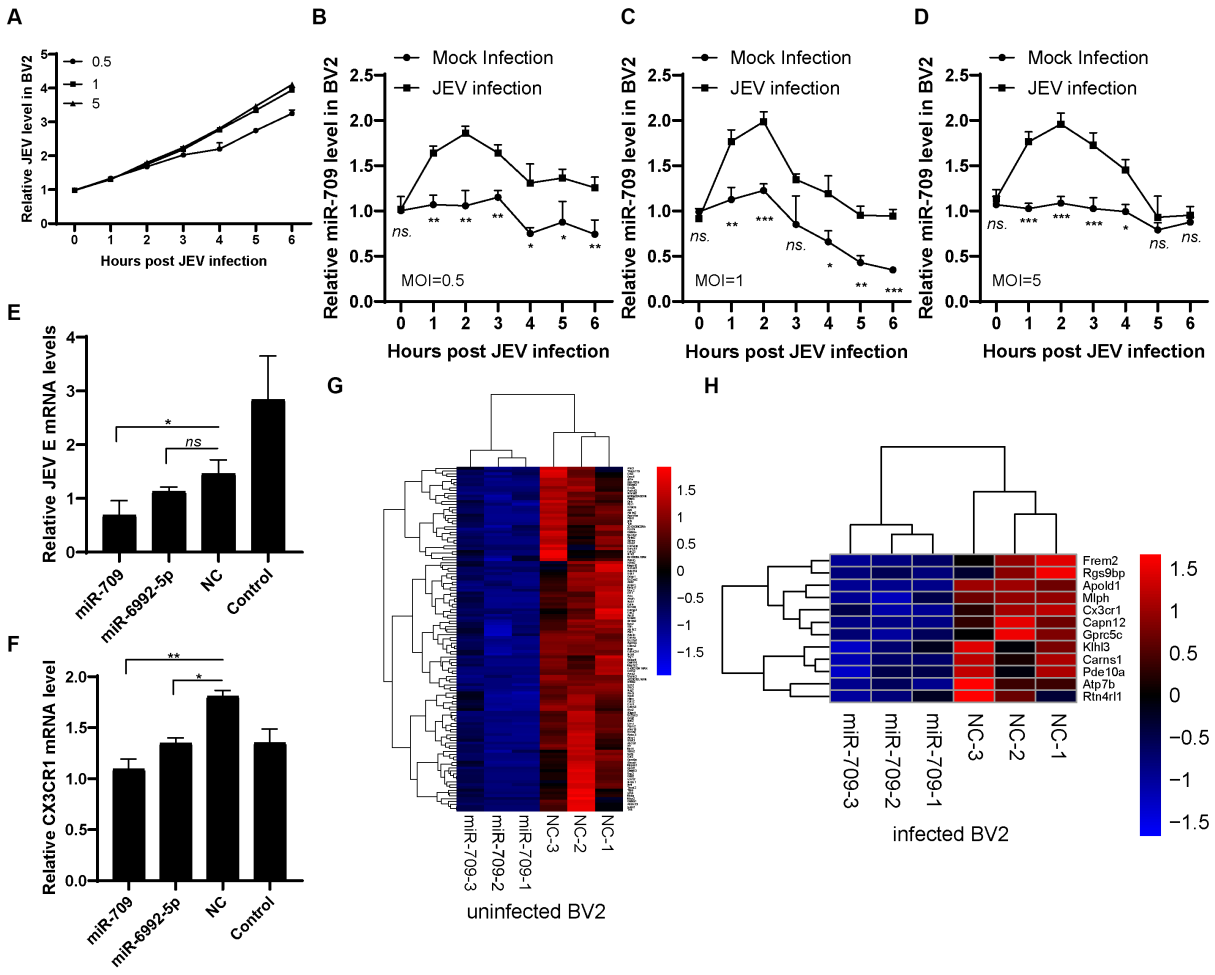

FIGURE 4
miR-709 targeted CX3CR1 during JEV infection. **(A)** JEV infection curve in BV2 cell. Three dose of JEV (MOI = 0.5, 1, 5) were inculated into BV2 cell, the infected or mock infected cells were collected at different time points. **(B–D)** miR-709 dynamic response after JEV infection in BV2 cell with different MOI. The infected or mock infected cells were collected at different time points, the relative expression of miR-709 was measured by qPCR. Data are shown as the mean ± standard error (SEM). The experiments were repeated three times. **(E)** JEV replication after miRNA transfection. miR-709, miR-6992-5p or NC were transfected in BV2 cell, JEV was inoculated at 24 h after transfection. 24 h post infection, cell samples were collected. **(F)** CX3CR1 mRNA changes after miRNA transfection. miR-709, miR-6992-5p or NC were transfected in BV2 cell, 24 h post transfection, cell samples were collected. *, $p < 0.05$ compared between groups. Data are shown as the mean ± standard error (SE). The experiments were repeated for three times. **(G)** Down-regulation of mRNAs of miR-709 transfected uninfected-BV2 cell. **(H)** Down-regulation of mRNAs of miR-709 transfected infected-BV2 cell. Red color represents up-regulations and blue colors represent down-regulatons. Difference were calculated as significant if a fold change >2 and a p value <0.05.

In circRNA-miRNA-mRNA interactions, miRNAs are intermediate molecules. miRNAs can be adsorbed on circRNA sponges and can target mRNAs to generate RNAi(Hansen et al., 2013). We believe that ceRNA analysis centered on miR-709 can explain and validate the circRNA-miRNA-mRNA pathway and its role. Therefore, we transfected miR-709 into BV2 cells and performed high-throughput RNA-seq of mRNAs from transfected cells. The results showed that the changes in CX3CR1 in BV2 cells were the same as the changes in CX3CR1 in mouse brain tissue. Based on the bifunctional chemokine role of CX3CR1, CX3CR1 may play an important role during JEV infection (Liu et al., 2018). Although there is no direct evidence that CX3CR1 is involved in viral inflammation caused by JEV infection, we speculate that changes in CX3CR1 may be associated with inflammation (Doggrell, 2011; Sutti et al., 2019). However, the clear mechanism needs to be further analyzed and verified. By transfecting miR-709 into BV2 cells, we found that miR-709 has a significant anti-JEV effect in BV2 cells. Bioinformatics analysis of the ceRNA network further proved that the antiviral effect of miR-709 is related to CX3CR1. miR-709 also has the potential to target other genes and thus suppress JEV infection (Surendran et al., 2016; Xiong et al., 2022), an issue that requires further experimental verification.

The ceRNA network consisting of circRNA-miRNA-mRNA is very complex, and ceRNAs within the cell generate many potential connections. The biological effects of these ceRNA networks are also complex and multiple. ceRNAs change depending on the organism or cellular state. There are many more ceRNA networks of circStrbp,

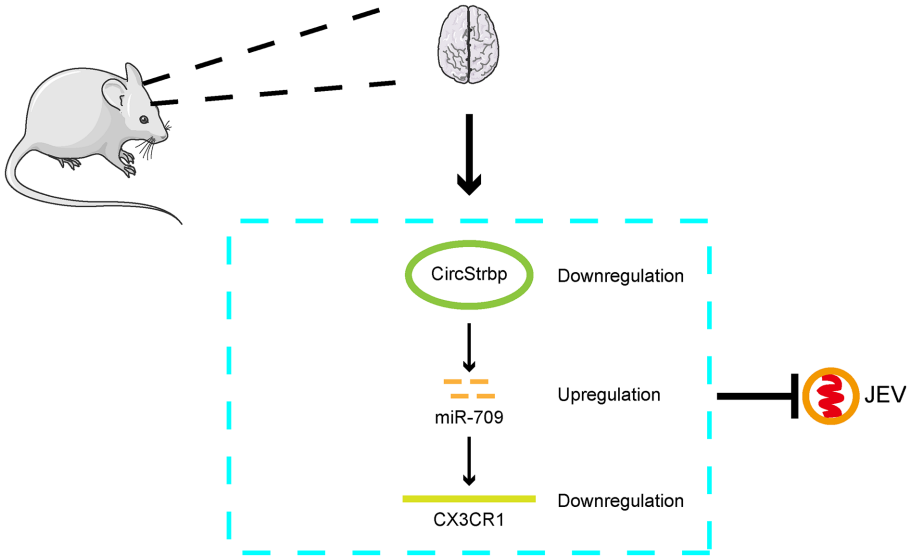

FIGURE 5
Mode pattern of the effect of CirStrbp-miR-709-CX3CR1 network on the JEV infection in mouse brain.

miR-709, and CX3CR1 were listed in this study (Tables 1, 2), and the changes of molecules related to these networks and the biological effects they produce may have potential roles in JEV infection, which need to be further investigated.

In conclusion, in this study, the circRNA-miRNA-mRNA interaction network in JEV-infected mouse brain tissue and JEV-infected mouse microglia cells was analyzed. The results indicate that the role of circRNA-miRNA-mRNA may change dynamically in different stages of infection and that the circStrbp-miR709-CX3CR1 pathway is associated with the JEV infection process (Figure 5).

Data availability statement

The authors confirm that the data supporting the findings of this study are available within the article/Supplementary material.

Ethics statement

Mouse experiments were performed in compliance with the Guidelines on the Human Treatment of Laboratory Animals (Ministry of Science and Technology of the People's Republic of China, Policy No. 2006 398) and were approved by the Institutional Animal Care and Use Committee at the Shanghai Veterinary Research Institute (IACUC No: Shvri-Pi-0124). The study was conducted in accordance with the local legislation and institutional requirements.

Author contributions

KL, ZM, and XF: conceived and designed the experiments, writing—review and editing. MC, LK, and TZ: performed the experiments. JZ and DC: data curation. DS, ZL, BL, JW, and YQ: writing—original draft. All authors contributed to the article and approved the submitted version.

Funding

The author(s) declare financial support was received for the research, authorship, and/or publication of this article. This study was supported by the Shanghai Natural Science Fund (no. 21ZR1477100), Shanghai Veterinary Research Institute 2022 Fund.

Conflict of interest

The authors declare that the research was conducted in the absence of any commercial or financial relationships that could be construed as a potential conflict of interest.

Publisher's note

All claims expressed in this article are solely those of the authors and do not necessarily represent those of their affiliated organizations, or those of the publisher, the editors and the reviewers. Any product that may be evaluated in this article, or claim that may be made by its manufacturer, is not guaranteed or endorsed by the publisher.

Supplementary material

The Supplementary material for this article can be found online at: https://www.frontiersin.org/articles/10.3389/fmicb.2023.1165378/full#supplementary-material

References

Bharucha, T., Cleary, B., Farmiloe, A., Sutton, E., Hayati, H., Kirkwood, P., et al. (2022). Mouse models of Japanese encephalitis virus infection: a systematic review and meta-analysis using a meta-regression approach. *PLoS Negl. Trop. Dis.* 16:e0010116. doi: 10.1371/journal.pntd.0010116

Bian, P., Ye, C., Zheng, X., Luo, C., Yang, J., Li, M., et al. (2020). RIPK3 promotes JEV replication in neurons via downregulation of IFI44L. *Front. Microbiol.* 11:368. doi: 10.3389/fmicb.2020.00368

Chen, L. L. (2016). The biogenesis and emerging roles of circular RNAs. *Nat. Rev. Mol. Cell Biol.* 17, 205–211. doi: 10.1038/nrm.2015.32

Chen, L., Li, G., Tian, Y., Zeng, T., Xu, W., Gu, T., et al. (2022). RNA sequencing reveals circRNA expression profiles in chicken DF1 cells infected with H5N1 influenza virus. *Animals (Basel)* 12. doi: 10.3390/ani12020158

Chen, Z., Zhong, D., and Li, G. (2019). The role of microglia in viral encephalitis: a review. *J. Neuroinflammation* 16:76. doi: 10.1186/s12974-019-1443-2

Daep, C. A., Munoz-Jordan, J. L., and Eugenin, E. A. (2014). Flaviviruses, an expanding threat in public health: focus on dengue, West Nile, and Japanese encephalitis virus. *J. Neurovirol.* 20, 539–560. doi: 10.1007/s13365-014-0285-z

Di, D., Li, C., Zhang, J., Hameed, M., Wang, X., Xia, Q., et al. (2020). Experimental infection of newly hatched domestic ducklings via Japanese encephalitis virus-infected mosquitoes. *Pathogens* 9:9050371. doi: 10.3390/pathogens9050371

Doggrell, S. A. (2011). CX3CR1 as a target for airways inflammation. *Expert Opin. Ther. Targets* 15, 1139–1142. doi: 10.1517/14728222.2011.597383

Hameed, M., Wahaab, A., Nawaz, M., Khan, S., Nazir, J., Liu, K., et al. (2021). Potential role of birds in Japanese encephalitis virus zoonotic transmission and genotype shift. *Viruses* 13:357. doi: 10.3390/v13030357

Hansen, T. B., Jensen, T. I., Clausen, B. H., Bramsen, J. B., Finsen, B., Damgaard, C. K., et al. (2013). Natural RNA circles function as efficient microRNA sponges. *Nature* 495, 384–388. doi: 10.1038/nature11993

Hu, Y., Xu, Y., Deng, X., Wang, R., Li, R., You, L., et al. (2021). Comprehensive analysis of the circRNA expression profile and circRNA-miRNA-mRNA network in the pathogenesis of EV-A71 infection. *Virus Res.* 303:198502. doi: 10.1016/j.virusres.2021.198502

Huang, Y. J., Higgs, S., Horne, K. M., and Vanlandingham, D. L. (2014). Flavivirus-mosquito interactions. *Viruses* 6, 4703–4730. doi: 10.3390/v6114703

Le Flohic, G., Porphyre, V., Barbazan, P., and Gonzalez, J. P. (2013). Review of climate, landscape, and viral genetics as drivers of the Japanese encephalitis virus ecology. *PLoS Negl. Trop. Dis.* 7:e2208. doi: 10.1371/journal.pntd.0002208

Li, Y., Ashraf, U., Chen, Z., Zhou, D., Imran, M., Ye, J., et al. (2020). Genome-wide profiling of host-encoded circular RNAs highlights their potential role during the Japanese encephalitis virus-induced neuroinflammatory response. *BMC Genomics* 21:409. doi: 10.1186/s12864-020-06822-5

Li, H., Tang, W., Jin, Y., Dong, W., Yan, Y., and Zhou, J. (2021). Differential CircRNA expression profiles in PK-15 cells infected with pseudorabies virus type II. *Virol. Sin.* 36, 75–84. doi: 10.1007/s12250-020-00255-w

Liu, K., Xiao, C., Wang, F., Xiang, X., Ou, A., Wei, J., et al. (2018). Chemokine receptor antagonist block inflammation and therapy Japanese encephalitis virus infection in mouse model. *Cytokine* 110, 70–77. doi: 10.1016/j.cyto.2018.04.022

Lu, S., Zhu, N., Guo, W., Wang, X., Li, K., Yan, J., et al. (2020). RNA-Seq revealed a circular RNA-microRNA-mRNA regulatory network in Hantaan virus infection. *Front. Cell. Infect. Microbiol.* 10:97. doi: 10.3389/fcimb.2020.00097

Memczak, S., Jens, M., Elefsinioti, A., Torti, F., Krueger, J., Rybak, A., et al. (2013). Circular RNAs are a large class of animal RNAs with regulatory potency. *Nature* 495, 333–338. doi: 10.1038/nature11928

Pichl, T., Wedderburn, C. J., Hoskote, C., Turtle, L., and Bharucha, T. (2022). A systematic review of brain imaging findings in neurological infection with Japanese encephalitis virus compared with dengue virus. *Int. J. Infect. Dis.* 119, 102–110. doi: 10.1016/j.ijid.2022.03.010

Shi, N., Zhang, S., Guo, Y., Yu, X., Zhao, W., Zhang, M., et al. (2021). CircRNA_0050463 promotes influenza a virus replication by sponging miR-33b-5p to regulate EEF1A1. *Vet. Microbiol.* 254:108995. doi: 10.1016/j.vetmic.2021.108995

Surendran, S., Jideonwo, V. N., Merchun, C., Ahn, M., Murray, J., Ryan, J., et al. (2016). Gene targets of mouse miR-709: regulation of distinct pools. *Sci. Rep.* 6:18958. doi: 10.1038/srep18958

Sutti, S., Bruzzi, S., Heymann, F., Liepelt, A., Krenkel, O., Toscani, A., et al. (2019). CX(3)CR1 mediates the development of monocyte-derived dendritic cells during hepatic inflammation. *Cells* 8:1099. doi: 10.3390/cells8091099

Wang, W., Xie, S., Yuan, D., He, D., Fang, L., and Ge, F. (2021). Systematic review with meta-analysis: diagnostic, prognostic and Clinicopathological significance of CircRNA expression in renal cancer. *Front. Oncol.* 12:158. doi: 10.3389/fonc.2021.773236

Xie, J., Jiang, H., Zhao, Y., Jin, X. R., Li, B., Zhu, Z., et al. (2022). Prognostic and diagnostic value of circRNA expression in prostate cancer: a systematic review and meta-analysis. *Front. Oncol.* 12:945143. doi: 10.3389/fonc.2022.945143

Xiong, J., Zhang, H., Wang, Y., Cheng, Y., Luo, J., Chen, T., et al. (2022). Rno_circ_0001004 acts as a miR-709 molecular sponge to regulate the growth hormone synthesis and cell proliferation. *Int. J. Mol. Sci.* 23:1413. doi: 10.3390/ijms23031413

Yang, X., Chen, C., Li, L., Xiao, T., Zou, Y. D., and Zheng, D. (2021). Current research advances in microRNA-mediated regulation of Kruppel-like factor 4 in cancer: a narrative review. *Ann Transl Med* 9:948. doi: 10.21037/atm-21-2347

Yun, S. I., and Lee, Y. M. (2014). Japanese encephalitis: the virus and vaccines. *Hum. Vaccin. Immunother.* 10, 263–279. doi: 10.4161/hv.26902

Zhao, W., Su, J., Wang, N., Zhao, N., and Su, S. (2021). Expression profiling and bioinformatics analysis of CircRNA in mice brain infected with rabies virus. *Int. J. Mol. Sci.* 22:22126537. doi: 10.3390/ijms22126537

Zheng, Y., Li, M., Wang, H., and Liang, G. (2012). Japanese encephalitis and Japanese encephalitis virus in mainland China. *Rev. Med. Virol.* 22, 301–322. doi: 10.1002/rmv.1710

Zhu, G., Chang, X., Kang, Y., Zhao, X., Tang, X., Ma, C., et al. (2021). CircRNA: a novel potential strategy to treat thyroid cancer (review). *Int. J. Mol. Med.* 48:5034. doi: 10.3892/ijmm.2021.5034

frontiers | Frontiers in Microbiology

TYPE Original Research
PUBLISHED 17 January 2024
DOI 10.3389/fmicb.2023.1324069

OPEN ACCESS

EDITED BY
James Weger-Lucarelli,
Virginia Tech, United States

REVIEWED BY
Pavle Banovic,
Pasteur Institute Novi Sad, Serbia
Pradip Barde,
National Institute of Research in Tribal Health (ICMR), India

*CORRESPONDENCE
Gaëlle Gonzalez
✉ gaelle.gonzalez@anses.fr
Sylvie Lecollinet
✉ sylvie.lecollinet@cirad.fr

†These authors have contributed equally to this work

RECEIVED 19 October 2023
ACCEPTED 28 December 2023
PUBLISHED 17 January 2024

CITATION
Fiacre L, Nougairède A, Migné C, Bayet M, Cochin M, Dumarest M, Helle T, Exbrayat A, Pagès N, Vitour D, Richardson JP, Failloux A-B, Vazeille M, Albina E, Lecollinet S and Gonzalez G (2024) Different viral genes modulate virulence in model mammal hosts and *Culex pipiens* vector competence in Mediterranean basin lineage 1 West Nile virus strains.
Front. Microbiol. 14:1324069.
doi: 10.3389/fmicb.2023.1324069

Different viral genes modulate virulence in model mammal hosts and *Culex pipiens* vector competence in Mediterranean basin lineage 1 West Nile virus strains

Lise Fiacre[1,2], Antoine Nougairède[3], Camille Migné[1], Maëlle Bayet[2], Maxime Cochin[3], Marine Dumarest[1], Teheipuaura Helle[1], Antoni Exbrayat[4], Nonito Pagès[2], Damien Vitour[1], Jennifer P. Richardson[1], Anna-Bella Failloux[5], Marie Vazeille[5], Emmanuel Albina[4], Sylvie Lecollinet[2*†] and Gaëlle Gonzalez[1*†]

[1]UMR VIRO, ANSES, ENVA, INRAE Virologie, Laboratoire de Santé Animale, Maisons-Alfort, France, [2]UMR ASTRE, CIRAD, Petit-Bourg, Guadeloupe, [3]Unité Des Virus Emergents (UVE), Aix-Marseille Université, IRD 190, INSERM 1207, Marseille, France, [4]ASTRE, CIRAD, INRAe, Université de Montpellier, Montpellier, France, [5]Institut Pasteur, Université Paris Cité, Arboviruses and Insects Vectors, Paris, France

West Nile virus (WNV) is a single-stranded positive-sense RNA virus (+ssRNA) belonging to the genus *Orthoflavivirus*. Its enzootic cycle involves mosquito vectors, mainly *Culex*, and wild birds as reservoir hosts, while mammals, such as humans and equids, are incidental dead-end hosts. It was first discovered in 1934 in Uganda, and since 1999 has been responsible for frequent outbreaks in humans, horses and wild birds, mostly in America and in Europe. Virus spread, as well as outbreak severity, can be influenced by many ecological factors, such as reservoir host availability, biodiversity, movements and competence, mosquito abundance, distribution and vector competence, by environmental factors such as temperature, land use and precipitation, as well as by virus genetic factors influencing virulence or transmission. Former studies have investigated WNV factors of virulence, but few have compared viral genetic determinants of pathogenicity in different host species, and even fewer have considered the genetic drivers of virus invasiveness and excretion in *Culex* vector. In this study, we characterized WNV genetic factors implicated in the difference in virulence observed in two lineage 1 WNV strains from the Mediterranean Basin, the first isolated during a significant outbreak reported in Israel in 1998, and the second from a milder outbreak in Italy in 2008. We used an innovative and powerful reverse genetic tool, e.g., ISA (*infectious subgenomic amplicons*) to generate chimeras between Israel 1998 and Italy 2008 strains, focusing on non-structural (NS) proteins and the 3'UTR non-coding region. We analyzed the replication of these chimeras and their progenitors in mammals, in BALB/cByJ mice, and

vector competence in *Culex (Cx.) pipiens* mosquitoes. Results obtained in BALB/cByJ mice suggest a role of the NS2B/NS3/NS4B/NS5 genomic region in viral attenuation in mammals, while NS4B/NS5/3′UTR regions are important in *Cx. pipiens* infection and possibly in vector competence.

KEYWORDS

***Culex pipiens*, host virulence, Mediterranean basin, reverse genetics, vector competence, West Nile virus lineage 1**

1 Introduction

West Nile virus (WNV) is a mosquito-borne single-stranded, positive-sense RNA virus. It belongs to the family *Flaviviridae*, genus *Orthoflavivirus*. It is transmitted through an enzootic cycle involving birds as amplifying hosts and mosquitoes as vectors, with occasional spillovers to such mammals as humans and horses, these latter being considered to be dead-end hosts (Kramer et al., 2007). It is the most widely spread encephalitic flavivirus, having been reported in Africa, Europe, the Middle East, Western Asia (Li et al., 2013; Chowdhury and Khan, 2021) and America, as well as in Australia. It was first isolated from a native woman of Uganda in 1937 (Smithburn et al., 1940) and Africa is most presumably the cradle of WNV strains that are regularly introduced in Europe and the Middle East through bird migration. WNV was first detected in Israel in 1951 (Bernkopf et al., 1953), during which a high seroprevalence rate was demonstrated in the human population (Melnick et al., 1951). WNV circulation was also documented in Europe in France, Portugal and Cyprus in the 1960s (Lecollinet et al., 2019). Silent or paucisymptomatic infections lasted for 30 years before important human outbreaks and horse epizootics were first reported in Europe, Romania, Italy and Russia in 1996, 1998, and 1999, respectively. Since the 1990s, and even more frequently since 2010, WNV has actively circulated in the Mediterranean basin on many occasions (Murgue et al., 2001), such as in Northern Africa (Morocco, Tunisia, Algeria), in the Middle East (Israel, Turkey) and in Southern Europe (Italy, France, Spain, Croatia, Greece). A highly virulent lineage 1 WNV strain, classified among the Israelo-American clade, emerged in Israel in 1998, causing 35 human neuroinvasive cases in 1998 (Green et al., 2005), as well as the death of domestic geese and wild migratory birds, and in particular storks (Malkinson et al., 2002). Closely-related WNV lineage 1 isolates reemerged in Israel in 2018 and caused epizootics in birds and horses. While lineage 1 WNV belonging to the Western Mediterranean clade was evidenced as early as 1998 in Italy in Tuscany, regular WNV outbreaks in Italy associated to the circulation of such WNV strains had not been observed before 2008 in North-Eastern Italy (Emilia-Romagna, Veneto, and Lombardy), or before 2010 in South Italy. Of note, during the last decade, WNV lineage 1 strains have circulated sporadically in Italy, being apparently replaced by lineage 2 WNV; the new introduction of a closely-linked lineage 1 WNV strain coincided with an increased incidence of WNV neuroinvasive disease in humans in 2021/2022 in Northern Italy (Barzon et al., 2022). Finally, WNV has been (re)emerging throughout Europe for decades giving rise to unpredictable outbreaks of varying intensity in equine, human and avian populations with higher incidence of severe WNV cases in humans and horses, especially in 2018 (Martin and Simonin, 2019) and 2022 (Riccardo et al., 2022).

Bird migrations are mainly responsible for long-distance transmission and spread of the virus (Komar, 2003). Due to its ability to rapidly adapt to local environmental conditions, WNV has spread and emerged all around the world. Its circulation has been evidenced on all continents with the exception of Antarctica. Intense and recurrent WNV outbreaks of meningitis and encephalitis in birds, horses and humans have been reported in America, Africa or Europe. Although the majority of infected people remain asymptomatic (80%), a small proportion will develop flu-like symptoms (20%) or severe forms of the disease (1%), e.g., West-Nile Neuroinvasive Disease (WNND) characterized by meningitis, encephalitis or acute flaccid paralysis (Fiacre et al., 2020). WNV pathogenesis and WNV-induced lesions in humans and other susceptible mammals have been thoroughly characterized (Donadieu et al., 2013; Clé et al., 2020). Yet, our knowledge of the mechanisms underlying the ability of the virus to spread, to be transmitted with efficiency by European mosquitoes or to modulate pathogenicity in birds and mammals needs to be assessed in order to refine risk assessment and preparedness for epidemics in Europe (Fiacre et al., 2020).

West Nile virus Israel 1998 (WNV IS98) and WNV Italy 2008 (WNV IT08) are two Mediterranean lineage 1 strains that have caused outbreaks of varying intensity in the avifauna. While IS98 was highly virulent in domestic and wild birds, IT08 induced low mortality in the wild avifauna. This observation led us and others (Dridi et al., 2013) to suspect that genetic differences between the two strains may have accounted for differential virulence in birds. Dridi and colleagues performed experimental infections of specific-pathogen free (SPF) chicks and confirmed that the two strains differed in virulence in an avian model of WNV infection (Dridi et al., 2013), IS98 being more virulent than IT08. We provided the first description of the molecular determinants of WNV driving increased avian pathology of IS98 by using for the first time a classical reverse genetic approach and the generation of IS98-IT08 chimeras (Fiacre et al., 2023). Reverse genetics has been used for decades to identify amino acids involved in WNV virulence and has led to significant progress in understanding viral pathogenesis (Aubry et al., 2015). We initially used a plasmid method to create chimeras between the two parental strains IS98 and IT08 by replacing the NS4A, NS4B, NS5, and/or 3′ UTR regions of IS98 by the corresponding regions of IT08 and conducted *in vivo* experiments in mammals (BALB/cByJ mice) and birds (SPF chicks) (Fiacre et al., 2023). Genetic motifs

implicated in differential pathogenesis in birds were consequently identified in the NS4A/NS4B/NS5 and 3′UTR regions. Our results suggest a role for the 3′ end of the WNV genome, especially the NS4A/NS4B/5′NS5 regions, in the decreased virulence of IT08 in SPF chickens, possibly due to the NS4B-E249D mutation. Other genetic markers could influence virulence of IS98 and IT08 in birds and mammals. Genome comparisons suggest a possible role of NS5-V258A, NS5-N280K, NS5-A372V, and NS5-R422K (not demonstrated) in attenuated phenotypes in mice.

A previous extensive review of the molecular determinants of WNV virulence in vertebrates and invertebrates indicated that critical motifs are disseminated all over the viral genome, not least in the 5′UTR and 3′UTR regions, and including key residues in the envelope (E) and non-structural 1 (NS1) proteins, E-159, NS1-175 or NS1-130 (Fiacre et al., 2020). Studies on molecular determinants of the virulence of European and Mediterranean WNV strains are scarce. In this context, the present study reports investigations on the role of structural and non-structural (NS) proteins, as well as non-coding genomic regions, in WNV transmission and virulence using the innovative reverse genetic ISA-method (*Infectious Subgenomic Method*) (Aubry et al., 2014). We designed six chimeric constructs between high- and low-virulence strains for birds, WNV IS98 and IT08, respectively, and tested them *in vitro* and *in vivo* on BALB/cByJ mice and on *Cx. pipiens*, the primary mosquito vector for WNV transmission in Europe and more specifically in the Mediterranean basin (Toma et al., 2008; Kampen et al., 2020; Tsioka et al., 2022).

2 Materials and methods

2.1 Cells lines

Vero (ATCC CCL81), HEK-293 (ATCC CRL1573) and HEK-293T cells (ATCC CRL3216) were maintained at 37°C, 5% CO_2 in Dulbecco Modified Eagle's Medium (DMEM, Thermo Fisher scientific, Montigny-le-Bretonneux, France) supplemented with 5% fetal bovine serum (FBS, Lonza), 1 mM sodium pyruvate, penicillin (1 U/mL)/streptomycin (1 µg/mL) and 2 mM L-glutamine. BHK-21 cells (ATCC CCL10) were maintained at 37°C in Dulbecco Modified Eagle's Medium (DMEM, Thermo Fisher scientific) supplemented with 10% fetal bovine serum (FBS, Lonza, France) and penicillin (1 U/mL)/streptomycin (1 µg/mL). C6/36 cells (ATCC CRL1660) were maintained at 28°C, in Leibowitz L-15 Medium supplemented with 1 mM sodium pyruvate, penicillin (1 U/mL)/streptomycin (1 µg/mL), 1 mL non-essential amino acids, and 2 mM L-glutamine (Thermo Fisher Scientific, France).

2.2 Generation of chimeric viruses using innovative reverse genetic ISA method

The procedure is described in detail in Aubry et al. (2014). Briefly, overlapping PCR fragments generated with a high-fidelity polymerase and reconstituting the entire WNV genome of IS98, IT08 or chimeric IS98-IT08 viruses were introduced by transfection of cells sustaining efficient WNV replication.

2.2.1 Preparation of PCR products for the ISA method

The complete genome, flanked at the 5′ and 3′ extremities by the human cytomegalovirus promoter (pCMV) and the hepatitis delta ribozyme, respectively, followed by the simian virus 40 polyadenylation signal [HDR/SV40p(A)], was amplified by PCR in 6 overlapping DNA fragments of approximately 2.5kb, 1.1 kb, 1.1 kb, 3.2 kb, 2.9 kb and 725 bp. The WNV IS98 strain was recovered from an infectious clone construct generated by Bahuon et al. (2012) (WNV IC-IS98). For WNV IC-IS98 and IT08, DNA fragments were obtained by RT-PCR from clarified cell supernatants. Total RNA was extracted using the MagVet Universal Isolation kit (ThermoFisher Scientific, Montigny-le-Bretonneux, France) according to the manufacturer's instructions and amplified using the Invitrogen™ SuperScript™ IV One-Step RT-PCR System with the Platinum SuperFi DNA polymerase (ThermoFisher Scientific, Montigny-le-Bretonneux, France) to minimize PCR mutations. Amplifications were performed on an AB 7300 Real-Time PCR thermocycler (Applied Biosystems) with the following conditions: (i) 50°C for 30 min (cDNA synthesis), (ii) 94°C for 2 min (pre-denaturation), (iii) 40 amplification cycles with 94°C for 15 s–64°C for 30 s–72°C for 2 min or more – depending on the expected fragment size (1 min/kb), (iiii) final elongation at 72°C for 10 min. The size of all PCR products was verified by gel electrophoresis and PCR products were purified using PCR PureLink™ purification kit (Invitrogen, Paris, France).

PCR fragments were amplified from WNV IC-IS98 (called WN-IS98) and WNV IT08 (WN-IT08) viral genomic RNA with the following primers listed in **Table 1**.

2.2.2 Cells transfection

Cell transfection was performed as previously described by Driouich et al. (2019). Briefly, 1 day before transfection, an equal number of HEK-293T and BHK-21 cells were plated in 96-well plates at the final density of 2×10^4 cells/well (1×10^4 HEK-293T cells + 1×10^4 BHK-21 cells). Transfection was performed using the Lipofectamine 3000 reagent (Invitrogen, Paris, France) and optiMEM (Gibco, ThermoFisher Scientific, Montigny-le-Bretonneux, France). Cells in each well were transfected with a 100 ng aliquot of an equimolar mix of the 8 DNA fragments (6 for the viral genome, 1 for pCMV and 1 for HDR/SV40p(A) ribozyme as previously described (Aubry et al., 2014). Each transfection was performed in 9 wells to ensure the production of the chimeric construct in at least one well. Transfected cells were incubated at 37°C, 5% CO_2 for 24 h. At 24 h post-transfection, cell supernatants were replaced by 100 µL of fresh DMEM medium supplemented with 5% fetal bovine serum (FBS, Lonza, France), 1 mM sodium pyruvate, penicillin (1 U/mL)/streptomycin (1 µg/mL) and 2 mM L-glutamine. Five days after transfection, cell supernatants were collected and then passaged once on confluent *Vero* cells plated in 96-well plates. After an incubation period of 5 h, cells were washed with PBS 1X and 100 µL of fresh medium was added per well. Cell supernatants were passaged twice on confluent *Vero* cells. Between each passage, cell supernatants were diluted 1/1000 to ensure that infectious viruses were produced. The resulting virus stocks, obtained after a total of 3 passages on *Vero* cells, were used to confirm the production of infectious particles by RT-qPCR, $TCID_{50}$ titration and whole-genome next-generation sequencing.

TABLE 1 Oligonucleotides sequences used for PCR amplification in the ISA method.

N PCR fragment	WN-IS98	WN-IT08
1	Forward-AGTAGTTCGCCTGTGTGAGCTG	Same as WN-IS98
	Reverse-AGCTCTTGCCGGCTGATGTCTATG	Same as WN-IS98
2	Forward-ACGTTTCTCGCAGTTGGAGGCCCAAC	Same as WN-IS98
	Reverse-AAGAACACGACCAGAAGGCCCAAC	Same as WN-IS98
3	Forward-CCCTCGTGCAGTCACAAGTGAA	Same as WN-IS98
	Reverse-GGTGGTCATGTCCCCCTTTTTGTA	Same as WN-IS98
4	Forward-ATGCTCAGAATGGTCTGTCTCGC	Forward-TCCTGCCCTCAGTAGTTGGAT
	Reverse-CCTCTTTGCGGTACCTAGTGAAC	Reverse-CCTCTTTGCGGTACCTAGTGAAC
5	Forward-TGAACGCAACAACTGCCATCG	Forward-ATTGGACTCTGCCACATCATGCG
	Reverse-CCGGCCTGACTTTTCTC	Reverse-CCGGCCTGACTTCCTCCTTAAA
6	Forward-CCGAGCCACGTGGGCAGAAAAYA	Same as WN-IS98
	Reverse-AGATCCTGTGTTCTCGCACCACC	Same as WN-IS98

For each genome (WN-IS98 and WN-IT08) six PCR fragments were generated.

2.3 Next-generation sequencing of chimeric viruses

Next-generation sequencing was performed using Ion PGM Instrument with the Torrent Suite 5.12 Software (ThermoFisher Scientific, France). Whole genome sequencing analyses were performed using the SISPA method initially developed for sequencing on Illumina platforms and further adapted to IonTorrent workflows (Gil et al., 2021). Briefly, the sequencing consisted of three steps: (i) library preparation using random amplification and PCR addition of library-adapters, (ii) library sizing quantification and quality assessment, and (iii) sequencing. Library preparation included a first step of random amplification. Briefly, a reverse transcription produced cDNA from RNA molecules using TagE_8N_HPLC random oligonucleotides (5′-CATCACATAGGCGTCCGCTGNNNNNNNN-3′) using the RevertAid First Strand cDNA Synthesis kit (Fisher Scientific, Les Ulis, France). Reverse transcription was followed by Klenow polymerization (Fisher Scientific, Les Ulis, France) and high-fidelity PCR with the Phusion High-Fidelity DNA Polymerase kit (Fisher Scientific, France). 4 PCR reactions per sample were performed to generate sufficient amplicons. The PCR mix (50 µl) consisted of 0.2 µM primer (TagEshort 5′-CATCACATAGGCGTCCGCTG-3′), 0.2 mM dNTPs, 1 × Phusion HF buffer, 0.5U of Phusion DNA polymerase and 5 µl of dsDNA obtained after Klenow polymerization. PCR parameters were as follows: 30 s at 98°C, 32 cycles of 10 s at 98°C, 20 s at 65°C, 60 s at 72°C, followed by a final elongation of 10 min at 72°C. PCR reactions from a given sample were pooled and purified with the NucleoSpin gel and PCR Clean-up (Macherey-Nagel, Hoerdt, France) following the manufacturer's instructions. Amplicons were eluted in 35 µl of ultra-pure water.

IonTorrent adapters (LigA_[n501-513], 5′-CCATCTCATCCC TGCGTGTCTCCGACT-3′ bound to 8-mer barcodes for the multiplexing of sequencing reactions) were added by PCR to TagE-flanked amplified dsDNA with the Ion Plus Fragment Library kit (ThermoFisher Scientific, Montigny-le-Bretonneux, France); the PCR mix consisted of 50 µL of Platinum PCR Supermix High Fidelity, 0.1 µM primers (LigA_[n501-513]-TagE and Lig2P1-TagE 5′-CCACTACGCCTCCGCTTTCCTCTCTA TGGGCAGTCGGTGATCATCACATAGGCGTCCGCTG-3′) and 7 µl of dsDNA. 4 PCR reactions per sample were carried out as follows: 5 min at 95°C, 8 cycles of 15 s at 95°C, 15 s at 58°C, 60 s at 70°C. PCR products from a given sample were pooled and purified with Agencourt AMPure XP (Fisher Scientific, France) following the manufacturer's instructions. Amplicons bound to IonTorrent adapters were eluted in 35 µl of ultra-pure water.

Library sizing was performed by gel electrophoresis with eGel Size-Select Agarose (Thermofisher Scientific, Montigny-le-Bretonneux, France) following the manufacturer's instructions. Bands of approximately 200 bp were excised from the agarose gel. Library concentrations were quantified and their quality assessed on the Bioanalyzer Instrument with an Agilent High Sensitivity PCR kit (Agilent Technologies, Waldbronn, Germany) following the manufacturer's instructions.

Libraries were multiplexed at equimolar ratios. The Ion OneTouch™ 2 System was used to prepare enriched, template-positive Ion PGM™ Hi-Q™ Ion Sphere™ Particles (ISPs) bound to insert libraries following the manufacturer's instructions (Thermofisher Scientific, Montigny-le-Bretonneux, France). Libraries were sequenced using the Ion PGM™ Hi-Q™ Sequencing Kit and Ion 316™ Chip v2 BC (Thermofisher Scientific, Montigny-le-Bretonneux, France) on an IonTorrent PGM instrument (Thermofisher Scientific, Montigny-le-Bretonneux, France).

Sequencing data were processed using a custom viral bioinformatics pipeline. Viral reads were identified and extracted through read mapping to the WN-IS98 genome (AF481864) using bwa-mem2 v2.0 (Vasimuddin et al., 2019). Adaptors, primer sequences, and low-quality bases (phred score threshold of 20) were trimmed from the raw reads, followed by removal of duplicate reads. Filtered datasets were assembled using SPAdes v3.15.5 (Prjibelski et al., 2020) using the default multiple kmer lengths and settings specific for Ion Torrent datasets. Resulting contigs were compared to the Pfam conserved domain DB- using blastx (Altschul et al., 1990). The shared regions within the chimeric virus

reconstruction is visualized through a Hive Plot built with d3.js (Bostock et al., 2011).

2.4 WNV plaque phenotype

Vero cells were seeded in 6-well plates and infected with parental WN-IS98 and WN-IT08 strains and the six chimeric viruses (**Figure 1**) at 100 PFU for 1 h 30 at 37°C, 5% CO_2, after which time media containing the virus was removed. Cells were overlaid with a semi-solid medium containing 2.4% Avicel, MEM 2X (ThermoFisher Scientific, Montigny-le-Bretonneux, France), 2.5% FBS (Lonza, France), 1% penicillin/streptomycin (ThermoFisher scientific, Montigny-le-Bretonneux, France) and 1% sodium pyruvate and incubated for 3 days at 37°C, 5% CO_2. The overlay was removed; cells were washed twice in PBS 1X and fixed with 4% paraformaldehyde and stained with 0.4% crystal violet for 24 h at room temperature.

2.5 Viral growth kinetics

Vero cells were seeded in 24-well plates and infected with parental WN-IS98 and WN-IT08 strains and the six chimeric viruses at MOI 0.1 in DMEM supplemented with 2% FBS. The cells were incubated at 37°C, 5% CO_2 and cell supernatants were harvested at the indicated times post-infection (17 h, 24 h, 48 h, and 72 h). Number of genome copies and infectious titers were determined as described below for all time points.

2.6 Quantitative RT-PCR

Total RNA was extracted using the MagVet^{TM} Universal Isolation kit (ThermoFisher scientific, Montigny-le-Bretonneux, France) according to the manufacturer's instructions. Reverse transcription and amplification were performed using the AgPath-ID One-Step RTPCR Kit (Applied Biosystems) as previously described in Linke et al. (2007). WNV amplification was achieved using the following specific primers (final concentration of 0.4 μM) WNproC-10 5′-CCTGTGTGAGCTGACAAACTTAGT-3′ and WNproC-132 5′-GCGTTTTAGCATATTGACAGCC-3′ and the probe (final concentration of 0.2 μM) 5′–FAM -CCTGGTTT CTTAGACATCGAGATCT–Tamra–3′. The housekeeping gene β -Actin was amplified using the primers (final concentration of 0.4 μM) ACTB-966 5′-CAGCACAATGAAGATCAAGATCATC-3′ and ACTB-1096 5′-CGGACTCATCGTACTCCTGCTT-3′ and the probe (final concentration of 0.2 μM) 5′-VIC-TCGCTGTCCACCTTCCAGCAGATGT-TAMRA-3′ (Toussaint et al., 2007). RT-PCR were run in an AB 7300 Real-Time PCR system (Applied Biosystems, Villebon sur Yvette, France) using the following program: 45°C for 10 min, 95°C for 10 min followed by 40 cycles of 95°C for 15 s and 60°C for 60 s. Genome copies per microliter were calculated based on the threshold cycle (CT) values of a standard curve generated using the standard RNA of WNV and normalized using the β-actin signal.

2.7 Infectious titer determination by $TCID_{50}$

$TCID_{50}$ was determined using 96-well cell culture plates seeded 1 day prior to infection with *Vero* cells at a density of 2.10^4 cells/well. Briefly, virus stocks were 10-fold serially diluted in DMEM and 50 μL of each dilution were inoculated into each well in quadruplicate. Plates were incubated for 3 days at 37°C, 5% CO_2 and 50% $TCID_{50}$ was determined by counting wells displaying viral cytopathic effect (CPE) using the methodology described by Reed and Munch.

2.8 Virulence in mice

Seven-week-old BALB/cByJ mice (Charles River Laboratories, L'Arbresle, France) were housed in an environmentally controlled room under biosafety level 3 conditions and were given food and water *ad libitum*. BALB/cByJ have long been used for studying WNV pathology and pathogenesis in mammals; they are highly susceptible to WNV clinical disease, due to impaired innate immunity associated with the absence of OAS1B expression (a premature STOP codon in the OAS1B gene is found in virtually all inbred mouse strains) and develop neurological signs and lesions mimicking the ones observed in humans and horses (Basset et al., 2020).

Groups of five mice were inoculated intraperitoneally with 10 PFU of WN-IS98, WN-IT08, chimera IS98-3′NS4B/NS5 or IS98-3′NS2B/NS3/NS4A/NS4B prepared in DMEM or with DMEM alone as a negative control. Every day, animals were weighed and monitored for the duration of the study (12 days) to detect the onset of signs of illness or suffering. Mice were euthanized by cervical dislocation when the end point was reached, that is, when at least two of the following clinical signs were observed: weight loss greater than 15%, anorexia, ruffled hair, curved back, loss of balance, paresis. The presence of viral RNA was confirmed by RT-qPCR in blood collected at 3-day pi (dpi) and in brain, heart and lung tissues, recovered shortly after their death and homogenized using the FastPrep Instrument (MP Biomedicals, Illkirch, France).

BALB/cByJ mice were housed at ANSES animal facilities (Maisons-Alfort, Paris). Work on animals was performed in compliance with French and European regulations on welfare and protection of animals used for scientific purposes (EC Directive 2010/63, French Law 2013-118, February 6th, 2013). All experiments were approved by the joint Anses-UPEC-Alfort Veterinary School ethics committee under the permit number 2022-11-15-11.

Biosecurity measures for the biocontainment of parental and chimeric viruses generated in this study have been reviewed and validated by the French Ministry of Higher Education, Research and Innovation under the DUO 10537.

2.9 Vector competence of *Cx. pipiens* mosquitoes

Infections of *Cx. pipiens* mosquitoes were performed at the Institut Pasteur, Paris, France. Briefly, 5- to 7-day-old female

10.3389/fmicb.2023.1324069

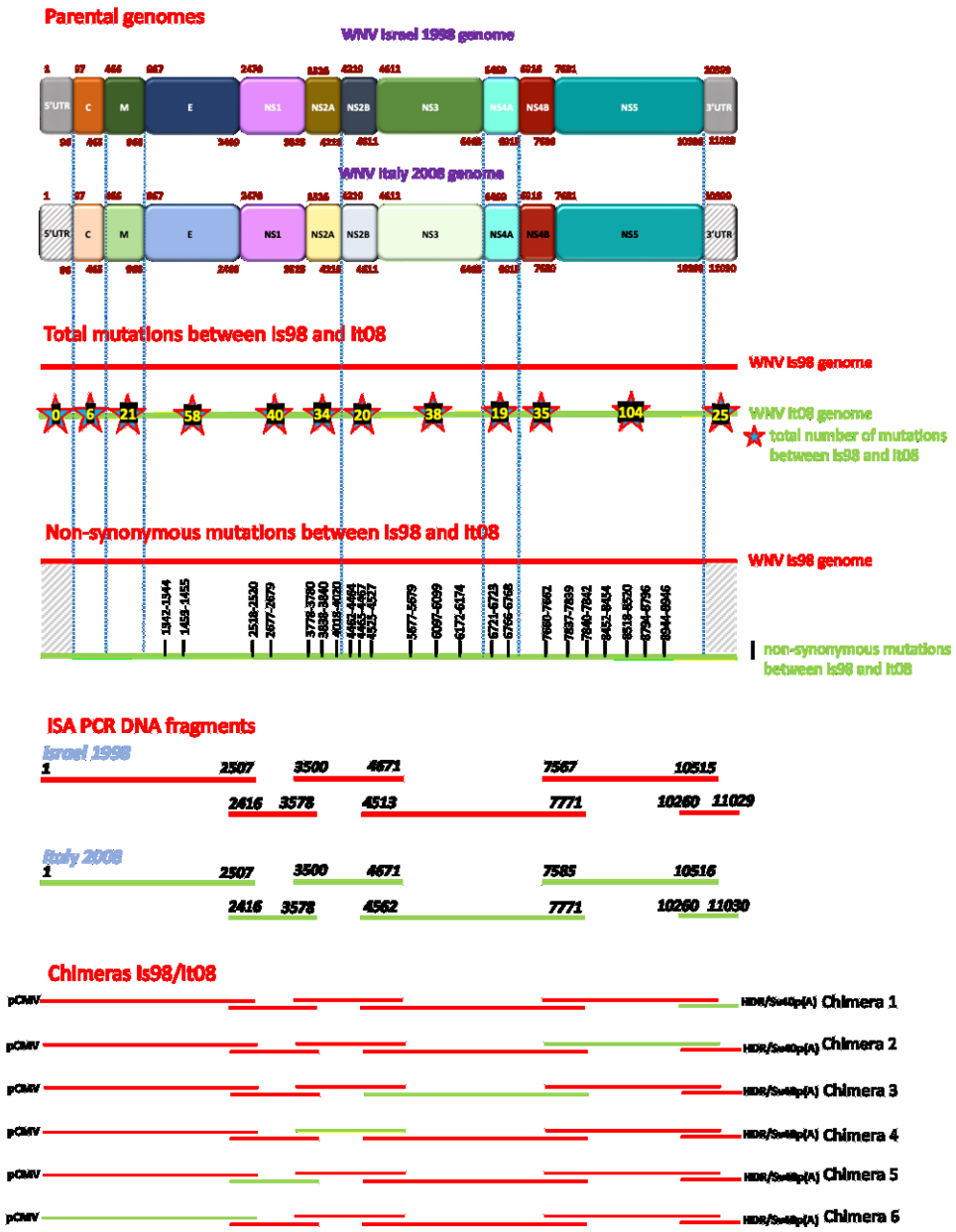

FIGURE 1
Schematic representation of chimeric constructs generated by the ISA method. Red lines represent WN-IS98 genome or corresponding PCR products. Green lines represent WN-IT08 genome or corresponding PCR products. The total number of synonymous and non-synonymous mutations between the two strains are reported inside stars on WN-IT08 genome. The exact start and end nucleotide positions are indicated for each ISA PCR DNA fragments. Chimeras are flanked at 5′ and 3′ ends by pCMV promoter and HDR/SV40p(A), respectively.

mosquitoes were transferred into plastic boxes and starved for 24 h in a biosafety level 3 insectarium before being orally infected with WN-IS98, WN-IT08, chimera IS98-3′UTR or IS98-3′NS4B/NS5 provided in a blood-meal corresponding to washed rabbit erythrocytes (2/3) mixed with a viral sample (1/3) at a final concentration of 10^7 $TCID_{50}$/mL. Adenosine triphosphate (ATP) (Sigma-Aldrich) was added as a phagostimulant at a final concentration of 5×10^{-3} M. Fully engorged females were maintained in cardboard boxes, at 28°C and 80% humidity for 14 days with a 12 L: 12 D circadian cycle and then processed for saliva collection (Amraoui et al., 2016). Batches of around twenty female mosquitoes were dissected at 14 days post-infection after cold anesthesia. Briefly, legs and wings of each mosquito were removed, and the proboscis was inserted into a 20 μL tip containing 5 μL of FBS for saliva collection. Head/thorax and body were separated from each mosquito and ground individually in DMEM (ThermoFisher Scientific, Montigny-le-Bretonneux, France). For each mosquito, abdomen was removed and processed alone to characterize infection. Head and thorax were processed together to characterize dissemination (crossing the intestinal barrier) and saliva was collected to characterize transmission. Each mosquito sample (abdomen, head and thorax, saliva) was analyzed separately. Abdomen and head/thorax were grinded in 500 uL of medium. The infection rate and dissemination efficiency were

assessed using RT-qPCR detection on body and head, respectively, whereas transmission efficiency was performed using $TCID_{50}$ viral titration on saliva. Infection rate corresponds to the percentage of mosquitoes presenting positive Ct after abdomen homogenization, compared to total mosquitoes dissected. Dissemination efficiency corresponds to the percentage of mosquitoes presenting positive Ct after head/thorax homogenization, compared to the total of mosquitoes positive for infection. Transmission efficiency corresponds to the percentage of positive saliva (evaluated by $TCID_{50}$ assay) compared to total mosquitoes positive for infection.

2.10 Statistical analysis

All statistical analyses were performed using GraphPad Prism software and the appropriated Kruskal-Wallis or Fisher's exact tests.

3 Results

3.1 Production of chimeric viruses between WN-IS98 and WN-IT08

Six chimeric viruses constructed by inserting different genomic fragments (3′UTR, 3′NS4B/NS5, 3′NS2B/NS3/NS4A/NS4B, NS2A/NS2B, NS1, 5′UTR/C/prM/E) from the low virulent WN-IT08 into the WN-IS98 genome were obtained by using ISA. Next-generation sequencing confirmed that chimeric constructs had indeed been obtained. Briefly, **Figure 2** corresponds to the hive plot representation of the sequencing data obtained for the 6 WN-IS98/IT08 chimeras generated. For each chimera, three axes are represented. The one on the left corresponds to WN-IS98 genome, the right axis corresponds to WN-IT08 genome and the other corresponds to the chimera sequence. Each colored curve represents genomic similarities between the parental viruses and the chimeric construct. Here, we confirm that chimeras comprised the WN-IS98 backbone with WN-IT08-derived fragments corresponding to the 3′UTR (IS98-3′UTR), 3′NS4B and NS5 (IS98-3′NS4B/NS5), 3′NS2B, NS3, NS4A and NS4B (IS98-3′NS2B/NS3/NS4A/NS4B), NS2A and NS2B (IS98-NS2A/NS2B), NS1 (IS98-NS1), and finally the 5′UTR, C, prM and E (IS98-5′UTR/C/prM/E). The sequence of WNV IC-IS98 and derived chimeras differed from the reference IS-98 STD strain (Genbank accession number AF481864.1) by 7 non-synonymous mutations: NS1-N17S; NS2A-R165G; NS2B-G82D; NS2B-E83G, NS3-P496L, NS3-E521D and NS5-N280K. These mutations probably reflect sequencing errors of the reference IS-98 STD strain or mutations having occurred during isolation and the first passages of the IS-98 STD strain, since the sequence of WNV IC-IS98 was determined to be identical to the parental WN-IS98 isolate used in our experimental assays. Of note, the replicative properties of IC-IS98 bearing these non-synonymous mutations were indistinguishable from those of the parental WN-IS98 isolate *in vitro* or *in vivo* (Bahuon et al., 2012).

Of note, a few mutations were introduced during the ISA procedure. Seven non-synonymous mutations have been identified by the sequencing of the complete genomes of the chimeras, that could have resulted from the amplification of naturally-occurring mutations in WN-IT08 and WN-IS98 isolates (quasi-species) or from the generation of errors during the amplification step. These mutations are: NS1-N207I (found on the chimera IS98-3′NS2B/NS3/NS4A/NS4B), NS3-R250K (found on chimera IS98-NS2A/NS2B), NS4B-C120F (found on chimera IS98-3′UTR), NS5-S54P (found on chimera IS98-3′NS2B/NS3/NS4A/NS4B and IS98-NS2A/NS2B), NS5-P431Q (found on chimera IS98-NS1), NS5-L432I (found on chimera IS98-5′UTR/C/prM/E) and NS5-V788I (found on chimera IS98-NS2A/NS2B).

In conclusion, six WN-IS98/WN-IT08 chimeric viruses were produced, with genomic sequences sharing more than 99.98% nt identity with the expected sequence.

3.2 Multiplication kinetics of the parental wild type (WT) isolates and chimeras in mammalian cell cultures

Replication kinetics were performed on *Vero* cells to compare the replicative fitness of each chimeric construct and parental strain in susceptible mammalian cells. *Vero* cells were infected at MOI 0.1 and cell culture supernatants were harvested at 17 h, 24 h, 48 h, and 72 h pi. Amounts of viral RNA and infectious particles were measured using RT-qPCR assay (number of genome copy/μL) and $TCID_{50}$, respectively. Replication kinetics of parental viruses were similar (**Figure 3**). Differences, however, were observed between chimeras, especially at 17 h and 24 h p.i. Of note, total viral RNA was significantly lower for IS98-3′NS2B/NS3/NS4A/NS4B than for IS98-3′NS4B/NS5 ($p < 0.05$) or IS98-NS1 ($p < 0.0001$) at 17 h and 24 h p.i only. This result was confirmed by a significantly lower infectious titer for IS98-3′NS2B/NS3/NS4A/NS4B than for IS98-NS1 at 17 h and 24 h p.i., but the difference between IS98-NS2B/NS3/NS4A/NS4B and IS98-3′NS4B/NS5 at 17 h p.i was not statistically significant (**Figure 4**).

These results suggest that the replication of IS98-3′NS2B/NS3/NS4A/NS4B is decreased at early time points of infection before reaching a similar level at later time points (48 h and 72 h p.i.).

The same observations were made when considering IS98-NS2A/NS2B and IS98-NS1. The quantity of total viral RNA was lower for IS98-NS2A/NS2B than for IS98-NS1 ($p < 0.01$) at 17 h and at 24 h p.i. ($p < 0.0001$) (**Figure 3**). Viral infectious titers confirmed these results only at 24 h p.i ($>10^6$ $TCID_{50}$/mL for IS98-NS2A/NS2B and $>10^8$ $TCID_{50}$/mL for IS98-NS1) (**Figure 4**). Surprisingly, quantification of total RNA at 48 h showed impaired replication of WN-IS98 and WN-IT08 in comparison with IS98-3′UTR and IS98-3′NS4B/NS5.

In sum, two chimeras demonstrated impaired replication kinetics in *Vero* cells, namely, IS98-3′NS2B/NS3/NS4A/NS4B and IS98-NS2A/NS2B, in comparison with chimeras IS98-NS1 and IS98-3′NS4B/NS5.

3.3 Replication of parental and chimeric viruses in BALB/cByJ mice

In vivo experiments performed in BALB/cByJ mice, which are highly susceptible to WNV, allowed us to

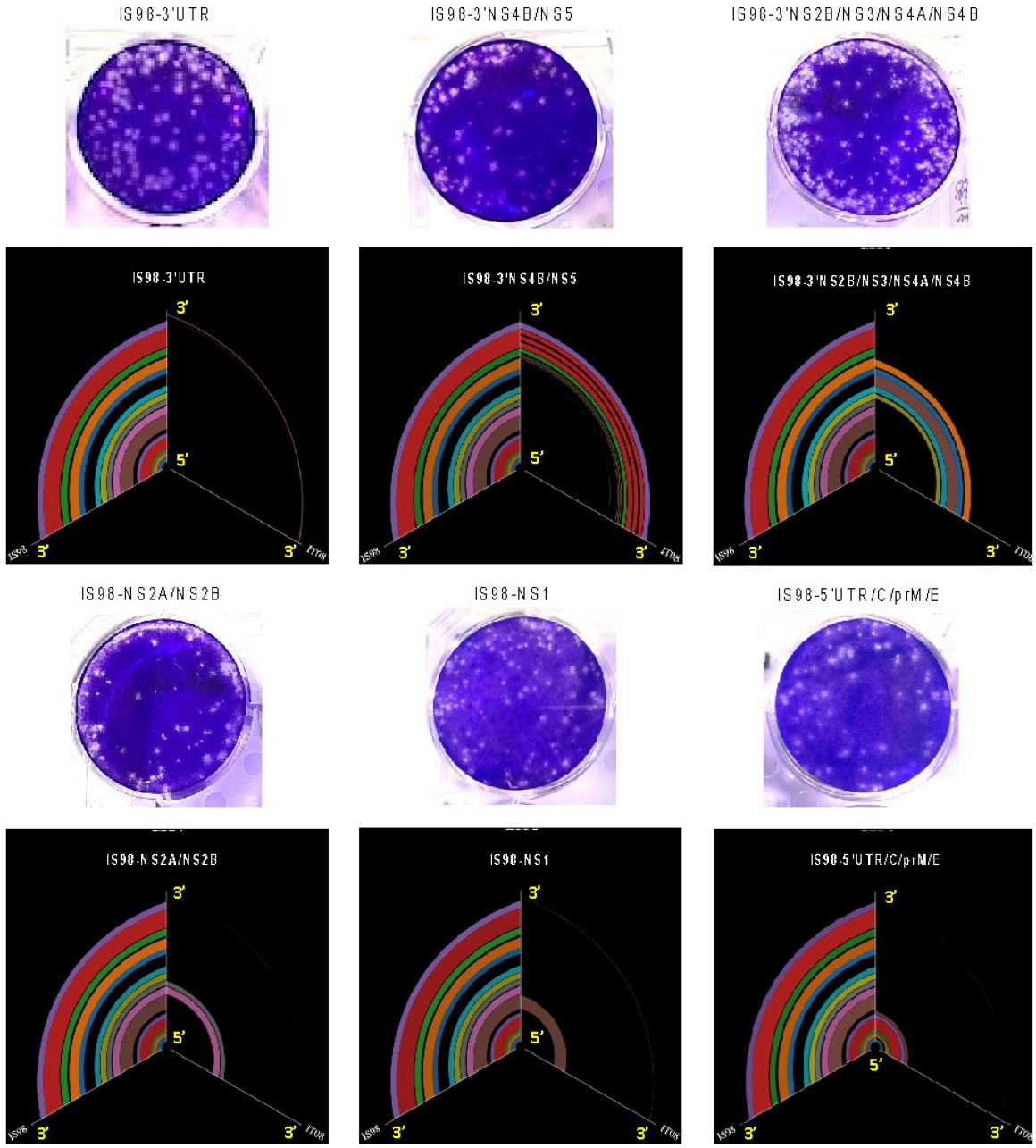

FIGURE 2
Hive plot representation of the sequence of the chimeric constructs. The middle axis represents the chimeric genome, the left axis the WN-IS98 genome – the line between the two represents the shared genomic regions, based on blastx alignment on the pfam conserved domain DB, the right axis is the WN-IT08 strain and lines between the middle and right axis represent shared regions between WN-IT08 and the chimeras.

characterize WNV pathogenicity regarding viremia, virus dissemination in peripheral tissues (data not shown), neuroinvasiveness and virulence. BALB/cByJ mice were infected by WN-IS98 and WN-IT08 strains and by chimeras IS98-3′NS4B/NS5 and IS98-3′NS2B/NS3/NS4A/NS4B, this latter having demonstrated decreased replication in comparison with IS98-3′NS4B/NS5 (control chimera) at early time points in mammalian cells. We hypothesized that such impaired replication of IS98-3′NS2B/NS3/NS4A/NS4B could affect early replication in mice and consequently decrease viremia.

As expected, a peak of viremia was reached at 3 days post-infection (data not shown). No significant differences were observed between the tested viruses. Nevertheless, IS98-3′NS2B/NS3/NS4A/NS4B tended to induce lower viremia ($<10^1$ RNA copy/μL) than WN-IS98 and IS98-3′NS4B/NS5 (Figure 5).

BALB/cByJ were monitored 12 days after i.p. inoculation. All mice infected with the parental strain WN-IS98 died at day 7 p.i., whereas only one mouse infected with WN-IT08 and 2 mice infected with IS98-3′NS4B/NS5 died at the same day p.i. Delayed death during infection by IS98-3′NS2B/NS3/NS4A/NS4B became evident on day 8 p.i. Kruskal-Wallis analysis at 7 days

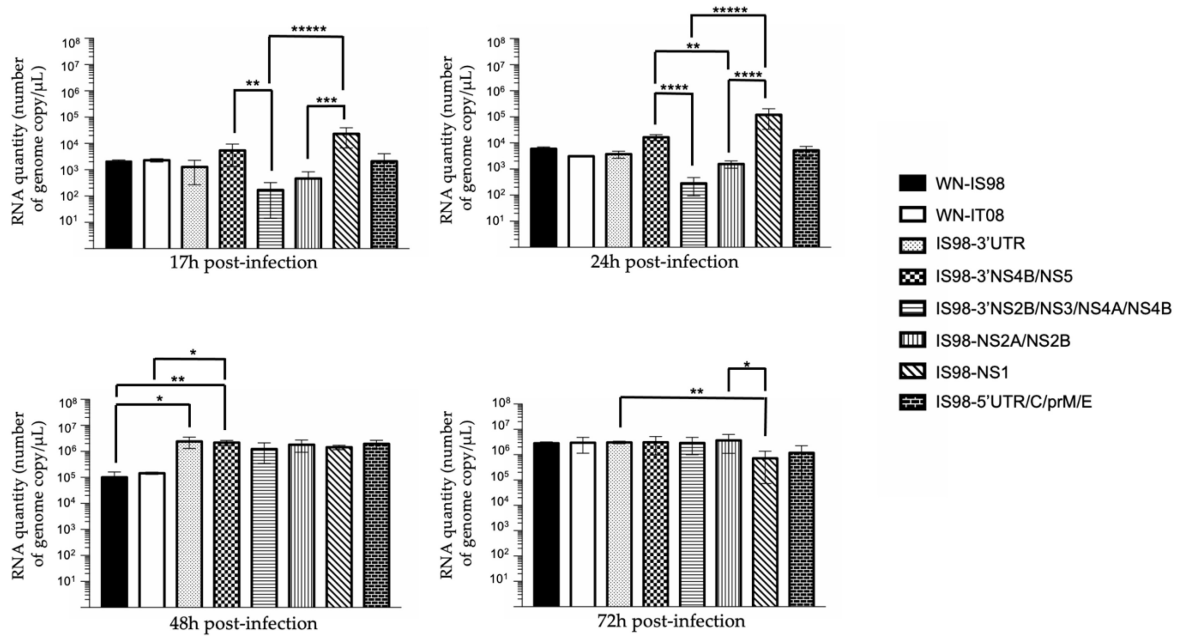

FIGURE 3
RT-qPCR analysis at 17 h, 24 h, 48 h, 72 h post-infection of parental strains and chimeras. *Vero* cells were infected with the indicated virus at multiplicity of infection (MOI) of 0.1. At the indicated time, cell culture supernatants were collected and analyzed by RT-qPCR. Number of genome copy/µL were quantified. Group statistical comparisons were performed by the non-parametrical Kruskal-Wallis test. Paired statistical comparisons were performed by Dunn's analysis. Results represent the mean of duplicate experiments, and in each experiment each point was performed in triplicate. The error bar indicates the standard deviation (SD) of duplicate measures. *0.05 < P < 0.1; **0.01 < P < 0.05; ***0.001 < P < 0.01; ****P < 0.001; *****P < 0.0001.

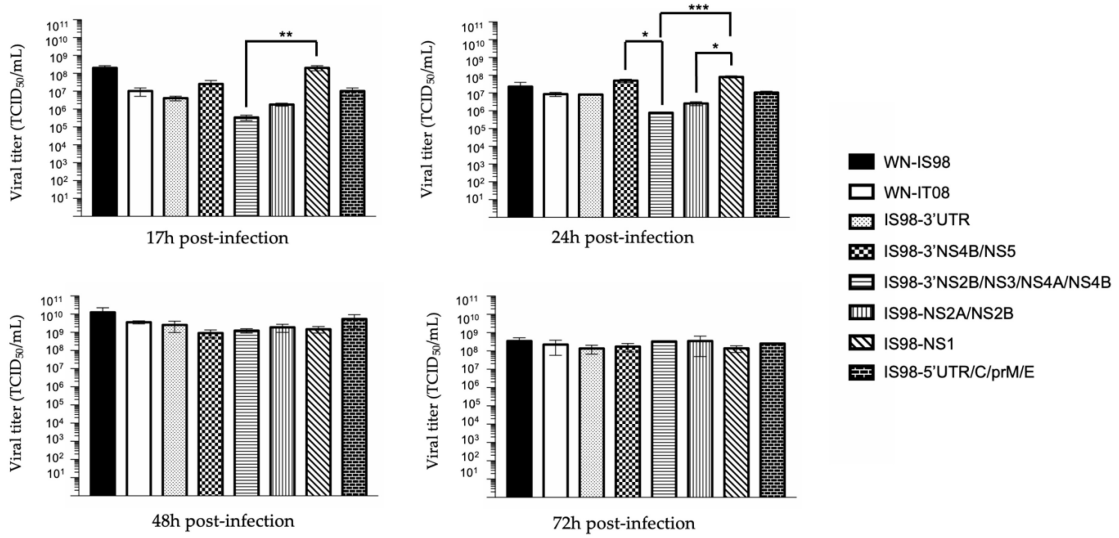

FIGURE 4
$TCID_{50}$ quantification at 17 h, 24 h, 48 h, and 72 h post-infection of parental strains and chimeras. *Vero* cells were infected with the indicate virus at multiplicity of infection (MOI) of 0.1. At the indicated time, cell culture supernatants were collected and analyzed by $TCID_{50}$ quantification. Infectious virus titers were expressed in $TCID_{50}$/mL. Each sample was analyzed in triplicate. Group statistical comparisons were performed by the non-parametrical Kruskal-Wallis test. Paired statistical comparisons were performed by Dunn's analysis. Results are represented as the mean of duplicate experiments, and in each experiment each point was performed in triplicate. The error bar indicates the standard error of the mean (SEM) of triplicate measures. *0.05 < P < 0.1; **0.01 < P < 0.05; ***0.001 < P < 0.01.

p.i. showed a significant difference in mortality between IS98-3′NS2B/NS3/NS4A/NS4B and WN-IS98 ($p < 0.01$) and between WN-IT08 and WN-IS98 ($p < 0.05$). No other differences were observed in mortality (Figure 6A).

Since WNV is a neurotropic virus, neuroinvasion and viral load in the CNS are relevant parameters to evaluate in the course of WNV infection. Total RNA in the brain was quantified by RT-qPCR. Although no statistical differences were observed in the level

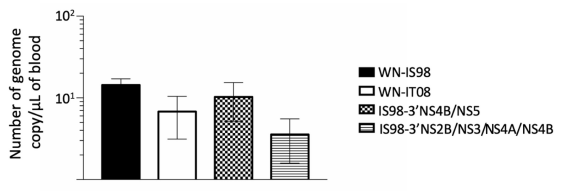

FIGURE 5
Viremia 3 days after intraperitoneal inoculation of female BALB/cByJ mice with 10 PFU of WNV IS98, WNV IT08 and chimeras IS98-3′NS4B/NS5 and IS98-3′NS2B/NS3/NS4A/NS4B. Viral RNA load in blood was quantified by RT-qPCR. The error bar indicates standard error of the mean (SEM).

of total RNA (Figure 6B), WNV was detected in the brains of animals belonging to all four groups. Although the quantity of total RNA in brain post-mortem was comparable for all four viruses, WN-IT08, IS98-3′NS4B/NS5 and IS98-3′NS2B/NS3/NS4A/NS4B seemed to induce delayed mortality in comparison with WN-IS98.

3.4 Multiplication kinetics of the parental wild type (WT) isolates and chimeras in insect cell cultures (C6/36)

Replication kinetics were assessed on the *Aedes albopictus* mosquito cell line, C6/36. In contrast to results obtained in *Vero* cells showing no impairment in replication of parental WNV isolates, the level of total viral RNA was significantly lower for the parental strain WN-IS98 than the IS98-3′NS4B/NS5 chimera at 17 h ($p < 0.0001$), 24 h ($p < 0.05$) and 48 h ($p < 0.05$) p.i. (Figure 7). Moreover, the quantity of total RNA seemed to be significantly reduced for IS98-3′UTR than for the parental strain WN-IT08 at 24 h ($p < 0.001$), 48 h ($p < 0.05$) p.i. and compared to WN-IS98 at 72 h p.i. ($p < 0.01$). IS98-3′UTR is the chimeric construct that demonstrated the lower RNA quantity when compared with other chimeras, especially with IS98-3′NS4B/NS5 at 17 h ($p < 0.0001$), 24 h ($p < 0.0001$), 48 h ($p < 0.0001$) and even 72 h p.i. ($p < 0.0001$). Moreover, IS98-3′NS4B/NS5 presented significantly higher viral RNA copies than IS98-5′UTR/C/prM/E at 17 h ($p < 0.05$), 24 h ($p < 0.05$), 48 h ($p < 0.05$) and 72 h ($p < 0.05$).

Cell supernatants of C6/36 mosquito cells infected at 0.1 MOI were collected at 17 h, 24 h, 48 h and 72 h p.i. IS98-3′UTR showed decreased replication in comparison with IS98-NS2A/NS2B and WN-IS98 at 17 h p.i. ($p < 0.1$) and with IS98-3′NS2B/NS3/NS4A/NS4B at 72 h p.i. ($p < 0.05$) (Figure 8). In conclusion, the insertion of the 3′UTR of the WN-IT08 strain in the WN-IS98 genome impaired IS98-3′UTR replication in C6/36 mosquito cells at most time points (17–72 h p.i.).

3.5 Replication of parental and chimeric viruses in *Cx. pipiens* mosquitoes

Compared to *in vitro* analyses, *in vivo* testing in mosquitoes allows evaluation of vector competence, regarding infection rate (IR), dissemination efficiency (DE) and transmission efficiency (TE).

In order to assess the differential ability of parental and chimeric viruses to cross the midgut barrier and spread in *Cx. pipiens* mosquitoes, the IR, DE, and TE were determined for parental strains WN-IS98 and WN-IT08, as well as for chimeras IS98-3′UTR and IS98-3′NS4B/NS5 (control chimera). IS98-3′UTR has been shown to replicate less efficiently in mosquito cells, and we hypothesized that such properties could decrease IR, DE or TE in *Cx. pipiens* mosquitoes. While IR reflects the infection rate of engorged female mosquitoes among tested individuals, DE is the proportion of infected females in which WNV was able to cross the midgut barrier and penetrate the mosquito haemocoel. Finally, the ability of each tested virus to reach the salivary glands was evaluated by determining the transmission efficiency (TE), which corresponds to the proportion of female mosquitoes that secrete infectious saliva among tested specimens.

The IRs were significantly higher for parental strains than for chimeric viruses IS98-3′UTR and IS98-3′NS4B/NS5 (Figure 9A).

Infection of *Cx. pipiens* was higher for WN-IS98 and WN-IT08 (67 and 73%, respectively) (Fisher's exact test) than for IS98-3′UTR (24%) ($p < 0.001$) and IS98-3′NS4B/NS5 (17%) ($p < 0.001$). No significant differences, however, were observed between parental viruses or between the chimeras as regards infection rates. Concerning the percentage of dissemination, significant differences were observed between IS98-3′UTR (43%) and IS98-3′NS4B/NS5 (80%) and between IS98-3′NS4B/NS5 (80%), WN-IS98 (42%) and WN-IT08 (43%). No significant differences in transmission, however, were observed among the four viruses, even though WN-IS98 and WN-IT08 tended to be more easily identified in saliva than IS98-3′UTR and IS98-3′NS4B/NS5 (Figure 9A). Similar viral RNA loads, between 10^5 and 10^6 RNA copies, were identified in abdomens (Figure 9B), heads and thorax (Figure 9C) after infection with parental and chimeric viruses. Although not statistically significant, differences in infectious viral titers in the saliva of infected mosquitoes were reported, with infectious titers for WN-IT08 and IS98-3′UTR (about 10^5 $TCID_{50}$/mL) being at least 10 times higher than those of WN-IS98 and IS98-3′NS4B/NS5 (about 10^3 $TCID_{50}$/mL) (Figure 9D).

In conclusion, the transmission risk of IS98-3′UTR by *Cx pipiens* mosquitoes was severely reduced (2/58, 3.4%), in comparison with WN-IS98 (10/54, 18.5%) and WN-It08 (13/60, 21.7%).

4 Discussion

Infectious subgenomic amplicons reverse genetics was successfully adapted to two lineage 1 Mediterranean strains of varying virulence, WN-IS98 and WN-IT08. Along with experimental infection of model hosts for WNV circulation in Europe, namely, *Cx. pipiens* mosquitoes and BALB/cByJ mice as a proxy for WNV infection in mammals, the method permitted identification of the molecular determinants of WNV virulence and pathogenicity and exploration of the mechanisms responsible for outbreaks of varying severity.

We recently identified the NS4A/NS4B/5'NS5 region of the viral genome as being implicated in increased bird mortality during

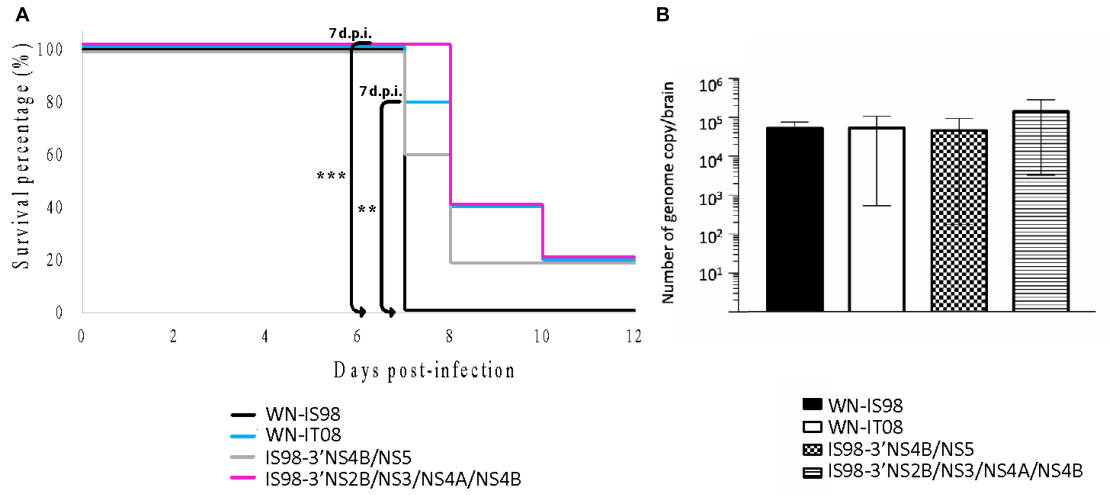

FIGURE 6
Neuroinvasive properties and neurovirulence of WN-IS98, WN-IT08 and their chimeras in 2-week-old female BALB/cByJ mice. Mice were infected intraperitoneally with 10 PFU and monitored for 12 dpi. **(A)** Survival growth. **(B)** Genome quantification in the brain of dead mice assessed by RT-qPCR. The error bar indicates standard error of the mean (SEM). **0.01 < *P* < 0.05; ***0.001 < *P* < 0.01.

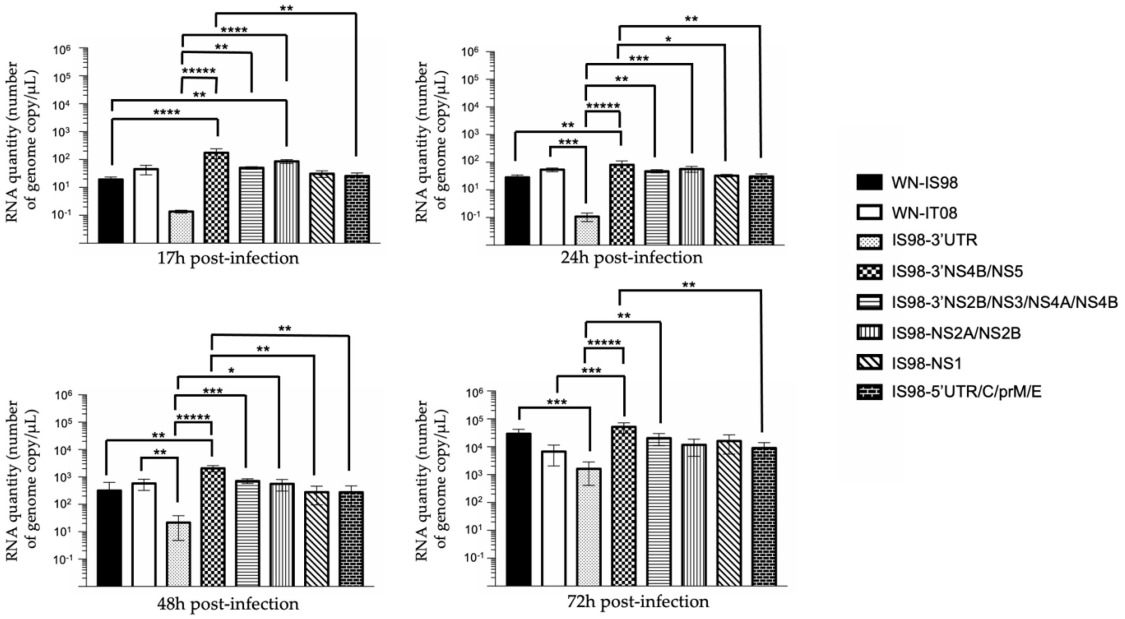

FIGURE 7
RT-qPCR analysis at 17 h, 24 h, 48 h, 72 h post-infection of parental strains and chimeras. C6/36 cells were infected with the indicated virus at multiplicity of infection (MOI) of 0.1. At the indicated time, cell culture supernatants were collected and analyzed by RT-qPCR. Number of genome copies/µL was quantified. Group statistical comparisons were performed by the non-parametrical Kruskal-Wallis test. Paired statistical comparisons were performed by Dunn's analysis. Each mean representation results from duplicate experiments, and in each experiment each point was performed in triplicate. The error bar indicates standard deviations (SD). *0.05 < *P* < 0.1; **0.01 < *P* < 0.05; ***0.001 < *P* < 0.01; ****$P < 0.001$; *****$P < 0.0001$.

Mediterranean WNV outbreaks (Fiacre et al., 2023). Here, we provide information on the role of other NS and structural proteins of WNV-IS98 and IT08 as virulence factors in mammalian hosts, as well as on factors modulating virus transmission in mosquito vectors.

Six chimeric viruses were constructed involving exchanges between WNV-IS98 and IT08, such that either structural (C, prM, E), non-structural (NS) or untranslated regions (UTR) of the WN-IS98 genome were replaced by the cognate regions of the IT08 strain. Chimeras were generated using the versatile infectious subgenomic amplicons (ISA) reverse genetic technology (Aubry et al., 2015). The ISA method avoids constraints associated with the use of infectious bacterial clones such as the propagation of potentially toxic cDNA copies of the viral genome in bacteria. Comparison of the replicative fitness of parental and chimeric viruses were carried out in mammalian and mosquito cell culture

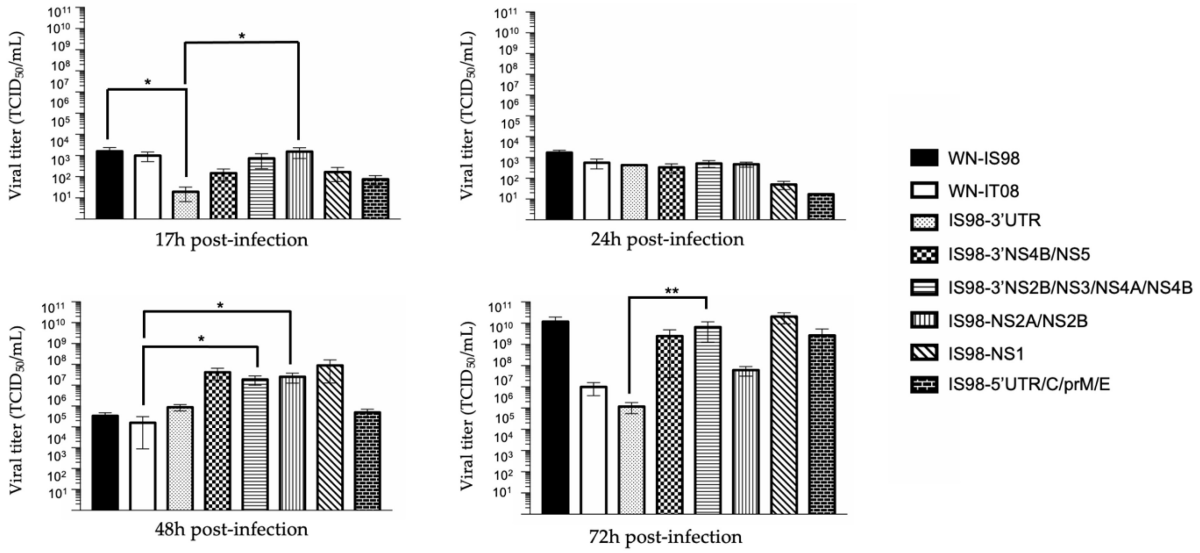

FIGURE 8
$TCID_{50}$ quantification at 17 h, 24 h, 48 h, and 72 h post-infection of parental strains and chimeras. C6/36 cells were infected with the indicated virus at multiplicity of infection (MOI) of 0.1. At the indicated time, cell culture supernatant was collected and analyzed by $TCID_{50}$ quantification. Viral quantities of infectious virus are expressed in $TCID_{50}$/mL. Each sample was analyzed in triplicate. Group statistical comparisons are performed by the non-parametrical Kruskal-Wallis test. Paired statistical comparisons are performed by Dunn's analysis. Results are represented as means od duplicate experiments, and in each experiment each point was performed in triplicate. The error bar indicates standard error of the mean (SEM) for each triplicate. *$0.05 < P < 0.1$; **$0.01 < P < 0.05$.

A

	% infection	% dissemination#	% transmission#	Total transmission/ Total engorged
WN-IS98	67% (36/54)	42% (15/36)	28% (10/36)	10/54
WN-IT08	73% (44/60)	43% (19/44)	30% (13/44)	13/60
IS98-3'UTR	24% (14/58)	43% (6/14)	14% (2/14)	2/58
IS98-3'NS4B/NS5	17% (10/60)	80% (8/10)	10% (1/10)	1/60

%Dissemination and transmission were calculated out of number of mosquitoes infected.

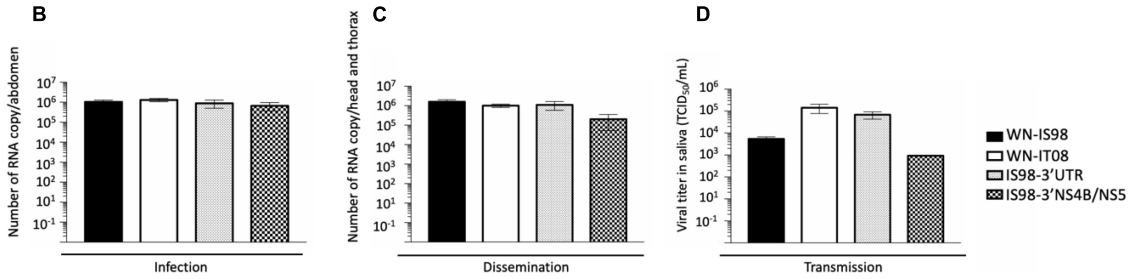

FIGURE 9
Infection, dissemination, and transmission rates after a blood meal with 10^7 $TCID_{50}$/mL of WN-IS98, WN-IT08, IS98-3′UTR and IS98-3′NS4B/NS5. **(A)** Percentage of mosquitoes presenting an infection, dissemination, or transmission. **(B)** Viral titer in abdomen assessed by RT-qPCR. **(C)** Viral titer in head and thorax assessed by RT-qPCR. **(D)** Viral titer in saliva assessed by $TCID_{50}$ titration. The error bar indicates standard error of the mean (SEM). *$0.05 < P < 0.1$; ****$P < 0.001$.

models, and virulence and viral transmission were assessed *in vivo* in mice and in *Cx. pipiens* mosquitoes, respectively.

Thirty-one mutations had been previously shown to be implicated in WNV virulence in mammalian models, including E-159, NS3-249 and NS1-175, but only a few of them, such as NS3-483, NS1-175 and NS1-207 (Fiacre et al., 2020), have been identified as molecular determinants of virus replication in mosquitos. Consequently, among the molecular markers implicated in the West Nile transmission cycle, those found not only in mammalian and avian hosts, but also in mosquito vectors, require further characterization.

We first investigated the viral fitness and pathogenicity of chimeric and parental viruses *in vitro* in *Vero* cells and *in vivo* in BALB/cByJByJ mice, respectively. Our results were indicative of a delayed replication of IS98-3′NS2B/NS3/NS4A/NS4B *in vitro*, a finding confirmed by an attenuated phenotype *in vivo*. Indeed, viral RNA loads and infectious viral titers were significantly lower than those of IS98-NS5 and IS98-NS1 at

17 h and 24 h p.i. (**Figures 8**, **9**). Surprisingly, reduced virus replication of IS98-3′NS2B/NS3/NS4A/NS4B was no longer observed from 48 h p.i onward. Such delayed replication of IS98-3′NS2B/NS3/NS4A/NS4B may have an impact on early stages of infection and therefore on the capacity for spread and potential for neuroinvasion of IS98-3′NS2B/NS3/NS4A/NS4B in mice. Indeed, WNV spread in model mice is intimately linked to the magnitude of viremia at early time points after peripheral virus inoculation. *In vivo*, viremia quantified at day 3 p.i tended to be lower in IS98-3′NS2B/NS3/NS4A/NS4B-infected mice than for other tested viruses. Furthermore, at 12 days p.i. the mortality rate of mice infected with IS98-3′NS2B/NS3/NS4A/NS4B or WN-IT08 was similar (80%), and inferior to that of mice infected with WN-IS98 (100%), thus confirming the attenuated phenotype of this chimeric construct. In contrast, while IS98-NS5 showed efficient early replication compared to WN-IS98 and WN- IT08 *in vitro*, this result was not confirmed *in vivo*. IS98-3′NS4B/NS5-infected mice exhibited a viremia as high as that of mice infected with parental viruses, even if the mortality rate of IS98-3′NS4B/NS5-infected mice was closer to that of WN-IT08. In conclusion, IS98-3′NS2B/NS3/NS4A/NS4B and IS98-3′NS4B/NS5 displayed a degree of attenuation comparable to that of WN-IT08 and lower than that of the highly virulent WN-IS98, both confirming our previous findings suggesting a role for NS5 and 3′UTR in determining virulence in mice and serving to identify additional virulence determinants in the 3′NS2B/NS3/NS4A/NS4B region (Fiacre et al., 2020).

IS98-3′NS2B/NS3/NS4A/NS4B displayed an attenuated phenotype *in vitro* on *Vero* cells and *in vivo* in BALB/cByJ mice. We previously reported (Fiacre et al., 2023) that IS98-NS4A/NSAB/5′NS5 showed an attenuated phenotype in SPF chickens but not mice. Our new findings suggest an essential role for 3′NS2B and NS3 genomic regions as well in and in modulating replication efficacy in mammals, presumably by determining interactions between viral components (protein or RNA) and cellular components. The role of specific mutations differing between WN-IS98 and WN-IT08 in 3′NS2B and NS3, namely, NS3-P496L and NS3-E521D, in WNV virulence should be further studied. This chimeric construct exhibited other non-synonymous substitutions located in NS1 [NS1-N207I known as a molecular factor implicated in virulence attenuation in mammals (Whiteman et al., 2010), and probably generated during *SuperFi* polymerase amplification in the ISA process] and in the NS4/NS5 genomic regions (NS4A-A85I, NS4A-P100S, and NS5-S54P).

Comparison of WN-IS98 and WN-IT08 genomes revealed 22 non-synonymous mutations, including E-V159I, also found on IS98-NS1, and NS4B-E249D. Kobayashi et al. (2020), demonstrated that E-I159V increased virulence in a mouse model. Here, the attenuated phenotype of WN-IT08 in mammals could be due to the E-V159I or the NS4B-E249D mutations, as well as to other modifications discussed earlier. In a previous study investigating chimeras between WN-IS98 and WN-IT08 focusing on the 3′ end of the genome (NS4A, NS4B, NS5, and 3′UTR regions), we showed that the NS4B-249 residue could be implicated in slightly decreased virulence in mice (Fiacre et al., 2023). However, we showed in Fiacre et al. (2023), that the IS98-NS4A/NS4B/5′NS5 chimera containing NS4B-E249G was not markedly attenuated in mice. Here, IS98-NS4B/NS5 containing NS4A from WN-IS98 is attenuated in the mice model, suggesting a role for cumulative molecular changes in host virulence and a possible role for NS4A in the modulation of virulence in mammals.

In order to gain deeper insight into the viral determinants modulating mosquito-borne transmission, we performed experiments in insect models, including *in vitro* assays in the C6/36 mosquito cell line and competence studies in *Cx. pipiens* mosquitoes. Replication kinetics performed in C6/36 cells are indicative of an attenuated phenotype of IS98-3′UTR, as evidenced by lower viral RNA quantities and a lower production of infectious virions at 17 h post-infection, compared to the parental viruses and chimera IS98-3′NS4B/NS5. Of note, IS98-3′NS4B/NS5 and IS98-3′NS2B/NS3/NS4A/NS4B, which demonstrated reduced virulence in mice, did not show reduced replication in insect cells. We further assessed the vector competence of *Cx. pipiens* mosquitoes with WN-IS98, WN-IT08, IS98-3′UTR and IS98-3′NS4B/NS5. Vector competence is defined as the ability of an arthropod to transmit a pathogen after infection. This combines the intrinsic ability of the virus to successfully enter, replicate within the vector, disseminate, and finally replicate in the salivary glands before being released at a concentration that suffices for infection of a naïve vertebrate host. Even if IS98-3′UTR and IS98-3′NS4B/NS5 infected less *Cx. pipiens* than WN-IS98 and WN-IT08, they disseminated as efficiently as their parental strains. Moreover, the transmission rate of chimeric constructs was 50% lower than that of parental strains. Our results imply that the 3′UTR and the NS5 genomic regions of WN-IS98 are essential virulence factors implicated in the infection of *Cx. pipiens* and the release of the virus in the saliva. All together, these results suggest that *Cx. pipiens* is less competent for the two chimeric viruses than for either parental viruses. The altered phenotype may result from the reassociation of genomic regions originating from two different parental strains leading to suboptimal functional interactions at the molecular level during the virus cycle or from single point mutations introduced unintentionally during the ISA procedure, even though such non-synonymous mutations have been infrequently documented when complete genome sequences of parental and chimeric constructs have been compared.

We hypothesize that the replacement of the 3′UTR region of WN-IS98 by the corresponding region in WN-IT08 altered genome interactions involved in the first steps of WNV replication in mosquitoes. The 5′ and 3′UTR can form conserved stem-loop structures (Brinton et al., 1986; Brinton and Dispoto, 1988) like the 5′CS/3′CSI (Hahn et al., 1987) or the 5′UAR/3′UAR interactions (Hahn et al., 1987). As no differences were observed in these regions in our two parental genomes, we propose that nt 10517, nt 10520, nt 10523, nt 10689, nt 10721, nt 10775, nt 10830, nt 10832, nt 10852, which differ between WN-IS98 and WN-IT08, could be responsible for the altered vector-pathogen interactions and reduced replication in *Cx. pipiens*. Moreover, IonTorrent sequencing of the IS98-3′UTR chimera revealed two substitutions, one non-synonymous (NS4B-C120F) and the other synonymous (NS5-N867N, that could also play a role in *Cx. pipiens* replication.

As previously discussed in Fiacre et al. (2023), the NS5 protein is composed of many important conserved sequences known to be implicated in viral replication. However, no differences in these

regions were observed between the sequences of WN-IS98 and WN-IT08. Other mutations found in WN-IT08 *vs.* WN-IS98 could be responsible for differences in replicative capacity in mammals and mosquitoes, such as NS5-H53Y, NS5-S54P, NS5-V258A, NS5-N280K, NS5-A732V and NS5-R422K. Moreover, IS98-3′NS4B/NS5 also contains the NS4B-E249G mutation identified in WN-IT08. The NS4B-249 residue is known to modulate WNV virulence in birds and mammals (Davis et al., 2004), but was also identified by Van Slyke et al. (2013) as a molecular marker implicated in enhanced transmission in *Cx. tarsalis,* in addition to prM-V156I and NS5-A804V (Davis et al., 2004). We demonstrated significantly enhanced transmission of IS98-3′NS4B/NS5 in comparison with parental viruses and IS98-3′UTR, which may question a role for NS4B-E249G in promoting the crossing of the midgut epithelium by WNV in *Cx. pipiens* mosquitoes.

Other non-synonymous mutations between WN-IS98 and IT08 have been previously shown to modify WNV replication in mosquitoes. As previously shown by Moudy et al. (2007), E protein modification at amino acid 159 (E-U159C, found in WN02) can be implicated in a shortening of the extrinsic incubation period. Our study did not reveal any difference in the replication capacity of WN-IS98 and WN-IT08 in C6/36 cells or in *Cx. pipiens*, suggesting that E-V159I cannot alone be responsible for modulating vector replication.

To conclude, our study improves knowledge about the molecular determinants that are responsible for the attenuated phenotype of WN-IT08 in mammalian hosts, namely, 3′NS2B/NS3/NS4A/NS4B and possibly NS3-P496L, NS3-E521D, NS4A-A85I and NS4A-P100S mutations. We cannot completely exclude the possibility that creation of the chimeras induced new mutations that possibly modulated mammalian virulence, such as the well-known molecular determinant NS1-N207A or the mutation NS5-S54P. As reported previously in Fiacre et al. (2023), NS5 mutations present in WN-IT08 can, through genomic interactions, participate in WNV attenuation. We also showed that no differences in vector competence were detected for WN-IS98 and WN-IT08, despite the fact that NS4B/NS5 and possibly the NS4B-E249G substitution improved dissemination in *Cx. pipiens*. Infection and transmission of viruses by *Culex* vectors seem to be influenced by interaction of NS4B/NS5 genes or proteins with the mosquito. Our results also suggest a role for the 3′UTR in vector infection/transmission, especially nt 10517, 10520, 10523, 10689, 10721, 10775, 10830, 10832 and 10852.

Finally, our study extends our understanding of genetic factors that may influence virulence of WN-IS98 and WN-IT08, two European WNV lineage 1 isolates differing in virulence for vertebrate hosts. This study has several limits. First, it was carried out on custom-generated chimeric viruses in order to modify and study the pathobiological properties of a considered virus. Secondly, we were constrained by the initial genetic differences between the WNV strains studied, with several mutations, non-synonymous or not, per fragment exchanged. Finally, the virulence factors of interest in vertebrate hosts differ between mammalian and avian species as described in Fiacre et al., 2020. An assessment of viral fitness and virulence need to be carried out on the considered species, modeling reservoir or clinically-susceptible hosts relevant for WNV epidemiology. Further studies are needed to understand the parallels and differences between infection dynamics in vectors and virulence in vertebrate hosts, and to identify vulnerable targets at every step of the WNV transmission cycle amenable to therapeutic and prophylactic interventions.

Data availability statement

The original contributions presented in the study are included in the article/supplementary material, further inquiries can be directed to the corresponding authors.

Ethics statement

The animal study was approved by the Joint Anses-UPEC-Alfort Veterinary School ethics committee under the permit number 2022-11-15-11. The study was conducted in accordance with the local legislation and institutional requirements.

Author contributions

LF: Data curation, Formal analysis, Investigation, Methodology, Writing—original draft. AN: Methodology, Writing—review and editing. CM: Methodology, Writing—review and editing. MB: Validation, Writing—review and editing. MC: Methodology, Writing—review and editing. MD: Methodology, Writing—review and editing. TH: Methodology, Writing—review and editing. AE: Formal analysis, Writing—review and editing. NP: Writing—review and editing. DV: Methodology, Writing—review and editing. JR: Writing—review and editing. A-BF: Methodology, Writing—review and editing. MV: Writing—review and editing, Methodology. EA: Funding acquisition, Resources, Supervision, Writing—review and editing. SL: Conceptualization, Data curation, Investigation, Methodology, Project administration, Resources, Supervision, Validation, Writing—review and editing, Funding acquisition. GG: Conceptualization, Data curation, Investigation, Methodology, Project administration, Resources, Supervision, Validation, Writing—review and editing.

Funding

The author(s) declare that no financial support was received for the research, authorship, and/or publication of this article.

Acknowledgments

We would like to thank Oceane Le Bidel and Alain Bernier for their availability during the animal experimentation.

Conflict of interest

The authors declare that the research was conducted in the absence of any commercial or financial relationships that could be construed as a potential conflict of interest.

Publisher's note

References

Altschul, S. F., Gish, W., Miller, W., Myers, E. W., and Lipman, D. J. (1990). Basic local alignment search tool. *J. Mol. Biol.* 215, 403–410. doi: 10.1016/S0022-2836(05)80360-2

Amraoui, F., Atyame-Nten, C., Vega-Rúa, A., Lourenço-de-Oliveira, R., Vazeille, M., and Failloux, A. (2016). Culex mosquitoes are experimentally unable to transmit Zika virus. *Euro Surveill.* 21:30333. doi: 10.2807/1560-7917.ES.2016.21.35.30333

Aubry, F., Nougairède, A., de Fabritus, L., Querat, G., Gould, E., and de Lamballerie, X. (2014). Single-stranded positive-sense RNA viruses generated in days using infectious subgenomic amplicons. *J. Gen. Virol.* 95 (Pt 11), 2462–2467. doi: 10.1099/vir.0.068023-0

Aubry, F., Nougairède, A., Gould, E., and de Lamballerie, X. (2015). Flavivirus reverse genetic systems, construction techniques and applications: A historical perspective. *Antiviral Res.* 114, 67–85. doi: 10.1016/j.antiviral.2014.12.007

Bahuon, C., Desprès, P., Pardigon, N., Panthier, J., Cordonnier, N., Lowenski, S., et al. (2012). IS-98-ST1 West Nile virus derived from an infectious cDNA clone retains neuroinvasiveness and neurovirulence properties of the original virus. *PLoS One* 7:e47666. doi: 10.1371/journal.pone.0047666

Barzon, L., Pacenti, M., Montarsi, F., Fornasiero, D., Gobbo, F., Quaranta, E., et al. (2022). Rapid spread of a new West Nile virus lineage 1 associated with increased risk of neuroinvasive disease during a large outbreak in northern Italy, 2022: One health analysis. *J. Travel. Med.* taac125. doi: 10.1093/jtm/taac125

Basset, J., Burlaud-Gaillard, J., Feher, M., Roingeard, P., Rey, F., and Pardigon, N. (2020). A molecular determinant of West Nile virus secretion and morphology as a target for viral attenuation. *J. Virol.* 94, e00086–20. doi: 10.1128/JVI.00086-20

Bernkopf, H., Levine, S., and Nerson, R. (1953). Isolation of West Nile virus in Israel. *J. Infect. Dis.* 93, 207–218. doi: 10.1093/infdis/93.3.207

Bostock, M., Ogievetsky, V., and Heer, J. (2011). D3: Data-driven documents. *IEEE Trans. Vis. Comput. Grap.* 17, 2301–2309. doi: 10.1109/TVCG.2011.185

Brinton, M. A., and Dispoto, J. H. (1988). Sequence and secondary structure analysis of the 5'-terminal region of flavivirus genome RNA. *Virology* 162, 290–299. doi: 10.1016/0042-6822(88)90468-0

Brinton, M. A., Fernandez, A. V., and Dispoto, J. H. (1986). The 3'-nucleotides of flavivirus genomic RNA form a conserved secondary structure. *Virology* 153, 113–121. doi: 10.1016/0042-6822(86)90012-7

Chowdhury, P., and Khan, S. (2021). Global emergence of West Nile virus: Threat & preparedness in special perspective to India. *Indian J. Med. Res.* 154, 36–50. doi: 10.4103/ijmr.IJMR_642_19

Clé, M., Eldin, P., Briant, L., Lannuzel, A., Simonin, Y., Van de Perre, P., et al. (2020). Neurocognitive impacts of arbovirus infections. *J. Neuroinflammation* 17:233. doi: 10.1186/s12974-020-01904-3

Davis, C., Beasley, D., Guzman, H., Siirin, M., Parsons, R., Tesh, R., et al. (2004). Emergence of attenuated West Nile virus variants in Texas, 2003. *Virology* 330, 342–350. doi: 10.1016/j.virol.2004.09.016

Donadieu, E., Bahuon, C., Lowenski, S., Zientara, S., Coulpier, M., and Lecollinet, S. (2013). Differential virulence and pathogenesis of West Nile viruses. *Viruses* 5, 2856–2880. doi: 10.3390/v5112856

Dridi, M., Rauw, F., Muylkens, B., Lecollinet, S., van den Berg, T., and Lambrecht, B. (2013). Setting up a SPF chicken model for the pathotyping of West Nile Virus (WNV) strains. *Transbound. Emerg. Dis.* 60 Suppl 2, 51–62. doi: 10.1111/tbed.12144

Driouich, J., Moureau, G., de Lamballerie, X., and Nougairède, A. (2019). Reverse genetics of RNA viruses: ISA-based approach to control viral population diversity without modifying virus phenotype. *Viruses* 11:666. doi: 10.3390/v11070666

Fiacre, L., Lowenski, S., Bahuon, C., Dumarest, M., Lambrecht, B., Dridi, M., et al. (2023). Evaluation of NS4A, NS4B, NS5 and 3'UTR genetic determinants of WNV lineage 1 virulence in birds and mammals. *Viruses* 15:1094. doi: 10.3390/v15051094

Fiacre, L., Pagès, N., Albina, E., Richardson, J., Lecollinet, S., and Gonzalez, G. (2020). Molecular determinants of West Nile virus virulence and pathogenesis in vertebrate and invertebrate hosts. *Int. J. Mol. Sci.* 21:9117. doi: 10.3390/ijms21239117

Gil, P., Dupuy, V., Koual, R., Exbrayat, A., Loire, E., et al. (2021). A library preparation optimized for metagenomics of RNA viruses. *Mol. Ecol. Resour.* 21, 1788–1807. doi: 10.1111/1755-0998.13378

Green, M., Weinberger, M., Ben-Ezer, J., Bin, H., Mendelson, E., Gandacu, D., et al. (2005). Long-term death rates, West Nile virus epidemic, Israel, 2000. *Emerg. Infect. Dis.* 11, 1754–1757. doi: 10.3201/eid1111.040941

Hahn, C. S., Hahn, Y. S., Rice, C. M., Lee, E., Dalgarno, L., Strauss, E. G., et al. (1987). Conserved elements in the 3' untranslated region of flavivirus RNAs and potential cyclization sequences. *J. Mol. Biol.* 198, 33–41. doi: 10.1016/0022-2836(87)90455-4

Kampen, H., Holicki, C., Ziegler, U., Groschup, M., Tews, B., and Werner, D. (2020). West Nile virus mosquito vectors (Diptera: Culicidae) in Germany. *Viruses* 12:493. doi: 10.3390/v12050493

Kobayashi, S., Kaneko, C., Kawakami, R., Hasebe, R., Sawa, H., Yoshii, K., et al. (2020). Amino acid 159 of the envelope protein affects viral replication and T-cell infiltration by West Nile virus in intracranial infection. *Sci. Rep.* 10:7168. doi: 10.1038/s41598-020-64199-7

Komar, N. (2003). West Nile virus: Epidemiology and ecology in North America. *Adv. Virus Res.* 61, 185–234. doi: 10.1016/s0065-3527(03)61005-5

Kramer, L., Li, J., and Shi, P. (2007). West Nile virus. *Lancet Neurol.* 6, 171–181. doi: 10.1016/S1474-4422(07)70030-3

Lecollinet, S., Pronost, S., Coulpier, M., Beck, C., Gonzalez, G., Leblond, A., et al. (2019). Viral equine encephalitis, a growing threat to the horse population in Europe? *Viruses* 12:23. doi: 10.3390/v12010023

Li, X., Fu, S., Liu, W., Wang, H., Lu, Z., Tong, S., et al. (2013). West Nile virus infection in Xinjiang, China. *Vector Borne Zoonotic Dis.* 13, 131–133. doi: 10.1089/vbz.2012.0995

Linke, S., Ellerbrok, H., Niedrig, M., Nitsche, A., and Pauli, G. (2007). Detection of West Nile Virus lineages 1 and 2 by real-time PCR. *J. Virol. Methods* 146, 355–358. doi: 10.1016/j.jviromet.2007.05.021

Malkinson, M., Banet, C., Weisman, Y., Pokamunski, S., King, R., Drouet, M., et al. (2002). Introduction of West Nile virus in the middle east by migrating white storks. *Emerg. Infect. Dis.* 8, 392–397. doi: 10.3201/eid0804.010217

Martin, M., and Simonin, Y. (2019). [West Nile virus historical progression in Europe]. *Virologie* 23, 265–270. doi: 10.1684/vir.2019.0787

Melnick, J. L., Paul, J. R., Riordan, J. T., Barnett, V. H., Goldblum, N., and Zabin, E. (1951). Isolation from human sera in Egypt of a virus apparently identical to West Nile Virus. *Proc. Soc. Exp. Biol. Med.* 77, 661–665. doi: 10.3181/00379727-77-18884

Moudy, R., Meola, M., Morin, L., Ebel, G., and Kramer, L. (2007). A newly emergent genotype of West Nile virus is transmitted earlier and more efficiently by culex mosquitoes. *Am. J. Trop. Med. Hyg.* 77, 365–370.

Murgue, B., Murri, S., Triki, H., Deubel, V., and Zeller, H. G. (2001). West Nile in the Mediterranean Basin: 1950-2000. *Ann. N. Y. Acad. Sci.* 951, 117–126. doi: 10.1111/j.1749-6632.2001.tb02690.x

Prjibelski, A., Antipov, D., Meleshko, D., Lapidus, A., and Korobeynikov, A. (2020). Using SPAdes De Novo Assembler. *Curr. Protoc. Bioinformatics* 70:e102. doi: 10.1002/cpbi.102

Riccardo, F., Bella, A., Monaco, F., Ferraro, F., Petrone, D., Mateo-Urdiales, A., et al. (2022). Rapid increase in neuroinvasive West Nile virus infections in humans, Italy, July 2022. *Euro Surveill.* 27:2200653. doi: 10.2807/1560-7917.ES.2022.27.36.2200653

Smithburn, K., Hughes, T., Burke, A., and Paul, J. (1940). A neurotropic virus isolated from the blood of a native of Uganda. *Am. J. Trop. Med. Hyg.* 20, 471–492.

Toma, L., Cipriani, M., Goffredo, M., Romi, R., and Lelli, R. (2008). First report on entomological field activities for the surveillance of West Nile Disease in Italy. *Vet. Ital.* 44, 483–497, 499–512.

Toussaint, J. F., Sailleau, C., Breard, E., Zientara, S., and De Clercq, K. (2007). Bluetongue virus detection by two real-time RT-qPCRs targeting two different genomic segments. *J. Virol. Methods* 140, 115–123. doi: 10.1016/j.jviromet.2006.11.007

Tsioka, K., Gewehr, S., Kalaitzopoulou, S., Pappa, S., Stoikou, K., Mourelatos, S., et al. (2022). Detection and molecular characterization of West Nile virus in culex pipiens mosquitoes in central Macedonia, Greece, 2019-2021. *Acta Trop.* 230:106391. doi: 10.1016/j.actatropica.2022.106391

Van Slyke, G., Jia, Y., Whiteman, M., Wicker, J., Barrett, A., and Kramer, L. (2013). Vertebrate attenuated West Nile virus mutants have differing effects on vector competence in culex tarsalis mosquitoes. *J. Gen. Virol.* 94 (Pt 5), 1069–1072. doi: 10.1099/vir.0.049833-0

Vasimuddin, M., Misra, S., Li, H., and Aluru, S. (2019). "Efficient architecture-aware acceleration of BWA-MEM for multicore systems," in *Proceedings of the 2019 IEEE international parallel and distributed processing symposium (IPDPS)*, Rio de Janeiro, 314–324. doi: 10.1109/IPDPS.2019.00041

Whiteman, M., Li, L., Wicker, J., Kinney, R., Huang, C., Beasley, D., et al. (2010). Development and characterization of non-glycosylated E and NS1 mutant viruses as a potential candidate vaccine for West Nile virus. *Vaccine* 28, 1075–1083. doi: 10.1016/j.vaccine.2009.10.112

Frontiers in Microbiology

Explores the habitable world and the potential of microbial life

The largest and most cited microbiology journal which advances our understanding of the role microbes play in addressing global challenges such as healthcare, food security, and climate change.

Discover the latest Research Topics

See more →

Frontiers

Avenue du Tribunal-Fédéral 34
1005 Lausanne, Switzerland
frontiersin.org

Contact us

+41 (0)21 510 17 00
frontiersin.org/about/contact